Behaviour of Trace Organics and Dissolved Organic Matter in Granular Activated Carbon Filters for Drinking Water Supply

A thesis
submitted in fulfilment
of the requirements for the degree
of
Doctor of Philosophy in Engineering
at
The University of Waikato
by
DANIEL RICHARD BERNSTEIN

THE UNIVERSITY OF
WAIKATO
Te Whare Wānanga o Waikato

2021

Abstract

Granular and biological activated carbon (GAC and BAC) filters are widely used to remove organic compounds from drinking water sources during municipal drinking water treatment. Common uses of GAC filters include removal of taste and odour (T&O) causing compounds such as geosmin and 2-methylisoborneol and reducing the concentration of dissolved organic matter (DOM) which contributes to the formation of disinfection by-products. GAC filters were installed at the Hamilton Drinking Water Treatment Station (HDWTS) in 2006 to address T&O issues and provide protection against cyanobacterial bloom events, and their effectiveness after such a long operational period was unknown. This study aimed to determine whether bacteria had colonised the GAC surface, compare full-scale GAC filters of different ages in their effectiveness in removing T&O compounds and different fractions of the DOM pool, and assess whether bacterially colonised GAC was able to remove high concentrations of T&O compounds during simulated, transient events after being subjected to steady state influent conditions. Results indicated that bacteria colonise the GAC surface quickly, and that T&O compounds and the humic fraction of the DOM are effectively removed. However, the extent to which humic substances were removed appeared to diminish relatively quickly as filters aged, and the protein fraction of the DOM appeared to be resistant to treatment across the entire treatment train.

Executive Summary

An investigation was undertaken into the performance of the granular activated carbon (GAC) filters used at the Hamilton Drinking Water Treatment Station (HDWTS) in terms of their removal of trace organic compounds and dissolved organic matter (DOM). GAC filters are widely used in water treatment for the removal of organic contaminants, and in the case of the HDWTS they were installed as a means to reduce the prevalence of taste and odour (T&O) compounds and problematic compounds associated with cyanobacterial blooms such as microcystins.

Prior to this study, information regarding the performance of the GAC filters present on-site was lacking, particularly information surrounding high concentration T&O events and with media that is partially depleted and operating as a biological activated carbon (BAC) filter. The main aim of this study was to provide the HWTS with an assessment on the performance of the GAC filters regarding the removal of the T&O compounds geosmin (GSM) and 2-methylisoborneol (2-MIB), particularly during transient, high concentration events, as well as the behaviour of the bulk DOM through the treatment train.

The GAC media was imaged with scanning electron microscopy (SEM) and its surface composition was determined with energy-dispersive x-ray spectroscopy (EDS). This revealed that the GAC surface is quickly colonised with bacteria (≤ 3 months), and that over time the surface becomes enriched with an inorganic layer that exhibited a high concentration of manganese (Mn) and oxygen (O). The high level of Mn on the older GAC media was confirmed using inductively coupled plasma mass spectrometry (ICP-MS). The presence of high levels of Mn and O on

the GAC surface indicates the presence of Mn(III/IV) oxides which may be a result of Mn(II) oxidising bacteria colonising the GAC surface. The presence of Mn(III/IV) oxides on the surface of the GAC media suggests some interesting implications for water treatment applications, considering the redox and adsorption properties of Mn oxides.

A quantitative GC-MS method was developed for the determination of GSM and 2-MIB and was applied to a survey of their distribution throughout the plant and in dosing experiments carried out using a pilot-scale GAC filter that was installed on site. The survey showed that the concentration of both compounds was significantly reduced during the flocculation stage and that they were not detected throughout the remainder of the treatment train. High concentration dosing experiments showed that the filter media was able to remove both compounds at concentrations up to 150 ng L^{-1}. A modelling investigation also showed that the filters were capable of dealing with a high concentration event, and that the empty bed contact time (EBCT) is a more important factor in removing these compounds rather than influent concentration.

The distribution of DOM was studied using total organic carbon (TOC) analysis and excitation emission fluorescence spectroscopy (EEMS) with parallel factor analysis (PARAFAC). TOC analysis showed significant reductions at the flocculation stage and at the GAC filters, although the removal at the GAC stage was related to filter age with the oldest filters providing no benefit with respect to TOC reduction. EEMS-PARAFAC showed that the DOM was comprised of three main components that were assigned as humic-like, tryptophan/protein-like and tyrosine/protein-like fluorophores. The humic-like fraction was strongly correlated

with TOC concentration and showed similar trends in removal across the plant. Behaviour in the GAC filters was also similar, with the reduction in humic-like fluorophores being related to the filter age, whilst the oldest filter provided no benefit with respect to the removal of humic substances. The protein-like fluorophores were found to be not as treatable, particularly the tyrosine-like fraction which was found to remain constant throughout treatment.

Acknowledgments

Firstly, I would like to express my deepest appreciation and gratitude to my chief supervisor Prof. Merilyn Manley-Harris. I have been incredibly lucky to have had you as a mentor since beginning as an undergraduate in the chemistry department, it has been a pleasure working with you over the last few years. Your experience has been invaluable during the course of writing this thesis, and I thank you for the time you have made for me in providing suggestions and feedback.

I would like to extend my sincere thanks to my supervisors Dr. Graeme Glasgow and Dr. Mark Lay. Graeme, I am grateful for being given the opportunity to work on this project, and your knowledge and guidance on water treatment processes has been invaluable. Mark, your technical help has been greatly appreciated, particularly with the modelling aspects. I thank you both for providing guidance and advice when needed, and in making time to review this work.

Many thanks to Sven Ericksen and Barry Hu at the Hamilton City Council for providing the project, organising access to the Waiora Water Treatment Station and their help throughout the course of the research program.

At the Waiora Water Treatment Station, a huge thank you to Rebecca Johnson, Oliver Bartley and Karl Hjelmstrom for their help with organising many aspects of this project alongside Dave, Kyle and Banda. Without your help, much of this research would have been impossible and I greatly appreciate how accommodating you have been over the course of the project.

Special thanks to Dr. Adam Hartland and Huma Saeed for their initial help with fluorescence spectroscopy, as well as Estelle Bezzina who helped with running the

fluorescence and TOC samples during her internship with the University of Waikato.

I would like to extend my thanks to the technical staff in the Chemistry Department. Firstly, Jenny Stockdill, your help over these last few years with all manner of things has been amazing and greatly appreciated, particularly with the GC-MS suite. Thank you also to Annie Barker, for being generally helpful and keeping our lab in order, as well as John Little and Karla Watson. Thanks to Steve Cameron for his help in developing the ICP-MS method and running the ICP-MS samples, and Dr. Megan Grainger for her helpful advice on the interpretation of the ICP-MS results.

Thank you to Helen Turner from the Division of Health, Engineering, Computing and Science for her help with everything SEM related. Also in the Engineering department, thanks to Pete Higgins for the welding work done on the pilot GAC column and also installing the column onsite, Brett Nichol for laser cutting parts for the pilot column and Shannon McMurray for help in coordinating site visits related to the installation of the pilot column. I would also like to thank Peter Jarman for his electrical work on the pilot column pump system.

I gratefully acknowledge the assistance of Kerstin Frazer and Activated Carbon Technologies NZ for donating initial samples of activated carbon which allowed the project to get started.

I am also grateful for the financial support provided by the University of Waikato through the School of Engineering Postgraduate Study Scholarship which allowed me to focus solely on my studies.

To my fellow grad students in the chemistry department, thanks for the much-needed distractions and discussions, I wish you all the best with your continuing studies and future endeavours.

Talia, cheers for putting up with me for these last few years. You're a fairly proficient project manager, so I'll probably keep you on for a bit longer.

To my Dad, thank you for your years of support. These last few years have been very challenging, and your love and support during this time has been an inspiration. Finally, I would like to thank my Mother who nurtured my life-long passion for learning – you will be dearly missed.

Table of Contents

List of Figures

List of Tables

List of Abbreviations

µGAC	Micro-Grain Activated Carbon
1-ADML	1-adamantanol
^{1}H-NMR	Proton Nuclear Magnetic Resonance Spectroscopy
2-MIB	2-methylisoborneol
A	Analyte
AC	Activated Carbon
ACN	Acetonitrile
ADDA	3-amino-9-methoxy-2,6,8-trimethyl-10-phenyldeca-4,6-dienoic acid
AHDS	Anthrahydroquinone-2,6-disulphonate
ANOVA	Analysis of Variance
AOP	Advanced Oxidation Process
AQDS	Anthraquinone-2,6-disulphonate
ASE	Accelerated Solvent Extraction
ATX-a	Anatoxin-a
ATXs	Anatoxins
BAC	Biological Activated Carbon
BET	Brunauer, Emmett, Teller Isotherm
BGAC	Biological Granular Activated Carbon
BIX	Freshness Index
BOM	Biodegradable Organic Matter
BSE	Back-scatter electron (imaging)
C1	Component 1
C2	Component 2
C3	Component 3
CI	Confidence Interval
cis-DHN	*cis*-decahydro-1-napthol
CLS	Closed Loop Stripping
COD	Chemical Oxygen Demand
CRM	Certified reference material
CYNs	Cylindrospermopsins
DBPFP	disinfection by-product formation potential
DI	De-ionised
DLLME	Dispersive liquid-liquid micro-extraction
DO	Dissolved Oxygen
DOM	Dissolved Organic Matter
DPB	Disinfection By-product
DPB	Disinfection By-Product
DWSNZ	Drinking Water Standards for New Zealand
DWTP	Drinking Water Treatment Plant
EBC	Equivalent Background Compound
EBCT	Empty Bed Contact Time
EC	Expanded Clay
ECD	Electron Capture Detection
ECs	Emerging Contaminants
EDCs	Endocrine Disrupting Chemicals
EEM	Excitation Emission Matrix
EEMS	Excitation-Emission Matrix Fluorescence Spectroscopy

EI	Electron Impact
EIC	Extracted ion chromatogram
ELISA	Enzyme-Linked Immunosorbent Assay
ER	Extraction Recovery
EtOH	Ethanol
EU	European Union
Ex_{max}/Em_{max}	Maximum Excitation/Emission Wavelength
fDOM	Fluorescence Dissolved Organic Matter
FI	Fluorescence Index
FLD	Fluorescence Detection
F_{max}	Fluorescence Maximum
GAC	Granular Activated Carbon
GC-MS	Gas Chromatography Mass Spectrometry
GC-SPE	Graphitised Carbon Solid Phase Extraction
GSM	Geosmin
GTX	Gonyautoxin
HAAFP	Haloacetic Acid Formation Potential
HAAs	Haloacetic Acids
HC1	Humic Component 1
HC2	Humic Component 2
HC3	Humic Component 3
HCC	Hamilton City Council
HDWTP	Hamilton Drinking Water Treatment Plant
HILIC	Hydrophilic Interaction Liquid Chromatography
HIX	Humification Index
HLR	Hydraulic Loading Rate
HWTS	Hamilton Water Treatment Station
IAST	Ideal Adsorbed Solution Theory
IDL	Instrument detection limit
IFE	Inner-Filter Effect
IPA	*iso*-propyl alcohol
IQL	Instrument quantitation limit
IS	Internal standard
K_{OW}	Octanol-Water Partition Coefficient
LDF	Linear Driving Force
LLE	Liquid-Liquid Extraction
LLME	Liquid-Liquid Micro-Extraction
LLOQ	Lower Limit of Quantitation
LOD	Limit of Detection
LSE	Liquid Sample Extraction
LVI	Large Volume Injection
MAV	Maximum Acceptable Value
MC-LR	Microcystin LR
MCs	Microcystins
MDL	Method detection limit
MeOH	Methanol
MQL	Method quantitation limit
nAchRs	Nicotinic Acetylcholine Receptors
NBR	Acrylonitrilebutadiene Rubber
NED	Needle-like Extraction Device

NMR	Nuclear Magnetic Resonance Spectroscopy
NOD	Nodularin
NOM	Natural Organic Matter
NPOC	Non-purgeable Organic Carbon
OCT	Odour Concentration Threshold
PAC	Powdered Activated Carbon
PARAFAC	Parallel Factor Analysis
PCA	Principle Component Analysis
PCA	Principal Component Analysis
PF	Preconcentration factor
PFO	Pseudo first order
PHP	Potassium Hydrogen Phthalate
PMAV	Provisional Maximum Acceptable Value
PMAVs	Provisional Maximum Acceptable Values
PMMA	Polymethylmethacrylate
PNEC	Predicted-no-effect Concentration
PPCPs	Pharmaceuticals and Personal Care Products
PSO	Pseudo second order
PSTs	Paralytic Shellfish Toxins
PT	Purge and Trap
QC	Quality Control
RSD	Relative Standard Deviation
RSE	Residual Standard Error
R.U.	Raman Units
S/N	Signal to noise
SBSE	Stir-bar Sorptive Extraction
SD	Standard Deviation
SEM	Scanning Electron Microscope
SHS	Static Headspace Extraction
SIM	Selected ion mode
SO	Second order
SOC	Synthetic Organic Contaminant
SPE	Solid Phase Extraction
SPME	Solid Phase Micro-Extraction
STXs	Saxitoxins
T&O	Taste and Odour
TCAA	Trichloroacetic Acid
TCC	Tucker's Congruence Coefficient
THMs	Trihalomethanes
t-NP	Technical Nonylphenol
TOC	Total Organic Carbon
TOX	Total Organic Halogens
UV	Ultraviolet
VALLME	Vortex Assisted Liquid-Liquid Microextraction
VSD	Variable Speed Drive
WRC	Waikato Regional Council
WTP	Water Treatment Plant
WTS	Water Treatment Station
WWTP	Wastewater Treatment Plant
SMPs	Soluble Microbial Products

Chapter 1:

Introduction

1 Introduction

For the city of Hamilton, municipal drinking water supply is sourced from the Waikato River, which is New Zealand's longest river (442 km). The catchment for the Waikato River begins prior to Lake Taupo, on the eastern side of Mount Ruapehu as the Upper Waikato Stream, which joins with the Tongariro River before entering Lake Taupo. The Waikato River in its current course flows in a northerly direction from Lake Taupo and onward through the Waikato district before discharging into the Tasman Sea at Port Waikato (**Figure 1-1**) ***[1]***.

Figure 1-1: Map outlining the course of the Waikato River beginning from the Upper Waikato Stream (Source: 38°49'33.41" S 175°55'33.85" E. GOOGLE EARTH. October 4, 2013. December 14, 2015).

The total catchment area encompasses 11013 km^2 which drains from and flows through land used for various purposes. Based on 2008 data, land use is predominantly pastoral (44%), planted forest (41%) and indigenous forest (9%) with a small percentage (6%) which may include scrub, horticulture, inland water, willows and poplar ***[1]***. However, there has recently been large scale conversion of

planted forest to pasture, so these figures will have changed somewhat. Due to the varied land use, and in particular the intensive agriculture carried out along the course of the river, there are numerous point and non-point sources throughout the river system that contribute to the overall water quality by the time it reaches Hamilton for drinking water treatment.

Prior to distribution, municipal drinking water is treated at the Hamilton City Council (HCC) Drinking Water Treatment Station (DWTS) (**Figure 1-2**). This plant was built in 1971 and was originally designed to produce 64 megalitres per day (ML D^{-1}). Over the years, the plant has been expanded to its current capacity, with a capability of producing 106 ML D^{-1} ***[2]***. The plant consists of a series of individual processes designed to purify the source water and deliver it to the consumer (**Figure 1-3**) in a form that adheres to the Drinking Water Standards for New Zealand (DWSNZ,***[3]***).

Figure 1-2: Aerial view of the Hamilton Drinking Water Treatment Station (Source: 37º48'33.96" S 175º18'12.50" E. GOOGLE EARTH. January 5, 2013. October 23, 2015).

The main functions of each process are follows:

- Screening: Physical removal of large and small debris such as pieces of wood, leaves, aquatic weeds, etc.
- Flocculation and Sedimentation: Chemical precipitation of microorganisms, fulvic acids, humic acids, metals and other inorganic/organic compounds.
- Sand Filtration: Physical filtration of residual floc and any large residual material remaining after flocculation/sedimentation.
- Granular Activated Carbon: Removal of taste and odour compounds, residual microorganisms, cyanotoxins and other organic compounds via physicochemical adsorption.
- UV Disinfection: Kills residual protozoa.
- Chlorine Disinfection: Kills any remaining bacteria. The chlorinated water is allowed to dwell in a reservoir to allow for maximum chlorine contact and effectiveness. Water pumped to the city reservoirs contains residual chlorine as extra protection against bacterial growth
- Fluoride Dosing: Addition of Fluoride (as hexafluorosilicic acid) as per Council policy and Ministry of Health recommendations.
- pH Correction: Addition of lime to return pH to neutral as flocculation lowers pH.

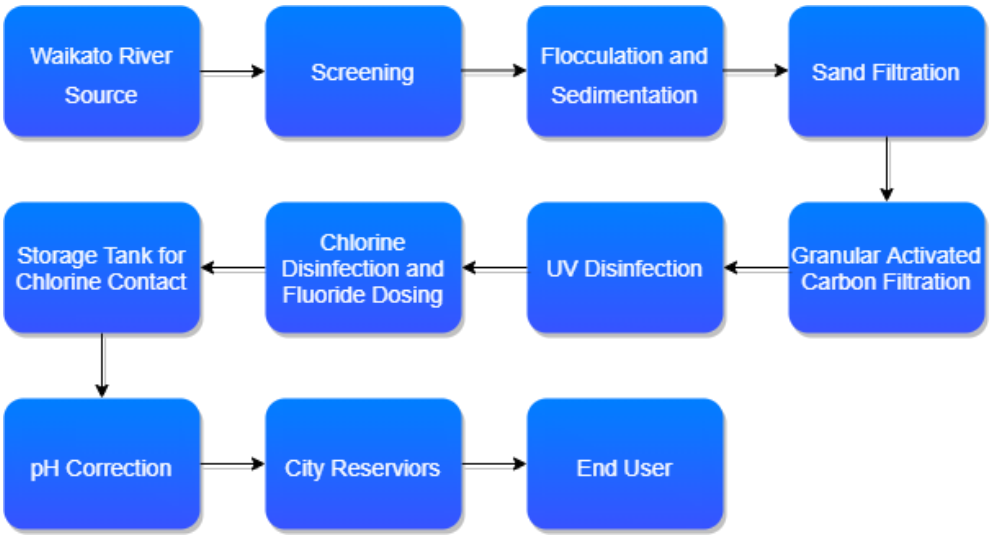

Figure 1-3: Basic process flow for the Hamilton City Council Drinking Water Treatment Station (adapted from *[2]*).

Prior to 2006, the plant employed no Granular Activated Carbon (GAC) filtration. However, following a significant algal bloom of cyanotoxin-producing cyanobacteria in 2003, GAC filtration was implemented as part of a plant upgrade in 2006. This was aimed at removing cyanotoxins from drinking water during seasonal algal blooms while at the same time managing taste and odour problems typically associated with the presence of certain species of cyanobacteria ***[1,2,4,5]***. Due to the prevalence of cyanobacterial blooms during low flow or drought conditions, the frequency and severity of such blooms is likely to increase in the future due to climate change/global warming and the prospect of longer, hotter summers in the region ***[5,6]***.

The GAC system at the HDWTS comprises six individual filters that run in parallel. These filters are fed from water exiting the rapid sand filters and the effluent from the GAC filters is combined before UV treatment (**Figure 1-4**).

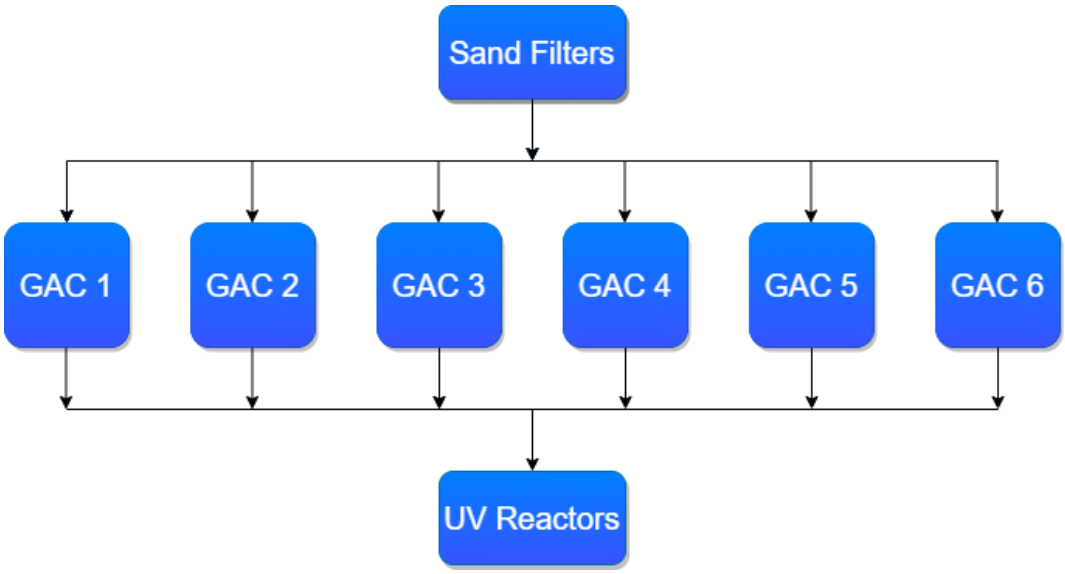

Figure 1-4: Diagram illustrating the arrangement of the GAC filters following sand filtration.

As the design of this particular GAC system makes replacement inherently difficult, and with GAC replacement being a rather expensive operation in general, the same

GAC is present in the filters as when the plant was initially implemented when this study was commenced. Therefore, the absorption capacity of the GAC was likely to be have been almost entirely exhausted and the current system is likely to be operating more akin to a biologically activated carbon (BAC) system with adsorption and transformation of chemical substrates present in the source water being carried out enzymatically by microorganisms attached to the GAC surface as a biofilm ***[7,8]***. Nevertheless, part-way through this study, the HCC decided to partially replace the GAC media by removing approximately half of the old GAC media and replacing it with new media. Media replacement was carried out in the order from first to last of GAC 6, GAC 1, GAC 2, GAC 3, GAC 4, GAC 5. While this resulted in some challenges regarding reworking sampling protocols that were initially proposed, it did provide an opportunity to investigate the performance of the GAC filters at various stages of their service life.

The GAC media used in the filters at the HDWTS is Acticarb BAC GA1000N 8 x 30 mesh (referred to throughout as GA1000N) which is a steam activated, coal-based activated carbon manufactured by Activated Carbon Technologies (Perth, Australia). The general properties as outlined by the manufacturer are given in **Table 1-1**. The properties of this GAC have been studied previously ***[9]***, and some further properties are given in **Table 1-2** to supplement **Table 1-1**.

Table 1-1: Acticarb BAC GA1000N properties as specified by Activated Carbon Technologies *[10]*.

Property	Value
Apparent density	0.35 – 0.45 g mL^{-1}
Moisture content (maximum)	2 %
Ash content (maximum)	6 %
Iodine number (minimum)	1000 mg g^{-1}
Surface area (minimum)	1000 m^2 g^{-1}
pH	5 - 8
Hardness index (minimum)	90 %

Table 1-2: Properties of Acticarb BAC GA1000N as determined in *[9]*.

Property	Value
Bulk density	564 kg m^{-3}
Mean 2D equivalent diameter	1.6 mm
Particle effective size	0.6 mm
Uniformity coefficient	< 1.8
Iodine number	1050 mg g^{-1}
BET surface area; based on Argon adsorption	1146 m^2 g^{-1}
Total porous volume	0.476 cm^3 g^{-1}
Microporous volume<2 nm	0.360 cm^3 g^{-1}
Mesoporous volume 2–50 nm	0.116 cm^3 g^{-1}

1.1 Thesis Objectives and Outline

Prior to commencing this study, a formal and comprehensive study of the behaviour of organic compounds in the HWTS had not been undertaken and knowledge relating to the performance of the GAC filters in relation to the removal of organic compounds was lacking or unknown, particularly after the filters had been in service for a long period of time. This thesis aimed to investigate the behaviour of organic compounds through the treatment train with a focus on the GAC filters following consultation with plant staff and engineers.

As the HDWTS has had issues historically with T&O compounds, as well as other cyanobacterial metabolites, geosmin and 2-MIB were selected as targets for gaining insight into the behaviour of specific, non-polar small organic compounds present at trace-level concentrations as they progress through the treatment train. Of

particular interest to the plant engineers was the behaviour of 2-MIB and GSM in the GAC filters during high concentration, transient events. Additionally, the behaviour of organic compounds at the bulk level was investigated to give further insight into the behaviour of organic compounds (e.g. humic acids and proteins) that are present at higher concentrations to supplement the information obtained from monitoring model compounds and assessing any differences in treatability between hydrophilic (e.g. proteins and peptides) and hydrophobic (e.g. humic acids) organic compounds. Specifically, this thesis aimed to answer or provide further information on the following questions:

- Have bacteria extensively colonised the GAC surface, causing the current filters to operate as BAC filters.
- Is the current treatment system adequate for removing T&O compounds, particularly during transient, high concentration events.
- How do different components of the DOM pool behave as they progress through the treatment train.

Chapter 2 comprises a literature review of the use of GAC in drinking water treatment in general as well as the behaviour and analysis of geosmin, 2-MIB and other cyanobacterial metabolites in drinking water treatment settings. This review also provides the basis for the development of a quantitative GC-MS method for geosmin and 2-MIB which is covered in chapter 4. This chapter also includes a review of the use of Excitation-Emission Matrix Fluorescence Spectroscopy (EEMS) for studying dissolved organic matter (DOM) as it relates to drinking water treatment to give some context on how the technique is used and what kind of information it can provide.

Chapter 3 provides the results of an investigation into the elemental composition and surface morphology of the GAC media at various stages of its service lifetime. The surface morphology was investigated using scanning electron microscopy (SEM), primarily in order to confirm the presence of microorganisms on the GAC surface. The elemental surface and bulk composition of the GAC was investigated using energy-dispersive x-ray spectroscopy (EDS) and inductively coupled plasma mass spectrometry (ICP-MS) respectively.

Chapter 4 describes the development of a quantitative GC-MS method for the analysis of the T&O compounds geosmin and 2-MIB. Standard methods for the analysis of these compounds are generally cumbersome and provide slow sample turn around which make them poorly suited for processing large amounts of samples. As such, a method that provided a quick and simple sample preparation procedure was developed and validated. The validated method was then applied to the research problem which is covered in chapter 5. This included a survey of the full-scale treatment process, the behaviour of 2-MIB and geosmin in a pilot scale GAC filter during high concentration, transient events and obtaining adsorption isotherms for use in modelling the removal of 2-MIB and geosmin in GAC filters.

Chapter 6 investigates the behaviour of total organic carbon (TOC) and fluorescent dissolved organic matter (fDOM) within the HWTS treatment train. A survey of the full-scale treatment train was then undertaken with the samples being analysed using EEMS in conjunction with parallel factor analysis (PARAFAC) with comparisons to results obtained from TOC analysis. The use of EEMS-PARAFAC

was then extended to include an investigation into the behaviour of fDOM in a pilot-scale GAC column.

Experimental methods and materials are included as part of their respective chapters. Each chapter includes a short conclusion relevant to the respective chapter, while final conclusions and recommendations for further research are included in chapter 7.

Chapter 2:

Literature Review†

† An abridged version of this review was originally published as a conference paper in Chemeca 2016: Chemical Engineering - Regeneration, Recovery and Reinvention. Melbourne, Vic.: Engineers Australia, **2016**: 815-827. See Appendix B-1

2 Literature Review

2.1 Review Structure and Search Methodology

A review of the relevant literature was conducted using SciFinder® with search terms constrained to the specific research topic. Initial searches were focused on review papers and book chapters to obtain an overview of the topic and from which more specific references could be gathered, read, and synthesised.

The first half of the review was focused on GAC and BAC filtration technologies and how cyanobacterial metabolites (particularly T&O compounds) are removed by such processes. This section of the review also looked for methods used for the quantitative analysis of cyanotoxins and T&O compounds.

The second half of the review looked at the current literature for the analysis of DOM in drinking water sources, treatment facilities and distribution networks in order to be able to assess the distribution of DOM in such systems. Initial searches identified that excitation-emission matrix fluorescence spectroscopy (EEMS) was the preferred and most widely used method for studying DOM in natural waters across a range of scientific disciplines.

Search terms for each major topic of the review are given in **Table 2-1**. Initial search terms included those given as well as Boolean combinations of phrases and single terms.

Table 2-1: Initial search terms used for each major topic included in the literature review.

Research Topic	Search terms
Removal of cyanobacterial metabolites from water using GAC and BAC filtration technologies	• BAC Drinking Water • BAC Drinking Water Treatment • GAC Drinking Water • GAC Drinking Water Treatment
Quantitative analysis of cyanotoxins and T&O compounds	• BAC Drinking Water • BAC Drinking Water Treatment • GAC Drinking Water • GAC Drinking Water Treatment
Distribution and analysis of DOM in natural waters and drinking water systems	• DOM Natural Water • DOM Drinking Water • DOM Analysis Water
Analysis of DOM in water using EEMS PARAFAC	• EEMS Drinking Water • EEMS DOM Water • EEMS PARAFAC • EEMS PARAFAC Drinking Water

2.2 Granular Activated Carbon

The use of carbon as a medium for the purification of water dates back to around 450 BC, with Hindu documents from this time making references to the use of sand and charcoal filters for these purposes. Studies of the wrecks of Phoenician trading ships dating from similar times (*ca.* 460-370 BC) have also shown that drinking water was stored in charred wooden barrels to keep it fresh. Initial uses likely arose empirically, with detailed scientific studies into the mechanisms of purification not being undertaken until the 19th century. The earliest use of activated carbon in water treatment was in 1910 for the purpose of dechlorinating chlorinated water, with subsequent application to a range of treatment problems throughout the 20th century including the removal of taste and odour (T&O) causing compounds, synthetic organic contaminants (SOCs) and disinfection by-products (DPBs) ***[7]***.

Activated carbons (ACs) are porous carbonaceous materials capable of adsorbing a wide range of aqueous phase solutes. Because of this porosity and the very high surface area this represents (500-1500 m^2g^{-1}), they have the potential to adsorb very large amounts of material ***[7,11]***.

Commercially available ACs are manufactured from a wide range of materials that have high carbon content including wood, peat, coconut shells and coal to name but a few. These raw materials are converted to ACs via two sequential processes; carbonisation and activation. Carbonisation involves drying and heating to remove unwanted components followed by pyrolysing the carbon material at high temperatures (600-800^{o}C) in an oxygen deficient atmosphere. The pyrolysed

material can then be activated thermally (high temperature steam or CO_2) or chemically (H_3PO_4, KOH or $ZnCl_2$) ***[7,11]***.

The nature of the starting material, carbonisation conditions and activation process all contribute to the properties of the AC produced. Such properties include porosity, pore size, pore size distribution, surface functionality, and ash content ***[7,11]***. The surface functionality of ACs plays an important role in the adsorption of organic solutes and is comprised mainly of oxygen based functional groups. Acidic groups include strong and weak carboxylic acids, phenols and carbonyls (α protons). Basic surface groups such as cyclic ethers are also generally present, with higher activation temperatures resulting in a more basic surface. Other components of ACs such as minerals (e.g. calcium, sulphate, and phosphate ions) and ash (silica, alumina, iron oxides, and alkaline earth metals) also contribute to the surface activity ***[7]***. Granular activated carbons generally have a particle size ranging from 0.2 – 5mm and are designated by mesh sizes such as 8/20, 20/40, or 8/30 for liquid phase applications such as drinking water treatment ***[7,12]***.

2.2.1 GAC in Drinking Water Treatment

The use of granular activated carbon (GAC) in drinking water treatment is a very common practice and is implemented with the aim of removing unwanted contaminants from source water intended for use as drinking water that cannot be removed via primary treatment ***[7,8,13]***. As such, the composition of the source water and the specific contaminants it may contain mean that GAC is employed for different reasons depending on location ***[7,8]***. In Hamilton, GAC filtration was introduced as a precautionary measure for the removal of cyanobacterial

metabolites, particularly cyanotoxins such as microcystins (**Figure 2-1**) and saxitoxins (**Figure 2-2**), that may pose serious health risks during future cyanobacterial blooms ***[4]***. Additionally, GAC is extremely effective in the removal of taste and odour (T&O) compounds such as geosmin and 2-methylisoborneol (2-MIB) ***[7]*** which are known to be present in the waters of the Waikato River (**Figure 2-3**).

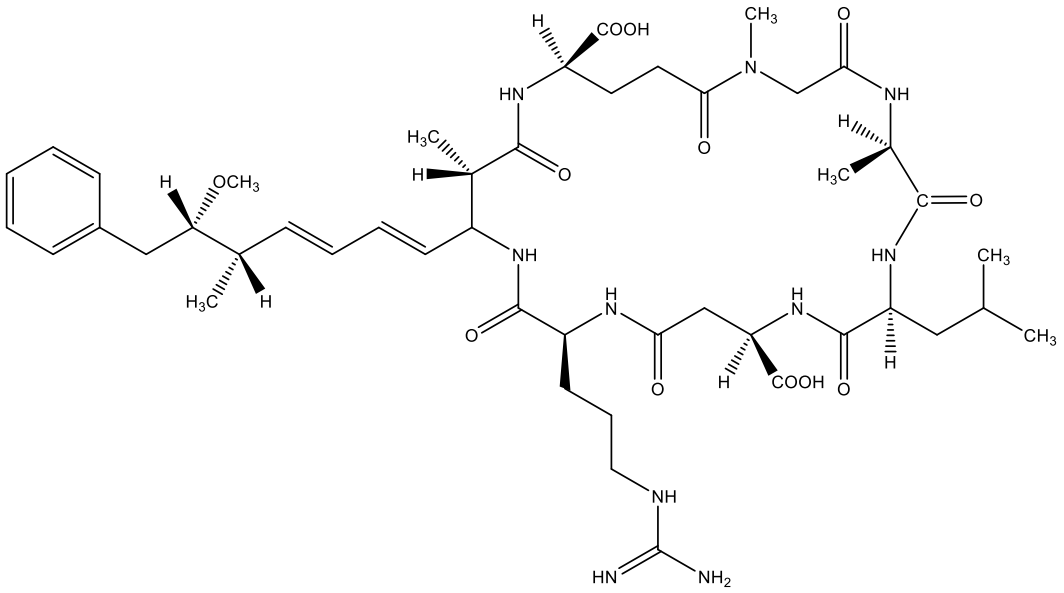

Figure 2-1: Molecular structure of Microcystin L-R.

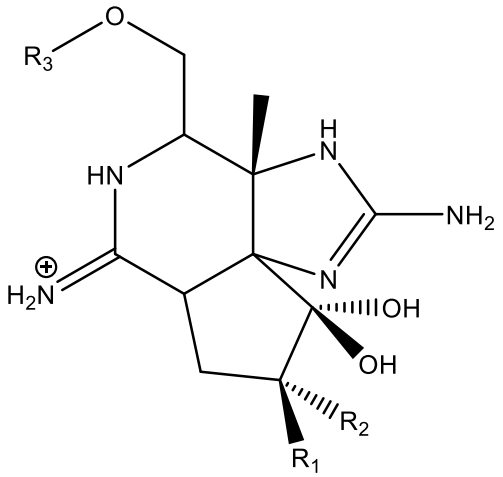

R_1 = H or OSO_3^-
R_2 = H or OSO_3^-
R_3 = $CONH_2$ or $CONHSO_3^-$

Figure 2-2: Molecular structure of the saxitoxin class of cyanotoxins.

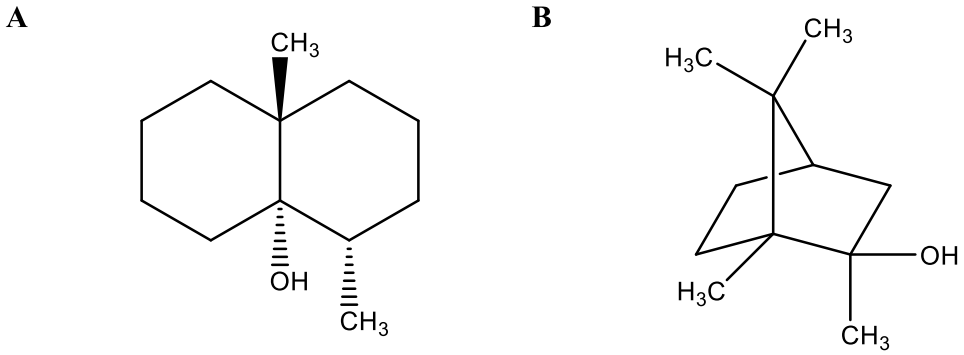

Figure 2-3: Molecular structures of Geosmin (A) and 2-methylisoborneol (B).

2.2.1.1 Adsorption on Granular Activated Carbon

The principal mechanisms for the removal of organic compounds on GAC are physical and chemical adsorption. The type of adsorption can be delineated by the binding energy of the interaction between the adsorbate and the adsorbent, with high binding energies reflecting chemical adsorption and lower binding energies reflecting physical adsorption. This correlates also to the reversibility of adsorption of a particular solute molecule ***[7,11,13]***.

The process of adsorption is influenced by several parameters related to the characteristics of the solid phase adsorbent, liquid phase solvent and adsorbate molecules. These include:

- Surface area of the adsorbent
- Physical and chemical properties of the adsorbate
- pH
- Temperature
- Porosity of the adsorbent
- Chemical properties of the adsorbent surface

Adsorption kinetics, or the rate of approach towards equilibrium of an analyte between the aqueous and solid phase, are generally limited by mass transport of the adsorbate to the adsorbing phase. Transport mechanisms include, bulk solution transport (advection), external diffusion, internal diffusion and finally adsorption to the carbon surface ***[7]***.

Adsorption kinetics can be described by carrying out adsorption experiments and interpreting the data using various adsorption isotherm models. The most commonly used and simplest of these include the BET (Brunauer, Emmett, Teller) model, the Freundlich isotherm and the Langmuir isotherm.

However, these models generally apply to only single solute cases; a situation not encountered in real world, drinking water applications. In multi-solute cases, the ideal adsorbed solution theory (IAST) and its modified versions which include the Freundlich equilibrium expression are often used, where the bi-solute (*N = 2)* case results in a pair of equations that can be solved simultaneously ***[8,14-16]***.

In the case of natural waters, the number of compounds making up the natural matter present is very large and, even if all those present could be identified, solving IAST models becomes computationally unfeasible. However, simplifications and assumptions can be made in order to obtain sufficiently accurate yet practical multi-solute adsorption models.

For example, types of natural organic matter (NOM) with similar adsorption characteristics can be defined as theoretical groups of compounds, significantly reducing the number of equations that need be solved simultaneously. For a system

of *N* components, the equilibrium expression for a solute *i* can be derived in the form;

$$C_{i,0} - q_i C_c - \left(\frac{q_i}{\sum_{j=1}^{N} q_j}\right)\left[\frac{\sum_{j=1}^{N} n_j q_j}{n_i K_i}\right]^{n_i} = 0 \qquad (2\text{-}1)$$

Where:
N = number of components
$C_{i,0}$ = initial concentration of compound *i*
C_c = carbon dose
q_i = equilibrium solid-phase concentration of *i*
n_i and K_i = single solute Freundlich parameters for *i*
j = other components in the system

Furthermore, the model can be simplified by assuming other organic matter that competes with target adsorbate can be represented as a single component, called the equivalent background compound (EBC). This approach relies on the Freundlich constants for the target compound and the EBC being between 0.1 and 1, and also that the concentration of the EBC far exceeds that of the target compound. If these criteria are met, the IAST can be simplified to give ***[8,15]***:

$$q_1 = C_{1,0}\left[C_c + \frac{1}{q_2}\left(\frac{n_2 q_2}{n_1 K_1}\right)^{n_1}\right]^{-1} \qquad (2\text{-}2)$$

Provided the above assumptions hold, the adsorption capacity for a trace compound can be determined by plotting the data from the adsorption isotherm of the trace compound on a log-log plot versus carbon dose from which the carbon dose for a required percentage removal can be calculated. In the case of geosmin and 2-MIB, concentrations of less than 1000 ng L^{-1} have been shown to give acceptable results ***[14,16]***. These concentrations are much higher than those typically encountered in the Waikato River, therefore such a model is likely to be applicable. However, in

the case where the adsorption capacity of the GAC surface is exhausted and biological degradation of trace compounds becomes a significant factor, adsorption models are likely to be less informative with respect to the performance of the GAC media in which biological degradation is likely to dominate.

2.3 Biological Activated Carbon

Removal of organic compounds from source waters using GAC is achieved via physicochemical adsorption. Hence, once the adsorptive capacity of the GAC is exhausted, adsorption can no longer occur and breakthrough is observed ***[13]***. To overcome this, the GAC must either be replaced or re-activated in order to restore its adsorption capacity. This is very labour intensive and costly, therefore in recent times, numerous investigations into the use of biological activated carbon (BAC or BGAC) have been carried out in various water treatment scenarios.

Biological activated carbon is activated carbon on which a biofilm has been allowed to accumulate with the aim of removing influent contaminants via biodegradation. Over the course of their lifetime, GAC filters are slowly converted to BAC as their adsorption capacity is depleted and a biofilm begins to accumulate. The term BAC (or BGAC) is also often used to refer to the combination of an advanced oxidation process (**Appendix B-2**)[†] with a BAC reactor as a coupled process. Obviously, the effectiveness of a BAC reactor is dependent on the biodegradability of the target compound. In the case of poorly or non-biodegradable compounds, the

[†] An article providing further information on this was originally published in Chemistry in New Zealand, 81(1), 13–18, **2017.** See Appendix B-2

implementation of an AOP prior to BAC aims to increase the biodegradability of the compounds by chemical oxidation ***[17,18]***.

In various parts of the World, some concerns have been raised by the public and regulatory bodies regarding the introduction of pathogens into the water supply via the sloughing of bacteria from biological filters. However, evidence suggests this concern is unwarranted ***[19]***. Furthermore, in the case of Hamilton's DWTP, UV disinfection is carried out directly following the GAC/BAC filters as a direct measure to remove pathogens such as cryptosporidium.

Although the ideal scenario is the biodegradation of target compounds leading to complete mineralisation, partial degradation by a change in molecular functionality to give compounds that impart no or reduced deleterious aesthetic or toxicological qualities to a treated water is also acceptable ***[20]***. However, the transformation of organic compounds into toxic or otherwise harmful products is a possibility that should not be overlooked.

2.3.1 Biodegradation and Enzyme Kinetics

Biodegradation of organic compounds is achieved through the metabolic processes of bacterial cells. The growth of bacteria requires an input of some energy source, which is generated via the transfer of electrons in oxidation/reduction reactions. This requires the presence of electron donors (oxidants; oxygen, nitrate, iron (III) etc.) or electron acceptors (reductants; NOM, trace organic compounds, ammonia etc.) to support cellular growth ***[20,21]***. This is defined as primary metabolism, with the compounds that promote primary metabolism being termed primary substrates. Additionally, metabolic processes may be carried out by bacteria on substrates that

do not contribute to cellular growth. This is termed secondary metabolism which acts upon secondary substrates. In general, secondary metabolism occurs when a compound is present at trace levels in the presence of a more concentrated primary substrate. Both primary and secondary metabolism can be exploited by using the metabolic transformations of target contaminants carried out by a bacterial colony attached to some support media (biofilm) as a means of removal. In the context of removing trace organic compounds from drinking water sources, secondary metabolism is important, as the compounds of interest are usually present in much lower concentration than the primary substrate (biodegradable organic matter or BOM). The primary metabolism of bacteria involved the metabolism of some primary substrate for utilisation in cell synthesis and simultaneous mass loss by endogenous decay can generally be described by the Monod relationship ***[20]***:

$$r_{syn} = Y_p \frac{\hat{q}_p S_p}{K_p + S_p} B \qquad (2\text{-}3)$$

Where:
r_{syn} = rate of new cell synthesis
Y_p = true yield coefficient for the primary substrate
$\hat{q}_p$ = maximum specific rate concentration for the primary
S_p = substrate
K_p = concentration of the primary substrate
B = half-maximum rate concentration for the primary substrate
concentration of active bacteria

And:

$$r_{dec} = -bB \qquad (2\text{-}4)$$

Where:
r_{dec} = rate of biomass decay
b = first-order decay coefficient

The rate of utilization of the secondary substrate can be derived from this equation, and provided the concentration of the secondary substrate is sufficiently small relative to the half-maximum rate concentration, the Monod expression can be simplified to give:

$$r_{ut} = -K_2 S_s B \tag{2-5}$$

Where: r_{ut} = rate of secondary substrate utilisation
S_s = secondary substrate concentration
K_2 = mixed second-order rate coefficient = $\frac{\hat{q}s}{Ks}$

Although the Monod relation is widely used in modelling bacterial growth, largely for practical reasons, it has no mechanistic basis ***[22]***. Other equations that attempt to model bacterial growth, such as logistic growth curves, together with the Michaelis-Menten mechanism of enzyme activity attempt to model secondary substrate utilisation on a more theoretical and mechanistic basis ***[23,24]***. The logistic equation is used to describe the growth of a population when there is an upper limit to the population density:

$$\frac{dB}{dt} = rB\left(\frac{1-B}{B_{max}}\right) \tag{2-6}$$

Where: r = maximum specific growth rate
B = population density
B_{max} = maximum population density

The Michaelis-Menten relationship can be used to describe rate of transformation of the substrate up to a maximum rate of substrate conversion which reflects the saturation of all available enzyme sites:

$$-\frac{dS}{dt} = \frac{V_{max}SB}{(K_m + S)} \quad (2\text{-}7)$$

Where: S = substrate concentration
B = population density
V_{max} = maximum specific reaction rate
K_m = half-saturation constant

Using these relationships, Schmidt *et al.* ***[23]*** developed 12 models describing the bacterial metabolism of secondary metabolites. These models can be used to describe bacterial populations exhibiting either logistic, exponential, linear or no growth at low, intermediate and high concentrations of secondary substrate. Biofilms that are growing attached to a biofilter (i.e. BAC) are often modelled as a steady-state biofilm, meaning that the growth and decay rates are equal giving no net growth ***[20,25]***. In this case, the growth function can be neglected ($B_0 = B_{max}$) and the model simplifies to a pseudo-first-order relationship (of the same form as the simplified Monod relationship; **Equation 2-5)** given that the number of cells do not change appreciably during the course of the reaction as the reactions are carried out catalytically by enzymes:

$$-\frac{dS}{dt} = k_1 S \quad (2\text{-}8)$$

$$k_1 = \frac{V_{max}B_0}{K_m} \quad (2\text{-}9)$$

Where: B_0 = initial population density

Of course, in the case of modelling continuous flow bioreactors, other factors need to be considered such as substrate concentration gradients, biomass population gradients, diffusion, and mass transport ***[20]***.

2.3.2 Biodegradation of 2-methylisoborneol

2-methylisoborneol (1,2,7,7-tetramethyl-*exo*-bicyclo[2.2.1]heptan-2-ol; 2-MIB) is a bridged cyclic alcohol produced by cyanobacteria and actinomycetes which imparts a muddy or musty taste and odour to natural waters ***[26,27]***. Many bacteria are capable of degrading 2-MIB, either as a primary or secondary substrate, and it is thought that the metabolic pathway may be similar to that of alicyclic alcohols and ketones ***[20]***.

In natural waters subject to BAC treatment, the concentration of 2-MIB is generally very low in comparison to NOM and trace compounds are metabolised as secondary substrates in such cases ***[7]***. Many studies have looked at the removal of 2-MIB in such scenarios, and it has been shown that the removal of 2-MIB can be significant.

In bioreactors, the biodegradation of 2-MIB has been investigated both as a primary substrate and as a secondary substrate in the presence of NOM. Generally, the biodegradation of 2-MIB (and other T&O compounds) is measured, or monitored, as a percentage removal of the influent concentration with little attention being paid to the actual biological transformations taking place. However, some work has been done on characterising the biotransformation products of 2-MIB following biodegradation by bacteria isolated from pilot or full-scale BAC filters and other bioreactors (sand, anthracite)

Biodegradation experiments in which 2-MIB has been studied as the primary substrate have shown that 2-MIB can be degraded by many strains of bacteria. Izaguirre *et al.* ***[26,28]*** demonstrated that 2-MIB could support bacterial cultures as a sole carbon source at mg L^{-1} concentrations. Additionally, the bacterial species implicated in the metabolism of 2-MIB were isolated and were found to be *Pseudomonas* spp. It was also shown that the degradation of 2-MIB was limited to mixed bacterial cultures in this case. Tanaka *et al.* ***[29]*** showed that bacteria of the *Pseudomonas* spp. and *Enterobacter* spp. isolated from the backwash water from a pilot scale biological filtration unit, were capable of biodegradation of 2-MIB and the authors also carried out structural elucidation of the biodegradation products. Bacterial culture extracts analysed by GC-MS and ^{1}H-NMR showed that 2-MIB was metabolised to 2-methylenebornane and 2-methylcamphene. The metabolite 2-methylcamphene was then further biodegraded to afford camphor and 1,7,7-trimethyl-3-oxacyclo- [2,2,1]-heptan-2-one (**Figure 2-4**).

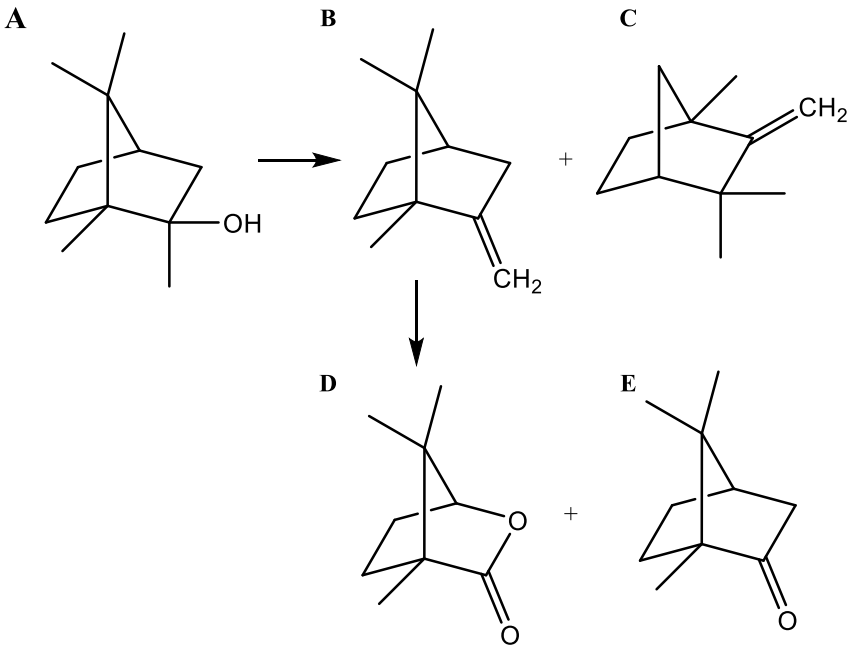

Figure 2-4: Biodegradation of 2-MIB (A) to give 2-methylenebornane (B), 2-methylcamphene (C), 1,7,7-trimethyl-3-oxacyclo[2,2,1]-heptan-2-one (D), and camphor (E).

Further work by Eaton *et al.*, showed that both camphor ***[30]*** and *R*-limonene ***[31]*** degrading bacteria were capable of metabolising 2-MIB as a primary substrate. Camphor degrading bacteria of the *Pseudomonas* spp. and *Rhodococcus* spp. were shown to degrade 2-MIB to hydroxyl- and keto-isoborneol derivatives. Similarly, *R*-limonene degrading bacteria from the *Pseudomonas* and *Sphingomonas* genera were shown to give hydroxylated isoborneol metabolites which were further transformed to give various keto-camphene, isoborneol and bornane products. The metabolites were separated and characterised from bacterial cultures using GC-MS and NMR for both studies.

The biodegradation rate constant of 2-MIB in biological sand filters has been shown to be between 0.10 and 0.36 d^{-1} when modelled as a pseudo-first-order reaction ***[32]***. Others who have investigated the biodegradation of organic compounds that are utilized as secondary substrates have also shown that such processes can be modelled as pseudo-first-order reactions, as the concentration of the primary substrate (BOM) is generally orders of magnitude greater (mg L^{-1} *cf.* ng L^{-1}) than the secondary substrate in drinking water scenarios and the number of metabolizing cells remain essentially constant throughout the process as they are acting catalytically (**section 2.3.1**) ***[23,33]***. The biodegradation rate was shown to be dependent on the initial concentration of the bacterial population and not the initial concentration of 2-MIB when the concentration of 2-MIB was between 50 and 200 ng L^{-1} ***[32]***. This makes sense, as the degradation of secondary substrates is dependent upon the active biomass which is determined by the availability of the primary substrate (BOM) ***[20]***.

These studies show that 2-MIB is readily biodegraded by both single strains and consortia of bacteria either as a primary or secondary substrate and that the metabolic pathway varies depending on the species of micro-organisms involved. In bioreactors (i.e. BAC), consortia of bacteria utilising 2-MIB as a secondary substrate is the most probable scenario, and it seems evident that bacterial communities are able to acclimatise to the presence of 2-MIB as a background component to the influent water source, allowing them to metabolise 2-MIB more effectively.

2.3.3 Biodegradation of Geosmin

Geosmin (2,6-dimethylbicyclo[4.4.0]decan-1-ol; (-)-geosmin; GSM) is a bicyclic alcohol with a characteristic earthy odour which is produced as a secondary metabolite by actinomycetes and cyanobacteria ***[27]***. It was first isolated from actinomycetes by Gerber *et al.* in 1965 ***[34]***. As with 2-MIB, biodegradation of geosmin is possible both as a primary and secondary substrate in the presence of single bacterial cultures or bacterial consortia ***[35-37]***.

Under laboratory conditions, geosmin has been shown to undergo biodegradation to form the two dehydration products 2,6-dimethylbicyclo[4.4.0]dec-1-ene and 6,10-dimethylbicyclo[4.4.0]dec-1-ene, of which the latter is then oxidised to give 6,10-dimethylbicyclo[4.4.0]dec-1-en-3-one (**Figure 2-5**) ***[38]***. Although the dehydration products are likely to be common metabolites of geosmin biodegradation due to the simplicity of the transformation, it is possible that other metabolites may be produced by other bacteria and consortia of bacteria capable of more extensive and complex biodegradation.

As with 2-MIB, the rate of biodegradation in bioreactors has been shown to be dependent on the initial concentration of bacteria present and not the initial geosmin concentration. Pseudo-first-order rate constants were found to be 0.12-0.58 d^{-1} for geosmin concentrations of 50-200 ng L^{-1} ***[32]***.

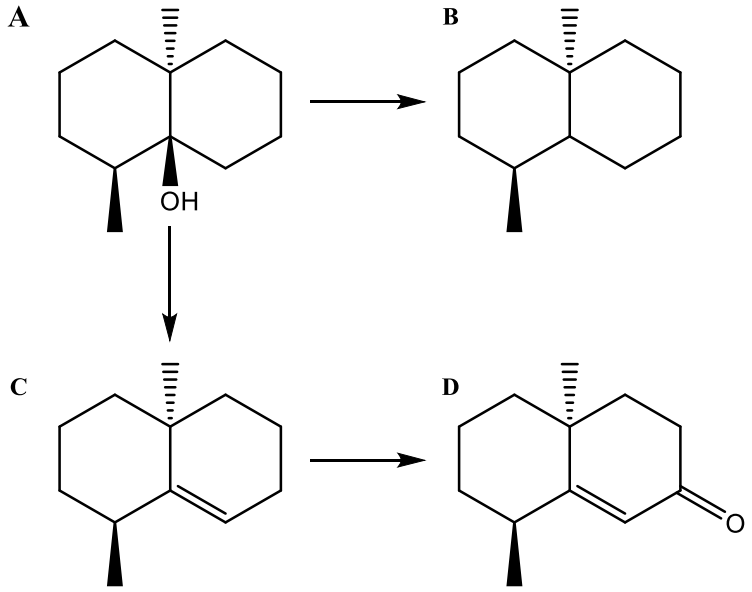

Figure 2-5: Biodegradation of geosmin (A) to give 2,6-dimethylbicyclo[4.4.0]dec-1-ene (B), 6,10-dimethylbicyclo[4.4.0]dec-1-ene (C) and 6,10-dimethylbicyclo[4.4.0]dec-1-en-3-one (D).

2.3.4 Removal of Taste and Odour Compounds Using BAC

Many studies have been conducted in order to assess the effectiveness of BAC as a removal technology for T&O compounds. These studies range from bench to full scale application and assess a wide range of operational conditions.

An early study by Yagi *et al.* ***[39]*** using bench scale GAC columns inoculated with *Bacillus subtilus* showed that biodegradation may indeed be a promising method for this purpose while at the same time extending the lifetime of GAC filters. This study investigated the biodegradation of geosmin and 2-MIB as a primary substrate at relatively high concentrations (2 mg L^{-1}) compared to that typically found in natural waters encountered in drinking water treatment. The study showed that

biodegradation of Geosmin and 2-MIB did indeed occur, indicating that the degradation of these compounds is possible as a sole carbon source.

A pilot scale investigation by Hrudey *et al.* ***[40]*** on raw waters containing geosmin at concentrations of 14 to 20 ng L^{-1} showed that BAC was effective at removing odour from the influent water when used in conjunction with pre-ozonation. However, bench scale studies carried out alongside the pilot study indicated that adsorption to the activated carbon may have been the primary mechanism for odour removal and it was concluded that biological removal of odours may not be a realistic approach. Despite this, more recent studies have indeed shown that the use of BAC is an effective treatment approach for T&O compounds.

An investigation by Nerenberg *et al.* ***[41]*** into the removal efficiency of a full scale plant employing conventional treatment with additional pre-ozonation and post-treatment BAC filtration showed that biological filtration was indeed effective in the removal of 2-MIB. The study was prompted after a survey of the treatment plants in the area (Chicago, IL), showed that all except one plant was experiencing seasonal odour issues, based on both quantitative analysis and consumer complaints. Most plants in the area relied on powdered activated carbon (PAC) dosing to remedy seasonal odour events, which was deemed to be ineffective at affordable or practical doses. However, the one plant in the area that employed pre-ozonation and BAC filtration had no consumer complaints. Tracing the concentration of 2-MIB through the treatment process showed that pre-ozonation removed 26% to 64% of the influent 2-MIB concentration, with the BAC removing

a further 36% - 65% of the 2-MIB remaining after pre-ozonation and conventional treatment.

Elhadi *et al.* ***[42]***carried out a study which investigated the transition from GAC to BAC using influent water containing spiked levels of 2-MIB (100 ng L^{-1}), geosmin (100 ng L^{-1}), and BOM (1000 μg L^{-1}; formaldehyde, glyoxal, formate, and acetate). Fresh GAC filters were monitored for their removal efficiency for geosmin and 2-MIB and, as expected, the removal efficiency decreased over time as the adsorption capacity of the GAC became exhausted. The removal efficiency was then shown to increase as more time passed, indicating the establishment of a biofilm that was capable of biodegrading geosmin and 2-MIB. Using fresh GAC, complete removal of both compounds was observed for the first 7 days, dropping off over a two-week period until it was clear that the adsorptive capacity had been compromised. After 42 days, the removal efficiencies of geosmin and 2-MIB were 76% and 47% respectively. The removal efficiency was then shown to increase, reaching removals of 87% for geosmin and 63% for 2-MIB by day 55 of the experiment. This suggested that biofilms are able to establish themselves and acclimatise to the presence of these T&O compounds resulting in enhanced biological removal. Further experiments showed that acclimatised biofilms were able to maintain high removal efficiencies during transient T&O events. The filters were run with a hydraulic loading rate (HLR) of 7.5 m h^{-1}, corresponding to an empty bed contact time (EBCT) of 5.6 min. In a follow-up study ***[43]***, BAC was compared to biologically active anthracite with respect to the ability to remove geosmin and 2-MIB in bench scale filter columns. The study also investigated the effect of temperature, geosmin/2-MIB concentration and BOM concentration on the

effectiveness of the two media types. Overall, BAC was found to be more effective in the removal of these T&O compounds. Additionally, higher temperatures (20ºC *cf.* 8ºC), higher BOM concentration and higher T&O concentration resulted in a greater percentage removal for geosmin and 2-MIB, although at higher temperatures, BOM concentration became less important. At the lowest T&O concentration investigated (25 ng L^{-1}), the removal efficiency at 20ºC was enough to produce an effluent water with concentrations of geosmin and 2-MIB that were within the odour concentration threshold for these compounds. At higher concentrations (100 ng L^{-1}), removals were found to be 60% for geosmin and 40% for 2-MIB.

Persson *et al.* ***[44,45]*** investigated the role of biodegradation on the removal of geosmin and 2-MIB by comparing BAC with biologically active expanded clay (EC). The removal efficiency of the BAC filter was found to be very high (≥ 97%) at low concentrations of influent geosmin and 2-MIB (20 ng L^{-1}) with an EBCT of 30 min and it was found to outperform the EC filter. In order to assess the extent of biodegradation, the filters were dosed with sodium azide (NaN_3) in order to suppress biological activity. Following this, the extent of removal in the EC filter was shown to diminish markedly, while the removal efficiency of the BAC remained largely unchanged (≥ 96%). This suggested that adsorption of T&O compounds to the GAC surface was still playing a major role even though the GAC medium had been in use for almost four years. As such, the results concerning the extent of biodegradation on the BAC filter in this study are complicated by the fact that significant adsorption was also occurring. It was concluded that the use of BAC as a filtration medium was the more viable option based on the added robustness

the GAC provided with the added removal mechanism of adsorption coupled with biodegradation.

Drikas *et al.* ***[46]*** noted, during a study of the removal of geosmin and 2-MIB using GAC filters, that the removal efficiency of both T&O compounds increased over time, rather than the expected decrease due to the exhaustion of the GAC adsorption sites. This was attributed to the development of a biofilm over the course of the experiment, with the GAC media removing geosmin and 2-MIB via both adsorption and biodegradation. It was also shown that longer EBCT's (20 min) were more effective, with an EBCT of 5 min resulting in breakthrough of geosmin and 2-MIB.

Ndiongue *et al.* ***[47]*** compared fresh GAC filters with GAC that had been in service for 3 years at various concentrations of geosmin and 2-MIB and also investigated the effect of the EBCT. Overall, it was found that at higher influent concentrations, the percentage removal was higher. Additionally, longer EBCTs afforded greater removal efficiencies (EBCT = 2.8, 3.4, 5.0 or 7.5 min), provided that the removal efficiency at the shortest EBCT was good. If the performance of the filter at low EBCTs was poor (< 20%), increasing the EBCT had reduced or no effect. This may have been influenced by prior experiments preloading the GAC and reducing the adsorption capacity prior to the longer EBCT experiments. For the used GAC filter (BAC) removals of geosmin increased from 38% to 78% while 2-MIB removal increased from 14% to 43% as the EBCT was increased. The fresh GAC filters were shown to be more effective at removing both compounds although none of the filters in this study were able to provide effluent water containing the compounds at levels below their respective odour concentration thresholds.

In a pilot scale study, Yang *et al.* ***[48]*** compared GAC with an O_3/BAC process and their respective efficiencies in removing geosmin and 2-MIB. GAC alone was found to remove 83.1% and 92.0% of geosmin and 2-MIB respectively compared with 100% and 96.3% for the O_3/BAC process. In this study, O_3 was applied preceding the BAC filter which was operated with an EBCT of 27.1 min. The raw water in this study also suffered from problems associated with trihalomethanes (THMs), haloacetic acids (HAAs) and saltwater intrusion (increased bromides and increased brominated disinfection by products) for which nano and ultrafiltration membranes were investigated in addition to GAC and O_3/BAC.

Other studies that investigate the use of biological removal by biofilms attached to other media (sand, anthracite, expanded clay, tube systems etc.) have also been shown to be effective in the removal of T&O compounds ***[20,21,32,37,43-45,49,50]***.

2.3.5 Biodegradation of Cyanotoxins

In freshwater environments, cyanotoxins are produced by cyanobacteria (sometimes called blue-green algae) ***[5]***. The most common types of cyanotoxins include Microcystins (MC), Cylindrospermopsins (CYN), Anatoxins (ATX), Saxitoxins (STX) and Nodularin (NOD), although NOD is generally found in brackish waters ***[5,51]***. The occurrence of cyanobacterial blooms may be dominated by a single species or contain several species and in both cases a range of toxic metabolites will be produced. Favourable conditions that can lead to blooms include; stagnant or low flow water conditions, warm water (15 – 30 ^oC), neutral to alkaline pH (6 – 9), and high nutrient content (eutrophic waters) ***[52]***. All

cyanotoxins are known to be amenable to biodegradation in natural waters, although there are some complications that may limit the effectiveness of BAC in the removal of these compounds ***[5]***. The DWSNZ state "Provisional Maximum Acceptable Values" (PMAVs) for cyanotoxins in treated water as listed in **Table 2-2** ***[3]***. In drinking water treatment, certain processes may increase the concentration of dissolved cyanotoxins due to the lysing of cell membranes causing intracellular cyanotoxins to become part of the bulk liquid. As such, processes like pre-ozonation that promote the lysing of cells prior to removing intact cells from solution, for example by sedimentation or sand filtration, should be avoided during cyanobacterial blooms ***[53]***.

Table 2-2: PMAVs for cyanotoxins as stated in the DWSNZ *[3]*.

Toxin	PMAV ($\mu g\ L^{-1}$)
Anatoxin-a	6.00
Anatoxin-a(S)	1.00
Homoanatoxin-a	2.00
Cylindrospermopsin	1.00
Microcystins*	1.00
Saxitoxins**	3.00

* as MC-LR equivalent concentration – see section **2.3.5.1**
** as STX equivalent concentration – see section **2.3.5.4**

2.3.5.1 Microcystins

Microcystins are a class of hepatotoxic cyclic peptides consisting of seven amino acids, two of which are variable giving a large number of possible derivatives. In the case of the most commonly reported MC, microcystin-LR (MC-LR), the variable groups are the side chain amino acids leucine and arginine (**Figure 2-1**). The toxicity of MCs is associated with the conjugated diene of the ADDA amino acid side chain (3-amino-9-methoxy-2,6,8-trimethyl-10-phenyldeca-4,6-dienoic acid; **Figure 2-6**) ***[5]***. MCs accumulate in the liver following ingestion which can lead to haemorrhage and death. The ability to accumulate in liver tissue also means

MCs can cause adverse effects following chronic, low level exposure ***[51]***. Although MC-LR is the most common cyanotoxin found in New Zealand waters ***[4]***, over 60 variants are known to exist and most cyanotoxin blooms produce a range of MC variants ***[51]***.

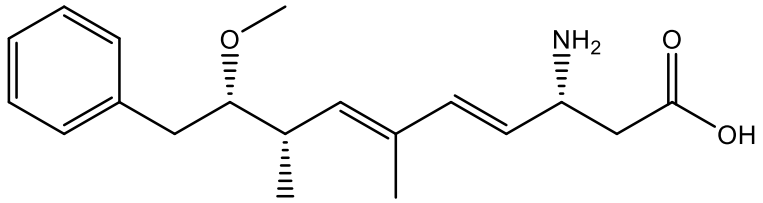

Figure 2-6: Molecular structure of ADDA.

Microcystins have been shown to be biodegraded in natural water sources ***[54-60]*** and a number of individual species of bacteria capable of degrading MCs have been isolated ***[61-63]***. The enzymatic pathway of biodegradation for MC-LR in *Sphingomonas* species was first put forward by Bourne *et al.* ***[63,64]***, showing the process involved at least three hydrolytic enzymes. The initial site of hydrolytic cleavage was shown to be at the ADDA-Arg peptide bond, resulting in ring opening and the loss of toxicity. The biodegradation products were found to be nontoxic from mouse bioassay analyses. Other researchers ***[62]*** have since postulated that alternative metabolic pathways exist for other bacterial species.

2.3.5.2 Cylindrospermopsins

Cylindrospermopsins are cytotoxic alkaloids produced by a range of cyanobacteria and are known to cause liver, kidney and intestinal damage at high concentrations. They have also been shown to inhibit protein synthesis, exhibit genotoxicity, and may also be carcinogenic ***[65,66]***. Three variants, cylindrospermopsin, 7-epicylindrospermopsin, and deoxycylindrospermopsin are known to exist

(**Figure 2-7**; ***[5]***). Of these, 7-epicylindrospermopsin is a minor, toxic metabolite whereas deoxycylindrospermopsin is considered to be non-toxic ***[67,68]***. Cylindrospermopsin has been shown to be produced by cyanobacteria in New Zealand waters ***[69]***.

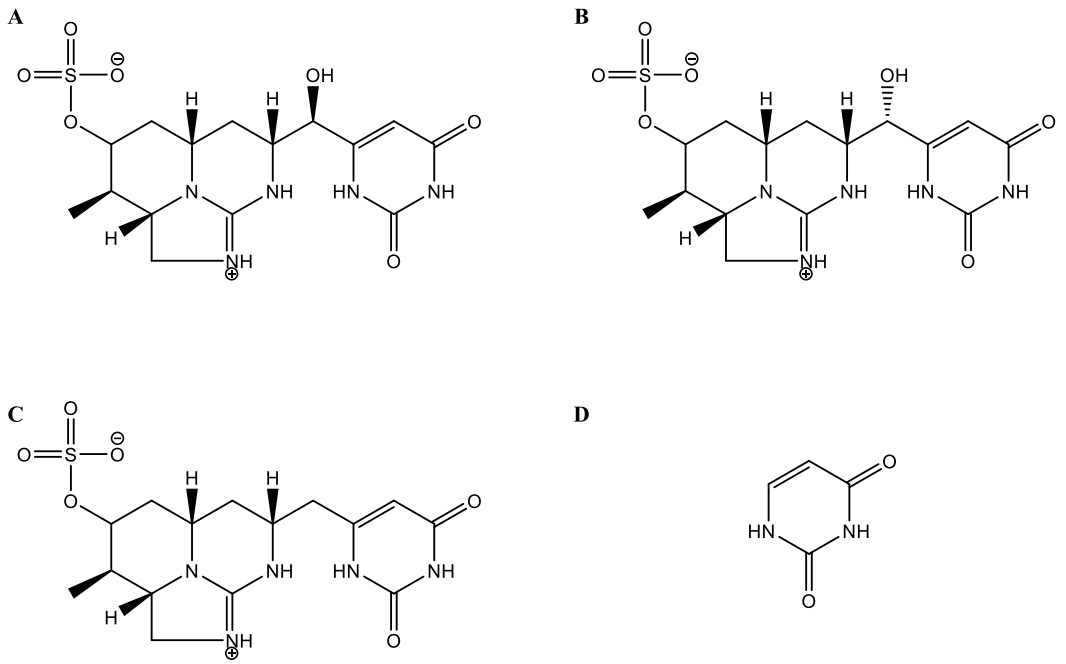

Figure 2-7: Molecular structures of cylindrospermopsin (A), 7-epicylindrospermopsin (B), deoxycylindrospermopsin (C), and uracil (D).

Although not as extensively studied as MCs, biodegradation of cylindrospermopsin has been shown to occur in natural waters and sludges ***[59,60,70,71]***. To date, no degradation pathway has been proposed, although it has been shown to be biodegraded by MC degrading bacteria ***[71]***.

It has been shown that the toxicity of this compound requires the uracil moiety to remain intact and that oxidation processes can cause ring cleavage, resulting in non-toxic products ***[72]***. The oxidants investigated in the study were chlorine, chlorine dioxide, and chloramine.

2.3.5.3 Anatoxins

Anatoxins are a class of low molecular weight neurotoxic alkaloids of which anatoxin-a (ATX-a) is the most common and widely reported. Other variants include homoanatoxin-a and anatoxin-a(S) (**Figure 2-8**) ***[51]***. Anatoxin-a and homoanatoxin-a act as agonists of nicotinic acetylcholine receptors (nAchRs), blocking these receptors due to irreversible binding and the inability of acetylcholinesterase to breakdown the anatoxin-a-nAchR complex. Anatoxin-a(S) is an anticholinesterase, which prevents the breakdown of the acetylcholine-nAchR complex by acetylcholinesterase due to irreversible inhibition ***[73]***.

There is only sparse information available on the biodegradation of these compounds, although there is some evidence to suggest it does occur in natural waters and sludges ***[5]***. Anatoxin-a and homoanatoxin-a are known to degrade in sunlight and at high pH to yield non-toxic dihydro and epoxy products ***[74,75]***.

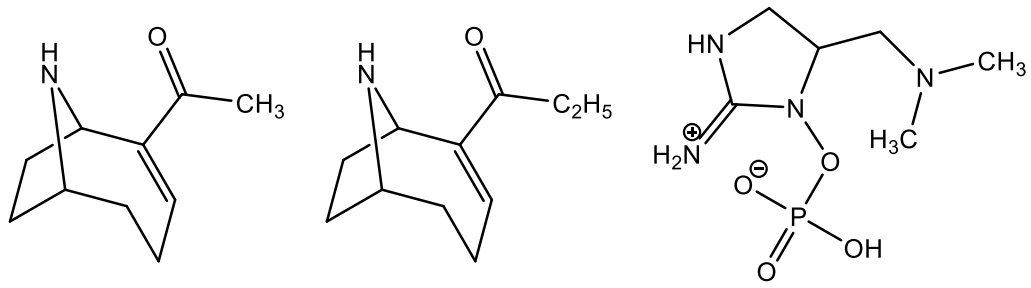

Figure 2-8: Molecular structures of (L-R): anatoxin-a, homoanatoxin-a, and anatoxin-a(S).

2.3.5.4 Saxitoxins

Saxitoxins are a class of neurotoxic alkaloids produced by cyanobacteria in aquatic environments and also in marine environments by dinoflagellates. Due to originally being isolated from marine shellfish, they are commonly referred to as paralytic shellfish toxins (PSTs) ***[5]***. More than 20 variants are known, categorised by four

subgroups; non-sulphated saxitoxins (STX; carbamate toxins), singly sulphated gonyautoxins (GTX), doubly sulphated C-toxins (*N*-sulfocarbamoyl toxins) and those with *N*-1-hydroxyl groups (decarbomoyl toxins) (**Figure 2-9**) ***[51,52,76,77]***. Although they are widely reported to act as sodium channel blockers, they have also been shown to act on multiple receptors including calcium channels, potassium channels, neuronal nitric oxide synthase, STX metabolising enzymes and transferrin-like proteins ***[78]***.

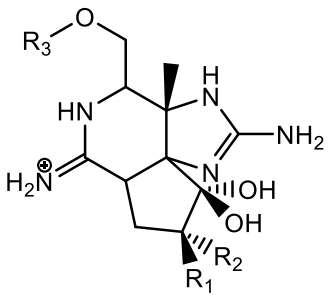

	Substituent Groups			
Toxin	R_1	R_2	R_3	TEF
STX	H	H	$CONH_2$	1.00
GTX2	H	OSO_3^-	$CONH_2$	0.40
GTX3	OSO_3^-	H	$CONH_2$	0.60
C1	H	OSO_3^-	$CONHSO_3^-$	0.01
C2	OSO_3^-	H	$CONHSO_3^-$	0.10
dcSTX	H	H	H	0.20
dcGTX2	H	OSO_3^-	H	0.40

Figure 2-9: General structure of saxitoxins, the substituents of some common analogues and their toxicity equivalency factors *[5,77,79]*.

At present, very little information on the biodegradation of saxitoxins in natural aquatic environments is available ***[80]*** with most investigations focussing on marine bacteria ***[81-84]***. A common theme in the biodegradation of saxitoxins is the transformation of less toxic variants to more toxic ones. For example, Kotaki *et al.* ***[80]*** showed that marine and freshwater bacteria transformed GTX2 and GTX3 into STX. Similar phenomena have been documented in BAC and other biofilter filter studies involving saxitoxins ***[85]***. It is also known that C-toxins spontaneously degrade to GTXs, causing waters contaminated with C-toxins to become more toxic over time as the concentration of GTX, and possibly STX, variants increase. Conversely, in a more recent study, Ho *et al*. ***[59]*** concluded that saxitoxins (C1, C2, GTX2, GTX3, STX) were non-biodegradable in an Australian source

water (Myponga Reservoir, South Australia) at 14 ºC and 24 ºC from batch biodegradation experiments. This indicates that the degradation of saxitoxins is dependent on local conditions and perhaps the bacterial species present.

2.3.6 Other Emerging Contaminants: EDCs and PPCPs

Endocrine disrupting chemicals (EDCs) are a class of natural hormones and synthetic chemicals that interfere with the endocrine (hormonal) system of organisms. Such chemicals include steroids like estradiol and synthetic steroid mimics like bisphenol-A (**Figure 2-10**). Another group of emerging contaminants (ECs), which may include some EDCs, are pharmaceuticals and personal care products (PPCPs). This group of ECs include, for example, prescribed drugs (e.g. anti-inflammatory drugs, antidepressants) and chemicals present in products like shampoos (surfactants etc.) and cosmetics.

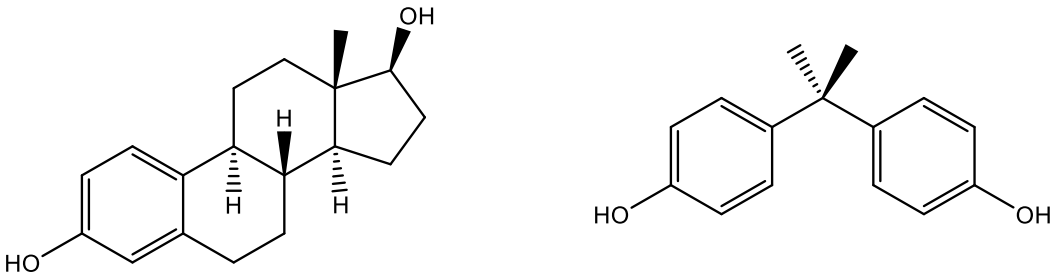

Figure 2-10: Molecular structures of estradiol (L) and bisphenol-A (R).

In 2013, the Cawthron Institute carried out a study for the Waikato Regional Council (WRC) on the presence of EDCs in the Waikato River between Lake Taupo and Tuakau and assessed endocrine disruption potential based upon the findings ***[86]***. In addition to investigating the presence of estrogenic and androgenic steroids, the study included industrially and domestically derived EDCs including; alkylphenols (nonyl- and octyl-), bisphenol-A, parabens (methyl-, ethyl-, propyl-,

butyl-, benzyl-), triclosan, methyl triclosan, o-phenylphenol, and chloroxylenol. For the steroids, none were detected above the method detection limit (MDL, 0.01-1.00 ng L^{-1}). Parabens were detected at five of the eight sites sampled, triclosan at five sites and alkylphenols were detected at two sites. Of these, technical nonylphenol (t-NP), which is an isomeric mixture of branched isomers, was present in the highest concentration (33.88 ng L^{-1}) although this is an order of magnitude below the predicted-no-effect concentration (PNEC) set by the European Union (EU). Similarly, for parabens and triclosan which were present at concentrations two orders of magnitude lower than their respective PNECs. The presence of t-NP downstream from Hamilton was stated to be consistent with widespread use in urban areas. Bisphenol-A was detected at all sites at concentrations ranging from 0.83 – 4.26 ng L-1 which is three orders of magnitude lower than the PNEC for this compound.

Although this suggests that only extremely low concentrations of steroids and their mimics are present, it is noted that the Waikato River receives inputs of steroids from diffuse agricultural sources in addition to WWTP point sources and that EDCs can elicit effects at very low concentrations. Additionally, the study states that the results are based on a one-off sampling regime and may not represent an annual flux of steroidal concentrations. It was concluded that organisms at localised sites may be negatively affected by steroids and EDCs, particularly those inhabiting areas near WWTP effluents.

The removal of EDCs and PPCPs using GAC and BAC has been demonstrated, particularly in the context of WWTPs where such compounds are generally present

at much higher concentrations compare with drinking water treatment. For example, using micro-grain activated carbon (μGAC) in fluidised beds, Mailler *et al.* ***[87]*** were able to reduce the concentrations of 62 pharmaceuticals and hormones and 57 other ECs by 50% to 90%. More relevant to the removal of trace pollutants using BAC, the biodegradation of bisphenol-A by bacteria immobilised on GAC has been shown to occur in batch experiments by Mita *et al.* ***[88]***. After 72 h, the concentration of bisphenol-A was reduced by more than 90%. How this translates to continuous flow BAC filters with much lower contact times remains to be seen. Others have noted in experiments using GAC for the removal of ECs that microbial activity had occurred, which resulted in extending service time of GAC filters. It was further postulated that biodegradation became the main removal mechanism provided the biofilm is allowed to develop sufficiently ***[89]***. The removal and biotransformation of estradiol in BAC filters has also been investigated, showing that estradiol and the biotransformation product estrone are readily removed using GAC and BAC ***[90]***.

Due to the low concentrations of steroids present in the Waikato River, it is unlikely to be possible or necessary to evaluate the performance of the Hamilton DWTP BAC filters in removing steroids at concentrations relevant to the source water. The performance with respect to bisphenol-A and alkylphenols may be relevant, as the concentration of these compounds is likely to increase as urban populations grow, resulting in the increased use of consumer products and industrial processes that contain or require them.

2.4 Analytical Methods for Cyanobacterial Metabolites

2.4.1 Quantitative Analysis of Geosmin and 2-Methylisoborneol

Quantitative analysis of geosmin and MIB can be achieved with good accuracy and very low limits of detection (LOD) by employing the use of Gas Chromatography Mass Spectrometry (GC-MS), which is the dominant chromatographic technique used in the quantitative analysis of T&O compounds ***[91-126]***.

Due to the very low odour concentration threshold (OCT) in humans for these types of chemicals (**Table 2-3**), the analytical method employed in the monitoring of processes designed to remove T&O compounds requires an LOD equal to, or preferably lower than, the OCT in order to ascertain whether the removal technology is performing acceptably. With GC-MS being by far the preferred instrumental technique, analytical methods in this area mainly differ in sample preparation and extraction methods.

Table 2-3: Odour concentration threshold values for geosmin and 2-MIB *[127]*.

Compound	Odour concentration threshold (ng L^{-1})
Geosmin	6-10
2-MIB	2-20

Due to the semi-volatile nature of both geosmin and MIB, headspace GC-MS analysis by solid phase micro-extraction (SPME) has been the method of choice for many researchers in this field of study ***[94,98,102,106,108,113-120]***. However, the use of SPME requires the use of expensive extraction fibres, gives long sample turn-around times and requires manual injection of the sample into the GC if a specialised auto-sampler is not available. Other methods such as those that employ closed loop stripping as the extraction method suffer from similar drawbacks, with

analysis being even more cumbersome and time consuming ***[91,92,125]***. Similarly, purge and trap (PT) extractions requires specialized apparatus ***[104,111]***.

Other extraction methods include stir-bar sorptive extraction (SBSE) ***[95]***, static headspace (SHS) extraction ***[101]*** and needle-like extraction devices (NED) ***[122]*** which are based upon adsorption of the analyte to activated carbon packed needles. Again, these methods all require specialised equipment.

In efforts to reduce analysis times without resorting to expensive consumables and apparatus, a range of liquid-liquid micro-extraction (LLME) methods have been developed ***[93,99,105,107,110,112,124]***. In general, these methods involve the partitioning of the target analytes from a water sample into a small volume of organic extracting solvent (e.g. pentane or hexane) by salting out the aqueous phase with high concentrations of inorganic salts (e.g. NaCl and K_2HPO_4) and mechanical agitation. These methods have the advantage of not requiring special auto-samplers like SMPE, which makes the analysis of large numbers of samples more feasible with the use of a standard auto-sampler. The use of organic solvents may be regarded as a disadvantage, but the volumes used are typically very small (3-1000 μL). Similarly, methods that employ solid phase extraction (SPE) also do not require specialised auto-samplers, but require numerous consumable SPE cartridges and can require quite large amounts of solvent ***[97,109,116,123]***.

Of the methods that have been developed to date, LODs are acceptable for most extraction procedures. Hence, the choice of method can be made based upon the available instrumentation or other restrictions regarding available apparatus or consumables. As many of these methods are also applicable to other T&O

compounds the specific needs of the analysis (fitness of purpose) also need to be considered. A summary of analytical methods available in the literature is presented in **Table 2-4**.

Table 2-4: Chromatographic techniques, extraction methods and limits of detection for analytical methods employed in the monitoring of 2-MIB and geosmin.

Separation and Detection	Extraction Method*	Limit of Detection (ng L^{-1}) 2-MIB	Geosmin	Reference
GC-FID/ECD	CLS	-	-	***[125]***
GC-MS	CLS	-	-	***[92]***
GC-MS	SPME	0.13	0.04	***[118]***
GC-MS	LVI-LLE	0.34	0.05	***[105]***
GC-MS	PT	1.40	0.08	***[111]***
GC-MS	SPE	0.10	0.10	***[97]***
GC-MS	LLME	0.10	0.10	***[99]***
GC-MS	SHS	0.36	0.14	***[101]***
GC-MS	SBSE	0.33	0.15	***[95]***
GC-MS	SPME	0.15	0.16	***[103]***
GC-MS	SPME	0.50	0.20	***[120]***
GC-MS	SPME	0.50	0.20	***[121]***
GC-MS	SPME	0.60	0.40	***[117]***
GC-IT-MS/MS	SPME	1.40	0.40	***[114]***
GC-MS	SPME	0.59-0.66	0.44-0.49	***[102]***
GC-MS	SPE	0.50	0.50	***[116]***
GC-MS	SPME	0.25	0.58	***[115]***
GC-MS	PT/SPE	0.87-1.00	0.50-0.62	***[109]***
GC-MS	CLS	0.80	0.80	***[91]***
GC-MS/MS	SPE	5.50	0.90	***[123]***
GC-IT-MS	LLME	1.00	1.00	***[93]***
GC-CI/EI-IT-MS	SPME	1.00	1.00	***[94]***
GC-MS	Ambersorb 572	1.00	1.00	***[96]***
GC-MS	SPME	1.00	1.00	***[108]***
GC-MS	LLE	5.00	1.00	***[107]***
GC-MS	LLME	1.00	1.10	***[112]***
GC-MS	NED	0.50	1.50	***[122]***
GC-MS	SPME	5.10	1.50	***[106]***
GC-MS	HF-LPME	1.30	1.90	***[124]***
GC-MS	PT	1.00	2.00	***[104]***
GC-MS/MS	SPME	8.00-20.00	0.10-2.00	***[113]***
GC-MS	SPME	4.12	3.60	***[119]***
GC-MS	USAD-LLME	9.00	5.00	***[110]***
GC-MS	LLE	20	20	***[126]***

* CLS = Closed Loop Stripping; LLE = Liquid-Liquid Extraction; SPME = Solid Phase Micro-extraction; SBSE = Stir-Bar Sorptive Extraction; SPE = Solid Phase Extraction; LLME = Liquid-Liquid Micro-extraction; PT = Purge and Trap; LVI = Large Volume Injection Liquid Liquid Extraction; USAD = Ultrasound Assisted Dispersive; NED = Needle-Like Extraction Device; HF-LMPE = Hollow-Fiber Liquid-Phase Microextraction

2.4.2 Quantitative Analysis of Cyanotoxins

Quantitative analysis of cyanotoxins is usually achieved through the use of High-Performance Liquid Chromatography (HPLC) with either MS (LC-MS) or Fluorescence detection (LC-FLD) depending on the class of the target cyanotoxin. These analytical techniques are known to provide good selectivity and low limits of detection. Other methods include mouse bioassays and various enzyme-linked immunosorbent assays (ELISA). However, while being simple to perform, these methods can suffer from numerous technical issues such as poor sensitivity, reproducibility, interferences, and false positive results ***[79,128]***. A range of analytical methods are summarised in **Table 2-5**.

2.4.2.1 Microcystins, Cylindrospermopsins and Anatoxins

These cyanotoxins are usually quantified in aquatic environments using LC-MS or LC-MS/MS. In order to remove matrix effects and interferences, sample preparation usually involves some kind of SPE protocol. While early methods could only screen for single toxins or classes of toxin, recent developments allow for the analysis of multiple toxins simultaneously. However, due to the vast number of cyanotoxin analogues, particularly MCs, and the high cost of analytical standards, analysing each individual compound can either be an unfeasible or financially prohibitive task. In such cases, a small number of the most common analogues from a subgroup can be analysed and taken as an estimate of the total subgroup concentration. This is often the case with microcystins, for which the concentration is often reported as the MC-LR equivalent concentration. This is generally less

problematic for ATXs and CYNs, as the number of known analogues is low, and each can be quantified directly.

2.4.2.2 Saxitoxins

Saxitoxins require a separate quantitative chromatographic method from other cyanotoxins due to the unique challenges associated with this class of toxins. Due to their highly polarity (zwitterionic), the retention of these compounds on traditional reversed phase (usually octadecylsilane; C18) columns is very poor. In order to overcome this, chromatography is achieved using an ion-pairing reagent. The drawback of this is that it precludes the use of MS detection due to the severe signal suppression that occurs in the presence of ion-pairing reagents. As the detection of these compounds requires very low limits of detection, one way of overcoming this is to employ fluorescence detection. However, STXs do not possess functional groups that exhibit fluorescence. This requires either pre- or post-column oxidation (periodic acid, hydrogen peroxide or *tert*-butyl-peroxide) in order to yield reaction products that exhibit fluorescence. More recently, the use of hydrophilic interaction liquid chromatography (HILIC) has allowed for successful chromatography of STXs without the need for ion-pairing reagents which allows the use of sensitive MS detection. This removes the need for pre/post oxidation of STX's while still providing low limits of detection. As with MCs, a large number of STX analogues exist and analytical standards are expensive. Although methods exist to analyse many of these analogues, this is not always feasible or practical.

Table 2-5: Chromatographic techniques, extraction methods and limits of detection for analytical methods employed in the monitoring of cyanotoxins.

Separation	Detection	Extraction	Toxins	LOD (μg L^{-1})	Reference
RP C18 Gradient	UV-DAD	SPE	MC-LR	100	***[129]***
RP C18 Gradient	ESI-MS/MS	SPE	MCs	0.01 - 0.03	***[130]***
RP C18 Gradient	ESI-MS/MS	SPE	MCs	0.0158 - 0.0317	***[131]***
RP C18 Gradient	ESI-MS/MS	ASE-SPE	MCs	0.01 - 0.012	***[132]***
CEX+AEX Gradient*	FLD + ESI-MS	LSE + Filtration	STXs	0.5 - 2	***[133]***
RP C18 Gradient	Pre-oxidation FLD	SPE	STXs	20 - 100	***[134]***
RP C18 Gradient	Post-oxidation FLD	LSE + Filtration	STXs	0.014 - 0.820	***[135]***
HILIC Amide Gradient	ESI-MS/MS	HILIC SPE	STXs	0.1 - 101.2	***[136]***
RP C18 Gradient	Pre-oxidation FLD	LSE	STXs	0.5 - 13	***[137]***
HILIC Amide Gradient	ESI-MS/MS	LSE + GC-SPE	STXs	0.03 - 1.17	***[79]***
RP PLRP-S Gradient*	ESI-MS	SPE	ATX, MCs	0.4 - 0.5	***[138]***
RP C18 Gradient	ESI-MS/MS	LSE	MCs, NOD	0.002 - 0.527	***[139]***
RP C18 Gradient	ESI-MS/MS	SPE	MCs, ATX,CYN	0.01 - 0.02	***[140]***
RP C18 Gradient	ESI-MS/MS	Filtration	MCs, ATX, CYN	0.17 - 0.21	***[141]***
HILIC Amide Gradient	ESI-MS/MS	LSE	STXs, ATX, CYN	0.002 - 0.527	***[139]***
RP C18 Gradient	ESI-MS	SPE	MCs, ATX, CYN, NOD	0.002 - 0.1	***[142]***
RP C18 Gradient	ESI-MS/MS	Filtration + LVI	MCs, ATX, CYN, NOD	0.1 - 0.5	***[143]***

* PLRP-S = Polymeric Reversed Phase; CEX = Cation Exchange; AEX = Anion Exchange

2.5 Excitation-Emission Matrix Fluorescence Spectroscopy and Dissolved Organic Matter

Excitation-emission matrix fluorescence spectroscopy (EEMS) is a widely used technique in water science in the study of dissolved organic matter (DOM) in both marine and freshwater environments. While most studies to date have focused on natural environments such as oceans, rivers and estuaries ***[144]***, comparatively little work has been done on the distribution and composition of DOM in drinking water plants using EEMS ***[145,146]***. Since the mid-1990's, the popularity of EEMS in water science has continued to increase ***[144,147,148]***, due to advantageous features such as quick analysis time, minimal sample preparation and the large amount of data obtained. These features, coupled with improvements in instrument technology and data processing capabilities has seen EEMS become the state-of-the-art technique for studying DOM.

The amount of DOM present in the source water is an important factor in drinking water treatment, as it impacts treatment parameters such as coagulant and disinfectant dose ***[149,150]***. Removing DOM during treatment is also important, as it can react with disinfectants to form disinfection by-products which cause adverse health effects in consumers. In WTPs, DOM is typically monitored using online total and dissolved organic carbon (TOC and DOC) and specific UV absorbance ($SUVA_{254}$) instruments. While these give indications of the total concentration of organic matter and its degree of aromaticity, these parameters provide no insight as to the overall composition of DOM present. The EEMS technique is able to provide

a more detailed view of DOM composition, which may inform more tailored water treatment processes for specific source waters. At present, EEMS is restricted to being a laboratory based technique, however current research indicates that it is amenable to implementation as an online monitoring tool in WTPs and early warning systems ***[151,152]***.

2.5.1 EEMS Technique

EEMS employs the use of fluorescence instruments that can scan a wide range of excitation and emission wavelengths to produce a 3D spectral map, or excitation emission matrix (EEM). Spectra are usually visualised as a contour map or surface plot of excitation wavelength vs. emission wavelength vs. fluorescence intensity (**Figure 2-11**).

EEMS typically requires little sample preparation, with filtration, pH adjustment and dilution being the usual level of sample processing required. While sample processing is minimal, each step is critical in acquiring good quality data. The main issues encountered with EEMS are chelation of certain compounds to metal ions, pH dependant fluorescence intensity and the inner-filter effect (IFE)***[153-158]***.

Humic substances are particularly affected by the presence of metal ions, as the numerous phenol and carboxylic acid groups are able to form organo-metallic complexes. This can alter the spectral properties of the compound of interest and may enhance or quench fluorescence. However, there is little evidence that this is a

major issue in aquatic systems, with most studies focusing on controlled, laboratory experiments ***[144]***.

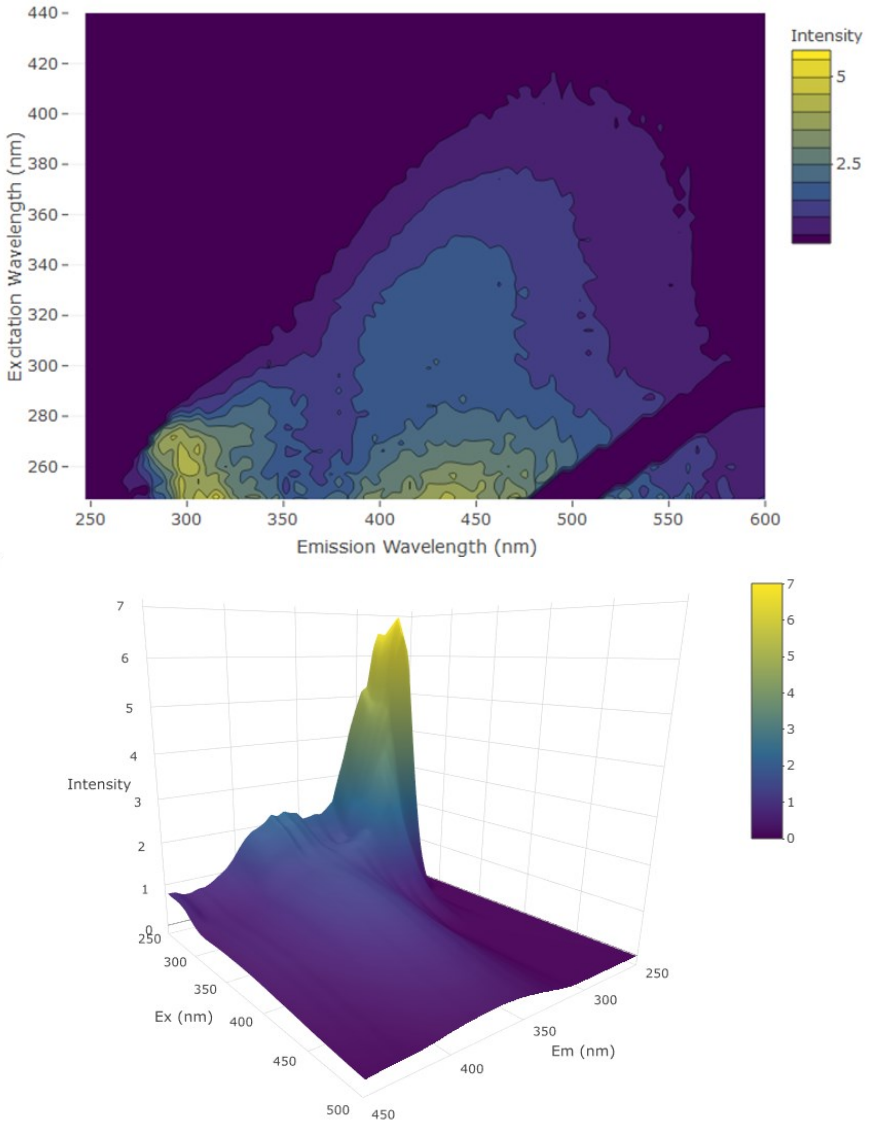

Figure 2-11: Examples of an EEM contour map (top) and surface plot (bottom).

The pH is also important, as it influences the spectral properties of common groups of compounds studied in DOM fluorescence. This is a result of conformational changes in the molecules as pH changes, hiding or exposing fluorescent groups. As such, it is common practice to adjust the pH of samples to account for the variation

between sampling locations and allow for data to be collected under similar conditions. Samples are commonly adjusted to pH 6 - 7 ***[144]***, although in some cases, the pH may be adjusted to as low as 2 in an effort to suppress the formation of complexes if this is deemed to be significant ***[159]***. Overall, the effect of pH on natural water samples is likely to be minimal in comparison to other factors ***[144]***.

The IFE is a signal attenuation effect that arises from the absorption of excitation and emission wavelength intensities (primary and secondary IFE) by the fluorophore or other chromophores in the sample. This can reduce fluorescence intensity and distort the shape of the spectra ***[153,154]***. The effect becomes more pronounced at higher concentrations and can often be mitigated by dilution of the sample prior to analysis ***[144,159]*** or the spectra can be corrected mathematically after acquisition ***[153,154]***. In the case of low concentration samples, the contribution of the IFE is negligible. Additionally, some modern instruments can correct for the IFE automatically.

2.5.2 Composition of DOM

DOM is a complex mixture of organic compounds derived from natural and anthropogenic sources. Natural DOM may enter aquatic systems in many ways such as run-off from surrounding land or may be created *in situ* by micro-organisms. Anthropogenic sources may include, for example; wastewater discharge sites, leaching or aerial dispersal. Consequently, the source of the DOM influences its composition and properties ***[144]***.

In the use of EEMS and other fluorescence-based techniques, the fluorescent DOM (fDOM) is the fraction of the DOM amenable to study. From EEMS studies of DOM, five major spectral regions are associated with three major components of DOM as first described by Coble *et.al.* (**Table 2-6, Figure 2-12**) ***[147]***. In general, the major fDOM component is comprised of humic-like material - a general term that represents a large group of molecules which exhibit a common structure comprised of aromatic groups linked together with phenolic, carboxylic and other substituents attached (**Figure 2-13**).

Table 2-6: Major fluorescent components present in natural waters and their characteristic spectral regions

Peak†	Peak‡	Ex_{max}(nm)	Em_{max}(nm)	Component type
C	α	330-350	420-480	Humic-like
A	α'	250-260	380-480	Humic-like
M	β	310-320	380-420	Marine humic-like
B	γ	270-280	300-320	Tyrosine-like, protein-like
T	δ	270-280	320-350	Tryptophan-like, protein-like or phenol-like

† Nomenclature as defined by Coble *et.al* ***[147]***
‡ Nomenclature as defined by Parlanti *et.al* ***[160]***

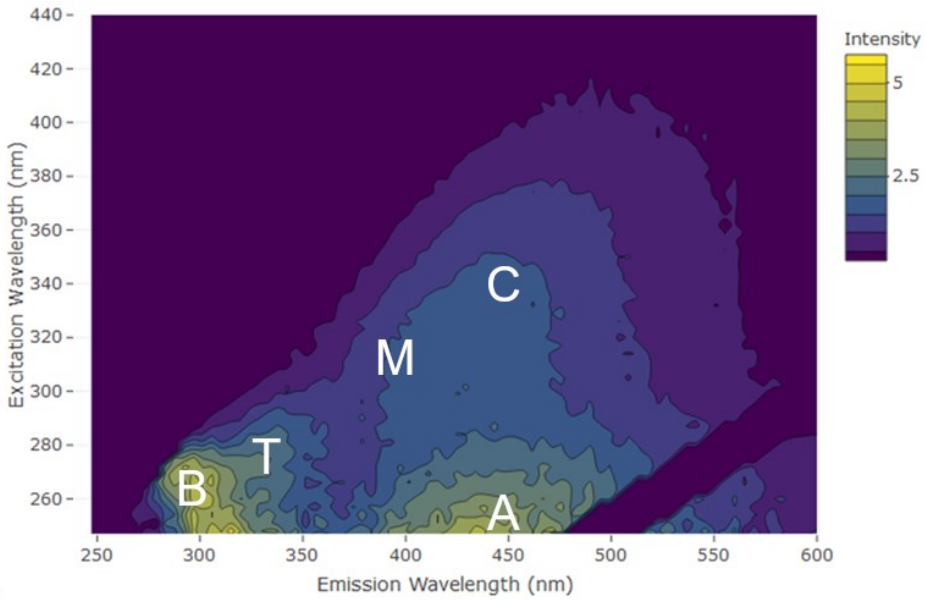

Figure 2-12: EEM contour plot indicating the spectral region of each major fluorescent group.

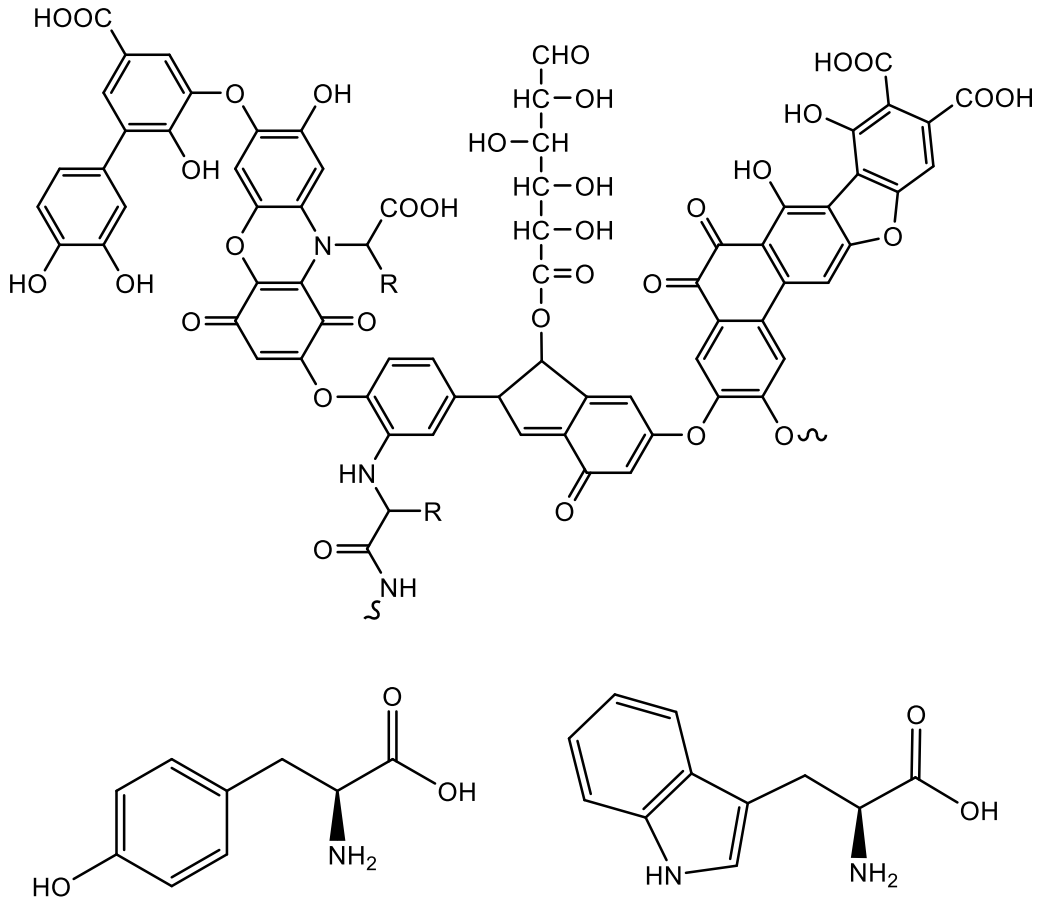

Figure 2-13: Chemical structures of a putative humic acid (top), tyrosine (bottom left) and tryptophan (bottom right).

The humic region of a typical fresh water EEM spectra is characterised by two peaks denoted A and C, while marine samples may also exhibit a third peak, M. Other major components of DOM include the protein derived fluorophores tryptophan (Peak T) and tyrosine (Peak B), which may be present as free amino acids or bound as polypeptides and proteins (**Figure 2-13**). While these are usually not as prominent as humic substances in typical natural water samples, they can sometimes become the major fDOM component, for example in wastewater and other waters that have high levels of biological activity or biological inputs such as

livestock runoff. As such, they have been used as markers for biological activity in some EEMS studies ***[160-162]***.

2.5.3 Data Processing: PARAFAC

As EEMS generally produces a large amount of spectroscopic data, appropriate methods for processing the data are required. Early work in this area made use of traditional "peak picking" techniques to identify excitation/emission (Ex_{max}/Em_{max}) maxima and used a range of parameters derived from these to interpret the complex spectra typically obtained ***[147]***. Nowadays, with readily accessible and highly capable computer and software systems, the analysis of EEM spectra has moved towards a more computationally intensive approach. At present, the current method of choice for many researchers is parallel factor analysis (PARAFAC), which was popularised by Bro in the late-1990s ***[163]*** and has since become more accessible, with specific packages for conducting EEMS PARAFAC now being available for software like MATLAB and *R*.

PARAFAC is a multi-way decomposition technique that is a generalisation of principle component analysis (PCA) that is applicable to higher order arrays; in the case of EEMS data, a three-way array (**Equation 2-10**).

$$x_{ijk} = \sum_{f=1}^{F} a_{if} b_{jf} c_{kf} + e_{ijk} \qquad (2\text{-}10)$$

In the context of EEM data, x_{ijk} refers to the fluorescence intensity of the *i*th sample at emission wavelength *j* and excitation wavelength *k*. This data matrix is decomposed by the PARAFAC algorithm into a set of trilinear terms (a_{if}, b_{jf}, c_{kf}) and a residual array (e_{ijk}). For a PARAFAC model with *F* components, a_{if} is proportional to the concentration of the *f*th component in sample *i*, and can therefore be used to quantify components if calibration is possible, or to identify trends in relative concentrations. Element b_{if} is linearly related to the fluorescence quantum efficiency of the *f*th component at emission wavelength *j*. Similarly, c_{kf} is linearly related to the specific absorption coefficient at excitation wavelength *k*. As such, *b* and *c* are able to be used as a modelled estimate of the *f*th component's EEM spectra in the *i*th sample. Element e_{ijk}, is the sum of squares residuals and the trilinear model is found that minimises this element ***[163,164]***.

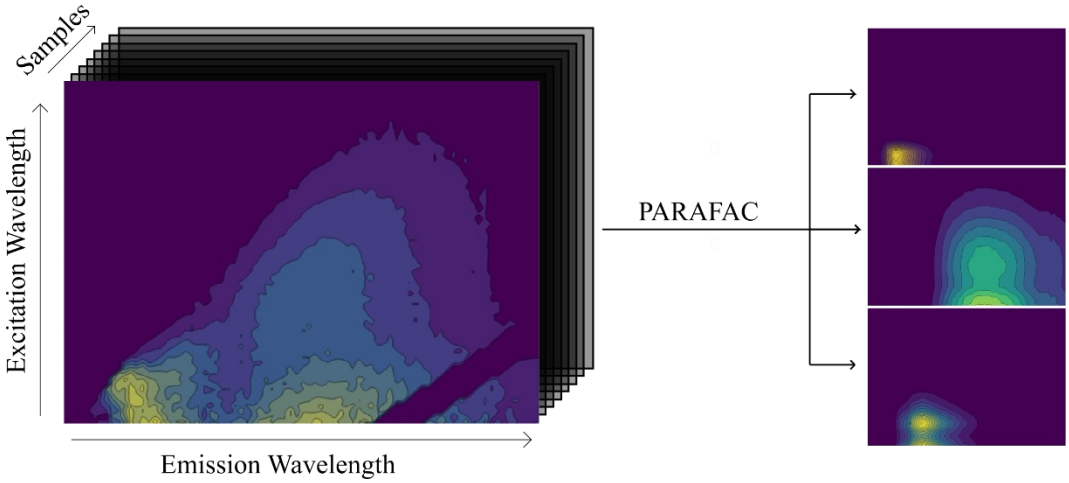

Figure 2-14: PARAFAC decomposition of raw fluorescence spectra yielding pure spectra of sample components in a three component model.

The use of PARAFAC for fluorescence data allows for pure spectra of each fluorescent component in a mixture to be obtained from the complex spectra

generated from raw samples (**Figure 2-14**), which affords simpler interpretation of the data in a more robust manner than traditional "peak picking" techniques. Further details on the theory and implementation of PARAFAC models can be found elsewhere ***[148,163]***.

In addition to the PARAFAC model, further methods must be employed to validate the model and arrive at the appropriate number of components to include to generate a stable model that fits the data satisfactorily. Usually, models are validated using a combination of split-half analysis, checking residuals, the core consistency diagnostic and by employing external experimental and chemical knowledge of the data being analysed ***[146,148,163,165]***.

2.5.4 Drinking Water Treatment Systems and EEMS PARAFAC

EEMS has become more prevalent in the study of drinking water in recent years, due to the advantages outlined earlier, as well as its potential to be implemented as an online monitoring tool. While EEMS has become more popular in this context, compared to other fields (e.g. marine chemistry) relatively little research has been conducted. This has been noted by researchers in this area ***[144,151,159]***, highlighting the need for further work to be carried out in order to ascertain a better understanding of the behaviour of DOM in water treatment plants (WTPs). The use of EEMS in studying drinking water systems is applicable to a number of important treatment problems including DOM removal efficiency/distribution ***[151,159,166]*** and disinfection by-product (DBP) formation ***[167,168]***, with some reviews

providing general overviews of the technique in such contexts ***[145,146,169,170]***. Commonly seen fDOM components in WTP studies include humic substances, tyrosine-protein like and tryptophan-protein like components, and some studies that have employed PARAFAC modelling have further decomposed humic fluorescence into sub-components ***[151,159]***.

2.5.4.1 DOM Removal Efficiency and Distribution

EEMS has been employed in various studies to investigate the distribution of humic and proteinaceous DOM in WTPs, which also give insight into the effectiveness of specific water treatment processes in removing specific DOM components. In general, commonly employed treatment processes are more effective in removing the humic fraction of fDOM compared to the proteinaceous fraction and good correlations have been found between TOC/DOC concentration, $SUVA_{254}$ and humic fluorescence.

2.5.4.1.1 Humic Substances

Overall, good removal of humic substances is achieved by usual water treatment practices with removals of 23–83 % being achieved during coagulation alone. Of the most commonly used coagulants, aluminium sulphate gives the highest percent removal of humic substances and is affected by dosing level and pH, with higher doses and pH close to 6 increasing effectiveness ***[145]***. Coagulation and flocculation are generally more efficient for the DOM fraction that exhibits higher hydrophobicity, aromaticity and charge, and high removals at this stage give some

indication of the DOM character of the source water. As humic substances are highly aromaticised and generally hydrophobic, it is not surprising that coagulation and flocculation are effective in removing them. Other primary treatment methods that usually follow coagulation and flocculation such as sand filtration, tend to have varying impact on the concentration of humic substances ***[152,171]***.

In many studies, the humic region of the EEM spectra has been modelled using PARAFAC and shown to be comprised of subsets of humic substances which exhibit differing properties and behaviours in WTPs. Commonly encountered PARAFAC components ascribed as humic substances were reviewed by Ishii *et.al* ***[172]***, and their general properties and behaviours in WTPs were grouped and catalogued. Three commonly encountered humic groups were looked at and assigned as components 1, 2 and 3 - however, these assignments were arbitrary as the naming of PARAFAC components differs between studies depending on the number of components modelled and the order in which researchers chose to label components. Also, not all of these components are always derived from PARAFAC modelling of natural water samples, and in some cases more subsets are found to be present. This reflects the variable nature of aquatic ecosystems and the need to assess water treatment approaches on a case-by-case basis regarding DOM removal.

Table 2-7: Commonly encountered humic groups as outlined by Ishii *et.al [172]*.

Humic Component	Peak	Classification	$Ex_{\lambda max}$	$Em_{\lambda max}$
1	A	UVC humic-like	< 230 - 260	400-500
2	A + C	UVC + UVA humic-like	< 240 - 275(339-420)*	434-520
3	A + M	UVC humic + UVA marine humic-like	< 240 - 260(295-380)*	374-450

* Parentheses indicate secondary peak.

Humic component 1 (HC1) is described as the UVC absorbing, low molecular weight fraction (mean highest molecular weight ≈ 665 Da) of humic material present in DOM. Data on HC1 in WTPs is limited, although it has been positively correlated with hydrophilicity while negatively correlated with alumina adsorption (pH 4) and benzo[*a*]pyrene binding in laboratory studies ***[172,173]***. In the absence of real WTP data, these experimental properties suggest that HC1 would be minimally affected by most treatment processes, with the exception of oxidation processes like O_3 or AOPs like O_3/H_2O_2 and O_3/UV. Humic component 2 (HC2) exhibits primary and secondary excitation peaks, with a primary peak similar to HC1. HC2 absorbs in both the UVC and UVA spectral regions and exhibits hydrophobic characteristics. HC2 is comprised of larger molecules, with apparent molecular weights > 1000 Da and has been described as "reduced quinone-like" after comparison with the model compound anthrahydroquinone-2,6-disulphonate (AHDS - **Figure 2-15**). The hydrophobicity and susceptibility of HC2 to photodegradation indicates that this component is likely to be removed to some degree by all common water treatment processes. This is reflected in research carried out in WTPs, which show reductions of HC2 throughout the treatment train, with the exception of sand filtration and water softening treatments. The removal of HC2 from water sources during treatment is important, as it has been strongly correlated with DBP formation potential (DBPFP). Like HC2, HC3 exhibits primary and secondary excitation peaks, and absorbs in the UVA and UVC spectral regions, as well as in the UVB region. HC3 has been compared to the model compound anthraquinone-2,6-disulphonate (AQDS - **Figure 2-15**), and described

as “oxidised quinone-like”. HC3 is found in the transphilic fraction of DOM, an indication of intermediate polarity between HC1 and HC2. Molecular weight is also regarded to be lower than that of HC2, evidenced by shorter excitation and emission wavelengths. Overall, HC3 behaves similarly to HC2 in WTPs, although is removed to a lesser extent due to lower susceptibility to photodegradation and increased hydrophilicity.

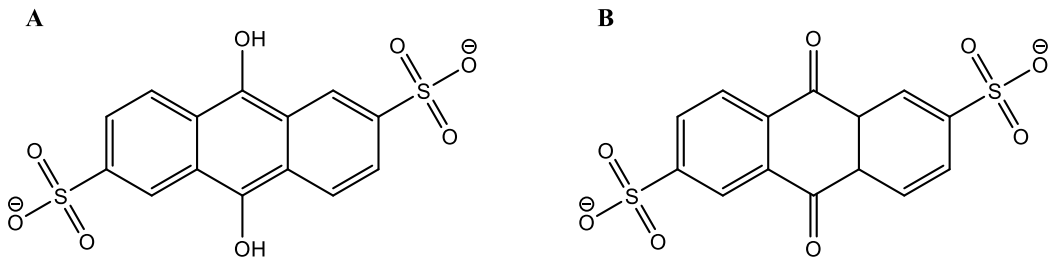

Figure 2-15: Anthrahydroquinone-2,6-disulphonate (A) and anthraquinone-2,6-disulphonate (B)

2.5.4.1.2 Proteinaceous DOM

In the context of drinking water treatment, the behaviour of proteinaceous DOM is less well documented, largely due to it being less prevalent or not detected in source waters. In WWTPs, tyrosine and tryptophan fluorescence is common, due to intense biological activity and biological treatment processes that produce biomolecules and biopolymers *in situ* ***[174]*** and the presence of tryptophan/tyrosine type protein fluorescence has been linked to biological processes in natural waters ***[160,161]***.

Protein derived fluorophores behave somewhat differently to humic substances in WTPs, and are in most cases are less treatable than terrestrial humic material ***[151]***, additionally the use of EEMS for assessing protein fluorescence during drinking

water treatment is complicated by a number of factors ***[169,174]***. Changes in protein fluorescence have been noted during water treatment processes, both increases and decreases. Changes in molecular structure and reactions during chlorination and ozonation can lead to increases in protein fluorescence in EEM spectra ***[169,174]***. Furthermore, the breakdown of humic components during chlorination into lower molecular weight fragments that fluoresce at shorter wavelengths can also increase fluorescence intensity in the protein fluorescence region of EEM spectra ***[174-176]***. These effects reflect an overall change in the composition of DOM during specific treatment processes, and not necessarily changes in total DOM concentration. Biological activity within the plant can also lead to increases in protein fluorescence due to *in situ* production of molecules containing tyrosine and tryptophan by microbes present in the system, for example during biological filtration processes. Reductions in protein fluorescence have been noted during GAC filtration ***[159]***, coagulation and membrane filtration ***[145,151]***.

2.5.4.2 Disinfection By-Product Formation

Disinfection by-products (DBPs) are a range of harmful reaction products formed during disinfection processes during drinking water treatment, the most notable being trihalomethanes (THMs) and haloacetic acids (HAAs). DBPs may be formed by the reaction between natural organic matter (NOM) and disinfectants (oxidising agents) such as chlorine, chloramine, chlorine dioxide and ozone. In New Zealand, the presence of certain DBPs are regulated as outlined in the Drinking Water Standards for New Zealand, each having an associated “maximum acceptable

value" (MAV) (**Table 2-8**) ***[3]***. Although 15 DBPs are regulated by the DWSNZ, many more DBPs have been identified. A review by Richardson *et.al* covered 85 DBPs, of which 74 were considered "emerging" DBPs ***[177]*** and over 600 DBPs have been reported in the literature ***[178,179]***. While THMs and HAAs are generally present in the highest concentration, some emerging DBPs are considered to be more genotoxic ***[177]***. Additionally, more than 50% of the total organic halogens (TOX) formed during chlorination are unaccounted for or unidentified, most of which are thought to be high molecular weight (> 500 Da) or highly polar compounds. It is hypothesised that this is due to most DBP studies employing solvent extraction based GC and GC-MS methods, which would be unable to detect such compounds leading to bias towards low molecular weight, volatile and semi-volatile DBPs ***[178]***.

Table 2-8: Regulated DBPs and their respective MAVs as outlined in the DWSNZ.

Chemical	MAV (mg/L)	Type	Source
Chlorate	0.8†	DBP	Chlorine dioxide
Chlorite	0.8†	DBP	Chlorine dioxide
Bromate	0.01†	DBP	Ozone
Cyanogen chloride	0.4	DBP	Chlorination
Monochloramine	3	DBP	Chlorination
Dibromoacetonitrile	0.08	DBP	Chlorination
Dichloroacetonitrile	0.02†	DBP	Chlorination
2,4,6-trichlorophenol	0.2	DBP	Chlorination
Dichloroacetic acid	0.05†	HAA	Chlorination
Monochloroacetic acid	0.02	HAA	Chlorination
Trichloroacetic acid	0.2	HAA	Chlorination
Bromodichloromethane	0.06	THM‡	Chlorination
Bromoform	0.1	THM‡	Chlorination
Chloroform	0.4	THM‡	Chlorination
Dibromochloromethane	0.15	THM‡	Chlorination

† Provisional maximum acceptable value (PMAV).
‡ The sum of the ratio of the concentration of each THM to its respective MAV must not exceed 1.

THMs can be formed via the haloform reaction between chlorine (Cl_2) and methyl ketones (**Figure 2-16)** or other groups of compounds that contain functional groups

that can be oxidised to a methyl ketone such as secondary alcohols, alkenes with activated double bonds, *m*-hydroxyphenols and β-diketones, (e.g. 2,4-pentadione) (**Table 2-9**) ***[179,180]***.

Table 2-9: Examples of important functional group precursors to THM and HAA formation *[179].*

Chemical group	Structure
Substituted benzene	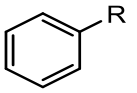
Substituted phenol	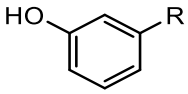
β - diketone	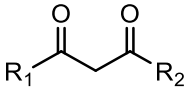
β - ketoacid	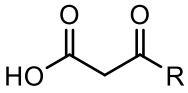
Amino acid	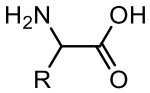

In natural waters used as drinking water sources, the dominant compounds susceptible to undergoing the haloform reaction during Cl_2 disinfection are humic and fulvic acids, which contain many precursor functional groups (**Figure 2-13**) and make up the largest proportion of DOM in most cases. Other reaction mechanisms that result in the formation of THMs are also possible, with susceptible substrates including carbohydrates, proteins, amino acids and carboxylic acids ***[179,181-183]***. It is also possible to form THMs from DOM during Cl_2 disinfection via other reaction mechanisms which also form HAAs (**Figure 2-17**) ***[179,184]***.

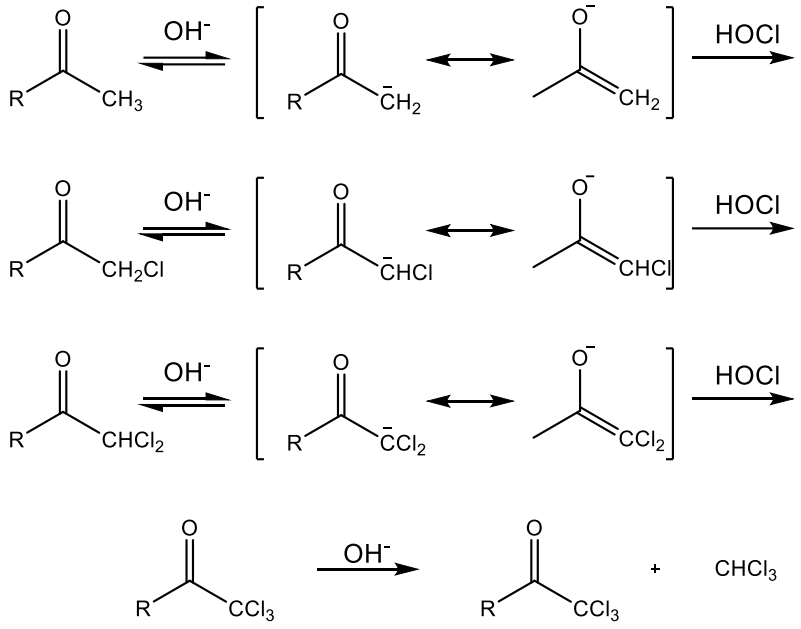

Figure 2-16: Generalised haloform reaction scheme between a methyl ketone and aqueous chlorine *[179]*.

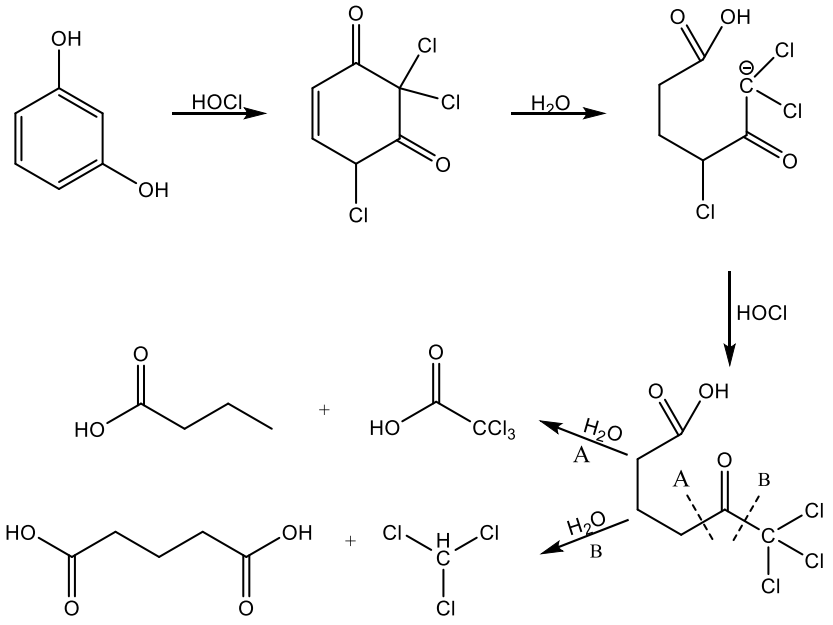

Figure 2-17: Reaction between resorcinol and aqueous chlorine to form trichloroacetic acid (TCAA) and chloroform *[179,185]*, a reaction relevant to the production of TCAA and chloroform from polyphenolic humic substances.

While the formation of THMs and HAAs are closely correlated with the humic and fulvic acid fraction of DOM, in most cases there is little correlation with the proteinaceous fraction ***[145]***. In general, bonded amino acids (proteins, polypeptides) have lower DBPFPs than free amino acids, due to the amine groups being unavailable to react with chlorine. Coupled with the fact that bonded amino acids are prevalent in much higher quantities than free amino acids in natural waters, the overall protein fraction of DOM has a lower DBPFP than the humic fraction. Nevertheless, in some cases the aromatic protein fraction of DOM has been correlated with chloroform yield, indicating that proteinaceous DOM does contribute to the DBPFP during drinking water treatment to some extent ***[169]***.

2.5.4.2.1 DBPs and EEMS-PARAFAC

As the main precursors to DBPs are humic and fulvic acids, EEMS has been used as a method for investigating the DBPFP in WTPs. The removal efficiency of these components of DOM via treatment (**Section 2.5.4.1.1**) are linked to DBPFP, where poor removal of humic and fulvic acids increases the risk of forming DPBs at the disinfection stage.

Johnstone *et.al.* ***[167]*** applied EEMS-PARAFAC to water samples collected during a peak DBP formation period. A three component PARAFAC model was validated with components being assigned as terrestrial humic (C1), microbial/marine humic (C2) and protein-like (C3). The component loadings were then correlated to DOC, chlorine consumption and individual DBP formation ($CHCl_3$, Cl_2AA and Cl_3AA)

using multiple linear regression. C1 showed strong correlations with DOC concentration (R^2 = 0.88) and Cl_2 consumption (R^2 = 0.85), while C2 and C3 together gave good correlations with individual DBPs ($CHCl_3$; R^2 = 0.77, Cl_2AA; R^2 = 0.61 and Cl_3AA; R^2 = 0.70). It should be noted that this study gave no information on correlations between component loadings and the modelled spectra of C3 (protein-like) exhibited considerable spectral information in the humic region ($Ex_\lambda \approx 220$ nm; $Em_\lambda = 450 - 550$). As such, there may have been some confounding factors that influenced the regression models produced.

Pifer *et.al.* ***[186]*** assessed EEMS-PARAFAC analysis as a means of improving $SUVA_{254}$ for DBP control. Validation of a PARAFAC model of 190 fluorescence spectra yielded a five-component model, although one component was attributed to instrument noise and was discarded leaving a four-component model that was used for further analysis. The four components were assigned as humic-like (C1; $Em/Ex_{\lambda max}$ = 238(329)/430), protein-like (C2; $Em/Ex_{\lambda max}$ = 231/362), humic-like (C3; $Em/Ex_{\lambda max}$ = 344(203, 228)/426) and humic-like (C4; $Em/Ex_{\lambda max}$ = 395(269,213)/471), where values in parentheses indicate secondary and tertiary excitation maxima. Of the DBPs included in the study (chloroform, bromodichloromethane, dibromochloromethane, bromoform, dichloroacetonitrile, trichloroacetonitrile, dibromoacetonitrile, and 1,1,1-trichloro-2-propanone), only four (chloroform, dichloroacetonitrile, bromodichloromethane, and 1,1,1-trichloro-2-propanone) were formed at quantifiable levels. Of these four, only correlations between DOM properties ($SUVA_{254}$, chlorine demand and F_{max} of PARAFAC

components) and chloroform yield could be established. The strongest correlations being found between chloroform yield and the humic components C1 (R^2 = 0.84) and C4 (R^2 = 0.76). Compared with the correlation with $SUVA_{254}$ (R^2 = 0.51), this was seen as a significant improvement over using $SUVA_{254}$ as a predictor of chloroform yield, with the fluorescence-based measurements representing chloroform precursors more accurately.

Nguyen *et.al.* ***[187]*** investigated spectral characteristics and DBPFPs following storm events using EEMS-PARAFAC. This study focused on raw river water collected during two rainfall events (major (152 mm) and minor (11 mm) rainfall) which were then subjected to a lab-based chlorination protocol and GC-MS analysis to quantify DBPs. Two components were identified from the PARAFAC analysis and were assigned as terrestrial humic-like (C1) and microbial humic-like (C2). It was found that C1 and C2 peak intensities increased during major rainfall events which peaked when the river level reached its maximum. The intensities of each component then decreased gradually after the rain event, but not as quickly as the river level dropped. The effect was found to be more pronounced for C1. An increase in trihalomethane formation potential (THMFP) and haloacetic acid formation potential (HAAFP) was also noted during storm events, with a more pronounced effect during major rainfall being found. DOC, $SUVA_{254}$, Fluorescence Index (FI) and C1 loading were all significantly correlated with THMFP and HAAFP. DOC, $SUVA_{254}$ and C1 loading exhibited strong positive correlations with THMFP and HAAFP, while FI exhibited weaker negative correlations for each

DBPFP. C2 was also correlated with DBPFP, although not as strongly as C2, with the authors attributing this to compounds containing more aromatic and condensed structures (C1) being more viable precursors to DBP formation.

Table 2-10: Correlation coefficients (R^2) between THMFP/HAAFP and some water quality parameters as determined by Nguyen *et.al [187].*

	THMFP	HAAFP
DOC	0.918	0.974
$SUVA_{254}$	0.912	0.921
C1	0.912	0.920
FI	0.340	0.446

Wu *et.al.* ***[188]*** looked at soluble microbial products (SMPs) discharged from upstream WWTPs and how they may impact DBPFP in downstream DWTPs after autochthonous microbial degradation in aerobic and anoxic conditions. Water samples were collected from a river that receives large wastewater inputs from municipal WWTPs. Samples were analysed using EEMS-PARAFAC and four components were identified from the PARAFAC analysis which were assigned as polyaromatic humic (C1), polycarboxylate humic (C2), fulvic acids (C3) and tryptophan-protein like (C4) components of DOM. Fluorescence intensity of C1 and C3 was shown to increase during aerobic biodegradation experiments, whereas no change was noted for these components under anoxic conditions. For C2 and C4, decreases in fluorescence intensity were observed in both aerobic and anoxic conditions. The results indicated that C1 and C3 were not fully biodegraded or assimilated under aerobic conditions, although they seemed to be degraded to some extent which resulted in an increase in fluorescence intensity. C2 and C4 were used during biodegradation. In conjunction with other techniques (infrared (IR) spectroscopy, GC-ECD and 16S rRNA sequencing), it was shown that aerobic

microbial degradation in the presence of SMPs decreased the DBPFP by 10%, however the DBP precursor reactivity (DPB yield) was greatly increased (≈ 35 %). DBPFP was reduced greatly by anoxic biodegradation (≈ 55 %), and DPB yield was also significantly reduced (≈ 50%). This showed that dissolved oxygen (DO) was a key factor in affecting microbial populations which degraded SMPs into compounds that influence DBPFP.

Chapter 3:

Surface Morphology and Elemental Composition of GAC

3 Surface Morphology and Elemental Composition of GAC

3.1 Introduction

This chapter aimed to determine whether bacteria had colonised the GAC surface, indicating a transition to BAC media, and whether the extent of bacterial colonisation was more apparent on older filter media. This involved a qualitative examination of the surface morphology of both used and fresh GAC media. Additionally, the surface and bulk composition, primarily in terms of metal concentrations, were investigated quantitatively. This was done to investigate the potential for GAC to become enriched with certain metals over time that may impact either the development of a stable biofilm over time or disposal following its use as a filtration media.

The Waikato River contains relatively high levels of some toxic heavy metals particularly arsenic (As) ***[189,190]***, due to the presence of geothermal activity upstream of the HWTS, including geothermal power generation. While coagulation, flocculation and sedimentation (CFS) processes remove the majority of these metals from the water prior to further treatment, a small fraction of the initial concentration remains in the aqueous phase or bound to small particles not completely precipitated during CFS. As such, it is likely that heavy metals will be captured by GAC filters due to the adsorptive nature of GAC and become enriched on the GAC surface over time. Further, after a long enough period, the GAC media may become so enriched that it may become inhibitory to biological growth and

metabolism. Therefore, if the GAC media is intended to act as a scaffold for the establishment of a biofilm and ultimately act as a biological filter (BAC), the presence of high concentrations of heavy metals may mean that this is not feasible over the long term. Additionally, the presence of high concentrations of certain metals within the GAC media may pose complications regarding disposal when it has reached the end of its service lifetime.

To investigate the surface morphology and elemental composition of the GAC media, scanning electron microscopy (SEM), energy dispersive x-ray spectroscopy (EDS) and inductively coupled plasma – mass spectrometry (ICP-MS) studies were carried out comparing the media originally present in the HWTS's GAC filters with fresh GAC and media that had been in use for only a short time.

3.2 Experimental

Virgin GAC (vGAC) and used GAC samples were imaged using scanning electron microscopy (SEM) as a means of investigating any differences in surface morphology and the presence of bacterial colonies. Samples were also analysed using energy-dispersive x-ray spectroscopy (EDS) to assess differences in the elemental composition of the carbon surface. Samples were also analysed using ICP-MS to investigate the concentrations of adsorbed elements more accurately.

3.2.1 SEM and EDS

Samples were collected from each full scale GAC filter at the HWTS and were analysed alongside vGAC (GA1000N 8 x 30 mesh). At the time of sampling, the

full-scale GAC filters were of different ages, with some having undergone partial media replacement. Samples were collected from GAC 5 (original filter media; ≈ 10 years old), GAC 6 (partial replacement; ≈ 6 months old) and a pilot scale column (fresh media; ≈ 3 months old).

3.2.2 ICP-MS

Fresh GAC was compared with GAC collected from the HWTS GAC filters using inductively coupled plasma mass spectrometry (ICP-MS). To assess the repeatability of the ICP-MS methodology, samples of GAC for preliminary screening were collected from the full-scale filters during routine maintenance while the filters were empty following a backwashing and air-scouring procedure and combined as a composite sample. These samples were compared with fresh GA1000N.

For further studies, carbon samples were collected using a sieve device prior to backwashing from the surface layer of the filter (0 - 20 cm) and during the back-wash procedure while the carbon media was being mixed. Samples were taken from each individual GAC filter and analysed in duplicate. Samples were collected from four old GAC filters (GAC2, GAC3, GAC4 and GAC 5) and one recently replaced filter (GAC 6) which were compared with GA1000N.

3.2.3 Materials and Instrumentation

Glutaraldehyde (25% solution), sodium cacodylate and molecular sieves (3Å) were obtained from Sigma-Aldrich (Auckland, New Zealand). Ethanol (EtOH; ACS grade, 100%) and hydrochloric acid (HCl; ACS grade, 37%), Nitric acid (HNO_3 65%; analytical grade) and hydrogen peroxide (H_2O_2 30%; analytical grade) were obtained from Merck (Auckland, New Zealand). Syringe filters (Minisart®, 0.45 µm, cellulose acetate) were obtained from Merck and digestion tubes (SCP DigiTUBEs® 50 mL) were obtained from SCP Science. Fresh GAC was supplied by Activated Carbon Technologies Ltd (GA1000N 8 x 30 mesh; Wellington, New Zealand). De-ionised water was prepared using a Barnstead E-Pure water purification system with a resistivity of 18 Ω (Thermo Fisher Scientific, New Zealand).

SEM was carried out using a Hitachi S-4700 equipped with an energy dispersive x-ray system. ICP-MS of samples collected for preliminary screening was carried out using a SCIEX ELAN DRC II ICP-MS instrument (Perkin-Elmer, New Zealand). All subsequent samples were analysed using an Agilent 8900 Triple Quadrupole ICP-MS instrument (Agilent, New Zealand).

3.2.4 Buffers and fixative solutions

A cacodylate buffer (0.1 M) was prepared by dissolving sodium cacodylate (21.41g) in de-ionised water (900 mL) followed by the addition of HCl (1M, 8mL) and making to volume in a volumetric flask (1 L).

Fixative solution was prepared by adding glutaraldehyde (10 mL) to the cacodylate buffer (90 mL).

3.2.5 Method

3.2.5.1 SEM sample preparation

Samples from the full-scale filters were collected prior to routine filter backwashing and transferred directly to a glass vial containing the pre-prepared fixative solution (7 mL). Samples were transported back to the laboratory where they were soaked in fresh fixative solution (4 x 30 min) prior to dewatering with ethanol as listed in **Table 3-1**. Samples were submitted for critical point drying (CPD) and sputter coating with platinum prior to imaging with SEM at 5.0kV and EDS at 20.0 kV.

Table 3-1: Dewatering procedure for GAC samples.

Solvent	Time	Repeats
Deionised water	30 min	4
50% EtOH	60 min	1
75% EtOH	60 min	1
95% EtOH	60 min	1
100% EtOH w/ 3Å mol. sieve	30 min	4

3.2.5.2 ICP-MS sample preparation

Samples of GAC (*ca.* 50 g) were frozen (liquid N_2) and freeze dried overnight (*ca.* 12 h). Sub-samples (1 ± 0.2 g) of freeze dried GAC were transferred to plastic digestion tubes in duplicate. To each digestion tube containing the carbon samples, HNO_3 (3 mL) and H_2O_2 (3 mL) was added. The samples were allowed to digest overnight before being transferred to a heating block (75 ºC, 90 min). The samples were allowed to cool before transferring an aliquot (50 µL) to a volumetric flask (10 mL) and making to volume with DI water. The diluted sample was filtered using a syringe filter (0.45 µm; cellulose acetate) prior to analysis by ICP-MS.

3.3 Results and Discussion

3.3.1 SEM Imaging and EDS

As a reference, images and spectra were collected from GA1000N vGAC. These images showed the carbon to have a relatively uniform surface (**Figure 3-1**) as well as uniform elemental composition as determined by EDS (**Figure 3-2**, **Figure 3-3**). As expected, C was the dominant element, accounting for approximately 90 % of the surface composition by weight. Traces of Al, Si, S, Ca, Mg, Cl and Fe were also present, with Si, Al and Ca being the next most abundant respectively after C.

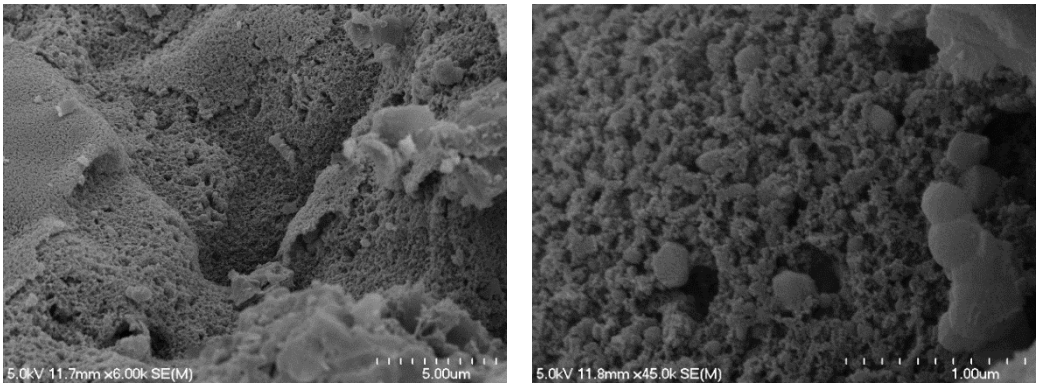

Figure 3-1: SEM images of the GA1000N surface.

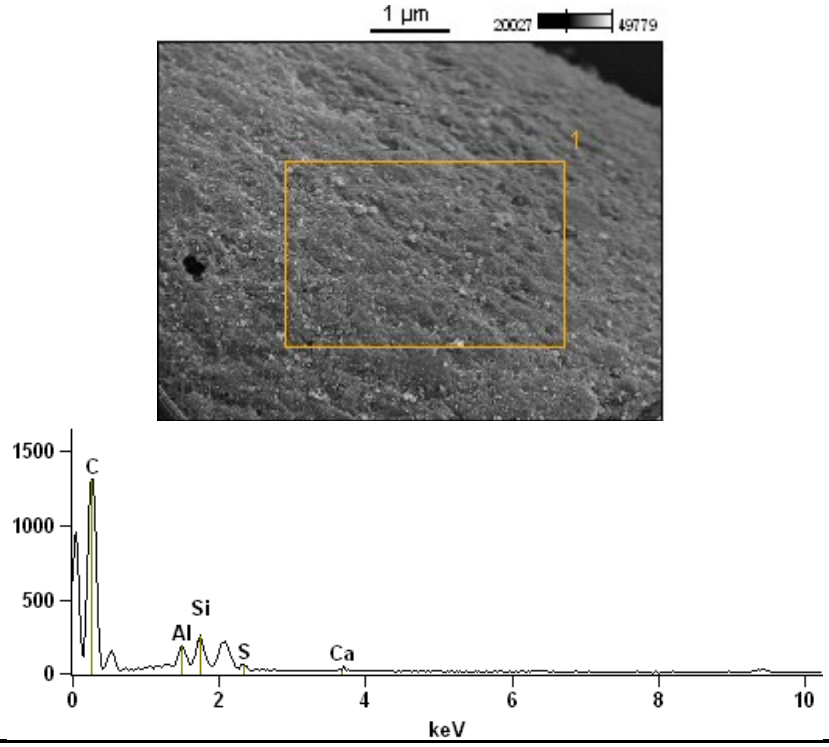

Weight %				
C	Al	Si	S	Ca
92.00 ± 0.89	2.33 ± 0.15	4.78 ± 0.2	0.32 ± 0.09	0.56 ± 0.09

Figure 3-2: SEM image, EDS spectra and elemental abundances of the GA1000N surface. The area from which the spectrum was collected is denoted by the orange rectangle.

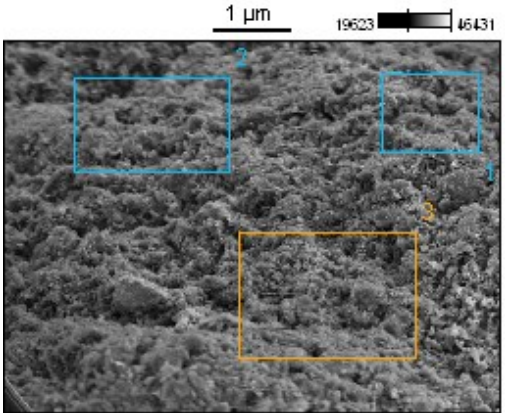

1

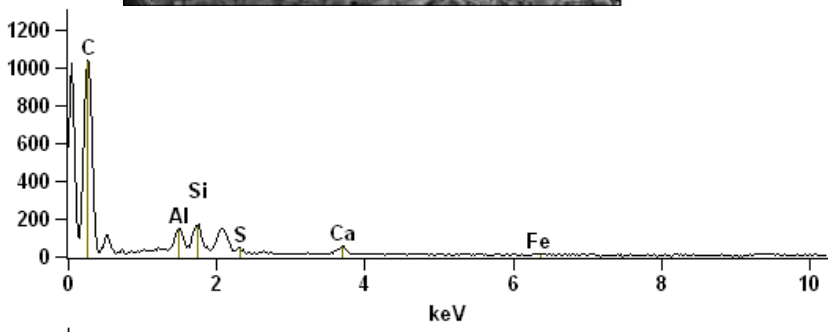

2

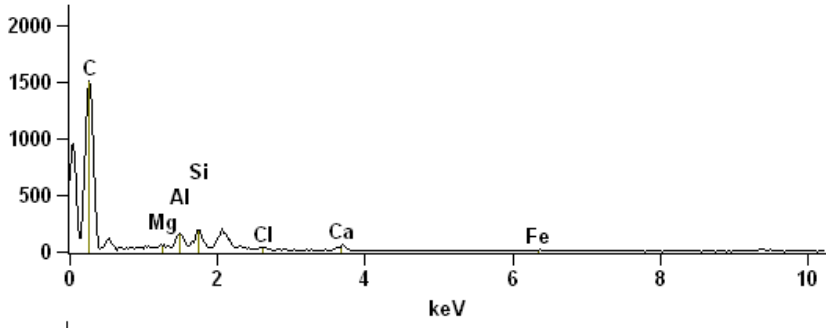

3

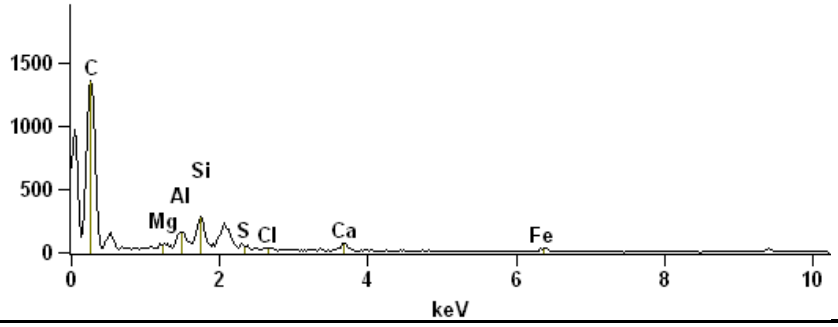

	Weight %							
Area	C	Mg	Al	Si	S	Cl	Ca	Fe
1	89.46 ± 0.98	-	2.72 ± 0.17	4.40 ± 0.21	0.27 ± 0.10	-	1.68 ± 0.13	1.47 ± 0.29
2	91.36 ± 0.83	0.21 ± 0.06	2.09 ± 0.16	3.46 ± 0.18	-	0.44 ± 0.07	1.39 ± 0.10	1.05 ± 0.22
3	88.05 ± 0.84	0.38 ± 0.06	2.28 ± 0.14	4.76 ± 0.18	0.17 ± 0.08	0.36 ± 0.07	1.78 ± 0.18	2.23 ± 0.22

Figure 3-3: Further EDS spectra illustrating the uniform composition of the GA1000N surface. Numbered rectangles indicate areas where each spectrum was collected.

Analysis of the filter media from the oldest filter (GAC5) gave markedly different results, in terms of both general appearance and elemental composition. The surface of the carbon appeared to consist of two areas of differing appearance. The first, and major region, was resolved as smooth, discrete regions that were closely grouped together, and resembled a smooth, mineralised surface (**Figure 3-4**). These regions exhibited high levels of O, Al and Mn, with low levels of C relative to the vGAC samples. No bacterial colonies were visible on these surfaces, and they appeared to dominate the bulk of the GAC particle surface.

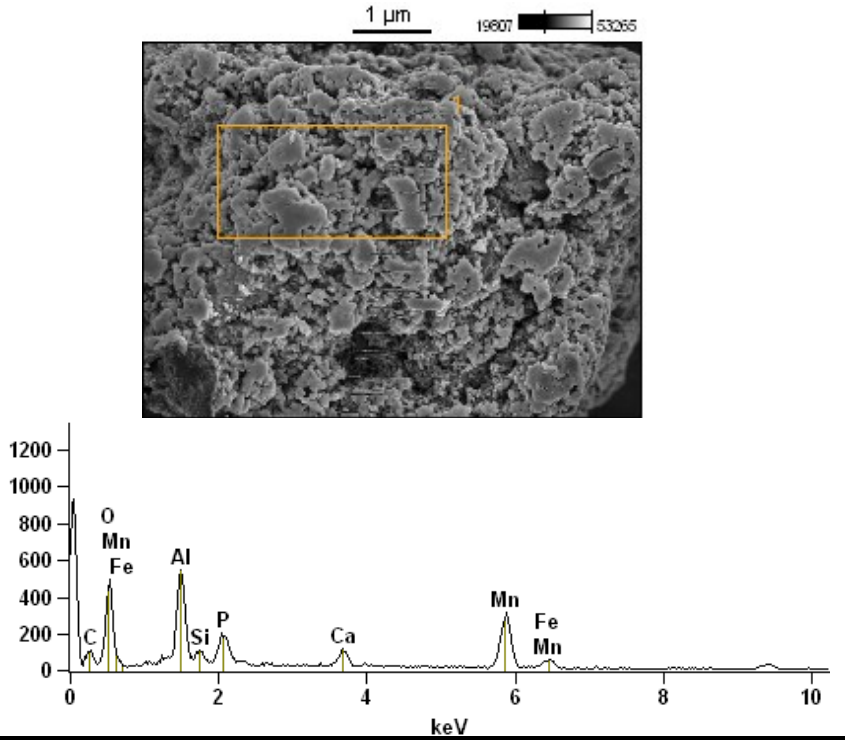

Weight %							
C	O	Al	Si	P	Ca	Mn	Fe
14.59	26.79	12.91	1.88	4.21	4.47	33.78	1.37
± 1.05	± 0.57	± 0.27	± 0.13	± 0.28	± 0.31	± 0.97	± 0.40

Figure 3-4: SEM image, EDS spectra and elemental composition of the major region of the GAC5 surface. The area from which the spectrum was collected is denoted by the orange rectangle.

The second major region appeared as the carbon surface similar to vGAC, but with colonies of bacteria present (**Figure 3-5**). In most cases, the presence of bacteria was quite dispersed, although some regions with dense colonisation were apparent (**Figure 3-6**). These regions exhibited a higher percentage of C than the mineralised regions due to the exposed carbon surface, but also had much higher amounts of other elements including O, Na, Al, P, Ca and Mn than the vGAC. A comparison of each region is shown in (**Figure 3-7**).

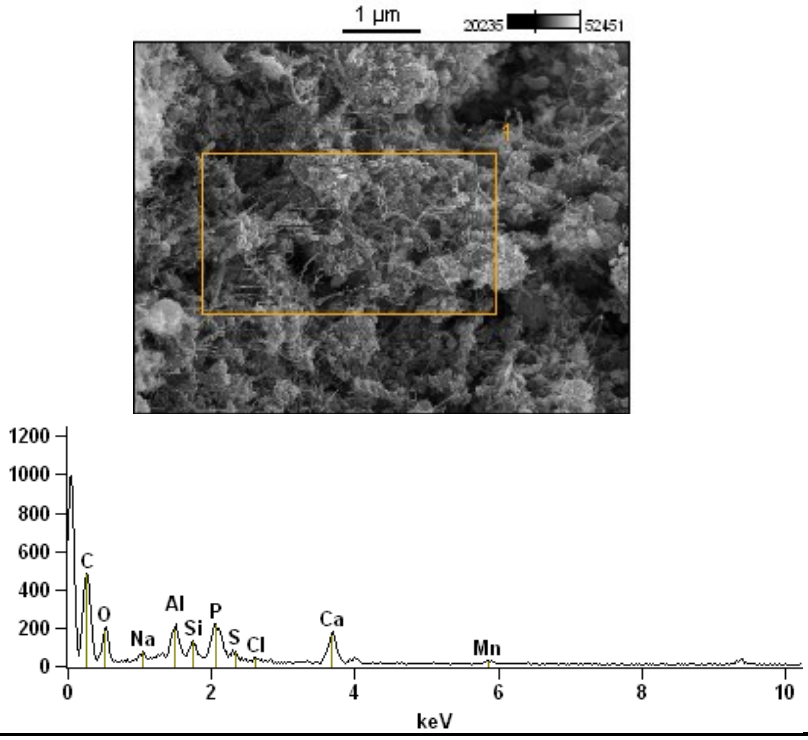

Weight %									
C	O	Na	Al	Si	P	S	Cl	Ca	Mn
58.12 ± 1.17	18.77 ± 0.59	1.58 ± 0.12	3.45 ± 0.19	1.91 ± 0.11	4.84 ± 0.29	0.04 ± 0.13	0.55 ± 0.10	7.93 ± 0.36	2.80 ± 0.54

Figure 3-5: SEM image, EDS spectra and elemental composition of the secondary region of the GAC5 surface. The area from which the spectrum was collected is denoted by the orange rectangle.

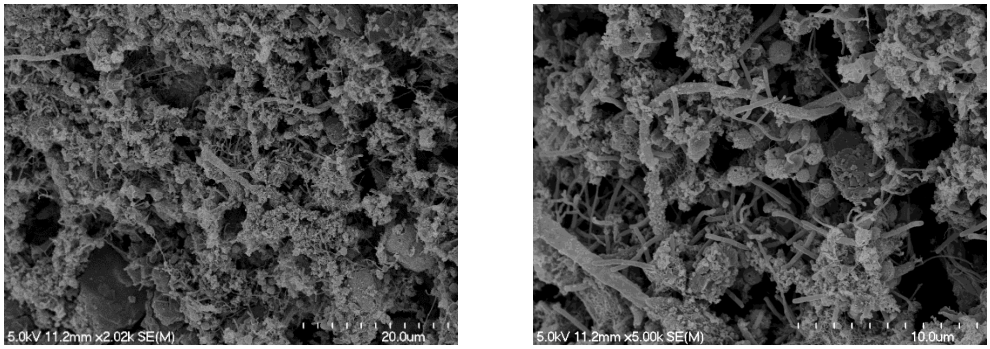

Figure 3-6: SEM image of the secondary region of the GAC5 surface showing dense bacterial colonisation with some areas of the exposed carbon surface

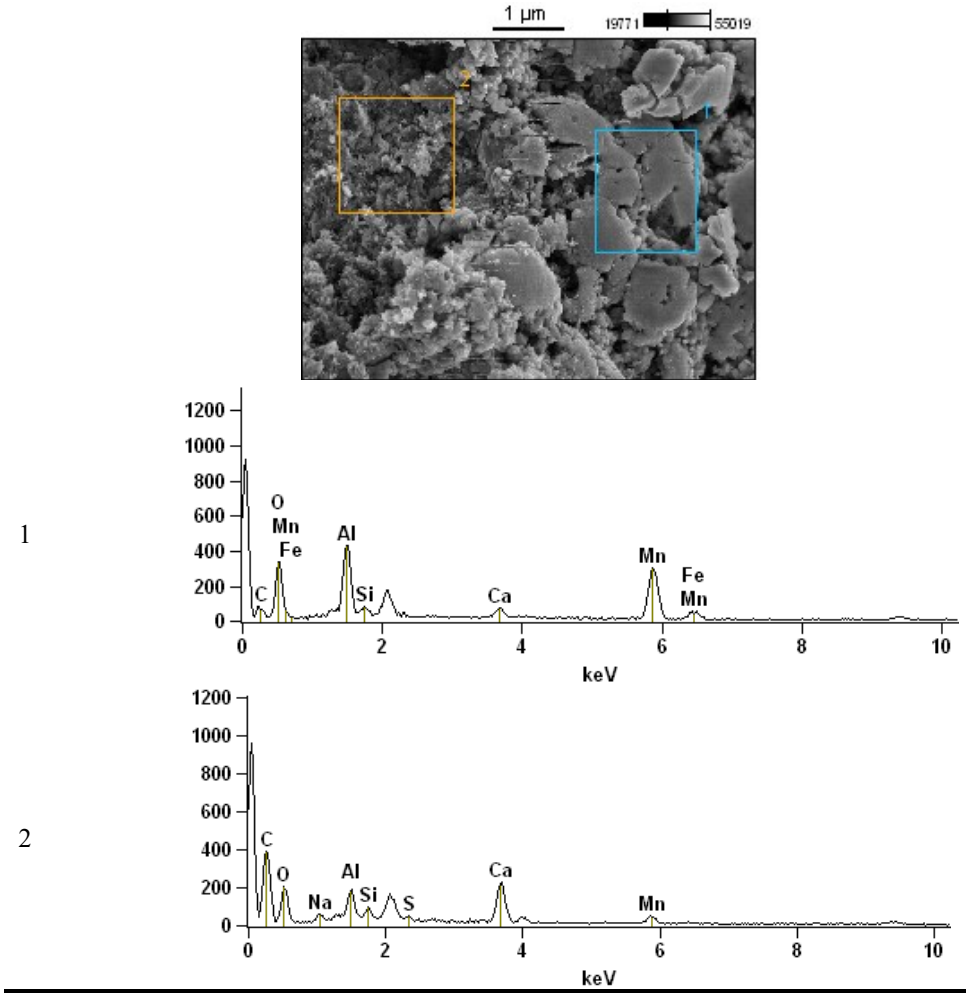

	Weight %									
Area	C	O	Na	Al	Si	S	Ca	Mn	Fe	Se
1	13.09 ± 1.06	21.65 ± 0.55	-	13.69 ± 0.36	2.92 ± 0.32	-	3.01 ± 0.31	41.46 ± 1.12	0.77 ± 0.45	3.40 ± 3.19
2	47.39 ± 1.12	26.36 ± 1.08	1.38 ± 0.25	3.68 ± 0.14	2.42 ± 0.26	0.20 ± 0.13	13.49 ± 0.48	5.10 ± 0.40	-	-

Figure 3-7: Comparison between regions 1 and 2 of the GAC5 surface. Numbered rectangles indicate areas where each spectrum was collected.

Overall, the presence of bacterial colonies appeared to be minimal on the GAC5 media, with the bulk of the surface exhibiting a mineralised coating. However, it is unclear whether bacteria was present beneath the mineralised layer, and the regions where the carbon surface and bacterial colonies are visible are where the mineralised layer had been dislodged as has been suggested elsewhere ***[191]***. It is possible that manganese oxide and hydroxide deposits are being formed by the bacteria themselves via the oxidation of soluble Mn(II) to insoluble Mn(III/IV) oxides ***[192,193]***.

Bacteria known to oxidise Mn(II) from phyla such as *Acidobacteria*, *Bacteroidetes*, *Nitrospira* and *Proteobacteria* ***[193,194]*** have also been found in GAC filters used for drinking water treatment ***[191,195-199]*** (**Table 3-2**). In fact, SEM images and EDS spectra described by White *et.al.* ***[191]*** indicated the presence of an inorganic layer devoid of bacteria comprising of C, O, S, Cl, Fe, Ca, As, Mn, and P coating the GAC particles. Much like the images presented here, areas where this layer was absent showed the presence of bacterial colonies, and some of the bacterial phyla found to be present, for example *Nitrospirae,* are capable of Mn(II) oxidation. While it was claimed that the inorganic layer was deposited via abiotic processes, the presence of Mn and O along with bacteria capable of Mn(II) oxidation means that biogenic Mn(III/IV) oxide deposition cannot be ruled out. Furthermore, attempts to assess the contribution of biodegradation and adsorption in the removal of organic compounds by BAC filters by stalling the biofilm with sodium azide or similar compounds ***[9,44,45,199]*** may be confounded by the adsorption capacity

and redox properties of Mn (III/IV) oxides if they are present on the BAC media under study.

Table 3-2: Phyla and genera known to contain Mn(II) oxidising species of bacteria *[193,194]* that have been found in BAC filters.

Phylum	Genus	Reference
Bacteroidetes		***[196,198,200,201]***
Chloroflexi		***[198]***
Nitrospirae	Nitrospira	***[191,202-205]***
Acidobacteria		***[198,206]***
Cyanobacteria		***[201]***
Actinobacteria		***[196,201]***
Firmicutes		***[196,201]***
Spirochaetes		***[198]***
Proteobacteria		***[195-198,200,201,203,206-210]***
Proteobacteria	Pseudomonas	***[196]***
Proteobacteria	Nitrosomonas	***[191,202]***

The results for GAC6 that had recently undergone partial media replacement provided an interesting case due to the presence of old carbon media similar to GAC5, and new media that had been in service for only a short time (**Figure 3-8**).

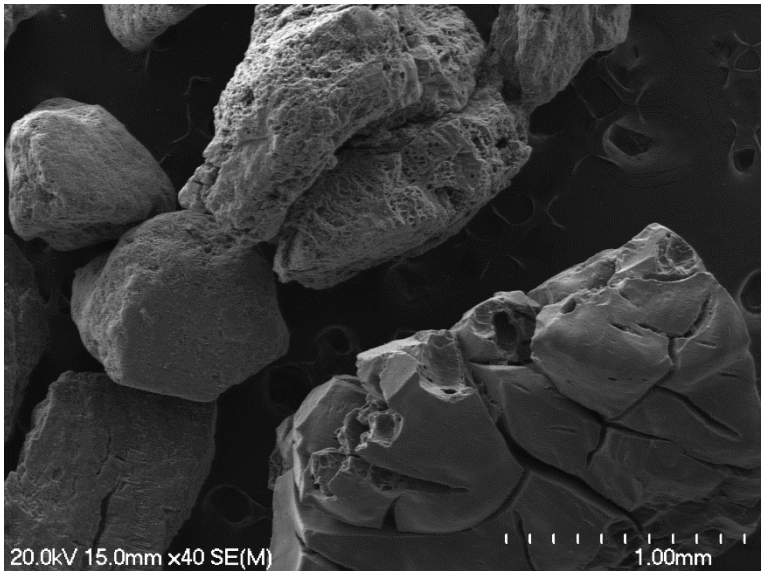

Figure 3-8: SEM image of the GAC6 media illustrating the presence of different particle types due to partial media replacement.

Similar to GAC5, some of the particles exhibited an inorganic layer high in O, Al and Si as well as regions of biological growth, indicating the presence of older GAC grains (**Figure 3-9**; **Figure 3-10**). All of the particles exhibited biological growth to some extent, indicating that bacteria colonise the recently added media quite quickly. However, as with GAC5, the extent of biological growth was sporadic and did not seem to cover the entire surface of the grains. Some particles produced EDS spectra that were similar to GA1000N, with mainly C being present in the spectra, consistent with the presence of recently added GAC media (**Figure 3-11**).

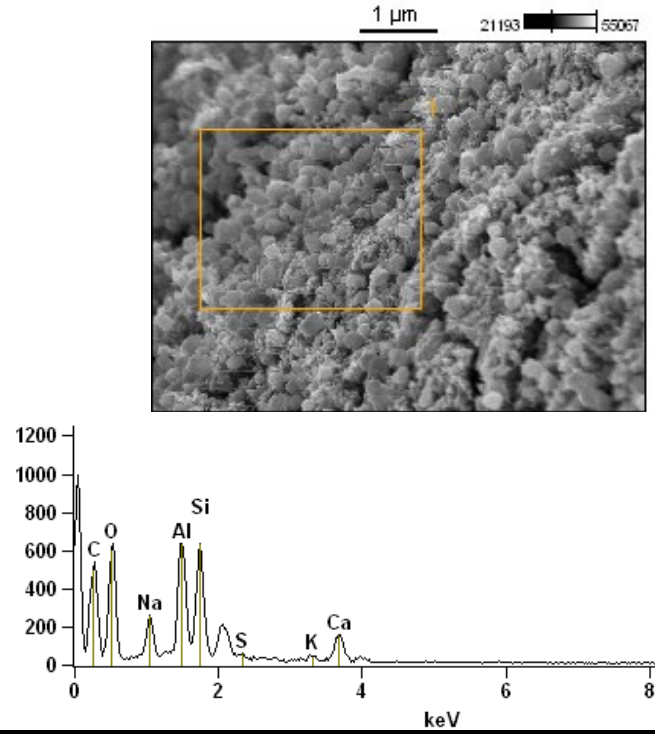

Weight %							
C	O	Na	Al	Si	S	K	Ca
42.53 ± 0.89	31.95 ± 0.59	4.21 ± 0.16	7.69 ± 0.16	9.08 ± 0.20	0.11 ± 0.07	0.54 ± 0.06	3.89 ± 0.20

Figure 3-9: SEM image, EDS spectra and elemental composition of GAC6 media exhibiting a similar composition to GAC5 media, indicating the presence of an older GAC grain. The area from which the spectrum was collected is denoted by the orange rectangle.

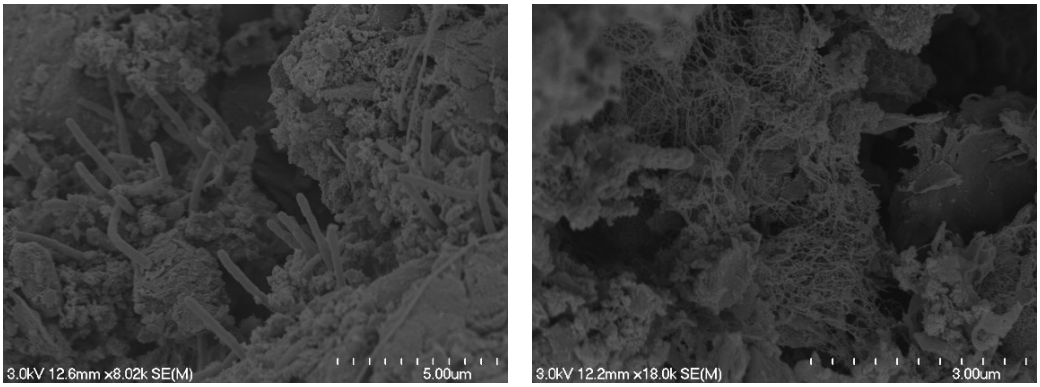

Figure 3-10: Biological growth on the GAC6 media surface.

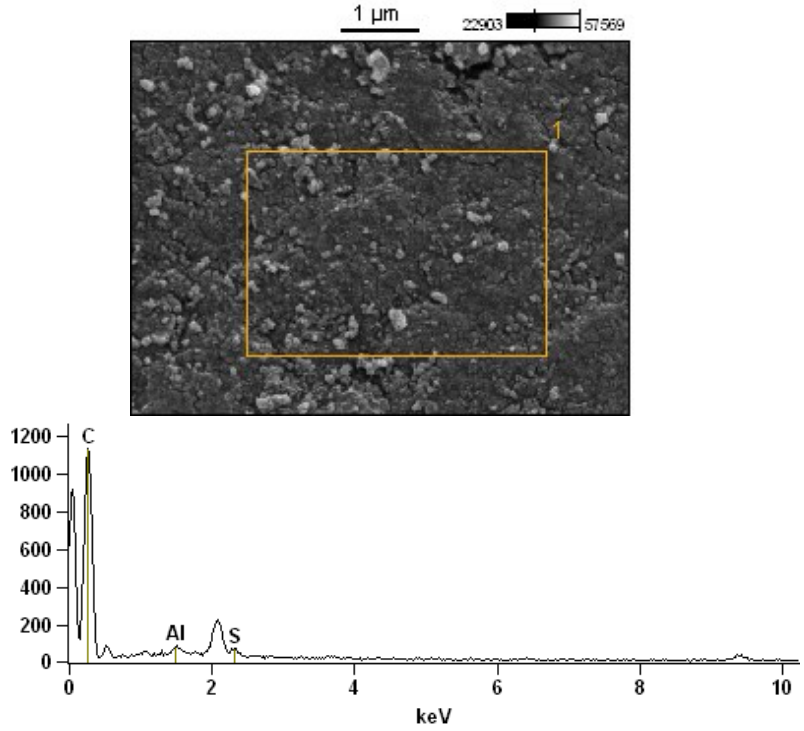

Weight %		
C	Al	S
98.02 ± 1.04	1.01 ± 0.11	0.97 ± 0.17

Figure 3-11: SEM image and EDS data of a GAC6 surface exhibiting a high proportion of C similar to GA1000N, indicating the prescence of new GAC grains. The area from which the spectrum was collected is denoted by the orange rectangle.

Some particles exhibited features not present on either the GA1000N samples or the GAC5 samples, most apparent was the presence of small, roughly cubic particles coating large areas of the GAC surface (**Figure 3-12**). Closer examination of these particles using EDS revealed they were high in O, Al and Si, indicating the

possible presence of silicate minerals (**Figure 3-13**). The difference in composition was also apparent using backscattered-electron (BSE) imaging (**Figure 3-14**). The shape of the particles and the EDS spectra suggest the particles may be the result of small particles of sand from the sand filters being passed through to the GAC filters, which are situated directly after the sand filters in the treatment train.

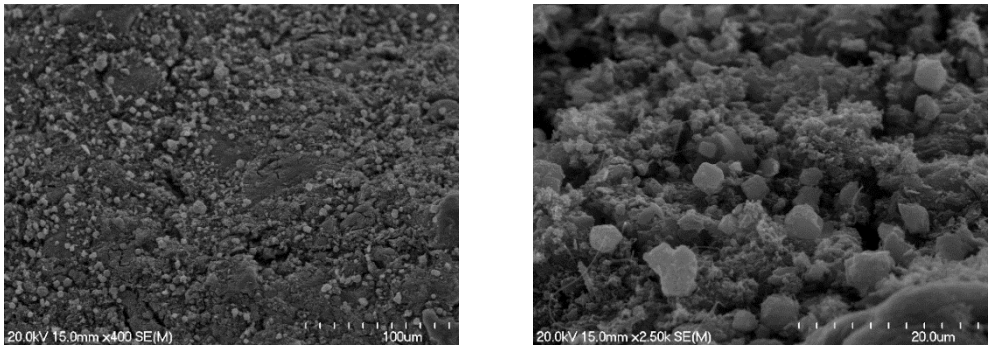

Figure 3-12: SEM image of GAC6 media coated in small, roughly cubic particles.

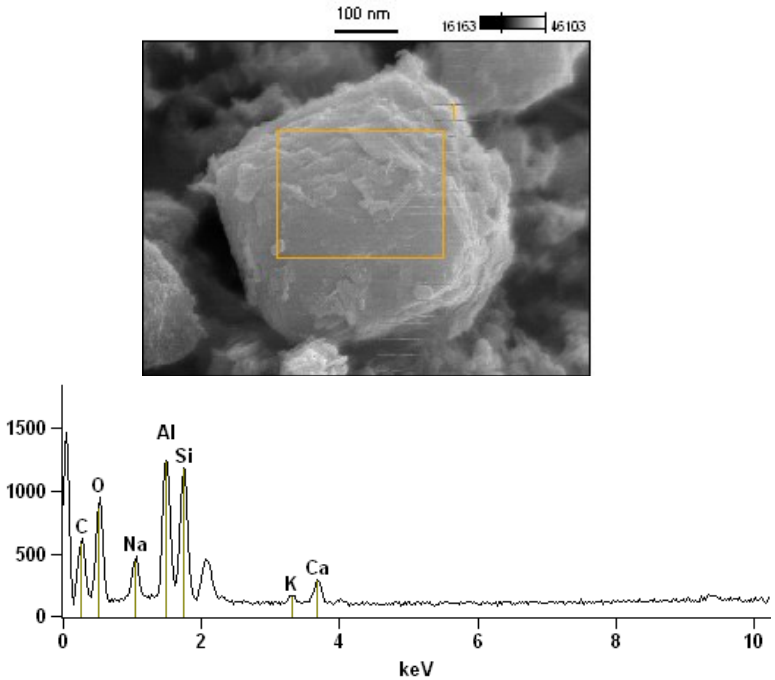

Weight %						
C	O	Na	Al	Si	K	Ca
38.26 ± 0.88	29.83 ± 0.53	4.75 ± 0.16	10.31 ± 0.18	12.42 ± 0.22	0.95 ± 0.08	3.49 ± 0.22

Figure 3-13: SEM image and EDS data of a particle on the GAC6 surface. The area from which the spectrum was collected is denoted by the orange rectangle.

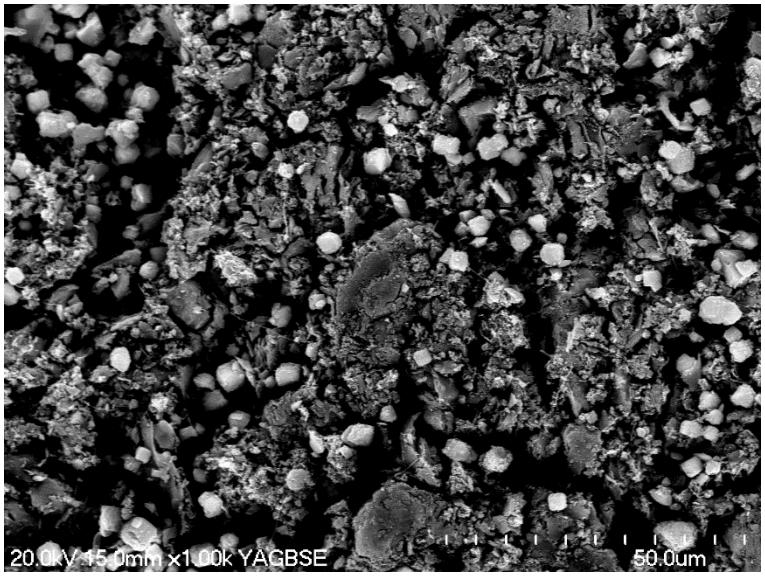

Figure 3-14: BSE image of particles present on the GAC6 surface.

Results from the pilot column showed that the surface was predominantly C, with small areas where bacteria had begun to colonise the surface (**Figure 3-15**). EDS indicated that while the surface composition of some areas was similar to GA1000N vGAC (**Figure 3-16**), other areas showed a change in surface composition, predominantly as a reduction in the relative proportion of C and an increase in O and other elements (**Figure 3-17**).

The presence of bacterial colonies after only a short period of operation (≈ 3 months) showed that bacterial colonisation is established quite soon after the filter media is commissioned, although at the time of sampling bacterial colonies were still very sparse in comparison to the full-scale filters.

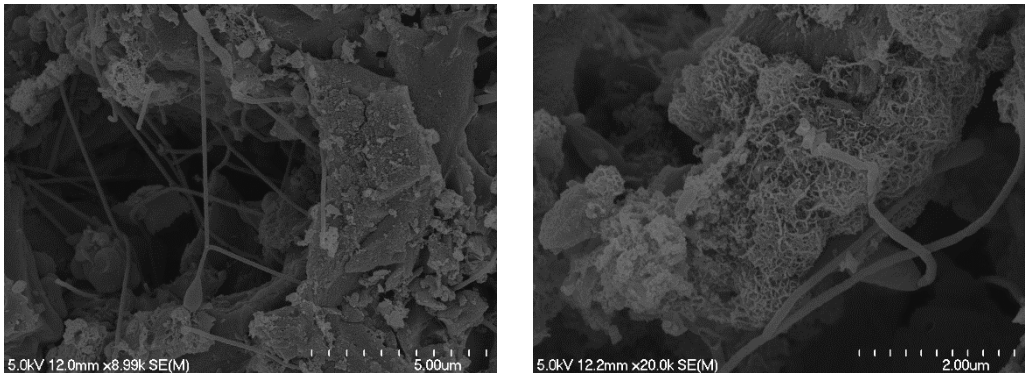

Figure 3-15: Bacterial growth on the pilot column media.

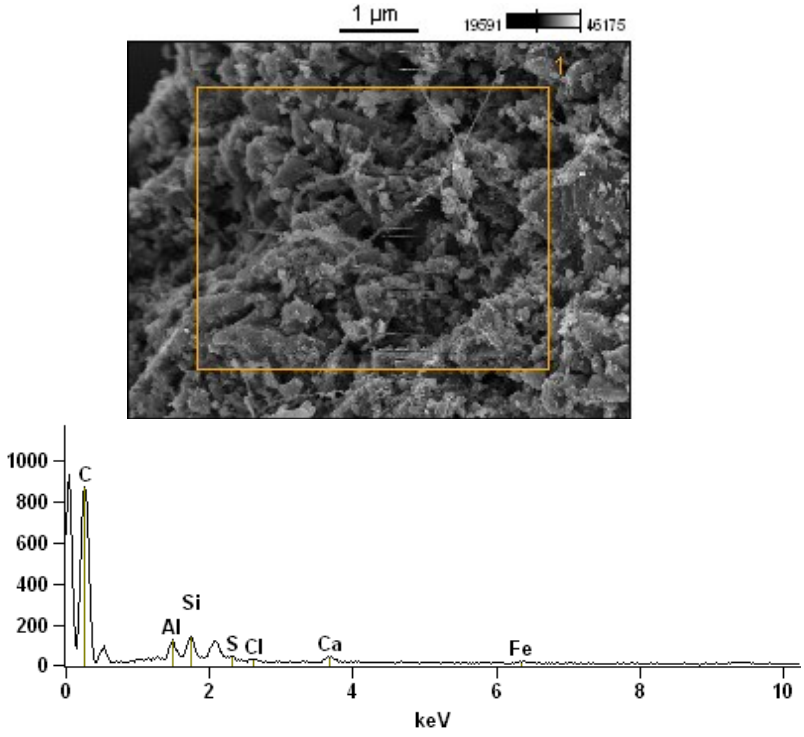

Weight %						
C	Al	Si	S	Cl	Ca	Fe
90.13 ± 1.07	2.00 ± 0.10	3.71 ± 0.22	0.45 ± 0.11	0.48 ± 0.10	1.75 ± 0.27	1.47 ± 0.29

Figure 3-16: A region of the pilot column media exhibiting a high proportion of C. The area from which the spectrum was collected is denoted by the orange rectangle.

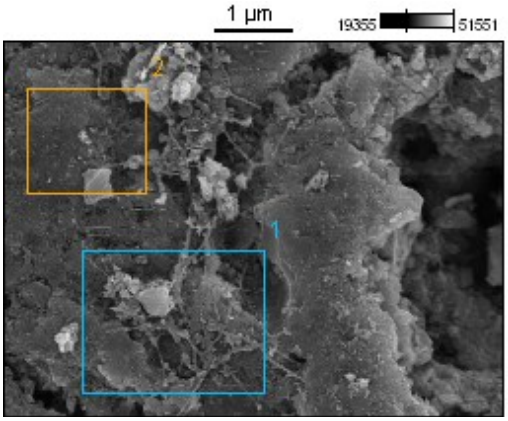

1

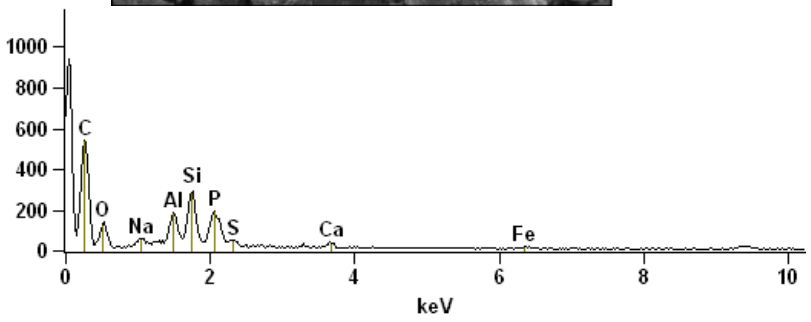

2

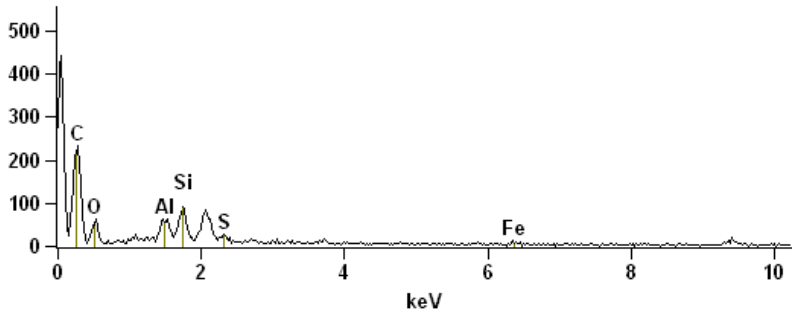

	Weight %								
Area	C	O	Na	Al	Si	P	S	Ca	Fe
1	68.45 ± 1.30	14.21 ± 0.88	1.01 ± 0.11	3.14 ± 0.22	6.46 ± 0.38	4.41 ± 0.12	0.27 ± 0.12	0.82 ± 0.12	1.23 ± 0.29
2	70.77 ± 1.71	16.71 ± 1.31	-	3.36 ± 0.31	6.14 ± 0.41	-	0.63 ± 0.19	-	2.38 ± 0.46

Figure 3-17: Two regions of the pilot media surface exhibiting lower levels of C and higher levels of O and other elements. Numbered rectangles indicate the area where each respective spectrum was collected.

Samples with similar surface compositions to GA1000N are shown in **Figure 3-18**. These samples included GAC grains from GAC6, which were likely to be newer grains added to the filters during partial replacement of the filter media. Some areas of GAC collected from the pilot column (C 1) also had similar surface compositions

to GA1000N, which was not surprising since the media had only been in service for a short time. Of these samples, C made up the bulk of the GAC surface, with minor contributions from other elements, particularly Al and Si.

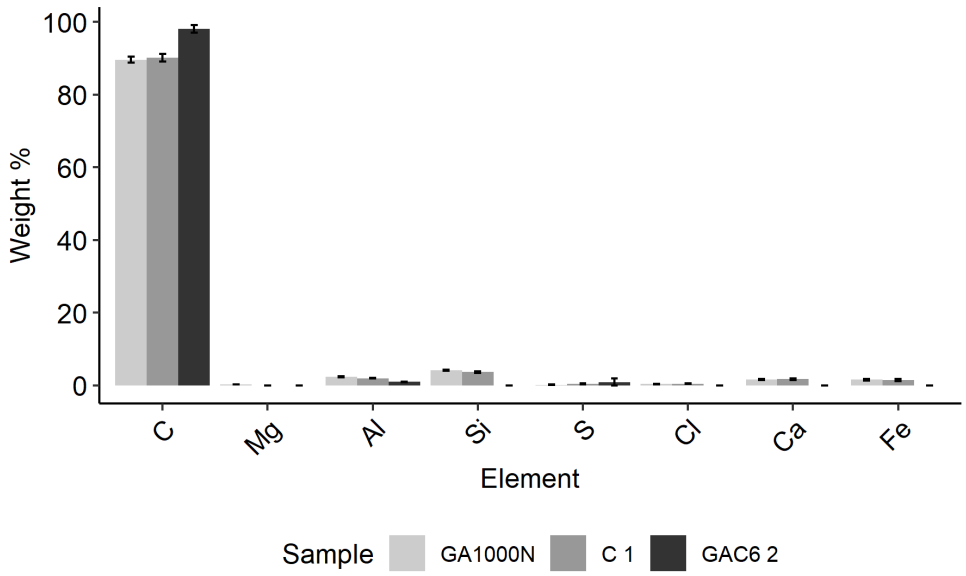

Figure 3-18: EDS results for samples with a similar surface composition to GA1000N. Error bars represent the error associated with the EDS measurement.

Samples with markedly different surface compositions to GA1000N included GAC5, some grains from GAC6 and some areas of grains from the pilot column (C 2) (**Figure 3-19**). The most apparent difference was a lower relative amount of C and a higher relative amount of O, indicating that the GAC surface had become enriched with O containing species, with the GA1000N sample containing no detected O. The other major difference was between GA1000N and the GAC5 samples, which had high levels of Mn that was not apparent in any other samples. As noted earlier, Mn was associated with the seemingly mineralised layer coating the old, original GAC media. Here, sample GAC5-1 relates to the GAC5 surface

covered in the mineralised layer, whereas GAC5-2 represents the areas where the carbon surface was exposed, and bacterial colonies were present.

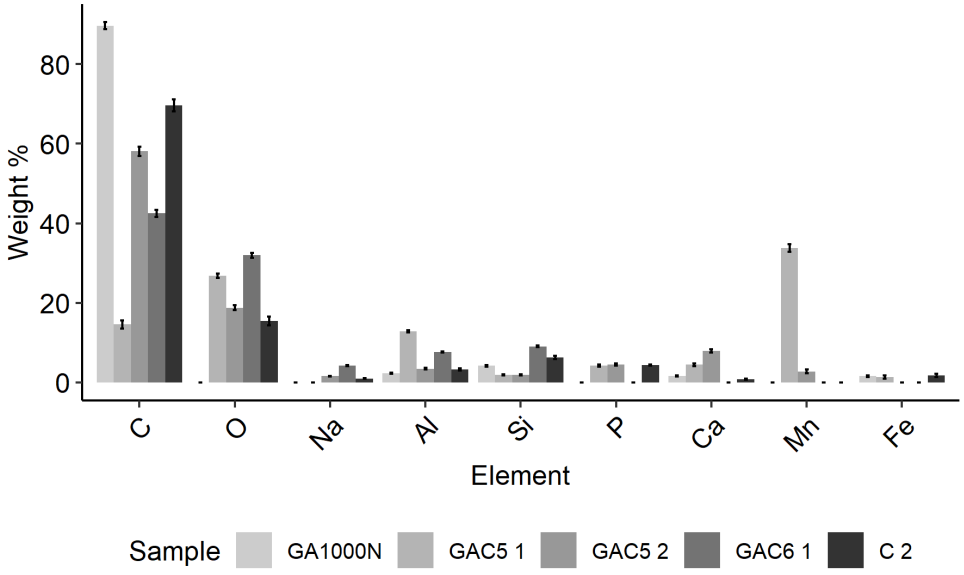

Figure 3-19: EDS results for samples with a different surface composition to GA1000N. Error bars represent the error associated with the EDS measurement.

While these results give some indication as to the changes in surface morphology and composition of the GAC media over time, the EDS results provide only an estimate of the relative amount of each element present on the particle surface. Further, the technique only provides information on the elements present in relatively high abundance and is therefore not suited to trace analysis. Therefore, ICP-MS was carried out in order to obtain more quantitative results on trace metals present in the GAC media.

3.3.2 ICP-MS Analysis of GAC Samples

3.3.2.1 Preliminary screening of GAC media and GA1000N

Overall, the GAC exhibited higher concentrations of nearly all of the elements that were tested for. Exceptions included Fe, Sn, and Cr where the difference was not obviously apparent (**Table 3-3**).

In some cases, the %RSD of the measurements was very high, for example the GA1000N results for Se, Ag and Cd. However, these represented results approaching the lower limit of detection for these elements on the instrument used and as such are generally interpreted as a "zero" result. In the cases where these elements are present in significantly higher concentrations on the GAC samples (e.g. Ag), the %RSD was much lower. In the case of Ag however, there was quite a large discrepancy between the GAC1 and GAC2 samples which casts some doubt over the accuracy of the result. As such, a larger sample set may be required in order to get a better idea of the concentration of Ag in the GAC media, especially considering the well-known anti-microbial properties of Ag ***[211]***.

In general, the results between replicates were in close agreement, indicating that the method produces relatively repeatable results.

Table 3-3: ICP-MS results for preliminary screening samples.

	Sample concentration (μg g^{-1} ± %RSD)*			
Element	GA1000N 1	GA1000N 2	GAC 1	GAC 2
B	5.31 (± 12.8)	5.28 (± 11.6)	10.40 (± 3.5)	12.08 (± 2.3)
Na	630.88 (± 2.2)	662.60 (± 1.9)	952.92 (± 2.8)	874.82 (± 0.6)
Mg	284.03 (± 2.5)	310.44 (± 1.7)	3415.16 (± 1.9)	3794.00 (± 1.5)
Al	3668.59 (± 2.6)	3887.77 (± 3.0)	20383.35 (± 1.4)	21468.56 (± 2.0)
K	225.19 (± 3.3)	235.06 (± 1.1)	662.76 (± 2.6)	639.66 (± 0.4)
Ca	2065.15 (± 1.6)	2009.81 (± 1.7)	36812.58 (± 3.0)	40953.24 (± 3.6)
V	7.98 (± 4.6)	8.75 (± 2.0)	17.66 (± 3.3)	17.96 (± 2.5)
Cr	7.32 (± 6.1)	11.78 (± 7.0)	10.71 (± 5.8)	11.45 (± 6.5)
Fe	1607.30 (± 2.8)	3633.23 (± 1.5)	1255.12 (± 3.8)	1424.25 (± 3.3)
Mn	20.31 (± 2.9)	24.31 (± 3.0)	12818.61 (± 3.0)	12802.18 (± 2.1)
Co	2.15 (± 6.1)	2.89 (± 1.3)	22.03 (± 1.4)	21.97 (± 3.0)
Ni	7.54 (± 6.0)	8.55 (± 1.9)	27.04 (± 3.4)	27.62 (± 2.8)
Cu	15.41 (± 3.4)	17.94 (± 2.7)	153.55 (± 2.4)	168.09 (± 2.9)
Zn	26.69 (± 12.3)	28.32 (± 4.1)	404.26 (± 2.1)	403.44 (± 3.1)
As	0.90 (± 7.2)	0.64 (± 29.0)	30.06 (± 1.5)	29.36 (± 1.7)
Se	-0.42 (± 105.4)	-0.52 (± 93.6)	2.44 (± 30.0)	2.86 (± 48.5)
Sr	84.49 (± 1.9)	82.20 (± 1.3)	298.43 (± 0.9)	341.08 (± 3.5)
Mo	0.31 (± 3.4)	0.30 (± 5.0)	2.98 (± 0.7)	3.39 (± 3.7)
Ag	0.03 (± 47.7)	0.02 (± 99.0)	4.67 (± 6.2)	0.76 (± 5.3)
Cd	0.14 (± 16.9)	0.04 (± 27.4)	0.87 (± 11.4)	0.90 (± 10.6)
Sn	0.31 (± 8.5)	0.35 (± 6.1)	0.55 (± 6.7)	0.09 (± 10.3)
Sb	0.07 (± 20.3)	0.06 (± 16.2)	0.13 (± 11.3)	0.15 (± 9.8)
Ba	183.78 (± 3.3)	191.94 (± 2.3)	1085.81 (± 3.9)	1259.60 (± 5.8)
Tl	0.00 (± 23.1)	0.01 (± 9.7)	6.09 (± 6.5)	7.42 (± 5.2)
Pb	1.48 (± 4.4)	2.32 (± 5.0)	6.42 (± 1.8)	6.56 (± 2.2)
U	0.58 (± 28.0)	0.70 (± 19.3)	7.66 (± 9.9)	9.32 (± 4.5)

* Error expressed as the percent relative standard deviation (%RSD) based on a triplicate analysis.

Results of samples analysed during preliminary screening are represented graphically below (**Figure 3-20**, **Figure 3-21**, **Figure 3-22**, **Figure 3-23**), illustrating that issues of repeatability were most prevalent for elements present at very low concentrations.

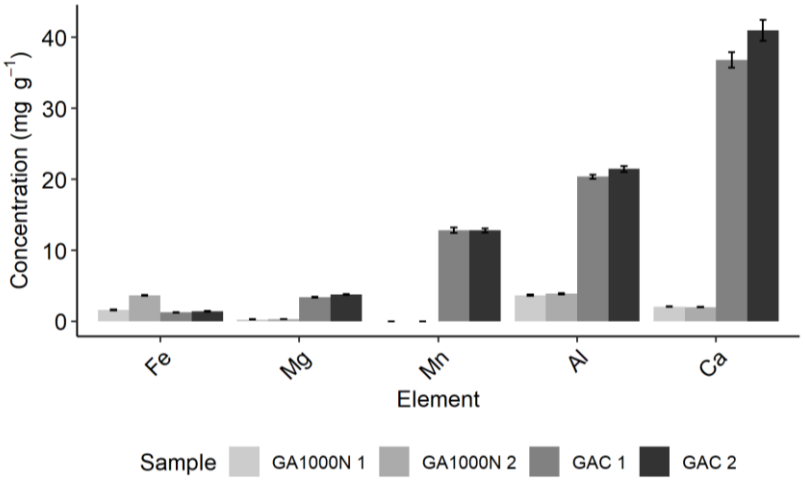

Figure 3-20: Preliminary ICP-MS results for Fe, Mg, Mn, Al and Ca. Error bars indicate the standard deviation.

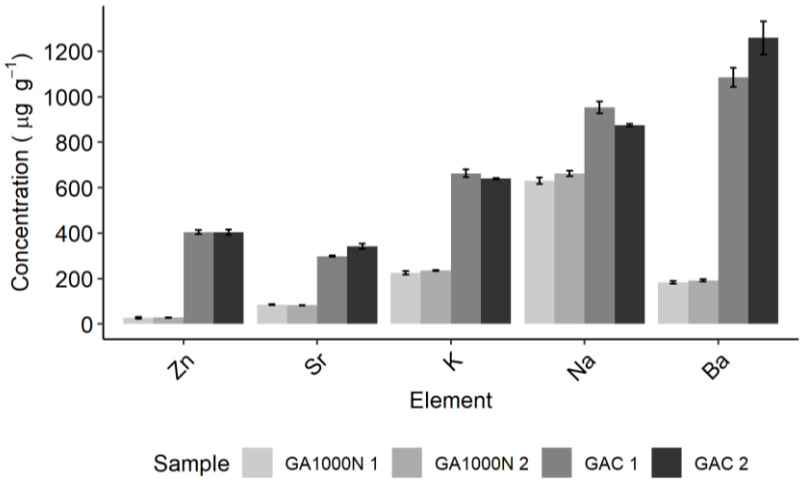

Figure 3-21: Preliminary ICP-MS results for Zn, Sr, K, Na and Ba. Error bars indicate the standard deviation.

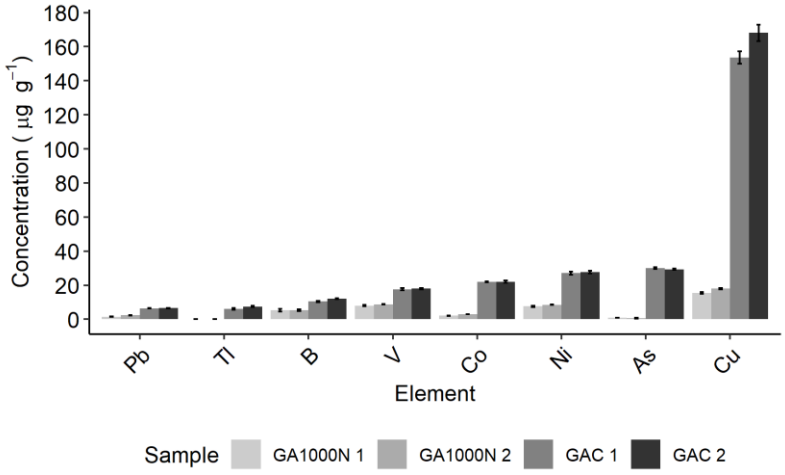

Figure 3-22: Preliminary ICP-MS results for Pb, Tl, B, V, Co, Ni, As and Cu. Error bars indicate the standard deviation.

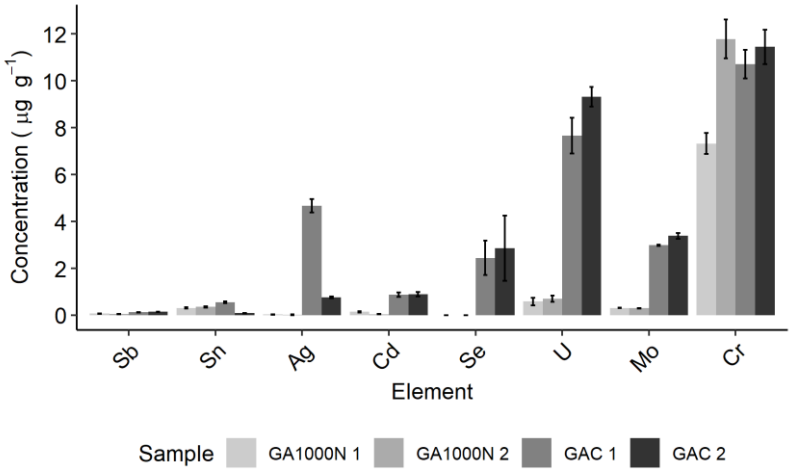

Figure 3-23: Preliminary ICP-MS results for Sb, Sn, Ag, Cd, Se, U, Mo and Cr. Error bars indicate the standard deviation.

Of particular interest was the clear and large increase of As on the GAC samples relative to vGAC. While this is somewhat expected due to the composition of the source water, this may have inhibitory effects on the potential to form, or maintain, a viable biofilm on the filter media. The level of arsenic present on the GAC (≈ 25 µg g^{-1}; ≈ 25 ppm) shows that the GAC is accumulating arsenic to levels significantly in excess of the influent water (≈ 0.022 g m^{-3}; ≈ 0.022 ppm ***[212-214]***). While this is to be expected due to the adsorptive nature of GAC systems, this does represent an increase in concentration of approximately 3 orders of magnitude which may be significant with respect to microbial growth. The accumulation of other metals that are known to be toxic to bacteria at high concentrations, for example Zn, Ba, Ni, Cu, Co and Tl ***[215-220]***, indicates further potential for the inhibition of microbial growth and metabolism.

Some elements were present in quite high concentrations on the used GAC media, notably Mn, Al and Ca, with combined concentration of these accounting for approximately 7 % of the carbon sample by mass. These elements were also

prevalent in EDS spectra as discussed previously and were enriched significantly on the GAC surface relative to GA1000N. The presence of high levels of Al is likely due to the use of $Al_2(SO_4)_3$ as a flocculant, where residual flocculant is adsorbed on the GAC surface over time. Similarly for Ca, where fairly high concentrations of dissolved Ca are present in the source water (≈ 6 – 12 mg L^{-1}) ***[213,214]***.

The high concentration of Mn is not as easily explained, as the concentration of Mn in the source water is generally quite low (≈ 7 – 30 µg L^{-1}) ***[213,214]***, and $KMnO_4$ is not used as part of the treatment process. As noted in the SEM and EDS results, the high concentration of Mn on the GAC media may be a result of Mn oxidising bacteria depositing Mn(III/IV) oxides and hydroxides.

Looking at the enrichment factor for each element, it becomes clear that the majority of the elements tested for were found in higher concentrations on the GAC media relative to GA1000N (**Figure 3-24**). Exceptions included Cr and Sn which were present at similar levels in both the GAC filter media and GA1000N and Fe which was present in higher levels in GA1000N relative to the filter media. The enrichment factor (EF) was defined as in **Equation 3-1.**

$$EF = \frac{C_i}{C_o} \tag{3-1}$$

Where: $C_i =$ GAC element concentration
$C_o =$ GA1000N element concentration

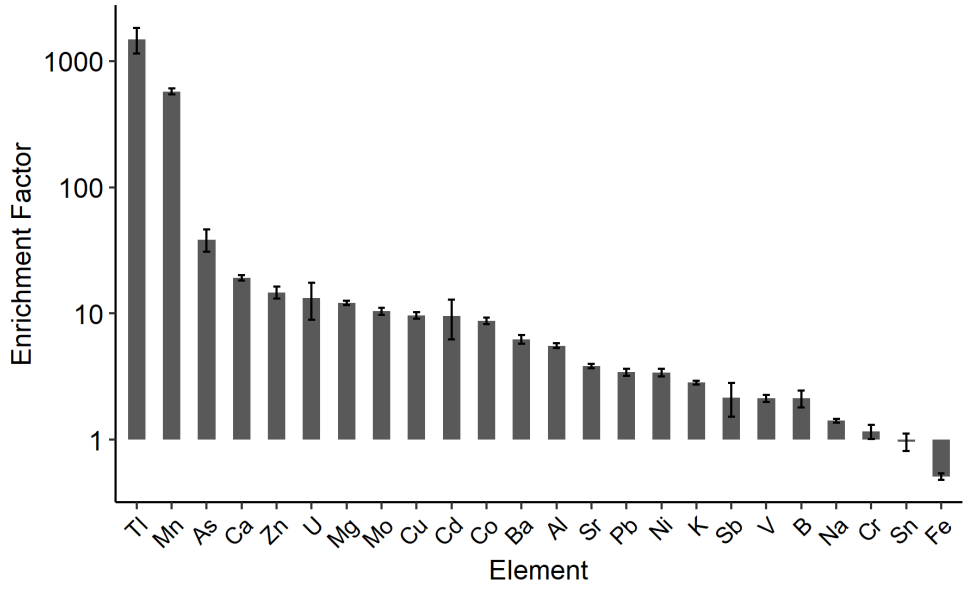

Figure 3-24: Enrichment factors for each element on the GAC media relative to GA1000N. Results are plotted on a $\log_{10}$ axis to account for the wide range in enrichment factors.

Thallium was enriched to the greatest extent, largely due to the very low level (0.0045 µg g^{-1}) present in the original media, with the level present in the used GAC media also being low at approximately 7 µg g^{-1}, far below toxic levels (LD_{50} = 10 – 15 mg kg^{-1}) ***[221]***. The increase in Ag concentration was highly variable, similar to the results for Ag as discussed earlier and is likely to be an erroneous result and was excluded from the dataset. Selenium was not detected in the GA1000N sample so was enriched to an infinite extent and is also not included here. Mn was enriched on the GAC media considerably (≈ 500 fold), and the concentration of Mn on the GAC media was high relative to most other elements.

Elements of concern, mainly with regard to disposal or other uses following use as a filter media, include As, Ba, Cd, Cr, Cu, Pb, Ni, Se, V and Zn, which have Environmental Guideline Values (EGVs) associated with them regarding soil contamination ***[222]***. Of these, As, Ba, Cu, Se, Tl and Zn were present at

concentrations above their respective EGVs. As such, disposal of the used GAC media should take this into account to ensure an appropriate level of dilution is reached, with consideration towards the background levels of these elements present at the disposal site. However, as these were only preliminary results, this should only be considered at estimate.

Table 3-4: Comparison of elements with associated EGVs to their respective concentrations on the GAC media *[222]*.

Element	EGV (mg kg^{-1})	GAC (mg kg^{-1} ± SD)
As	12	29.7 (± 0.5)
Ba	750	1172.7 (± 56.9)
Cd	1.4	0.9 (± 0.1)
Cr	64	11.1 (± 0.7)
Cu	63	160.8 (± 4.3)
Pb	70	6.5 (± 0.1)
Ni	50	27.3 (± 0.8)
Se	1	2.7 (± 0.4)
Tl	1	6.8 (± 0.4)
V	130	17.8 (± 0.5)
Zn	200	403.9 (± 10.5)

3.3.2.2 ICP-MS of individual GAC filters

High concentrations of Ca, Al, Mn and Mg were found to be present on the old GAC media (GAC 2, 3 4 and 5; **Figure 3-25**), accounting for 10.7 ± 1.4 % of the GAC media by weight and 92.0 ± 1 % of the total elements tested for. These elements were also found in high concentration in GAC 6, accounting for 6.3 ± 0.1 % of the GAC media by weight (80 ± 1% total elements). It is likely that the majority of these elements are associated with the old media still present in the filter. Indeed, as the filters were replenished with approximately 50 % new media

during media replacement, the change in total amount of the major elements found on the filter media is close to what would be expected.

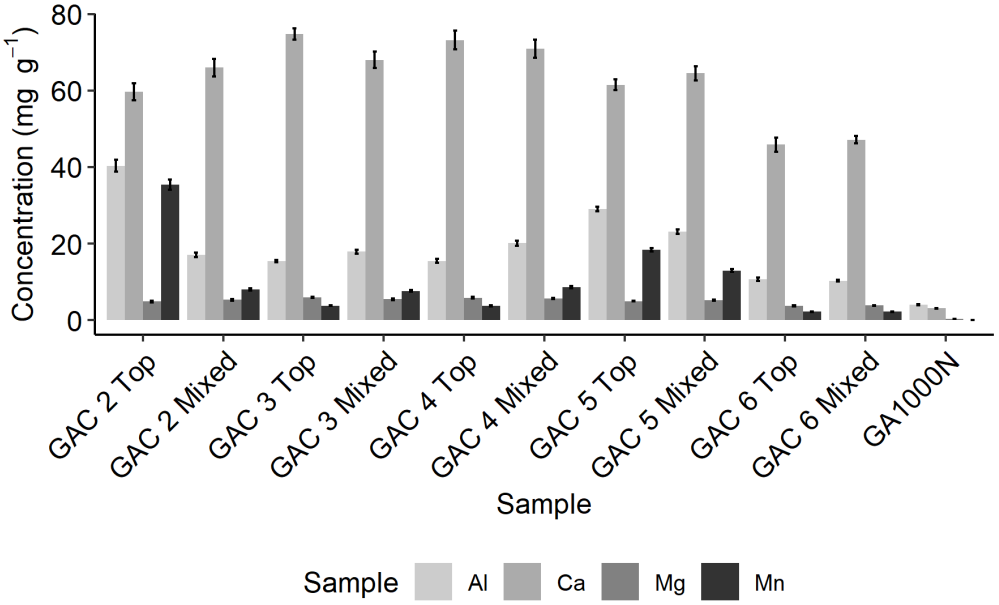

Figure 3-25: ICP-MS results for Al, Ca, Mg and Mn for individual GAC filters. Error bars indicate the standard deviation.

In general, the old GAC filter media exhibit higher concentrations of all elements that were tested for. However, there were some exceptions, with the most prominent being B, S, Fe and Sn. For all of these elements, a similar trend was noted, with much higher levels of each being found in the GAC 6 samples than in either GAC 5 or GA1000N (**Figure 3-26**; **Figure 3-27**; **Figure 3-28**; **Figure 3-29**). In the case of Fe, both the older GAC filters and GA1000N exhibited similar concentrations. For Sn, GA1000N had higher levels than the old GAC media, and the concentration of Sn was also quite high on GA1000N relative to the GAC 6 media.

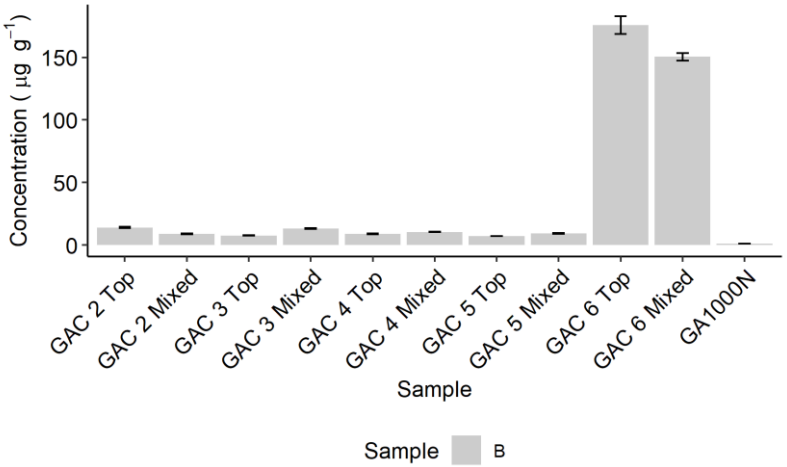

Figure 3-26: ICP-MS results for B from individual GAC filters. Error bars indicate the standard deviation.

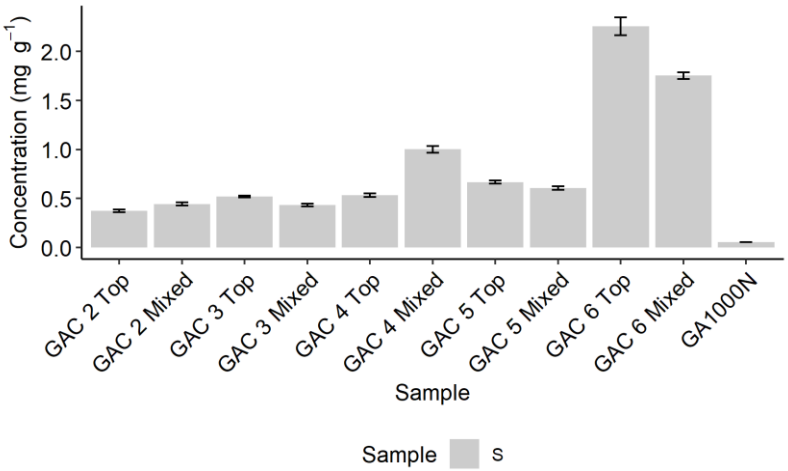

Figure 3-27: ICP-MS results for S from individual GAC filters. Error bars indicate the standard deviation.

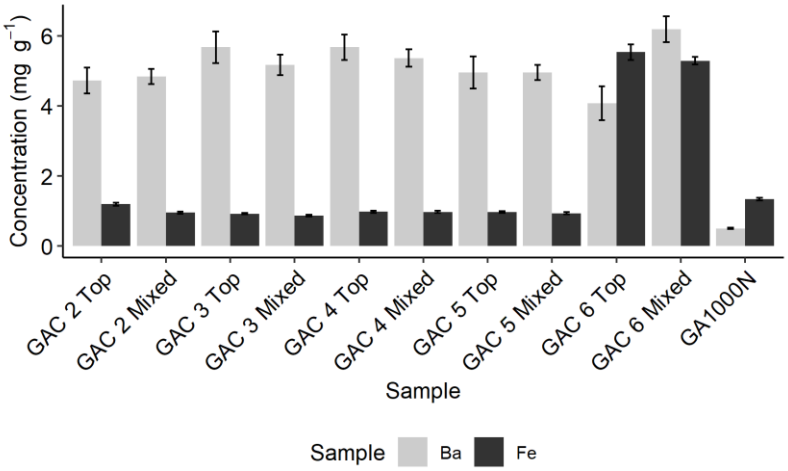

Figure 3-28: ICP-MS results for Ba and Fe from individual GAC filters. Error bars indicate the standard deviation.

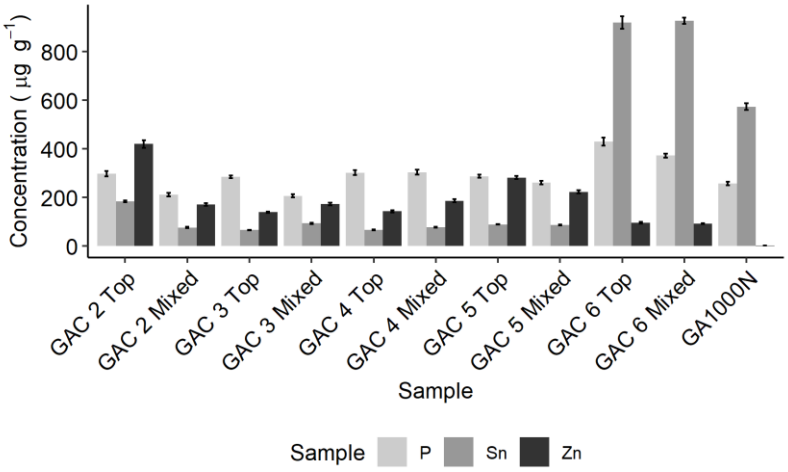

Figure 3-29: ICP-MS results for P, Sn and Zn from individual GAC filters. Error bars indicate the standard deviation.

As GAC 6 had higher levels of these elements relative to the old GAC media, this suggests that these elements are adsorbed quickly during the early stages of the GAC lifespan, and are slowly displaced by other elements and compounds over time until an equilibrium concentration is reached, similar to the concentrations found on the old GAC media. For instance, the concentration of Ba is similar between GAC 6 and the old GAC media, indicating that Ba reaches an equilibrium concentration soon after the media is commissioned for use, and is enriched significantly relative to GA1000N. Conversely, the concentration of P is similar for all three media types, suggesting that P concentration remains constant over the lifetime of the GAC media. A corollary to this is that the concentration of P on its own may not be useful as an indicator of biological growth in GAC filters.

Results for the remainder of the elements present at low concentrations are displayed in **Figure 3-30** to **Figure 3-34**. Similar trends were noted as with the elements present at high concentrations, with higher concentrations being present on the old GAC media as would be expected.

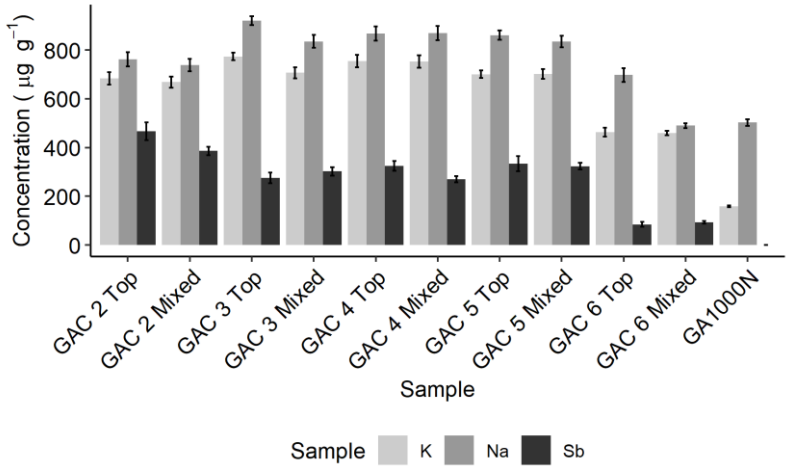

Figure 3-30: ICP-MS results for K, Na and Sb from individual GAC filters. Error bars indicate the standard deviation.

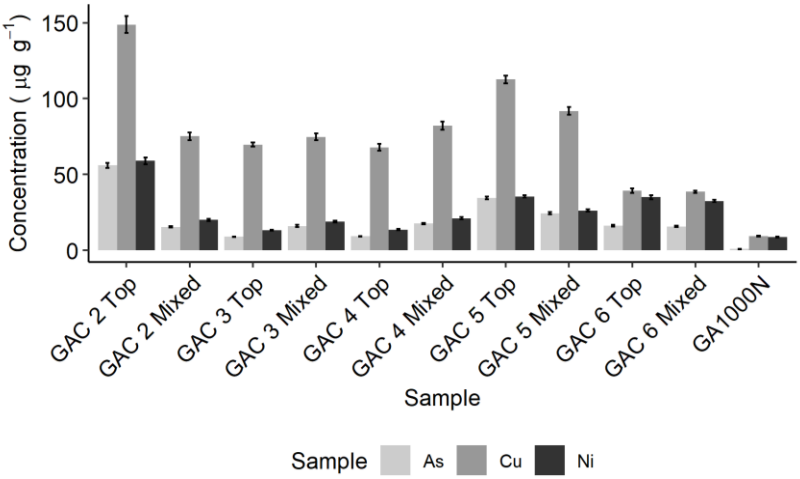

Figure 3-31: ICP-MS results for As, Cu and Ni from individual GAC filters. Error bars indicate the standard deviation.

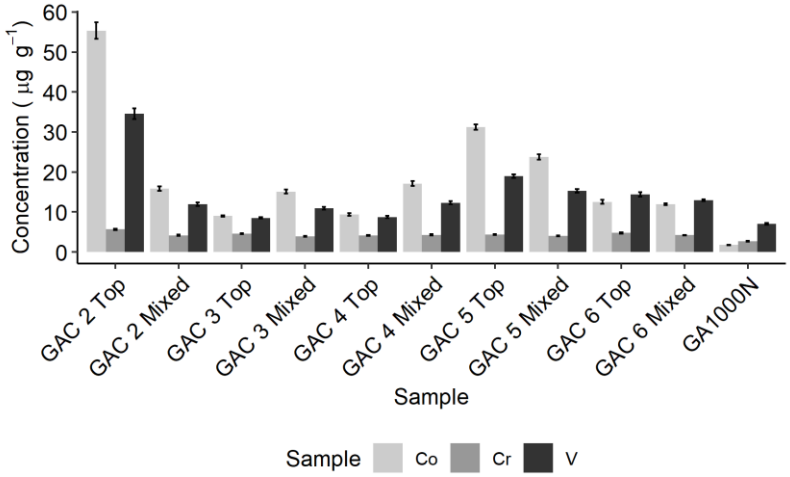

Figure 3-32: ICP-MS results for Co, Cr and V from individual GAC filters. Error bars indicate the standard deviation.

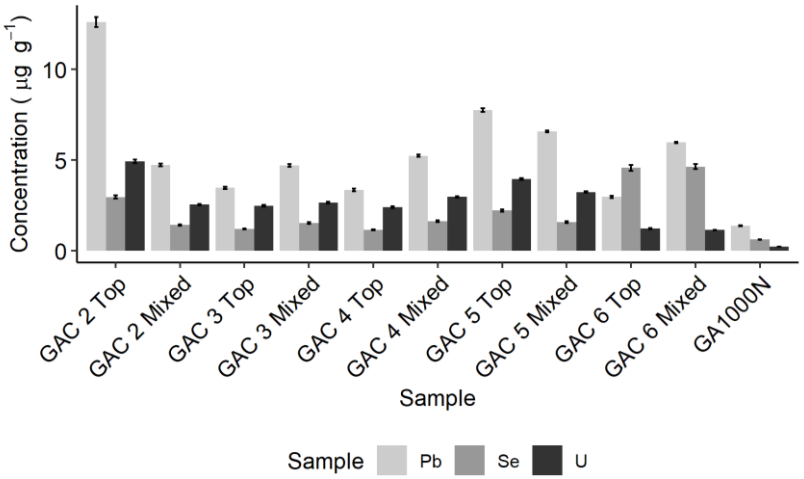

Figure 3-33: ICP-MS results for Pb, Se and U from individual GAC filters. Error bars indicate the standard deviation.

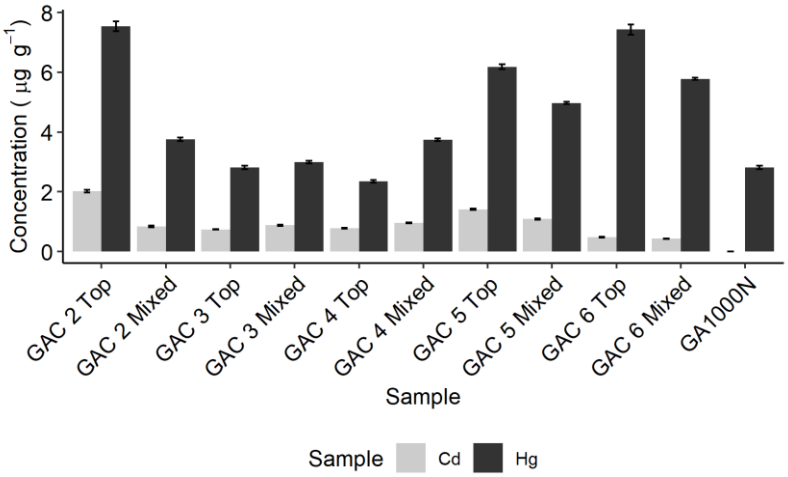

Figure 3-34: ICP-MS results for Cd and Hg from individual GAC filters. Error bars indicate the standard deviation.

Similar to the screening results, the elements enriched to the greatest extent on the old GAC media were Mn, Zn, As, Ca, Mg and U. Thallium was not tested for in this experiment, and the screening results for Ag were confirmed to be erroneous. The enrichment of each element was similar between the old GAC media and the mixed GAC media from GAC 6, with the exceptions being S, B, Ni, Se, Fe and Sn which were enriched to a greater extent on the GAC 6 media relative to the old GAC media. As outlined earlier, these may represent concentrations present on the GAC media prior to equilibrium, steady state concentrations being reached.

As with previous screening experiments, As, Ba, Cu, Se and Zn were present at levels in excess of their associated EGVs. As noted in the preliminary results, this may have implications regarding disposal or alternative uses of the media following its use as a filter medium.

Table 3-5: Mean concentrations of elements on GAC media in comparison to their associated EGVs. GAC concentrations are expressed as the average concentration ± the standard deviation of the pooled result.

Element	EGV (mg kg^{-1})	GAC (mg kg^{-1} ± SD)
As	12	22.8 (± 15.8)
Ba	750	5171.5 (± 368.4)
Cd	1.4	1.1 (± 0.4)
Cr	64	4.4 (± 0.5)
Cu	63	90.4 (± 27.7)
Ni	70	25.9 (± 15.1)
Pb	50	6.1 (± 3.0)
Se	1	1.7 (± 0.6)
V	130	15.2 (± 8.6)
Zn	200	216.9 (± 94.1)

The concentration of some elements was found to vary widely between the four old GAC filters. Of the elements found to be present at high concentrations, wide ranges in Al and Mn were noted, with % RSDs of 39% and 85% respectively (**Table 3-6**; **Figure 3-35**). The reason for the wide range in concentrations was mainly due to the high concentration of these elements in the GAC 2 Top sample. This sample had the highest concentration for 19 of the 26 elements tested for and also had the highest total elements of all the samples. Why this was the case is unclear, as the concentrations of the duplicate analyses were in close agreement for all samples indicating that sample preparation or sampling was not an issue. Further, as larger variations were apparent for only some elements, this may just indicate natural variation in the concentrations present in the GAC filters.

Table 3-6: Mean concentration of elements on used GAC filter media (GAC 2, 3, 4 and 5).

Element	Mean Concentration (µg g^{-1})	% RSD
Ca	67327.7	8.1
Al	22307.7	38.5
Mn	12300.7	85.3
Mg	5396.8	7.4
Ba	5171.5	7.1
Fe	974.4	9.9
Na	836.1	7.2
K	718.0	5.3
S	573.2	34.5
Sb	335.2	19.3
P	269.0	14.7
Zn	216.9	43.4
Sn	92.2	41.7
Cu	90.4	30.7
Ni	25.9	58.3
As	22.8	69.3
Co	22.1	69.2
V	15.2	56.5
B	9.9	25.1
Pb	6.1	50.0
Cr	4.4	12.3
Hg	4.3	42.1
U	3.2	28.0
Mo	3.0	93.4
Se	1.7	35.1
Cd	1.1	39.7

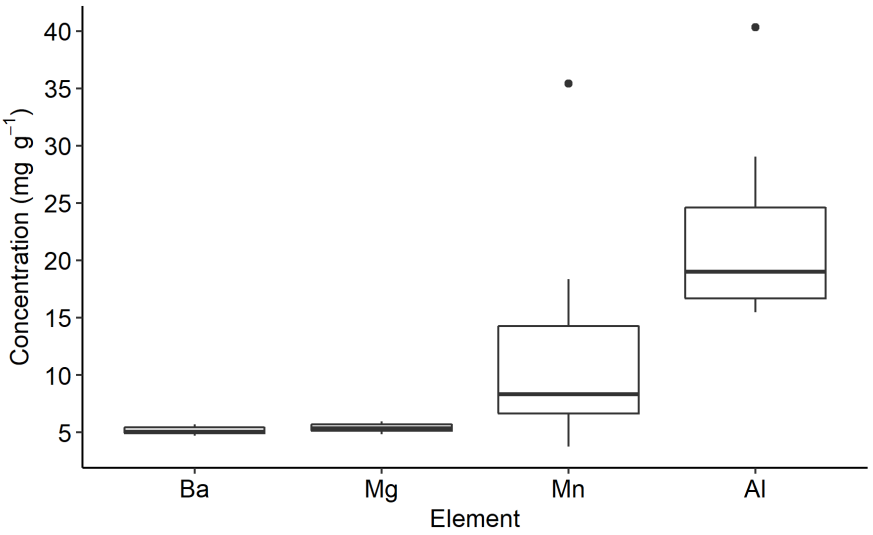

Figure 3-35: Boxplot illustrating the wide spread in results for Al and Mn relative to other elements found at comparable concentrations. The very high concentrations for Mn and Al were both associated with GAC 2 Top.

The mean total elements was found not to differ between samples collected from the surface and those collected from mixed GAC media ($p = 0.383$), indicating that adsorbed metals are distributed somewhat evenly throughout the filter media, and are not preferentially concentrated at the surface. Due to Ca, Al, Mn and Mg making up > 90 % of the total elements present on GAC media, looking at changes in total elements essentially looks at the change in the total concentration of these four elements, as the total is heavily influenced by the concentration of these elements. However, no discernible trend was observed for individual elements, indicating that after such a long time in service, the filter media was at its saturation capacity for all elements.

The possibility that Mn(II) oxidising bacteria may be present in GAC filters raises some interesting questions and possibilities for this technology. For instance, the properties of Mn(IV) oxides provide beneficial properties in the context of water treatment, most notably their sorption and redox capacities. While it has been hypothesized ***[191]*** that mineralised deposits on GAC particles are formed due to abiotic processes, which are sheared off during backwashing and redeposited between backwash cycles, in this case that seems to be an unlikely scenario. Even assuming that all of the Mn present in the source water is transported through to the GAC filters, it would take an estimated 100 to 400 days to accumulate the observed levels of Mn assuming the plant is operating at maximum capacity (106 ML/day) and based on the concentration of Mn in the source water (7 – 30 $\mu g\ L^{-1}$). This is also assuming complete oxidation of soluble Mn(II) to insoluble Mn(IV) oxides. In

practice, as the plant is not usually run at full capacity and the oxidation of Mn(II) to Mn(IV) has quite a high activation energy, the time required to reach the concentrations observed here is likely to be significantly longer assuming abiotic processes only. Further, as any Mn present in the source water as Mn(IV) would be likely to be present as suspended particulates due to the low solubility of Mn(IV) it would be effectively removed during coagulation and flocculation meaning that the amount of Mn reaching the GAC filters would be further reduced, increasing the time it would take to build appreciable concentrations on the GAC. Overall, this suggests that inorganic coatings on GAC particles are not replenished between backwashing cycles and are built up slowly over time and are in fact quite robust and resilient to repeated backwashing.

At low pH and in the absence of oxygen, Mn(II) is the thermodynamically favoured form of Mn in solution, although Mn(II) can exist in natural waters even in the presence of oxygen ***[194]***. Sources of Mn in rivers and streams include weathering processes that supply suspended sediment and leachate from soils and ground waters which supply soluble Mn(II) ***[223]***. Suspended sediments are likely to be removed from the source water during coagulation, flocculation and sand filtration, resulting in the majority of Mn reaching the GAC filters in the form of soluble Mn(II). The water reaching the GAC filters is well oxygenated, and remains so through the filter bed, although it is depleted to some extent (**Figure 3-36**) meaning that O_2 concentration would not be a limiting factor in Mn(II) oxidation and the pH remains relatively constant and close to neutral throughout the plant. The

conversion of Mn(II) to Mn(IV) in natural waters is quite slow, and increased rates of Mn(II) oxidation are associated with biological oxidation ***[192-194,223]***. For example, solutions of Mn(II) in the absence of a catalyst have been shown to be stable for seven years, and the kinetics of Mn(II) oxidation in the presence of a catalysts at environmentally realistic concentrations predict that Mn(II) concentrations remain effectively stable (half-life $= 10^5$ days). In contrast, direct measurement of Mn(II) depletion in natural waters show typical a typical half-life of 1-100 days, and the increased rate of oxidation has been attributed to microbial catalysis ***[223]***. Whether the contact time in the GAC filters is sufficient for abiotic Mn(II) oxidation to occur is unknown, but with bacteria being present on the GAC media, it is likely that Mn(II) oxidation is facilitated via biological processes.

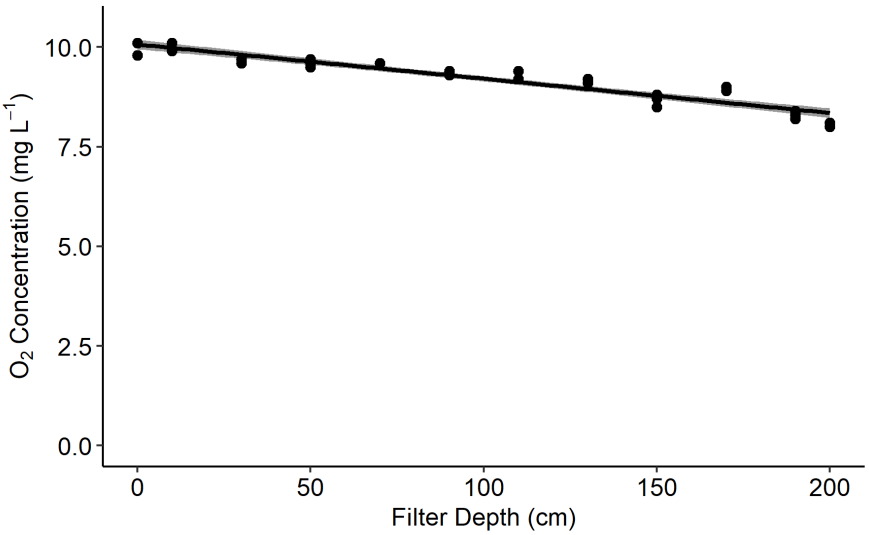

Figure 3-36: Dissolved oxygen concentration through the depth of the pilot column filter media ($T = 11.5\ ^oC$, $R^2 = 0.895$, $p = 2.2E^{-16}$).

Regardless of the mechanism of deposition, the presence of Mn and O on the GAC surface strongly suggests the presence of Mn(III/IV) oxides, which has some interesting implications. Firstly, Mn(III/IV) oxides have good adsorption properties and high surface areas with high negative charges which facilitate cation exchange processes ***[194]***. This allows the adsorption of a wide range of metal cations which can also be incorporated into the crystal lattice allowing Mn(III/IV) oxide to act as a sink for metal cations ***[192,193]***. This includes many of the metals found to be present in the HWTS GAC filters such as Ca, As, Zn and Cu amongst others. Secondly, Mn oxides are relatively strong oxidising agents which are capable of degrading a range of organic compounds including components of natural organic matter (**Figure 3-37**) as well as anthropogenic pollutants ***[194,224]***. Oxidation at the Mn oxide surface can occur via several mechanisms including free radical oxidation, nucleophilic addition and dealkylation and the Mn oxides can facilitate biodegradation by functioning as electron acceptors ***[194]***. Indeed, Mn oxides have found use in water treatment situations ***[225]*** and the removal of Mn(II) has been reported in BAC filters ***[224]*** and other types of biofilters ***[226,227]***, and deposits of Mn(III/IV) oxides on bacteria present in biofilters and biofilms have also been reported ***[227,228]***.

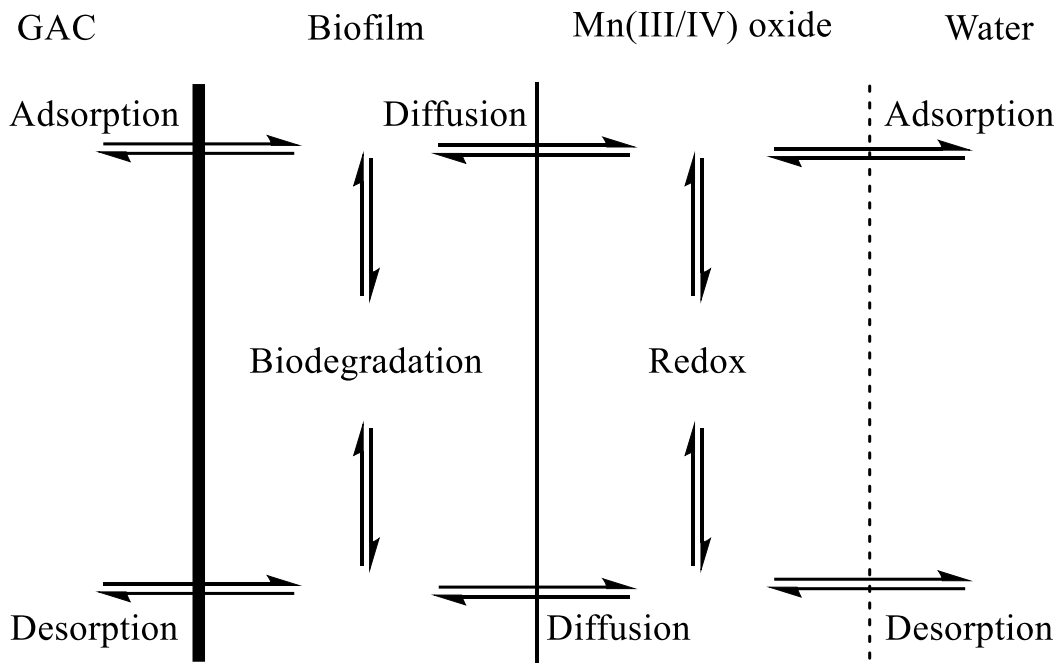

Figure 3-37: Possible scheme for the cycling of organic molecules on GAC media colonised with bacteria in the presence of an Mn(III/IV) oxide surface layer.

3.4 Conclusion

The surface morphology and composition of the GAC media as determined with SEM imaging and EDS was found to change significantly with filter age, with the oldest GAC media exhibiting a mineralised surface comprising of O, Mn, Al, Ca and Si with low levels of C relative to the original GA1000N media and was interspersed with bacterial colonies. Further elemental analysis of the GAC media using ICP-MS also showed high levels of Ca, Al and Mn. The presence of high concentrations on Mn and O strongly suggests the presence of Mn(III/IV) oxides on the GAC surface, and along with the presence of bacterial colonies in close

proximity, it seems probable that Mn oxides are being deposited by Mn oxidising bacteria present in the GAC biological community[†].

[†] DNA sequencing work aimed at investigating the biological community present in the HWTS GAC filters was attempted, but laboratory closures and other factors related to the COVID-19 pandemic resulted in this aspect of the project remaining incomplete.

Chapter 4:

Development of a Quantitative GC-MS Method for the Analysis of Geosmin and 2-MIB in Water Samples.

4 Development of a Quantitative GC-MS Method for the Analysis of Geosmin and 2-MIB in Water Samples.

4.1 Introduction

A GC-MS method was adapted from the available literature (**Chapter 2**, **section 2.4.1**) and validated as a means of quantifying geosmin (GSM) and 2-MIB in water samples. The method needed to provide very low limits of detection due to the generally very low concentration of the analytes in natural water systems, coupled with the ability of humans to perceive them in drinking water at these low concentrations. Additionally, the method needed to involve relatively simple and rapid sample preparation to provide an effective and practical means of monitoring pilot and full-scale GAC filters on a daily basis. This would require the method to be useful for a single operator extracting and analysing between 10 and 50 samples per day, including sample collection.

4.2 Method Development

4.2.1 Chemicals and Reagents

GSM, 2-MIB (Certified Reference Materials; CRMs) and 1-adamantanol (1-ADML; internal standard) were purchased from Sigma-Aldrich (Auckland, New Zealand; **Figure 4-1**). Methanol, ethanol, acetone, acetonitrile, isopropyl alcohol, *n*-heptane and *n*-hexane were HPLC or spectroscopy grade and were also purchased from Sigma-Aldrich (Auckland, New Zealand). De-ionised water was prepared

using a Barnstead E-Pure water purification system with a resistivity of 18 Ω (Thermo Fisher Scientific, New Zealand).

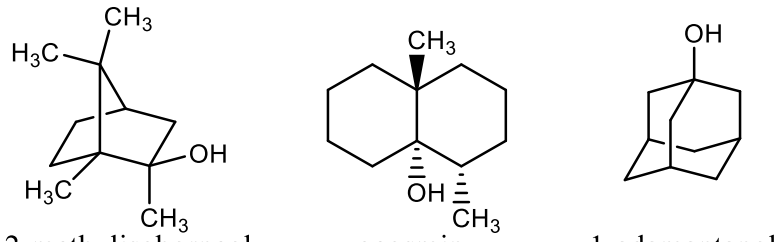

2-methylisoborneol geosmin 1-adamantanol

Figure 4-1: Structural formulae for 2-MIB, GSM and 1-ADML.

4.2.2 Analytical Standards and Calibration

Stock standard solutions of GSM and 2-MIB were prepared by transferring the supplied CRM (100 μg mL^{-1}) to a 100 mL volumetric flask and making up to volume with acetone to yield a final concentration of 1 mg L^{-1}. Each stock standard was then transferred to a glass bottle with a screw cap and stored at -18°C in the dark. The stability of GSM and 2-MIB has been shown to exceed 6 months in organic solvents under such conditions ***[229]***.

Calibration standards were prepared for each analysis day by transferring the appropriate volume of stock or intermediate standard to a 5 or 10 mL volumetric flask and making to volume with *n*-hexane (**Table 4-1**). An appropriate aliquot of 1-ADML IS was added to each calibration standard to give a final 1-ADML concentration of 5 μg L^{-1}. Other compounds were trialled as potential internal standards, including *cis*-decahydro-1-napthol (*cis*-DHN) and nopol ((1R)-6,6-dimethylbicyclo[3.1.1]hept-2-ene-2-ethanol) due to their similarity to

GSM and 2-MIB (**Figure 4-2**), but these were found to produce excessive peak tailing in the GC-MS trace.

Table 4-1: Scheme for the preparation of calibration standards of GSM and 2-MIB

Concentration	V(stock)	V(1-ADML)	V(flask)
50 µg L^{-1}	250 µL	25 µL	5 mL
35 µg L^{-1}	175 µL	25 µL	5 mL
20 µg L^{-1}	100 µL	25 µL	5 mL
10 µg L^{-1}	50 µL	25 µL	5 mL
5 µg L^{-1}	25 µL	25 µL	5 mL
2.5 µg L^{-1}	12.5 µL	25 µL	5 mL
0.25 µg L^{-1}	2.5 µL	50 µL	10 mL

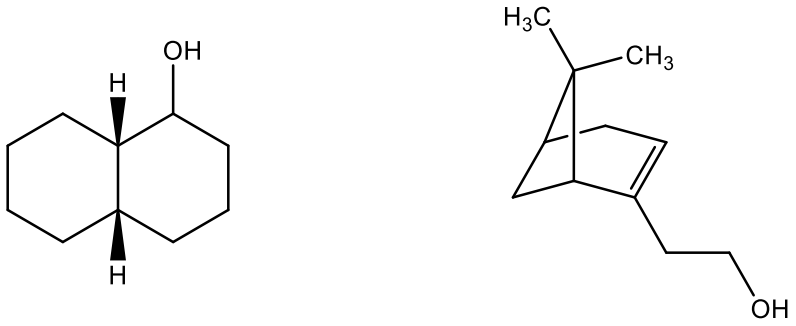

Figure 4-2: *cis*-decahydro-1-napthol (left) and nopol (right).

Early trials using *n*-heptane as a solvent showed baseline interference with 2-MIB at the lower end of the calibration range due to trace contaminants in the solvent that would elute at similar times even when a range of GC-MS parameters were trialled (oven programs, SIM ion choice etc.). Hence, *n*-heptane was abandoned as a suitable solvent for this method.

Response factors of the analyte compared to the internal standard were determined, where the ratio of concentration between each analyte (A) and the IS was plotted against the ratio of the peak area between each analyte and the IS. This yielded a linear calibration graph with gradient *m* described by **Equation 4-1**;

$$\frac{(Peak\ Area\ A)}{(Peak\ Area\ IS)} = m\frac{(Concentration\ A)}{(Concentration\ IS)} \quad (4\text{-}1)$$

The calibration plot was forced through zero after confirmation that a blank solvent injection yielded a peak response indistinguishable from the baseline noise. Representative calibration plots for 2-MIB and GSM are shown in **Figure 4-3**.

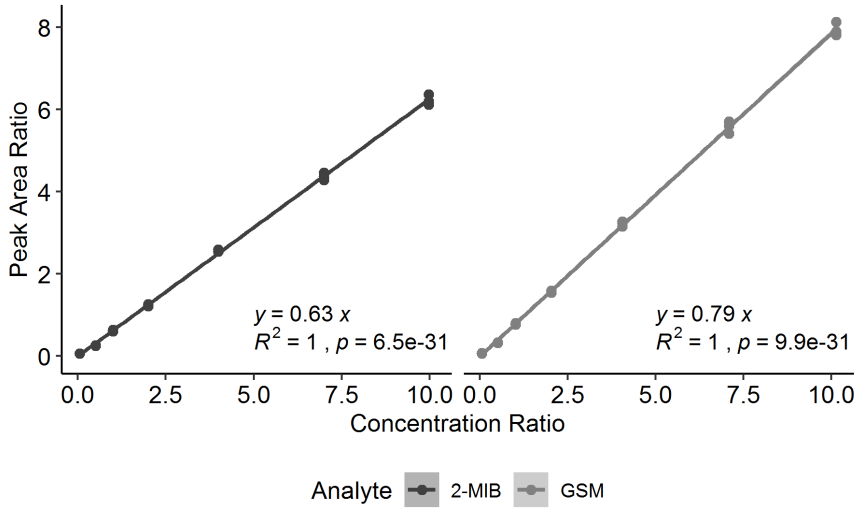

Figure 4-3: Representative calibration plots for 2-MIB (left) and GSM (right).

The signal response of each analyte was optimised by varying the MS source voltage and inspecting the peak area and signal-to-noise ratio (S/N). Experiments were carried out at concentrations at the low end (0.25 µg L^{-1}) and middle (10 µg L^{-1}) of the calibration range. Voltage tests showed that a MS source voltage of 2.1 kV gave the highest peak areas and S/N (**Figure 4-4** to **Figure 4-7**).

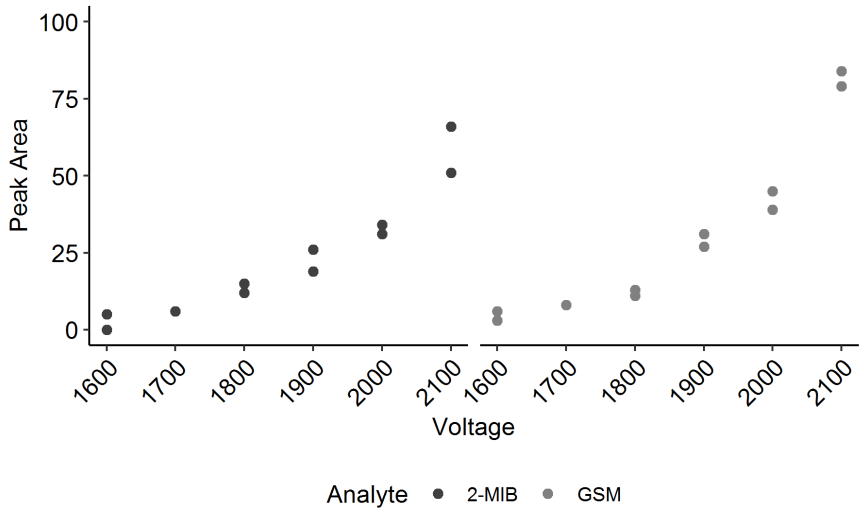

Figure 4-4: Peak area response of each analyte at 0.25 µg L^{-1} at various MS source voltages.

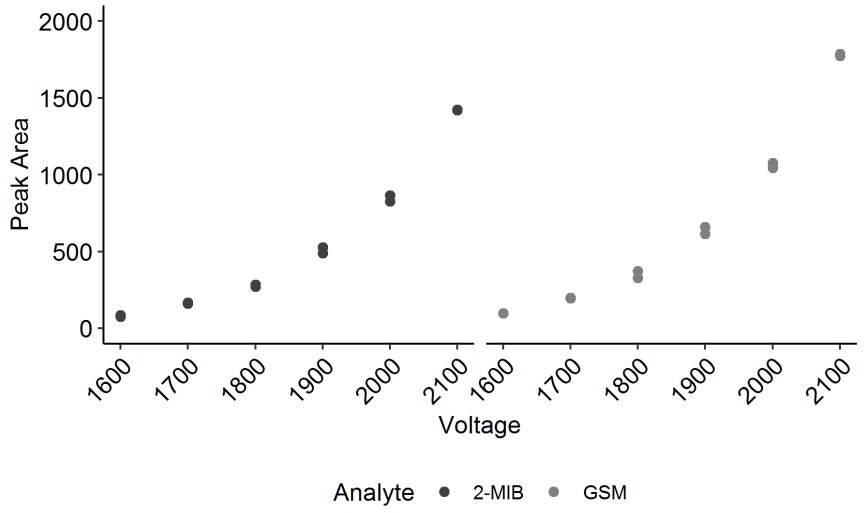

Figure 4-5: Peak area response of each analyte at 10 µg L-1 at various MS source voltages.

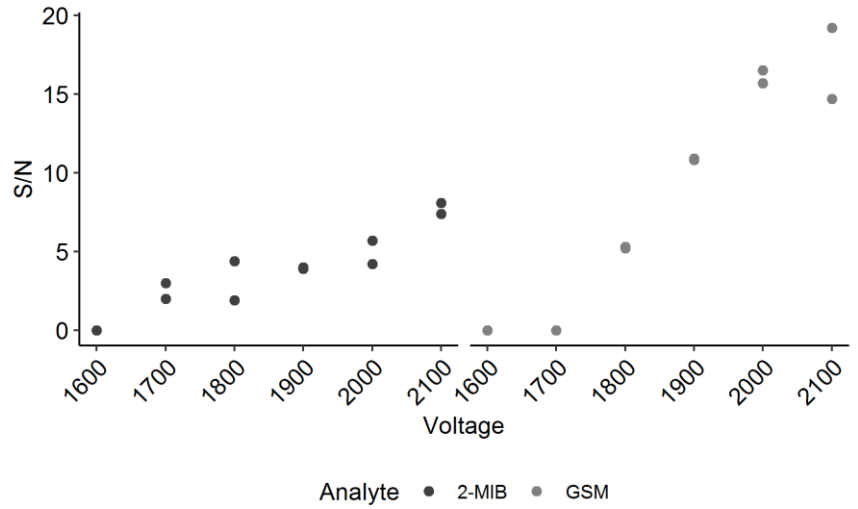

Figure 4-6: S/N of each analyte at 0.25 µg L^{-1} at various MS source voltages.

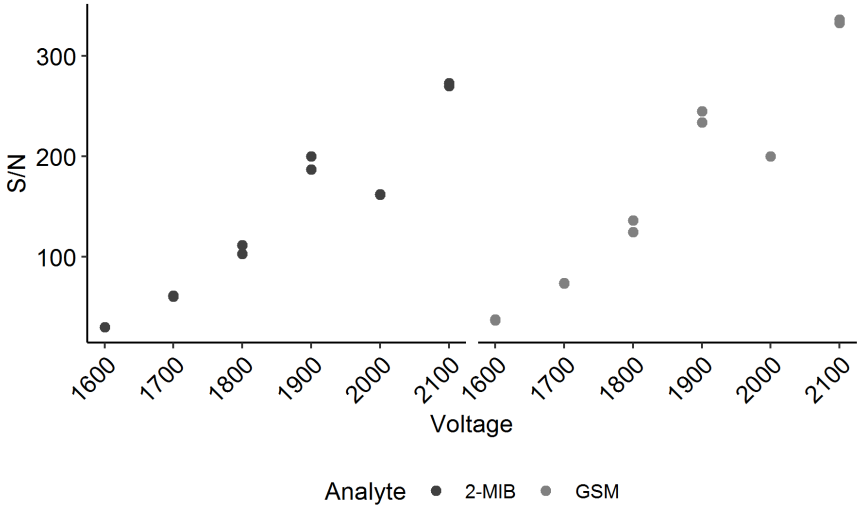

Figure 4-7: S/N of each analyte at 10 µg L^{-1} at various MS source voltages.

4.2.3 GC-MS Instrument Parameters

Analyses were carried out using an Agilent 7890A/5795C GC-MS system (Agilent Technologies, New Zealand) equipped with a Phenomenex ZB-5 column (30 m x 0.25 mm x 0.25 µm; Phenomenex, New Zealand). The injector was maintained at 250 °C and operated in the splitless mode with a purge time of 0.70 min at 25 mL min^{-1} and an injection volume of 2 µL. Helium was used as the carrier gas at a flow rate of 1.0 mL min^{-1}. The column oven was set at an initial temperature

of 35 ºC for 3 min, then programmed to ramp at 5 ºC min^{-1} to 150 ºC where it was held for 2 min followed by a 100 ºC min^{-1} ramp to 300 ºC for 3 min. The instrument was operated in the SIM acquisition mode with quantitative and confirmatory ions specified as listed in Table **4-2** with the MS source set at 2100V and 230 ºC. A fairly long run time (32.5 min) was implemented following preliminary screening of raw water extracts that showed significant background interference at the retention times of the target analytes.

Table 4-2: Quantitative and confirmatory ions* used for SIM GC-MS of GSM, 2-MIB and 1-ADML and their associated retention times.

Compound	Ion 1 m/z	Ion 2 m/z	Ion 3 m/z	Time Slice	Retention Time
2-MIB	95	107	108	3.5 – 19.50 min	18.39 min
1-ADML	95	152	N/A	19.50 – 23.5 min	20.45 min
GSM	111	112	125	23.5 – 32.5 min	24.51 min

* Ion 1 indicates ions used for quantitation while ions 2 and 3 indicate confirmatory ions.

Quantitative and confirmatory ions were selected after running each standard at high concentration (1 mg L^{-1}) and assessing the full scan GC-MS spectrum obtained for each compound (**Figure 4-8**). Discussions on the electron impact mass spectrometry (EI-MS) fragmentation patterns for 2-MIB, GSM and similar cyclic alcohols can be found elsewhere ***[230,231]***. A representative extracted ion (EIC) SIM GC-MS chromatogram is shown in **Figure 4-9**.

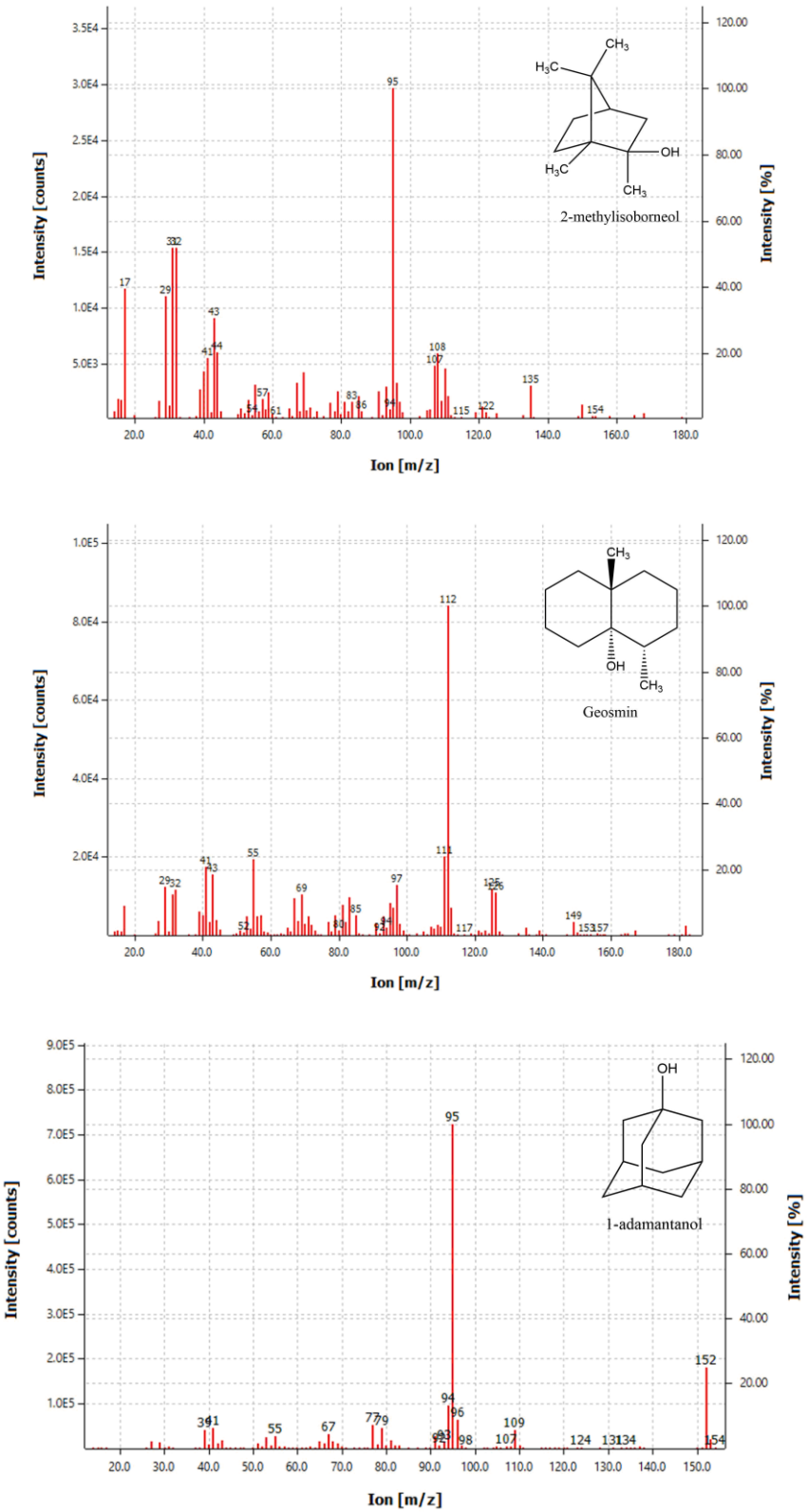

Figure 4-8: Full scan GC-MS spectra for 2-MIB (top), GSM (middle), and 1-ADML (bottom).

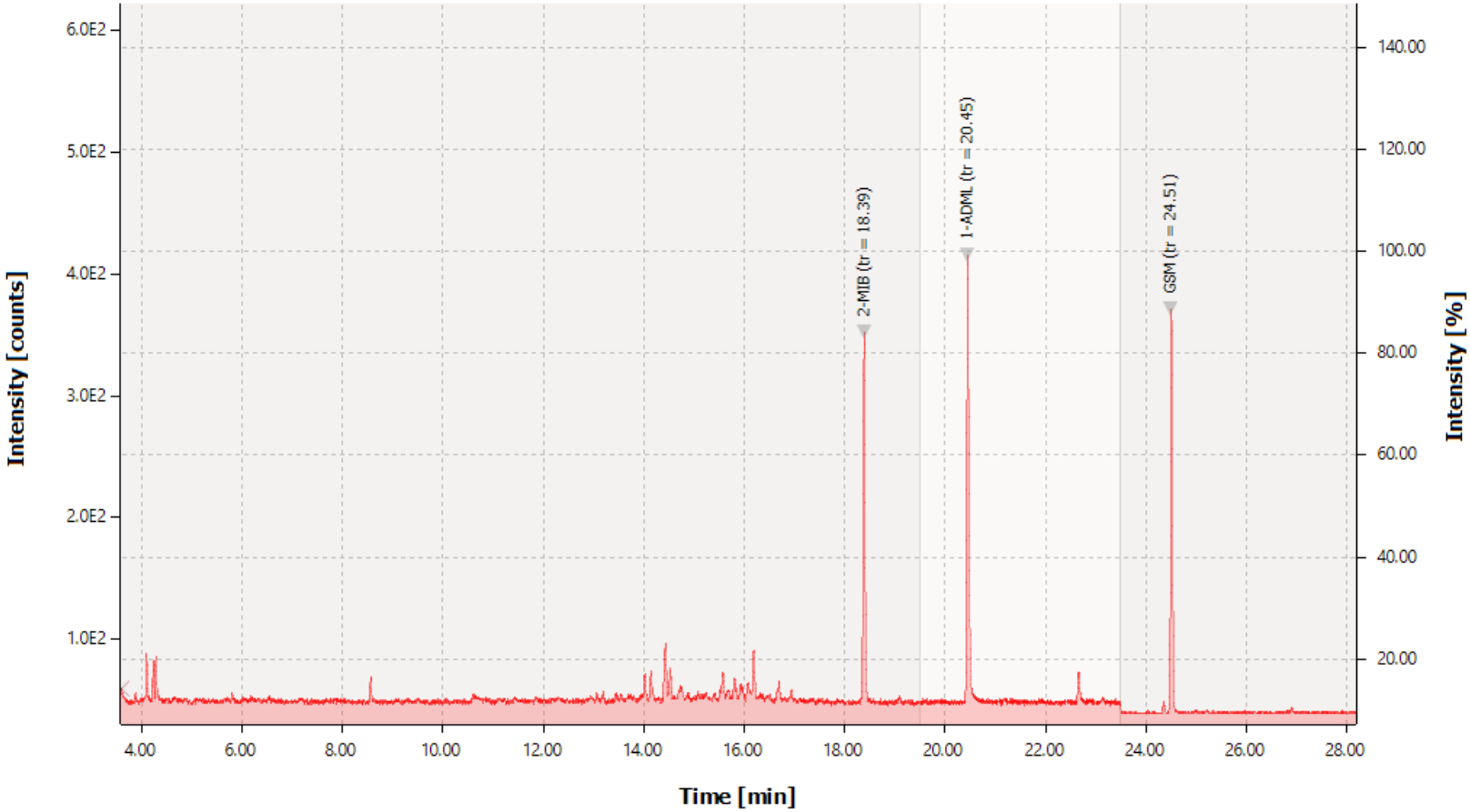

Figure 4-9: EIC SIM GC-MS chromatogram for a 2-MIB (t_r = 18.39) and GSM (t_r = 24.51) calibration standard (10 µg L^{-1}) containing 1-ADML (t_r = 20.45) as internal standard (5 µg L^{-1}).

4.2.4 Vortex Assisted Liquid-Liquid Micro-Extraction

As outlined in **section 2.4.1**, many extraction methods have been applied to the trace analysis of 2-MIB and GSM. As for any application of an analytical method, the overall protocol must be fit for purpose and usable on a practical basis. In the case of this study, a low-cost method that could achieve low detection limits while also allowing a fast sample turnaround was required. As such, extraction methods such as PT, CLS, SPME were deemed to be unsuitable due to their reliance on expensive equipment and slow rate of sample processing. Similarly, conventional LLE was seen as being too reliant on large amounts of organic solvents while SPE requires numerous disposable cartridges which become costly when large numbers of samples need to be processed. This led to micro-extraction techniques being seen as the most promising candidates for the extraction and pre-concentration of 2-MIB and GSM. Of these techniques, Dispersive Liquid-Liquid Micro-Extraction (DLLME) was chosen as the basis for developing an appropriate extraction methodology due to it requiring very low volumes of organic solvents and a minimal amount of specialised equipment while providing fast sample turnaround and large analyte enrichment factors which correspond to low detection limits.

DLLME provides a simple and rapid extraction procedure that also minimises solvent use. The use of DLLME, in conjunction with sonication, was employed by Cortada *et al.* ***[110],*** which showed that this type of extraction was indeed effective in the extraction and pre-concentration of 2-MIB, GSM, and other odour compounds. Further to this, the use of vortex mixing as a means to finely disperse

the extraction solvent throughout the sample matrix has also been employed in the analysis of these compounds (Vortex Assisted Liquid-Liquid Micro-Extraction; VALLME) ***[232]***. The use of such micro-extraction techniques reflects the current trend in analytical chemistry towards miniaturisation and minimisation of solvents and reagents reflecting an overall trend towards "greener" methodologies ***[233,234]***. Usually, DLLME procedures employs the use of a chlorinated extraction solvent (e.g. dichloromethane, tetrachloroethylene) along with a disperser solvent (e.g. methanol, acetonitrile, isopropanol) which allows the extraction solvent to be dispersed as micro-droplets throughout an aqueous sample matrix. This provides a large surface area that facilitates the mass transfer of analyte between the aqueous and extracting phase, providing very short extraction times. The mixture can then be centrifuged and the extracting phase is recovered for analysis which is facilitated by the use of high density, chlorinated solvents and the use of conical centrifuge tubes. Due to the small amounts of solvent used for DLLME extractions (typically 10 – 100 μL), not only is solvent consumption greatly reduced compared with conventional liquid-liquid or Soxhlet extractions, large analyte enrichment factors can also be achieved which is very useful for trace analyses ***[235-239]***. The use of sonication or vortex mixing as a means of a dispersion can remove the need for a disperser solvent, further reducing solvent consumption. Additionally, in efforts to reduce the reliance on environmentally harmful chlorinated solvents, the use of solvents such as cyclohexane, *n*-heptane and *n*-octane has been investigated in pesticide analysis as possible replacements ***[240]***. Based on this, a micro-extraction

procedure was investigated as a means of extracting and pre-concentrating 2-MIB and GSM from water samples for GC-MS analysis using non-chlorinated solvents.

4.2.4.1 Choice of Solvent Dispersion Technique

A range of dispersion solvents were trialled in order to maximise extraction solvent recovery and minimise the variation in the volume of recovered extraction solvent. This was carried out as low recovery of the extraction solvent correlates with low analyte extraction recoveries, while high variations in the recovered volume results in highly variability (low precision) extraction recovery of the analyte. Five dispersion solvents were trialled; acetone, acetonitrile (ACN), isopropyl alcohol (IPA), methanol (MeOH) and ethanol (EtOH).

Initial trials showed that IPA was unsuitable as a dispersion solvent when using *n*-hexane as the extraction solvent, as the volume of extraction solvent recovered was very low which resulted in very low recoveries of the targets. Additionally, while ACN and acetone provided reasonable recoveries, the volume of recovered extraction solvent varied substantially between replicates and resulted in highly variable recoveries. While MeOH and EtOH both provided more repeatable recoveries of the extraction solvent than the other dispersion solvents trialled, the volumes recovered using EtOH were consistently higher and a superior emulsion was formed during the DLLME procedure, resulting in higher analyte recoveries. Overall however, the use of a dispersion solvent resulted in highly variable volumes of extraction solvent being recovered which resulted in high variability in the

percent recovery of the target analytes. As a comparison, the dispersion of *n*-hexane in the aqueous phase was achieved through the use of vortex mixing without the use of a dispersion solvent; this proved to give superior recovery of the extraction solvent and the target analytes, while also providing lower variability in percentage recovery and lower baseline noise. This may be explained by the fact that introduction of a water miscible organic dispersion solvent (EtOH, MeOH etc.) into the aqueous phase results in an increase in the solubility of the target analytes in the aqueous phase, altering the equilibrium partition coefficient and resulting in less mass transfer of the target species to the organic extracting phase. As such, vortex assisted extraction was employed as the extraction method of choice for this analytical method and further, more rigorous recovery and validation studies.

4.2.4.2 Choice of Extraction Solvent

Both *n*-hexane and *n*-heptane proved effective at extracting 2-MIB and GSM from water samples, however as noted earlier (**Section 4.2.2**), *n*-heptane introduced interference to the 2-MIB SIM GC-MS signal and *n*-hexane was used instead. Other solvents such as xylene, toluene and ethyl acetate either produced emulsions that were too stable to allow for sufficient separation of the extraction solvent during centrifugation or became almost entirely solubilised when introduced to the water sample in the presence of a dispersion solvent. As such, *n*-hexane was selected as the most suitable candidate for extraction recovery experiments.

4.2.4.3 Effect of Salt Addition

While initial trials showed that the addition of salt (NaCl) did not have a particularly great effect on the recovery of either analyte, it did provide better phase separation during centrifugation. This allowed for more repeatable volumes of extraction solvent to be recovered and eliminated the thin emulsified layer that persisted between layers when salt was not used. As such, the addition of NaCl and H_2KPO_4 to water samples in similar proportions to Shin *et al.* ***[99]*** was incorporated into the VALLME procedure as a means of reducing variability between samples.

4.2.4.4 VALLME Method

A water sample (10 ± 0.02 mL, room temperature) was transferred to a screw-top, glass centrifuge tube (15 mL) containing NaCl (1.0 ± 0.2 g) and KH_2PO_4 (200 ± 10 mg). The sample was mixed using a vortex mixer until the salts dissolved after which *n*-hexane (100 µL) was added. The sample was vortexed (1 min, 40 Hz) and centrifuged (5 min, 2800 rpm) after which the lower aqueous layer was carefully removed via syringe, making sure not to disturb the organic, supernatant phase. The sample was centrifuged a second time (5 min, 2800 rpm) after which any remaining aqueous phase was removed via syringe. The volume of the organic, supernatant phase was recorded (V_{sup}) and an aliquot (V_E = 50 µL) was transferred to a GC vial equipped with a glass low volume vial insert (100 µL). The sample was amended with 1-ADML IS (V_{IS} = 10 µL, 30 µg L^{-1}) to give a final volume of 60 µL (V_T) and an IS concentration of 5 µg L^{-1} (C_{IS}). The sample was introduced to the GC-MS

system (**Section 4.2.3**) via an auto-sampler. A diagram illustrating the extraction procedure is given in **Figure 4-10**.

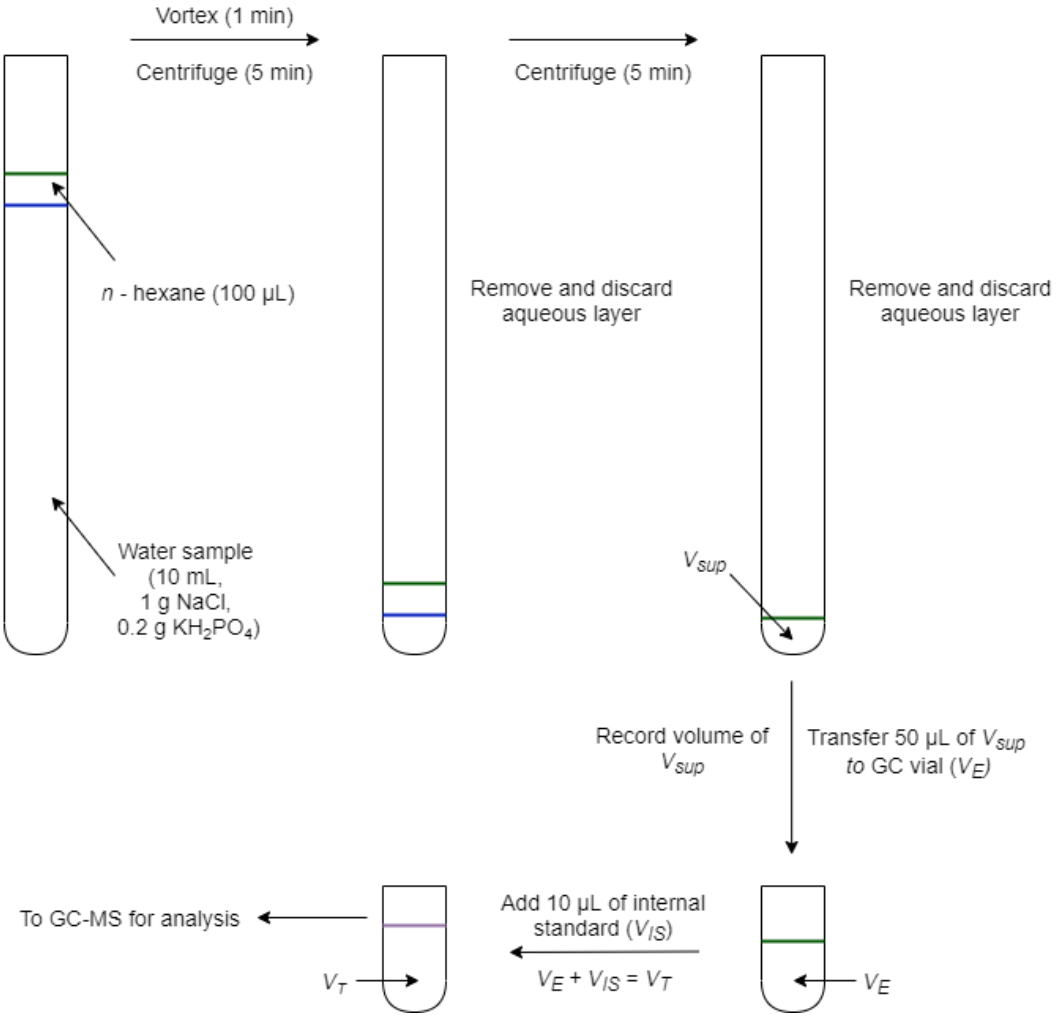

Figure 4-10: Diagram illustrating the VALLME procedure.

4.2.4.5 Method Validation

4.2.4.5.1 Extraction Recovery Efficiency

For VALLME and other micro-extraction techniques with solvents of lower density than the sample solvent (water), the extraction recovery (ER) efficiency is based upon the calculated concentration of analyte present in the initial sample as

measured in the supernatant extracting phase (C_f) and the actual concentration of analyte spiked into the recovery sample (C_o) ***[238]***. This can be expressed as a percentage:

$$ER = \frac{C_f}{C_o} \times 100 \quad (4\text{-}2)$$

The concentration of a given sample is calculated from the calibration curve using **Equation 4-3**. This involves calculating the concentration present in the extract from the calibration plot, correcting for the volume of internal standard added to the extract, accounting for the volume of the extracting phase recovered, the volume of the initial water sample and converting to units of ng L^{-1}. For a full example of the calculations involved, see **Appendix A-2**.

$$C_f = C_{IS} \frac{R}{RF} \frac{V_T}{V_E} \frac{V_{sup}}{V_s} \times 1000\, ng\, \mu g^{-1} \quad (4\text{-}3)$$

$$R = \frac{PA_A}{PA_{IS}} \quad (4\text{-}4)$$

Where: C_f = Concentration of the analyte in the sample (µg L^{-1})
C_{IS} = Concentration of the internal standard in the extract (4.9 µg L^{-1})
R = Peak area ratio of analyte to internal standard
RF = Response factor (slope of calibration plot)
PA_A = Peak area of the analyte A
PA_{IS} = Peak area of the internal standard (IS)
V_T = Volume of extract and IS measured (60 µL)
V_E = Volume of extract measured (50 µL)
V_{sup} = Volume of extract (µL)
V_S = Volume of water sample (10000 µL)

The value of V_{sup} was monitored over the course of subsequent recovery experiments (n = 30) in order to assess the variability of the recovered volume of extraction solvent. The pre-concentration factor (PF) was also monitored during this time (**Table 4-3**).

Table 4-3: V_{sup} and PF values for the VALLME method.

Parameter	Mean	%RSD
V_{sup} (μL)	73.6	3.5
PF (2-MIB)	134.2	12.4
PF (GSM)	149.5	8.9

Inter and intra-day recovery experiments were carried out over three separate days. Outliers were detected and removed using Rosner's generalised ESD procedure for outliers (n = 30, k = 3, α = 0.05, ***[241]***) after the data was tested for normality using the Shapiro-Wilk test (α = 0.05; **Figure 4-11**; **Figure 4-12; *[242,243]***).

No outliers were detected across all three days. Inter-day results were compared using a single factor ANOVA test (α = 0.05). Recovery data for each of the three days are shown in **Table 4-4** and **Table 4-5**. Overall, GSM (110.0 ± 9.6 %) was extracted more effectively than 2-MIB (98.6 ± 11.4 %), likely due to the higher hydrophobicity of GSM (K_{OW} = 3.57) relative to 2-MIB (K_{OW} = 3.31) ***[244]***. Results of the ANOVA test showed no statistical difference in mean percentage recovery between days and are displayed in **Table 4-6** and **Table 4-7**.

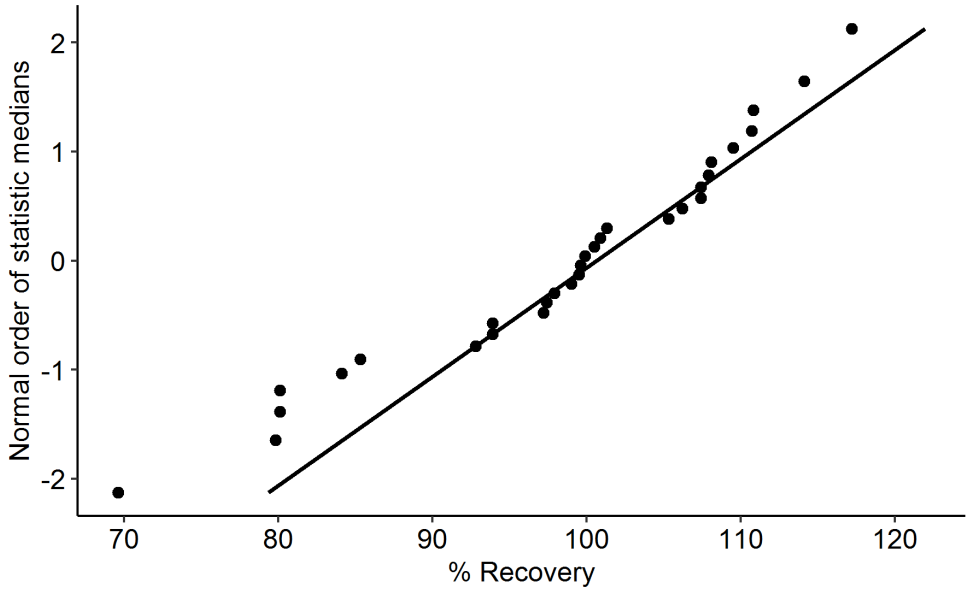

Figure 4-11: Normal probability plot for 2-MIB percent recovery (p=0.10).

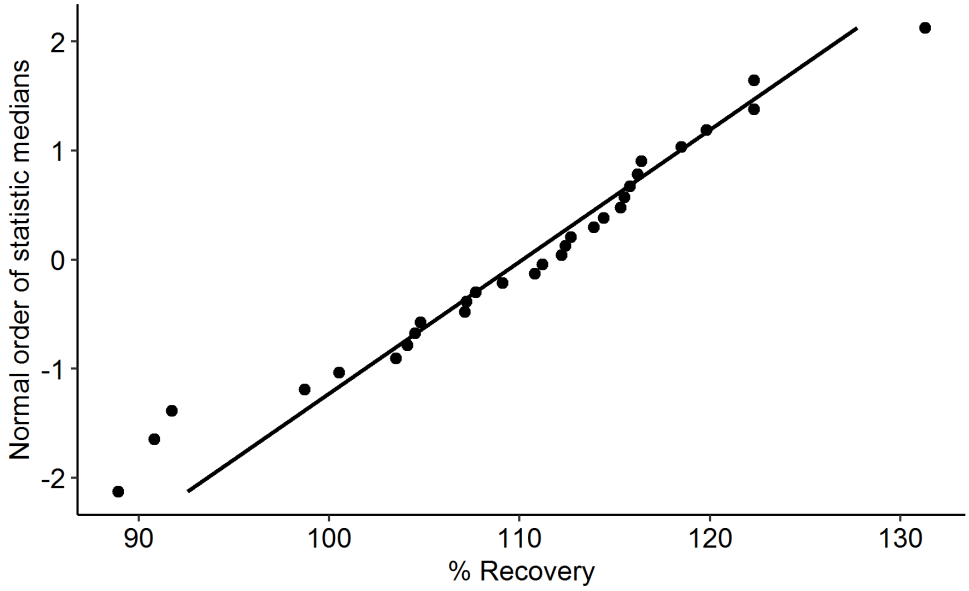

Figure 4-12: Normal probability plot for GSM percent recovery (p=0.36).

Table 4-4: Percentage recovery of 2-MIB and GSM from spiked water samples over three days.

	2-MIB Recovery (%)			GSM Recovery (%)		
Replicate	13/06/2017	4/07/2017	7/07/2017	13/06/2017	4/07/2017	7/07/2017
1	80.1	110.8	100.9	98.7	88.9	104.5
2	80.1	107.9	69.6	116.4	107.1	104.8
3	84.1	93.9	79.8	110.8	100.5	91.7
4	100.5	108.1	117.2	113.9	115.3	122.3
5	93.9	97.9	92.8	114.4	119.8	103.5
6	99.9	99.6	101.3	112.7	122.3	116.2
7	107.4	99.5	106.2	115.8	112.2	112.4
8	97.2	109.5	110.7	104.1	111.2	115.5
9	85.3	99.0	107.4	90.8	109.1	118.5
10	97.4	105.3	114.1	107.7	107.2	131.3
Mean	92.6	103.1	100.0	108.5	109.4	112.1
Median	95.5	102.5	103.7	111.8	110.1	113.9
SD	9.5	5.8	15.2	8.4	9.6	11.3
% RSD	10.3	5.7	15.2	7.7	8.8	10.1
95% CI	5.9	3.6	9.4	5.2	6.0	7.0
% Bias	-7.42	3.14	-0.02	8.53	9.35	12.06

Table 4-5: Overall recovery statistics for 2-MIB and GSM over all three days.

	2-MIB	GSM
Mean	98.6	110.0
Median	99.8	111.7
SD	11.4	9.6
% RSD	11.6	8.7
95% CI	4.1	3.6
% Bias	-1.43	+9.98

Table 4-6: Single factor ANOVA results for 2-MIB recovery across three days.

SUMMARY						
Groups	Count	Sum	Average	Variance		
13/06/17	10	925.8	92.6	91.0		
03/07/17	10	1031.4	103.1	34.1		
07/07/17	10	999.8	100.0	231.9		
ANOVA						
Source of Variation	SS	df	MS	F	P-value	F crit
Between Groups	587.6	2	293.8	2.5	0.10	3.4
Within Groups	3212.6	27	119.0			
Total	3800.2	29				

Table 4-7: Single factor ANOVA results for GSM recovery across three days.

SUMMARY						
Groups	Count	Sum	Average	Variance		
13/06/17	10	1085.3	108.5	70.2		
03/07/17	10	1093.5	109.4	92.3		
07/07/17	10	1120.6	112.1	127.1		
ANOVA						
Source of Variation	SS	df	MS	F	P-value	F crit
Between Groups	68.2	2	34.1	0.4	0.71	3.4
Within Groups	2606.2	27	96.5			
Total	2674.4	29				

Recovery experiments were carried out using DI water samples spiked with either 5 ng L^{-1}, 50 ng L^{-1} or 500 ng L^{-1} of both 2-MIB and GSM using the previously described VALLME and GC-MS methods. Quality control (QC) blanks containing 2-MIB (10 µg L^{-1}), GSM (10 µg L^{-1}) and 1-ADML (5 µg L^{-1}) were inserted into the GC sequence every five samples to assess any drift or departure from the calibration of the GC-MS instrument. A representative chromatogram of a spiked water sample is shown in **Figure 4-13**.

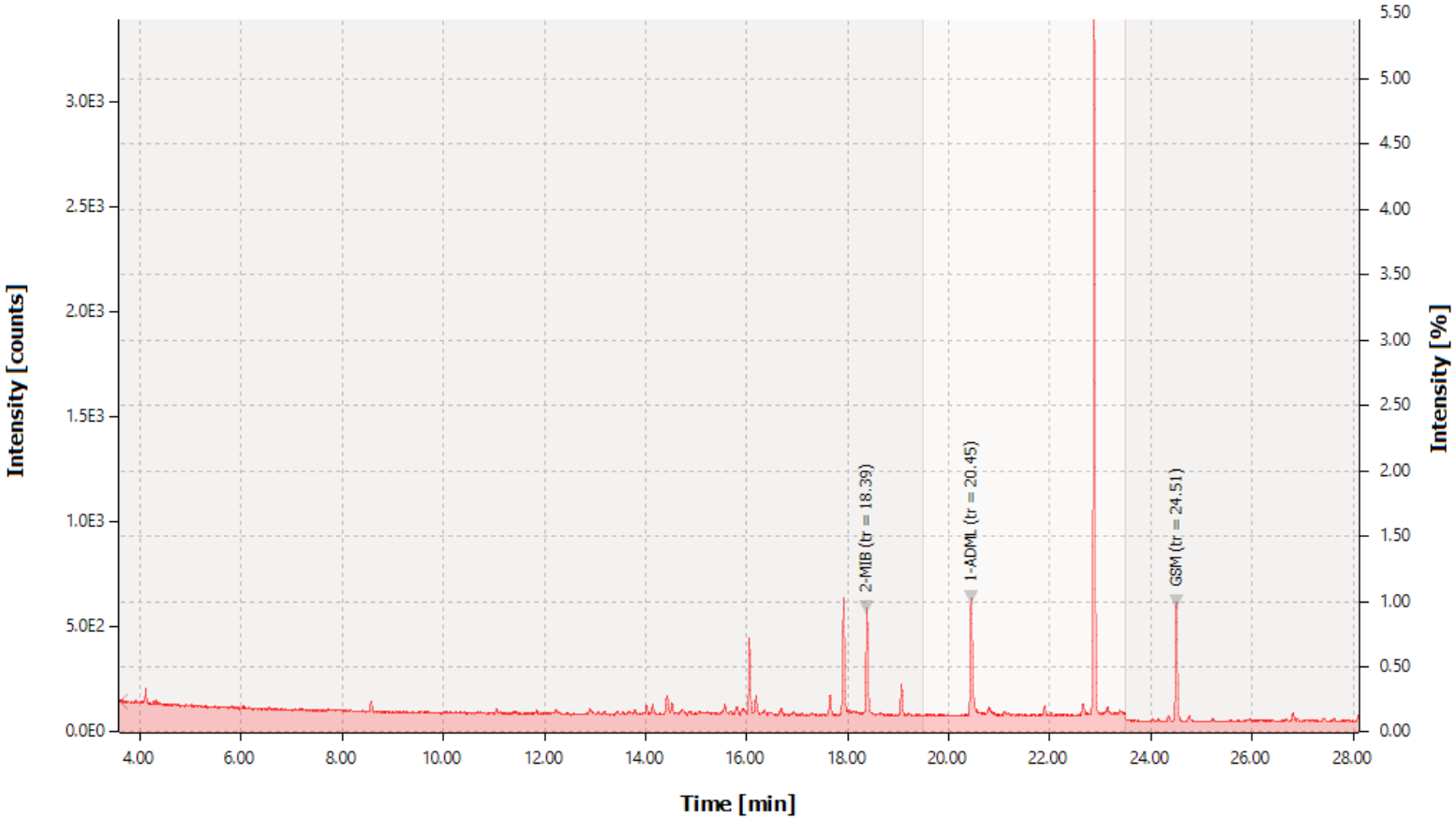

Figure 4-13: GC-MS EIC SIM chromatogram of a VALLME extract at 50 ng L^{-1}.

4.2.4.5.2 Limits of Detection and Quantification

The limit of detection was initially estimated after running standard solutions of 2-MIB and GSM at low concentrations and assessing the signal-to-noise (S/N) of the peaks of each analyte. This was found to be approximately 3 to 5 ng L^{-1} after applying the approximately 100-fold pre-concentration step included in the VALLME extraction method, with the instrument detection limit (IDL) being approximately 300 to 500 ng L^{-1}. Method detection and quantification limits (MDL and MQL; **Table 4-8**) were more accurately estimated from the standard deviation obtained by running nine replicates through the VALLME method at a low concentration close to the estimated limit of detection (5 ng L^{-1}) using **Equations 4-5** and **4-6** ***[245]***.

$$MDL = \frac{3 \times SD}{S} \quad (4\text{-}5)$$

$$MQL = \frac{10 \times SD}{S} \quad (4\text{-}6)$$

Where: SD = standard deviation
S = slope of the calibration plot

Table 4-8: Detection and quantification limits of the GC-MS instrument and the VALLME method.

Compound	MDL (ng L^{-1})	MQL (ng L^{-1})
2-MIB	2.8	9.3
GSM	2.1	6.9

4.2.4.5.3 Linearity and Range

While linearity had already been demonstrated for the GC-MS instrument (**Figure 4-3**) linearity of the entire method was also tested. Spiked water samples at 3 concentration levels (5, 50 and 500 ng L^{-1}) were subjected to the VALLME method and analysed by GC-MS in triplicate across two days. Taking into account

the pre-concentration factor of approximately 100 included in the DLLME method, this is equivalent to the calibration range of 0.5 to 50 μg L^{-1}. Across this range, the method was found to be linear for both 2-MIB and GSM and that the ER was the same within acceptable experimental error across this range (**Table 4-9)**. The calibration range was chosen to reflect the concentrations of 2-MIB and GSM expected to be found in environmental water samples, with samples at concentrations greater than 500 ng L^{-1} being unlikely to be encountered. In the case of samples too concentrated that fall outside the calibration range, it may be necessary to dilute the sample prior to analysis.

Table 4-9: Linearity and associated ER results across three concentration levels (5, 50 and 500 ng L^{-1}).

Compound	Linearity (R^2)	ER (%)	RSD (%)
2-MIB	0.9991	92.0	10.8
GSM	0.9987	108.6	8.9

4.2.5 Further Remarks on the Analytical Method

The method developed here provides a simple, fast and cost-effective technique for the quantitation of GSM and 2-MIB at trace levels commonly encountered in natural waters. The limits of detection are comparable to those of previously developed methods, and the method is capable of detecting the target compounds at the level of their respective OCTs. The use of low solvent volumes and minimal reliance on plastic consumables (e.g. SPE cartridges) results in a very cost-effective method which does not rely on specialised equipment (e.g. CLS, SPME). Samples can be processed quickly by a single analyst, with sample preparation of batches 24 samples taking approximately 1.5 to 2 hours. The limiting step was found to be the

length of the GC-MS run, with each run being 30 minutes leading to long run times for large batches of samples. Improvements could easily be made in this respect, for example the use of a longer column or GC-MS/MS, as this would provide a way to avoid interfering co-eluting compounds which were the reason for implementing such a long GC-MS program. The use of GC-MS/MS would also improve the detection limits, and allow for a greater degree of selectivity in the case of co-elution.

Overall, the method was found to be fit-for-purpose and was subsequently used to study various aspects of the behaviour of 2-MIB and GSM in the HWTS.

Chapter 5:

Behaviour of Taste and Odour Compounds in Full-scale and Pilot-scale Systems

5 Behaviour of Taste and Odour Compounds in Full-scale and Pilot-scale Systems

The quantitative GC-MS method that was developed and documented in chapter 4 was applied to studying the behaviour GSM and 2-MIB within the HDWTS. Historically, the HWTS has had issues with T&O compounds, and this study aimed to answer some questions regarding their behaviour within the plant. Firstly, a sampling survey of the entire plant was undertaken to assess baseline levels of GSM and 2-MIB and to discern where the bulk of these compounds are removed by the current treatment system. Second, dosing experiments were carried out using a pilot-scale GAC column to simulate high concentration, transient events which were of particular interest to the plant operators and engineers, and to investigate if biodegradation products of 2-MIB or GSM could be detected. Finally, using isotherm data and data collected during dosing experiments, adsorption models were used to predict the effect of varying influent concentrations and empty bed contact times (EBCTs) on the removal of these compounds, and whether such models could be used to predict bed life.

5.1.1 Removal of Geosmin and 2-MIB in Full Scale GAC Filters

The influent and effluent of the GAC filters at the HWTS were monitored over a period of 30 days to assess their performance in the removal of T&O compounds. Samples were taken from various points throughout the treatment train to assess the concentration of 2-MIB and GSM throughout the system and determine the percent removal being contributed by the GAC filters themselves. Samples were collected from the river intake, post-settling, post-sand filtration, post-GAC filtration and post-UV treatment (**Figure 5-1**).

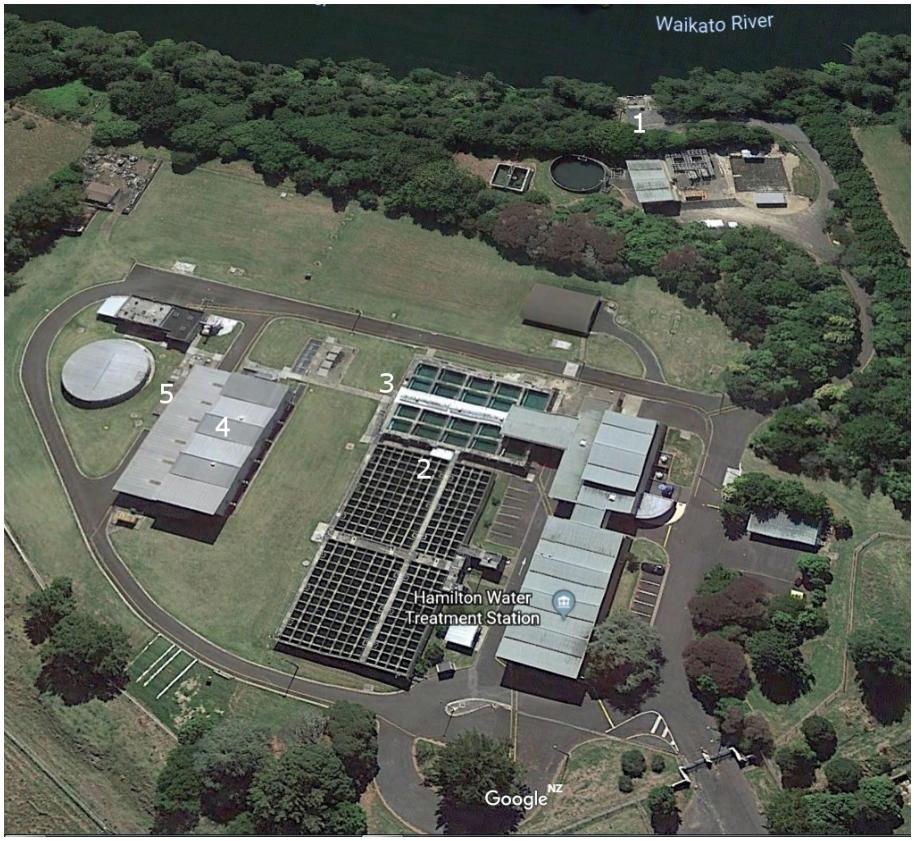

Figure 5-1: Aerial view of the HWTS showing sampling locations. (1) River intake; (2) Post-settling; (3) Post-sand; (4) Post-GAC and pilot column; (5) Post-UV. (Source: 37°48'39" S 175°18'16" E. GOOGLE EARTH. April 24, 2018).

Post-GAC samples were collected from each individual GAC filter to investigate any differences between the filters. Samples were also collected from a pilot scale

GAC filter which was connected to the same influent source as the full-scale filters as a comparison (GAC depth = 1.8m, EBCT = 15 min). Samples were collected from 27/02/18 and 28/03/18 between 12:00 and 13:00 for each sampling day. At this time, the GAC filters were at various stages of use, having been partially replaced with fresh media (≈ 50%) sequentially in the time leading up to sampling being carried out. At the time of sampling, the age of the filters from oldest to newest was GAC5 > GAC6 > GAC1 > GAC2 > GAC3 > GAC4. However, GAC 5 was taken out of service 7 days into sampling for media replacement and therefore could not be sampled for the entire time. The range of filter ages spanned from approximately 7 months for GAC6 to approximately 2 weeks for GAC4, while GAC5 had been in service since 2007 (≈ 10 years).

5.1.1.1 Experimental

5.1.1.1.1 Method

Water samples (≈ 50 mL) were collected daily from each sampling location using plastic centrifuge tubes (50 mL). Sample tubes were transferred to polystyrene boxes and stored on ice while transported to the laboratory where they were frozen prior to being processed for analysis by VALLME GC-MS. Sub-samples (10 mL) were taken from each water sample in duplicate after bringing the frozen samples to room temperature in a water bath at ambient temperature. The thawed samples were extracted using the VALMME method and analysed by GC-MS. Spiked water samples (≈ 50 ng L^{-1}) were also included in each run to assess the extraction efficiency across each day. QC standards were also run to assess any drift from the

current instrument calibration at a concentration near the middle of the calibration range (10 µg L^{-1}).

Water temperature, TOC, and DOC measurements were collected from instruments and meters installed on-site at the HWTS which are calibrated periodically by site staff. Weather data was obtained from New Zealand's National Climate Database ***[246]*** using data from the closest available weather station to the HWTS.

5.1.1.2 Results and Discussion

Across all samples, 2-MIB was only observed at levels above the MDL (2.8 ng L^{1}) on one day (14/03/18) in the raw river sample and was not observed above the MDL in any of the samples collected from within the treatment train. The approximate concentration of 2-MIB detected on this day was also very low (≈ 3.3 ng L^{-1}), being only barely above the MDL and at the lower end of the OCT for 2-MIB (2 - 20 ng L^{-1}; ***[127]***) . While accurate quantitation was not possible at this level using this analytical method, it did give some indication that the concentration of 2-MIB in the source water is generally very low. The fact that 2-MIB was only present at very low background levels in the source water and was not detected anywhere throughout the treatment train suggests that the current treatment process is able to easily deal with these concentrations of 2-MIB. Due to the low concentration of 2-MIB in the source water and the inability to quantify accurately at such low levels, no further analysis of the data was possible.

Geosmin was detected in the source water at levels above the MQL of 6.4 ng L^{-1} on all but one sample (**Figure 5-2**). Over the sampling period, the GSM concentration

for accurately quantifiable samples ranged 7.5 to 25 ng L^{-1}. The lowest detected concentration in the source water was estimated to be approximately 5.2 ng L^{-1} on 07/03/18. With the OCT of GSM being 6-10 ng L^{-1} ***[127]***, most of the samples exhibited GSM at the higher end or above the OCT for GSM. No large spikes in the concentration of GSM were observed during the 30 period of the trial, suggesting that the concentration of GSM is somewhat stable in the source water. However, as no algal blooms, heavy rainfall events or other environmental events occurred during the trial, it is still possible that large spikes in GSM concentration do occur at times over the course of the year.

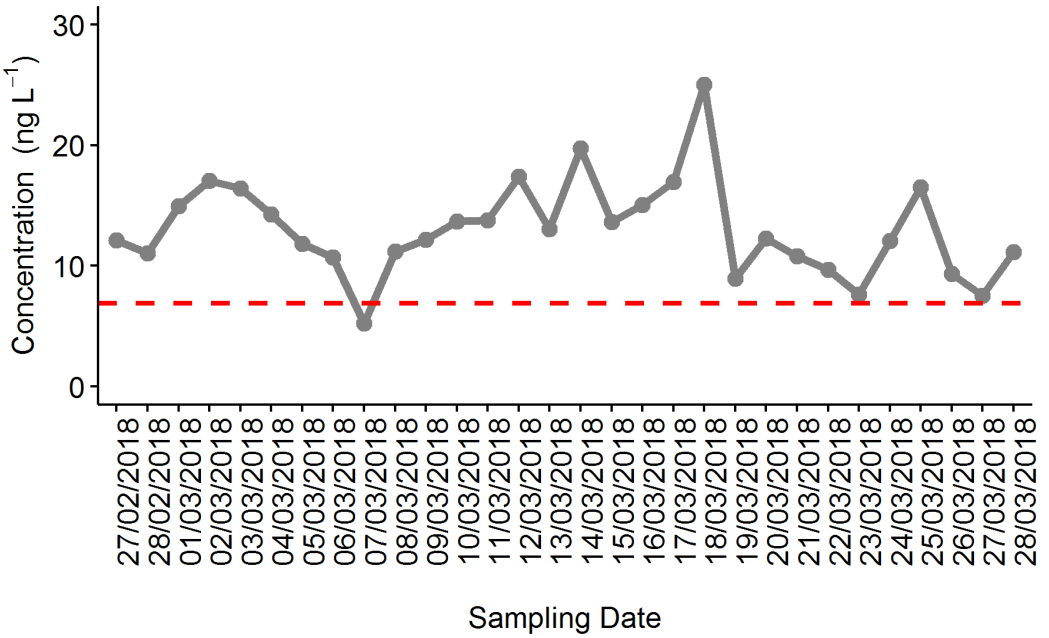

Figure 5-2: Geosmin concentration in source water across all sampling days. Note: - - - Indicates the MQL for GSM (6.9 ng L^{-1}).

Regression analysis showed that the concentration of GSM was not significantly correlated with TOC ($p = 0.27$) or DOC ($p = 0.27$) concentration, river level ($p = 0.91$), river flow rate ($p = 0.85$), water temperature ($p = 0.36$) or relative humidity ($p = 0.15$). However, there was a significant correlation with ambient temperature ($p = 0.009$; **Figure 5-3**), with higher temperatures predicting lower

GSM concentrations. This may in part be due to higher temperatures allowing more GSM to volatilise, leaving the aqueous phase and entering the gas phase resulting in a lower aqueous phase concentration. The correlation was weak however, with only a small percentage of the variation in GSM concentration being explained by the regression model ($R^2 = 0.22$). It is likely that other factors play a greater role in the flux in GSM concentration, such as daily variation in GSM producing microbial populations, rainfall and runoff.

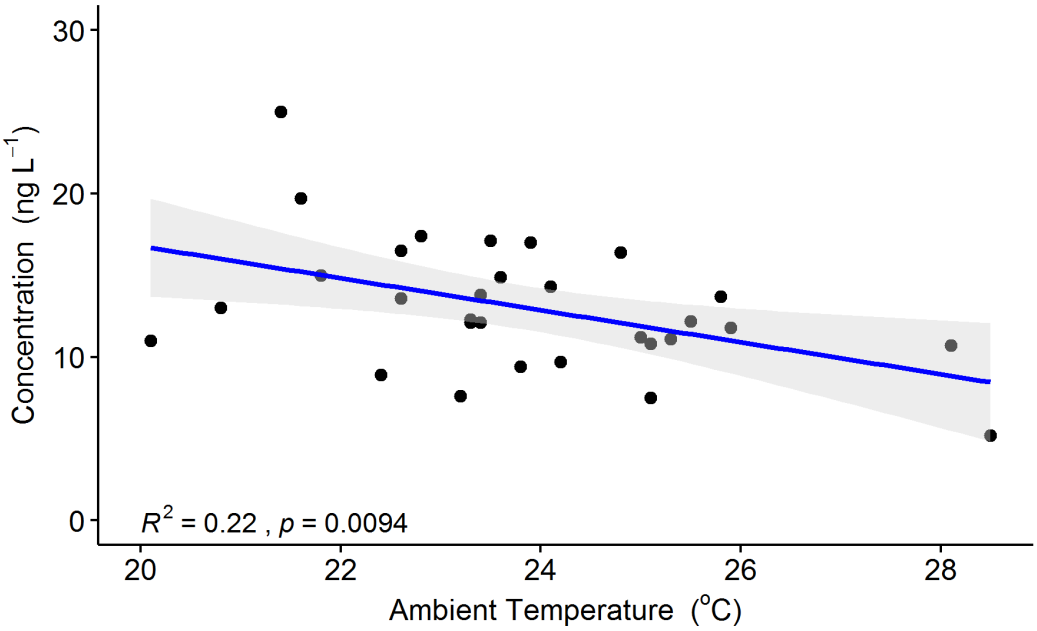

Figure 5-3: Regression plot of geosmin concentration against ambient temperature.

Geosmin was also detected in the settled water and post-sand filtration, although at significantly reduced levels. In all cases, the concentration of GSM was below the MQL (6.4 ng L^{-1}), and in many cases was also below the MDL (2.1 ng L^{-1}). Geosmin was not detected in any samples following GAC filtration, indicating that the current state of the GAC filters is sufficient for removing GSM at these concentration levels. The greatest reduction in the concentration of GSM was noted at the flocculation stage, with an approximate reduction in GSM concentration of

80 %. Note that this is only an estimate in the reduction of GSM at the flocculation stage, as the concentration of GSM was below the MQL on all of the settled water samples, meaning accurate quantitation was not possible. No significant change in GSM concentration was noted during sand filtration, while all remaining GSM was removed during GAC filtration.

As a large proportion of GSM was removed during flocculation, it raises some questions as to how GSM, and likely 2-MIB, are partitioned within natural waters. As the flocculation stage is designed to precipitate colloidal material and is particularly effective for large, hydrophobic compounds like humic substances, this could imply that GSM and 2-MIB are strongly associated with such components. As these classes of compounds are significantly removed during flocculation, it is possible that small, trace level molecules that are strongly associated with the hydrophobic fraction of suspended and dissolved organic matter are precipitated along with them. The hydrophobic nature of GSM and 2-MIB is illustrated by how effectively they are extracted from the aqueous phase during sample preparation with *n*-hexane. Further, as the extraction method used here included the addition of salt, it is likely that any GSM and 2-MIB that is associated with bacterial cells is released during the extraction process. While this GSM and 2-MIB would not be present in water as free dissolved molecules, the majority would also be precipitated during the flocculation and settling stage.

5.1.2 Adsorption Isotherms

5.1.2.1 Experimental

Adsorption experiments were carried out on GAC media collected from the pilot column as the same time as dosing experiments. This was carried out to assess the adsorption capacity of the GAC after 12 months of operation and to obtain adsorption parameters for the current state of the GAC media that could be used for modelling of GSM and 2-MIB concentrations within the GAC filter.

5.1.2.1.1 Chemicals and Reagents

GSM, 2-MIB (Certified Reference Materials; CRMs) and 1-adamantanol (1-ADML; internal standard) were purchased from Sigma-Aldrich (Auckland, New Zealand). Spectroscopy grade *n*-hexane was also purchased from Sigma-Aldrich (Auckland, New Zealand). De-ionised water was prepared using a Barnstead E-Pure water purification system with a resistivity of 18 Ω (Thermo Fisher Scientific, New Zealand). Activated carbon (GA1000N 8 x 30 mesh) used in the pilot column was supplied by Activated Carbon Technologies Ltd. (Wellington, New Zealand).

5.1.2.1.2 Method

Mixed solutions of GSM and 2-MIB were prepared at a range of concentrations (100, 250, 500, 1000 and 2000 ng L^{-1}) in DI water and an aliquot (50 mL) was transferred to a conical flask in duplicate. Each flask was spiked with GAC (20 mg L^{-1}), sealed, mixed and transferred to an incubator (15 ^{o}C). Flasks were kept at 15^{o}C for 7 days with daily mixing prior to analysis by VALLME-GCMS.

Adsorption parameters were estimated for Freundlich and Langmuir isotherms from **Equations 5-1** and **5-2**.

$$C_s^* = KC^{*n} \quad (5\text{-}1)$$

where; C_s^* = Equilibrium solid phase analyte concentration (ng cm^{-3})
C^* = Equilibrium liquid phase analyte concentration (ng cm^{-3})
K = Freundlich equilibrium constant ((ng cm^{-1}) (cm^3 ng $^{-1})^n$))
n = Freundlich factor

$$C_s^* = \frac{QbC^*}{1 + bC^*} \quad (5\text{-}2)$$

where; C_s^* = Equilibrium solid phase analyte concentration (ng cm^{-3})
C^* = Equilibrium liquid phase analyte concentration (ng cm^{-3})
Q = Adsorbate saturation concentration (ng cm^{-3})
b = Langmuir isotherm constant

5.1.2.1.3 Results

Isotherms were fitted using a non-linear least squares algorithm which gave estimations of the adsorption parameters for Langmuir and Freundlich isotherms (**Table 5-1**). Isotherms obtained for 2-MIB and GSM are displayed in **Figure 5-4** and **Figure 5-5**. While the GAC used for these experiments had been in use for approximately 12 months, appreciable adsorption capacity was still clearly evident. As the carbon was dried prior to testing, all biological activity was assumed to have ceased, with the isotherm data representing adsorption processes only. Also, despite the media being partially depleted due to previous use, the saturation point of the GAC was not reached. This was most likely due to the low concentrations of GSM and 2-MIB relative to GAC concentration, albeit much higher than those measured onsite, and the very high surface area of GAC (> 1000 m^2 g^{-1}).

Table 5-1: Langmuir and Freundlich isotherm parameters for GSM and 2-MIB at 15° C

	Langmuir			Freundlich	
	GSM	2-MIB		GSM	2-MIB
Q	4.28×10^5	4.31×10^5	K	1.43×10^6	4.36×10^5
b	28.85	2.989	n	0.5956	0.6676
R^2	0.9850	0.9933	R^2	0.9740	0.9869
RSE	1.84×10^4	1.02×10^4	RSE	2.45×10^4	1.17×10^4

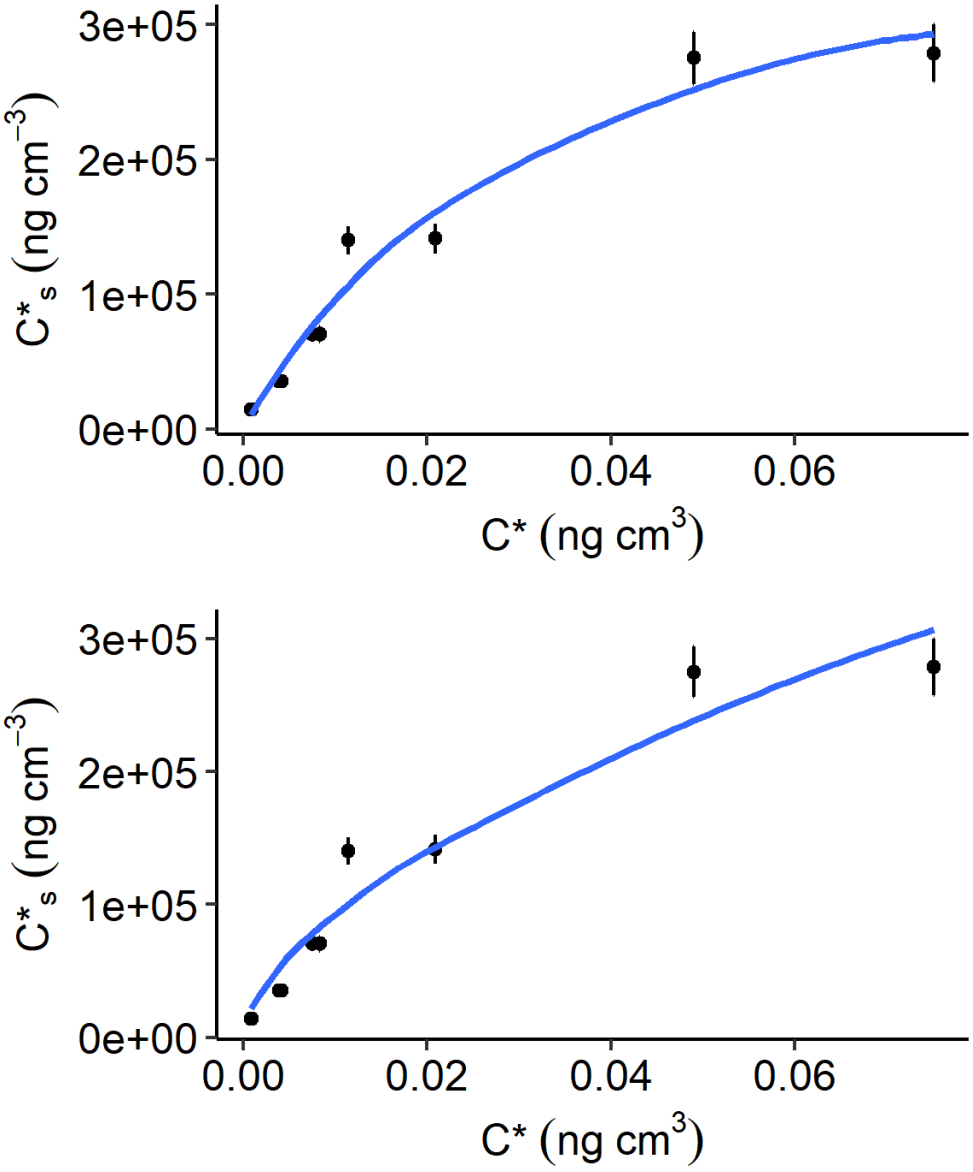

Figure 5-4: Langmuir (top) and Freundlich (bottom) isotherms for GSM at 15° C

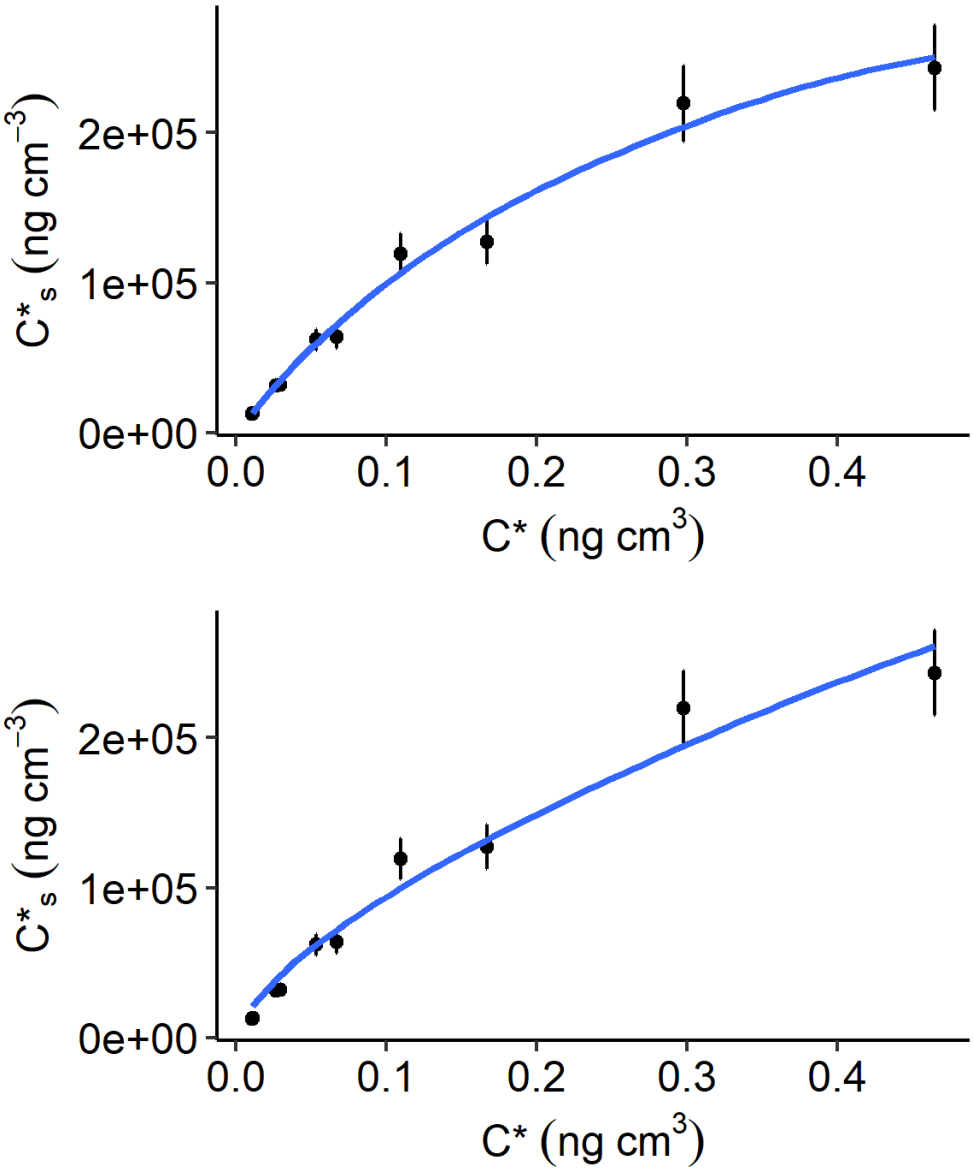

Figure 5-5: Langmuir (top) and Freundlich (bottom) isotherms for 2-MIB at 15° C

The data indicated that adsorption was more favourable for GSM than 2-MIB, with GSM having higher *b* and lower *n* values for the Langmuir and Freundlich models respectively. The Langmuir model appeared to fit the data better, giving higher R^2 and lower *RSE* values than the respective Freundlich model. The adsorbate saturation concentration was also estimated to still be relatively high compared to typical environmental concentrations of GSM and 2-MIB, despite the media having been in use for approximately 12 months. Based on the Langmuir model, the

monolayer saturation concentration of the filter media was approximately 500,000 ng cm^{-3} GAC for each analyte (≈ 1.5 mg g^{-1} GAC). While this indicates that the filter medium is still capable of adsorbing a large quantity of either GSM of 2-MIB, this assumes only a single analyte is present. In practice, adsorption sites will be depleted by other compounds present in the source water that compete for adsorption sites which will mean that the saturation capacity will be reached at a lower concentration than indicated by this isotherm data.

5.1.3 Pilot Scale Dosing Experiments

Dosing experiments were carried out on a pilot scale GAC column installed on-site at the HWTS in order to model the performance of the full-scale GAC filters under the conditions of a high concentration GSM and 2-MIB event. The column was installed in early 2018 and run for approximately 12 months in order to somewhat deplete the adsorption capacity of the GAC media and allow bacterial colonisation to occur. Signs of bacterial growth were noted in SEM images acquired approximately 3 months after commissioning the column (**Figure 5-6**). As such, 12 months was deemed ample time to allow a stable bacterial population to develop.

While some unavoidable interruptions in the operation of the GAC occurred during this time (pump issues, electrical faults etc.), the filter bed was kept submerged at all times and not allowed to dry.

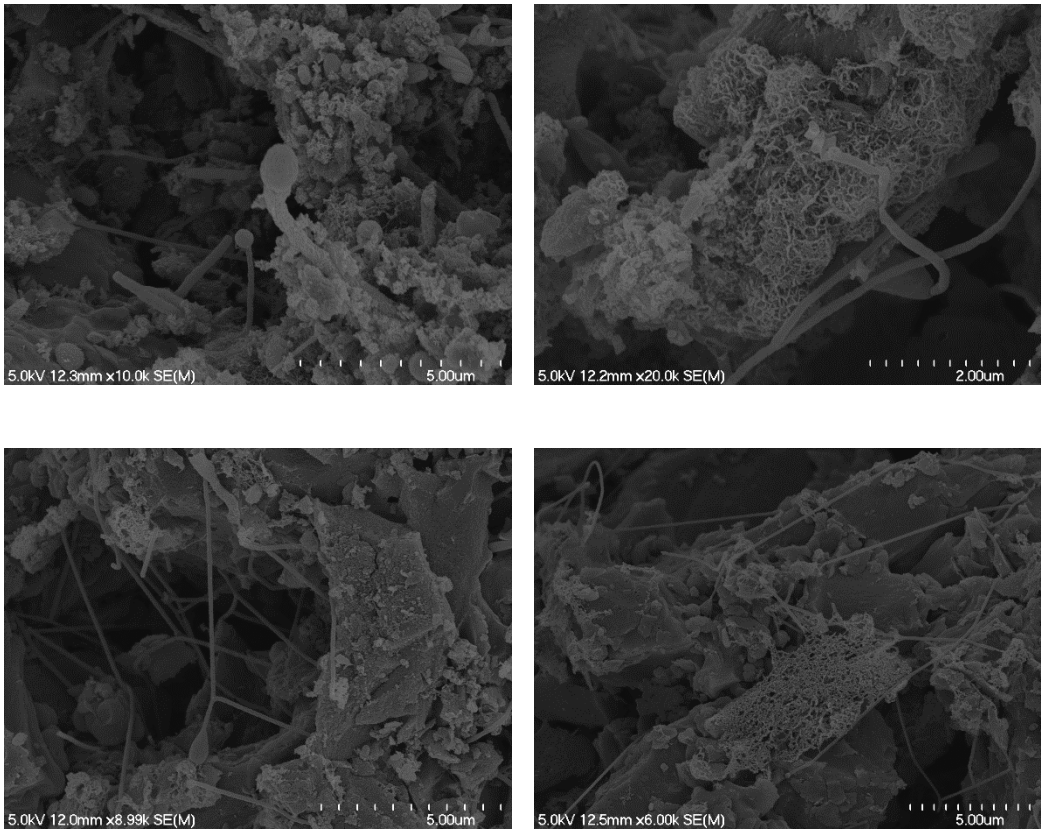

Figure 5-6: SEM images of pilot column filter media after approximately 3 months.

5.1.3.1 Column Design and Operating Parameters

The pilot filter was constructed of square 316 stainless steel tube (0.1 x 0.1 m) sections (4 x 1m and 1 x 0.5 m; 4.5 m total length) bolted together and sealed with NBR (acrylonitrile butadiene rubber) gaskets. The column was packed to a depth of 180 cm with 15 L of fresh GAC (GA1000N 8 x 30 mesh; Activated Carbon Technologies Ltd; Wellington, New Zealand) supported upon a perforated PMMA (poly(methyl methacrylate)) grate and graded gravel and sand (30 cm). Sampling ports were installed at 10 cm intervals along the depth of the filter media (0 - 180 cm depth). The column was fed with source water diverted from the full-scale GAC filters via a peristaltic pump and operated with an EBCT of 15 min (1.0 ± 0.1 L min^{-1}). The column was also fitted to a backwashing system comprising

of a centrifugal pump connected to a variable speed drive (VSD) that was fed from a continuously replenished reservoir fed from the influent water system. During experimental work, the column was backwashed at 2-week intervals at a rate of approximately 8 L min^{-1} to yield a bed expansion of 20 - 25 %.

The dosing system consisted of a constant flow HPLC pump fed from a glass reservoir containing a stock solution of GSM and 2-MIB (50 µg L^{-1} each) delivered to the influent water at a rate of up to 4 mL min^{-1}, yielding a maximum dosing concentration of 200 ng L^{-1}.

A simplified diagram illustrating the experimental set up of the pilot column is presented in **Figure 5-7**. More detailed measurements and design images can be found in **Appendix A-2**.

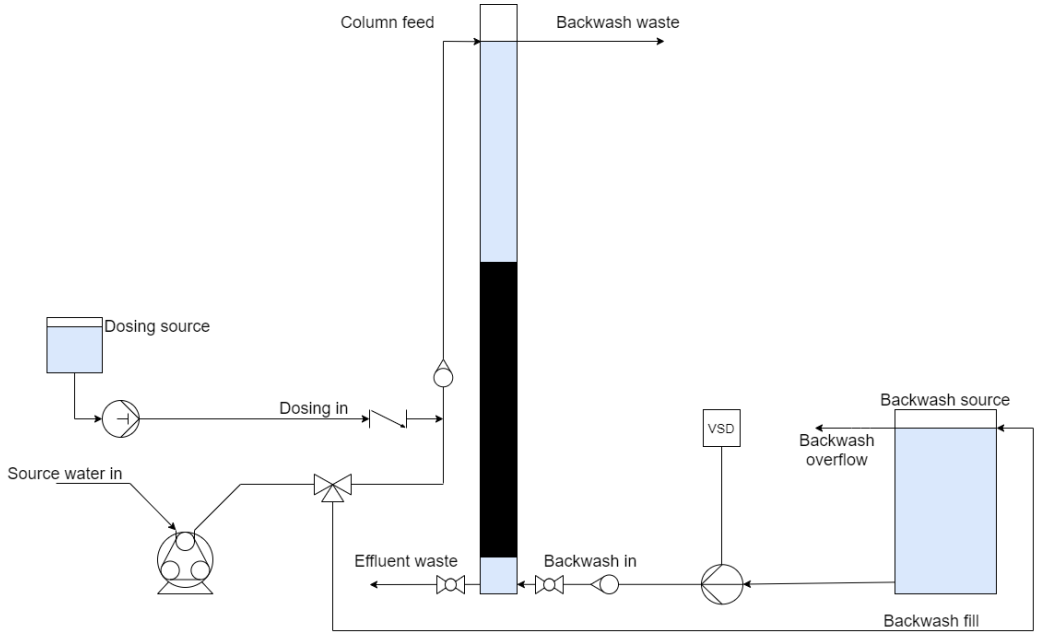

Figure 5-7: Diagram illustrating the experimental setup of the pilot scale GAC filter column.

5.1.3.2 Dosing regime and sampling

The flow rate of the dosing pump was increased at steady rate (0.2 mL min^{-1} min^{-1}) until the required flow rate was reached in order to achieve the target dosing concentration. After the maximum flow rate was reached, the concentration of 2-MIB and GSM was allowed to equilibrate (15 min = EBCT) to allow the spiked analytes to be transported though the delivery system and distributed throughout the column media. Samples were collected from each sampling point along the depth of the filter bed (50 mL per sample) at two intervals following the stabilisation of the 2-MIB and GSM concentration (EBCT + 0 and + 30 min). Samples were stored on ice prior to being transported to the laboratory where they were analysed immediately or frozen (-18 ºC) for later analysis. The experiment was carried out at initial 2-MIB and GSM concentrations of 50 and 150 ng L^{-1}.

5.1.3.3 Modelling

5.1.3.3.1 Model Formulation

The concentration of 2-MIB and GSM through the depth of the filter column was modelled in *R* to solve a system of delay differential equations (DDEs) for the liquid and solid phase concentration. The equations were derived from the advection-dispersion equation using either Freundlich or Langmuir isotherms with either the pseudo first order (PFO or linear driving force (LDF) equation ***[247,248]***) or pseudo second order (PSO ***[249]***) kinetic adsorption models.

The liquid phase concentration can be described by the advection-dispersion (1D plug-flow axial dispersion) equation which describes the transport of a solute in

saturated porous media and is commonly used for modelling fixed bed adsorption processes ***[250-254]***:

$$\frac{\partial C}{\partial t} = \frac{\partial C}{\partial x}\frac{u}{\varepsilon} + D\frac{\partial^2 C}{\partial x^2} - \frac{\partial C_s}{\partial t}\frac{(1-\varepsilon)}{\varepsilon} \quad (5\text{-}3)$$

where; C = Liquid phase analyte concentration (ng cm^{-3})
C_s = Solid phase analyte concentration (ng cm^{-3})
x = Depth (cm)
ε = Void fraction of the filter medium
u = Velocity (cm min^{-1})

By modelling the column as a series of well mixed tanks with a constant influent concentration, the dispersion term is accounted for and **Equation 5-3** can be simplified:

$$D\frac{\partial^2 C}{\partial x^2} = 0 \quad (5\text{-}4)$$

$$\frac{\partial C}{\partial t} = \frac{\partial C}{\partial x}\frac{u}{\varepsilon} - \frac{\partial C_s}{\partial t}\frac{(1-\varepsilon)}{\varepsilon} \quad (5\text{-}5)$$

Considering the pilot column as a series of *i* stages of height *x*, the change in liquid phase concentration across each stage can be approximated by the difference **Equation 5-6** for sufficiently small values of *x*:

$$\frac{dC}{dx} = (C_{i-1} - C_i)\frac{u}{\Delta x \varepsilon} \quad (5\text{-}6)$$

$$u = \frac{Q}{A} \quad (5\text{-}7)$$

$$\frac{dC}{dt} = (C_{i-1} - C_i)\frac{Q}{\mathrm{A}\Delta x \varepsilon} - \frac{dC_s}{dt}\frac{(1-\varepsilon)}{\varepsilon} \quad (5\text{-}8)$$

where; Q = Volumetric flow rate (cm^3 min^{-1})
A = Cross sectional area (cm^2)
Height of the *i*th stage (cm)

$\Delta x =$

The solid phase concentration can be derived from the PFO or PSO kinetic adsorption models and either the Freundlich or Langmuir isotherms:

Freundlich isotherm and PFO kinetics:

$$C_s^* = KC^{*n} \tag{5-9}$$

$$\frac{dC_s}{dt} = k_1(C_s^* - C_s) = k_1(KC_i{}^n - C_s) \tag{5-10}$$

where; C_s^* = Equilibrium solid phase analyte concentration (ng cm^{-3})
C^* = Equilibrium liquid phase analyte concentration (ng cm^{-3})
k_1 = Pseudo first order rate constant (min $^{-1}$)

Freundlich isotherm and PSO kinetics:

$$C_s^* = KC^{*n} \tag{5-11}$$

$$\frac{dC_s}{dt} = k_2(C_s^* - C_s)^2 = k_2(KC_i{}^n - C_s)^2 \tag{5-12}$$

where; k_2 = Pseudo second order rate constant (cm^3 ng^{-1} min $^{-1}$)

Langmuir isotherm and PFO kinetics:

$$C_s^* = \frac{QbC^*}{1 + bC^*} \tag{5-13}$$

$$\frac{dC_s}{dt} = k_1(C_s^* - C_s) = k_1\left(\frac{QbC_i}{1 + bC_i} - C_s\right) \tag{5-14}$$

where; Q = Adsorbate saturation concentration (ng cm^3)
b = Langmuir isotherm constant

Langmuir isotherm and PSO kinetics:

$$C_s^* = \frac{QbC^*}{1 + bC^*} \tag{5-15}$$

$$\frac{dC_s}{dt} = k_2(C_s^* - C_s)^2 = k_2\left(\frac{QbC_i}{1+bC_i} - C_s\right)^2 \quad (5\text{-}16)$$

where; k_2 = Pseudo second order rate constant ($cm^3\ ng^{-1}\ min^{-1}$)

Equations 5-10, 5-12, 5-14 and **5-16** can be substituted into **Equation 5-8** to give the following equations:

Freundlich PFO model:

$$\frac{dC}{dt} = (C_{i-1} - C_i)\frac{Q}{A\Delta x\varepsilon} - k_1(KC_i^{\,n} - C_s)\frac{(1-\varepsilon)}{\varepsilon} \quad (5\text{-}17)$$

Freundlich PSO model:

$$\frac{dC}{dt} = (C_{i-1} - C_i)\frac{Q}{A\Delta x\varepsilon} - k_2(KC_i^{\,n} - C_s)^2\frac{(1-\varepsilon)}{\varepsilon} \quad (5\text{-}18)$$

Langmuir PFO model:

$$\frac{dC}{dt} = (C_{i-1} - C_i)\frac{Q}{A\Delta x\varepsilon} - k_1\left(\frac{QbC_i}{1+bC_i} - C_s\right)\frac{(1-\varepsilon)}{\varepsilon} \quad (5\text{-}19)$$

Langmuir PSO model:

$$\frac{dC}{dt} = (C_{i-1} - C_i)\frac{Q}{A\Delta x\varepsilon} - k_2\left(\frac{QbC_i}{1+bC_i} - C_s\right)^2\frac{(1-\varepsilon)}{\varepsilon} \quad (5\text{-}20)$$

Equations 5-17 to **5-20** were modelled in *R* using the *R* package deSolve, which includes a range of solvers for initial value problems of specific classes of differential equations such as ordinary differential equations (ODEs), differential algebraic equations (DAEs), and delay differential equations (DDEs) ***[251,252,255]***. Models were fitted to the data collected from the pilot column and parameters were

estimated using the *R* package FME ***[256]***. Fitting was performed on data points that were present at concentrations above the MQL of the GC-MS method to ensure that the model was fitted to accurate data points. An example of the *R* code can be found in **Appendix A-2.**

5.1.3.4 Results and Discussion

5.1.3.4.1 Dosing Experiments

At both concentration levels, the pilot column was able to successfully remove GSM to concentrations below the MDL (2.1 ng L^{-1}). At an influent concentration of ≈ 150 ng L^{-1}, GSM was reduced to below the MDL within the top 50 cm of the filter bed, while at ≈ 50 ng L^{-1} the concentration was reduced to below the MDL within the top 40 cm.

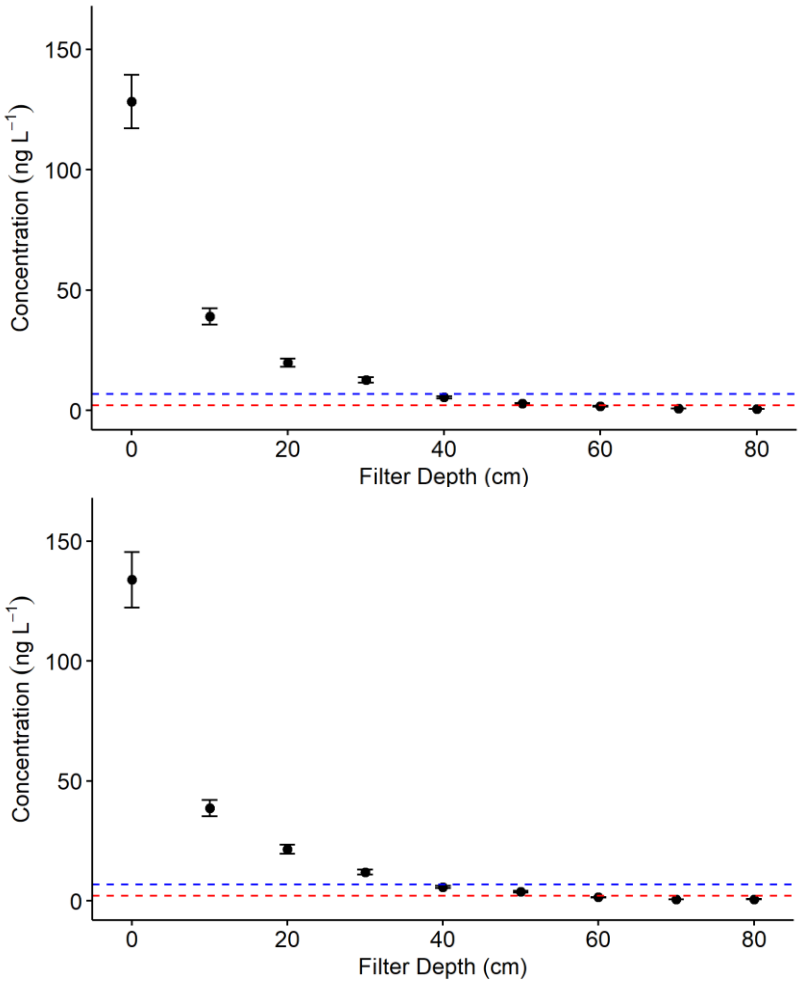

Figure 5-8: GSM concentration through the depth of the filter media at an influent concentration of 150 ng L^{-1} at t = 0 min (top) and t = 30 min (bottom). Error bars = SD. Note: --- indicates the MQL and --- indicates the MDL.

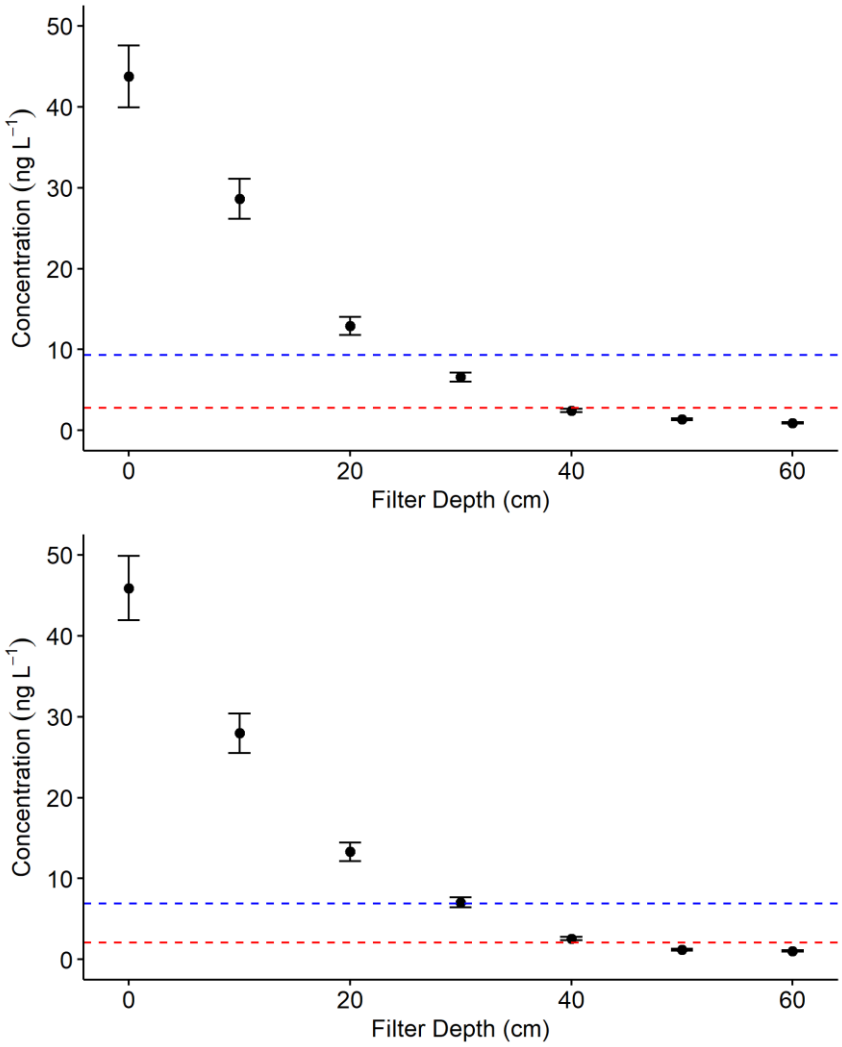

Figure 5-9: GSM concentration through the depth of the filter media at an influent concentration of 50 ng L^{-1} at t = 0 min (top) and t = 30 min (bottom). Error bars = SD. Note: --- indicates the MQL and --- indicates the MDL.

Similar results were also obtained for 2-MIB, although more residence time was required to achieve a similar level of removal. At ≈ 150 ng L^{-1}, 2-MIB was reduced to below the MDL in the top 90 cm of the filter bed, while at ≈ 50 ng L^{-1} it was reduced to below the MDL in the top 60 cm. These concentrations are much higher than would be normally encountered and were used in order to simulate a transient, high concentration event.

Taking into account the percentage of 2-MIB and GSM removed at the flocculation stage (≈ 80 %), the doses tested in these experiments would equate source water

concentrations of approximately 250 and 750 ng L^{-1}; 10 to 100 times the concentrations found in the analysis of river water samples (**Section 5.1.1.2**). These results indicate that the GAC filters are sufficient for removing 2-MIB and GSM even at relatively high concentrations.

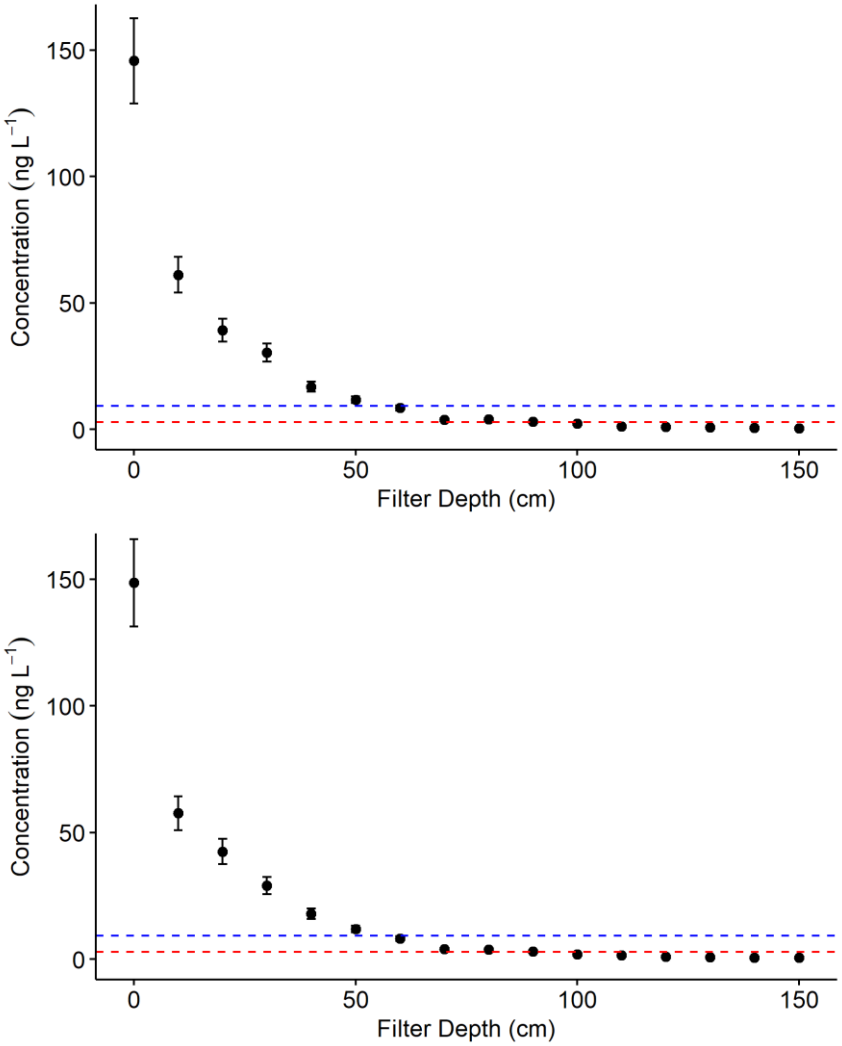

Figure 5-: 2-MIB concentration through the depth of the filter media at an influent concentration of 150 ng L^{-1} at t = 0 min (top) and t = 30 min (bottom). Error bars = SD. Note: --- indicates the MQL and --- indicates the MDL.

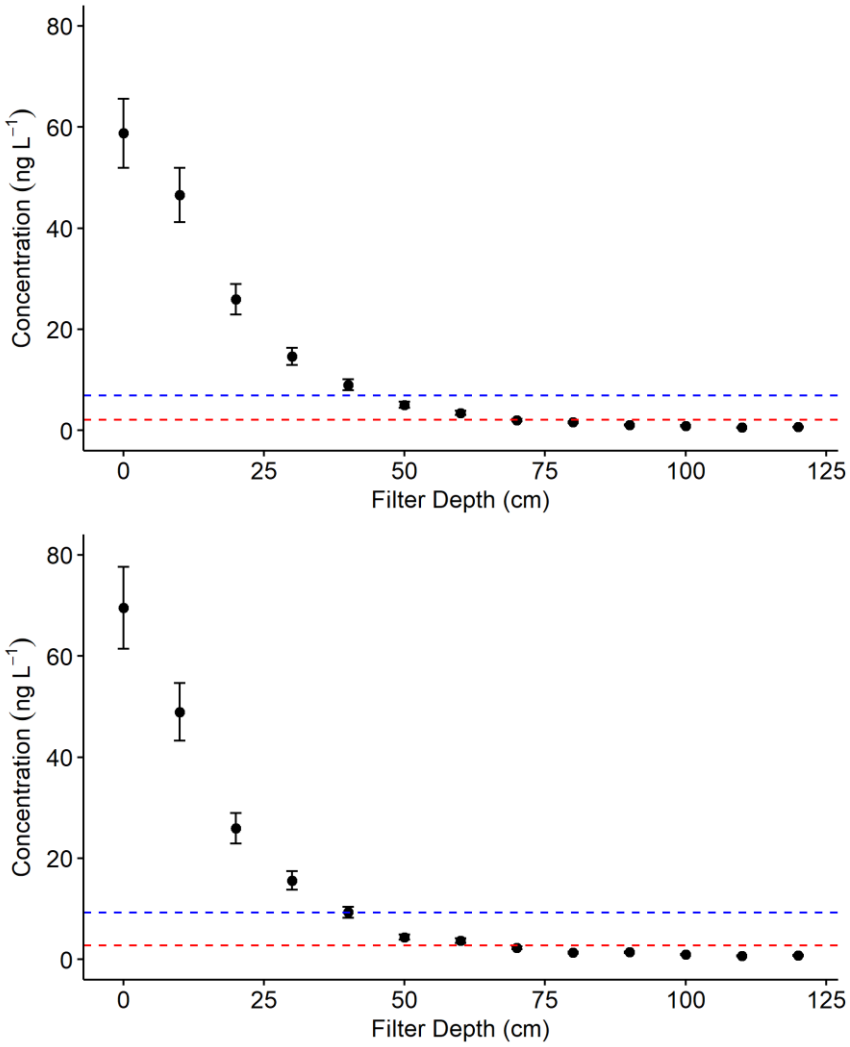

Figure 5-10: 2-MIB concentration through the depth of the filter media at an influent concentration of 50 ng L^{-1} at t = 0 min (top) and t = 30 min (bottom). Error bars = SD. Note: --- indicates the MQL and --- indicates the MDL.

There was also no difference between samples collected at t = 0 and t = 30 mins following column stabilisation (**Figure 5-11**, **Figure 5-12**), with very similar trend in removal being observed for both groups for both GSM and 2-MIB. This suggested that there was no lag time associated with a sudden increase in 2-MIB and GSM concentration with respect to removal efficiency.

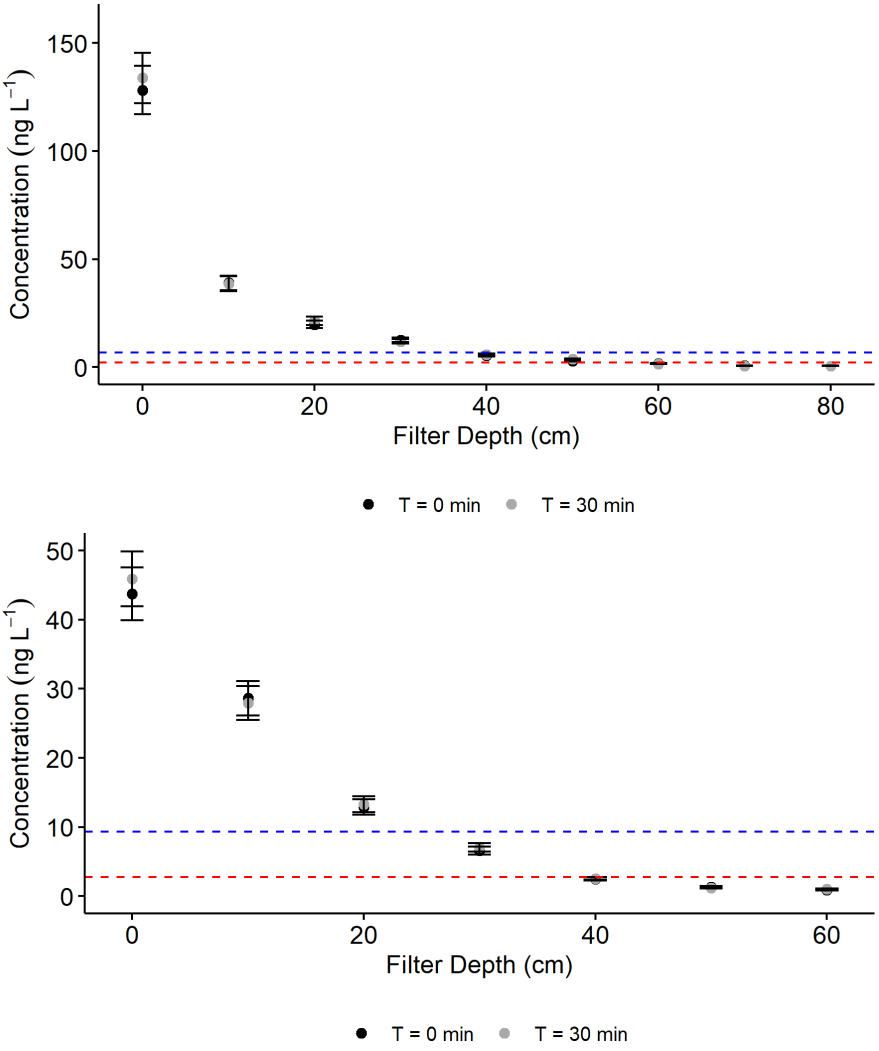

Figure 5-11: Comparison of GSM concentrations through the depth of the filter media at t = 0 min and t = 30 min at influent concentrations of 150 ng L^{-1} (top) and 50 ng L^{-1} (bottom). Error bars = SD. Note: --- indicates the MQL and --- indicates the MDL.

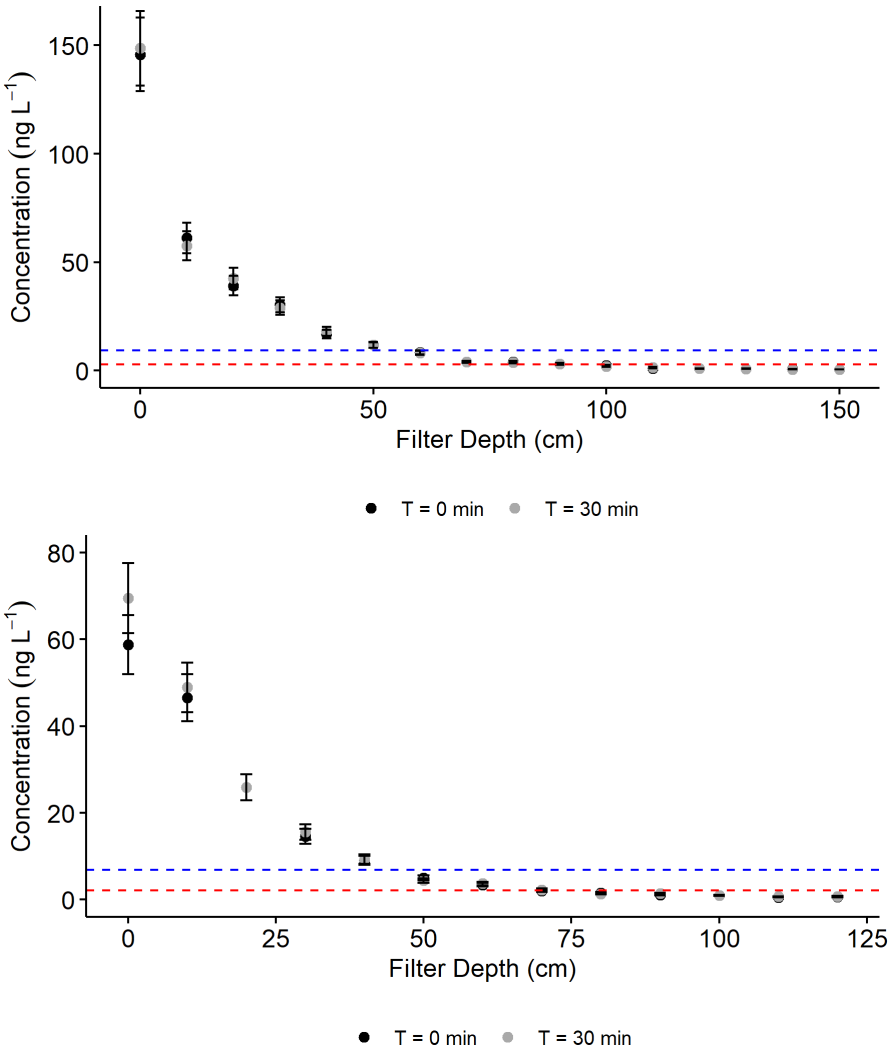

Figure 5-12: Comparison of 2-MIB concentrations through the depth of the filter media at t = 0 min and t = 30 min at influent concentrations of 150 ng L^{-1} (top) and 50 ng L^{-1} (bottom). Error bars = SD. Note: --- indicates the MQL and --- indicates the MDL.

The high removal efficiency, alongside the isotherm data also suggests that significant adsorption sites remain available even after approximately 12 months of operation. The slower rate of 2-MIB removal relative to GSM is likely to be a result of GSM being more hydrophobic than 2-MIB, causing it to diffuse from the liquid to solid phase more slowly than GSM ***[244]***. Furthermore, the biodegradation products of 2-MIB are all norbornyl derivatives, which all exhibit the characteristic m/z 95 norbornyl cation in their EI mass spectrum (**Figure 5-13**, **Figure 5-14**).

Major biodegradation products of 2-MIB include camphor and borneol, both of which can be detected by the GC-MS method used (**Figure 5-15**).

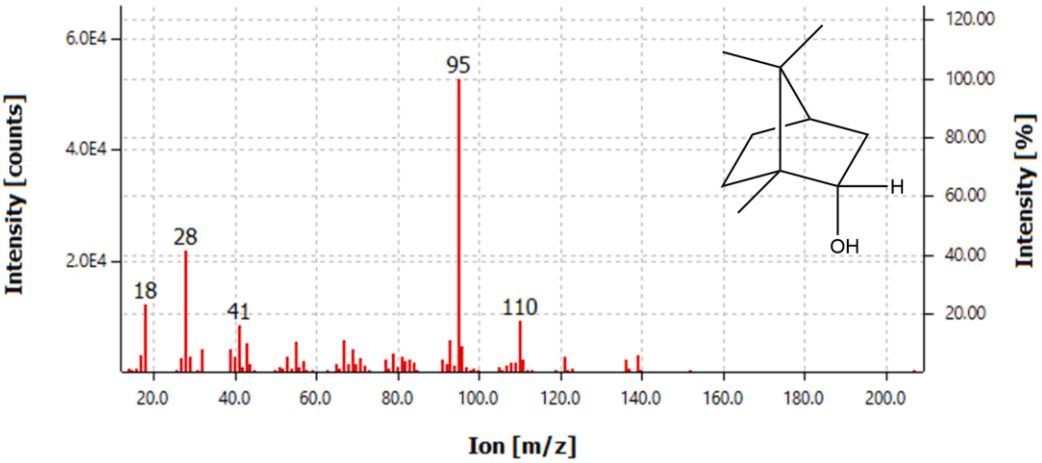

Figure 5-13: EI-MS spectrum of borneol showing the characteristic m/z 95 norbornyl ion.

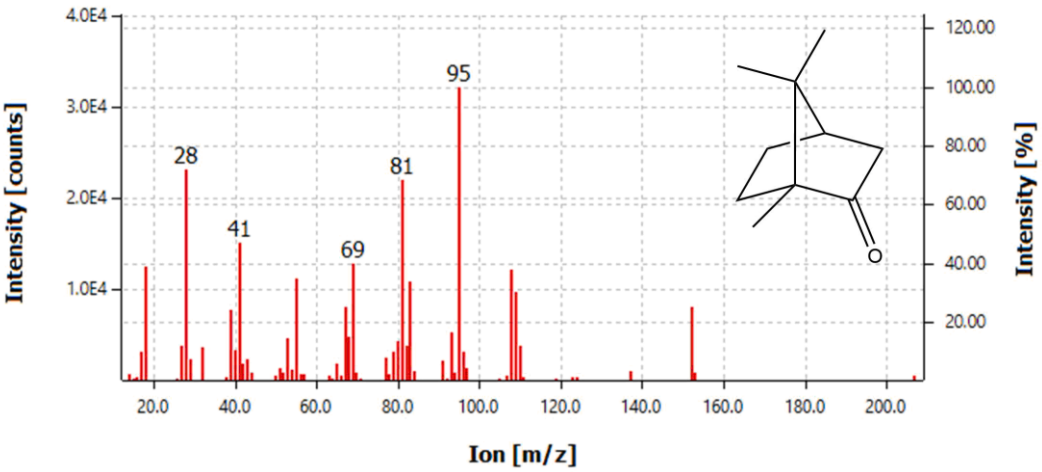

Figure 5-14: EI-MS spectrum of camphor showing the characteristic m/z 95 norbornyl ion.

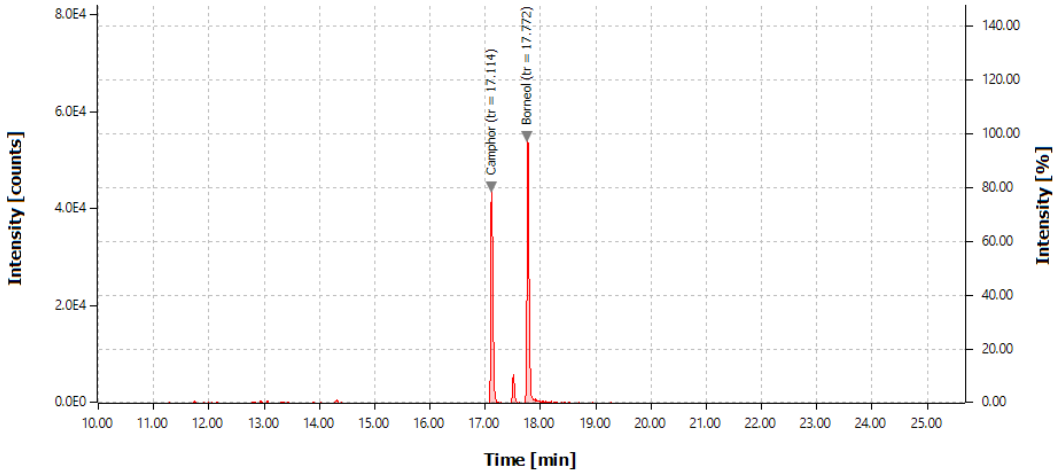

Figure 5-15: GC-MS chromatogram of camphor (t_r = 17.114 min) and borneol (t_r = 17.772 min) standards.

Neither camphor nor borneol were detected in increasing amounts as the concentration of 2-MIB decreased through the column, even though it might be expected that the transformation of 2-MIB to borneol or camphor would be associated with an increase in the observed chromatogram peak area for each degradation product as the peak area of 2-MIB decreased. This effect was not observed at either the 50 ng L^{-1} or 150 ng L^{-1} levels or at the t = 0 min or t = 30 min levels. Additionally, no other GC-MS signals exhibiting the m/z 95 ion were observed in increasing amounts through the depth of the filter in any of the samples. However, as the filter media was shown to exhibit considerable adsorption capacity, biodegradation products may have been re-adsorbed to the GAC and would therefore not be detected in the GC-MS water extracts. Also, if a large suite of biodegradation products is produced, each individual compound may be at concentrations too low to detect.

The filter seemed to preferentially remove GSM over 2-MIB, as evidenced by the lower residence time required to reduce GSM to levels below the MDL and the more favourable isotherm data for GSM. As such, it is expected that breakthrough

of 2-MIB would occur before GSM, both in terms of an unusually high concentration of 2-MIB in the source water and over time with the associated depletion of adsorptive sites.

5.1.3.4.2 Modelling

Models were evaluated for each analyte at each concentration level for each isotherm type and kinetic model to give 16 models in total. Estimated values for the rate constants k_1 (PFO models) and k_2 (PSO models) and their respective model fit output are given in **Table 5-2.**

Table 5-2: Estimated rate constants and model fit values for GSM and 2-MIB models with PFO and PSO kinetics.

Dataset	Isotherm	Kinetics	k_1 (min^{-1})	k_2 ($cm^3\ ng^{-1}\ min^{-1}$)	*RSE*	*SSR*
GSM 0.15 ng cm^{-3}	Freundlich	PFO	1.4×10^{-6}	-	1.0×10^{-2}	7.6×10^{-4}
GSM 0.15 ng cm^{-3}	Freundlich	PSO	-	4.5×10^{-12}	4.6×10^{-3}	1.5×10^{-4}
GSM 0.15 ng cm^{-3}	Langmuir	PFO	1.5×10^{-6}	-	1.1×10^{-2}	9.1×10^{-4}
GSM 0.15 ng cm^{-3}	Langmuir	PSO	-	5.0×10^{-12}	6.6×10^{-3}	3.0×10^{-4}
GSM 0.05 ng cm^{-3}	Freundlich	PFO	4.9×10^{-7}	-	1.2×10^{-3}	9.9×10^{-6}
GSM 0.05 ng cm^{-3}	Freundlich	PSO	-	3.5×10^{-12}	3.1×10^{-3}	6.8×10^{-5}
GSM 0.05 ng cm^{-3}	Langmuir	PFO	4.5×10^{-7}	-	1.1×10^{-3}	8.5×10^{-6}
GSM 0.05 ng cm^{-3}	Langmuir	PSO		2.4×10^{-12}	2.5×10^{-3}	4.3×10^{-5}
2-MIB 0.15 ng cm^{-3}	Freundlich	PFO	3.5×10^{-6}	-	1.3×10^{-2}	2.2×10^{-3}
2-MIB 0.15 ng cm^{-3}	Freundlich	PSO	-	4.2×10^{-11}	5.9×10^{-3}	4.5×10^{-4}
2-MIB 0.15 ng cm^{-3}	Langmuir	PFO	3.5×10^{-6}	-	1.0×10^{-2}	1.4×10^{-3}
2-MIB 0.15 ng cm^{-3}	Langmuir	PSO	-	4.9×10^{-11}	3.7×10^{-3}	1.8×10^{-4}
2-MIB 0.05 ng cm^{-3}	Freundlich	PFO	1.8×10^{-6}	-	3.5×10^{-3}	1.1×10^{-4}
2-MIB 0.05 ng cm^{-3}	Freundlich	PSO	-	3.7×10^{-11}	5.2×10^{-3}	2.5×10^{-4}
2-MIB 0.05 ng cm^{-3}	Langmuir	PFO	2.1×10^{-6}	-	4.0×10^{-3}	1.4×10^{-4}
2-MIB 0.05 ng cm^{-3}	Langmuir	PSO	-	4.7×10^{-11}	6.6×10^{-3}	3.9×10^{-4}

For the GSM 0.15 ng cm^{-3} dataset, the Freundlich PSO model gave the closest fit to the data. A graphical comparison of each model for this dataset is displayed in **Figure 5-16**. As can be seen, the PFO models were found to fit the data poorly in comparison the PSO models.

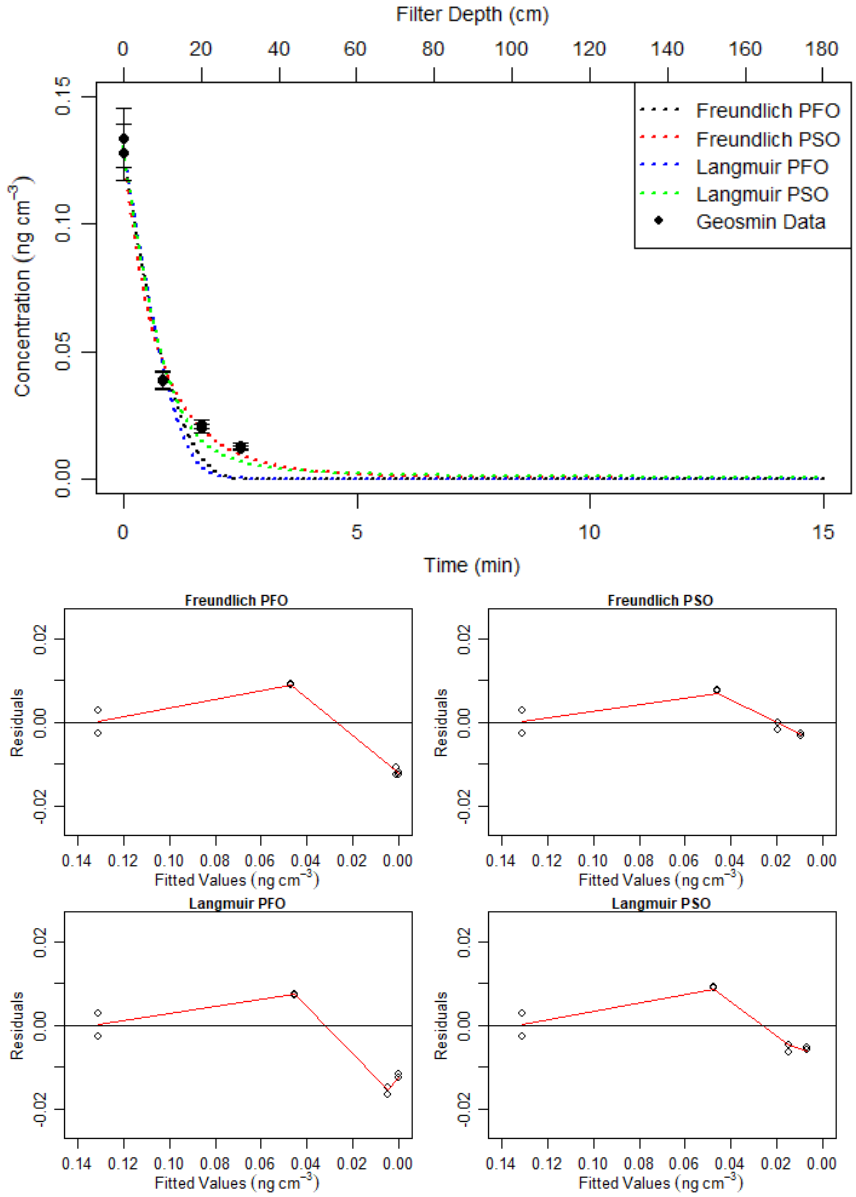

Figure 5-16: Comparison of GSM PFO and PSO models at an influent concentration of approximately 0.15 ng cm^{-3} (top) and corresponding residual plots (bottom).

In contrast, the PFO models were found to fit the lower concentration GSM data (0.05 ng cm^{-3}) data better than the PSO models (**Figure 5-17**). However, unlike the 0.15 ng cm^{-3} data, the Freundlich PSO model also gave an adequate fit to the data. For both the PFO and PSO models, the rate constant was found to be dependent on the initial liquid phase concentration.

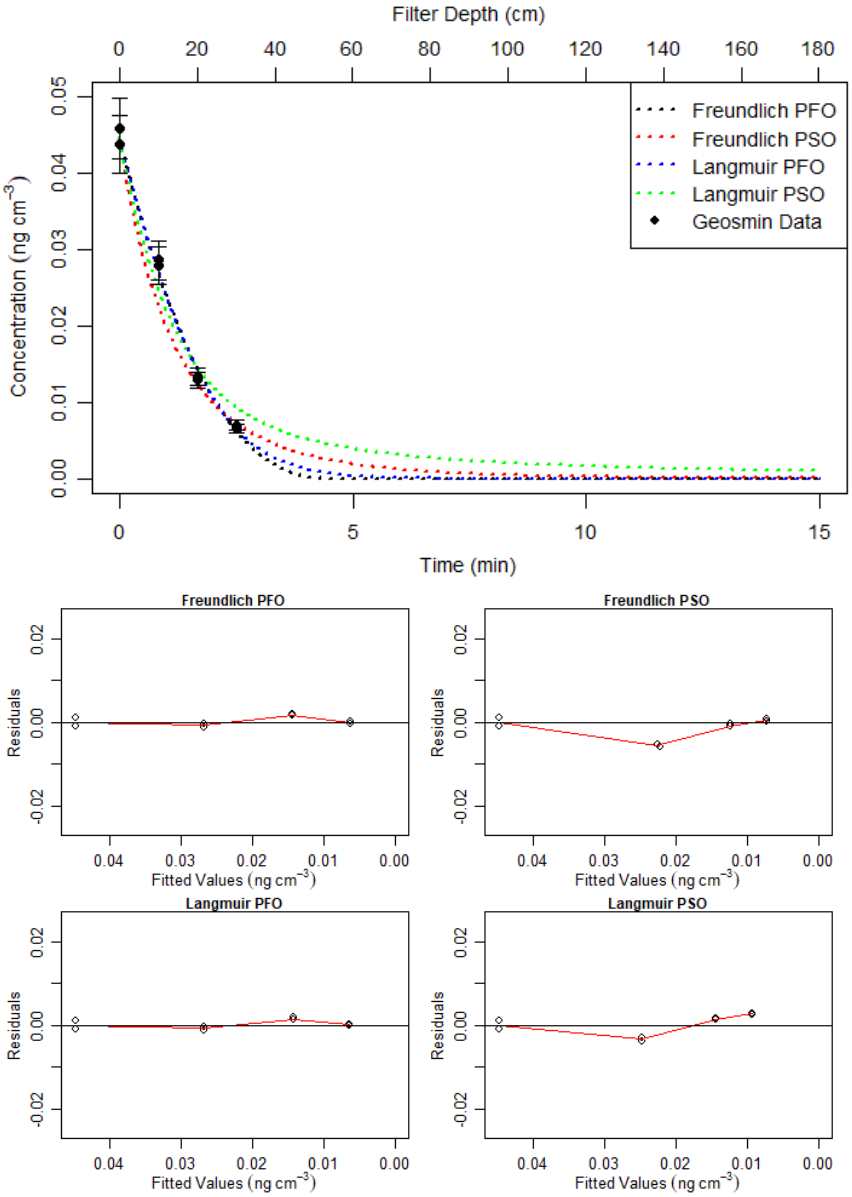

Figure 5-17: Comparison of GSM PFO and PSO models at an influent concentration of approximately 0.05 ng cm^{-3} (top) and corresponding residual plots (bottom).

As with the high concentration GSM models, the Freundlich PSO model was found to fit the high concentration 2-MIB (0.15 ng cm^{-3}) data best (**Figure 5-18**). Also, as noted for the GSM models, the PFO models gave a poor fit to the data for the high concentration data, while the PFO models gave a better fit for the low concentration data (**Figure 5-19**), although the Freundlich PSO also closely fit the data . The rate

constants for 2-MIB were found to be less affected by the initial concentration of 2-MIB than was apparent for GSM.

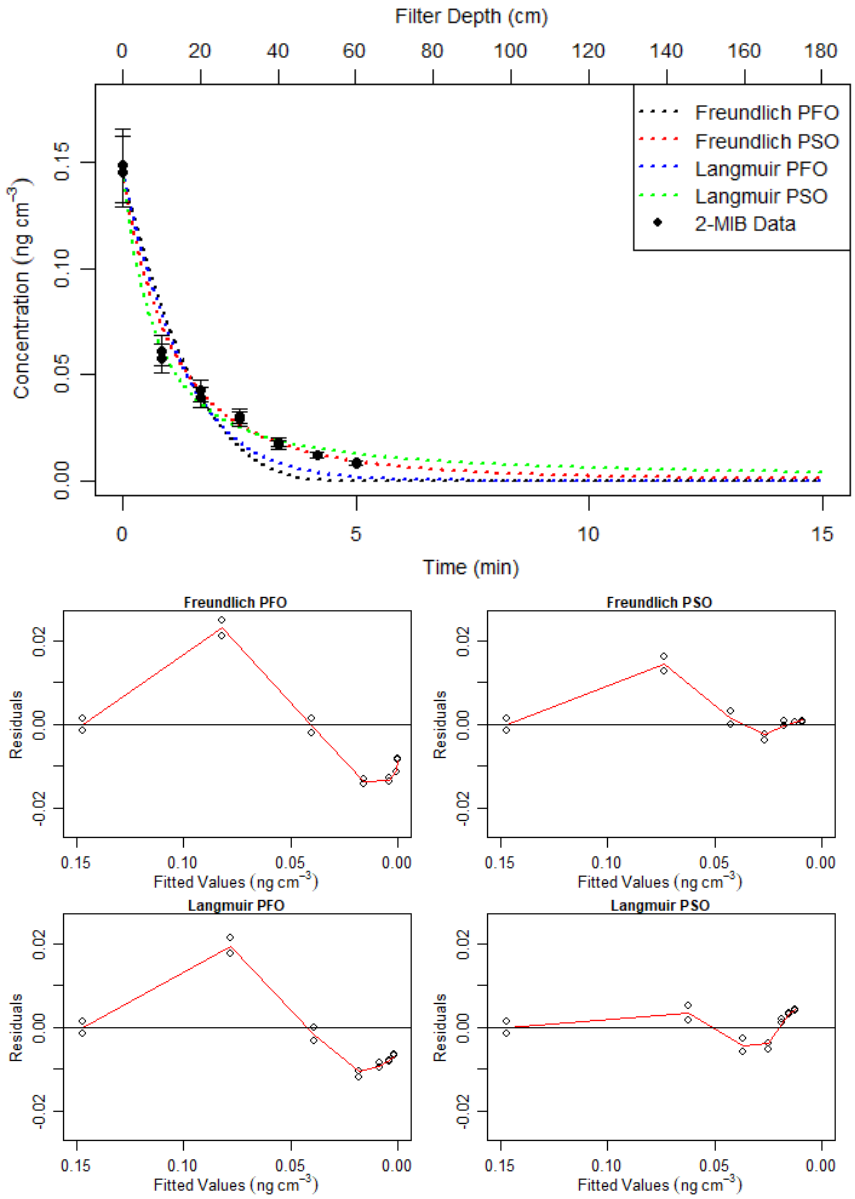

Figure 5-18: Comparison of 2-MIB PFO and PSO models at an influent concentration of approximately 0.15 ng cm^{-3} (top) and corresponding residual plots (bottom).

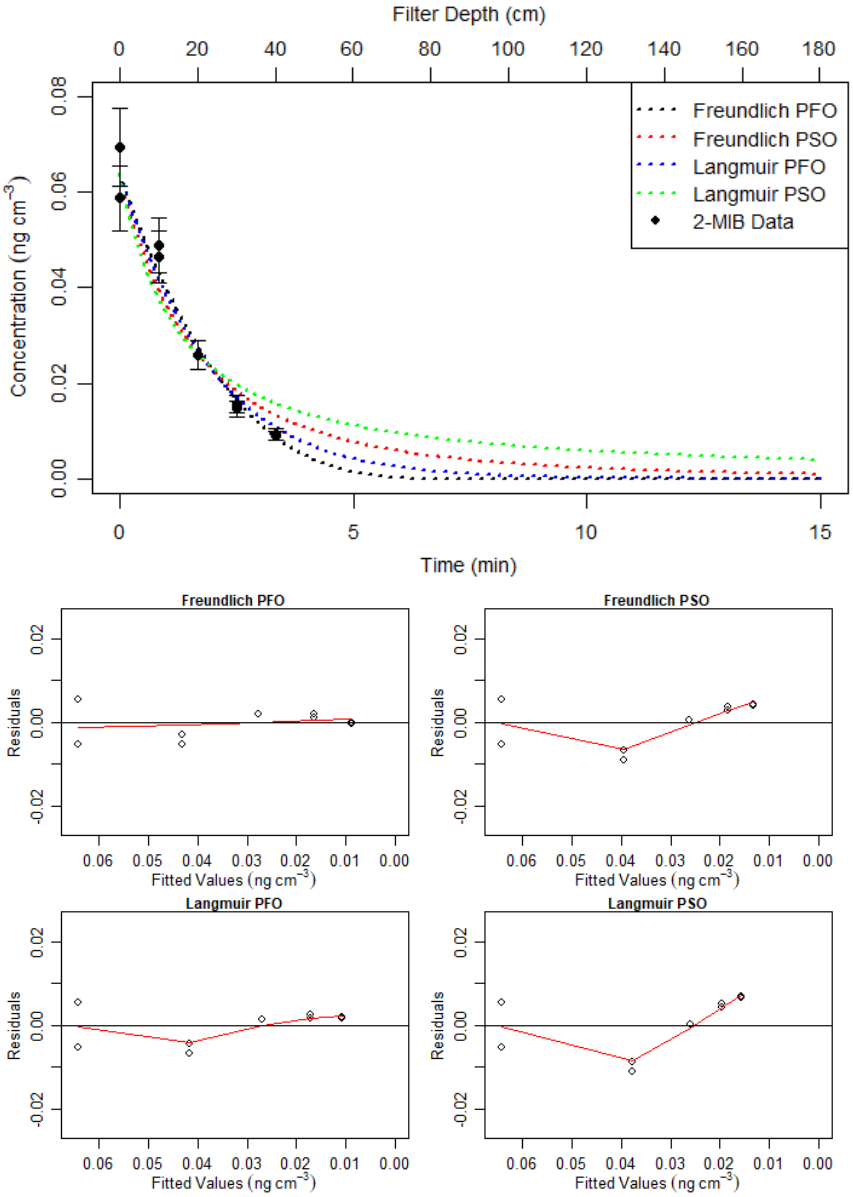

Figure 5-19: Comparison of 2-MIB PFO and PSO models at an influent concentration of approximately 0.05 ng cm^{-3} (top) and corresponding residual plots (bottom).

Due to different kinetic models fitting the different concentration data sets, and the seemingly concentration dependant rate constants, particularly for GSM, the kinetic model was reformulated to include the liquid phase concentration of the analyte in an effort to find a model that would capture the behaviour of each analyte at both concentration levels. This was done by modifying **Equation 5-10** to include the liquid phase concentration to give the second order (SO) rate **Equation 5-21**

[253,254] and assuming that the rate of desorption is negligible or zero. The appropriate isotherm equation can then be substituted as outlined previously (**Section 5.1.3.3.1**).

$$\frac{dC_s}{dt} = k_s C_i (C_s^* - C_s) \quad (5\text{-}21)$$

where; $k_s =$ Second order rate constant ($cm^3\ ng^{-1}\ min^{-1}$)

Estimated values for the rate constants for the second order rate constant for each isotherm type and their respective model fit output are given in **Table 5-3.** As can be seen, the difference in the rate constant between each concentration level were found to be in closer agreement in comparison to the PFO and PSO models.

As with the PFO and PSO models, the Freundlich isotherm was found to give the best fit to the data, although the difference between the two isotherms was minimal when used in conjunction with the SO kinetic model.

Table 5-3: Estimated rate constants and model fit values for GSM and 2-MIB models with second order kinetics.

Dataset	Isotherm	Kinetics	k_s ($cm^3\ ng^{-1}\ min^{-1}$)	*RSE*	SSR
GSM 0.15 ng cm^{-3}	Freundlich	Second order	2.2×10^{-5}	1.7×10^{-3}	1.9×10^{-5}
GSM 0.15 ng cm^{-3}	Langmuir	Second order	2.2×10^{-5}	2.1×10^{-3}	3.1×10^{-5}
GSM 0.05 ng cm^{-3}	Freundlich	Second order	1.9×10^{-5}	3.4×10^{-3}	7.9×10^{-5}
GSM 0.05 ng cm^{-3}	Langmuir	Second order	1.7×10^{-5}	3.4×10^{-3}	8.0×10^{-5}
2-MIB 0.15 ng cm^{-3}	Freundlich	Second order	5.1×10^{-5}	3.4×10^{-3}	1.5×10^{-4}
2-MIB 0.15 ng cm^{-3}	Langmuir	Second order	5.2×10^{-5}	3.8×10^{-3}	1.9×10^{-4}
2-MIB 0.05 ng cm^{-3}	Freundlich	Second order	4.8×10^{-5}	6.2×10^{-3}	3.4×10^{-4}
2-MIB 0.05 ng cm^{-3}	Langmuir	Second order	5.3×10^{-5}	6.8×10^{-3}	4.2×10^{-4}

For the GSM 0.15 ng cm^{-3} data, both the Langmuir and Freundlich isotherms fit the data very well, which is illustrated in **Figure 5-20**. At the 0.05 ng cm^{-3} concentration level, while both isotherms gave similar output, the fit did not capture the data as well, and was found to diverge at low concentrations **Figure 5-21**.

This outcome was similar to what was found for the PSO kinetic model, however, as the rate constant between concentration levels was found to similar, the SO model may be of more use for predicting behaviour at different concentration levels.

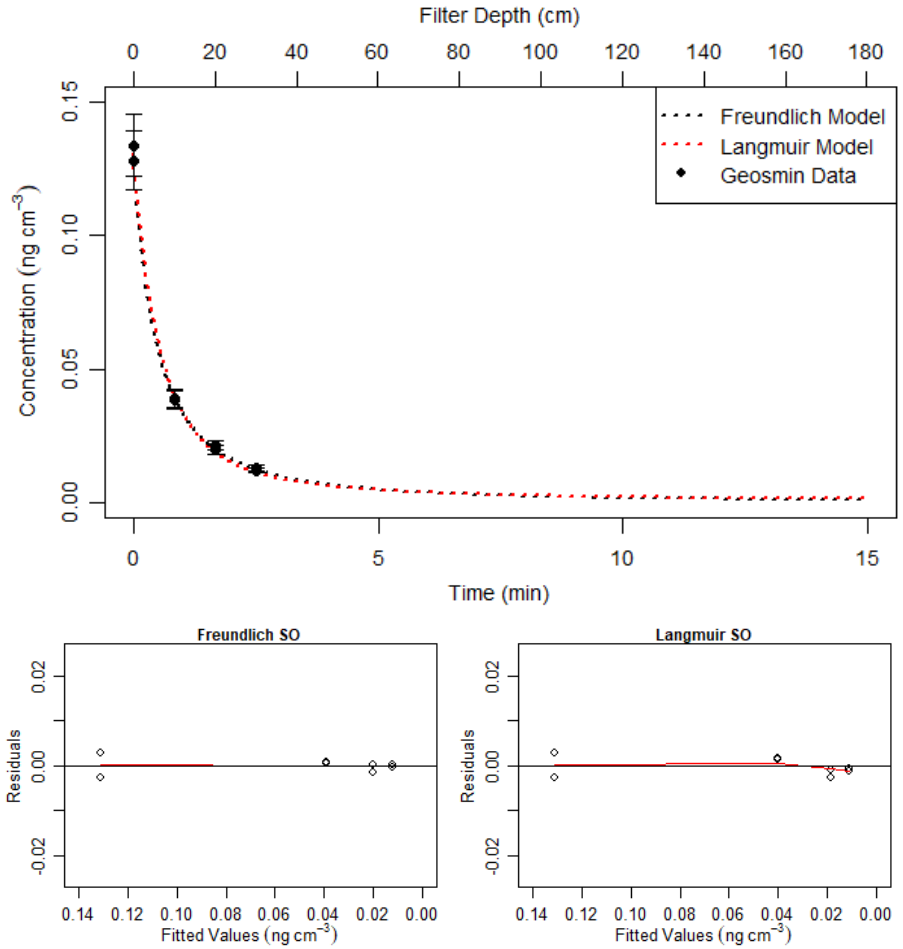

Figure 5-20: Comparison of GSM SO models at an influent concentration of approximately 0.15 ng cm^{-3} (top) and corresponding residual plots (bottom).

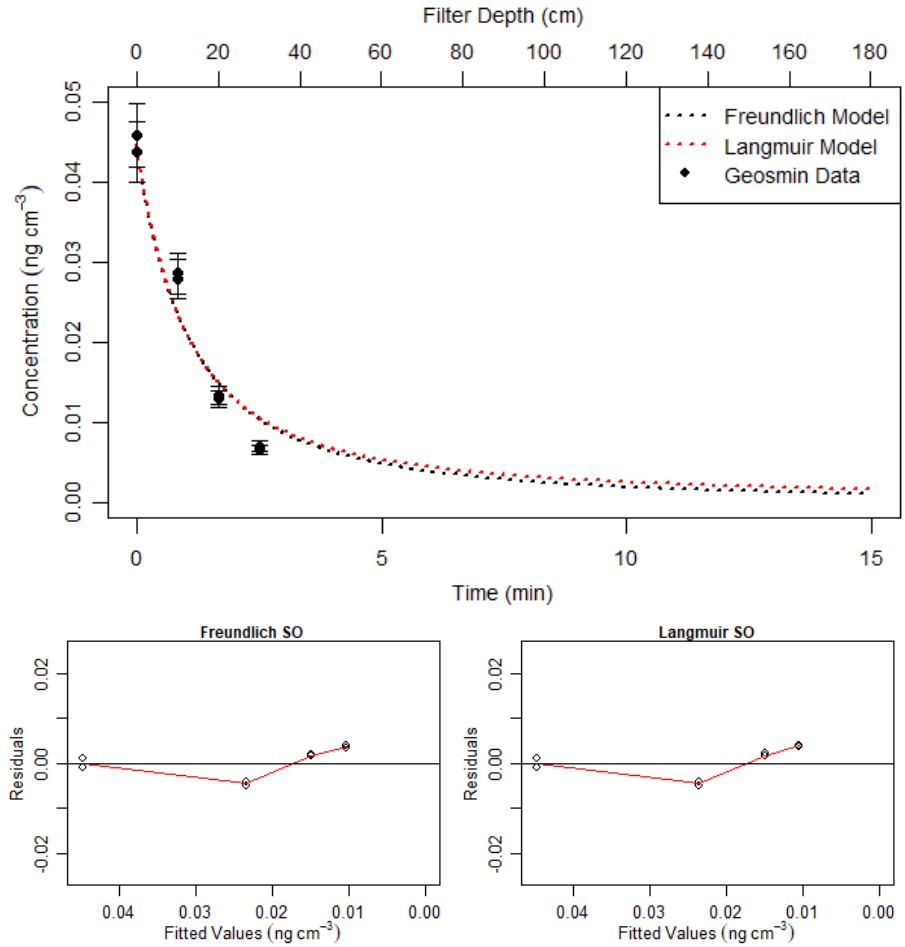

Figure 5-21: Comparison of GSM SO models at an influent concentration of approximately 0.05 ng cm^{-3} (top) and corresponding residual plots (bottom).

Similar results were obtained for 2-MIB, with both the Langmuir and Freundlich isotherms describing the 0.15 ng cm^{-3} data well (**Figure 5-22**), while a poorer fit was found for the 0.05 ng cm^{-3} data (**Figure 5-23**). As the rate constants for 2-MIB were found to be similar for the PSO models, the SO model did not provide much benefit for predicting 2-MIB concentration, although the model fit in terms of *RSE* and *SSR* were slightly more favourable for the SO models.

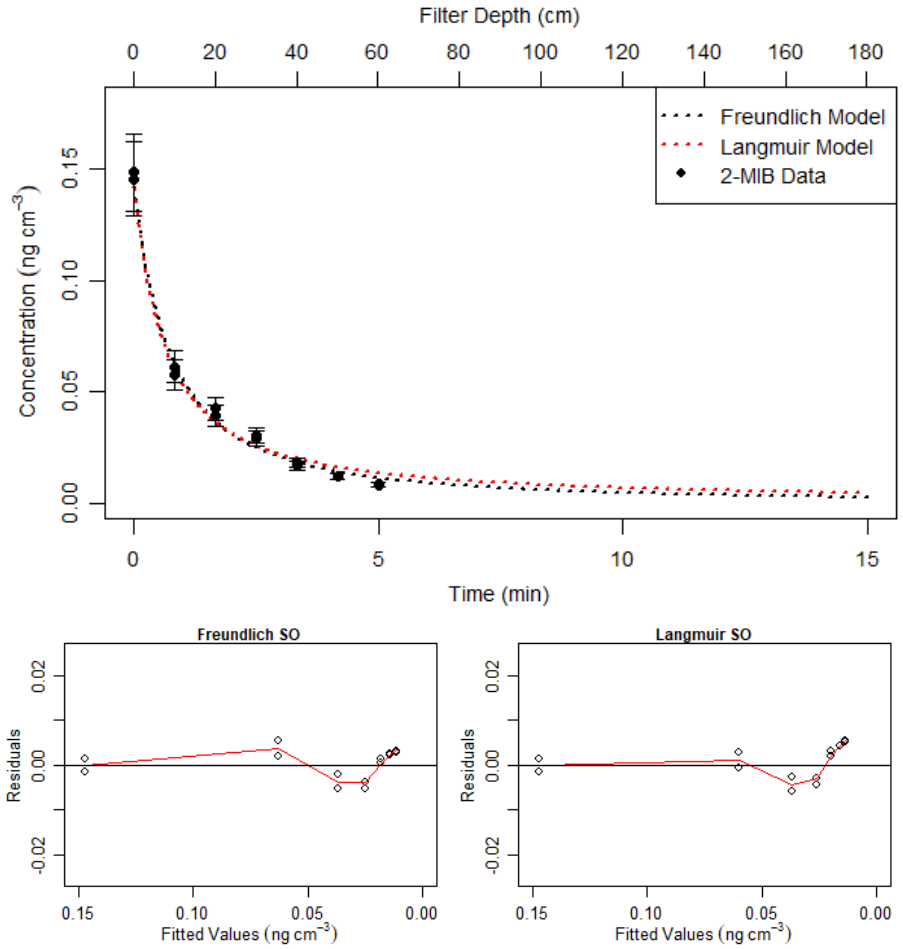

Figure 5-22: Comparison of 2-MIB SO models at an influent concentration of approximately 0.15 ng cm^{-3} (top) and corresponding residual plots (bottom).

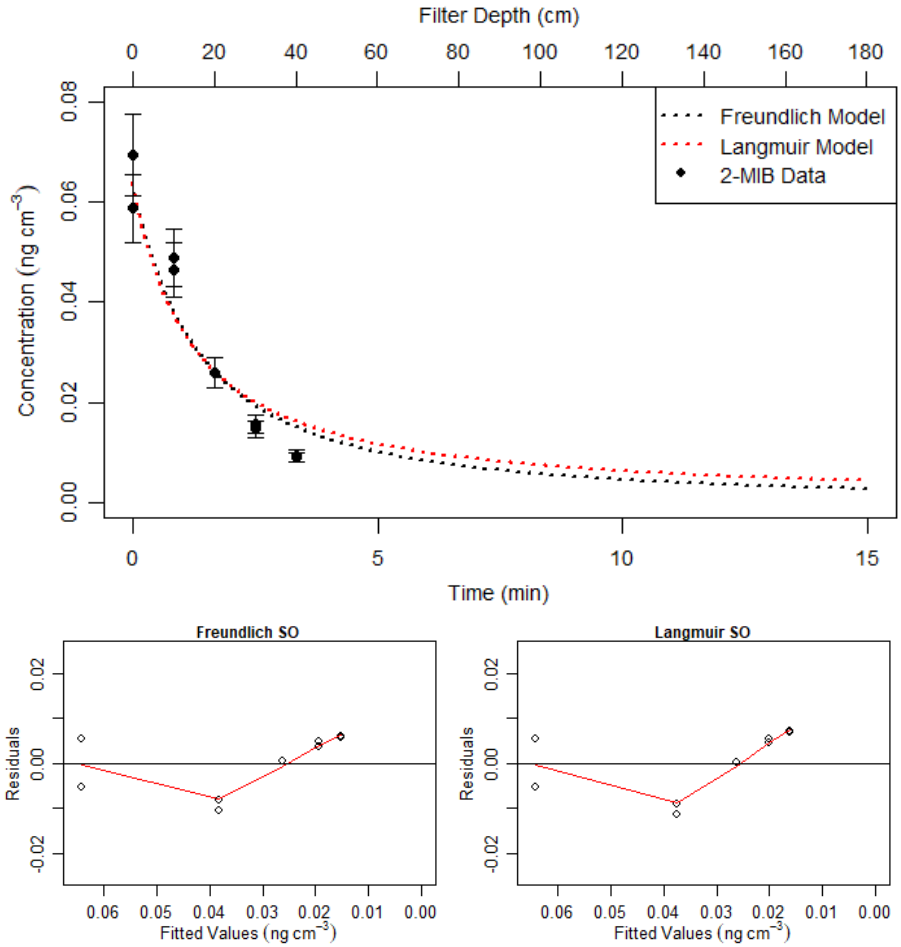

Figure 5-23: Comparison of 2-MIB SO models at an influent concentration of approximately 0.015 ng cm^{-3} (top) and corresponding residual plots (bottom).

While the PSO and SO models gave a poorer fit for the low concentration data, for both GSM and 2-MIB the fit was still quite good and allowed for the same model formulation to describe all the data while minimising the range in the *RSE* and *SSR* between data sets. The mean *RSE* and *SSR* for all models and data sets are given in **Figure 5-24** and **Figure 5-25** to illustrate this, and show that the SO models provided the lowest mean *RSE* and *SSR*.

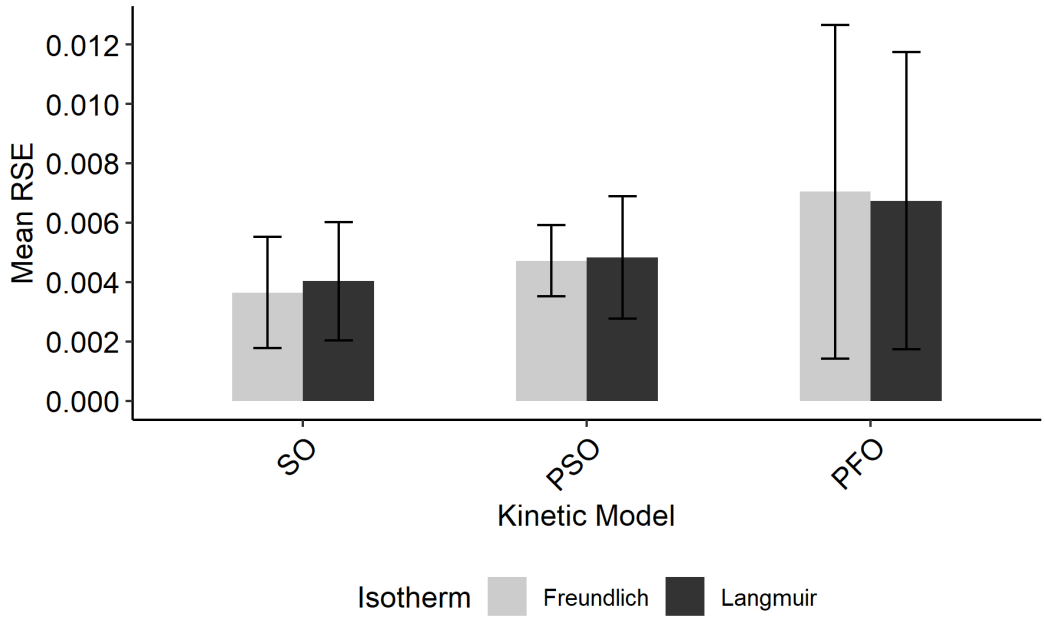

Figure 5-24: Mean *RSE* across all models and each analyte at each concentration level (error bars = SD).

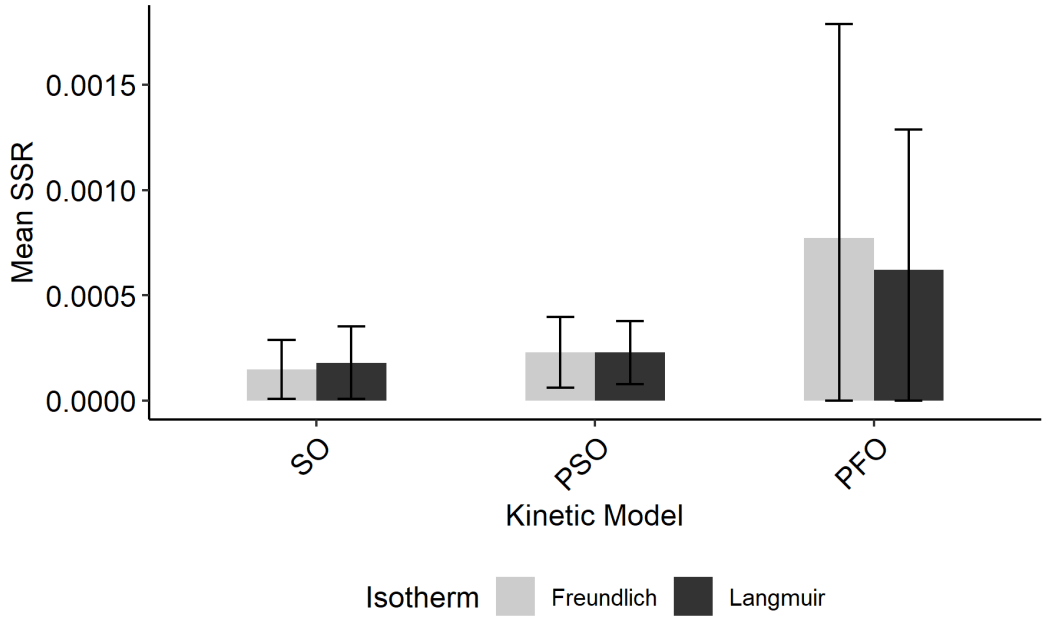

Figure 5-25: Mean *SSR* across all models and each analyte at each concentration level (error bars = SD).

For the PFO models, the high mean *RSE* and *SSR* reflect the poor fit to the high concentration data, while the large spread (indicated by the standard deviation) arises due to the difference between the poor fit of the high concentration data and the very good fit of the low concentration data. The low mean *RSE* and *SSR*, and the low degree of spread, for the SO and PSO models indicate that these models gave a better degree of fit across all the datasets relative to the PFO models.

In the case of using these models for predicting the behaviour of GSM and 2-MIB in GAC filters, the SO and PSO models are likely to be more useful for simulating high concentration events. At low concentrations, the PFO model may be more appropriate. In this case, as high concentration events were more pertinent, the SO model was selected for simulating high concentration events and other scenarios due the concentration dependant rate constant associated with the PSO model particularly for GSM.

Simulating influent concentrations of GSM up to 1.0 ng cm^{-3} (1.0 µg L^{-1}) indicated that the residence time required to reduce the concentration to below the OCT for GSM was only marginally increased (**Figure 5-26**, **Figure 5-27**).

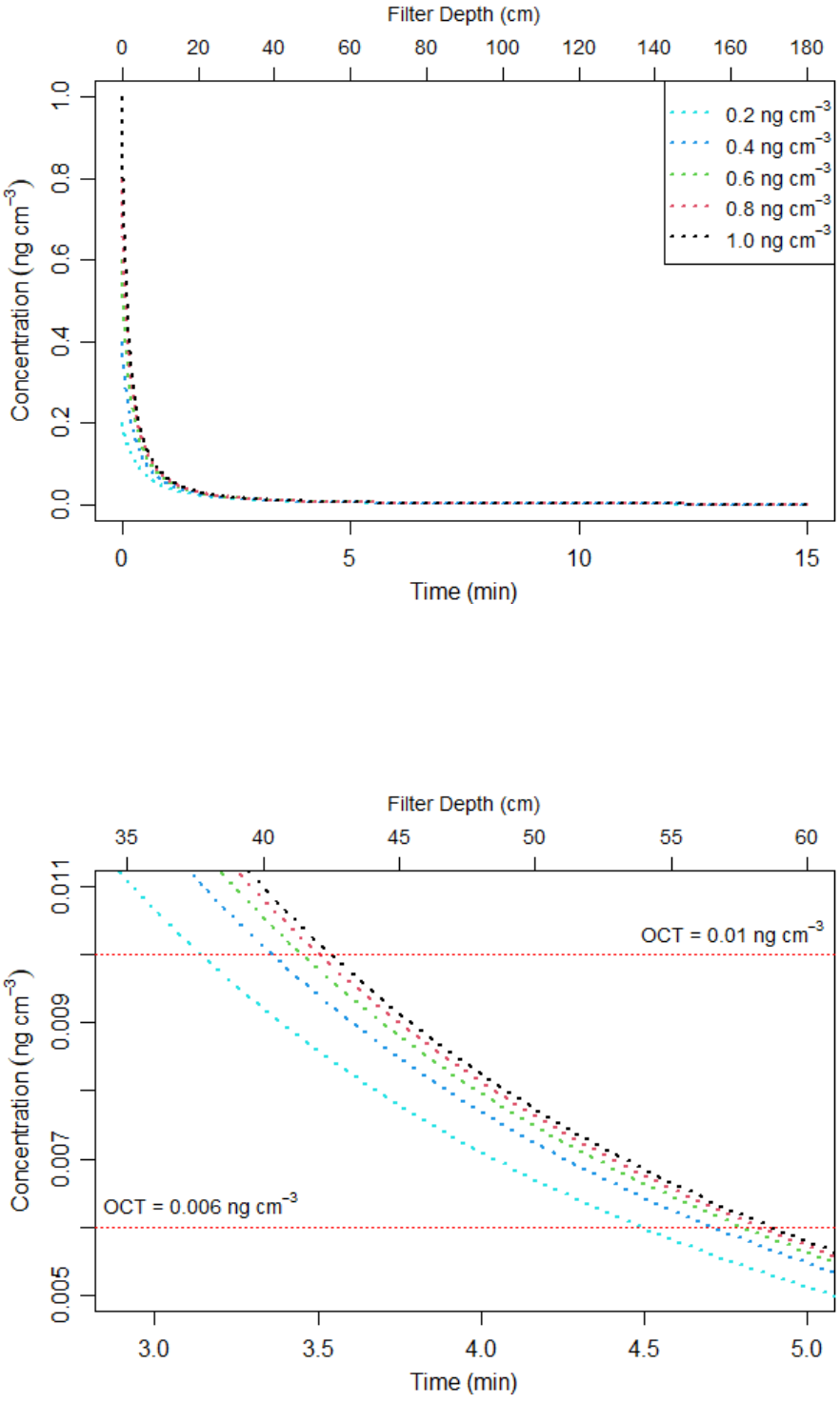

Figure 5-26: Second order Freundlich model output at varying GSM influent concentrations (top) and a magnified version of the same plot indicating the OCT for GSM (bottom).

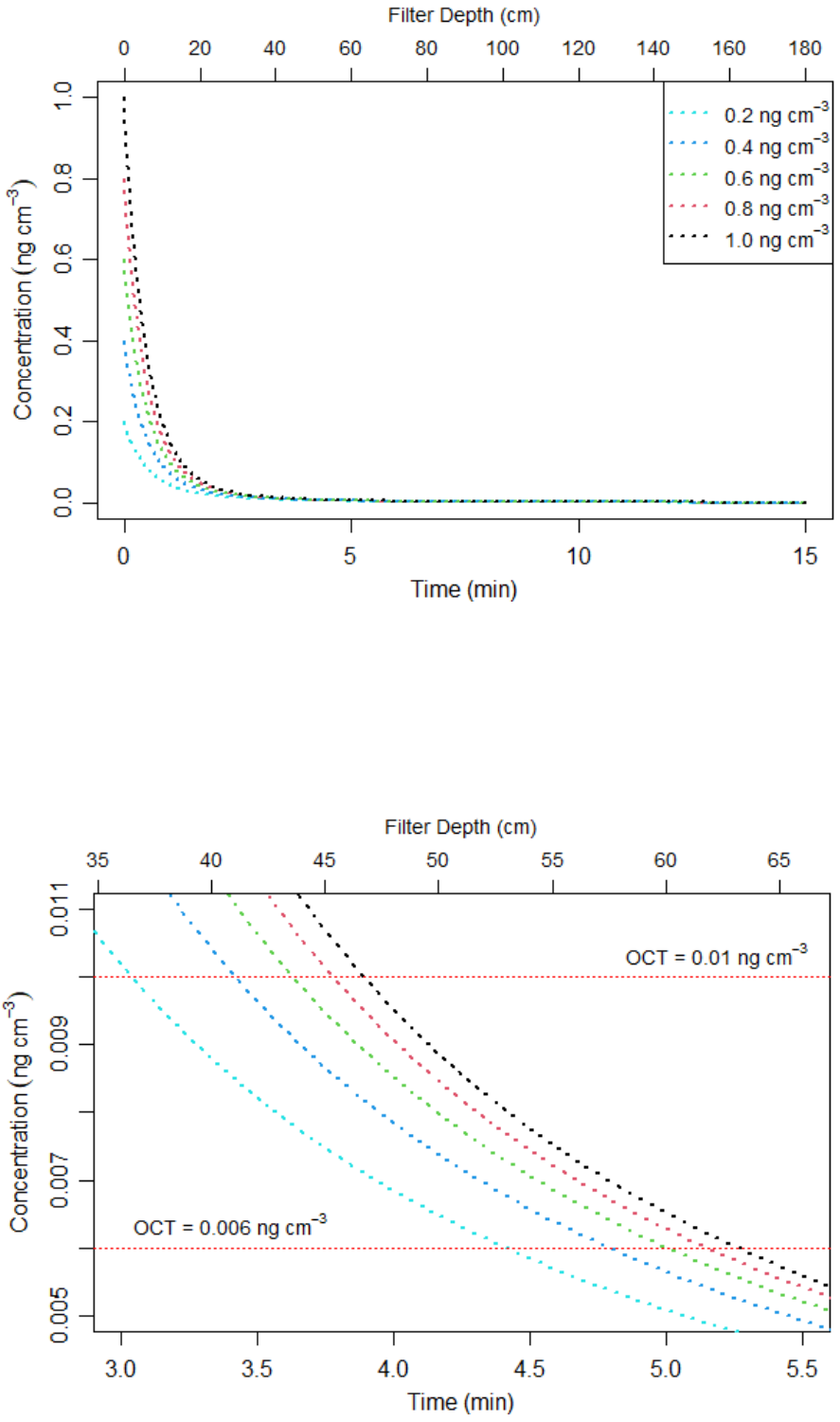

Figure 5-27: Second order Langmuir model output at varying GSM influent concentrations (top) and a magnified version of the same plot indicating the OCT for GSM (bottom).

For 2-MIB, while the model predicted that the concentration would be reduced to below the upper limit of the OCT for 2-MIB, the concentration would not be reduced to below the lower limit of the OCT even with an EBCT of 15 min (**Figure 5-28**, **Figure 5-29**).

The concentration of 2-MIB was predicted to decline very slowly once the concentration reached very low levels, which is a consequence of the less favourable adsorption behaviour of 2-MIB relative to GSM as determined from adsorption isotherm experiments. The range of the OCT is also much greater for 2-MIB than it is for GSM, with the lower limit being substantially lower. The combination of poorer adsorptivity and a lower OCT means that 2-MIB is likely to be less treatable that GSM in the event of a high concentration event.

It should be noted that the concentrations simulated here are much higher than those that would be expected to occur in the Waikato river with any degree of regularity. Furthermore, as the data obtained from sampling the entire plant indicated, much of the GSM and 2-MIB present in the source water are removed during flocculation. This would mean that the concentration of GSM and 2-MIB in the source water would need to be exceedingly high before the scenarios presented here become relevant. In conjunction with the dosing results reported earlier, this shows that the GAC filters are capable of removing GSM and 2-MIB quite effectively even at fairly high concentrations at an EBCT of 15 min.

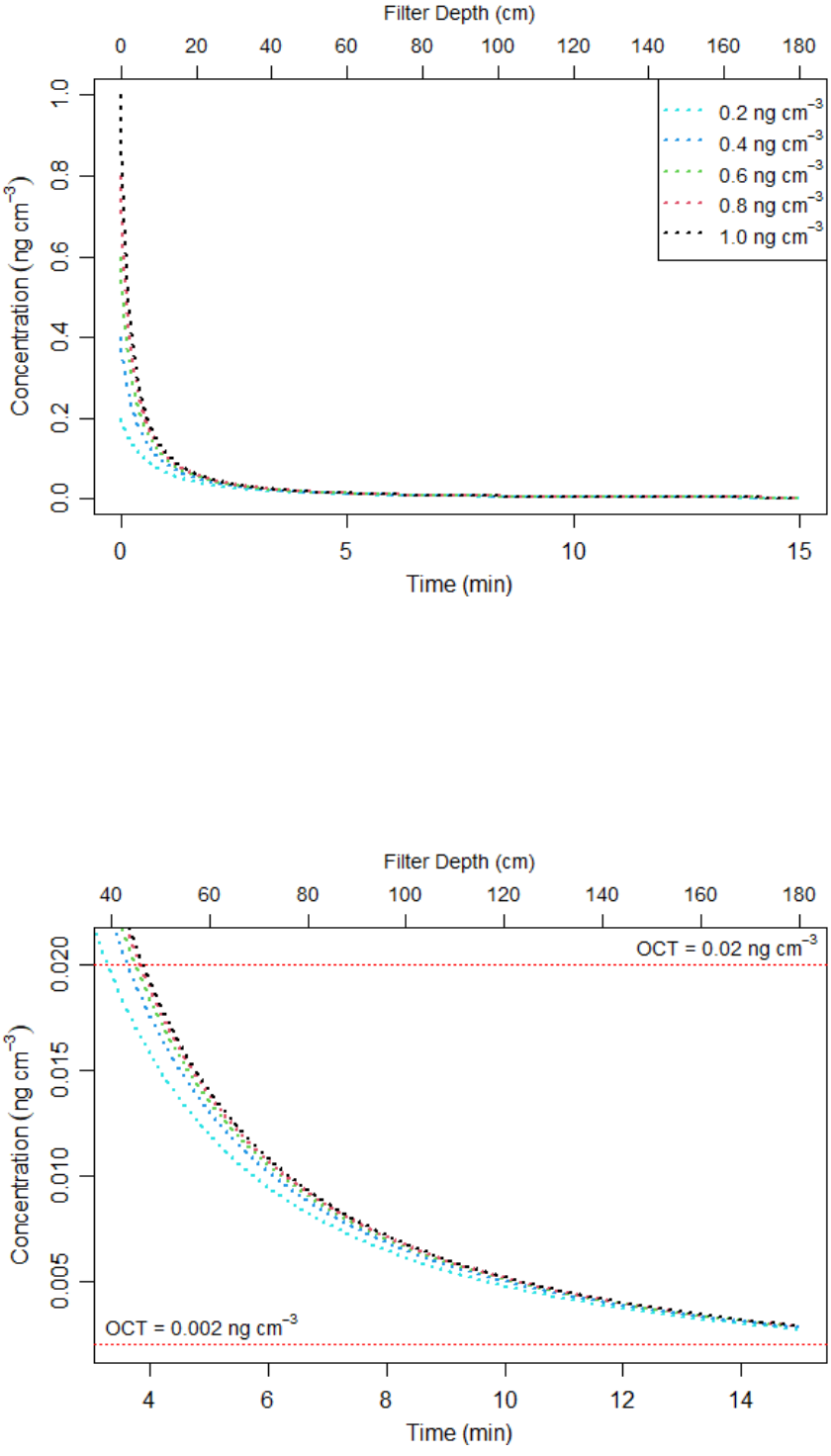

Figure 5-28: Second order Freundlich model output at varying 2-MIB influent concentrations (top) and a magnified version of the same plot indicating the OCT for 2-MIB (bottom).

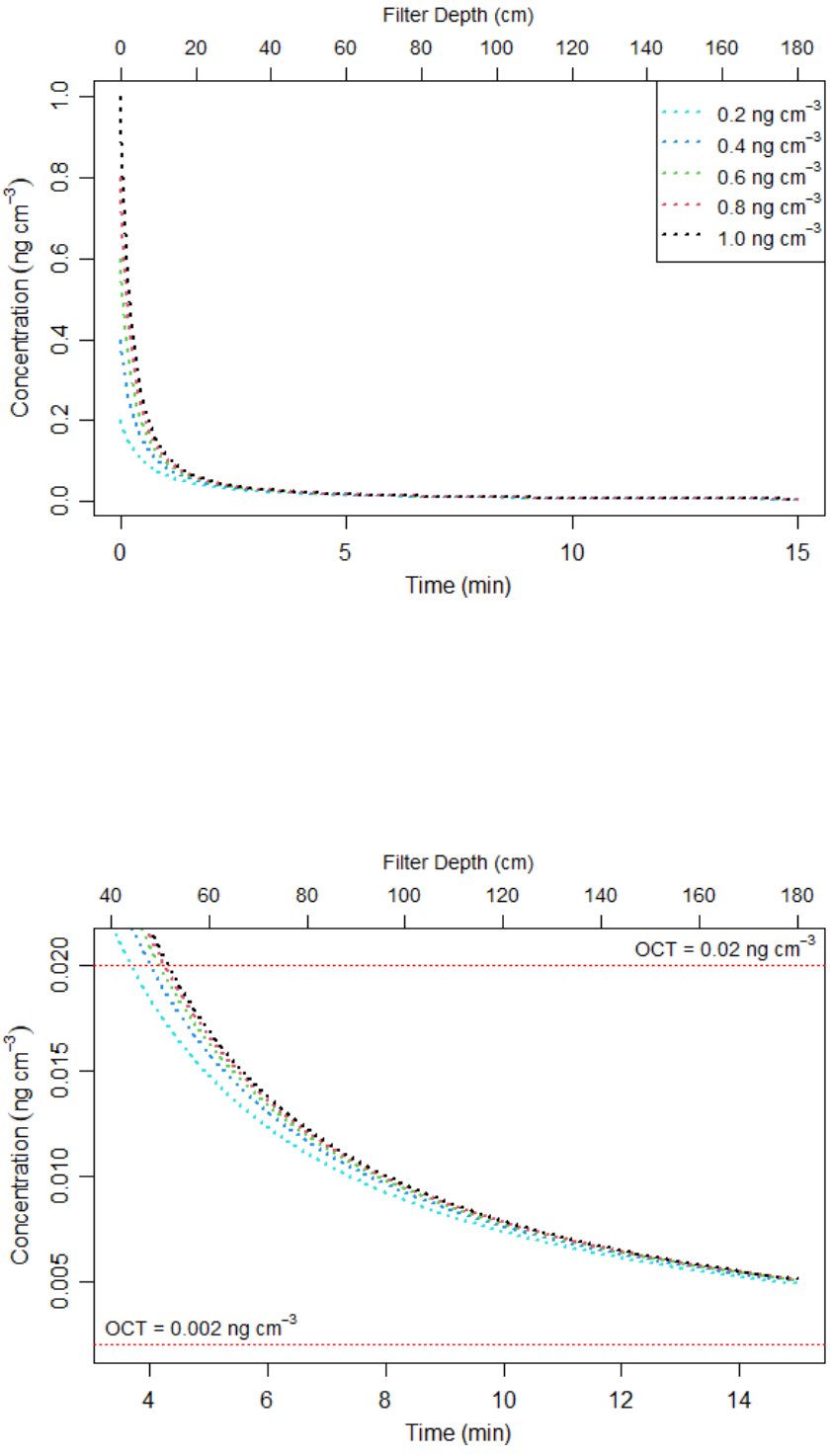

Figure 5-29: Second order Langmuir model output at varying 2-MIB influent concentrations (top) and a magnified version of the same plot indicating the OCT for 2-MIB (bottom).

Investigating the effect of changes to the EBCT indicated that this has a marked effect on the removal of 2-MIB and GSM. Changes in the EBCT during operation of the full-scale filters occur routinely, for example when one filter is out of operation for backwashing or maintenance, or when the throughput of the plant needs to be increased due to increased demand.

Examples of the predicted behaviour of GSM at an influent concentration of 0.15 ng cm^{-3} (150 ng $^{L-}$1) at various EBCTs are shown in **Figure 5-30**. The predictions indicate that a wide range of EBCTs allow for removal of GSM to below its respective OCT, with breakthrough above the OCT becoming apparent when the EBCT is lowered from 7.5 min to 5 min.

Predictions between the Freundlich and Langmuir models were quite similar and indicate that the operational range of EBCTs of 10 to 15 mins used at the HWTS ***[257]*** are appropriate for removing GSM, particularly when real concentrations of GSM in the source water are generally much lower than those considered here.

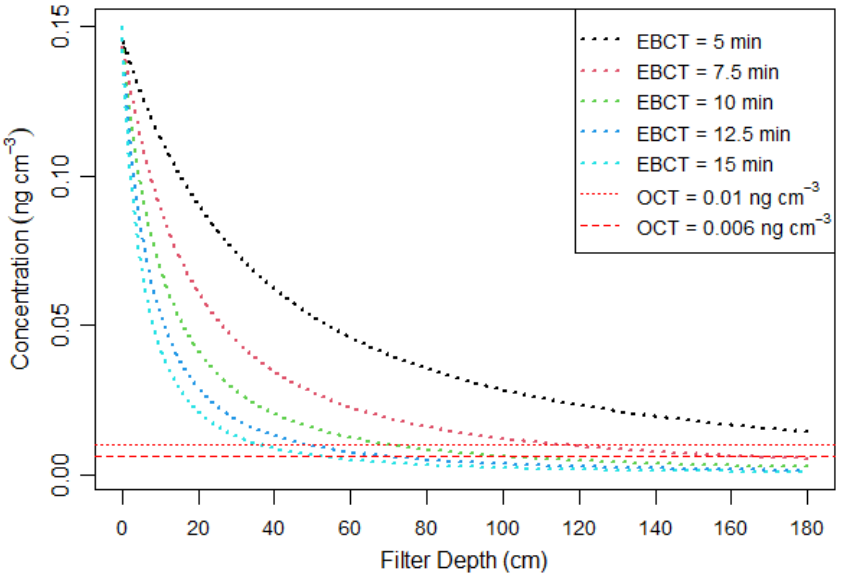

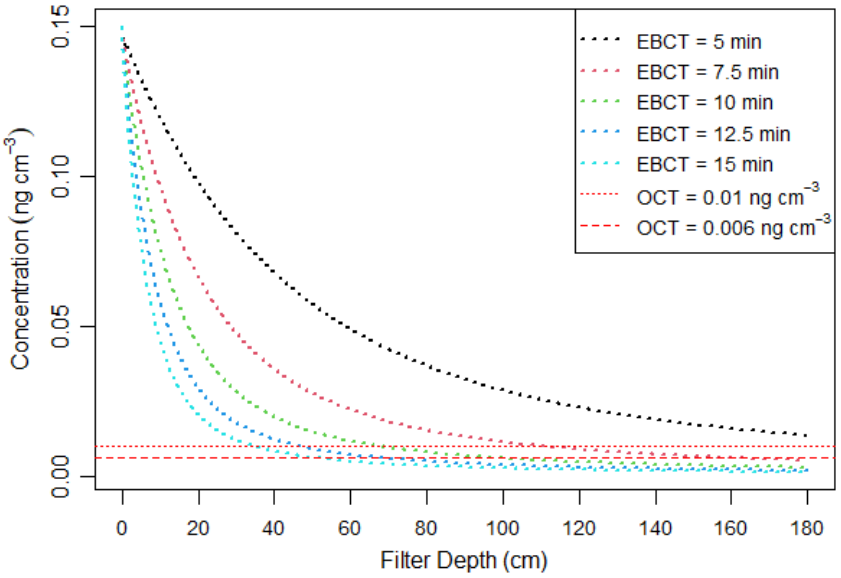

Figure 5-30: Predicted effect on the removal of GSM at an influent concentration of 0.15 ng cm^{-3} at various EBCTs using the Freundlich model (top) and the Langmuir model (bottom).

The effect for 2-MIB was more pronounced, due to it less favourable adsorption behaviour and its lower minimum OCT. As noted when simulating various influent concentrations, the very low minimum OCT was not reached at an influent concentration of 0.2 ng cm^{-3} even at a EBCT of 15 min, and similarly here at 0.15 ng cm^{-3} the minimum OCT is not predicted to be reached at an EBCT of 15 min.

At lower EBCT's the upper OCT is also predicted not to be reached, with the both the Freundlich and Langmuir models predicting breakthrough when the EBCT is reduced below approximately 7.5 min. While this is the same prediction as for GSM, the wider range of the 2-MIB OCT and its very low minimum OCT may mean that consumers that are more sensitive to 2-MIB may perceive the presence of 2-MIB when it is only removed to below its upper OCT. However, the generally lower levels of 2-MIB present in the Waikato river relative to GSM as noted during the survey of the full-scale plant indicates that very high concentrations of 2-MIB are unlikely to occur.

As with GSM, the operational range of EBCTs of 10 to 15 mins used at the HWTS are likely to be appropriate for removing 2-MIB during a high concentration event to below the upper OCT, while the removal of 2-MIB to below its lower OCT may not be possible at these concentration levels, even at an EBCT of 15 min.

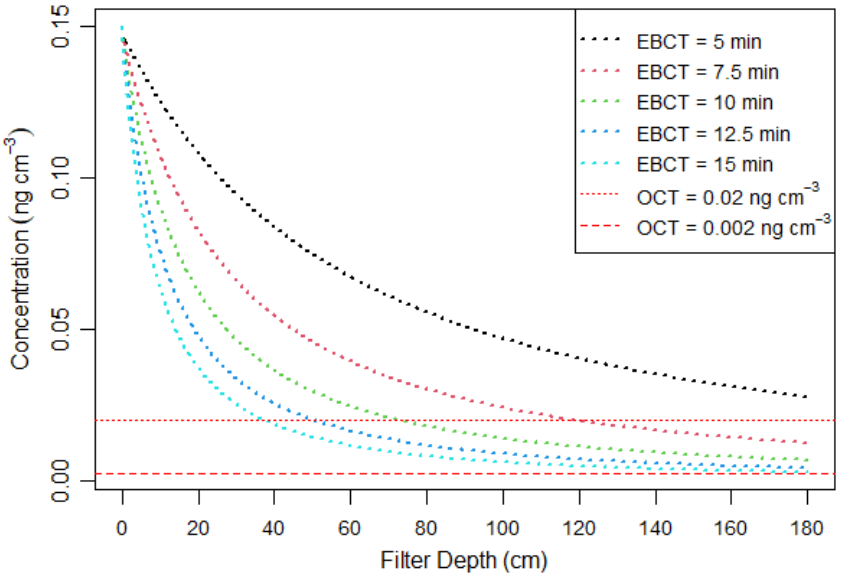

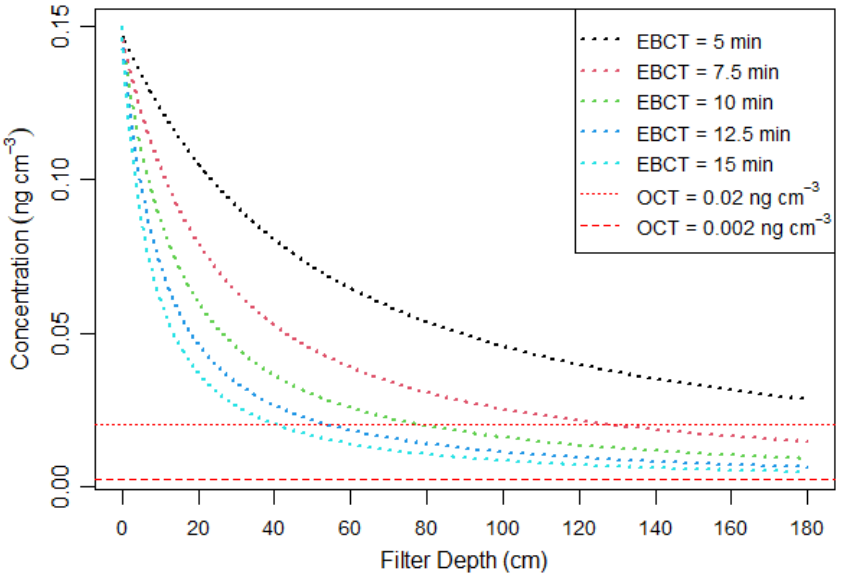

Figure 5-31: Predicted effect on the removal of 2-MIB at an influent concentration of 0.15 ng cm-3 at various EBCTs using the Freundlich model (top) and the Langmuir model (bottom).

Predicting the effect of a reduction in adsorption capacity over time proved to be more complicated as it depends of a range of unknown factors. One main factor is the competition for adsorption sites by other compounds present in the bulk DOM. As will be covered in Chapter 5, the bulk of the DOM in the Waikato river consists of humic substances which have been used in the past as a surrogate for competing molecules in conjunction with ideal adsorbed solution theory (IAST) where humic substances represent an effective background compound (EBC) ***[258]***. However, the molecular size of humic substances means that they do not compete for the same adsorption sites, with 2-MIB and GSM adsorption occurring in micropores that humic substances cannot access (**Figure 5-32**), with use of the full DOM profile as the EBC greatly overestimating competitive effects ***[258]***.

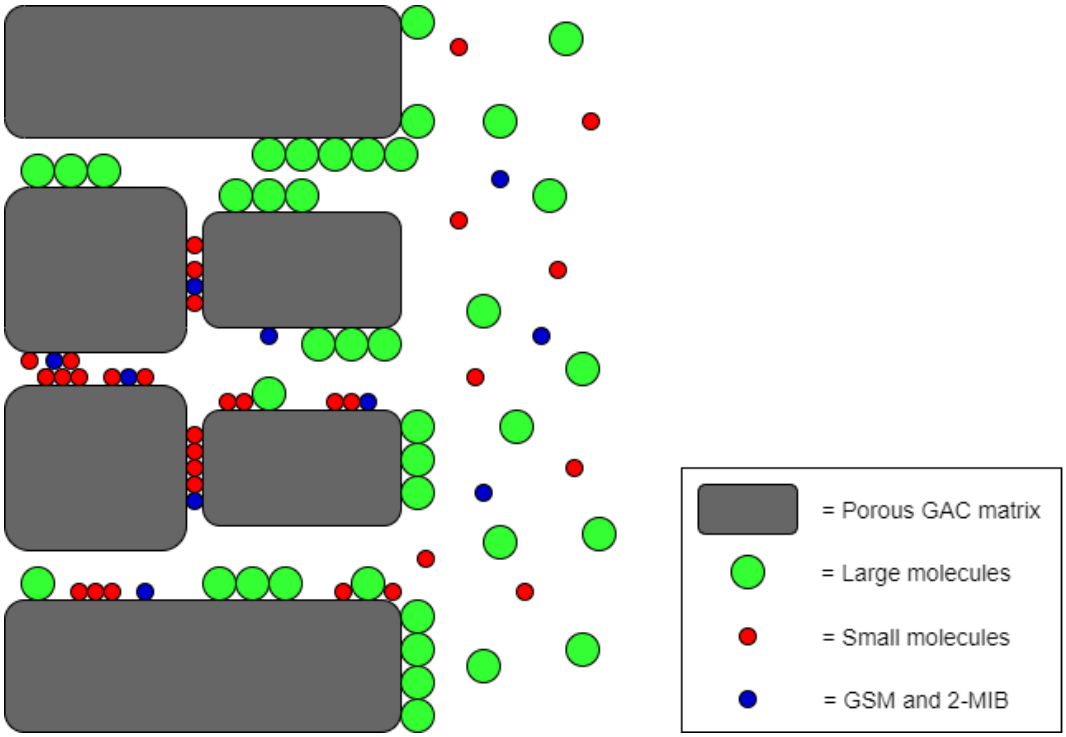

Figure 5-32: Diagram illustrating competition for adsorption sites between small molecules and T&O compounds in micropores where larger molecules are excluded.

As demonstrated in ***[258]***, an EBC approach using a "fictive compound" approach provided the best prediction of competitive effects, where the fictive compound

represents the fraction of DOM that is highly adsorbable and is of a molecular size that allows it to compete for the same adsorption sites. This was shown to account for approximately 0.45% of the total DOM for the waters studied. This would equate to approximately 7 μg L^{-1} for the Waikato river water (TOC ≈ 1.5 mg L^{-1}), or 4 μg L^{-1} for the GAC filter influent (TOC ≈ 0.9 mg L^{-1}), however the development of a fictive compound relevant to the Waikato river source water would be necessary to achieve valid results. Furthermore, due to the low concentration of GSM and 2-MIB in the source water, and that based on the survey of the full-scale plant which showed that no GSM and 2-MIB were reaching the GAC filters, any reduction in the adsorption capacity of the GAC is likely to be a result of other compounds present in the DOM taking up adsorption sites. Therefore, in order to predict the loss of adsorption capacity over time, an investigation into small, highly adsorbable compounds that are likely to compete with GSM and 2-MIB for adsorption sites would need to be undertaken.

As will be demonstrated in Chapter 5, significant loss of capacity in relation to the removal of humic substances was noted from data obtained from samples collected at the same time as 2-MIB and GSM dosing experiments were carried out, while the dosing experiments showed that 2-MIB and GSM were still quickly removed at the upper region of the filter media. This further suggests that the humic fraction of the DOM does not have a significant impact on the removal of GSM and 2-MIB and is therefore unlikely to be a suitable candidate for a competitive adsorption surrogate.

As competitive adsorption experiments were not carried out here, further investigations would be required in order to implement competitive adsorption effects into the models presented above in order to predict the behaviour of GSM and 2-MIB as the filter media becomes exhausted. This would require the development of a fictive compound tailored to the Waikato river DOM composition. However, as these experiments showed that significant adsorption was still occurring in the upper layers of the GAC bed after 12 months of service time, coupled with the generally low concentrations of GSM and 2-MIB present in the Waikato river, it seems reasonable to assume that GSM and 2-MIB are unlikely to cause problems in the future, particularly if a program of media replacement is implemented and maintained.

5.2 Conclusion

The method developed here for the quantitative analysis of GSM and 2-MIB was applied to investigating their behaviour in the HWTS. A survey of the full-scale plant showed that the background levels of GSM and 2-MIB were quite low in the source water, and a large proportion was removed during flocculation with no residual GSM or 2-MIB reaching the GAC filters. Pilot-scale dosing experiments aimed at simulating high concentration events showed that the filters were quite capable of removing these compounds at influent concentrations of up to 150 ng L^{-1} within the upper region of the GAC filter, with adsorption isotherm experiments indicating that significant adsorption capacity remained after 12 months of operation. A modelling investigation based on models fitted to the dosing and adsorption data indicated that the pilot filter was capable of removing high

concentrations (200 – 1000 ng L-1) of both target compounds at an EBCT of 15 min, and varying the EBCT with a fixed concentration of 150 ng L^{-1} showed that breakthrough may occur at EBCTs lower than 7.5 min.

The concentrations investigated during dosing experiments and simulated using models were much higher than would be expected during routine operation of the plant. High levels of GSM and 2-MIB are only likely to be present during an algal bloom, during which it would be expected that the plant operators would be aware of such a situation due to the associated risks of cyanobacterial toxins. As such, on a daily operational basis, the current range of EBCTs used are appropriate for removal of GSM and 2-MIB. In the case of a cyanobacterial bloom, daily monitoring would be required to ensure compliance with the DWSNZ, at which time analysis of GSM and 2-MIB could be carried out if it was deemed to be of sufficient importance and changes to the plants operating parameters could be made accordingly.

Chapter 6:

Excitation-Emission Matrix Fluorescence Spectroscopy of Municipal Drinking Water Samples

6 Excitation-Emission Matrix Fluorescence Spectroscopy of Municipal Drinking Water Samples

6.1 Introduction

The distribution of DOM throughout the HWTS treatment train was investigated using TOC analysis and EEMS-PARAFAC. This was undertaken to assess the extent to which TOC is removed by the current treatment process with the use of EEMS-PARAFAC providing insight into how different groups of the DOM pool behave relative to each other and how they are correlated to the TOC. Further, EEMS can provide information as to which stages of the treatment train are effective at removing different classes of DOM components. As the major groups of the DOM pool amenable to study using EEMS are humic substances and proteins/amino acids, this technique is able to provide some information as to the behaviour of non-polar (humics) and polar (proteins, peptides, amino acids) and their relative removal at each treatment stage. This study also looked at the difference in TOC removal by the GAC filters at different stages of their service life, as well as the changes in the behaviour of DOM components as the filters age using EEMS.

EEMS-PARAFAC was also used to study the change in DOM composition within a pilot-scale GAC filter. This was undertaken at the same time as T&O dosing experiments were carried out. The aim was to assess how different components of the DOM pool changed throughout the depth of the filter column, and how this may differ from the behaviour of low molecular weight, trace level compounds.

6.2 Experimental

6.2.1 Materials

Potassium hydrogen phthalate (PHP; 99 %) was obtained from Sigma-Aldrich (Auckland, New Zealand). Sodium peroxodisulphate (Emsure®, ≥ 99 %), orthophosphoric acid (Emprove®, 85 %) and hydrochloric acid (Suprapur®, 36 %) were purchased from Merck (Auckland, New Zealand). Syringe filters (Sartorius® 0.45 µm, cellulose acetate) were purchased from Thermo Fisher Scientific (Auckland, New Zealand). De-ionised water was prepared using a Barnstead E-Pure water purification system with a resistivity of 18 Ω (Thermo Fisher Scientific, Auckland, New Zealand).

6.2.2 TOC Analysis

Total organic carbon (TOC) is often used as a marker for the efficacy of treatment in municipal water treatment plants. TOC data was collected alongside EEMS data to allow for comparisons and to identify any correlations that may be present.

Samples were analysed using an OI Analytical Aurora 1030 TOC analyser operating in the NPOC mode. Instrument reagents (0.84 M sodium peroxodisulphate and 5 % H_3PO_4) and DI water were replenished each analysis day. The instrument was calibrated daily from a 5-point calibration curve including a blank (DI water). Calibration standards (0.25 - 3 mg/L) were prepared from a 1000 mg/L carbon stock solution of PHP (0.2218 g/100 mL). Water samples and standards (20 mL) were transferred to acid washed (10 % v/v HCl) autosampler vials and analysed in duplicate (5 mL per replicate).

6.2.3 EEMS Analysis

All EEM spectra were recorded on a Horiba Aqualog Fluorometer. Samples (≈ 2 mL) were prepared by filtering through a pre-rinsed 0.45 µm syringe filter directly into a 1 mL quartz cuvette. Samples were analysed undiluted due to the low TOC concentration of the samples (< 2 mgC L^{-1}) and spectra were recorded at excitation wavelengths from 239 nm to 800 nm with 3 nm increments. Blank spectra were obtained using DI water, and the recorded blank spectra was subtracted from each subsequent sample and also used for Raman normalisation. Samples were analysed without pH adjustment, as the water in the Waikato River and throughout treatment remains relatively stable (pH = 6.5 ± 0.4).

Processing of spectra and PARAFAC modelling were conducted in *R **[259]*** using the eemR and staRdom packages ***[260-262]***. PARAFAC models were validated using split-half analysis, core consistency and correlation coefficients.

6.2.4 Sampling and context

At the time that this study was carried out, the GAC filters contained media that was of different ages as some of them had been partially replaced with new media over a period of approximately 10 months prior to commencing sampling. Filter ages ranged from the oldest, GAC5 (≈ 10 years or 120 months) which had no new media and was operating as a purely biological BAC filter, to GAC4 (≈ 2 months) which had undergone partial media replacement. The filters GAC1, GAC2, GAC3, GAC4 and GAC6 had undergone partial media replacement, meaning that half of the old GAC media was left in place while the rest of the filter was topped up with

fresh GAC in an effort to improve the efficiency of the filters. As such, it was assumed that these filters were operating in a combined adsorption-biological filtration mode, as the old media was known to possess little adsorption capacity while being densely colonised with microbes (**Figure 6-1**). The ages of the replaced filters ranged from 2 to 10 months in the order from oldest to newest; GAC6 > GAC1 > GAC2 > GAC3 > GAC4.

Samples were collected on fifteen separate days between 05/01/18 and 17/03/18. Samples were collected from 12 locations around the plant in order to track the contribution of key treatment stages to the removal of TOC. The sampling locations were the river, settled water (post-coagulation), post-sand filtration (re-lift), post-GAC, post-UV and the finished water. The post-GAC samples were collected from each individual GAC filter present on site (6 filters). Water samples were also collected from a pilot scale GAC filter present on site during this time. Sampling locations and abbreviations used are given in **Table 6-1** and **Figure 6-2**.

Figure 6-1: Scanning electron micrograph showing microbial colonisation of the GAC surface (GAC 5).

Table 6-1: Sampling locations and abbreviations.

Location ID	Sampling Location	Abbreviation
1	River	R
2	Settled water (post-coagulation)	S
3	Post-sand filtration (re-lift)	RL
4	Post-GAC1	G1
4	Post-GAC2	G2
4	Post-GAC3	G3
4	Post-GAC4	G4
4	Post-GAC5	G5
4	Post-GAC6	G6
4	Post-pilot column	C
5	Post-UV	PUV
6	Finished Water	F

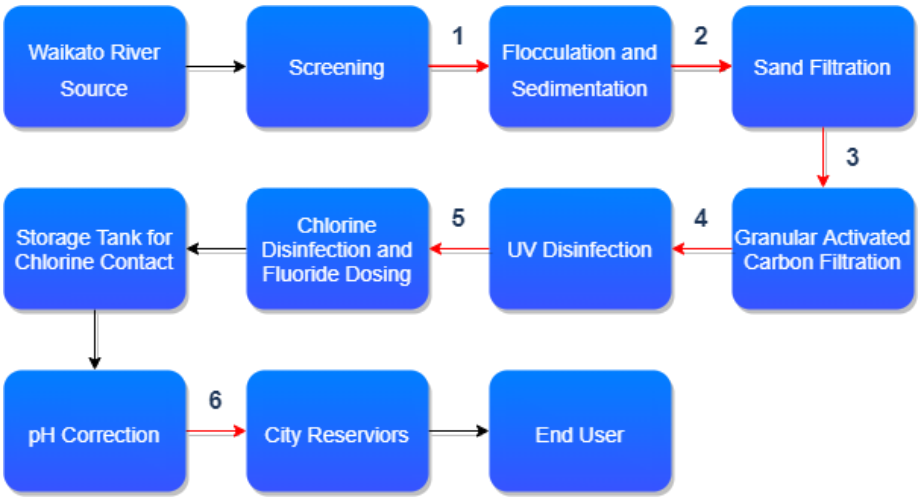

Figure 6-2: Basic process flow for the Hamilton Water Treatment Station with sampling locations in red.

Further water samples were collected from the pilot GAC column in March 2019, after the filter had been in use for approximately 12 months. These samples were collected in order to assess changes in the fluorescent components of DOM across the depth of GAC filters in greater detail. Samples (n = 60) were collected on three separate days at various depths across the filter bed from sampling ports installed on the column (0 - 180 cm at 10 cm intervals).

6.3 Results and Discussion

6.3.1 Total Organic Carbon

The result of the TOC analysis for each day can be found in **Appendix A-3**. Outliers were removed from the data using Dixon's Q test for outliers ($\alpha = 0.05$, ***[263-265]***) for each sample location prior to further statistical analyses after the data was shown to adhere to a normal distribution by using the Shapiro-Wilk's test ($\alpha = 0.05$). In some cases, samples were not able to be collected due to plant maintenance or specific areas being inaccessible or out of service on a particular day.

The mean TOC concentration at each sampling point is shown in **Figure 6-3**; the pilot column results were not included at this stage, as the column was not part of the main treatment process and is discussed later.

In this case, as the GAC filters run in parallel and the effluent water from these filters is combined prior to UV treatment, taking the mean of the GAC results yields a clearer estimate of TOC reduction throughout the plant (**Figure 6-4**). As expected, there was an overall trend of reduced TOC concentration as the water progressed through the plant, with TOC being reduced by 67 ± 6 %.

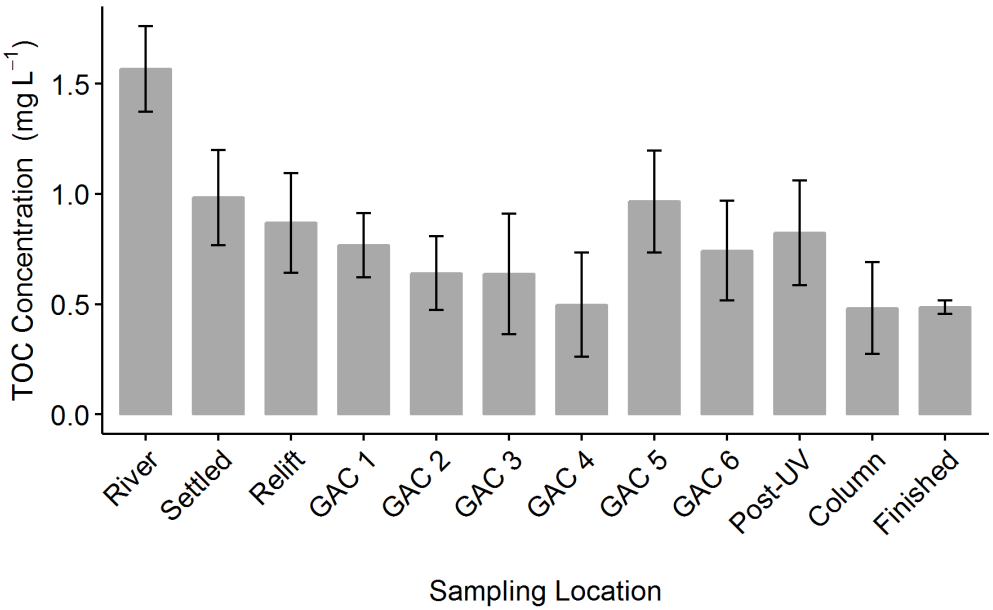

Figure 6-3: Mean TOC concentration across all sampling locations and all sampling days (error bars = standard deviation).

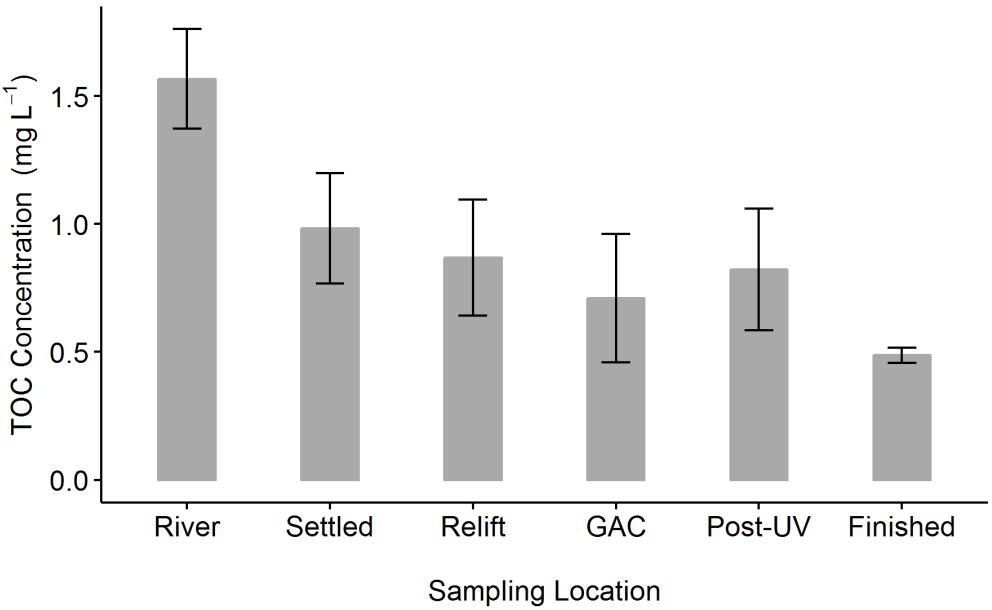

Figure 6-4: Mean TOC concentration across all sampling locations and all sampling days with mean GAC concentration (error bars = standard deviation).

As can be seen in **Figure 6-5**, GAC 5 seemed to be less effective than the other 5 GAC filters, having a higher TOC concentration than the others following GAC filtration. Overall, the mean TOC concentration following GAC 5 was shown to be higher than the mean influent (Relift) TOC concentration, suggesting that GAC 5 was increasing the TOC content of the water. In order to determine whether this

was a real effect or not, a one-way analysis of variance (ANOVA; $\alpha = 0.05$) was carried out on the GAC TOC data, including the pilot column which was included as a control (**Appendix A-3**). The results of the ANOVA gave a p-value much less than 0.05 ($p = 8.66E^{-05}$) which indicated that one or more of the mean TOC results for each GAC filters was different from the at least one of the others. Mean TOC concentrations following GAC filtration including the pilot column are shown in **Figure 6-5**.

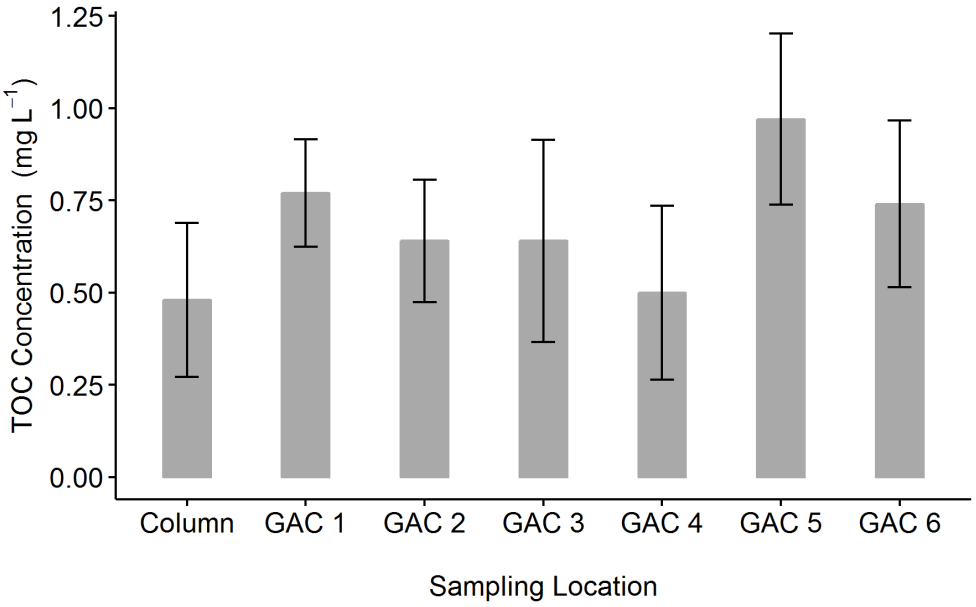

Figure 6-5: Mean TOC concentration following GAC filtration and pilot column filtration (error bars = standard deviation).

The ANOVA was then extended in order to find which filters were in fact different in mean effectiveness by carrying out a Tukey HSD test ***[266]***. This showed that the mean TOC following each filter was different for some of the filters, indicating that some were performing better than others with respect to TOC removal (**Appendix A-3**). In this case, it suggested that GAC5 was different to GAC2, GAC3, GAC4 and the pilot column. As the mean TOC value for GAC5 was higher than these four filters, this indicated that GAC5 was not performing as well. This

makes sense, as GAC 5 had been in service for much longer than the rest of the filters and was assumed to be operating as a purely biological filter (BAC) which is known to be less effective than purely adsorptive GAC filters for removing TOC. Additionally, the pilot column, was shown to differ from GAC1 and GAC5. As the pilot column had been recently installed with fresh GAC (compared to the partial GAC replacement of the full scale GAC filters), it was somewhat expected that the pilot column would perform better (lower mean TOC). When plotted in order of increasing filter age, the reduction in mean effectiveness became more apparent (**Figure 6-6**).

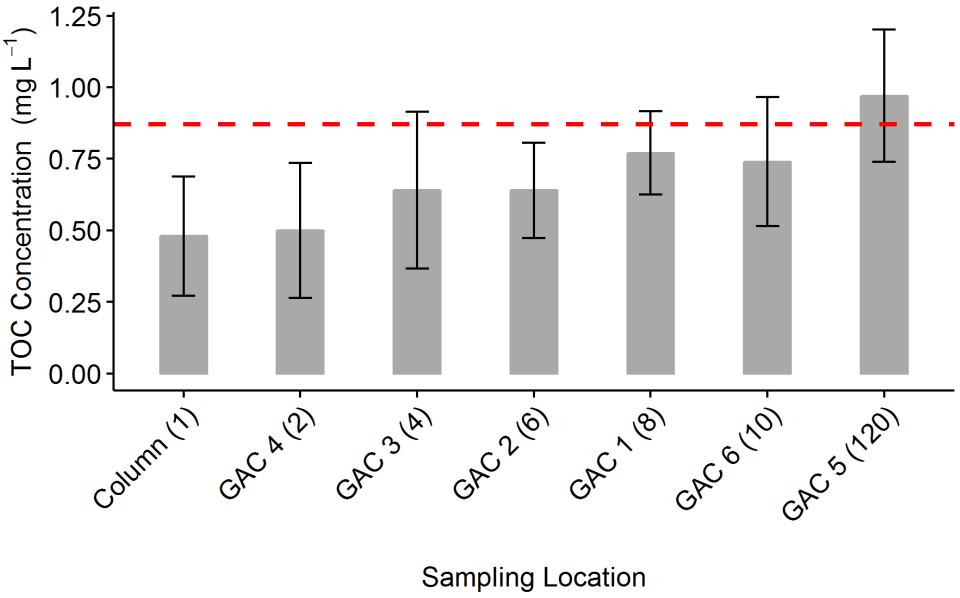

Figure 6-6: TOC concentration following each GAC filter in order of ascending filter age (error bars = standard deviation). Approximate age denoted in months in brackets. Dotted line indicates mean influent TOC concentration.

6.3.2 EEM Fluorescence Spectroscopy

As expected of a natural water source, the untreated samples collected directly from the Waikato River displayed peaks arising from humic substances (**Figure 6-7**; peaks C and A - see **Table 2-6**). There were also strong peaks arising from tryptophan/tyrosine-protein type fluorescent material that can be associated with recent autochthonous biological activity (**Figure 6-7**; peaks B and T; ***[160,161]***).

A preliminary assessment of the absorption maxima of these peaks gave some indication that the B and T peaks remained largely unchanged in their intensity across the treatment process, while the peaks associated with humic-like material (peaks C and A) were reduced significantly.

Examples of the EEM spectra obtained across the plant are displayed in **Figure 6-8** and **Figure 6-9,** and show a clear reduction in the intensity of peaks C and A throughout treatment. Exceptions to this appeared to be GAC 6 and particularly GAC 5, which still exhibited clear C and A peaks following filtration. However, the impact of this seemed to be negligible overall, as the effluent of the combined GAC filters as measured in the post-UV spectrum showed almost no fluorescence arising from peaks C and A. The spectra also show the persistence and high intensity of peaks B and T throughout treatment.

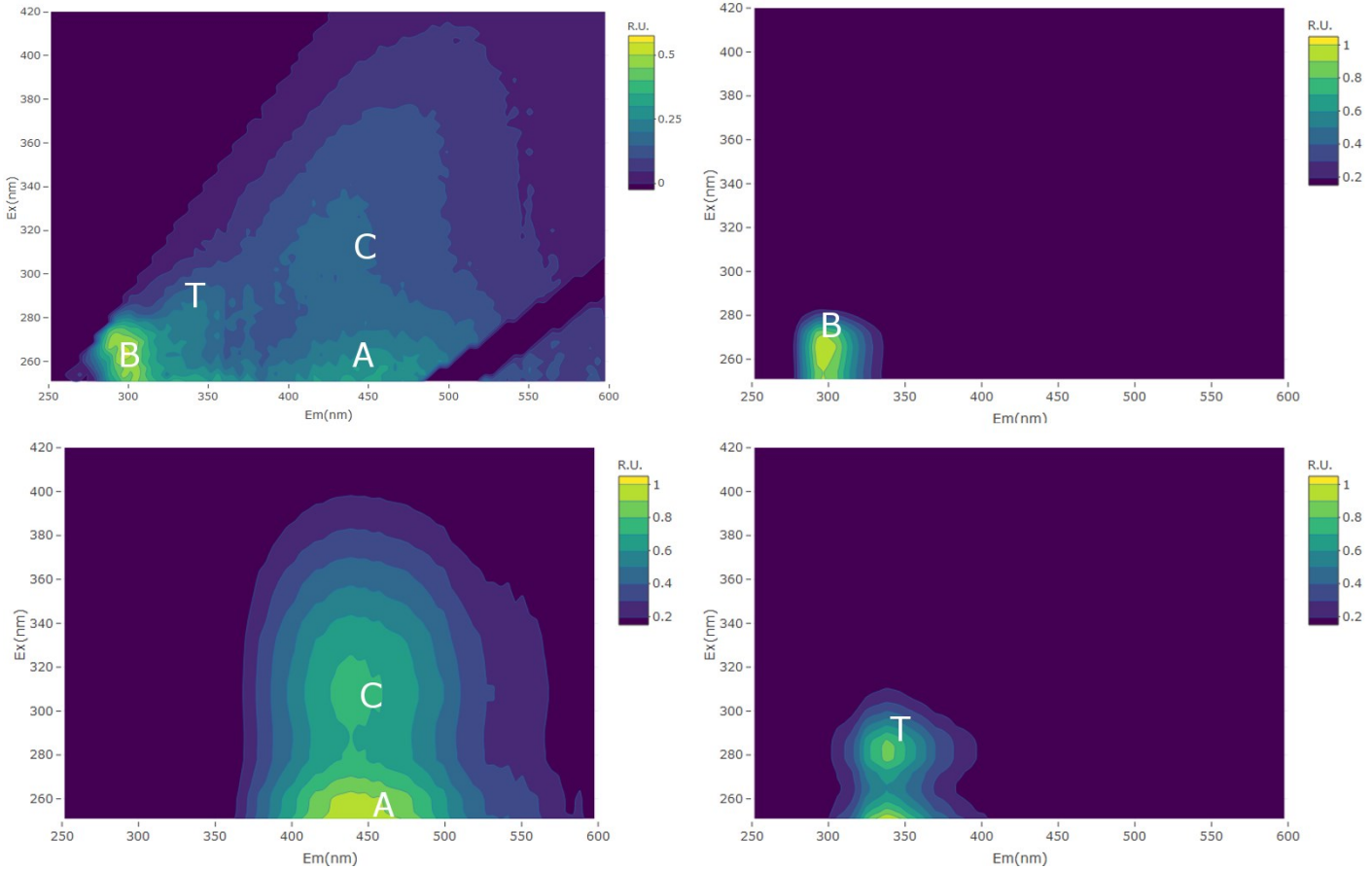

Figure 6-7: EEM contour plots of raw river water (top right) and PARAFAC components: C1 (tyrosine-like; top left), C2 (humic-like; bottom left) and C3 (tryptophan-like; bottom right). PARAFAC derived spectra have been normalised to λ_{max} = 1 R.U.

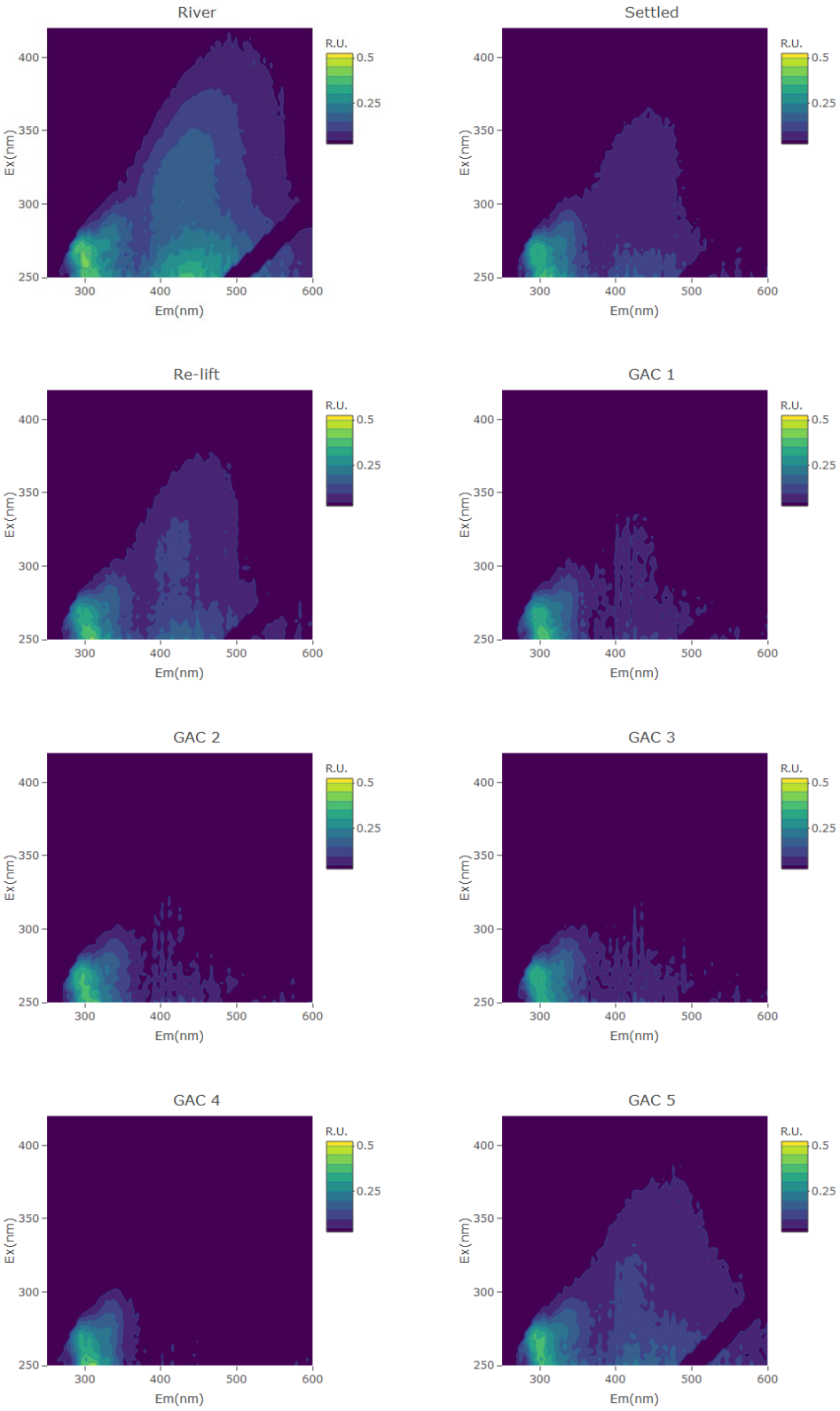

Figure 6-8: Fluorescence EEM spectra across each sampling point for samples collected 02/03/2018 (Continued in Figure 6-9).

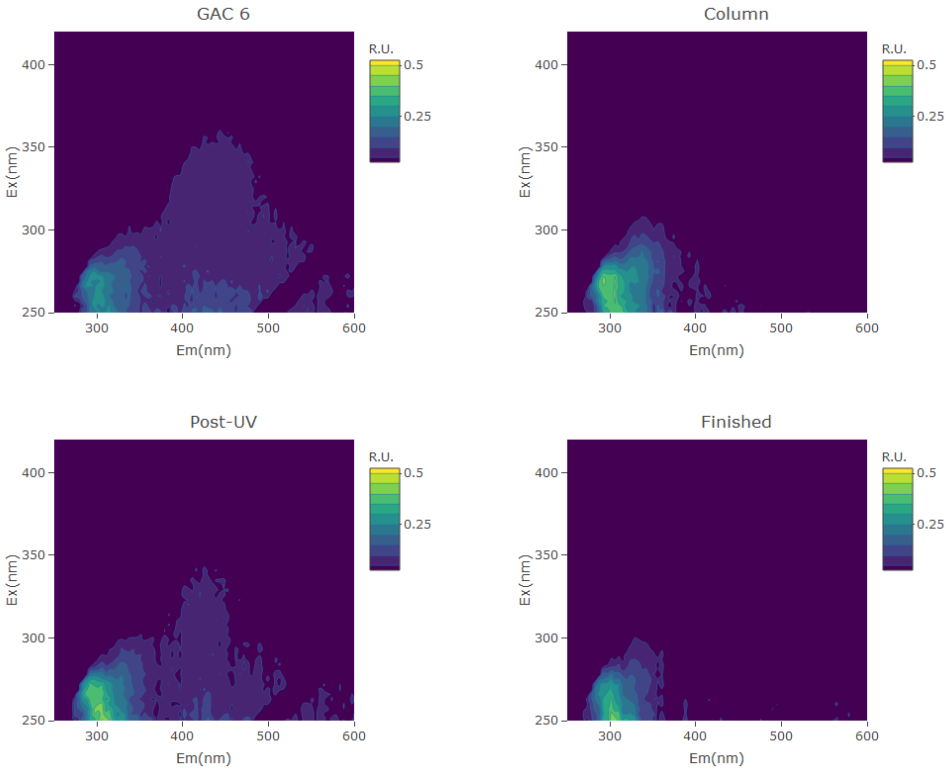

Figure 6-9: Fluorescence EEM spectra across each sampling point for samples collected 02/03/2018 (Continued from Figure 6-8).

The spectral data obtained was investigated in a more robust manner using PARAFAC modelling, which yielded a three-component model. The three components (**Table 6-2**, **Figure 6-7**) were assigned as tyrosine-protein like (Peak B; Component 1 - C1), humic-like (Peaks C and A; Component 2 - C2) and tryptophan-protein like (Peak T; Component 3 - C3). The positions of C1 and C3 in optical space closely resemble those outlined by Baghoth *et.al* (C7 and C4 respectively ***[159]***), which were also assigned as proteinaceous or amino acid fluorescence.

Table 6-2: Fluorescence maxima and characteristics of PARAFAC components in this study.

Component	$Ex_{\lambda max}$ (nm) †	$Em_{\lambda max}$ (nm)	Coble Peak ID †	Identification
1	266	296	B	Tyrosine-like
2	251 (305)	443	A (C)	Humic-like
3	251 (281)	342	T	Tryptophan-like

† Secondary fluorescence maxima in parentheses

Comparison of C1 to the fluorescence spectrum of a pure tyrosine standard showed that C1 exhibited similar spectral characteristics to tyrosine, but with some degree of spectral shift indicating a difference in electronic environment (**Table 6-3**, **Figure 6-11**). The position of the C1 peak in optical space also closely matched the position of tyrosine protein-like fluorescence as reported in numerous other studies. As such, C1 was assigned as being representative of protein fluorescence arising from the tyrosine fluorophore, with the shift in $Ex_{\lambda max}$ and $Em_{\lambda max}$ arising from the differing electronic environment of tyrosine as present in proteins and peptides as opposed to free tyrosine. The spectrum of C1 also appeared to exhibit a secondary peak at $Ex_{\lambda max} \approx 250$ nm, which suggested that another component present in the samples was being modelled as an interfering component, indicating that C1 was not purely the result of tyrosine fluorescence.

Table 6-3: Excitation and emission maxima (nm) of C1 and tyrosine.

Spectrum	$Ex_{\lambda max}$ (nm)	$Em_{\lambda max}$ (nm)
C1	266	296
Tyrosine	275	301

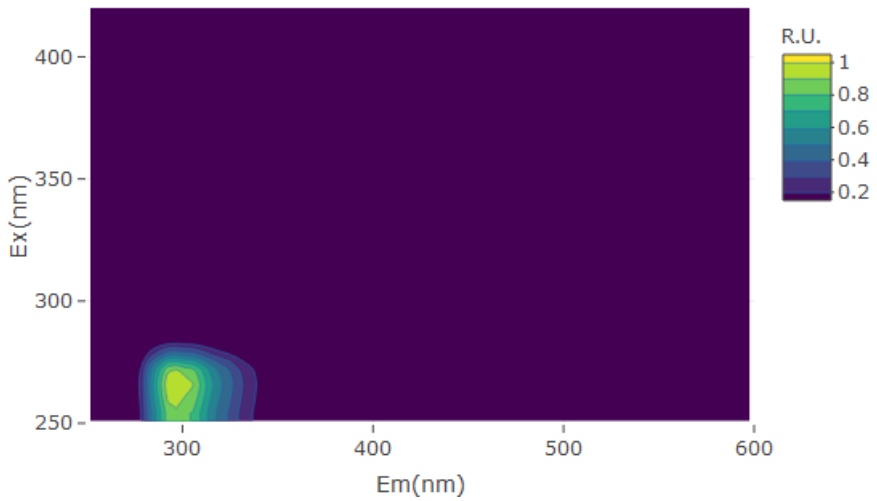

Figure 6-10: Normalised (λ_{max} = 1 R.U.) PARAFAC derived spectrum of C1.

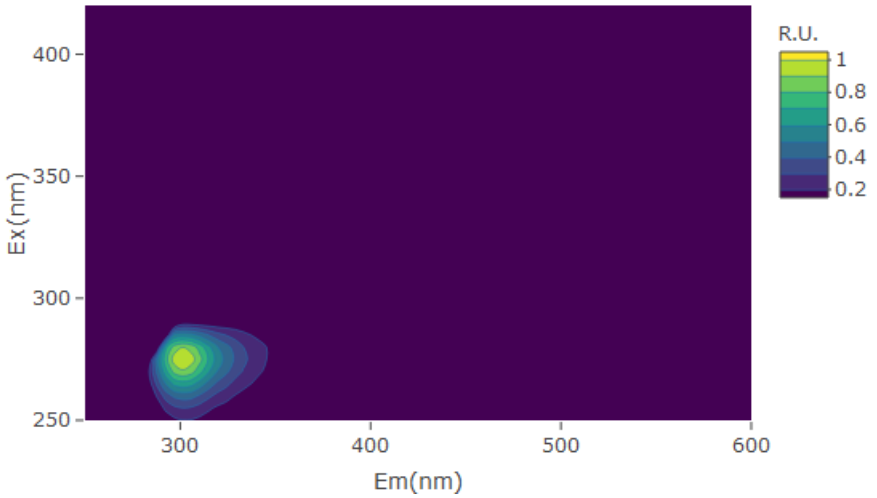

Figure 6-11: Normalised (λ_{max} = 1 R.U.) fluorescence spectrum of tyrosine.

Whereas others have obtained PARAFAC models which indicate multiple types of humic fluorescence ***[151,159]***, the humic fraction was only able to be validated as a single component here. According to ***[172]*** (**Table 2-7**), the humic component found in this study would fall between HC2 and HC3, indicating characteristics similar to UVC and UVA humic-like material, as well as UVA marine humic-like material. Such humic-like components are expected to be somewhat susceptible to photodegradation, and to exhibit intermediate molecular size and intermediate hydrophobicity compared to the other humic-like groups. Such DOM components have been found previously in forest streams, agricultural streams, seawater and swimming pools ***[267,268]***. This group will be referred to as humic-like or C2 here.

The PARAFAC derived spectrum for component C3 (**Figure 6-12**) was compared with the spectrum obtained from a pure standard of tryptophan (**Figure 6-13**). The PARAFAC derived spectrum differed somewhat to that of the standard, most notably the presence of a second excitation maximum of higher fluorescence intensity at approximately 251 nm, similar yet more pronounced than that which was present in the modelled spectrum of tyrosine like fluorescence as noted earlier.

Excitation and emission maxima of C3 and tryptophan are presented in (**Table 6-4**). The $Ex_{\lambda max}$/ $Em_{\lambda max}$ pair at 281/342 nm closely matched the fluorescence maxima of pure tryptophan, while the second peak indicated the presence of a component that was not able to be separated by the PARAFAC algorithm.

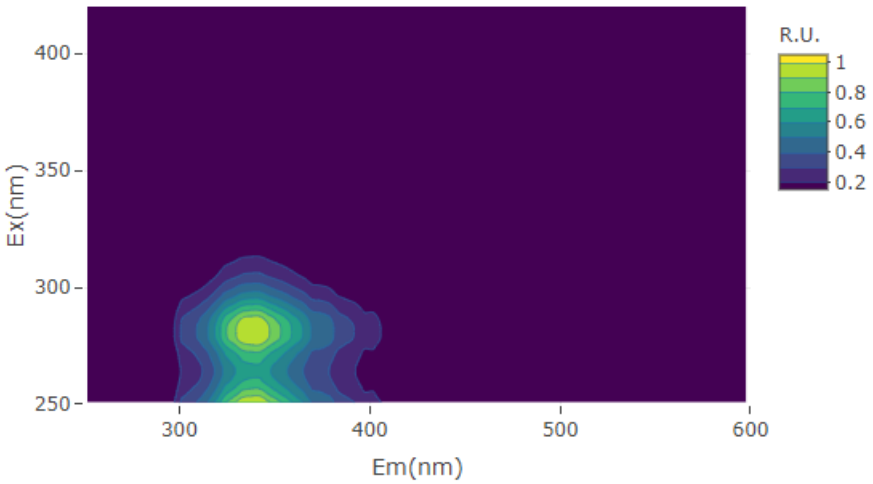

Figure 6-12: Normalised (λ_{max} = 1 R.U.) PARAFAC derived spectrum of C3.

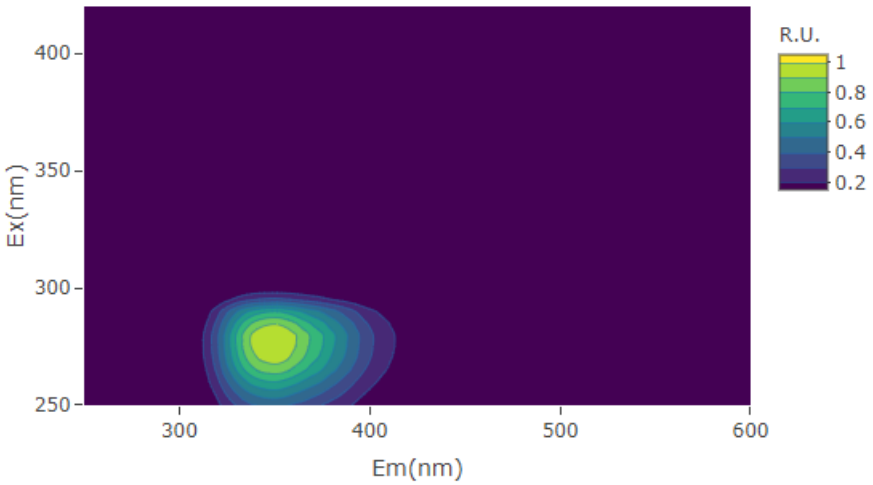

Figure 6-13: Normalised (λ_{max} = 1 R.U.) spectrum of tryptophan.

Table 6-4: Excitation and emission maxima (nm) of C3, tryptophan (secondary peaks indicated in parentheses) and tannic acid.

Spectrum	$Ex_{\lambda max}$ (nm)	$Em_{\lambda max}$ (nm)
C3	251 (281)	342
Tryptophan	280	351
Tannic Acid	260	346

Comparison of the C3 and tryptophan spectra with the spectrum of a tannic acid standard gave some indication that the second peak in the C3 spectrum may be interference from tannic acid (**Table 6-4; Figure 6-15**), lignin or simple phenolic acids (e.g. gallic, vanillic or syringic acid - **Figure 6-16; Figure 6-17**) and other breakdown products of tannins or lignin ***[269]***.

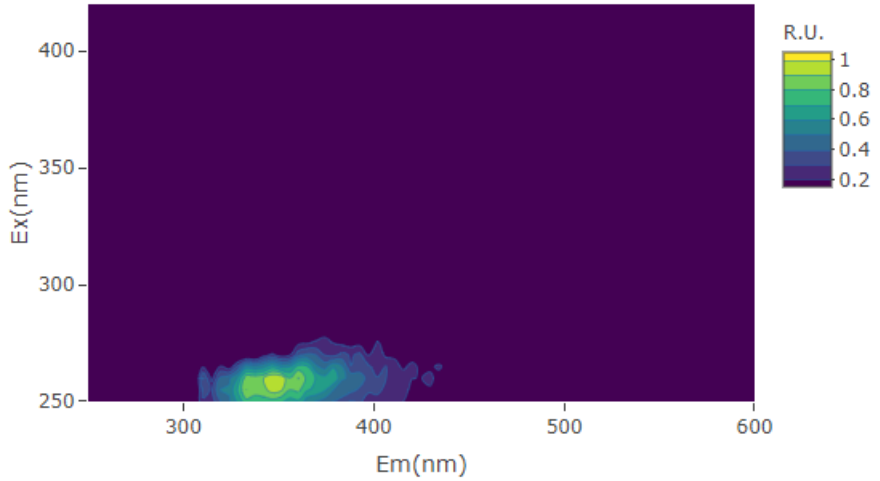

Figure 6-14: Normalised (λ_{max} = 1 R.U.) spectrum of tannic acid.

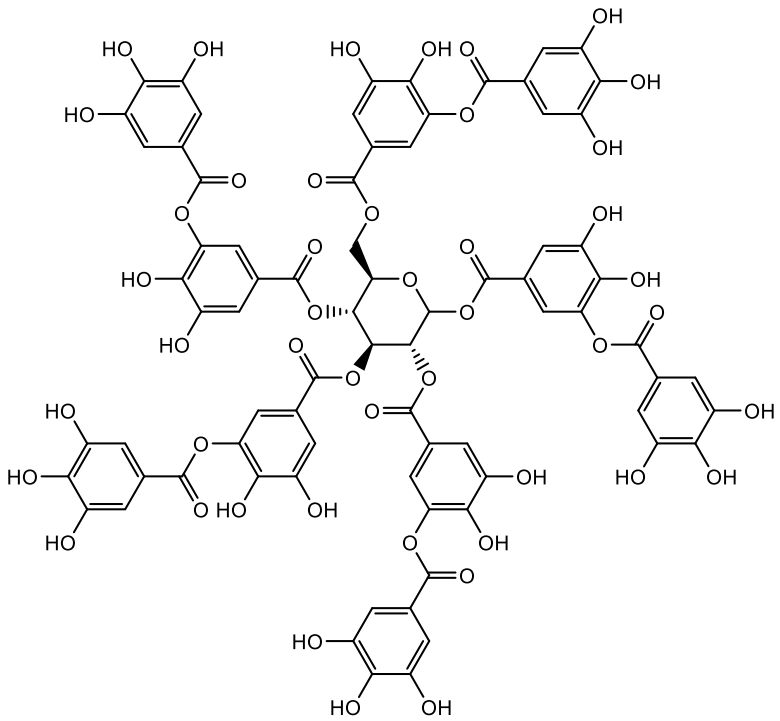

Figure 6-15: Chemical structure of a tannic acid (gallotannin), a tannin derived from gallic acid.

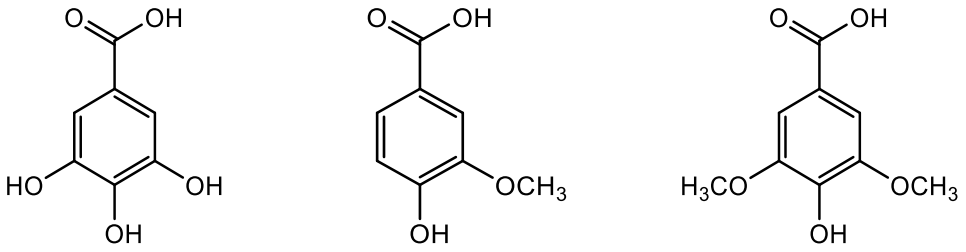

Figure 6-16: Chemical structures of gallic acid (left), vanillic acid (centre) and syringic acid (right).

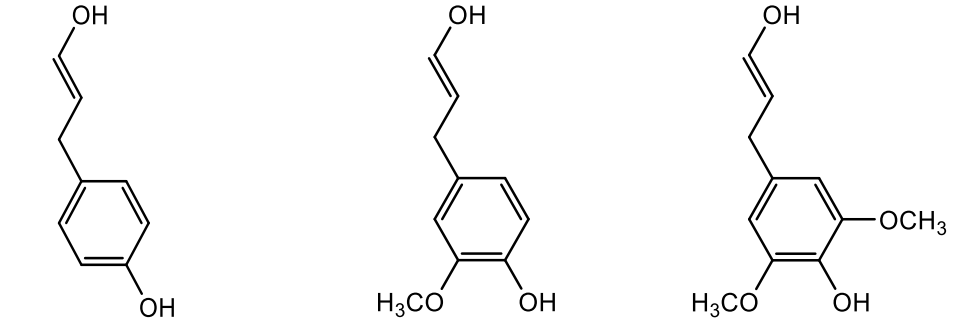

Figure 6-17: Chemical structure of some common monolignols: paracoumaryl alcohol (left), coniferyl alcohol (centre), and sinapyl alcohol (right).

The spectral overlap of C3, and also C1, with tyrosine, tryptophan and tannic acid can be further illustrated by comparing the maximum excitation and emission lines of each spectrum (**Figure 6-18**). Due to their similar spectral properties, and perhaps high degree of correlation, this may have prevented these from being modelled as individual components using PARAFAC. In fact, peak T, which is the spectral position of C3 here, has been split using size exclusion chromatography into two components of distinct molecular weights ***[270]*** and shown to be a combination of protein and phenolic material, and it is possible that this is the case here.

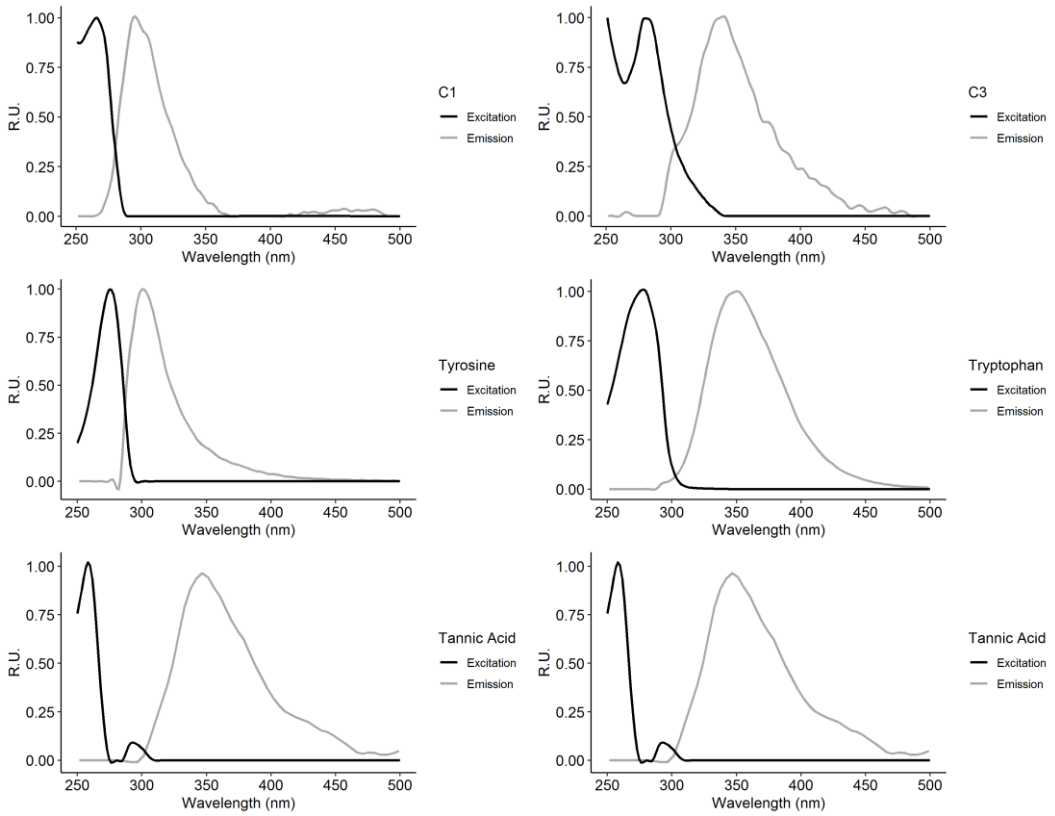

Figure 6-18: Excitation and emission maxima plots for C1, C3, tryptophan, tyrosine and tannic acid.

As a secondary fluorescence maximum was also noted in component C1, it is also possible that peak B (spectral position of C1) is a combination of more than one chemically distinct group, and not due to protein-like fluorescence alone. As such, it may not be valid to assess PARAFAC components present in the protein region of the spectrum as being purely of proteinaceous origin, particularly in natural fresh waters where inputs from plant material are likely and where the derived components have spectral features such as shoulders or secondary fluorescence maxima that are not features of tyrosine or tryptophan fluorescent residues.

6.3.2.1 PARAFAC Modelling and Validation

A total of 155 spectra were included in the PARAFAC model after preliminary analysis to remove outliers and artefacts. PARAFAC analyses with 1-10 components were carried out, with split-half validation being carried out on each of the models generated. Of these, only the three-component model could be validated by means of the core consistency diagnostic (**Figure 6-19**), split-half analysis (**Figure 6-20**) and assessment of Tucker's congruence coefficients (TCC ≥ 0.95; **Table 6-5;** ***[260,262]***).

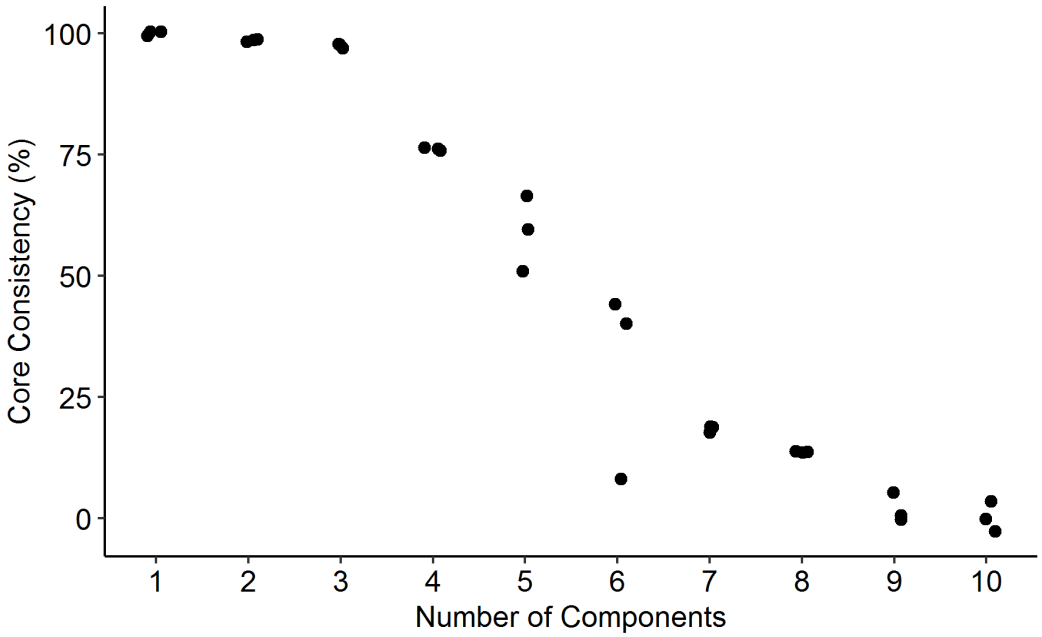

Figure 6-19: Core consistency validation plot of all modelled components. The core consistency diagnostic is used to assess the "appropriate" number of components to include in a PARAFAC model. For a one component model, the core consistency is always 100% and will drop off slowly until the maximum number of appropriate components are reached and the core consistency will drop off more abruptly *[165]*. It is generally used in conjunction with other validation tools, as have been used here.

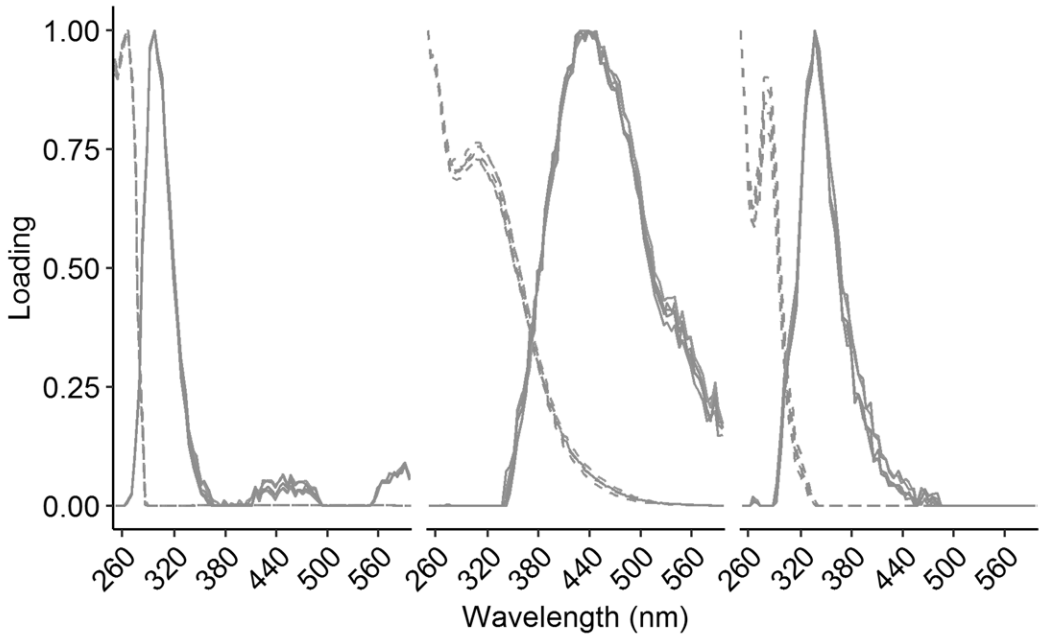

Figure 6-20: Split-half validation plots of the three component model (C1 -left, C2 -middle, C3 - right). The dataset is split into four subsamples (A, B, C, D) which are then combined (AB, CD, AC, BD, AD, BC) and modelled using PARAFAC. The model output for each combination is then plotted and compared. Due to the uniqueness property of PARAFAC models, the results of each split should be essentially the same if the correct number of components is chosen.

Table 6-5: TCC values for three component PARAFAC split-half analysis. TCC values can be used as a quantitative measure of the similarity between each split (AB vs. CD, AC vs. BD, AD vs. BC), with a maximum value of 1.000 indicating complete similarity *[260,262]*.

Component	Split-half combination	TCC(Ex λ)	TCC(Em λ)
1	ABvsCD	1.000	0.999
1	ACvsBD	0.999	0.996
1	ADvsBC	1.000	0.998
2	ABvsCD	1.000	1.000
2	ACvsBD	1.000	0.999
2	ADvsBC	0.999	0.999
3	ABvsCD	0.999	0.996
3	ACvsBD	0.996	0.995
3	ADvsBC	0.996	0.990

6.3.2.2 Overall Component Loadings and Trends

Extraction of the component loadings from the three-component PARAFAC model revealed some trends in apparent removal and persistence of specific DOM components. Overall mean loadings of each component at each sampling point are displayed in **Figure 6-21**.

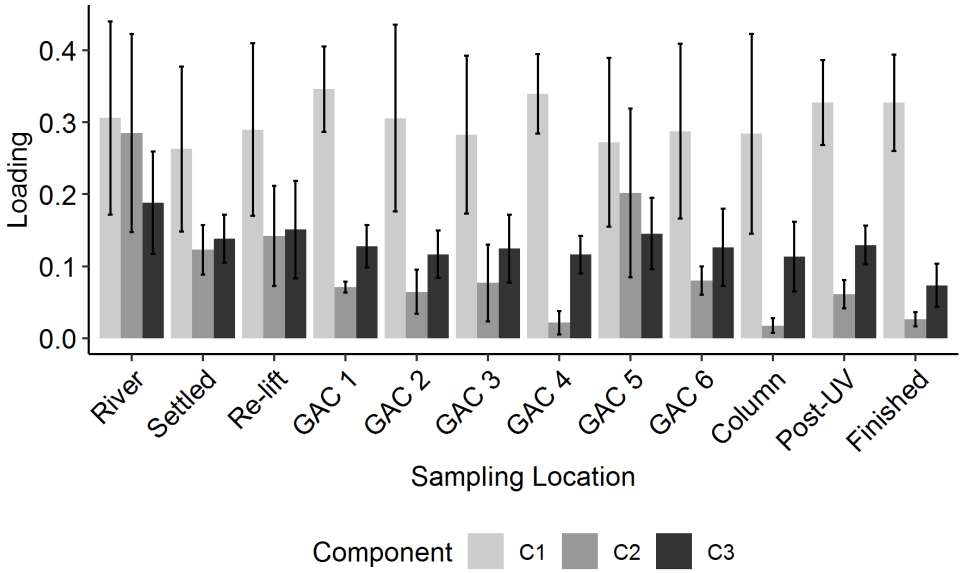

Figure 6-21: Mean PARAFAC component loadings across all sampling locations (Error bars = standard deviation).

For C2 (peaks C and A), the data indicated that the current treatment process is effective in removing humic-like compounds from the influent water source. The exception to this was GAC 5, which seems to increase C2 loading, similar to what was noted in the TOC results. Plotting the TOC results against C2 further illustrates this (**Figure 6-22**).

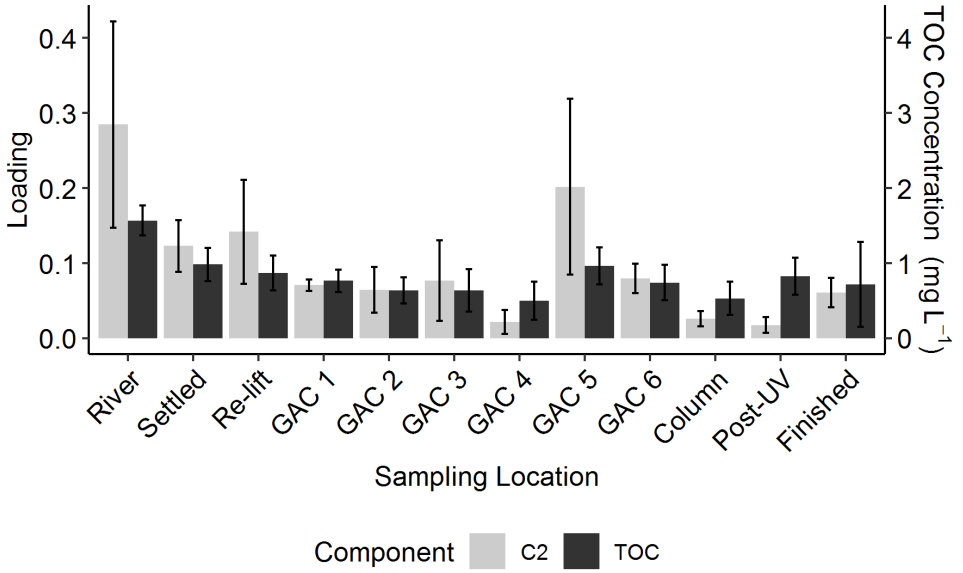

Figure 6-22: Mean C2 loading and mean TOC concentration across all sampling locations (Error bars = standard deviation).

Regression analysis of TOC concentration against C2 loading gave a good correlation (R^2 = 0.62, p = $1.1E^{-24}$; **Figure 6-24**), suggesting that TOC measurements are strongly influenced by the humic fraction of the DOM. C3 was also significantly correlated with TOC concentration, although not as strongly as C2 (R^2 = 0.14, p = $4.8E^{-5}$, **Figure 6-25**). C1 was not correlated with TOC concentration (R^2 = 0.0015, p = 0.69, **Figure 6-23**). Of course, the non-fluorescent fraction of the DOM also contributes to the TOC and could account for discrepancies in the regression analysis, but humic substances are known to make up a large fraction of DOM and are likely to be the major factor here. Strong correlations between humic loading against TOC, DOC and $SUVA_{254}$ measurements have also been found elsewhere ***[151,159,187]***.

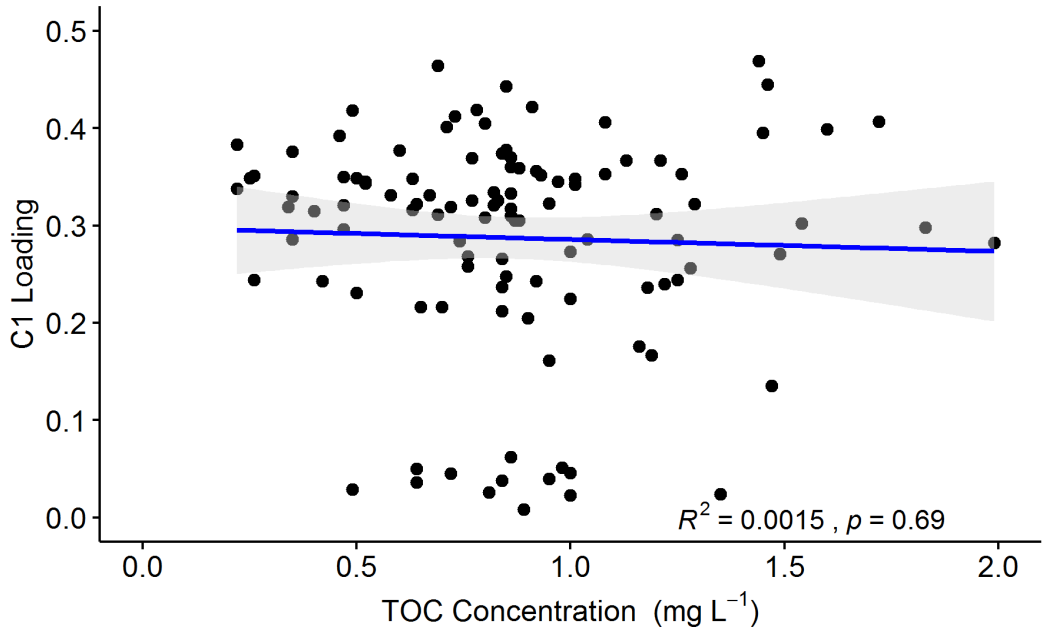

Figure 6-23: Linear regression of C1 loading and TOC concentration.

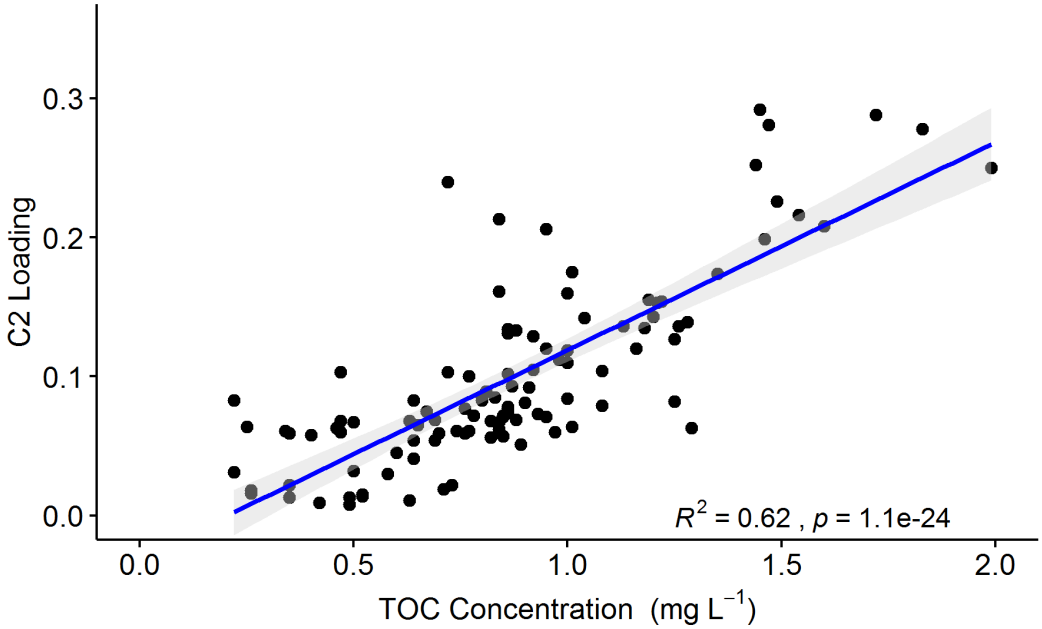

Figure 6-24: Linear regression of C2 loading and TOC concentration.

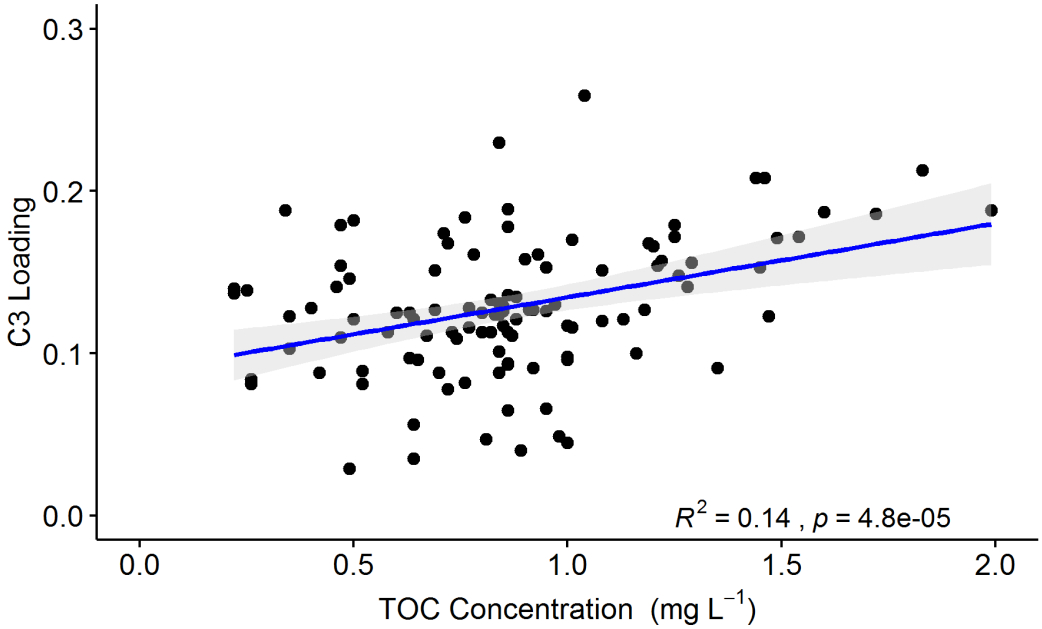

Figure 6-25: Linear regression of C3 loading and TOC concentration.

As with the TOC results, the loading of C2 following GAC filtration was also somewhat related to the age of the filter, although the effect was most apparent with GAC 5, where mean C2 loading was higher than that of the mean C2 loading of the influent water (**Figure 6-27**). Filter age appeared to have no effect on C1 and C3 loading following filtration (**Figure 6-26** and **Figure 6-28**).

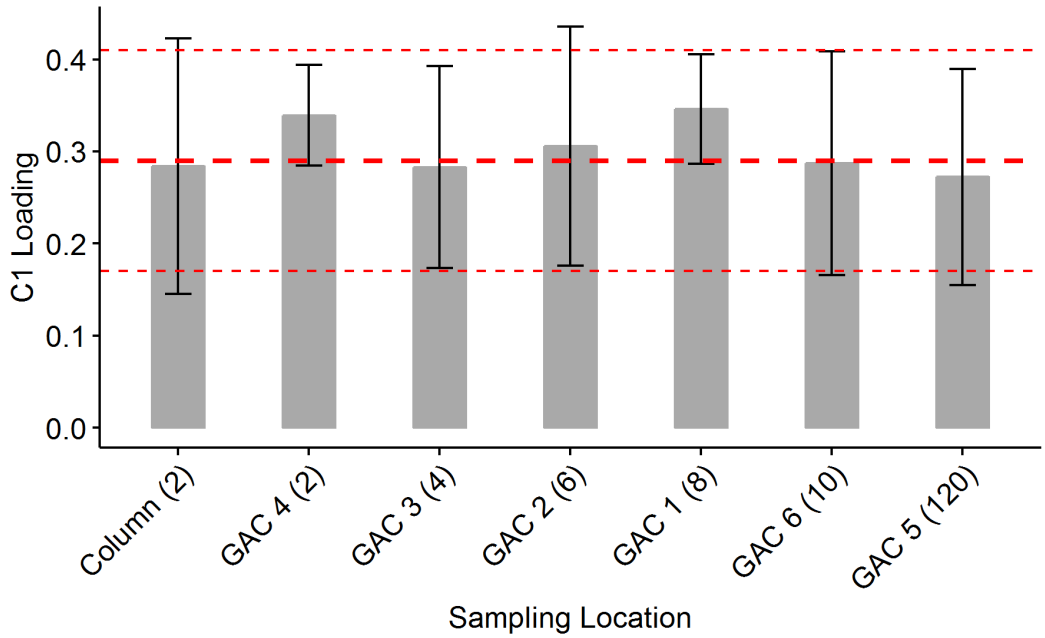

Figure 6-26: C1 loading following each GAC filter in order of ascending filter age. Approximate age denoted in months in brackets. Dotted lines indicate mean influent C1 loading ± SD.

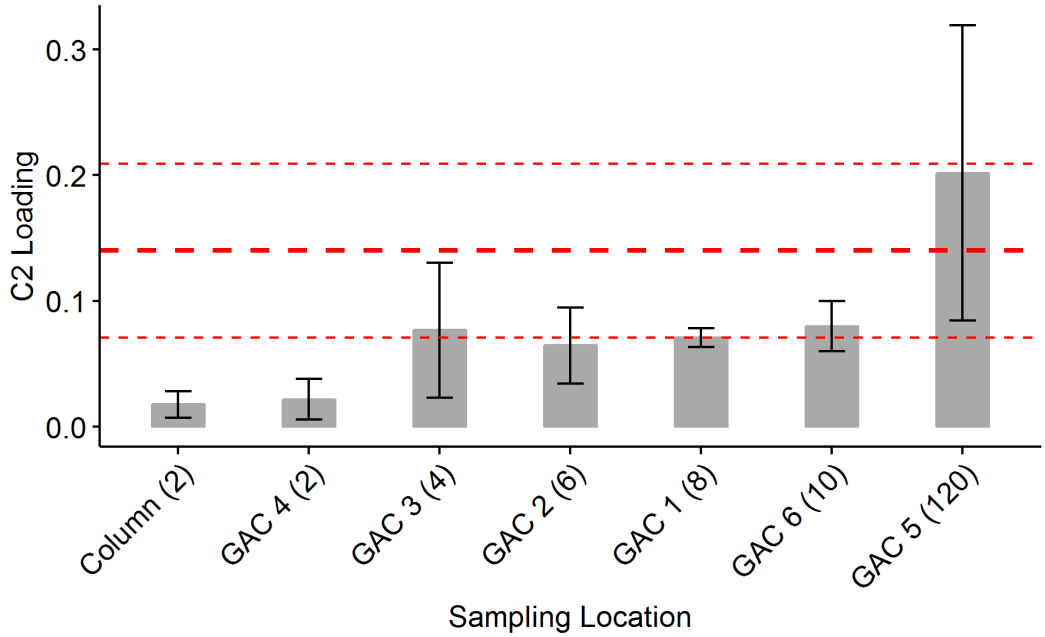

Figure 6-27: C2 loading following each GAC filter in order of ascending filter age. Approximate age denoted in months in brackets. Dotted lines indicate mean influent C2 loading ± SD.

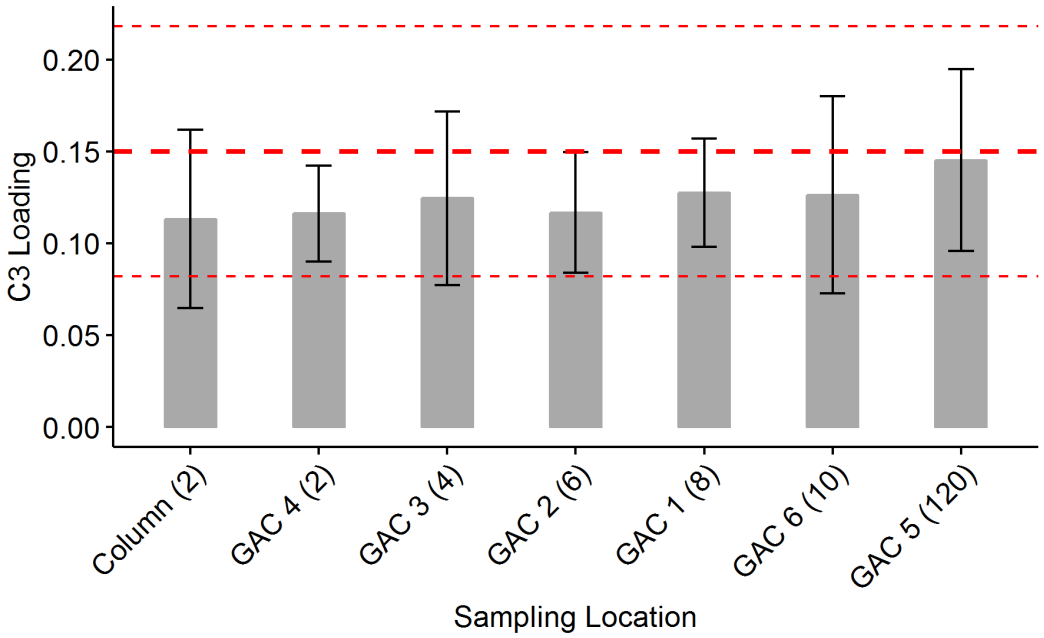

Figure 6-28: C3 loading following each GAC filter in order of ascending filter age. Approximate age denoted in months in brackets. Dotted lines indicate mean influent C3 loading ± SD.

To investigate this effect further, multiple comparisons testing was carried out following an assessment of equal variances (Levene's test ***[271]***) and adherence to normality (Shapiro-Wilk's test ***[242,243]***). Levene's test indicated that each component for each group displayed equal variances (C1; $p = 0.49$, C2; $p = 0.07$, C3; $p = 0.71$), however each group was shown not to adhere to a normal distribution (C1; $p = 1.60E^{-07}$, C2; $p = 1.63E^{-12}$, C3; $p < 0.01$). As such, non-parametric tests were used for comparison testing and multiple comparison testing (Kruskal-Wallis and Kruskal-Wallace multiple comparison tests).

Based on the Kruskal-Wallace test, C1 ($p = 0.83$) and C3 ($p = 0.58$) showed no difference between each filter, including the pilot column. This indicated that there was no statistical difference in the effectiveness of each filter in the removal of C1 and C3. Moreover, based on the mean fluorescence of C1 and C3 following filtration in relation to the influent C1 and C3 fluorescence (**Figure 6-26** and

Figure 6-28), it seems apparent that the GAC filters are ineffective at removing proteinaceous DOM.

The Kruskal-Wallace test for C2 indicated that there were significant differences between each filter ($p = 1.40E^{-11}$), so the Kruskal-Wallace multiple comparisons test at significance levels of $\alpha = 0.05$ and $\alpha = 0.01$ was used to give an indication of which filters differed from each other. Pairwise comparisons which showed statistically significant differences are listed in **Table 6-6**.

Table 6-6: Statistically significant Kruskal-Wallace multiple comparisons of C2 loading following each GAC filter.

Comparison	Difference ($\alpha = 0.05$)	Difference ($\alpha = 0.01$)
GAC1 - Column	True	True
GAC3 - Column	True	False
GAC5 - Column	True	True
GAC6 - Column	True	True
GAC1 - GAC4	True	True
GAC3 - GAC4	True	False
GAC5 - GAC4	True	True
GAC6 - GAC4	True	True
GAC2 - GAC5	True	True
GAC3 - GAC5	True	True

The newest filter (pilot column) was significantly different to the three oldest filters (GAC 5, GAC 6 and GAC 1) at the $\alpha = 0.05$ and $\alpha = 0.01$ significance levels, while a newer filter, GAC 3, also differed from the pilot column, but only at the $\alpha = 0.05$ level. As the pilot column had been recently filled with fresh GAC media, it would be expected to perform better than filters that had been in use for longer periods of time (GAC 5, GAC 6 and GAC 1). The column was also filled with pure GAC media, while the full-scale filters contained either mixed GAC/BAC media (GAC 1 and GAC 6), or purely BAC media (GAC 5). While GAC 3 also exhibited a significant difference at the $\alpha = 0.05$ level, an older filter (GAC 2) did not. However, this was not apparent at the $\alpha = 0.01$ level.

The newest full scale filter (GAC4) was significantly different to the three oldest filters (GAC 5, GAC 6 and GAC 1) at the $\alpha = 0.05$ and $\alpha = 0.01$ significance levels, while the next two newest filters (GAC 3 and GAC 2) were only significantly different to the oldest filter (GAC 5). This lends further evidence to the conclusion that new filters perform better than older filters regarding C2 removal. An exception to this is between GAC 3 and GAC 4, where a statistical difference was apparent at the $\alpha = 0.05$ level. These filters were of a similar age (approximately 4 and 2 months old respectively), and would be assumed to have behave similarly, although this seemed not to be the case. However, this effect was not discernible at the $\alpha = 0.01$ level and may also have been an artefact of the high variability in the GAC 3 results. Of note here, is that a noticeable effect is produced between filters that show relatively small difference in ages. For example, the age difference between GAC 4 and GAC 1 was only 4 months, but a reduction in the effectiveness of GAC 1 relative to GAC 4 was statistically discernible at both the $\alpha = 0.05$ and $\alpha = 0.01$ levels. This suggests that the mean effectiveness of the filters following partial media replacement begins to decline quite quickly. As a general trend, older filters tended to differ from newer filters, while those of similar age tended to exhibit similar performance, as would be expected. This trend is similar to that shown for the GAC TOC results (**Appendix A-3**, **Figure 6-6**), as would be expected considering the strong correlation between TOC concentration and C2 fluorescence.

In the case of GAC 5, the increase in C2 loading following filtration relative to influent loading may be of some concern, as humic acids are implicated in the formation of disinfection by-products (DBPs) ***[146]***. It is also likely that this effect will become apparent with the other filters as they age following media replacement.

However, at the time of sampling it seemed clear that partial replacement of the filter media provided a significant improvement in filter performance.

Regarding peptide derived fluorophores the overall treatment seemed ineffective towards C1, with the loadings of C1 increasing slightly through the treatment train, following a slight reduction at the flocculation stage (**Figure 6-21**). However, as the EEM technique measures the fluorescence of tyrosine and tryptophan only, the breakdown of longer polypeptides and proteins (e.g. biodegradation) is not accounted for. Regarding peak T, it is possible that the concentration of specific biopolymers is reduced, while the concentration of tyrosine and tryptophan remain constant in the form of shorter peptides or monomers. However, others researchers have noted that the protein fraction of the fluorescent DOM is removed to some degree during flocculation, particularly tyrosine fractions ***[159]***. This may be due to the nature of the source water, flocculation conditions, the overall makeup of the DOM such as hydrophobicity and chain length. In this case, it may be that the peptide fraction of the DOM is made up of short chain length molecules that are minimally affected by flocculation and sand filtration, and their polar nature would mean that GAC filtration would also be ineffective.

Looking at mean component loadings across sampling sites associated with the plant only (ignoring the pilot column) and grouping the GAC filters as a parallel process, the change in the prevalence of each component becomes somewhat clearer (**Figure 6-29**). On average, this gives a picture of a decreasing C2 fluorescence (peaks A and C), with a less dramatic decrease in C3 (peak T) fluorescence throughout the treatment train. C1 (peak B) dropped slightly following

coagulation/flocculation, then increased marginally for the remainder of the treatment process.

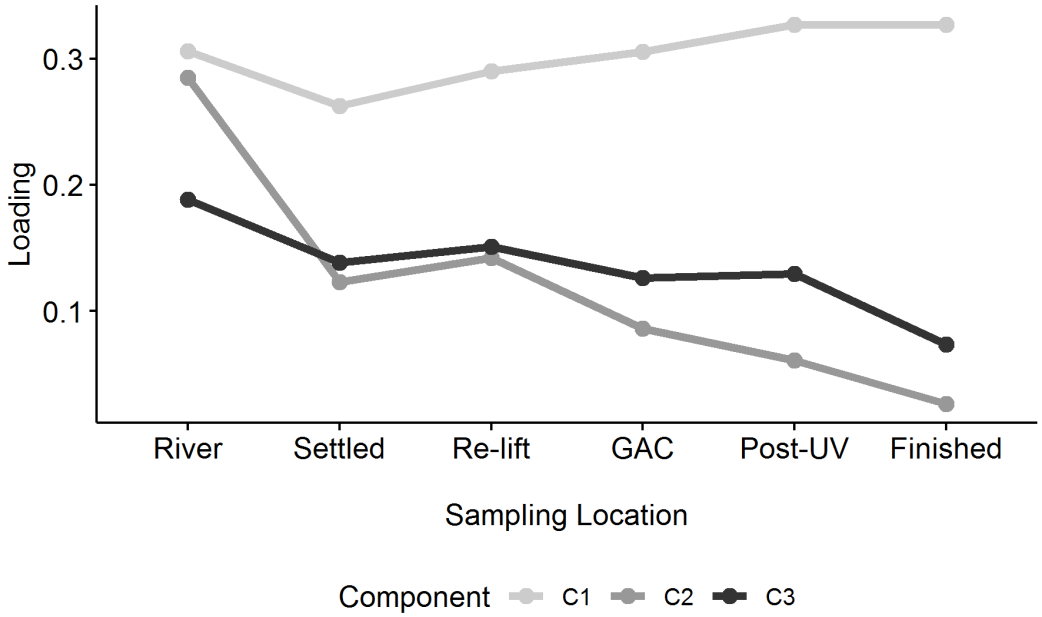

Figure 6-29: Mean component loadings across plant specific sampling sites and mean GAC results.

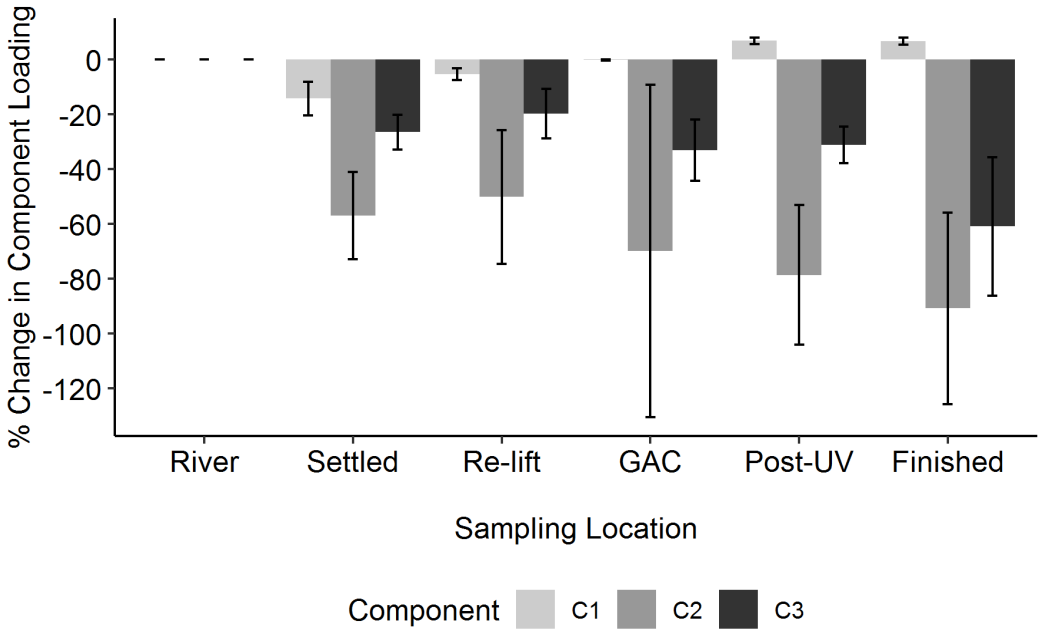

Figure 6-30: Mean percent change in component loadings at each plant specific sampling point (error bars = standard deviation).

Cumulative percent removal based on component loadings also illustrates this (**Figure 6-30)**, indicating an approximate 90 % reduction in C2 humic-like fluorescence, and 60 % decrease in C3 tryptophan/protein-like fluorescence. C1 tyrosine/protein fluorescence showed an approximate 15 % reduction following coagulation/flocculation, which steadily rose to a 6 % overall increase at the final stage of treatment.

The removal of C2 was quite variable across the plant, particularly following GAC filtration. The high variability of the pooled GAC results can be attributed to the much higher C2 fluorescence following GAC 5 and the lower fluorescence of GAC 4, resulting in a large spread of C2 fluorescence when pooling the GAC results. However, as the GAC filtered water is combined following this treatment stage, this does not represent the range of C2 fluorescence following GAC filtration prior to UV treatment.

While the current treatment process is effective in reducing humic-like fluorescence, the results for protein-like fluorescence displayed mixed effectiveness. The behaviour of protein-like fluorophores is known to vary across different DWTPs with the properties of the source water and the specific treatment types used playing a greater role. Further, the steady increase in C1 could indicate autochthonous production of tyrosine containing biological products, which would make sense following biological GAC filtration. Nevertheless, an increase in C1 was seen throughout treatment, and no sudden increase in C1 was noted following GAC filtration. Some reasons for this could include the lysing of cells during coagulation, biological activity in the rapid sand filters, and changes to molecular structure that

influence fluorescence intensity, for example during UV irradiation or reactions during disinfection with chlorine ***[169,174]***. While the slight decrease in C1 loading at the settled water stage may be attributed to the slight decrease in pH at this stage (**Figure 6-31)**, as the pH remains stable for the rest of the treatment train, this does not account for the continued increase in C1 loading through the remainder of the plant.

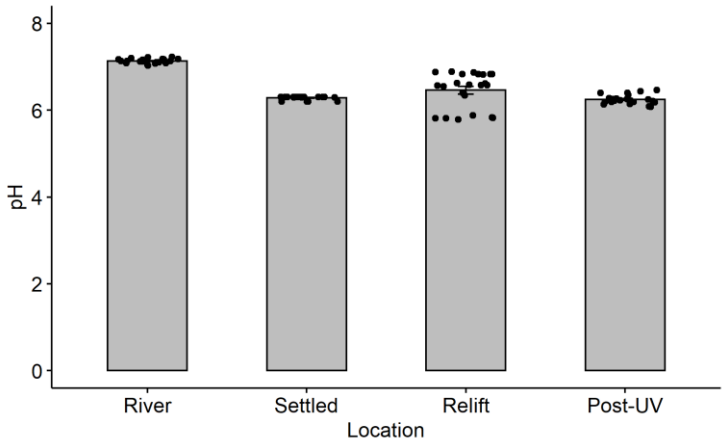

Figure 6-31: pH at various stages through the treatment train as measured by online instruments installed onsite.

Additionally, the possibility that both C1 and C3 exhibit some amount of tannin or phenolic fluorescence as discussed earlier, may have an influence on their apparent removal through the plant. Some of these components are quite hydrophobic, and the fact that C3 appeared to exhibit a greater spectral contribution from phenolic-type fluorescence may explain why C3 appeared to be removed more effectively than C1. In this case, the hydrophobic phenolic component would be preferentially removed, while the more soluble protein fraction would remain in greater relative proportions.

Overall, the changes in TOC concentration and the fluorescence of specific components indicate that changes in TOC are largely due to the removal of humic

substances and other DOM components that do not fluoresce. Others have also noted that humic substances correlate well with TOC and DOC measurements. The residual TOC may be considered as an estimate of the concentration of protein derived fluorophores, although this residual fraction will also contain non-fluorescent species, for example carbohydrates. The fact that strong proteinaceous fluorescence was observed on each day samples were collected indicates that proteins and peptide make up a significant amount of the DOM present in the Waikato River. Other studies that have looked at fluorescence in water treatment plants seem to indicate much lower protein fluorescence relative to humic fluorescence. As fluorescence arising from proteins is generally regarded as being indicative of recent biological activity, this suggests that the Waikato River is highly populated with active biological communities on an ongoing basis which may be due to the high degree of agricultural land use in the area.

The polar nature of dissolved peptides and proteins suggests that other polar compounds may be unaffected by the current treatment processes used at the HWTS. This may be of some concern, considering that cyanotoxins are either cyclic peptides (e.g. microcystins) or small, highly polar molecules (e.g. saxitoxins). In the event of future cyanobacterial blooms, monitoring of these compounds would still be required in order to ensure compliance with the DWSNZ, as it cannot be assumed that these compounds are sufficiently removed by the current treatment process.

6.3.3 EEMS of DOM Distribution in a Pilot Scale GAC filter

Samples collected from the pilot column in March 2019 during GSM and 2-MIB dosing experiments were analysed in a similar manner to samples collected from the entire plant as previously discussed. PARAFAC modelling yielded a three-component model, which was validated using split-half analysis and the core consistency diagnostic. The components yielded from the column model indicated the presence of tyrosine-protein like fluorescence (B; Component 1 - C1), humic-like fluorescence (C and A; Component 2 - C2) and tryptophan-protein like fluorescence (T; Component 3 - C3).

Raw fluorescence spectra (**Figure 6-32**) and the position and spectral appearance of each fluorescence group closely resembled those found during the analysis of samples collected from the entire plant in 2018, indicating that the general composition of fDOM in the Waikato River during late summer is similar on a yearly basis. Further, it was found that humic fluorescence was reduced significantly relative to protein fluorescence, while protein fluorescence was minimally affected during GAC filtration. Additionally, the intensity of protein fluorescence through the filter column appeared to be highly variable, suggesting that the amount of protein and amino acids present in the water system may vary considerably over short time frames.

In contrast to the data obtained in 2018, the overall performance of the pilot column appeared to have deteriorated, with reduced effectiveness in the removal of humic substances becoming apparent, although the removal of humic material was still significant compared with protein derived fluorophores. This was to be expected,

as the column had been in use for approximately 12 months, and the adsorption capacity of the GAC media would be depleted to some extent.

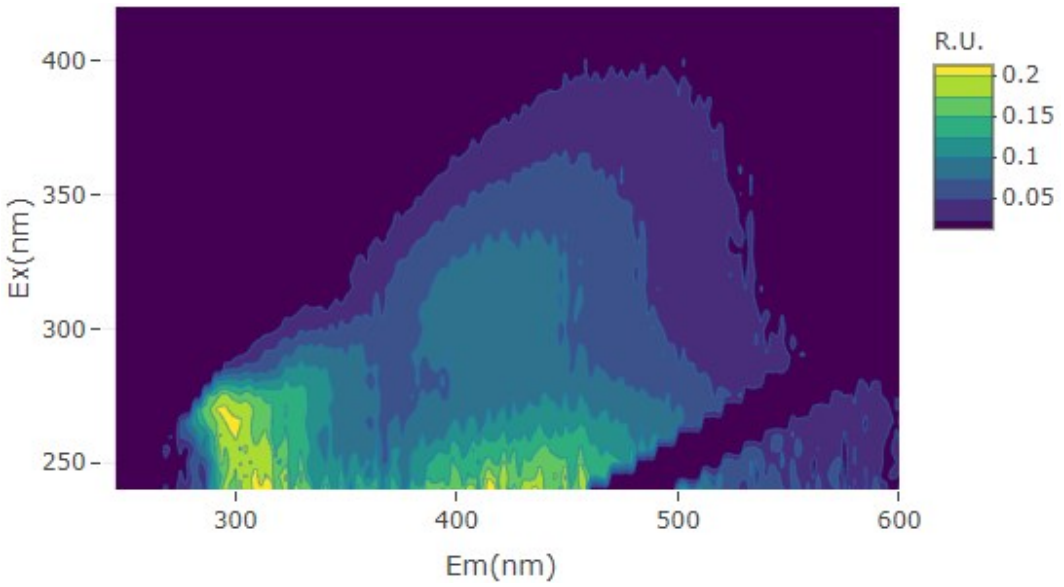

Figure 6-32: EEM fluorescence spectrum of influent water collected during column monitoring experiments.

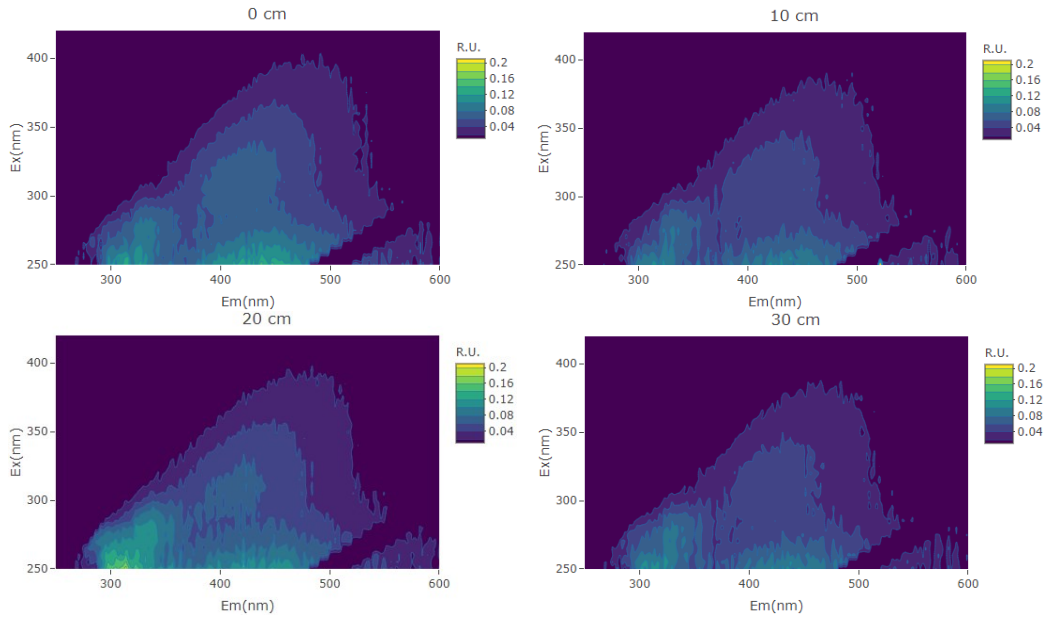

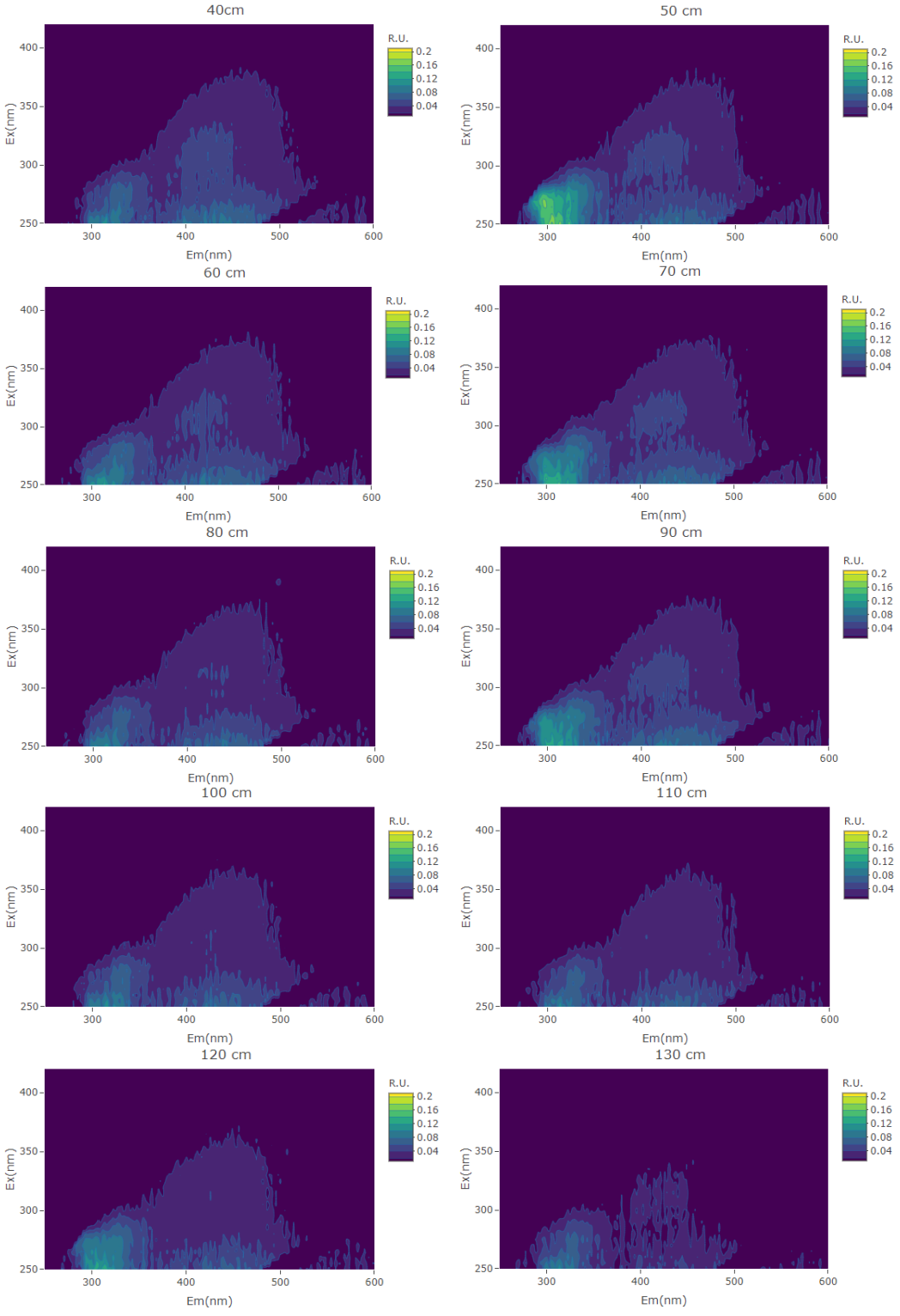
40cm
50 cm
60 cm
70 cm
80 cm
90 cm
100 cm
110 cm
120 cm
130 cm
Ex(nm)
Em(nm)
R.U.
0.2
0.16
0.12
0.08
0.04
250
300
350
400
500
600

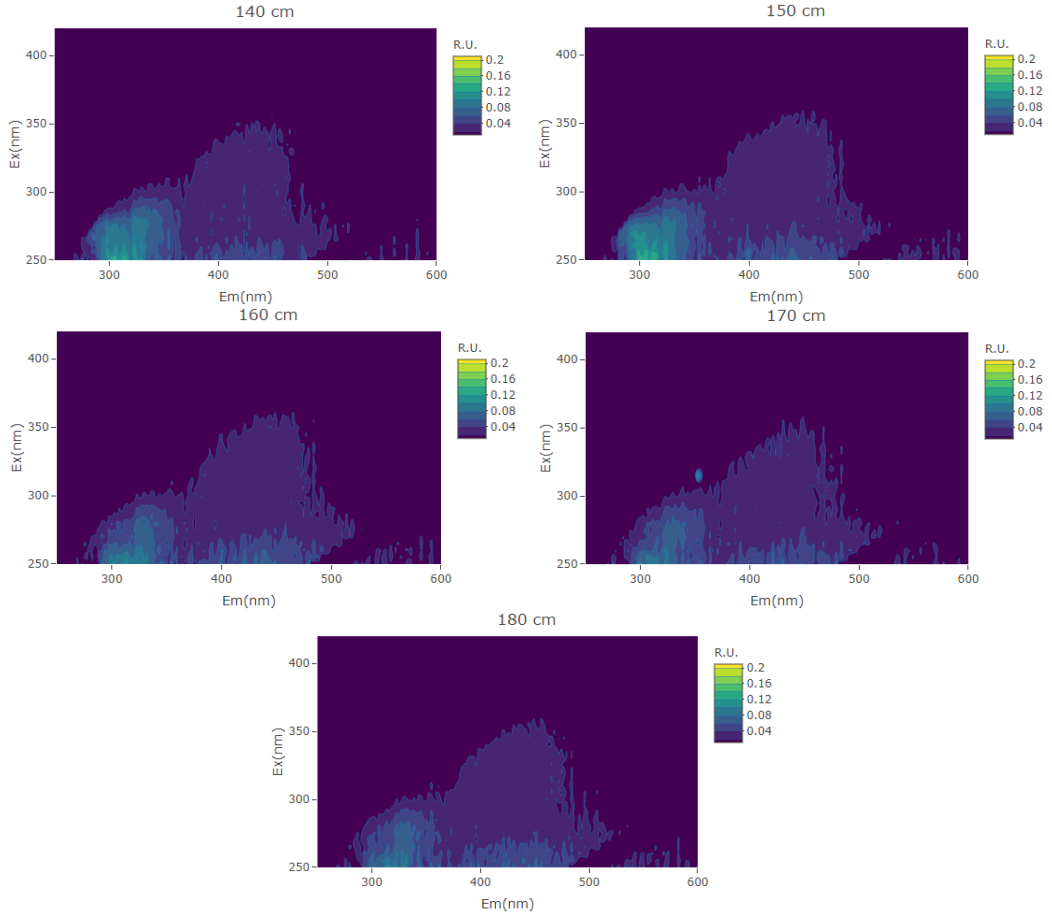

Figure 6-33: EEM spectra of water samples collected across the depth of the pilot GAC column.

6.3.3.1 PARAFAC Modelling and Validation

A total of 60 spectra were included in the PARAFAC model after preliminary analysis to remove outliers and artefacts. PARAFAC analyses with 1-10 components were carried out, with core consistency and split-half validation being carried out on each model. As with the samples collected across the entire plant, only the three-component model could be validated by means of the core consistency diagnostic, split-half analysis and assessment of Tucker's congruence coefficients (TCC ≥ 0.95) (**Figure 6-34, Figure 6-35, Table 6-7**).

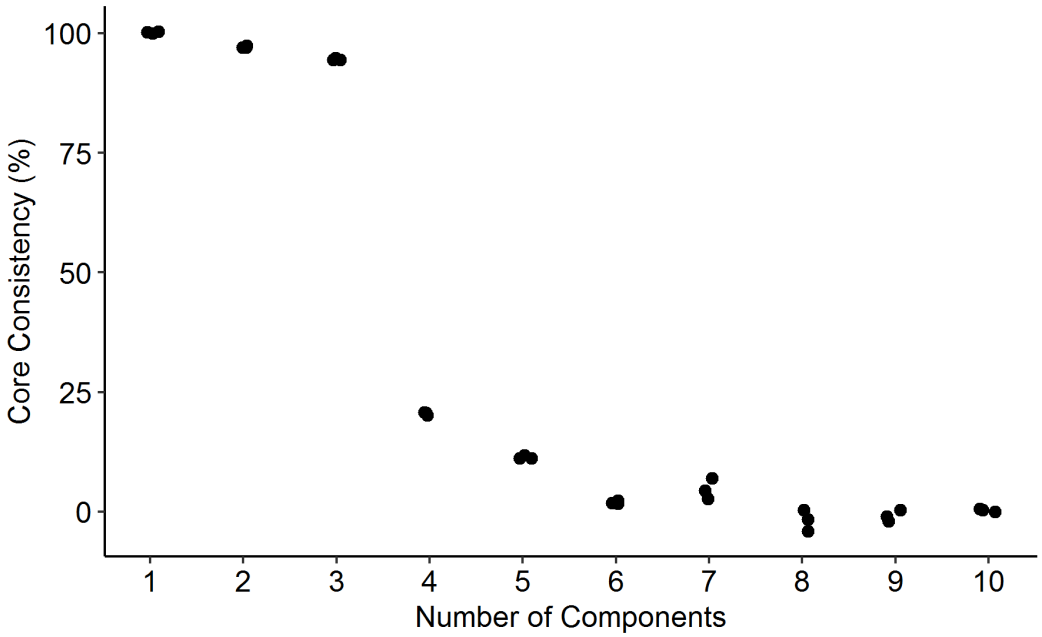

Figure 6-34: Core consistency validation plot of 1 - 10 component PARAFAC models obtained from pilot column data.

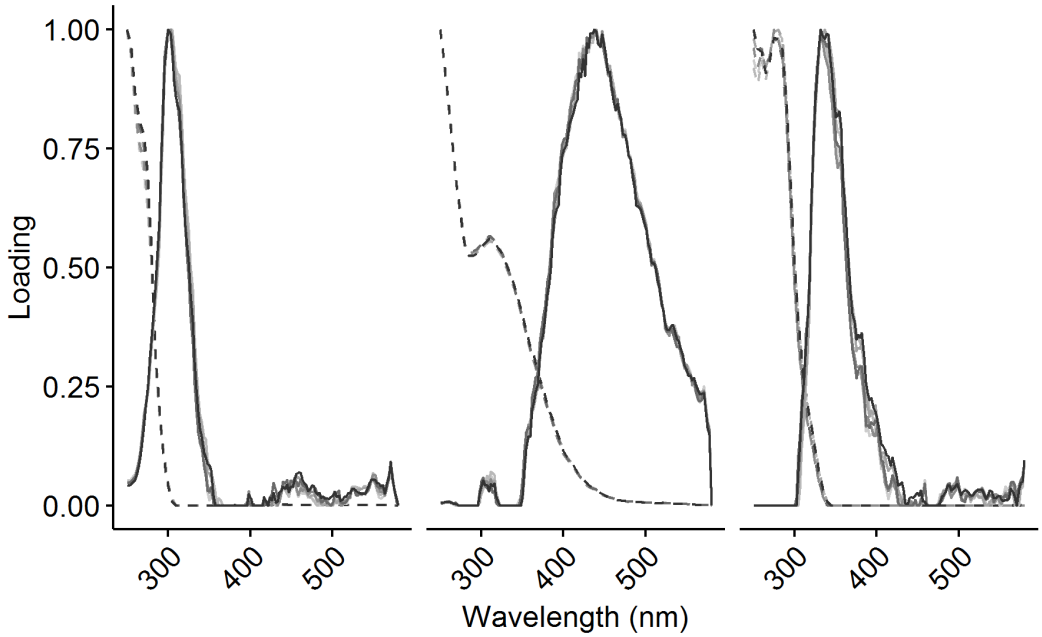

Figure 6-35: Split-half validation plot obtained from the pilot column data.

Table 6-7: TCC values (4 d.p.) for the three component PARAFAC split-half analysis of the pilot column data.

Component	Split-half combination	TCC(Ex λ)	TCC(Em λ)
1	ABvsCD	0.9998	0.9995
1	ACvsBD	1.0000	0.9995
1	ADvsBC	1.0000	0.9997
2	ABvsCD	0.9990	0.9973
2	ACvsBD	0.9996	0.9947
2	ADvsBC	0.9999	0.9981
3	ABvsCD	0.9991	0.9953
3	ACvsBD	0.9983	0.9941
3	ADvsBC	0.9994	0.9962

6.3.3.2 Overall Component Loadings and Trends

The results for C1, reflecting tyrosine-like fluorescence, were somewhat difficult to describe in simple terms of an overall reduction of fluorescence intensity, displaying features that were not present in the results for C2 or C3. Based on considering only the influent and effluent C1 loading, it could be concluded that C1 loading was reduced slightly across the filter bed. Comparing the behaviour in reduction of C1 across the filter bed with the results obtained during sampling in 2018, it seems apparent that the reduction of C1 loading is highly variable (**Figure 6-36**), which is illustrated further by comparing mean percent C1 reductions between years (**Figure 6-37**). Additionally, the influent loading of C1 was generally lower during 2019 sampling than 2018 (**Figure 6-38**), although two days from 2018 had comparable influent loadings as well as percent C1 removal (**Figure 6-39**). Although this indicates that the filter was performing better during 2019, the highly variable influent loading coupled with highly variable percent reduction makes reaching a clear conclusion difficult. In this case, carrying out sampling on more days, particularly in 2019 may have alleviated this issue.

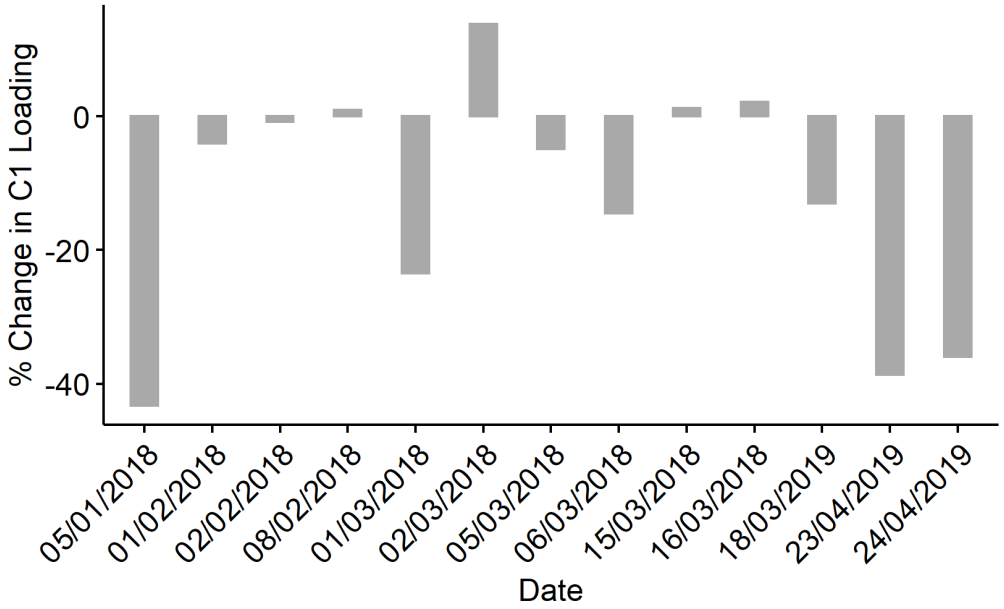

Figure 6-36: Percent change in column influent and effluent C1 loading across all sampling days from 2018 and 2019.

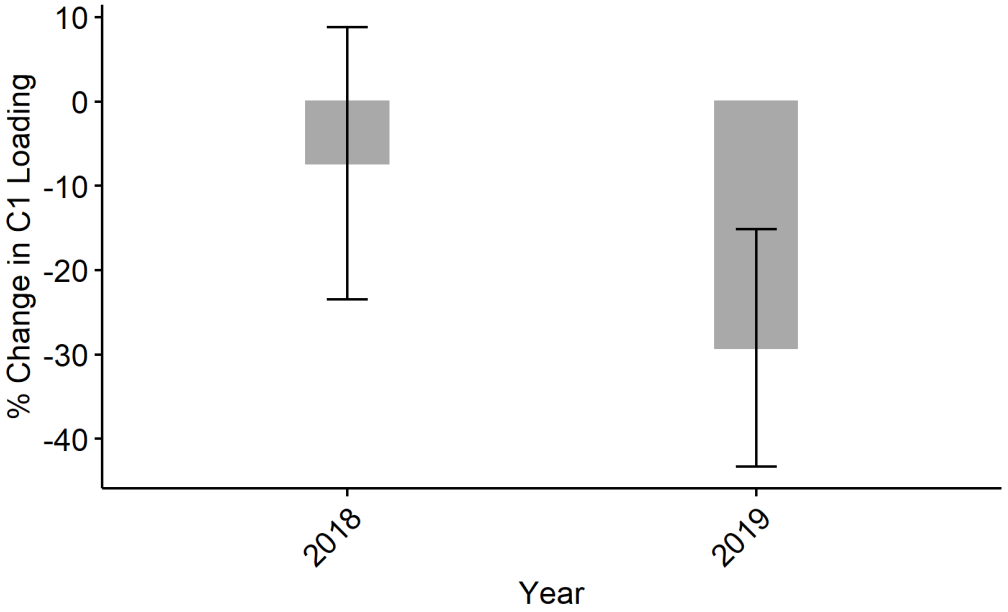

Figure 6-37: Mean percent change in column C1 loading from (n = 10) and 2019 (n = 3) (error bars = standard deviation).

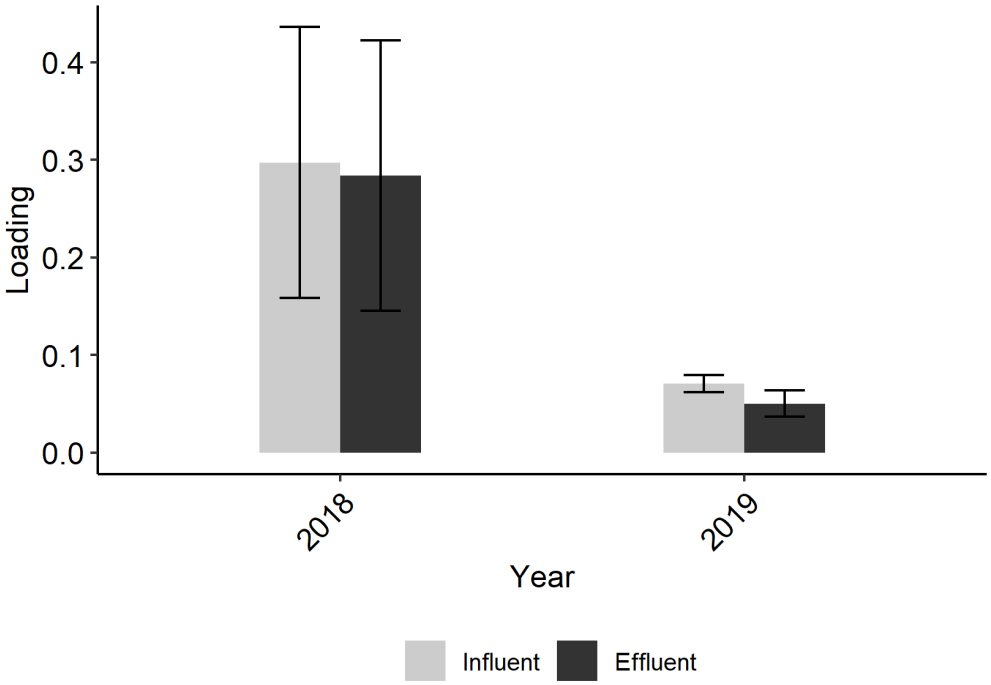

Figure 6-38: Mean influent and effluent C1 loading from 2018 (n = 10) and 2019 (n = 3) (error bars = standard deviation).

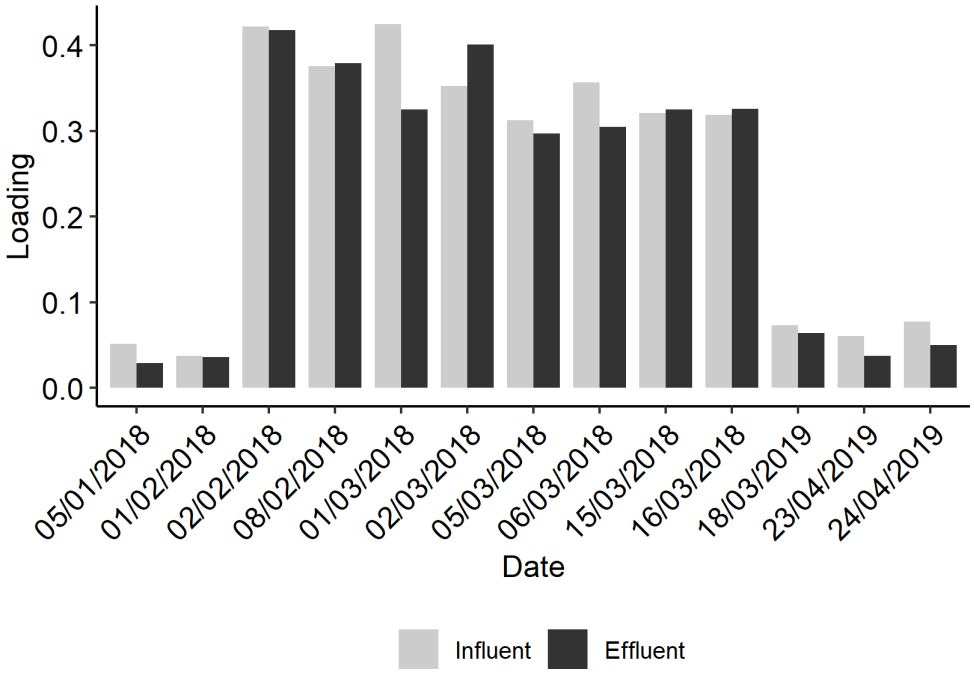

Figure 6-39: Column influent and effluent C1 loading across all sampling days from 2018 and 2019.

Looking in more detail at the C1 results through the depth of the column, spikes in the loading of C1 were observed a various stages (**Figure 6-40**). Why this was the case is unclear. Initially, this was thought to be an artefact of the PARAFAC

modelling, however, sharp increases in the raw fluorescence spectra in the region occupied by C1 could be easily discerned, indicating that this was in fact a real effect present in the sample data. This can be visualised by peak picking F_{max} for peak B in the raw spectra and plotting the data, from which a similar trend to that obtained from the PARAFAC data is observed (**Figure 6-41**).

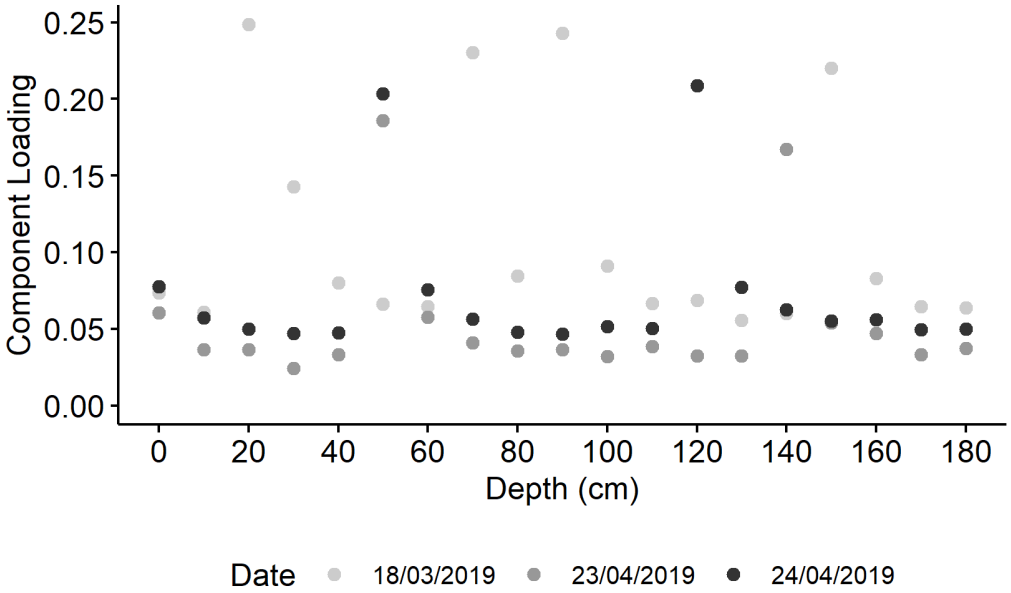

Figure 6-40: C1 loading across the column depth for each sampling day.

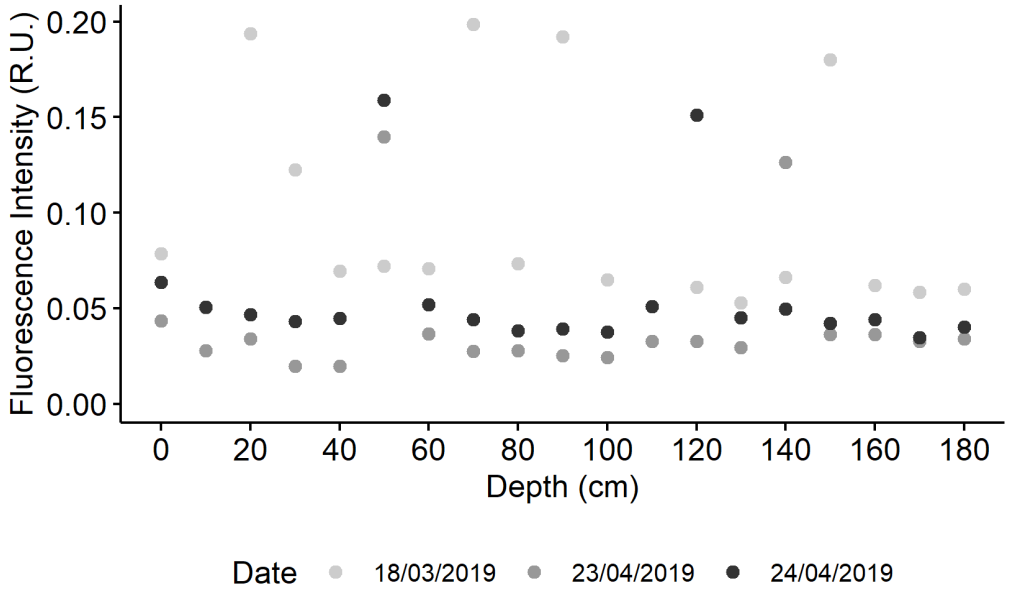

Figure 6-41: Peak B intensity across the column depth for each sampling day.

Looking at the position of Ex_{max} at an emission wavelength of 300 nm provided some more insight as to what was occurring to produce spikes in the data. All of the high C1 loading points correlated with an Ex_{max} of approximately 265 nm, while the baseline C1 loading correlated with an Ex_{max} of approximately 250 nm (**Figure 6-42**).

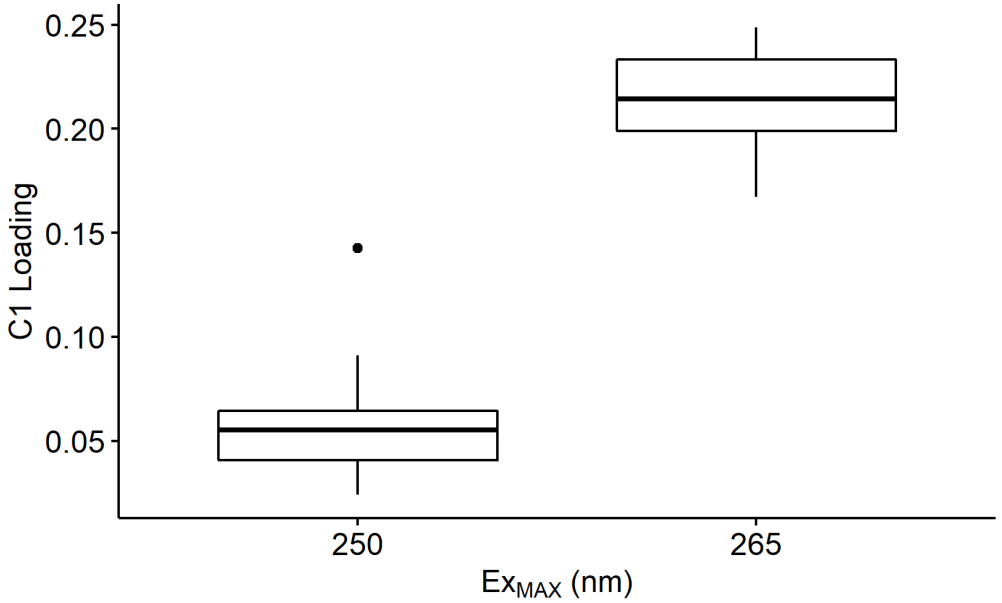

Figure 6-42: Distribution of C1 loadings at respective Ex_{max} values.

As noted for C1 and C3 in the PARAFAC analysis of the full-scale plant data, the modelled components seem to include a second Ex_{max} peak at approximately 250 nm, which is not indicative of amino acid type fluorescence, but may be the result of tannic acid, lignin or phenolic acid fluorescence ***[269]***. It appears in this case, that the high intensity spikes across the column arise from tyrosine-like fluorescence ($Ex_{max}/Em_{max} \approx 265/300$ nm), while the residual fluorescence arises from other species present in the water that exhibit phenolic acid type fluorescence. However, this does not explain the presence of spikes in tyrosine-like fluorescence. Without carrying out further experiments to specifically investigate this phenomenon, robust conclusions cannot be made. Some speculative reasons include

dislodgement of bacteria or bacterial exudate from the GAC surface during sample collection, which may have been exacerbated by recent backwashing. Indeed, this effect was more pronounced for samples collected on 18/03/19, which was one day after the most recent back wash of the filter.

Humic fluorescence (component C2) was found to decrease across the filter bed depth, indicating that after 12 months of operation the filter medium was still effective at removing humic substances from the influent water delivered post sand filtration (re-lift) to some extent. Visualising C2 loading across the column depth for each sampling day showed a clear trend in the reduction of C2 through the column (**Figure 6-43, Figure 6-44**).

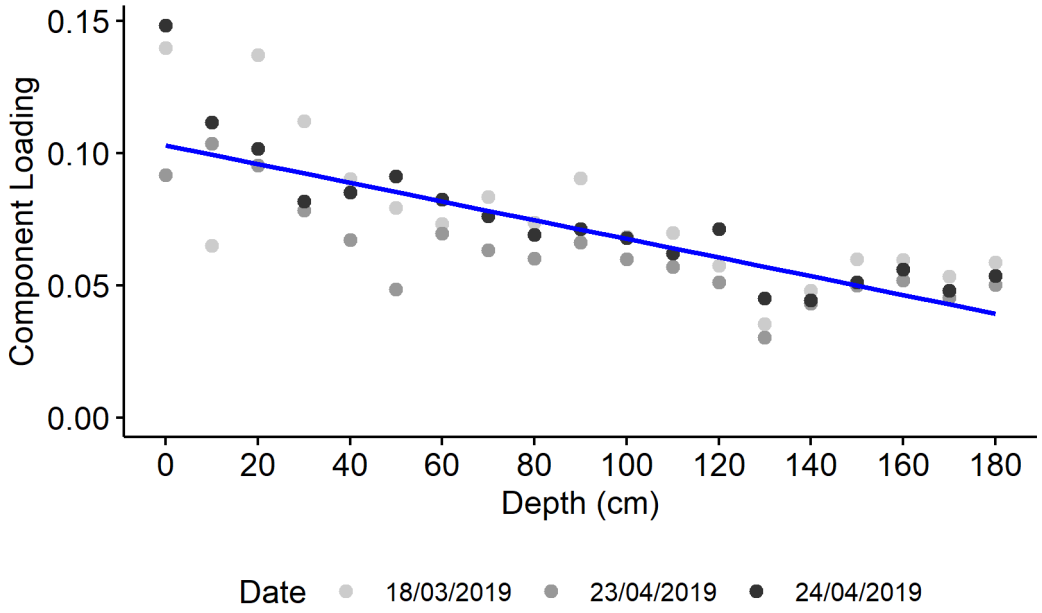

Figure 6-43: C2 loading across the column depth for each sampling day fitted to a linear model (R^2 = 0.6127; p = 6.3E^{-13}).

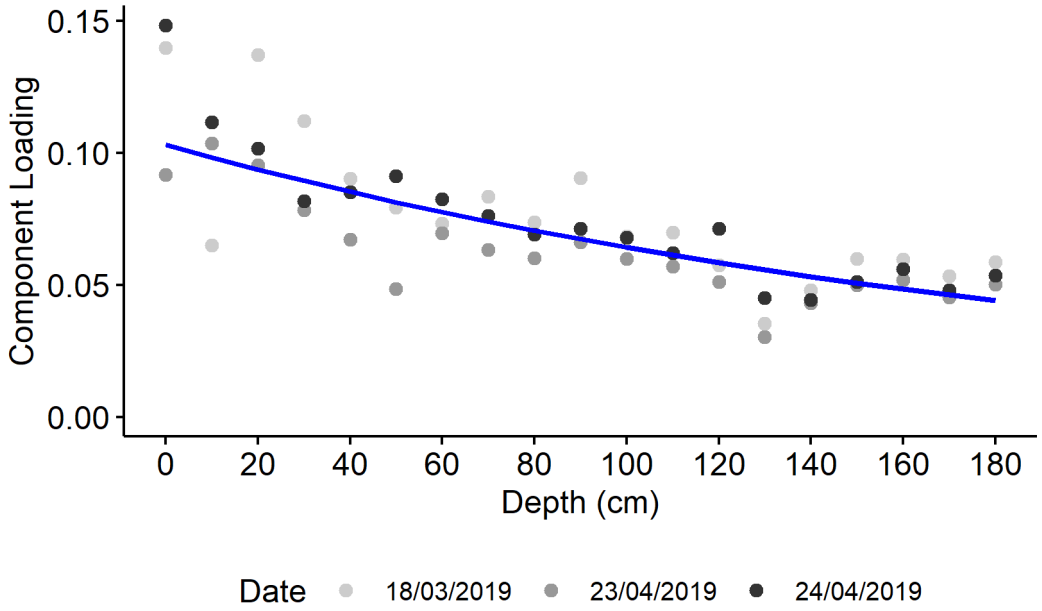

Figure 6-44: C2 loading across the column depth for each sampling day fitted to an exponential model (R^2 = 0.6294; p = 1.86E^{-13}).

However, comparing the overall reduction in humic fluorescence (influent vs. effluent) with the data gathered previously from the entire plant when the column media was fresh showed that the effectiveness of the column had degraded significantly in this respect (**Figure 6-45**). While the influent C2 loading was comparable between each year (0.13 ± 0.03), the effluent loading was significantly higher for the samples collected in 2019 (0.054 ± 0.004) compared with 2018 (0.018 ± 0.010) (**Figure 6-46**). This was further compared by looking at the percent reduction in C2 loading between the column influent and effluent, which showed a decline from 86.6 ± 5.5 % reduction in 2018 to 55.8 ± 9.5 % reduction in 2019 (**Figure 6-47, Figure 6-48**).

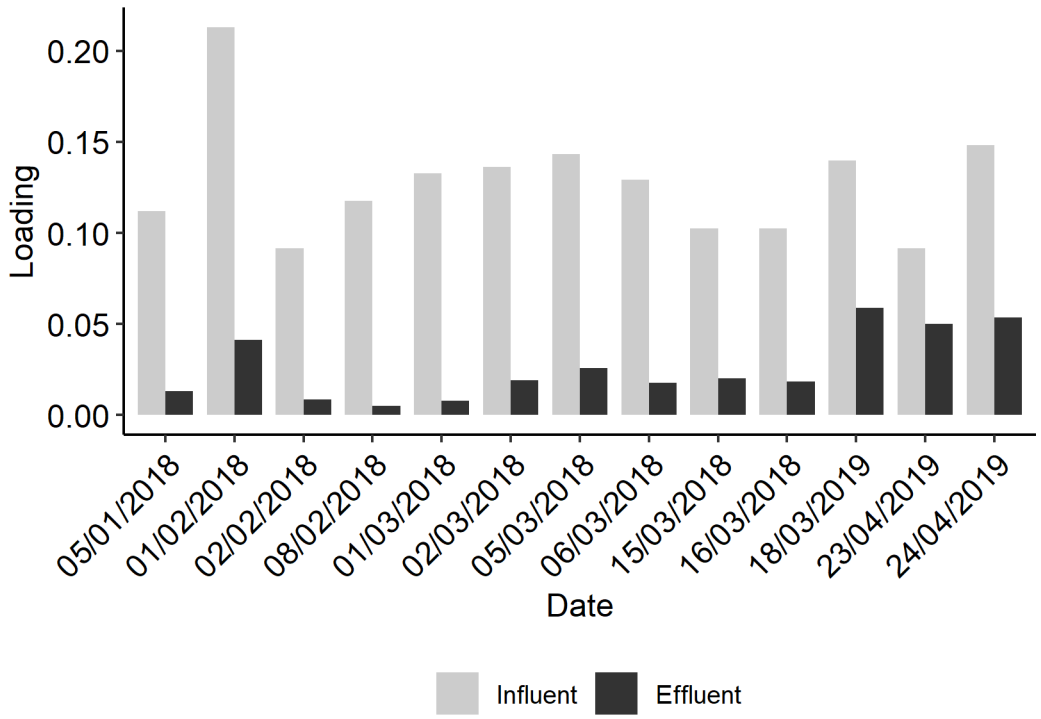

Figure 6-45: Column influent and effluent C2 loading across all sampling days from 2018 and 2019.

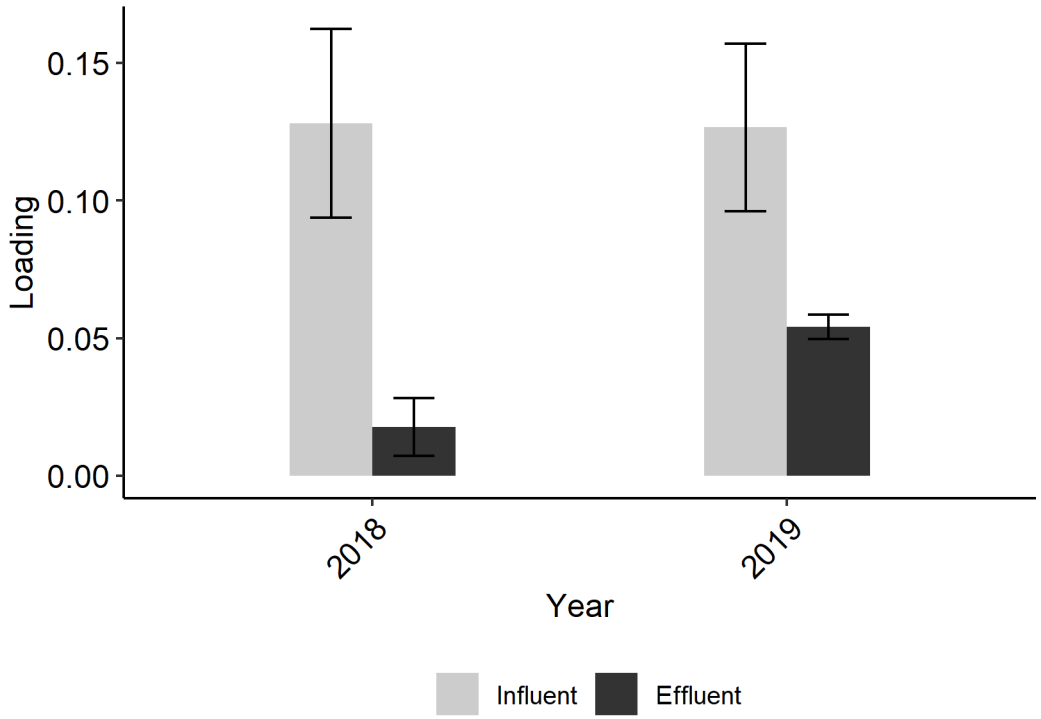

Figure 6-46: Mean influent and effluent C2 loading from 2018 (n = 10) and 2019 (n = 3) (error bars = standard deviation).

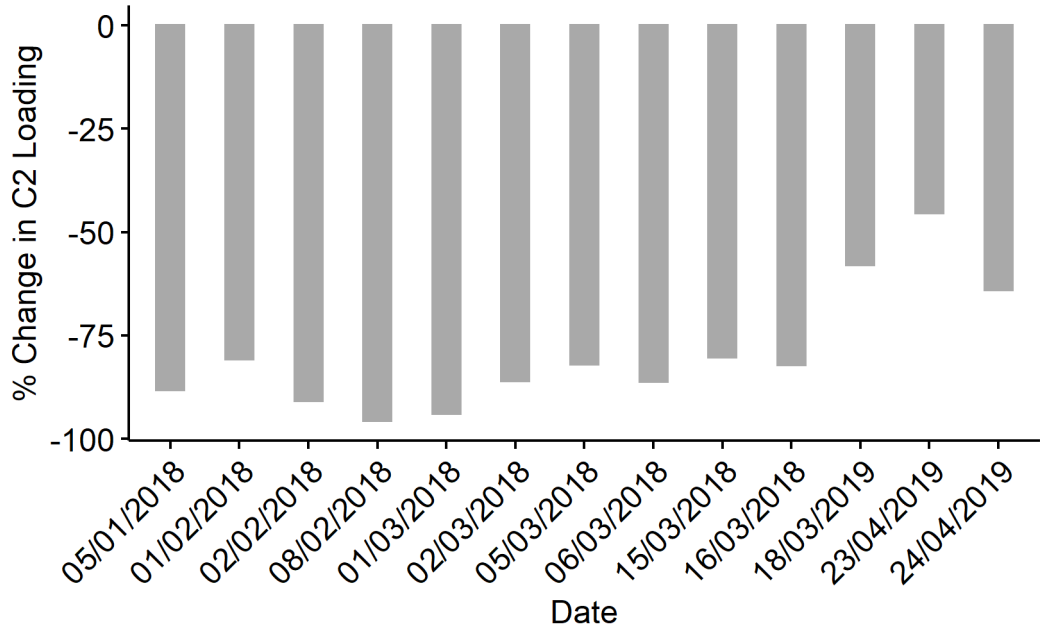

Figure 6-47: Percent change in column influent and effluent C2 loading across all sampling days from 2018 and 2019.

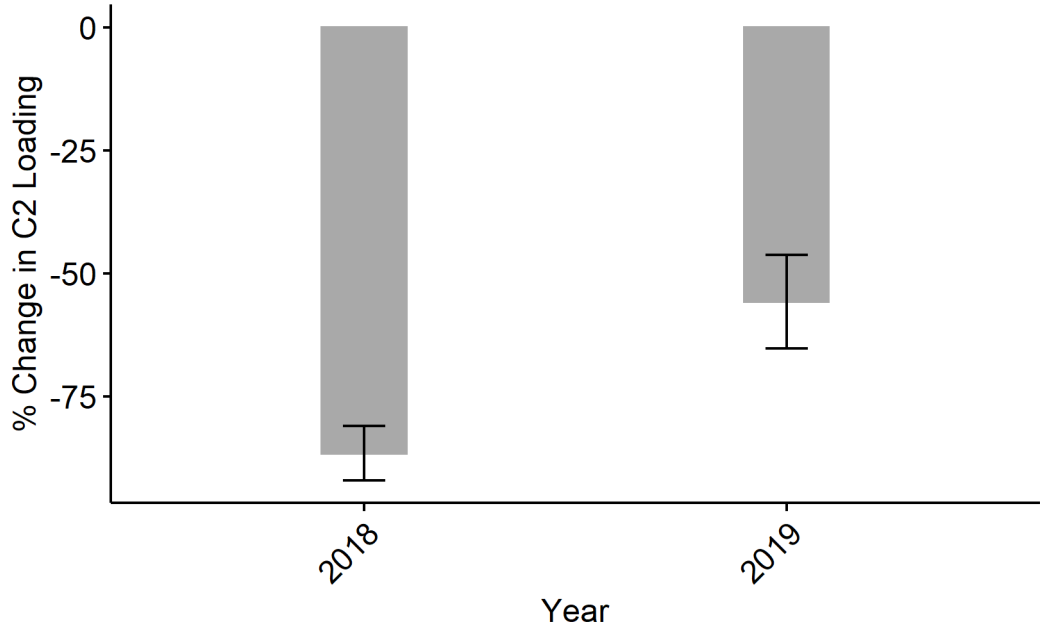

Figure 6-48: Mean percent change in column C2 loading from 2018 (n = 10) and 2019 (n = 3) (error bars = standard deviation)

Component C3, representative of tryptophan-type fluorescence, was also removed to some extent by the pilot column, although to a lesser extent than C2. C3 loading also appeared to be more variable across the column depth, with only a loose

correlation between C3 loading and column depth being evident (**Figure 6-49**, **Figure 6-50**). This was also apparent in the data gathered in 2018, where the removal of C3 by the pilot column was also highly variable, similar to what was observed for C1. Unlike C1, no spikes were observed across the filter bed depth and a uniform, although scattered, decrease in C3 loading was observed.

One point of note is that the filter appeared to be more effective at removing C3 after 12 months of operation. However, as the data collected in 2018 covered more sampling days, more of the day-to-day variation of C3 loading and removal was covered, while the influent loading in 2019 was more uniform. Overall, the maximum removal in 2019 was similar to that of 2019, with the data from 2018 being skewed by days where no apparent removal was noted. Increasing the number of sampling days in 2019 may have been beneficial in this case, as was noted for the C1 results.

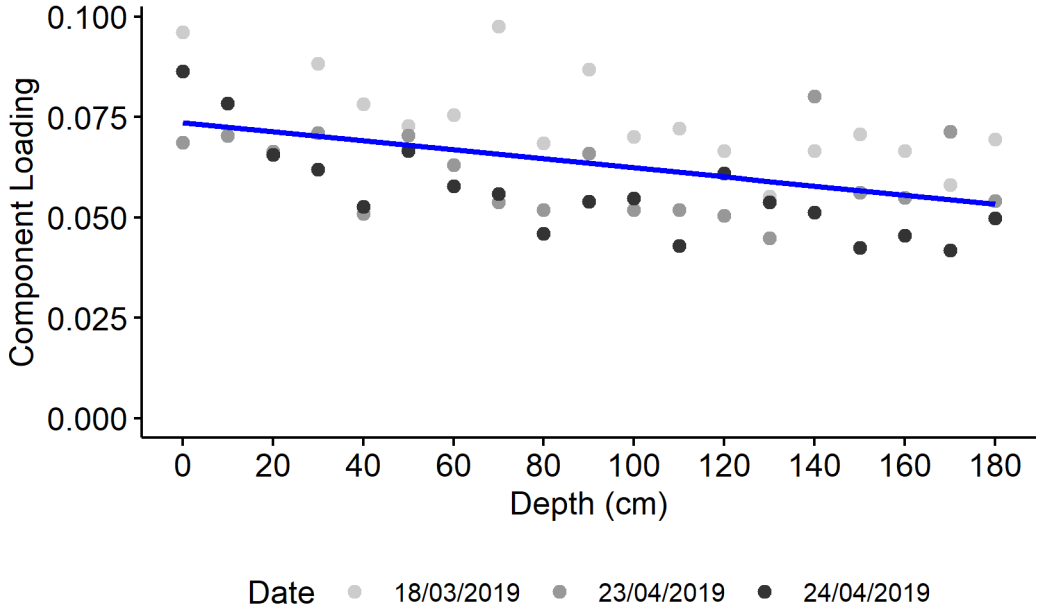

Figure 6-49: C3 loading across the column depth for each sampling day fitted to a linear model (R2 = 0.2006; p = 0.00032).

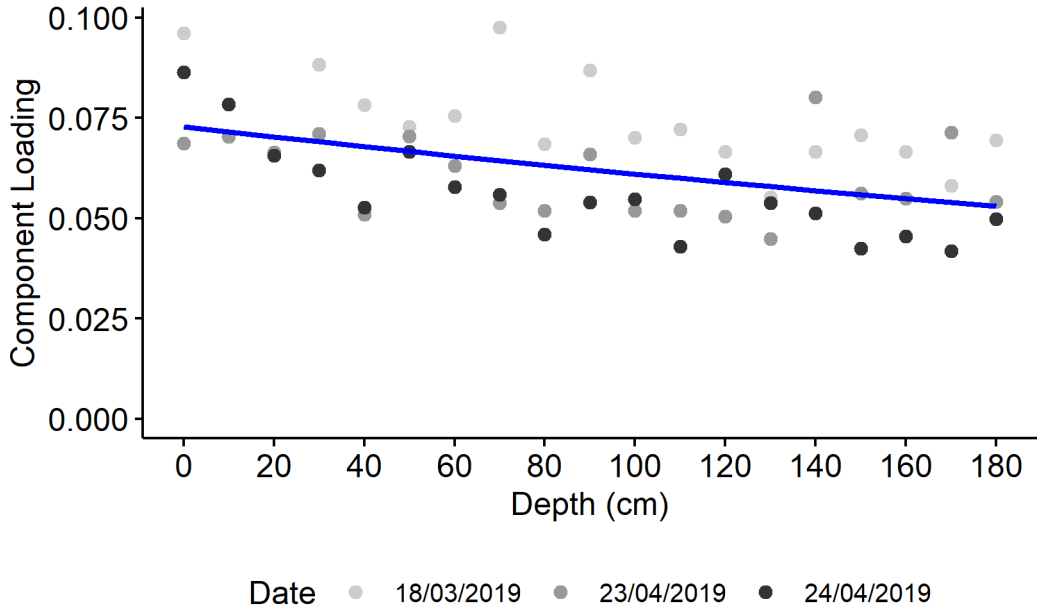

Figure 6-50: C3 loading across the column depth for each sampling day fitted to an exponential model (R2 = 0.2037; p = 0.00028).

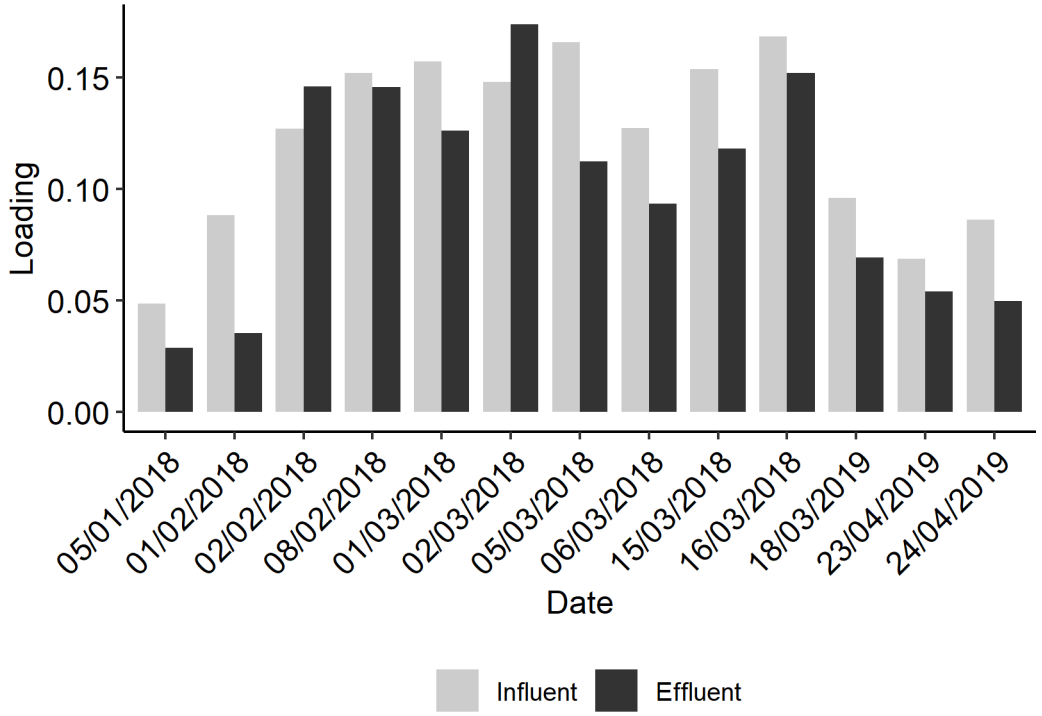

Figure 6-51: Column influent and effluent C3 loading across all sampling days from 2018 and 2019.

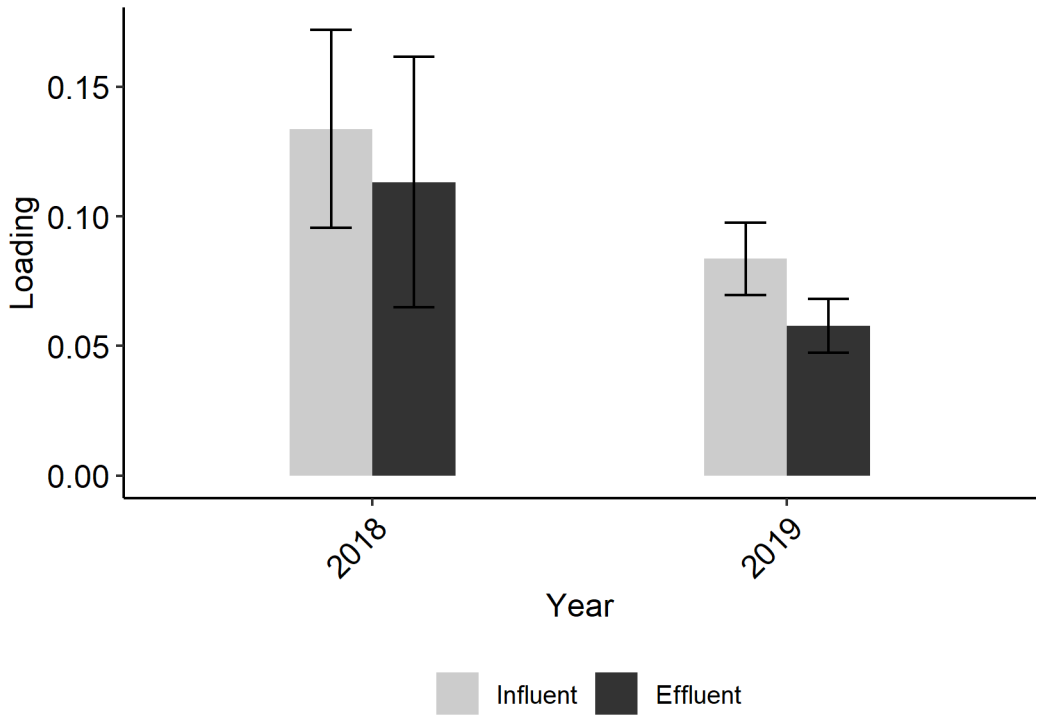

Figure 6-52: Mean influent and effluent C3 loading from 2018 (n = 10) and 2019 (n = 3) (error bars = standard deviation).

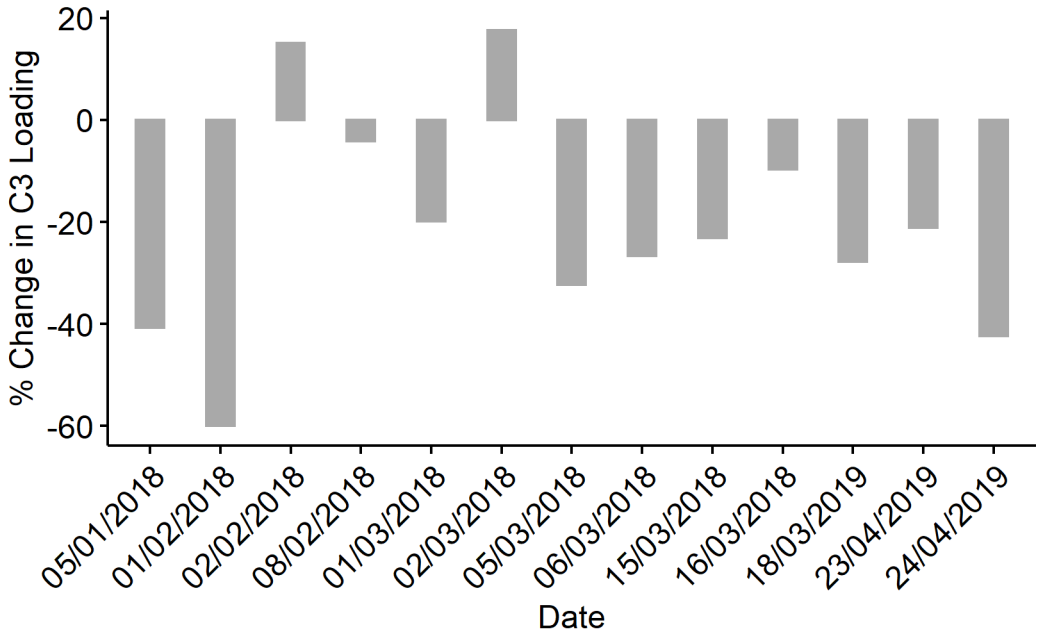

Figure 6-53: Percent change in column influent and effluent C3 loading across all sampling days from 2018 and 2019.

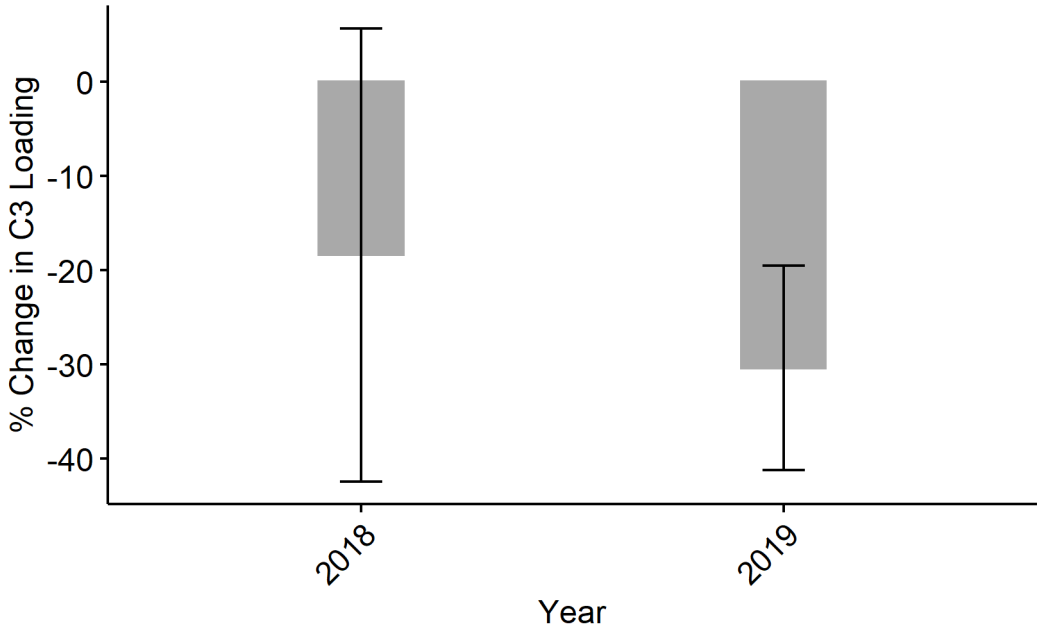

Figure 6-54: Mean percent change in column C3 loading from 2018 (n = 10) and 2019 (n = 3) (error bars = standard deviation)

6.4 Conclusion

The current treatment process at the HWTS seems to be adequate for removing the hydrophobic fraction of DOM present in the source water. TOC was significantly reduced through the treatment train, and was significantly correlated with humic-like fluorescence, humic-like substances being major contributors to the hydrophobic DOM fraction. TOC concentration was reduced by ≈ 67 ± 6 % and was strongly correlated with humic-like fluorescence while being weakly, or uncorrelated with protein-like fluorescence, indicating that the treatment process was more effective for hydrophobic compounds than polar compounds. Humic-like fluorescence was shown to decrease by ≈ 90 ± 35 %, while tryptophan-like fluorescence was shown to be reduced by ≈ 60 ± 25 % and tyrosine-like fluorescence was shown to increase by ≈ 6 ± 1 %. However, the results for tyrosine-like, and particularly tryptophan-like fluorescence are unlikely to be representative

of protein-like fluorescence only, as the modelled spectra indicated that these components included some proportion of other fluorescence groups, perhaps related to tannins, lignins or other phenolic compounds. This finding is an important consideration when using PARAFAC as a method for monitoring WTPs processing natural waters, as proteins and phenolics are likely to have markedly different properties and behaviours when subjected to specific treatment processes.

Reduction in both TOC concentration and humic-like fluorescence within the GAC filters was strongly influenced by filter age, with newer filters performing better than older filters. The oldest GAC filter at the time this study was carried out was shown to cause an increase in both TOC and humic-like fluorescence following filtration, which may be of some concern if all of the filters are allowed to reach their maximum lifespan simultaneously, as this may increase the risk of DBP formation from such precursors. Similarly, the varied behaviour of protein-like fluorescent groups may also be of concern regarding the possibility of cyanobacterial blooms and the subsequent production of cyanotoxins. Due to the protein-like, or highly polar structures of these toxins, it is likely that they will behave similarly to proteins already present in the source water. As such, they may not be removed consistently, or removed at all by the current treatment process. As DBPs arising from proteins and the reactions of proteins with other DOM molecules, for example carbohydrates, are not currently regulated, there is little concern with these compounds being present in the source water on a day-to-day operational basis unless new DBPs are added to the regulations outlined in the DWSNZ.

The behaviour of fluorescent DOM within the pilot column was shown to give similar results to those obtained from the survey of the full-scale plant, with humic-like fluorescence being reduced to a greater extent than protein-like fluorescence. The column media was shown to have reduced effectiveness after 12 months of operation, with the reduction in humic-like fluorescence decreasing from 86.6 ± 5.5 % reduction in 2018 to 55.8 ± 9.5 % in 2019. As with the full-scale plant, protein-like fluorescence was found to be highly variable, particularly for tyrosine-like fluorescence. This may be due to the presence of tannins/lignins within these fluorescent groups, but more work would be required in order to reach robust conclusions.

Chapter 7:

Final Conclusions and Recommendations

7 Final conclusions and recommendations for further research

7.1 Conclusion

The Hamilton Drinking Water Treatment Station relies on GAC filters as a means of removing organic compounds from the Waikato River source water following primary treatment of coagulation, flocculation and sand filtration. These filters were installed in 2006 as a means of removing cyanobacterial metabolites. At the time this study was commenced, the filters had been in service for approximately 10 years and were assumed to be operating at biological activated carbon filters. During the course of this study, the HCC commenced work to partially replace the GAC media which allowed for some comparisons of the GAC filters at various stages of their service life regarding physical properties and performance.

This research first looked at the surface morphology and elemental composition of GAC media from filters of different ages including media from a pilot scale GAC filter that was installed onsite in comparison to fresh GAC samples. SEM images and EDS showed marked differences between the old and new media both in terms of appearance and elemental composition. Newer media was found to resemble the fresh GAC media, although accumulations of what appeared to be sand from the sand filters were apparent on the GAC surface, and sparse colonies of bacteria could be discerned even after relative short service times (≈ 3 months). The oldest GAC media exhibited what appeared to be extensive mineralised deposits high in Mn and O interspersed with bacterial colonies. The presence of Mn and O indicates that Mn(III/IV) may be accumulating on the GAC surface over time, and may in fact be a result of bacterial colonies present in the GAC media as some bacteria known to

colonise GAC filters are also known Mn(II) oxidisers. The presence of high levels of Mn was confirmed with ICP-MS, and while other elements present at high concentrations in the GAC media could be explained by high concentrations in the source water (e.g. Ca) or their presence in coagulant (e.g. Al), the high level of Mn appeared to be anomalous considering its low concentration in the source water. This gives some indication that the deposition of Mn is being driven by some other factor, which may be the presence of Mn(II) oxidising bacteria. While the work detailed in this chapter was able to show that bacteria were able to colonise the GAC surface rapidly, more detailed work such as DNA sequencing was unable to be completed due to restrictions imposed during the COVID-19 epidemic. However, the results surrounding high concentrations of Mn, and possibly Mn(II/IV) oxides, on the GAC surface in proximity to bacterial colonies may provide some interesting future research opportunities, particularly regarding the mechanism of biological degradation within BAC filters.

Of particular interest was the behaviour of T&O compounds, specifically GSM and 2-MIB, in relation to the performance of the GAC filters. This work was covered in chapters 4 and 5, which included the development of a quantitative GC-MS method (chapter 4) and its application to experimental work aimed at evaluating the performance of the GAC filters during high-concentration events (chapter 5). The analytical method was developed following a review of the literature surrounding the determination of these compounds, and a method based on a liquid-liquid micro extraction technique was chosen in order to afford a method that provided low detection limits and fast sample processing times. The method was first applied to a survey of the entire plant process over the course of 30 days in order to assess the

prevalence of GSM and 2-MIB on a daily basis and how they are distributed through the plant. This survey found that the levels of both compounds were generally quite low, particularly for 2-MIB which was not present at levels above the MQL on any of the 30 days. This survey also showed that the concentration of these compounds was reduced significantly at the flocculation stage, which raised some questions regarding the partitioning of these compounds in natural waters. It is likely that, due to their hydrophobic nature, they are associated with the hydrophobic fraction of the DOM or bacterial cells which are precipitated during flocculation. Further, due to the loss of these compounds during flocculation, no detectable levels were found in the influent water fed to the GAC filters which allowed no further insights to be gained into the distribution of GSM and 2-MIB throughout the plant. This led to the use of a pilot-scale GAC filter for simulating a high concentration event. The dosing experiments showed that the GAC media was capable of removing GSM and 2-MIB at concentrations up to 150 ng L^{-1} at an EBCT of 15 min even after 12 months of use. Analysis of the GAC media collected during dosing experiments revealed that the GAC still exhibited significant adsorption capacity, indicating that while biological processes may contribute to the removal of organic compounds during this timeframe, the effect of adsorption is likely to be much greater. Biodegradation products of GSM or 2-MIB were not observed, although due to the high adsorption capacity of the GAC, it is likely that biodegradation products become adsorbed to the GAC following enzymatic transformation. A modelling study also indicated that the GAC could deal with high concentrations of GSM and 2-MIB, and that changes in the EBCT were a more important factor when considering the removal of these compounds. Overall, if the HCC were to continue

with a program of periodic partial replacement of the GAC media, these results indicate that GSM and 2-MIB are unlikely to prove problematic in future even at very high concentrations, unless the EBCT is reduced drastically. Overall, this study found that the full-scale GAC filters were sufficient for removing GSM and 2-MIB at typical levels present in the Waikato river, largely due to the concentration of these compounds is significantly reduced at the flocculation stage. Similarly, pilot-scale studies showed that the filter media was capable of removing high concentrations of 2-MIB and GSM after 12 months of operation. Additional work would need to be carried out to develop the adsorption models further, particularly to include competitive adsorption from compounds that are likely to be present at much higher concentrations than GSM and 2-MIB.

Investigations into the distribution of DOM throughout the treatment train produced some interesting results, particularly for the EEMS work. Regarding TOC, the concentration was found to decline through the treatment train with large decreases apparent at the flocculation and GAC stages as expected. However, the reduction at the GAC stage was found to depend on the age of the GAC filter, due to loss of adsorption capacity, and in the case of the oldest filter the effluent concentration was found to be higher than the influent concentration. This was investigated further with EEMS-PARAFAC, which indicated that the DOM was comprised of three major fluorescent groups – humic-like (C2), tyrosine-like (C1) and tryptophan-like (C3). Component C2 was found to be highly correlated with TOC concentration, which indicated that the majority of the reduction in TOC was a result in the reduction of the humic fraction of the DOM. Similar to the TOC results, the reduction of C2 at the GAC stage was found to be dependent on filter age, again

with the oldest filter showing an increase in C2 following GAC filtration. A reason for this may be that the influent concentration of TOC or humic material traverses the depth of the filter media unchanged, while simultaneously, previously adsorbed humic material is being desorbed due to competitive adsorption from other compounds or metals in solution. The result being a measured net increase in TOC and humic-like fluorescence in the effluent of the older GAC filters. This may have some negative implications regarding DPBFP in the future, particularly if all of the filters are allowed to reach their adsorption capacity simultaneously. Furthermore, while old GAC filters may be operating as BAC filters which perform some degree of treatment via biodegradation, once the filters become too old, the increase in humic-like material in the effluent may actually result in an overall reduction in water quality at the bulk level. As such, any benefit arising from biological transformation would be negated in such a scenario. The protein-like fluorophores C1 and C3 were found to be less treatable than the humic fraction, particularly C1 which was found to remain at constant levels through the treatment train. This may be due to the polar nature of amino acids and proteins, as GAC adsorption is known to be more favourable in the adsorption of hydrophobic compounds. If so, this would have implications regarding the removal of cyanotoxins during a cyanobacterial bloom, as some of them are cyclic peptides, and all of them are polar. Similar results were obtained from EEMS-PARAFAC experiments that concentrated on the pilot-scale GAC column, although the results for C1 were somewhat inconclusive and gave some further indication that this spectral group was comprised of both amino acid-based fluorophores and possibly phenolic compounds. This study strongly suggests that different fractions of the DOM pool

exhibit markedly different levels of treatability, with hydrophobic compounds being removed far more effectively compared with hydrophilic compounds. This may have implications in future, either regarding DBPs or cyanotoxins, and may provide a starting point for future research in this area.

7.2 Recommendations for further research

Chapter 3 found that high levels of Mn were present in close proximity to bacterial colonies, suggested follow up research may include:

- Confirmation that the Mn is present as Mn(III/IV) oxides, perhaps using x-ray diffraction (XRD) or some other suitable technique.
- Genomic sequencing of bacteria present on the filter media, with a focus on Mn(II) oxidising bacteria.
- Depending on the outcome of the suggestions above, an investigation into the redox and adsorption properties of Mn(III/IV) oxides present in GAC filters associated with biological colonisation.

The outcomes of these experiments would provide added evidence to the biogenic origin of Mn(III/IV) oxides present on the surface of the GAC, and would also provide further insight as to biological mechanisms for removing organic contaminant in such systems.

Analysis of 2-MIB and GSM in chapter 5 showed that the filters were effective at removing these compounds, even at high concentration. However, in order to produce a more accurate model that can predict the depletion of adsorption capacity, further experiments would be required as follows:

- Further refinement of the GC-MS method to give lower detection limits. This would give more data points at the lower concentration range to ensure the model produces accurate results at very low concentrations.
- Formulation of a "fictive compound" tailored to the Waikato River source water that can be used for competitive adsorption experiments.
- Competitive adsorption experiments using a fictive compound IAST approach to assess any inhibition in GSM and 2-MIB adsorption due to competitive adsorption.
- Incorporation of the outcomes from the above suggestions into the models described in chapter 5.
- Extension of the GC-MS method and model to include other compounds of concern, for example endocrine disruptors and other synthetic organic contaminants.

While chapter 6 provided some insights into the distribution of DOM through the treatment train, there are still many opportunities for further research. These may provide information relevant to public health outcomes in the future and inform the HCC regarding potential upgrades or changes to the current treatment system depending on the outcomes of such a research program.

- An investigation into the apparent increase in TOC and humic substances in the effluent of old GAC filters. This would require waiting for the filters to become extensively aged and may not be possible if the HCC continues to replenish the GAC media at regular intervals.
- Separation and characterisation of each fluorescent group identified using EEMS-PARAFAC. This may include chromatographic separation using size exclusion chromatography with fluorescence detection while collecting each separated fraction. The fractions could then be investigated further using mass spectrometry, nuclear magnetic resonance (NMR) spectroscopy and gel electrophoresis.

- An investigation into the DPBs formed from proteins and peptides during disinfection. As protein derived fluorophores were not significantly removed during flocculation or GAC filtration, they may be reaching the disinfection stage in higher concentrations than humic substances which are considered to be the main precursors to DBPs. While DBPs derived from proteins and peptides are not currently regulated, the information gained from such a study may be useful in future.
- The EEMS-PARAFAC results indicated that the current treatment process is poorly suited to removing polar compounds. As such, a study similar to that carried out in chapter 5 may be of value, particularly to provide information on the behaviour of cyanotoxins. As dosing experiments of cyanotoxins using the on-site pilot GAC column would be precluded due to health and safety concerns, lab-based column experiments may be used. In addition, carefully selected, non-toxic model compounds or non-toxic cyanotoxin analogues could be used for on-site dosing experiments. Analysis of polar compounds could be achieved with high-performance liquid chromatography coupled mass spectrometry (LC-MS or LC-MS/MS).

References

1. Collier, J. C.; Hamilton, D. P.; Vant, W. N.; Howard-Williams, C. Ed. *The Waters of the Waikato: Ecology of New Zealand's Longest River.* Environment Waikato and the Centre for Bioiversity and Ecology Research (The University of Waikato): Hamilton, New Zealand, 2010.

2. Hamilton City Council. River to the Tap: A guide to Hamilton's Water Supply. http://www.hamilton.govt.nz/our-services/water/water/Documents/RIVER%20TO%20TAP%20FOR%20WEB.pdf (accessed 23 October 2015)

3. Ministry of Health Drinking-Water Standards for New Zealand 2005 (Revised 2008). Government of New Zealand: Wellington (NZ), 2008.

4. Kouzminov, A.; Ruck, J.; Wood, S. A. New Zealand risk management approach for toxic cyanobacteria in drinking water. *Aust. N.Z. J. Public Health* **2007**, *31*, 275-281.

5. Ho, L.; Sawade, E.; Newcombe, G. Biological treatment options for cyanobacteria metabolite removal – A review. *Water Res.* **2012**, *46*, 1536-1548.

6. Clark, A.; Mullan, B.; Porteous, A. "Scenarios of Regional Drought under Climate Change," NIWA, 2011.

7. Cecen, F.; Aktas, O. *Activated Carbon for Water and Wastewater Treatment: Integration of Adsorption and Biological Treatment*; Wiley-VCH: Weinheim, Germany, 2012.

8. American Water Works Association *Water Quality and Treatment: A Handbook of Community Water Supplies. 5th Ed*; McGraw-Hill Publishing Co., 1999.

9. Rattier, M.; Reungoat, J.; Gernjak, W.; Joss, A.; Keller, J. Investigating the role of adsorption and biodegradation in the removal of organic micropollutants during biological activated carbon filtration of treated wastewater. *Journal of Water Reuse and Desalination* **2012**, *2*, 127-139.

10. Activated Carbon Technologies Acticarb BAC GA1000N - Specification Sheet. Victoria, Australia, 2017.

11. Marsh, H.; Rodriguez-Reinoso, F. *Activated Carbon*; Elsevier: Amsterdam; London, 2006.

12. Davis, M. L. *Water and Wastewater Engineering*; McGraw-Hill: New York, 2010.

13. Digiano, F. A. Adsorption of Organic Substances in Drinking Water. In *Control of Organic Substances in Water and Wastewater*; B. B. Berger, Ed.; Noyes Data Corporation: NJ, USA, 1987.

14. Graham, M. R.; Summers, R. S.; Simpson, M. R.; Macleod, B. W. Modeling equilibrium adsorption of 2-methylisoborneol and geosmin in natural waters. *Water Res.* **2000**, *34*, 2291-2300.

15. Knappe, D. R. U.; Matsui, Y.; Snoeyink, V. L.; Roche, P.; Prados, M. J.; Bourbigot, M.-M. Predicting the Capacity of Powdered Activated Carbon for Trace Organic Compounds in Natural Waters. *Environ. Sci. Technol.* **1998**, *32*, 1694-1698.

16. Gillogly, T. E. T.; Snoeyink, V. L.; Elarde, J. R.; Wilson, C. M.; Royal, E. P. 14C-MIB adsorption on PAC in natural water. *J. - Am. Water Works Assoc.* **1998**, *90*, 98-108.

17. Black & Veatch Corporation *White's Handbook of Chlorination and Alternative Disinfectants (5th Edition)*; John Wiley & Sons, Inc., 2010.

18. Linden, K. G.; Mohseni, M. Advanced Oxidation Processes: Applications in Drinking Water Treatment. In *Comprehensive Water Quality and Purification*; S. Ahuja, Ed.; Elsevier: Waltham, 2014; pp 148-172.

19. Zhu, I. X.; Getting, T.; Bruce, D. Review of biologically active filters in drinking water applications. *J. - Am. Water Works Assoc.* **2010**, *102*, 67-77.

20. Rittmann, B. E., Gantzer, C.J., Montiel, A. Biological treatment to control taste-and-odor compounds in drinking water treatment. In *Advances in Taste-and-Odor Treatment and Control*; I. H. Suffet, Mallevialle, J., Kawczynski, E. , Ed.; American Water Works Association Research Foundation: Denver, USA, 1995; pp 290-246.

21. Urfer, D.; Huck, P. M.; Booth, S. D. J.; Coffey, B. M. Biological filtration for BOM and particle removal: a critical review. *J. - Am. Water Works Assoc.* **1997**, *89*, 83-98.

22. Merchuk, J. C.; Asenjo, J. A. The Monod equation and mass transfer. *Biotechnol. Bioeng.* **1995**, *45*, 91-94.

23. Schmidt, S. K.; Simkins, S.; Alexander, M. Models for the kinetics of biodegradation of organic compounds not supporting growth. *Appl. Eviron. Microbiol.* **1985**, *50*, 323-331.

24. Engel, T.; Reid, P. *Physical Chemistry*, 3 ed.; Pearson Education, Inc.: San Francisco, CA, 2006.

25. Rittmann, B. E.; McCarty, P. L. Model of steady-state-biofilm kinetics. *Biotechnol. Bioeng.* **1980**, *22*, 2343-2357.

26. Izaguirre, G.; Wolfe, R. L.; Means, E. G. Degradation of 2-Methylisoborneol by Aquatic Bacteria. *Appl. Eviron. Microbiol.* **1988**, *54*, 2424-2431.

27. Izaguirre, G.; Taylor, W. D. A guide to geosmin- and MIB-producing cyanobacteria in the United States. *Water Sci. Technol.* **2004**, *49*, 19-24.

28. Izaguirre, G.; Wolfe, R. L.; Means, E. G. Bacterial degradation of 2-methylisoborneol. *Water Sci. Technol.* **1988**, *20*, 205-210.

29. Tanaka, A.; Oritani, T.; Uehara, F.; Saito, A.; Kishita, H.; Niizeki, Y.; Yokota, H.; Fuchigami, K. Biodegradation of a musty odor component, 2-methylisoborneol. *Water Res.* **1996**, *30*, 759-761.

30. Eaton, R. W.; Sandusky, P. Biotransformations of 2-methylisoborneol by camphor-degrading bacteria. *Appl. Environ. Microbiol.* **2009**, *75*, 583-588.

31. Eaton, R. W. Dehydration of the off-flavor chemical 2-methylisoborneol by the R-limonene-degrading bacteria *Pseudomonas* sp. strain 19-rlim and *Sphingomonas* sp. strain BIR2-rlima. *Biodegradation* **2012**, *23*, 253-261.

32. Ho, L.; Hoefel, D.; Bock, F.; Saint, C. P.; Newcombe, G. Biodegradation rates of 2-methylisoborneol (MIB) and geosmin through sand filters and in bioreactors. *Chemosphere* **2007**, *66*, 2210-2218.

33. Andreozzi, R.; Cesaro, R.; Marotta, R.; Pirozzi, F. Evaluation of biodegradation kinetic constants for aromatic compounds by means of aerobic batch experiments. *Chemosphere* **2006**, *62*, 1431-1436.

34. Gerber, N. N.; Lechevalier, H. A. Geosmin, an Earthy-Smelling Substance Isolated from Actinomycetes. *Appl. Microbiol.* **1965**, *13*, 935-938.

35. Hoefel, D.; Ho, L.; Aunkofer, W.; Monis, P. T.; Keegan, A.; Newcombe, G.; Saint, C. P. Cooperative biodegradation of geosmin by a consortium comprising three gram-negative bacteria isolated from the biofilm of a sand filter column. *Lett. Appl. Microbiol.* **2006**, *43*, 417-423.

36. Hoefel, D.; Ho, L.; Monis, P. T.; Newcombe, G.; Saint, C. P. Biodegradation of geosmin by a novel Gram-negative bacterium; isolation, phylogenetic characterisation and degradation rate determination. *Water Res.* **2009**, *43*, 2927-2935.

37. McDowall, B.; Hoefel, D.; Newcombe, G.; Saint, C. P.; Ho, L. Enhancing the biofiltration of geosmin by seeding sand filter columns with a consortium of geosmin-degrading bacteria. *Water Res.* **2009**, *43*, 433-440.

38. Saito, A.; Tokuyama, T.; Tanaka, A.; Oritani, T.; Fuchigami, K. Microbiological degradation of (-)-geosmin. *Water Res.* **1999**, *33*, 3033-3036.

39. Yagi, M.; Nakashima, S.; Muramoto, S. Biological degradation of musty odor compounds, 2-methylisoborneol and geosmin, in a bio-activated carbon filter. *Water Sci. Technol.* **1988**, *20*, 255-260.

40. Hrudey, S. E.; Huck, P. M.; Mitton, M. J.; Kenefick, S. L. Evaluation of odor removal by pilot-scale biological treatment process trains during spring runoff in an ice-covered river. *Water Sci. Technol.* **1995**, *31*, 195-201.

41. Nerenberg, R.; Rittmann, B. E.; Soucie, W. J. Ozone/biofiltration for removing MIB and geosmin. *J. - Am. Water Works Assoc.* **2000**, *92*, 85-95.

42. Elhadi, S. L. N.; Huck, P. M.; Slawson, R. M. Removal of geosmin and 2-methylisoborneol by biological filtration. *Water Sci. Technol.* **2004**, *49*, 273-280.

43. Elhadi, S. L. N.; Huck, P. M.; Slawson, R. M. Factors affecting the removal of geosmin and MIB in drinking water biofilters. *J. - Am. Water Works Assoc.* **2006**, *98*, 108-119.

44. Uhl, W., Persson, F., Heinicke, G., Hermansson, M., and Hedberg, T. Removal of geosmin and MIB in biofilters-on the role of biodegradation and adsorption. In *Recent progress in slow sand and alternative biofiltration processes*; R. Gimbel; N. Graham and M. R. Collins, Eds.; IWA Publishing: London, UK, 2006.

45. Persson, F.; Heinicke, G.; Hedberg, T.; Hermansson, M.; Uhl, W. Removal of geosmin and MIB by biofiltration - an investigation discriminating between adsorption and biodegradation. *Environ. Technol.* **2007**, *28*, 95-104.

46. Drikas, M.; Dixon, M.; Morran, J. Removal of MIB and geosmin using granular activated carbon with and without MIEX pre-treatment. *Water Res.* **2009**, *43*, 5151-5159.

47. Ndiongue, S.; Anderson, W. B.; Tadwalkar, A.; Rudnickas, J.; Lin, M.; Huck, P. M. Using pilot-scale investigations to estimate the remaining geosmin and MIB removal capacity of full-scale GAC-capped drinking water filters. *Water Qual. Res. J. Can.* **2006**, *41*, 296-306.

48. Yang, J.-S.; Yuan, D.-X.; Weng, T.-P. Pilot study of drinking water treatment with GAC, O3/BAC and membrane processes in Kinmen Island, Taiwan. *Desalination* **2010**, *263*, 271-278.

49. Hattori, K. Water treatment systems and technology for the removal of odor compounds. *Water Sci. Technol.* **1988**, *20*, 237-244.

50. Lundgren, B. V.; Grimvall, A.; Saevenhed, R. Formation and removal of off-flavor compounds during ozonation and filtration through biologically active sand filters. *Water Sci. Technol.* **1988**, *20*, 245-253.

51. World Health Organization *Toxic Cyanobacteria in Water: A Guide to their Public Health Consequences, Monitoring and Managment*, 1st ed.; E & FN Spon: London, 1999.

52. Clark, S.; Smith, D. W. Cyanobacteria toxins and the current state of knowledge on water treatment options: a review. *J. Environ. Eng. Sci.* **2004**, *3*, 155-185.

53. Merel, S.; Walker, D.; Chicana, R.; Snyder, S.; Baurès, E.; Thomas, O. State of knowledge and concerns on cyanobacterial blooms and cyanotoxins. *Environ. Int.* **2013**, *59*, 303-327.

54. Cousins, I. T.; Bealing, D. J.; James, H. A.; Sutton, A. Biodegradation of microcystin-LR by indigenous mixed bacterial populations. *Water Res.* **1996**, *30*, 481-485.

55. Jones, G. J.; Negri, A. P. Persistence and degradation of cyanobacterial paralytic shellfish poisons (PSPs) in freshwaters. *Water Res.* **1997**, *31*, 525-533.

56. Christoffersen, K.; Lyck, S.; Winding, A. Microbial activity and bacterial community structure during degradation of microcystins. *Aquat. Microb. Ecol.* **2002**, *27*, 125-136.

57. Holst, T.; Jorgensen, N. O. G.; Jorgensen, C.; Johansen, A. Degradation of microcystin in sediments at oxic and anoxic, denitrifying conditions. *Water Res.* **2003**, *37*, 4748-4760.

58. Bourne, D. G.; Blakeley, R. L.; Riddles, P.; Jones, G. J. Biodegradation of the cyanobacterial toxin microcystin LR in natural water and biologically active slow sand filters. *Water Res.* **2006**, *40*, 1294-1302.

59. Ho, L.; Tang, T.; Monis, P. T.; Hoefel, D. Biodegradation of multiple cyanobacterial metabolites in drinking water supplies. *Chemosphere* **2012**, *87*, 1149-1154.

60. Maghsoudi, E.; Fortin, N.; Greer, C.; Duy, S. V.; Fayad, P.; Sauvé, S.; Prévost, M.; Dorner, S. Biodegradation of multiple microcystins and cylindrospermopsin in clarifier sludge and a drinking water source: Effects of particulate attached bacteria and phycocyanin. *Ecotoxicol. Environ. Saf.* **2015**, *120*, 409-417.

61. Hu, L. B.; Yang, J. D.; Zhou, W.; Yin, Y. F.; Chen, J.; Shi, Z. Q. Isolation of a Methylobacillus sp that degrades microcystin toxins associated with cyanobacteria. *N. Biotechnol.* **2009**, *26*, 205-211.

62. Manage, P. M.; Edwards, C.; Singh, B. K.; Lawton, L. A. Isolation and identification of novel microcystin-degrading bacteria. *Appl. Eviron. Microbiol.* **2009**, *75*, 6924-6928.

63. Bourne, D. G.; Jones, G. J.; Blakeley, R. L.; Jones, A.; Negri, A. P.; Riddles, P. Enzymatic pathway for the bacterial degradation of the cyanobacterial cyclic peptide toxin microcystin LR. *Appl. Eviron. Microbiol.* **1996**, *62*, 4086-4094.

64. Bourne, D. G.; Riddles, P.; Jones, G. J.; Smith, W.; Blakeley, R. L. Characterisation of a gene cluster involved in bacterial degradation of the cyanobacterial toxin microcystin LR. *Environ. Tox.* **2001**, *16*, 523-534.

65. Chong, M. W. K.; Wong, B. S. F.; Lam, P. K. S.; Shaw, G. R.; Seawright, A. A. Toxicity and uptake mechanism of cylindrospermopsin and lophyrotomin in primary rat hepatocytes. *Toxicon* **2002**, *40*, 205-211.

66. Shen, X.; Lam, P. K. S.; Shaw, G. R.; Wickramasinghe, W. Genotoxicity investigation of a cyanobacterial toxin, cylindrospermopsin. *Toxicon* **2002**, *40*, 1499-1501.

67. Norris, R. L.; Eaglesham, G. K.; Pierens, G.; Shaw, G. R.; Smith, M. J.; Chiswell, R. K.; Seawright, A. A.; Moore, M. R. Deoxycylindrospermopsin, an analog of cylindrospermopsin from Cylindrospermopsis raciborskii. *Environ. Tox.* **1999**, *14*, 163-165.

68. Banker, R.; Teltsch, B.; Sukenik, A.; Carmeli, S. 7-Epicylindrospermopsin, a toxic minor metabolite of the cyanobacterium Aphanizomenon ovalisporum from Lake Kinneret, Israel. *J. Nat. Prod.* **2000**, *63*, 387-389.

69. Stirling, D. J.; Quilliam, M. A. First report of the cyanobacterial toxin cylindrospermopsin in New Zealand. *Toxicon* **2001**, *39*, 1219-1222.

70. Smith, M. J.; Shaw, G. R.; Eaglesham, G. K.; Ho, L.; Brookes, J. D. Elucidating the factors influencing the biodegradation of cylindrospermopsin in drinking water sources. *Environ. Tox.* **2008**, *23*, 413-421.

71. Mohamed, Z. A.; Alamri, S. A. Biodegradation of cylindrospermopsin toxin by microcystin-degrading bacteria isolated from cyanobacterial blooms. *Toxicon* **2012**, *60*, 1390-1395.

72. Banker, R.; Carmeli, S.; Werman, M.; Teltsch, B.; Porat, R.; Sukenik, A. Uracil moiety is required for toxicity of the cyanobacterial hepatotoxin cylindrospermopsin. *J. Toxicol. Environ. Health A* **2001**, *62*, 281-288.

73. Aráoz, R.; Molgó, J.; Tandeau de Marsac, N. Neurotoxic cyanobacterial toxins. *Toxicon* **2010**, *56*, 813-828.

74. James, K. J.; Furey, A.; Sherlock, I. R.; Stack, M. A.; Twohig, M.; Caudwell, F. B.; Skulberg, O. M. Sensitive determination of anatoxin-a, homoanatoxin-a and their degradation products by liquid chromatography with fluorimetric detection. *J. Chromatogr. A* **1998**, *798*, 147-157.

75. James, K. J.; Crowley, J.; Hamilton, B.; Lehane, M.; Skulberg, O.; Furey, A. Anatoxins and degradation products, determined using hybrid quadrupole time-of-flight and quadrupole ion-trap mass spectrometry: Forensic investigations of cyanobacterial neurotoxin poisoning. *Rapid Commun. Mass Spectrom.* **2005**, *19*, 1167-1175.

76. Vale, P. New saxitoxin analogues in the marine environment: developments in toxin chemistry, detection and biotransformation during the 2000s. *Phytochem. Rev.* **2010**, *9*, 525-535.

77. Quilliam, M. A.; Janecek, M.; Lawrence, J. F. Characterization of the oxidation products of paralytic shellfish poisoning toxins by liquid chromatography/mass spectrometry. *Rapid Commun. Mass Spectrom.* **1993**, *7*, 482-487.

78. Llewellyn, L. E. Saxitoxin, a toxic marine natural product that targets a multitude of receptors. *Nat. Prod. Rep.* **2006**, *23*, 200-222.

79. Boundy, M. J.; Selwood, A. I.; Harwood, D. T.; McNabb, P. S.; Turner, A. D. Development of a sensitive and selective liquid chromatography–mass spectrometry method for high throughput analysis of paralytic shellfish toxins using graphitised carbon solid phase extraction. *J. Chromatogr. A* **2015**, *1387*, 1-12.

80. Kotaki, Y. Screening of bacteria which convert gonyautoxin 2, 3 to saxitoxin. *Nippon Suisan Gakk.* **1989**, *55*, 1293-1293.

81. Smith, E. A.; Grant, F.; Ferguson, C. M. J.; Gallacher, S. Biotransformations of paralytic shellfish toxins by bacteria isolated from bivalve molluscs. *Appl. Environ. Microbiol.* **2001**, *67*, 2345-2353.

82. Vasama, M.; Kumar, H.; Salminen, S.; Haskard, C. A. Removal of paralytic shellfish toxins by probiotic lactic acid bacteria. *Toxins* **2014**, *6*, 2127-2136.

83. Donovan, C. J.; Ku, J. C.; Quilliam, M. A.; Gill, T. A. Bacterial degradation of paralytic shellfish toxins. *Toxicon* **2008**, *52*, 91-100.

84. Kotaki, Y.; Oshima, Y.; Yasumoto, T. Bacterial transformation of paralytic shellfish toxins in coral reef crabs and a marine snail. *Nippon Suisan Gakk.* **1985**, *51*, 1009-1013.

85. Kayal, N.; Newcombe, G.; Ho, L. Investigating the fate of saxitoxins in biologically active water treatment plant filters. *Environ. Tox.* **2008**, *23*, 751-755.

86. Tremblay, L. A.; Northcott, G. L. "Analysis of Waikato River Water Samples for Selected Endocrine Disruptor Chemicals and Hormonal Activity. Prepared for Waikato Regional Council, Cawthron Report No. 2422," 2013.

87. Mailler, R.; Gasperi, J.; Coquet, Y.; Bulete, A.; Vulliet, E.; Deshayes, S.; Zedek, S.; Mirande-Bret, C.; Eudes, V.; Bressy, A.; Caupos, E.; Moilleron, R.; Chebbo, G.; Rocher, V. Removal of a wide range of emerging pollutants from wastewater treatment plant discharges by micro-grain activated carbon in fluidized bed as tertiary treatment at large pilot scale. *Sci. Total Environ.* **2016**, *542*, 983-996.

88. Mita, L.; Grumiro, L.; Rossi, S.; Bianco, C.; Defez, R.; Gallo, P.; Mita, D. G.; Diano, N. Bisphenol A removal by a Pseudomonas aeruginosa immobilized on granular activated carbon and operating in a fluidized bed reactor. *J. Hazard. Mater.* **2015**, *291*, 129-135.

89. Katsigiannis, A.; Noutsopoulos, C.; Mantziaras, J.; Gioldasi, M. Removal of emerging pollutants through Granular Activated Carbon. *Chem. Eng. J.* **2015**, *280*, 49-57.

90. Li, F.; Yuasa, A.; Tanaka, H.; Katamine, Y. Adsorption and biotransformation of 17β-estradiol in biological activated carbon adsorbers. *Adsorption* **2008**, *14*, 389-398.

91. Hwang, C. J.; Krasner, S. W.; McGuire, M. J.; Moylan, M. S.; Dale, M. S. Determination of subnanogram-per-liter levels of earthy-musty odorants in water by the salted closed-loop stripping method. *Environ. Sci. Technol.* **1984**, *18*, 535-539.

92. Hayes, K. P.; Burch, M. D. Odorous compounds associated with algal blooms in South Australian waters. *Water Res.* **1989**, *23*, 115-121.

93. Bao, M.-L.; Barbieri, K.; Burrini, D.; Griffini, O.; Pantani, F. Determination of trace levels of taste and odor compounds in water by microextraction and gas chromatography-ion-trap detection-mass spectrometry. *Water Res.* **1997**, *31*, 1719-1727.

94. McCallum, R.; Pendleton, P.; Schumann, R.; Trinh, M.-U. Determination of geosmin and 2-methylisoborneol in water using solid-phase microextraction and gas chromatography-chemical ionization/electron impact ionization-ion-trap mass spectrometry. *Analyst* **1998**, *123*, 2155-2160.

95. Nakamura, S.; Nakamura, N.; Ito, S. Determination of 2-methylisoborneol and geosmin in water by gas chromatography-mass spectrometry using stir bar sorptive extraction. *J. Sep. Sci.* **2001**, *24*, 674-677.

96. Palmentier, J. P. F. P.; Taguchi, V. Y. The determination of six taste and odour compounds in water using Ambersorb 572 and high resolution mass spectrometry. *Analyst* **2001**, *126*, 840-845.

97. Ikai, Y.; Honda, S.; Yamada, N.; Onuma, S.; Tomita, B.-i.; Kawamura, N.; Miyazaki, Y. Determination of geosmin and 2-methylisoborneol in water using solid phase extraction and headspace-GC/MS. *J. Mass. Spectrom. Soc. Jpn.* **2003**, *51*, 174-178.

98. Lin, T.-F.; Liu, C.-L.; Yang, F.-C.; Hung, H.-W. Effect of residual chlorine on the analysis of geosmin, 2-MIB and MTBE in drinking water using the SPME technique. *Water Res.* **2003**, *37*, 21-26.

99. Shin, H.-S.; Ahn, H.-S. Simple, rapid, and sensitive determination of odorous compounds in water by GC-MS. *Chromatographia* **2004**, *59*, 107-113.

100. American Public Health Association 6040D Solid Phase Microextraction (SMPE). In *Standard methods for the examination of water and wastewater*; A. D. Eaton; American Water Works Association and Water Environment Federation, Eds.; APHA-AWWA-WEF: Washington, D. C., 2005.

101. Nakamura, S.; Sakui, N.; Tsuji, A.; Daishima, S. Determination of 2-methylisoborneol and geosmin in aqueous samples by static headspace-gas chromatography-mass spectrometry with ramped inlet pressure. *J. Sep. Sci.* **2005**, *28*, 2511-2516.

102. Sung, Y.-H.; Li, T.-Y.; Huang, S.-D. Analysis of earthy and musty odors in water samples by solid-phase microextraction coupled with gas chromatography/ion trap mass spectrometry. *Talanta* **2005**, *65*, 518-524.

103. Zhang, L.; Hu, R.; Yang, Z. Simultaneous picogram determination of "earthy-musty" odorous compounds in water using solid-phase microextraction and gas chromatography–mass spectrometry coupled with initial cool programmable temperature vaporizer inlet. *J. Chromatogr. A* **2005**, *1098*, 7-13.

104. Salemi, A.; Lacorte, S.; Bagheri, H.; Barceló, D. Automated trace determination of earthy-musty odorous compounds in water samples by on-line purge-and-trap–gas chromatography–mass spectrometry. *J. Chromatogr. A* **2006**, *1136*, 170-175.

105. Zhang, L.; Hu, R.; Yang, Z. Routine analysis of off-flavor compounds in water at sub-part-per-trillion level by large-volume injection GC/MS with programmable temperature vaporizing inlet. *Water Res.* **2006**, *40*, 699-709.

106. Boutou, S.; Chatonnet, P. Rapid headspace solid-phase microextraction/gas chromatographic/mass spectrometric assay for the quantitative determination of some of the main odorants causing off-flavours in wine. *J. Chromatogr. A* **2007**, *1141*, 1-9.

107. Ma, X.; Gao, N.; Chen, B.; Li, Q.; Zhang, Q.; Gu, G. Detection of geosmin and 2-methylisoborneol by liquid-liquid extraction-gas chromatograph mass spectrum (LLE-GCMS) and solid phase extraction-gas chromatograph mass spectrum (SPE-GCMS). *Front. Environ. Sci. Eng.* **2007**, *1*, 286-291.

108. Chang, J.; Biniakewitz, R.; Harkey, G. Determination of geosmin and 2-MIB in drinking water by SPME-PTV-GC-MS. *LC-GC Eur.* **2008**, 11-12.

109. Sibali, L. L.; Schoeman, C.; Morobi, J. S.; Molalatladi, B. S. Comparison of two selective methods for determination of geosmin (1,2,7,7-tetramethyl-2-norborneol) and 2-MIB (2-methylisoborneol) in drinking and raw water samples by capillary gas chromatography-mass spectrometry. *Water Qual. Res. J. Can.* **2010**, *45*, 491-497.

110. Cortada, C.; Vidal, L.; Canals, A. Determination of geosmin and 2-methylisoborneol in water and wine samples by ultrasound-assisted dispersive liquid-liquid microextraction coupled to gas chromatography-mass spectrometry. *J. Chromatogr. A* **2011**, *1218*, 17-22.

111. Deng, X.; Liang, G.; Chen, J.; Qi, M.; Xie, P. Simultaneous determination of eight common odors in natural water body using automatic purge and trap coupled to gas chromatography with mass spectrometry. *J. Chromatogr. A* **2011**, *1218*, 3791-3798.

112. Ma, J.; Lu, W.; Li, J.; Song, Z.; Liu, D.; Chen, L. Determination of geosmin and 2-methylisoborneol in water by headspace liquid-phase microextraction coupled with gas chromatography-mass spectrometry. *Anal. Lett.* **2011**, *44*, 1544-1557.

113. Machado, S.; Gonçalves, C.; Cunha, E.; Guimarães, A.; Alpendurada, M. F. New developments in the analysis of fragrances and earthy–musty compounds in water by solid-phase microextraction (metal alloy fibre) coupled with gas chromatography–(tandem) mass spectrometry. *Talanta* **2011**, *84*, 1133-1140.

114. Parinet, J.; Rodriguez, M. J.; Serodes, J.; Proulx, F. Automated analysis of geosmin, 2-methyl-isoborneol, 2-isopropyl-3-methoxypyrazine, 2-isobutyl-3-methoxypyrazine and 2,4,6-trichloroanisole in water by SPME-GC-ITDMS/MS. *Int. J. Environ. Anal. Chem.* **2011**, *91*, 505-515.

115. Ma, K.; Zhang, J. N.; Zhao, M.; He, Y. J. Accurate analysis of trace earthy-musty odorants in water by headspace solid phase microextraction gas chromatography-mass spectrometry. *J. Sep. Sci.* **2012**, *35*, 1494-1501.

116. Sun, W.; Jia, R.; Gao, B. Simultaneous analysis of five taste and odor compounds in surface water using solid-phase extraction and gas chromatography-mass spectrometry. *Front. Environ. Sci. Eng.* **2012**, *6*, 66-74.

117. Chen, X.; Luo, Q.; Yuan, S.; Wei, Z.; Song, H.; Wang, D.; Wang, Z. Simultaneous determination of ten taste and odor compounds in drinking water by solid-phase microextraction combined with gas chromatography-mass spectrometry. *J. Environ. Sci.* **2013**, *25*, 2313-2323.

118. Peng, S.; Ding, Z.; Xia, W.; Zheng, H.; Xia, Y.; Chen, X. Orthogonal design study on factors affecting the determination of common odors in water samples by headspace solid-phase microextraction coupled to GC/MS. *J. Anal. Methods Chem.* **2013**, 340658, 340610 pp.

119. Yuan, B.; Li, F.; Xu, D.; Fu, M.-L. Comparison of two methods for the determination of geosmin and 2-methylisoborneol in algae samples by stable isotope dilution assay through purge-and-trap or headspace solid-phase microextraction combined with GC/MS. *Anal. Methods* **2013**, *5*, 1739-1746.

120. Ding, Z.; Peng, S.; Xia, W.; Zheng, H.; Chen, X.; Yin, L. Analysis of five earthy-musty odorants in environmental water by HS-SPME/GC-MS. *Int. J. Anal. Chem.* **2014**, *2014*, 11.

121. Peng, S.; Ding, Z.; Zhao, L.; Fei, J.; Xuan, Z.; Huang, C.; Chen, X. Determination of seven odorants in purified water among worldwide brands by HS-SPME coupled to GC–MS. *Chromatographia* **2014**, *77*, 729-735.

122. Ueta, I.; Mitsumori, T.; Kawakubo, S.; Saito, Y. Determination of musty-odor compounds in water by gas chromatography-mass spectrometry with a needle-type sample-preparation device. *Anal. Sci.* **2014**, *30*, 979-983.

123. Wright, E.; Daurie, H.; Gagnon, G. A. Development and validation of an SPE-GC-MS/MS taste and odour method for analysis in surface water. *Int. J. Environ. Anal. Chem.* **2014**, *94*, 1302-1316.

124. Yu, S.; Xiao, Q.; Zhu, B.; Zhong, X.; Xu, Y.; Su, G.; Chen, M. Gas chromatography–mass spectrometry determination of earthy–musty odorous compounds in waters by two phase hollow-fiber liquid-phase microextraction using polyvinylidene fluoride fibers. *J. Chromatogr. A* **2014**, *1329*, 45-51.

125. Jüttner, F. Dynamics of the volatile organic substances associated with cyanobacteria and algae in a eutrophic shallow lake. *Appl. Eviron. Microbiol.* **1984**, *47*, 814-820.

126. Brownlee, B. G.; Gammie, L.; Gummer, W. D.; MacInnis, G. A. A simple extraction procedure for moderately volatile taste and odor compounds such as geosmin and 2-methylisoborneol - method and applications. *Water Sci. Technol.* **1988**, *20*, 91-97.

127. Omur-Ozbek, P.; Little, J. C.; Dietrich, A. M. Ability of humans to smell geosmin, 2-MIB and nonadienal in indoor air when using contaminated drinking water. *Water Sci. Technol.* **2007**, *55*, 249-256.

128. Kaushik, R.; Balasubramanian, R. Methods and Approaches Used for Detection of Cyanotoxins in Environmental Samples: A Review. *Crit. Rev. Env. Sci. Technol.* **2013**, *43*, 1349-1383.

129. de Andrade, F. M.; de Macedo, A. N.; Vieira, E. M. Determination of microcystin-LR in cyanobacterial blooms from the Mogi Guacu River (Brazil) by high-performance liquid chromatography. *J. Liq. Chromatogr. Relat. Technol.* **2014**, *37*, 1310-1319.

130. Mekebri, A.; Blondina, G. J.; Crane, D. B. Method validation of microcystins in water and tissue by enhanced liquid chromatography tandem mass spectrometry. *J. Chromatogr. A* **2009**, *1216*, 3147-3155.

131. Rodrigues, M. A.; Reis, M. P.; Mateus, M. C. Liquid chromatography/negative electrospray ionization ion trap MS2 mass spectrometry application for the determination of microcystins occurrence in Southern Portugal water reservoirs. *Toxicon* **2013**, *74*, 8-18.

132. Zastepa, A.; Pick, F. R.; Blais, J. M.; Saleem, A. Analysis of intracellular and extracellular microcystin variants in sediments and pore waters by accelerated solvent extraction and high performance liquid chromatography-tandem mass spectrometry. *Anal. Chim. Acta* **2015**, *872*, 26-34.

133. Jaime, E.; Hummert, C.; Hess, P.; Luckas, B. Determination of paralytic shellfish poisoning toxins by high-performance ion-exchange chromatography. *J. Chromatogr. A* **2001**, *929*, 43-49.

134. Lawrence, J. F.; Niedzwiadek, B. Quantitative determination of paralytic shellfish poisoning toxins in shellfish by using prechromatographic oxidation and liquid chromatography with fluorescence detection. *J. AOAC Int.* **2001**, *84*, 1099-1108.

135. Diener, M.; Erler, K.; Hiller, S.; Christian, B.; Luckas, B. Determination of paralytic shellfish poisoning (PSP) toxins in dietary supplements by application of a new HPLC/FD method. *Eur. Food. Res. Technol.* **2006**, *224*, 147-151.

136. Turrell, E.; Stobo, L.; Lacaze, J.-P. Optimization of hydrophilic interaction liquid chromatography/mass spectrometry and development of solid-phase extraction for the determination of paralytic shellfish poisoning toxins. *J. AOAC Int.* **2008**, *91*, 1372-1386.

137. Harwood, D. T.; Boundy, M.; Selwood, A. I.; van Ginkel, R.; MacKenzie, L.; McNabb, P. S. Refinement and implementation of the Lawrence method (AOAC 2005.06) in a commercial laboratory: Assay performance during an Alexandrium catenella bloom event. *Harmful Algae* **2013**, *24*, 20-31.

138. Hormazabal, V.; Ostensvik, O.; Underdal, B.; Skulberg, O. M. Simultaneous determination of the cyanotoxins anatoxin a, microcystin desmethyl-3, LR, RR, and YR in fish muscle using liquid chromatography-mass spectrometry. *J. Liq. Chromatogr. Relat. Technol.* **2000**, *23*, 185-196.

139. Lajeunesse, A.; Segura, P. A.; Gelinas, M.; Hudon, C.; Thomas, K.; Quilliam, M. A.; Gagnon, C. Detection and confirmation of saxitoxin analogues in freshwater benthic Lyngbya wollei algae collected in the St. Lawrence River (Canada) by liquid chromatography-tandem mass spectrometry. *J. Chromatogr. A* **2012**, *1219*, 93-103.

140. Fayad, P. B.; Roy-Lachapelle, A.; Duy, S. V.; Prevost, M.; Sauve, S. On-line solid-phase extraction coupled to liquid chromatography tandem mass spectrometry for the analysis of cyanotoxins in algal blooms. *Toxicon* **2015**, *108*, 167-175.

141. Oehrle, S. A.; Southwell, B.; Westrick, J. Detection of various freshwater cyanobacterial toxins using ultra-performance liquid chromatography tandem mass spectrometry. *Toxicon* **2010**, *55*, 965-972.

142. Yen, H.-K.; Lin, T.-F.; Liao, P.-C. Simultaneous detection of nine cyanotoxins in drinking water using dual solid-phase extraction and liquid chromatography-mass spectrometry. *Toxicon* **2011**, *58*, 209-218.

143. Pekar, H.; Westerberg, E.; Bruno, O.; Lääne, A.; Persson, K. M.; Sundström, L. F.; Thim, A.-M. Fast, rugged and sensitive ultra high pressure liquid chromatography tandem mass spectrometry method for analysis of cyanotoxins in raw water and drinking water—First findings of anatoxins, cylindrospermopsins and microcystin variants in Swedish source waters and infiltration ponds. *J. Chromatogr. A* **2016**, *1429*, 265-276.

144. Hudson, N.; Baker, A.; Reynolds, D. Fluorescence analysis of dissolved organic matter in natural, waste and polluted waters—a review. *River Res. Appl.* **2007**, *23*, 631-649.

145. Yang, L.; Hur, J.; Zhuang, W. Occurrence and behaviors of fluorescence EEM-PARAFAC components in drinking water and wastewater treatment systems and their applications: a review. *Environ. Sci. Pollut. R.* **2015**, *22*, 6500-6510.

146. Markechová, D.; Tomková, M.; Sádecká, J. Fluorescence excitation-emission matrix spectroscopy and parallel factor analysis in drinking water treatment: A review. *Pol. J. Environ. Stud.* **2013**, *22*, 1289-1295.

147. Coble, P. G. Characterization of marine and terrestrial DOM in seawater using excitation-emission matrix spectroscopy. *Mar. Chem.* **1996**, *51*, 325-346.

148. Murphy, K. R.; Stedmon, C. A.; Graeber, D.; Bro, R. Fluorescence spectroscopy and multi-way techniques. PARAFAC. *Anal. Methods* **2013**, *5*, 6557-6566.

149. Sharp, E. L.; Parsons, S. A.; Jefferson, B. Seasonal variations in natural organic matter and its impact on coagulation in water treatment. *Sci. Total Environ.* **2006**, *363*, 183-194.

150. Kim, H.-C.; Yu, M.-J. Characterization of natural organic matter in conventional water treatment processes for selection of treatment processes focused on DBPs control. *Water Res.* **2005**, *39*, 4779-4789.

151. Shutova, Y.; Baker, A.; Bridgeman, J.; Henderson, R. K. Spectroscopic characterisation of dissolved organic matter changes in drinking water treatment: From PARAFAC analysis to online monitoring wavelengths. *Water Res.* **2014**, *54*, 159-169.

152. Stedmon, C. A.; Seredynska-Sobecka, B.; Boe-Hansen, R.; Le Tallec, N.; Waul, C. K.; Arvin, E. A potential approach for monitoring drinking water quality from groundwater systems using organic matter fluorescence as an early warning for contamination events. *Water Res.* **2011**, *45*, 6030-6038.

153. Mendonça, A.; Rocha, A. C.; Duarte, A. C.; Santos, E. B. H. The inner filter effects and their correction in fluorescence spectra of salt marsh humic matter. *Anal. Chim. Acta* **2013**, *788*, 99-107.

154. Larsson, T.; Wedborg, M.; Turner, D. Correction of inner-filter effect in fluorescence excitation-emission matrix spectrometry using Raman scatter. *Anal. Chim. Acta* **2007**, *583*, 357-363.

155. Ohno, T. Fluorescence Inner-Filtering Correction for Determining the Humification Index of Dissolved Organic Matter. *Environ. Sci. Technol.* **2002**, *36*, 742-746.

156. Osburn, C. L.; Del Vecchio, R.; Boyd, T. J. Physicochemical Effects on Dissolved Organic Matter Fluorescence in Natural Waters. In *Aquatic Organic Matter Fluorescence*; A. Baker; D. M. Reynolds; J. Lead; P. G. Coble and R. G. M. Spencer, Eds.; Cambridge University Press: Cambridge, 2014; pp 233-277.

157. Gilchrist, J. R.; Reynolds, D. M. Optical Spectroscopy Instrumentation Design, Quality Assurance, and Control. In *Aquatic Organic Matter Fluorescence*; A. Baker; D. M. Reynolds; J. Lead; P. G. Coble and R. G. M. Spencer, Eds.; Cambridge University Press: Cambridge, 2014; pp 147-189.

158. Conmy, R. N.; Del Castillo, C. E.; Downing, B. D.; Chen, R. F. Experimental Design and Quality Assurance. In *Aquatic Organic Matter Fluorescence*; A. Baker; D. M. Reynolds; J. Lead; P. G. Coble and R. G. M. Spencer, Eds.; Cambridge University Press: Cambridge, 2014; pp 190-230.

159. Baghoth, S. A.; Sharma, S. K.; Amy, G. L. Tracking natural organic matter (NOM) in a drinking water treatment plant using fluorescence excitation–emission matrices and PARAFAC. *Water Res.* **2011**, *45*, 797-809.

160. Parlanti, E.; Worz, K.; Geoffroy, L.; Lamotte, M. Dissolved organic matter fluorescence spectroscopy as a tool to estimate biological activity in a coastal zone submitted to anthropogenic inputs. *Org. Geochem.* **2000**, *31*, 1765-1781.

161. Hudson, N.; Baker, A.; Ward, D.; Reynolds, D. M.; Brunsdon, C.; Carliell-Marquet, C.; Browning, S. Can fluorescence spectrometry be used as a surrogate for the Biochemical Oxygen Demand (BOD) test in water quality assessment? An example from South West England. *Sci. Total Environ.* **2008**, *391*, 149-158.

162. Saadi, I.; Borisover, M.; Armon, R.; Laor, Y. Monitoring of effluent DOM biodegradation using fluorescence, UV and DOC measurements. *Chemosphere* **2006**, *63*, 530-539.

163. Bro, R. PARAFAC. Tutorial and applications. *Chemom. Intell. Lab. Syst.* **1997**, *38*, 149-171.

164. Stedmon, C. A.; Markager, S.; Bro, R. Tracing dissolved organic matter in aquatic environments using a new approach to fluorescence spectroscopy. *Mar. Chem.* **2003**, *82*, 239-254.

165. Bro, R.; Kiers, H. A. L. A new efficient method for determining the number of components in PARAFAC models. *J. Chemom.* **2003**, *17*, 274-286.

166. Bieroza, M.; Baker, A.; Bridgeman, J. Relating freshwater organic matter fluorescence to organic carbon removal efficiency in drinking water treatment. *Sci. Total Environ.* **2009**, *407*, 1765-1774.

167. Johnstone, D. W.; Sanchez, N. P.; Miller, C. M. Parallel Factor Analysis of Excitation-Emission Matrices to Assess Drinking Water Disinfection Byproduct Formation During a Peak Formation Period. *Environ. Eng. Sci.* **2009**, *26*, 1551-1559.

168. Yang, L.; Kim, D.; Uzun, H.; Karanfil, T.; Hur, J. Assessing trihalomethanes (THMs) and N-nitrosodimethylamine (NDMA) formation potentials in drinking water treatment plants using fluorescence spectroscopy and parallel factor analysis. *Chemosphere* **2015**, *121*, 84-91.

169. Bridgeman, J.; Bieroza, M.; Baker, A. The application of fluorescence spectroscopy to organic matter characterization in drinking water treatment. *Rev. Environ. Sci. Bio/Technol.* **2011**, *10*, 277-290.

170. Matilainen, A.; Gjessing, E. T.; Lahtinen, T.; Hed, L.; Bhatnagar, A.; Sillanpaa, M. An overview of the methods used in the characterisation of natural organic matter (NOM) in relation to drinking water treatment. *Chemosphere* **2011**, *83*, 1431-1442.

171. Baghoth, S. A.; Sharma, S. K.; Guitard, M.; Heim, V.; Croue, J. P.; Amy, G. L. Removal of NOM-constituents as characterized by LC-OCD and F-EEM during drinking water treatment. *J. Water Supply: Res. Technol.--AQUA* **2011**, *60*, 412-424.

172. Ishii, S. K. L.; Boyer, T. H. Behavior of reoccurring PARAFAC components in fluorescent dissolved organic matter in natural and engineered systems: a critical review. *Environ. Sci. Technol.* **2012**, *46*, 2006-2017.

173. Baker, A.; Tipping, E.; Thacker, S. A.; Gondar, D. Relating dissolved organic matter fluorescence and functional properties. *Chemosphere* **2008**, *73*, 1765-1772.

174. Bieroza, M. Z.; Bridgeman, J.; Baker, A. Fluorescence spectroscopy as a tool for determination of organic matter removal efficiency at water treatment works. *Drinking Water Eng. Sci.* **2010**, *3*, 63-70.

175. Świetlik, J.; Sikorska, E. Application of fluorescence spectroscopy in the studies of natural organic matter fractions reactivity with chlorine dioxide and ozone. *Water Res.* **2004**, *38*, 3791-3799.

176. Korshin, G. V.; Kumke, M. U.; Li, C.-W.; Frimmel, F. H. Influence of Chlorination on Chromophores and Fluorophores in Humic Substances. *Environ. Sci. Technol.* **1999**, *33*, 1207-1212.

177. Richardson, S. D.; Plewa, M. J.; Wagner, E. D.; Schoeny, R.; DeMarini, D. M. Occurrence, genotoxicity, and carcinogenicity of regulated and emerging disinfection by-products in drinking water: A review and roadmap for research. *Mutat. Res.* **2007**, *636*, 178-242.

178. Richardson, S. D. Disinfection By-Products: Formation and Occurrence in Drinking Water. In *Encyclopedia of Environmental Health*; J. O. Nriagu, Ed.; Elsevier Science Inc.: Burlington, MA, 2011; pp 110-136.

179. Bond, T.; Goslan, E. H.; Parsons, S. A.; Jefferson, B. A critical review of trihalomethane and haloacetic acid formation from natural organic matter surrogates. *Environmental Technology Reviews* **2012**, *1*, 93-113.

180. Moore, D. R. J. *Ambient Water Quality Criteria for Organic Carbon in British Columbia*; Environment and Resource Management Department: British Colombia, 1998.

181. Navalon, S.; Alvaro, M.; Garcia, H. Carbohydrates as trihalomethanes precursors. Influence of pH and the presence of Cl- and Br- on trihalomethane formation potential. *Water Res.* **2008**, *42*, 3990-4000.

182. Trehy, M. L.; Yost, R. A.; Miles, C. J. Chlorination byproducts of amino acids in natural waters. *Environ. Sci. Technol.* **1986**, *20*, 1117-1122.

183. Dotson, A.; Westerhoff, P.; Krasner, S. W. Nitrogen enriched dissolved organic matter (DOM) isolates and their affinity to form emerging disinfection by-products. *Water Sci. Technol.* **2009**, *60*, 135-143.

184. National Research Council The Chemistry of Disinfectants in Water: Reactions and Products. In *Safe Drinking Water Committee. Drinking Water and Health: Volume 2*; National Academies Press: Washington (DC), 1980.

185. Rook, J. J. Chlorination reactions of fulvic acids in natural waters. *Environ. Sci. Technol.* **1977**, *11*, 478-482.

186. Pifer, A. D.; Fairey, J. L. Improving on SUVA254 using fluorescence-PARAFAC analysis and asymmetric flow-field flow fractionation for assessing disinfection byproduct formation and control. *Water Res.* **2012**, *46*, 2927-2936.

187. Nguyen, H. V.-M.; Lee, M.-H.; Hur, J.; Schlautman, M. A. Variations in spectroscopic characteristics and disinfection byproduct formation potentials of dissolved organic matter for two contrasting storm events. *J. Hydrol. (Amsterdam, Neth.)* **2013**, *481*, 132-142.

188. Wu, M.; Liang, Y.; Peng, H.; Ye, J.; Wu, J.; Shi, W.; Liu, W. Bioavailability of soluble microbial products as the autochthonous precursors of disinfection by-products in aerobic and anoxic surface water. *Sci. Total Environ.* **2019**, *649*, 960-968.

189. McLaren, S. J.; Kim, N. D. Evidence for a seasonal fluctuation of arsenic in New Zealand's longest river and the effect of treatment on concentrations in drinking water. *Environ. Pollut.* **1995**, *90*, 67-73.

190. Piper, J.; Kim, N. "Arsenic in Groundwater of the Waikato Region," Environment Waikato, 2006.

191. White, C. P.; DeBry, R. W.; Lytle, D. A. Microbial survey of a full-scale, biologically active filter for treatment of drinking water. *Appl. Environ. Microbiol.* **2012**, *78*, 6390-6394.

192. Learman, D.; Voelker, B.; Vazquez-Rodriguez, A.; Hansel, C. Formation of manganese oxides by bacterially generated superoxide. *Nat. Geosci.* **2011**, *4*, 95-98.

193. Tebo, B. M.; Johnson, H. A.; McCarthy, J. K.; Templeton, A. S. Geomicrobiology of manganese(II) oxidation. *Trends Microbiol.* **2005**, *13*, 421-428.

194. Tebo, B. M.; Bargar, J. R.; Clement, B. G.; Dick, G. J.; Murray, K. J.; Parker, D.; Verity, R.; Webb, S. M. Biogenic Manganese Oxides: Properties and Mechanisms of Formation. *Annu. Rev. Earth Planet. Sci* **2004**, *32*, 287-328.

195. Kasuga, I.; Shimazaki, D.; Kunikane, S. Influence of backwashing on the microbial community in a biofilm developed on biological activated carbon used in a drinking water treatment plant. *Water Sci. Technol.* **2007**, *55*, 173-180.

196. Magic-Knezev, A.; Wullings, B.; Van der Kooij, D. Polaromonas and Hydrogenophaga species are the predominant bacteria cultured from granular activated carbon filters in water treatment. *J. Appl. Microbiol.* **2009**, *107*, 1457-1467.

197. Niemi, R. M.; Heiskanen, I.; Heine, R.; Rapala, J. Previously uncultured β-Proteobacteria dominate in biologically active granular activated carbon (BAC) filters. *Water Res.* **2009**, *43*, 5075-5086.

198. Li, X.; Upadhyaya, G.; Yuen, W.; Brown, J.; Morgenroth, E.; Raskin, L. Changes in the structure and function of microbial communities in drinking water treatment bioreactors upon addition of phosphorus. *Appl. Environ. Microbiol.* **2010**, *76*, 7473-7481.

199. Doederer, K.; De Vera, G. A.; Espino, M. P.; Pype, M.-L.; Gale, D.; Keller, J. MIB and geosmin removal during adsorption and biodegradation phases of GAC filtration. *Water Supply* **2017**, *18*, 1449-1455.

200. Sack, E. L. W.; van der Wielen, P. W. J. J.; van der Kooij, D. Polysaccharides and proteins added to flowing drinking water at microgram-per-liter levels promote the formation of biofilms predominated by bacteroidetes and proteobacteria. *Appl. Eviron. Microbiol.* **2014**, *80*, 2360-2371.

201. Tian, J.; Lu, J.; Zhang, Y.; Li, J.-C.; Sun, L.-C.; Hu, Z.-L. Microbial community structures and dynamics in the O3/BAC drinking water treatment process. *Int. J. Environ. Res. Public Health* **2014**, *11*, 6281-6290, 6210 pp.

202. Feng, S.; Xie, S.; Zhang, X.; Yang, Z.; Ding, W.; Liao, X.; Liu, Y.; Chen, C. Ammonium removal pathways and microbial community in GAC-sand dual media filter in drinking water treatment. *J. Environ. Sci. (Beijing, China)* **2012**, *24*, 1587-1593.

203. Kaarela, O. E.; Harkki, H. A.; Palmroth, M. R. T.; Tuhkanen, T. A. Bacterial diversity and active biomass in full-scale granular activated carbon filters operated at low water temperatures. *Environ. Technol.* **2015**, *36*, 681-692.

204. La Para, T. M.; Wilkinson, K. H.; Strait, J. M.; Hozalski, R. M.; Sadowksy, M. J.; Hamilton, M. J. The bacterial communities of full-scale biologically active, granular activated carbon filters are stable and diverse and potentially contain novel ammonia-oxidizing microorganisms. *Appl. Environ. Microbiol.* **2015**, *81*, 6864-6872.

205. Xu, J.; Tang, W.; Ma, J.; Wang, H. Comparison of microbial community shifts in two parallel multi-step drinking water treatment processes. *Appl. Microbiol. Biotechnol.* **2017**, *101*, 5531-5541.

206. Liao, X.; Chen, C.; Chang, C.-H.; Wang, Z.; Zhang, X.; Xie, S. Heterogeneity of microbial community structures inside the up-flow biological activated carbon (BAC) filters for the treatment of drinking water. *Biotechnol. Bioprocess Eng.* **2012**, *17*, 881-886.

207. Tung, H.-H.; Regan, J. M.; Unz, R. F.; Xie, Y. F. Microbial community structure in a drinking water GAC filter. *Water Sci. Technol.: Water Supply* **2006**, *6*, 267-271.

208. Liao, X.; Chen, C.; Wang, Z.; Wan, R.; Chang, C.-H.; Zhang, X.; Xie, S. Pyrosequencing analysis of bacterial communities in drinking water biofilters receiving influents of different types. *Process Biochem. (Oxford, U. K.)* **2013**, *48*, 703-707.

209. Liao, X.; Chen, C.; Wang, Z.; Wan, R.; Chang, C.-H.; Zhang, X.; Xie, S. Changes of biomass and bacterial communities in biological activated carbon filters for drinking water treatment. *Process Biochem. (Oxford, U. K.)* **2013**, *48*, 312-316.

210. Liao, X.; Chen, C.; Zhang, J.; Dai, Y.; Zhang, X.; Xie, S. Operational performance, biomass and microbial community structure: impacts of backwashing on drinking water biofilter. *Environ Sci Pollut Res Int* **2015**, *22*, 546-554.

211. Maillard, J.-Y.; Hartemann, P. Silver as an antimicrobial: facts and gaps in knowledge. *Crit. Rev. Microbiol.* **2013**, *39*, 373-383.

212. Environment Waikato. Changes in arsenic. https://www.waikatoregion.govt.nz/Environment/Natural-resources/ Water/Rivers/WaikatoRiver/Downstream-change-to-water-quality/Changes-in-arsenic/ (accessed 29 June 2017)

213. Hamilton City Council *Waikato river and treated drinking water comprehensive analysis report 2013/14*: Hamilton, New Zealand, 2014.

214. Hamilton City Council *Hamilton City Council Water Supply Annual Compliance Report 2018/2019*: Hamilton, New Zealand, 2019.

215. Bruins, M. R.; Kapil, S.; Oehme, F. W. Microbial Resistance to Metals in the Environment. *Ecotoxicol. Environ. Saf.* **2000**, *45*, 198-207.

216. Silver, S. Bacterial resistances to toxic metal ions - a review. *Gene* **1996**, *179*, 9-19.

217. Blencowe, D. K.; Morby, A. P. Zn(II) metabolism in prokaryotes. *FEMS Microbiology Reviews* **2003**, *27*, 291-311.

218. Finney, L. A.; O'Halloran, T. V. Transition Metal Speciation in the Cell: Insights from the Chemistry of Metal Ion Receptors. *Science* **2003**, *300*, 931-936.

219. McDevitt, C. A.; Ogunniyi, A. D.; Valkov, E.; Lawrence, M. C.; Kobe, B.; McEwan, A. G.; Paton, J. C. A Molecular Mechanism for Bacterial Susceptibility to Zinc. *PLoS Pathogens* **2011**, *7*, e1002357.

220. Baldi, F.; Pepi, M.; Burrini, D.; Kniewald, G.; Scali, D.; Lanciotti, E. Dissolution of Barium from Barite in Sewage Sludges and Cultures of Desulfovibrio desulfuricans. *Appl. Eviron. Microbiol.* **1996**, *62*, 2398-2404.

221. Thompson, L. J. CHAPTER 16 - Thallium. In *Handbook of Toxicology of Chemical Warfare Agents*; R. C. Gupta, Ed.; Elsevier Inc, 2009; pp 225-227.

222. Ministry for the Environment. Environmental Guideline Value (EGV) database. https://www.mfe.govt.nz/land/risks-contaminated-land/managing-contaminated-land/contaminated-land-management-guidelines-0 (accessed 11th June 2020)

223. Davison, W. Iron and manganese in lakes. *Earth-Sci. Rev.* **1993**, *34*, 119-163.

224. Greenstein, K. E.; Lew, J.; Dickenson, E. R. V.; Wert, E. C. Investigation of biotransformation, sorption, and desorption of multiple chemical contaminants in pilot-scale drinking water biofilters. *Chemosphere* **2018**, *200*, 248-256.

225. Thirunavukkarasu, O. S.; Phommavong, T.; Jin, Y. C.; Ferris, S. A. Performance of reverse osmosis and manganese greensand plants in removing naturally occurring substances in drinking water. *Water Qual. Res. J.* **2013**, *49*, 72-81.

226. Burger, M. S.; Mercer, S. S.; Shupe, G. D.; Gagnon, G. A. Manganese removal during bench-scale biofiltration. *Water Res.* **2008**, *42*, 4733-4742.

227. Katsoyiannis, I. A.; Zouboulis, A. I. Biological treatment of Mn(II) and Fe(II) containing groundwater: kinetic considerations and product characterization. *Water Res.* **2004**, *38*, 1922-1932.

228. Duckworth, O. W.; Rivera, N. A.; Gardner, T. G.; Andrews, M. Y.; Santelli, C. M.; Polizzotto, M. L. Morphology, structure, and metal binding mechanisms of biogenic manganese oxides in a superfund site treatment system. *Environ. Sci. Process Impacts* **2017**, *19*, 50-58.

229. Korth, W.; Ellis, J.; Bowmer, K. The stability of geosmin and MIB and their deuterated analogs in surface waters and organic solvents. *Water Sci. Technol.* **1992**, *25*, 115-122.

230. Mosley, J. D.; Young, J. W.; Agarwal, J.; Schaefer, H. F., III; Schleyer, P. v. R.; Duncan, M. A. Structural isomerization of the gas-phase 2-norbornyl cation revealed with infrared spectroscopy and computational chemistry. *Angew. Chem., Int. Ed.* **2014**, *53*, 5888-5891.

231. Kwart, H.; Blazer, T. A. Analysis of mass spectral fragmentation patterns in various bicyclic alcohols. *J. Org. Chem.* **1970**, *35*, 2726-2731.

232. Lu, J.; Wu, Z.-P.; Che, W.-J.; Xian, Y.-P.; Guo, X.-D.; Lv, J.-X.; Li, H. Determination of earthy-musty odorous compounds in drinking water by vortex assisted dispersive liquid-liquid microextraction combined with gas chromatography tandem mass spectrometry. *Anal. Sci.* **2016**, *32*, 407-411.

233. Mahugo-Santana, C.; Sosa-Ferrera, Z.; Torres-Padrón, M. E.; Santana-Rodríguez, J. J. Application of new approaches to liquid-phase microextraction for the determination of emerging pollutants. *TrAC, Trends Anal. Chem.* **2011**, *30*, 731-748.

234. Berton, P.; Lana, N. B.; Ríos, J. M.; García-Reyes, J. F.; Altamirano, J. C. State of the art of environmentally friendly sample preparation approaches for determination of PBDEs and metabolites in environmental and biological samples: A critical review. *Anal. Chim. Acta* **2016**, *905*, 24-41.

235. Leong, M.-I.; Fuh, M.-R.; Huang, S.-D. Beyond dispersive liquid–liquid microextraction. *J. Chromatogr. A* **2014**, *1335*, 2-14.

236. Jain, R.; Singh, R. Applications of dispersive liquid–liquid micro-extraction in forensic toxicology. *TrAC, Trends Anal. Chem.* **2016**, *75*, 227-237.

237. Saraji, M.; Boroujeni, M. K. Recent developments in dispersive liquid-liquid microextraction. *Anal. Bioanal. Chem.* **2014**, *406*, 2027-2066.

238. Rezaee, M.; Yamini, Y.; Faraji, M. Evolution of dispersive liquid–liquid microextraction method. *J. Chromatogr. A* **2010**, *1217*, 2342-2357.

239. Zgoła-Grześkowiak, A.; Grześkowiak, T. Dispersive liquid-liquid microextraction. *TrAC, Trends Anal. Chem.* **2011**, *30*, 1382-1399.

240. Cristina Henriques Alves, A.; Margarida Pontes Boavida Gonçalves, M.; Manuel Serrano Bernardo, M.; Simões Mendes, B. Dispersive liquid–liquid microextraction of organophosphorous pesticides using nonhalogenated solvents. *J. Sep. Sci.* **2012**, *35*, 2653-2658.

241. Rosner, B. Percentage Points for a Generalized ESD Many-Outlier Procedure. *Technometrics* **1983**, *25*, 165-172.

242. Shapiro, S. S.; Wilk, M. B. An Analysis of Variance Test for Normality (Complete Samples). *Biometrika* **1965**, *52*, 591-611.

243. Royston, J. P. An Extension of Shapiro and Wilk's W Test for Normality to Large Samples. *J. Roy. Stat. Soc. C Appl. Stat.* **1982**, *31*, 115-124.

244. Matsui, Y.; Nakao, S.; Sakamoto, A.; Taniguchi, T.; Pan, L.; Matsushita, T.; Shirasaki, N. Adsorption capacities of activated carbons for geosmin and 2-methylisoborneol vary with activated carbon particle size: Effects of adsorbent and adsorbate characteristics. *Water Res.* **2015**, *85*, 95-102.

245. ICH Expert Working Group Tripartite Guideline - Validation of Analytical Procedures: Text and Methodology Q2(R1). In *International Conference On Harmonisation Of Technical Requirements For Registration Of Pharmaceuticals For Human Use* ICH, 2005.

246. NIWA. New Zealand National Climate Database (CliFlo). https://cliflo.niwa.co.nz/ (accessed 20 February 2019)

247. Glueckauf, E.; Coates, J. I. 241. Theory of chromatography. Part IV. The influence of incomplete equilibrium on the front boundary of chromatograms and on the effectiveness of separation. *J. Chem. Soc.* **1947**, 1315-1321.

248. Sircar, S.; Hufton, J. R. Why Does the Linear Driving Force Model for Adsorption Kinetics Work? *Adsorption* **2000**, *6*, 137-147.

249. Ho, Y. S.; McKay, G. Pseudo-second order model for sorption processes. *Process Biochem.* **1999**, *34*, 451-465.

250. Knox, J. C.; Ebner, A. D.; LeVan, M. D.; Coker, R. F.; Ritter, J. A. Limitations of Breakthrough Curve Analysis in Fixed-Bed Adsorption. *Ind. Eng. Chem. Res.* **2016**, *55*, 4734-4748.

251. Soetaert, K.; Meysman, F.; Petzoldt, T. Solving differential equations in R. *R J.* **2010**, *2*, 5-15.

252. Soetaert, K.; Cash, J.; Mazzia, F. *Solving Differential Equations in R*; Springer Berlin Heidelberg, 2012.

253. Chase, H. A. Prediction of the performance of preparative affinity chromatography. *J. Chromatogr. A* **1984**, *297*, 179-202.

254. Hagel, L.; Jagschies, G.; Sofer, G. 10 - Optimization of Chromatographic Separations. In *Handbook of Process Chromatography (Second Edition)*; L. Hagel; G. Jagschies and G. Sofer, Eds.; Academic Press: Amsterdam, 2008; pp 237-298.

255. Soetaert, K.; Petzoldt, T.; Stetzer, W. deSolve: Solvers for Initial Value Problems of Differential Equations. 2019. R package version 1.24. http://desolve.r-forge.r-project.org/

256. Soetaert, K.; Petzoldt, T. FME: A Flexible Modelling Environment for Inverse Modelling, Sensitivity, Identifiability and Monte Carlo Analysis. 2019. R package version 1.3.6.1. http://fme.r-forge.r-project.org/

257. Porter, M.; Rose, R. Hamilton's water treatment plant - a review of recent performance. In *Water New Zealand's Annual Conference & Expo*: Rotorua, New Zealand, 2011.

258. Graham, M. R.; Summers, R. S.; Simpson, M. R.; Macleod, B. W. Modeling equilibrium adsorption of 2-methylisoborneol and geosmin in natural waters. *Water Res.* **2000**, *34*, 2291-2300.

259. R Core Team. R: A language and environment for statistical computing. 2018. R package version https://www.R-project.org/

260. Matthias, P.; Daniel, G. staRdom: PARAFAC Analysis of EEMs from DOM. 2018. R package version 1.0.8. https://github.com/MatthiasPucher/staRdom

261. Massicotte, P. eemR: Tools for Pre-Processing Emission-Excitation-Matrix (EEM) Fluorescence Data. 2017. R package version 0.1.5. https://CRAN.R-project.org/package=eemR

262. Pucher, M.; Wünsch, U.; Weigelhofer, G.; Murphy, K.; Hein, T.; Graeber, D. staRdom: Versatile software for analyzing spectroscopic data of dissolved organic matter in R. *Water* **2019**, *11*, 2366.

263. Dixon, W. J. Analysis of Extreme Values. *Ann. Math. Stat.* **1950**, *21*, 488-506.

264. Dixon, W. J. Ratios Involving Extreme Values. *Ann. Math. Stat.* **1951**, *22*, 68-78.

265. Rorabacher, D. B. Statistical treatment for rejection of deviant values: critical values of Dixon's "Q" parameter and related subrange ratios at the 95% confidence level. *Anal. Chem.* **1991**, *63*, 139-146.

266. Tukey, J. W. Comparing Individual Means in the Analysis of Variance. *Biometrics* **1949**, *5*, 99-114.

267. Seredynska-Sobecka, B.; Stedmon, C. A.; Boe-Hansen, R.; Waul, C. K.; Arvin, E. Monitoring organic loading to swimming pools by fluorescence excitation-emission matrix with parallel factor analysis (PARAFAC). *Water Res.* **2011**, *45*, 2306-2314.

268. Stedmon, C. A.; Markager, S. Resolving the variability in dissolved organic matter fluorescence in a temperate estuary and its catchment using PARAFAC analysis. *Limnol. Oceanogr.* **2005**, *50*, 686-697.

269. Stedmon, C. A.; Cory, R. M. Biological Origins and Fate of Fluorescent Dissolved Organic Matter in Aquatic Environments. In *Aquatic Organic Matter Fluorescence*; A. Baker; D. M. Reynolds; J. Lead; P. G. Coble and R. G. M. Spencer, Eds.; Cambridge University Press: Cambridge, 2014; pp 278-300.

270. Maie, N.; Scully, N. M.; Pisani, O.; Jaffé, R. Composition of a protein-like fluorophore of dissolved organic matter in coastal wetland and estuarine ecosystems. *Water Res.* **2007**, *41*, 563-570.

271. Brown, M. B.; Forsythe, A. B. Robust Tests for the Equality of Variances. *J. Am. Stat. Assoc.* **1974**, *69*, 364-367.

Appendix A - Supplementary Information

A-1 Chapter 3 Supplementary Information

Preliminary ICP-MS Data

Sample	Element	Concentration (μg L^{-1})	Mass (g)	V (L)	Dilution	Concentration (μg g^{-1})	SD
GA1000N 1	B	4.901	1.108	0.2	6	5.3	0.7
GA1000N 1	Na	582.508	1.108	0.2	6	630.9	13.9
GA1000N 1	Mg	262.256	1.108	0.2	6	284.0	7.1
GA1000N 1	Al	3387.328	1.108	0.2	6	3668.6	95.4
GA1000N 1	K	207.93	1.108	0.2	6	225.2	7.4
GA1000N 1	Ca	1906.818	1.108	0.2	6	2065.2	33
GA1000N 1	V	7.365	1.108	0.2	6	8.0	0.4
GA1000N 1	Cr	6.758	1.108	0.2	6	7.3	0.4
GA1000N 1	Fe	1484.076	1.108	0.2	6	1607.3	45
GA1000N 1	Mn	18.757	1.108	0.2	6	20.3	0.6
GA1000N 1	Co	1.981	1.108	0.2	6	2.2	0.1
GA1000N 1	Ni	6.958	1.108	0.2	6	7.5	0.5
GA1000N 1	Cu	14.226	1.108	0.2	6	15.4	0.5
GA1000N 1	Zn	24.646	1.108	0.2	6	26.7	3.3
GA1000N 1	As	0.835	1.108	0.2	6	0.9	0.1
GA1000N 1	Se	0.000	1.108	0.2	6	0.0	0
GA1000N 1	Sr	78.015	1.108	0.2	6	84.5	1.6
GA1000N 1	Mo	0.289	1.108	0.2	6	0.3	0
GA1000N 1	Ag	0.028	1.108	0.2	6	0.0	0
GA1000N 1	Cd	0.133	1.108	0.2	6	0.1	0
GA1000N 1	Sn	0.289	1.108	0.2	6	0.3	0
GA1000N 1	Sb	0.065	1.108	0.2	6	0.1	0
GA1000N 1	Ba	169.688	1.108	0.2	6	183.8	6.1
GA1000N 1	Tl	0.003	1.108	0.2	6	0.0	0
GA1000N 1	Pb	1.366	1.108	0.2	6	1.5	0.1
GA1000N 1	U	0.54	1.108	0.2	6	0.6	0.2
GA1000N 2	B	4.539	1.0311	0.2	6	5.3	0.6
GA1000N 2	Na	569.341	1.0311	0.2	6	662.6	12.6
GA1000N 2	Mg	266.746	1.0311	0.2	6	310.4	5.3
GA1000N 2	Al	3340.568	1.0311	0.2	6	3887.8	116.6
GA1000N 2	K	201.979	1.0311	0.2	6	235.1	2.6
GA1000N 2	Ca	1726.929	1.0311	0.2	6	2009.8	34.2
GA1000N 2	V	7.522	1.0311	0.2	6	8.8	0.2
GA1000N 2	Cr	10.122	1.0311	0.2	6	11.8	0.8
GA1000N 2	Fe	3121.856	1.0311	0.2	6	3633.2	54.5
GA1000N 2	Mn	20.886	1.0311	0.2	6	24.3	0.7
GA1000N 2	Co	2.485	1.0311	0.2	6	2.9	0
GA1000N 2	Ni	7.348	1.0311	0.2	6	8.6	0.2
GA1000N 2	Cu	15.417	1.0311	0.2	6	17.9	0.5
GA1000N 2	Zn	24.33	1.0311	0.2	6	28.3	1.1
GA1000N 2	As	0.548	1.0311	0.2	6	0.6	0.2
GA1000N 2	Se	0	1.0311	0.2	6	0	0
GA1000N 2	Sr	70.629	1.0311	0.2	6	82.2	1.1
GA1000N 2	Mo	0.256	1.0311	0.2	6	0.3	0
GA1000N 2	Ag	0.018	1.0311	0.2	6	0.0	0
GA1000N 2	Cd	0.035	1.0311	0.2	6	0.0	0
GA1000N 2	Sn	0.303	1.0311	0.2	6	0.4	0
GA1000N 2	Sb	0.048	1.0311	0.2	6	0.1	0
GA1000N 2	Ba	164.924	1.0311	0.2	6	191.9	4.4
GA1000N 2	Tl	0.005	1.0311	0.2	6	0.0	0
GA1000N 2	Pb	1.991	1.0311	0.2	6	2.3	0.1
GA1000N 2	U	0.602	1.0311	0.2	6	0.7	0.1
GAC 1	B	9.236	1.0662	0.2	6	10.4	0.4
GAC 1	Na	846.667	1.0662	0.2	6	952.9	26.7
GAC 1	Mg	3034.368	1.0662	0.2	6	3415.2	64.9
GAC 1	Al	18110.605	1.0662	0.2	6	20383.4	285.4
GAC 1	K	588.862	1.0662	0.2	6	662.8	17.2
GAC 1	Ca	32707.976	1.0662	0.2	6	36812.6	1104.4
GAC 1	V	15.691	1.0662	0.2	6	17.7	0.6
GAC 1	Cr	9.513	1.0662	0.2	6	10.7	0.6
GAC 1	Fe	1115.175	1.0662	0.2	6	1255.1	47.7
GAC 1	Mn	11389.332	1.0662	0.2	6	12818.6	384.6
GAC 1	Co	19.574	1.0662	0.2	6	22.0	0.3

GAC 1	Ni	24.023	1.0662	0.2	6	27.0	0.9
GAC 1	Cu	136.426	1.0662	0.2	6	153.5	3.7
GAC 1	Zn	359.189	1.0662	0.2	6	404.3	8.5
GAC 1	As	26.708	1.0662	0.2	6	30.1	0.5
GAC 1	Se	2.17	1.0662	0.2	6	2.4	0.7
GAC 1	Sr	265.153	1.0662	0.2	6	298.4	2.7
GAC 1	Mo	2.65	1.0662	0.2	6	3.0	0
GAC 1	Ag	4.15	1.0662	0.2	6	4.7	0.3
GAC 1	Cd	0.775	1.0662	0.2	6	0.9	0.1
GAC 1	Sn	0.488	1.0662	0.2	6	0.5	0
GAC 1	Sb	0.112	1.0662	0.2	6	0.1	0
GAC 1	Ba	964.743	1.0662	0.2	6	1085.8	42.3
GAC 1	Tl	5.407	1.0662	0.2	6	6.1	0.4
GAC 1	Pb	5.703	1.0662	0.2	6	6.4	0.1
GAC 1	U	6.807	1.0662	0.2	6	7.7	0.8
GAC 2	B	10.272	1.0202	0.2	6	12.1	0.3
GAC 2	Na	743.745	1.0202	0.2	6	874.8	5.2
GAC 2	Mg	3225.53	1.0202	0.2	6	3794.0	56.9
GAC 2	Al	18251.855	1.0202	0.2	6	21468.6	429.4
GAC 2	K	543.815	1.0202	0.2	6	639.7	2.6
GAC 2	Ca	34817.076	1.0202	0.2	6	40953.2	1474.3
GAC 2	V	15.27	1.0202	0.2	6	18.0	0.4
GAC 2	Cr	9.731	1.0202	0.2	6	11.4	0.7
GAC 2	Fe	1210.85	1.0202	0.2	6	1424.3	47
GAC 2	Mn	10883.988	1.0202	0.2	6	12802.2	268.8
GAC 2	Co	18.677	1.0202	0.2	6	22.0	0.7
GAC 2	Ni	23.485	1.0202	0.2	6	27.6	0.8
GAC 2	Cu	142.905	1.0202	0.2	6	168.1	4.9
GAC 2	Zn	342.992	1.0202	0.2	6	403.4	12.5
GAC 2	As	24.964	1.0202	0.2	6	29.4	0.5
GAC 2	Se	2.433	1.0202	0.2	6	2.9	1.4
GAC 2	Sr	289.973	1.0202	0.2	6	341.1	11.9
GAC 2	Mo	2.88	1.0202	0.2	6	3.4	0.1
GAC 2	Ag	0.648	1.0202	0.2	6	0.8	0
GAC 2	Cd	0.761	1.0202	0.2	6	0.9	0.1
GAC 2	Sn	0.079	1.0202	0.2	6	0.1	0
GAC 2	Sb	0.125	1.0202	0.2	6	0.1	0
GAC 2	Ba	1070.874	1.0202	0.2	6	1259.6	73.1
GAC 2	Tl	6.312	1.0202	0.2	6	7.4	0.4
GAC 2	Pb	5.575	1.0202	0.2	6	6.6	0.1
GAC 2	U	7.921	1.0202	0.2	6	9.3	0.4

Full ICP-MS Data

Sample	Element	Concentration ($\mu g\ L^{-1}$)	Mass (g)	V (L)	Dilution	Concentration ($\mu g\ g^{-1}$)	SD
GAC 2 Top	B	11.8335	1.02055	0.2	6	13.9	0.5
GAC 2 Top	Na	648.27	1.02055	0.2	6	761.9	28.6
GAC 2 Top	Mg	4120.52	1.02055	0.2	6	4842.1	181.6
GAC 2 Top	Al	34353.55	1.02055	0.2	6	40332.7	1512.5
GAC 2 Top	P	253.42	1.02055	0.2	6	297.7	11.2
GAC 2 Top	S	319.12	1.02055	0.2	6	374.2	14
GAC 2 Top	K	582.20	1.02055	0.2	6	684.0	25.7
GAC 2 Top	Ca	50795.31	1.02055	0.2	6	59664.7	2237.4
GAC 2 Top	V	29.46	1.02055	0.2	6	34.6	1.3
GAC 2 Top	Cr	4.81	1.02055	0.2	6	5.6	0.2
GAC 2 Top	Mn	30176.50	1.02055	0.2	6	35409.1	1327.8
GAC 2 Top	Fe	1019.45	1.02055	0.2	6	1196.0	44.9
GAC 2 Top	Co	47.131	1.02055	0.2	6	55.3	2.1
GAC 2 Top	Ni	50.20	1.02055	0.2	6	59.0	2.2
GAC 2 Top	Cu	126.6675	1.02055	0.2	6	148.8	5.6
GAC 2 Top	Zn	357.518	1.02055	0.2	6	419.9	15.7
GAC 2 Top	As	47.7045	1.02055	0.2	6	56.0	1.6
GAC 2 Top	Se	2.5245	1.02055	0.2	6	3.0	0.1
GAC 2 Top	Mo	7.696	1.02055	0.2	6	9.0	0.3
GAC 2 Top	Ag	0.042	1.02055	0.2	6	0.1	0
GAC 2 Top	Cd	1.724	1.02055	0.2	6	2.0	0
GAC 2 Top	Sn	156.182	1.02055	0.2	6	184.0	4
GAC 2 Top	Sb	397.3995	1.02055	0.2	6	467.3	36
GAC 2 Top	Ba	4022.9235	1.02055	0.2	6	4725.3	363.8
GAC 2 Top	Hg	6.4115	1.02055	0.2	6	7.5	0.2

GAC 2 Top	Pb	10.7445	1.02055	0.2	6	12.6	0.3
GAC 2 Top	U	4.197	1.02055	0.2	6	4.9	0.1
GAC 2 Mixed	B	7.4485	1.00545	0.2	6	8.9	0.3
GAC 2 Mixed	Na	618.17	1.00545	0.2	6	737.8	25.5
GAC 2 Mixed	Mg	4443.76	1.00545	0.2	6	5303.6	183
GAC 2 Mixed	Al	14296.17	1.00545	0.2	6	17060.3	588.6
GAC 2 Mixed	P	177.42	1.00545	0.2	6	211.8	7.3
GAC 2 Mixed	S	372.86	1.00545	0.2	6	444.8	15.3
GAC 2 Mixed	K	560.28	1.00545	0.2	6	668.7	23.1
GAC 2 Mixed	Ca	55320.07	1.00545	0.2	6	66023.6	2277.8
GAC 2 Mixed	V	10.01	1.00545	0.2	6	11.9	0.4
GAC 2 Mixed	Cr	3.51	1.00545	0.2	6	4.2	0.1
GAC 2 Mixed	Mn	6710.31	1.00545	0.2	6	8006.2	276.2
GAC 2 Mixed	Fe	797.48	1.00545	0.2	6	951.7	32.8
GAC 2 Mixed	Co	13.278	1.00545	0.2	6	15.8	0.5
GAC 2 Mixed	Ni	16.80	1.00545	0.2	6	20.0	0.7
GAC 2 Mixed	Cu	63.019	1.00545	0.2	6	75.2	2.6
GAC 2 Mixed	Zn	142.945	1.00545	0.2	6	170.6	5.9
GAC 2 Mixed	As	12.944	1.00545	0.2	6	15.4	0.5
GAC 2 Mixed	Se	1.186	1.00545	0.2	6	1.4	0
GAC 2 Mixed	Mo	1.734	1.00545	0.2	6	2.1	0.1
GAC 2 Mixed	Ag	0	1.00545	0.2	6	0.0	0
GAC 2 Mixed	Cd	0.7035	1.00545	0.2	6	0.8	0
GAC 2 Mixed	Sn	63.7655	1.00545	0.2	6	76.1	2.4
GAC 2 Mixed	Sb	323.3655	1.00545	0.2	6	386.0	17.4
GAC 2 Mixed	Ba	4057.0675	1.00545	0.2	6	4842.0	217.9
GAC 2 Mixed	Hg	3.1405	1.00545	0.2	6	3.7	0.1
GAC 2 Mixed	Pb	3.9615	1.00545	0.2	6	4.7	0.1
GAC 2 Mixed	U	2.135	1.00545	0.2	6	2.5	0
GAC 3 Top	B	6.414	1.00545	0.2	6	7.5	0.1
GAC 3 Top	Na	783.42	1.02105	0.2	6	920.7	18
GAC 3 Top	Mg	5070.94	1.02105	0.2	6	5959.7	116.2
GAC 3 Top	Al	13163.26	1.02105	0.2	6	15470.3	301.7
GAC 3 Top	P	241.55	1.02105	0.2	6	283.9	5.5
GAC 3 Top	S	442.92	1.02105	0.2	6	520.5	10.1
GAC 3 Top	K	658.44	1.02105	0.2	6	773.8	15.1
GAC 3 Top	Ca	63628.65	1.02105	0.2	6	74780.2	1458.2
GAC 3 Top	V	7.23	1.02105	0.2	6	8.5	0.2
GAC 3 Top	Cr	3.90	1.02105	0.2	6	4.6	0.1
GAC 3 Top	Mn	3187.53	1.02105	0.2	6	3746.2	73.1
GAC 3 Top	Fe	783.53	1.02105	0.2	6	920.8	18
GAC 3 Top	Co	7.6575	1.02105	0.2	6	9.0	0.2
GAC 3 Top	Ni	11.32	1.02105	0.2	6	13.3	0.3
GAC 3 Top	Cu	59.302	1.02105	0.2	6	69.7	1.4
GAC 3 Top	Zn	118.3205	1.02105	0.2	6	139.1	2.7
GAC 3 Top	As	7.638	1.02105	0.2	6	9.0	0.2
GAC 3 Top	Se	1.027	1.02105	0.2	6	1.2	0
GAC 3 Top	Mo	0.571	1.02105	0.2	6	0.7	0
GAC 3 Top	Ag	0	1.02105	0.2	6	0.0	0
GAC 3 Top	Cd	0.631	1.02105	0.2	6	0.7	0
GAC 3 Top	Sn	55.8585	1.02105	0.2	6	65.6	1.1
GAC 3 Top	Sb	234.069	1.02105	0.2	6	275.1	22
GAC 3 Top	Ba	4829.148	1.02105	0.2	6	5675.5	454
GAC 3 Top	Hg	2.3875	1.02105	0.2	6	2.8	0.1
GAC 3 Top	Pb	2.9485	1.02105	0.2	6	3.5	0.1
GAC 3 Top	U	2.115	1.02105	0.2	6	2.5	0.1
GAC 3 Mixed	B	11.19	1.01295	0.2	6	13.2	0.4
GAC 3 Mixed	Na	705.34	1.01295	0.2	6	835.6	26.3
GAC 3 Mixed	Mg	4575.40	1.01295	0.2	6	5419.6	170.7
GAC 3 Mixed	Al	15077.37	1.01295	0.2	6	17855.9	562.5
GAC 3 Mixed	P	173.93	1.01295	0.2	6	206.0	6.5
GAC 3 Mixed	S	369.11	1.01295	0.2	6	435.5	13.7
GAC 3 Mixed	K	596.48	1.01295	0.2	6	706.6	22.3
GAC 3 Mixed	Ca	57429.21	1.01295	0.2	6	68030.7	2143
GAC 3 Mixed	V	9.24	1.01295	0.2	6	10.9	0.3
GAC 3 Mixed	Cr	3.33	1.01295	0.2	6	3.9	0.1
GAC 3 Mixed	Mn	6425.12	1.01295	0.2	6	7607.6	239.6
GAC 3 Mixed	Fe	732.91	1.01295	0.2	6	868.1	27.3
GAC 3 Mixed	Co	12.7595	1.01295	0.2	6	15.1	0.5
GAC 3 Mixed	Ni	16.03	1.01295	0.2	6	19.0	0.6
GAC 3 Mixed	Cu	63.1655	1.01295	0.2	6	74.8	2.4
GAC 3 Mixed	Zn	146.303	1.01295	0.2	6	173.3	5.5

GAC 3 Mixed	As	13.545	1.01295	0.2	6	16.0	0.6
GAC 3 Mixed	Se	1.288	1.01295	0.2	6	1.5	0.1
GAC 3 Mixed	Mo	1.395	1.01295	0.2	6	1.7	0.1
GAC 3 Mixed	Ag	0.054	1.01295	0.2	6	0.0	0
GAC 3 Mixed	Cd	0.7435	1.01295	0.2	6	0.9	0
GAC 3 Mixed	Sn	78.5815	1.01295	0.2	6	93.2	2.4
GAC 3 Mixed	Sb	255.2955	1.01295	0.2	6	302.2	16.9
GAC 3 Mixed	Ba	4368.0155	1.01295	0.2	6	5174.0	289.7
GAC 3 Mixed	Hg	2.5245	1.01295	0.2	6	3.0	0.1
GAC 3 Mixed	Pb	3.976	1.01295	0.2	6	4.7	0.1
GAC 3 Mixed	U	2.247	1.01295	0.2	6	2.7	0
GAC 4 Top	B	7.543	1.0211	0.2	6	8.8	0.3
GAC 4 Top	Na	738.57	1.0211	0.2	6	867.4	29.1
GAC 4 Top	Mg	4951.39	1.0211	0.2	6	5819.0	194.9
GAC 4 Top	Al	13157.90	1.0211	0.2	6	15462.6	518
GAC 4 Top	P	256.32	1.0211	0.2	6	301.3	10.1
GAC 4 Top	S	446.18	1.0211	0.2	6	533.7	17.9
GAC 4 Top	K	642.98	1.0211	0.2	6	755.4	25.3
GAC 4 Top	Ca	62273.49	1.0211	0.2	6	73185.3	2451.7
GAC 4 Top	V	7.42	1.0211	0.2	6	8.7	0.3
GAC 4 Top	Cr	3.54	1.0211	0.2	6	4.2	0.1
GAC 4 Top	Mn	3189.56	1.0211	0.2	6	3747.3	125.5
GAC 4 Top	Fe	830.50	1.0211	0.2	6	976.5	32.7
GAC 4 Top	Co	7.9995	1.0211	0.2	6	9.4	0.3
GAC 4 Top	Ni	11.56	1.0211	0.2	6	13.6	0.5
GAC 4 Top	Cu	57.701	1.0211	0.2	6	67.8	2.3
GAC 4 Top	Zn	121.2395	1.0211	0.2	6	142.5	4.8
GAC 4 Top	As	7.8555	1.0211	0.2	6	9.2	0.2
GAC 4 Top	Se	0.974	1.0211	0.2	6	1.1	0
GAC 4 Top	Mo	0.5635	1.0211	0.2	6	0.7	0
GAC 4 Top	Ag	0	1.0211	0.2	6	0.0	0
GAC 4 Top	Cd	0.664	1.0211	0.2	6	0.8	0
GAC 4 Top	Sn	56.658	1.0211	0.2	6	66.5	1.5
GAC 4 Top	Sb	277.7405	1.0211	0.2	6	324.6	20.6
GAC 4 Top	Ba	4832.978	1.0211	0.2	6	5677.4	360.5
GAC 4 Top	Hg	2.001	1.0211	0.2	6	2.4	0.1
GAC 4 Top	Pb	2.8585	1.0211	0.2	6	3.4	0.1
GAC 4 Top	U	2.0405	1.0211	0.2	6	2.4	0.1
GAC 4 Mixed	B	8.91	1.02065	0.2	6	10.5	0.4
GAC 4 Mixed	Na	739.13	1.02065	0.2	6	869.2	29.1
GAC 4 Mixed	Mg	4814.40	1.02065	0.2	6	5661.8	189.7
GAC 4 Mixed	Al	17124.08	1.02065	0.2	6	20134.8	674.5
GAC 4 Mixed	P	257.57	1.02065	0.2	6	303.3	10.2
GAC 4 Mixed	S	847.07	1.02065	0.2	6	1002.0	33.6
GAC 4 Mixed	K	640.55	1.02065	0.2	6	753.3	25.2
GAC 4 Mixed	Ca	60324.49	1.02065	0.2	6	70935.1	2376.3
GAC 4 Mixed	V	10.46	1.02065	0.2	6	12.3	0.4
GAC 4 Mixed	Cr	3.64	1.02065	0.2	6	4.3	0.1
GAC 4 Mixed	Mn	7340.95	1.02065	0.2	6	8626.9	289
GAC 4 Mixed	Fe	827.26	1.02065	0.2	6	973.7	32.6
GAC 4 Mixed	Co	14.562	1.02065	0.2	6	17.1	0.6
GAC 4 Mixed	Ni	17.94	1.02065	0.2	6	21.1	0.7
GAC 4 Mixed	Cu	69.7965	1.02065	0.2	6	82.1	2.7
GAC 4 Mixed	Zn	158.288	1.02065	0.2	6	186.1	6.2
GAC 4 Mixed	As	14.9665	1.02065	0.2	6	17.6	0.4
GAC 4 Mixed	Se	1.382	1.02065	0.2	6	1.6	0
GAC 4 Mixed	Mo	1.639	1.02065	0.2	6	1.9	0
GAC 4 Mixed	Ag	0	1.02065	0.2	6	0.0	0
GAC 4 Mixed	Cd	0.821	1.02065	0.2	6	1.0	0
GAC 4 Mixed	Sn	65.39	1.02065	0.2	6	76.6	1.8
GAC 4 Mixed	Sb	229.4715	1.02065	0.2	6	269.7	12.7
GAC 4 Mixed	Ba	4565.027	1.02065	0.2	6	5368.0	252.3
GAC 4 Mixed	Hg	3.1875	1.02065	0.2	6	3.7	0.1
GAC 4 Mixed	Pb	4.4555	1.02065	0.2	6	5.2	0.1
GAC 4 Mixed	U	2.527	1.02065	0.2	6	3.0	0
GAC 5 Top	B	6.20	1.04285	0.2	6	7.1	0.2
GAC 5 Top	Na	749.38	1.04285	0.2	6	861.2	19.4
GAC 5 Top	Mg	4312.08	1.04285	0.2	6	4959.7	111.6
GAC 5 Top	Al	25233.03	1.04285	0.2	6	29030.0	653.2
GAC 5 Top	P	249.84	1.04285	0.2	6	287.1	6.5
GAC 5 Top	S	588.30	1.04285	0.2	6	668.0	15
GAC 5 Top	K	608.93	1.04285	0.2	6	700.5	15.8

GAC 5 Top	Ca	53441.26	1.04285	0.2	6	61481.2	1383.3
GAC 5 Top	V	16.46	1.04285	0.2	6	18.9	0.4
GAC 5 Top	Cr	3.82	1.04285	0.2	6	4.4	0.1
GAC 5 Top	Mn	15950.61	1.04285	0.2	6	18350.3	412.9
GAC 5 Top	Fe	842.15	1.04285	0.2	6	971.1	21.9
GAC 5 Top	Co	27.1195	1.04285	0.2	6	31.2	0.7
GAC 5 Top	Ni	30.81	1.04285	0.2	6	35.5	0.8
GAC 5 Top	Cu	97.819	1.04285	0.2	6	112.6	2.5
GAC 5 Top	Zn	244.631	1.04285	0.2	6	281.5	6.3
GAC 5 Top	As	30.046	1.04285	0.2	6	34.6	0.9
GAC 5 Top	Se	1.927	1.04285	0.2	6	2.2	0.1
GAC 5 Top	Mo	4.1525	1.04285	0.2	6	4.8	0.1
GAC 5 Top	Ag	0.006	1.04285	0.2	6	0.0	0
GAC 5 Top	Cd	1.2285	1.04285	0.2	6	1.4	0
GAC 5 Top	Sn	77.0555	1.04285	0.2	6	89.2	1.1
GAC 5 Top	Sb	289.592	1.04285	0.2	6	333.1	30.8
GAC 5 Top	Ba	4304.6905	1.04285	0.2	6	4951.9	458.1
GAC 5 Top	Hg	5.374	1.04285	0.2	6	6.2	0.1
GAC 5 Top	Pb	6.7245	1.04285	0.2	6	7.7	0.1
GAC 5 Top	U	3.438	1.04285	0.2	6	4.0	0
GAC 5 Mixed	B	8.48	1.09055	0.2	6	9.3	0.3
GAC 5 Mixed	Na	759.10	1.09055	0.2	6	834.9	23.8
GAC 5 Mixed	Mg	4736.17	1.09055	0.2	6	5209.1	148.5
GAC 5 Mixed	Al	21046.28	1.09055	0.2	6	23114.8	658.8
GAC 5 Mixed	P	236.80	1.09055	0.2	6	260.9	7.4
GAC 5 Mixed	S	558.48	1.09055	0.2	6	607.2	17.3
GAC 5 Mixed	K	637.97	1.09055	0.2	6	701.5	20
GAC 5 Mixed	Ca	58649.31	1.09055	0.2	6	64520.6	1838.8
GAC 5 Mixed	V	13.94	1.09055	0.2	6	15.3	0.4
GAC 5 Mixed	Cr	3.67	1.09055	0.2	6	4.0	0.1
GAC 5 Mixed	Mn	11780.13	1.09055	0.2	6	12911.7	368
GAC 5 Mixed	Fe	849.12	1.09055	0.2	6	936.8	26.7
GAC 5 Mixed	Co	21.67	1.09055	0.2	6	23.8	0.7
GAC 5 Mixed	Ni	23.80	1.09055	0.2	6	26.1	0.7
GAC 5 Mixed	Cu	83.573	1.09055	0.2	6	91.9	2.6
GAC 5 Mixed	Zn	202.8205	1.09055	0.2	6	222.6	6.3
GAC 5 Mixed	As	22.321	1.09055	0.2	6	24.5	0.8
GAC 5 Mixed	Se	1.427	1.09055	0.2	6	1.6	0.1
GAC 5 Mixed	Mo	2.8225	1.09055	0.2	6	3.1	0.1
GAC 5 Mixed	Ag	0	1.09055	0.2	6	0.0	0
GAC 5 Mixed	Cd	0.995	1.09055	0.2	6	1.1	0
GAC 5 Mixed	Sn	79.0605	1.09055	0.2	6	86.4	1.4
GAC 5 Mixed	Sb	292.3	1.09055	0.2	6	323.3	13.9
GAC 5 Mixed	Ba	4509.4415	1.09055	0.2	6	4957.6	213.2
GAC 5 Mixed	Hg	4.5075	1.09055	0.2	6	5.0	0
GAC 5 Mixed	Pb	5.9995	1.09055	0.2	6	6.6	0.1
GAC 5 Mixed	U	2.9455	1.09055	0.2	6	3.2	0
GAC 6 Top	B	152.00	1.0379	0.2	6	175.8	7
GAC 6 Top	Na	600.70	1.0379	0.2	6	697.6	27.9
GAC 6 Top	Mg	3194.82	1.0379	0.2	6	3695.4	147.8
GAC 6 Top	Al	9210.90	1.0379	0.2	6	10653.4	426.1
GAC 6 Top	P	371.95	1.0379	0.2	6	429.8	17.2
GAC 6 Top	S	1949.34	1.0379	0.2	6	2257.4	90.3
GAC 6 Top	K	400.31	1.0379	0.2	6	463.1	18.5
GAC 6 Top	Ca	39632.67	1.0379	0.2	6	45848.6	1833.9
GAC 6 Top	V	12.47	1.0379	0.2	6	14.4	0.6
GAC 6 Top	Cr	4.12	1.0379	0.2	6	4.8	0.2
GAC 6 Top	Mn	1888.63	1.0379	0.2	6	2185.1	87.4
GAC 6 Top	Fe	4791.33	1.0379	0.2	6	5535.3	221.4
GAC 6 Top	Co	10.8305	1.0379	0.2	6	12.5	0.5
GAC 6 Top	Ni	30.32	1.0379	0.2	6	35.0	1.4
GAC 6 Top	Cu	34.031	1.0379	0.2	6	39.4	1.6
GAC 6 Top	Zn	83.0575	1.0379	0.2	6	96.1	3.8
GAC 6 Top	As	14.0315	1.0379	0.2	6	16.2	0.6
GAC 6 Top	Se	3.9575	1.0379	0.2	6	4.6	0.2
GAC 6 Top	Mo	1.159	1.0379	0.2	6	1.3	0
GAC 6 Top	Ag	0	1.0379	0.2	6	0.0	0
GAC 6 Top	Cd	0.4125	1.0379	0.2	6	0.5	0
GAC 6 Top	Sn	795.917	1.0379	0.2	6	919.9	25.3
GAC 6 Top	Sb	72.8765	1.0379	0.2	6	84.4	10.1
GAC 6 Top	Ba	3522.7345	1.0379	0.2	6	4075.1	487
GAC 6 Top	Hg	6.379	1.0379	0.2	6	7.4	0.2

GAC 6 Top	Pb	2.567	1.0379	0.2	6	3.0	0.1
GAC 6 Top	U	1.052	1.0379	0.2	6	1.2	0
GAC 6 Mixed	B	138.661	1.1055	0.2	6	150.5	3
GAC 6 Mixed	Na	483.676	1.1055	0.2	6	490.1	9.8
GAC 6 Mixed	Mg	3509.039	1.1055	0.2	6	3807.3	76.1
GAC 6 Mixed	Al	9472.904	1.1055	0.2	6	10281.1	205.6
GAC 6 Mixed	P	347.424	1.1055	0.2	6	372.0	7.4
GAC 6 Mixed	S	1616.524	1.1055	0.2	6	1754.7	35.1
GAC 6 Mixed	K	432.256	1.1055	0.2	6	458.9	9.2
GAC 6 Mixed	Ca	43437.359	1.1055	0.2	6	47123.7	942.5
GAC 6 Mixed	V	11.955	1.1055	0.2	6	13.0	0.3
GAC 6 Mixed	Cr	3.95	1.1055	0.2	6	4.2	0.1
GAC 6 Mixed	Mn	1999.928	1.1055	0.2	6	2170.9	43.4
GAC 6 Mixed	Fe	4873.395	1.1055	0.2	6	5289.6	105.8
GAC 6 Mixed	Co	10.996	1.1055	0.2	6	11.9	0.2
GAC 6 Mixed	Ni	30.016	1.1055	0.2	6	32.5	0.7
GAC 6 Mixed	Cu	35.887	1.1055	0.2	6	38.6	0.8
GAC 6 Mixed	Zn	86.203	1.1055	0.2	6	92.2	1.8
GAC 6 Mixed	As	14.523	1.1055	0.2	6	15.7	0.4
GAC 6 Mixed	Se	4.317	1.1055	0.2	6	4.6	0.1
GAC 6 Mixed	Mo	1.287	1.1055	0.2	6	1.1	0
GAC 6 Mixed	Ag	<0.000	1.1055	0.2	6	0.0	0
GAC 6 Mixed	Cd	0.409	1.1055	0.2	6	0.4	0
GAC 6 Mixed	Sn	866.185	1.1055	0.2	6	927.0	12.1
GAC 6 Mixed	Sb	159.488	1.1055	0.2	6	93.2	5.6
GAC 6 Mixed	Ba	3793.801	1.1055	0.2	6	6186.2	371.2
GAC 6 Mixed	Hg	4.02	1.1055	0.2	6	5.8	0
GAC 6 Mixed	Pb	3.075	1.1055	0.2	6	6.0	0
GAC 6 Mixed	U	1.066	1.1055	0.2	6	1.2	0
GA1000N	B	1.00	1.0337	0.2	6	1.1	0
GA1000N	Na	433.43	1.0337	0.2	6	502.8	13.3
GA1000N	Mg	215.86	1.0337	0.2	6	250.6	6.6
GA1000N	Al	3469.77	1.0337	0.2	6	4027.1	106.7
GA1000N	P	220.87	1.0337	0.2	6	257.0	6.8
GA1000N	S	94.10	1.0337	0.2	6	55.9	1.5
GA1000N	K	136.91	1.0337	0.2	6	158.9	4.2
GA1000N	Ca	2639.66	1.0337	0.2	6	3064.5	81.2
GA1000N	V	6.07	1.0337	0.2	6	7.0	0.2
GA1000N	Cr	2.32	1.0337	0.2	6	2.7	0.1
GA1000N	Mn	22.45	1.0337	0.2	6	26.1	0.7
GA1000N	Fe	1153.82	1.0337	0.2	6	1339.0	35.5
GA1000N	Co	1.5025	1.0337	0.2	6	1.7	0
GA1000N	Ni	7.58	1.0337	0.2	6	8.8	0.2
GA1000N	Cu	7.9855	1.0337	0.2	6	9.3	0.2
GA1000N	Zn	1.195	1.0337	0.2	6	1.4	0
GA1000N	As	0.7005	1.0337	0.2	6	0.8	0
GA1000N	Se	0.539	1.0337	0.2	6	0.6	0
GA1000N	Mo	0.4035	1.0337	0.2	6	0.5	0
GA1000N	Ag	0	1.0337	0.2	6	0.0	0
GA1000N	Cd	0.003	1.0337	0.2	6	0.0	0
GA1000N	Sn	494.2215	1.0337	0.2	6	573.1	14
GA1000N	Sb	0	1.0337	0.2	6	0.0	0
GA1000N	Ba	434.266	1.0337	0.2	6	504.1	23.7
GA1000N	Hg	2.4185	1.0337	0.2	6	2.8	0.1
GA1000N	Pb	1.1905	1.0337	0.2	6	1.4	0
GA1000N	U	0.1935	1.0337	0.2	6	0.2	0

A-2 Chapter 4 Supplementary Information

Voltage, peak area and S/N data

Analyte	Voltage	Concentration (µg L^{-1})	Peak Area	S/N Ratio
2-MIB	1600	0.25	0	0
2-MIB	1600	0.25	5	0
2-MIB	1700	0.25	6	3
2-MIB	1700	0.25	6	2
2-MIB	1800	0.25	12	1.9
2-MIB	1800	0.25	15	4.4
2-MIB	1900	0.25	26	3.9
2-MIB	1900	0.25	19	4
2-MIB	2000	0.25	31	4.2
2-MIB	2000	0.25	34	5.7
2-MIB	2100	0.25	51	8.1
2-MIB	2100	0.25	66	7.4
GSM	1600	0.25	3	0
GSM	1600	0.25	6	0
GSM	1700	0.25	8	0
GSM	1700	0.25	8	0
GSM	1800	0.25	13	5.2
GSM	1800	0.25	11	5.3
GSM	1900	0.25	27	10.9
GSM	1900	0.25	31	10.8
GSM	2000	0.25	45	15.7
GSM	2000	0.25	39	16.5
GSM	2100	0.25	79	14.7
GSM	2100	0.25	84	19.2
2-MIB	1600	10.00	84	30
2-MIB	1600	10.00	76	30
2-MIB	1700	10.00	166	61.5
2-MIB	1700	10.00	160	60.5
2-MIB	1800	10.00	285	111.5
2-MIB	1800	10.00	270	102.7
2-MIB	1900	10.00	526	199.9
2-MIB	1900	10.00	488	187.1
2-MIB	2000	10.00	865	162.4
2-MIB	2000	10.00	828	162.1
2-MIB	2100	10.00	1423	270
2-MIB	2100	10.00	1419	272.8
GSM	1600	10.00	99	37.9
GSM	1600	10.00	99	36.9
GSM	1700	10.00	199	73.9
GSM	1700	10.00	195	73.4
GSM	1800	10.00	373	136.1
GSM	1800	10.00	329	124.8
GSM	1900	10.00	660	244.8
GSM	1900	10.00	616	233.8
GSM	2000	10.00	1076	199.8
GSM	2000	10.00	1045	199.8
GSM	2100	10.00	1772	332.9
GSM	2100	10.00	1787	336.2

VALLME calculations:

From the GC-MS peak area data and the calibration data, the concentration of the analyte (A) in the extract (C_i) can be calculated as:

$$C_i = C_{IS}\frac{R}{RF}$$

$$R = \frac{PA_A}{PA_{IS}}$$

Where C_i = Concentration of the analyte in the extract (µg L^{-1})
C_{IS} = Concentration of the internal standard in the extract (4.9 µg L^{-1})
R = Peak area ratio of analyte to internal standard
RF = Response factor (slope of calibration plot)
PA_A = Peak area of the analyte A
PA_{IS} = Peak area of the internal standard

Because a certain volume of the internal standard (*IS*) is added to a fixed volume of the extract, C_i must be corrected for to give the actual concentration of A in the extract (E):

$$C_i = C_{IS}\frac{R}{RF}\frac{V_T}{V_E}$$

Where V_T = Sum of E and *IS* volume (60 µL)
V_E = Volume of E (50 µL)

The preconcentration factor (PF) is simply the ratio of C_i to the spiked concentration in the initial water sample (C_o). Note that both C_i and C_o must be in the sample concentration units:

$$PF = \frac{C_i}{C_o}$$

To obtain the concentration of A in the initial water sample (C_f), C_i must be corrected for the initial concentration of the water sample (V_s), the volume of the supernatant extracting phase recovered (V_{sup}) and a conversion to units of ng L^{-1}:

$$C_f = C_i\frac{V_{sup}}{V_s} \times 1000\ ng\ \mu g^{-1}$$

Where V_{sup} = Volume of supernatant extracting phase (µL)
V_s = Volume of water sample (10000 µL)

Overall, C_f can be calculated as:

$$C_f = C_{IS}\frac{R}{RF}\frac{V_T}{V_E}\frac{V_{sup}}{V_s} \times 1000\ ng\ \mu g^{-1}$$

The extraction recovery percentage (ER) can be obtained from C_f and C_o:

$$ER = \frac{C_f}{C_o} \times 100$$

As an example, taken from the first line of the next table of extraction recovery data:

Date	Analyte	PA_A	PA_{IS}	RF	C_{IS} (ug L^{-1})	C_o (ng L^{-1})	V_{sup} (µL)	C_i (ug L^{-1})	C_f (ng L^{-1})	ER	PF
13/06/17	2-MIB	105	1556	0.7291	4.9	4.89	72	0.5	3.9	80.1	111.3

$$R = \frac{PA_A}{PA_{IS}} = \frac{105}{1556} = 0.06745\ (4\ s.f.)$$

$$C_i = C_{IS}\frac{R}{RF}\frac{V_T}{V_E} = 4.9\ \mu g\ L^{-1} \times \frac{0.06745}{0.7291} \times \frac{60\ \mu L}{50\ \mu L} = 0.5442\ \mu g\ L^{-1}\ (4\ s.f.)$$

$$PF = \frac{C_i}{C_o} = \frac{0.5442\ \mu g\ L^{-1}}{\left(\frac{4.89\ ng\ L^{-1}}{1000\ ng\ \mu g^{-1}}\right)} = 111.3\ (1\ d.p.)$$

$$C_f = C_i\frac{V_{sup}}{V_s} \times 1000\ ng\ \mu g^{-1}$$

$$= 0.5442\ \mu g\ L^{-1} \times \left(\frac{72\ \mu L}{10000\ \mu L}\right) \times 1000\ ng\ \mu g^{-1}$$

$$= 3.918\ ng\ L^{-1}\ (4\ s.f.) = 3.9\ ng\ L^{-1}\ (1\ d.p.)$$

$$ER = \frac{C_f}{C_o} \times 100 = \frac{3.918\ ng\ L^{-1}}{4.89\ ng\ L^{-1}} \times 100 = 80.1\ \%\ (1\ d.p.)$$

Extraction recovery, pre-concentration factor and V_{sup} data:

Date	Analyte	PA_A	PA_{IS}	RF	C_{IS} (ug L^{-1})	C_o (ng L^{-1})	V_{sup} (µL)	C_i (ug L^{-1})	C_f (ng L^{-1})	ER	PF
13/06/17	2-MIB	105	1556	0.7291	4.9	4.89	72	0.5	3.9	80.1	111.3
13/06/17	2-MIB	95	1448	0.7291	4.9	4.89	74	0.5	3.9	80.1	108.2
13/06/17	2-MIB	107	1511	0.7291	4.9	4.89	72	0.6	4.1	84.1	116.8
13/06/17	2-MIB	1340	1628	0.7291	4.9	48.9	74	6.6	49.1	100.5	135.7
13/06/17	2-MIB	1213	1619	0.7291	4.9	48.9	76	6.0	45.9	93.9	123.6
13/06/17	2-MIB	1372	1721	0.7291	4.9	48.9	76	6.4	48.9	99.9	131.5
13/06/17	2-MIB	13479	1573	0.7291	4.9	489	76	69.1	525.2	107.4	141.3
13/06/17	2-MIB	13192	1702	0.7291	4.9	489	76	62.5	475.1	97.2	127.8
13/06/17	2-MIB	12771	1828	0.7291	4.9	489	74	56.3	416.9	85.3	115.2
13/06/17	2-MIB	8687	1088	0.7291	4.9	489	74	64.4	476.5	97.4	131.7
4/07/17	2-MIB	70	864	0.6157	4.9	4.89	70	0.8	5.4	110.8	158.2
4/07/17	2-MIB	88	1147	0.6157	4.9	4.89	72	0.7	5.3	107.9	149.8
4/07/17	2-MIB	78	1233	0.6157	4.9	4.89	76	0.6	4.6	93.9	123.5
4/07/17	2-MIB	811	1084	0.6157	4.9	48.9	74	7.1	52.9	108.1	146.1
4/07/17	2-MIB	810	1196	0.6157	4.9	48.9	74	6.5	47.9	97.9	132.3
4/07/17	2-MIB	783	1136	0.6157	4.9	48.9	74	6.6	48.7	99.6	134.6
4/07/17	2-MIB	9852	1276	0.6157	4.9	489	66	73.7	486.7	99.5	150.8
4/07/17	2-MIB	9980	1317	0.6157	4.9	489	74	72.4	535.5	109.5	148.0
4/07/17	2-MIB	8184	1195	0.6157	4.9	489	74	65.4	484.0	99.0	133.8
4/07/17	2-MIB	7290	892	0.6157	4.9	489	66	78.0	515.1	105.3	159.6
7/07/17	2-MIB	40	575	0.6136	4.9	4.89	74	0.7	4.9	100.9	136.3
7/07/17	2-MIB	40	833	0.6136	4.9	4.89	74	0.5	3.4	69.6	94.1
7/07/17	2-MIB	51	927	0.6136	4.9	4.89	74	0.5	3.9	79.8	107.8
7/07/17	2-MIB	617	784	0.6136	4.9	48.9	76	7.5	57.3	117.2	154.2
7/07/17	2-MIB	631	1013	0.6136	4.9	48.9	76	6.0	45.4	92.8	122.1
7/07/17	2-MIB	662	948	0.6136	4.9	48.9	74	6.7	49.5	101.3	136.8
7/07/17	2-MIB	773	1056	0.6136	4.9	48.9	74	7.0	51.9	106.2	143.4
7/07/17	2-MIB	844	1136	0.6136	4.9	48.9	76	7.1	54.1	110.7	145.6
7/07/17	2-MIB	761	1000	0.6136	4.9	48.9	72	7.3	52.5	107.4	149.1
7/07/17	2-MIB	6099	775	0.6136	4.9	489	74	75.4	558.1	114.1	154.2
13/06/17	GSM	133	1556	0.7378	4.9	4.97	72	0.7	4.9	98.7	137.1
13/06/17	GSM	142	1448	0.7378	4.9	4.97	74	0.8	5.8	116.4	157.3
13/06/17	GSM	145	1511	0.7378	4.9	4.97	72	0.8	5.5	110.8	153.9
13/06/17	GSM	1563	1628	0.7378	4.9	49.7	74	7.7	56.6	113.9	154.0
13/06/17	GSM	1520	1619	0.7378	4.9	49.7	76	7.5	56.9	114.4	150.5
13/06/17	GSM	1592	1721	0.7378	4.9	49.7	76	7.4	56.0	112.7	148.3
13/06/17	GSM	14948	1573	0.7378	4.9	497	76	75.7	575.6	115.8	152.4
13/06/17	GSM	14538	1702	0.7378	4.9	497	76	68.1	517.4	104.1	137.0
13/06/17	GSM	13990	1828	0.7378	4.9	497	74	61.0	451.3	90.8	122.7
13/06/17	GSM	9081	892	0.7378	4.9	497	66	81.1	535.5	107.7	163.2
4/07/17	GSM	72	864	0.7766	4.9	4.97	70	0.6	4.4	88.9	127.0
4/07/17	GSM	112	1147	0.7766	4.9	4.97	72	0.7	5.3	107.1	148.8
4/07/17	GSM	107	1233	0.7766	4.9	4.97	76	0.7	5.0	100.5	132.2
4/07/17	GSM	1109	1084	0.7766	4.9	49.7	74	7.7	57.3	115.3	155.9
4/07/17	GSM	1271	1196	0.7766	4.9	49.7	74	8.0	59.5	119.8	161.9
4/07/17	GSM	1232	1136	0.7766	4.9	49.7	74	8.2	60.8	122.3	165.2
4/07/17	GSM	14250	1277	0.7766	4.9	497	66	84.5	557.6	112.2	170.0
4/07/17	GSM	12990	1317	0.7766	4.9	497	74	74.7	552.6	111.2	150.3
4/07/17	GSM	11565	1195	0.7766	4.9	497	74	73.3	542.2	109.1	147.4
4/07/17	GSM	10343	1088	0.7766	4.9	497	74	72.0	532.6	107.2	144.8
7/07/17	GSM	53	575	0.7725	4.9	4.97	74	0.7	5.2	104.5	141.2
7/07/17	GSM	77	833	0.7725	4.9	4.97	74	0.7	5.2	104.8	141.6
7/07/17	GSM	75	927	0.7725	4.9	4.97	74	0.6	4.6	91.7	123.9
7/07/17	GSM	824	784	0.7725	4.9	49.7	76	8.0	60.8	122.3	161.0
7/07/17	GSM	901	1013	0.7725	4.9	49.7	76	6.8	51.5	103.5	136.2
7/07/17	GSM	972	948	0.7725	4.9	49.7	74	7.8	57.8	116.2	157.0
7/07/17	GSM	1047	1056	0.7725	4.9	49.7	74	7.5	55.8	112.4	151.8
7/07/17	2-MIB	1127	1136	0.7725	4.9	49.7	76	7.6	57.4	115.5	151.9
7/07/17	2-MIB	1075	1000	0.7725	4.9	49.7	72	8.2	58.9	118.5	164.6
7/07/17	2-MIB	8976	775	0.7725	4.9	497	74	88.2	652.4	131.3	177.4

HWTS GSM and 2-MIB Survey Results (Note: Positive results only):

Date	Analyte	Sample	PA_A	PA_{IS}	RF	C_{IS} (µg L^{-1})	V_{sup} (µL)	C_f (ng L^{-1})	± (ng L^{-1})
27/02/18	2-MIB	R 1	201.2	5893	0.8726	4.9	68	1.6	0.2
27/02/18	2-MIB	S 1	141.9	6813	0.8726	4.9	66	0.9	0.1
27/02/18	2-MIB	R 2	282.5	8914	0.8726	4.9	68	1.5	0.2
27/02/18	2-MIB	S 2	274.4	8986	0.8726	4.9	68	1.4	0.2
28/02/18	2-MIB	R 1	206.4	5749	0.8681	4.9	66	1.6	0.2
28/02/18	2-MIB	S 1	205.6	6696	0.8681	4.9	68	1.4	0.2
28/02/18	2-MIB	RL 1	159.8	7246	0.8681	4.9	68	1	0.1
28/02/18	2-MIB	R 2	245.6	9002	0.8681	4.9	72	1.3	0.2
28/02/18	2-MIB	S 2	203.5	8860	0.8681	4.9	62	1	0.1
28/02/18	2-MIB	RL 2	188.2	9263	0.8681	4.9	66	0.9	0.1
1/03/18	2-MIB	R 1	185.1	6342	0.8726	4.9	66	1.3	0.2
1/03/18	2-MIB	S 1	179.8	7235	0.8726	4.9	68	1.2	0.1
1/03/18	2-MIB	RL 1	156	7202	0.8726	4.9	70	1	0.1
1/03/18	2-MIB	R 2	317.6	8490	0.8726	4.9	74	1.9	0.2
1/03/18	2-MIB	S 2	252.6	9531	0.8726	4.9	58	1.1	0.1
1/03/18	2-MIB	RL 2	217.1	5832	0.8726	4.9	70	1.8	0.2
2/03/18	2-MIB	R 1	204.9	6252	0.8675	4.9	68	1.5	0.2
2/03/18	2-MIB	S 1	125.9	6984	0.8675	4.9	72	0.9	0.1
2/03/18	2-MIB	RL 1	154.5	7450	0.8675	4.9	72	1	0.1
2/03/18	2-MIB	R 2	291.7	10136	0.8675	4.9	68	1.3	0.2
2/03/18	2-MIB	S 2	181.4	9275	0.8675	4.9	70	0.9	0.1
3/03/18	2-MIB	R 1	190.4	6429	0.8675	4.9	68	1.4	0.2
3/03/18	2-MIB	S 1	144.8	6952	0.8675	4.9	68	1	0.1
3/03/18	2-MIB	RL 1	101.4	7647	0.8675	4.9	70	0.6	0.1
3/03/18	2-MIB	R 2	540	9758	0.8675	4.9	68	2.6	0.3
3/03/18	2-MIB	S 2	299	9597	0.8675	4.9	62	1.3	0.2
4/03/18	2-MIB	R 1	180.3	7944	0.8681	4.9	70	1.1	0.1
4/03/18	2-MIB	S 1	111.8	7538	0.8681	4.9	72	0.7	0.1
4/03/18	2-MIB	RL 1	107.7	8055	0.8681	4.9	70	0.6	0.1
4/03/18	2-MIB	R 2	335.7	9001	0.8681	4.9	70	1.8	0.2
4/03/18	2-MIB	S 2	186	9073	0.8681	4.9	74	1	0.1
4/03/18	2-MIB	RL 2	123.6	7548	0.8681	4.9	70	0.8	0.1
5/03/18	2-MIB	R 1	109.9	3896	0.8232	4.9	72	1.5	0.2
5/03/18	2-MIB	S 1	106.1	5389	0.8232	4.9	74	1.1	0.1
5/03/18	2-MIB	RL 1	73.9	6361	0.8232	4.9	74	0.6	0.1
5/03/18	2-MIB	R 2	231.6	8057	0.8232	4.9	64	1.3	0.2
5/03/18	2-MIB	S 2	155	9957	0.8232	4.9	74	0.8	0.1
5/03/18	2-MIB	RL 2	176.9	9146	0.8232	4.9	72	1	0.1
6/03/18	2-MIB	R 1	269	7730	0.8232	4.9	70	1.8	0.2
6/03/18	2-MIB	S 1	276.2	8143	0.8232	4.9	70	1.7	0.2
6/03/18	2-MIB	RL 1	165.6	9130	0.8232	4.9	72	0.9	0.1
6/03/18	2-MIB	R 2	352.9	13550	0.8232	4.9	68	1.3	0.1
6/03/18	2-MIB	S 2	170.2	12351	0.8232	4.9	72	0.7	0.1
6/03/18	2-MIB	RL 2	267.3	11674	0.8232	4.9	74	1.2	0.1
7/03/18	2-MIB	R 1	125.4	5290	0.8901	4.9	68	1.1	0.1
7/03/18	2-MIB	S 1	81.3	6733	0.8901	4.9	66	0.5	0.1
7/03/18	2-MIB	RL 1	128.5	6795	0.8901	4.9	72	0.9	0.1
7/03/18	2-MIB	R 2	160.8	7235	0.8901	4.9	72	1.1	0.1
7/03/18	2-MIB	S 2	194.9	7666	0.8901	4.9	72	1.2	0.1
7/03/18	2-MIB	RL 2	136.8	8514	0.8901	4.9	76	0.8	0.1
8/03/18	2-MIB	R 1	166.1	4663	0.8901	4.9	70	1.7	0.2
8/03/18	2-MIB	R 2	176.7	6935	0.8901	4.9	72	1.2	0.1
9/03/18	2-MIB	R 1	267.2	6477	0.8836	4.9	70	1.9	0.2
9/03/18	2-MIB	R 2	311	9313	0.8836	4.9	74	1.7	0.2
9/03/18	2-MIB	S 2	123.6	9891	0.8836	4.9	72	0.6	0.1

9/03/18	2-MIB	RL 2	164.5	10033	0.8836	4.9	72	0.8	0.1
10/03/18	2-MIB	R 1	224.8	5655	0.8901	4.9	68	1.8	0.2
10/03/18	2-MIB	S 1	120.1	6118	0.8901	4.9	70	0.9	0.1
10/03/18	2-MIB	R 2	297.2	10365	0.8901	4.9	72	1.4	0.2
10/03/18	2-MIB	S 2	258.1	11378	0.8901	4.9	68	1	0.1
10/03/18	2-MIB	RL 2	212.1	11191	0.8901	4.9	74	0.9	0.1
11/03/18	2-MIB	R 1	246.9	7117	0.8873	4.9	66	1.5	0.2
11/03/18	2-MIB	R 2	290.8	11159	0.8873	4.9	72	1.3	0.1
11/03/18	2-MIB	S 2	164	9077	0.8873	4.9	70	0.8	0.1
12/03/18	2-MIB	R 1	233.8	5052	0.8836	4.9	66	2.1	0.2
12/03/18	2-MIB	S 1	144.1	7572	0.8836	4.9	72	0.9	0.1
12/03/18	2-MIB	RL 1	169.4	8318	0.8836	4.9	66	0.9	0.1
12/03/18	2-MIB	R 2	295.2	9264	0.8836	4.9	72	1.5	0.2
12/03/18	2-MIB	S 2	115.9	9154	0.8836	4.9	72	0.6	0.1
13/03/18	2-MIB	R 1	174.7	4008	0.8755	4.9	64	1.9	0.2
13/03/18	2-MIB	R 2	202.6	8903	0.8755	4.9	68	1.1	0.1
13/03/18	2-MIB	RL 2	251.5	7897	0.8755	4.9	60	1.3	0.2
14/03/18	2-MIB	R 1	351.1	4843	0.8384	4.9	64	3.3	0.4
14/03/18	2-MIB	S 1	231.1	6033	0.8384	4.9	68	1.9	0.2
14/03/18	2-MIB	RL 1	439.3	5795	0.8384	4.9	68	3.7	0.4
14/03/18	2-MIB	R 2	469.8	6672	0.8384	4.9	68	3.4	0.4
14/03/18	2-MIB	S 2	349	7704	0.8384	4.9	74	2.4	0.3
14/03/18	2-MIB	RL 2	412.2	8181	0.8384	4.9	68	2.4	0.3
15/03/18	2-MIB	R 1	275.9	5561	0.8726	4.9	56	1.9	0.2
15/03/18	2-MIB	S 1	159.6	5804	0.8726	4.9	58	1.1	0.1
15/03/18	2-MIB	RL 1	144.1	6033	0.8726	4.9	62	1	0.1
15/03/18	2-MIB	R 2	272.5	7836	0.8726	4.9	56	1.3	0.2
15/03/18	2-MIB	S 2	238	9114	0.8726	4.9	72	1.3	0.1
15/03/18	2-MIB	RL 2	235	8791	0.8726	4.9	62	1.1	0.1
16/03/18	2-MIB	R 1	170.4	5432	0.8512	4.9	64	1.4	0.2
16/03/18	2-MIB	S 1	159.4	7252	0.8512	4.9	68	1	0.1
16/03/18	2-MIB	RL 1	168.1	7320	0.8512	4.9	68	1.1	0.1
16/03/18	2-MIB	R 2	251.9	8241	0.8512	4.9	70	1.5	0.2
16/03/18	2-MIB	S 2	142.1	8492	0.8512	4.9	68	0.8	0.1
16/03/18	2-MIB	RL 2	168.3	8692	0.8512	4.9	70	0.9	0.1
17/03/18	2-MIB	R 1	259.3	7160	0.8512	4.9	70	1.8	0.2
17/03/18	2-MIB	S 1	158.2	7325	0.8512	4.9	66	1	0.1
17/03/18	2-MIB	RL 1	130.8	8148	0.8512	4.9	70	0.8	0.1
17/03/18	2-MIB	R 2	325.2	7474	0.8512	4.9	70	2.1	0.2
17/03/18	2-MIB	S 2	121.2	2118	0.8512	4.9	78	3.1	0.4
17/03/18	2-MIB	RL 2	197.6	9520	0.8512	4.9	74	1.1	0.1
18/03/18	2-MIB	R 1	39.6	1292.3	0.8649	4.9	64	1.4	0.2
18/03/18	2-MIB	S 1	19.6	1691.2	0.8649	4.9	68	0.5	0.1
18/03/18	2-MIB	RL 1	22	1705.9	0.8649	4.9	66	0.6	0.1
18/03/18	2-MIB	R 2	47.8	2122.1	0.8649	4.9	64	1	0.1
18/03/18	2-MIB	S 2	38.3	2317.3	0.8649	4.9	72	0.8	0.1
18/03/18	2-MIB	RL 2	26.2	739.5	0.8649	4.9	64	1.6	0.2
19/03/18	2-MIB	R 1	13.2	1292.3	0.6694	4.9	66	0.6	0.1
19/03/18	2-MIB	S 1	17.1	1533.6	0.6694	4.9	66	0.7	0.1
19/03/18	2-MIB	RL 1	32.8	1630.2	0.6694	4.9	66	1.2	0.1
19/03/18	2-MIB	R 2	24.1	1787.4	0.6694	4.9	66	0.8	0.1
19/03/18	2-MIB	S 2	21.9	1831.7	0.6694	4.9	70	0.7	0.1
19/03/18	2-MIB	RL 2	32.2	1844.9	0.6694	4.9	66	1	0.1
20/03/18	2-MIB	R 1	20	1215.3	0.6694	4.9	62	0.9	0.1
20/03/18	2-MIB	S 1	20.3	1582.1	0.6694	4.9	66	0.8	0.1
20/03/18	2-MIB	RL 1	20.3	1782.9	0.6694	4.9	70	0.7	0.1
20/03/18	2-MIB	R 2	52.8	1906.9	0.6694	4.9	60	1.5	0.2
20/03/18	2-MIB	S 2	33.8	1994.2	0.6694	4.9	68	1	0.1

21/03/18	2-MIB	R 1	55.4	1528.6	0.8649	4.9	62	1.5	0.2
21/03/18	2-MIB	S 1	22.7	1654.4	0.8649	4.9	66	0.6	0.1
21/03/18	2-MIB	RL 1	34.8	1802.7	0.8649	4.9	66	0.9	0.1
21/03/18	2-MIB	R 2	49.1	2038	0.8649	4.9	68	1.1	0.1
21/03/18	2-MIB	S 2	34.1	2414.3	0.8649	4.9	66	0.6	0.1
21/03/18	2-MIB	RL 2	37.7	2019.4	0.8649	4.9	68	0.9	0.1
22/03/18	2-MIB	R 1	54.4	1556.9	0.8649	4.9	68	1.6	0.2
22/03/18	2-MIB	S 1	25.4	1850.7	0.8649	4.9	68	0.6	0.1
22/03/18	2-MIB	RL 1	18	1628.1	0.8649	4.9	68	0.5	0.1
22/03/18	2-MIB	R 2	43.1	1738.5	0.8649	4.9	68	1.2	0.1
22/03/18	2-MIB	S 2	23.5	1899.7	0.8649	4.9	70	0.6	0.1
23/03/18	2-MIB	R 1	218	6728	0.8477	4.9	72	1.6	0.2
23/03/18	2-MIB	S 1	83.4	8598	0.8477	4.9	74	0.5	0.1
23/03/18	2-MIB	RL 1	114	9955	0.8477	4.9	76	0.6	0.1
23/03/18	2-MIB	R 2	297.1	11106	0.8477	4.9	76	1.4	0.2
23/03/18	2-MIB	S 2	195.7	11780	0.8477	4.9	76	0.9	0.1
23/03/18	2-MIB	RL 2	180.4	10666	0.8477	4.9	68	0.8	0.1
23/03/18	2-MIB	R 1	331.8	8149	0.8349	4.9	68	2	0.2
24/03/18	2-MIB	S 1	225	10135	0.8349	4.9	68	1.1	0.1
24/03/18	2-MIB	RL 1	122.1	10692	0.8349	4.9	72	0.6	0.1
24/03/18	2-MIB	R 2	483.9	12269	0.8349	4.9	74	2.1	0.2
24/03/18	2-MIB	S 2	227.5	9351	0.8349	4.9	74	1.3	0.1
24/03/18	2-MIB	R 1	60.2	1452.3	0.8502	4.9	64	1.9	0.2
25/03/18	2-MIB	S 1	29.3	1715.3	0.8502	4.9	62	0.7	0.1
25/03/18	2-MIB	RL 1	25.4	1871.3	0.8502	4.9	66	0.6	0.1
25/03/18	2-MIB	R 2	49.4	2201	0.8502	4.9	70	1.1	0.1
25/03/18	2-MIB	S 2	28.6	2051.6	0.8502	4.9	70	0.7	0.1
25/03/18	2-MIB	RL 2	29.1	2045.9	0.8502	4.9	66	0.7	0.1
25/03/18	2-MIB	R 1	379.7	9138	0.8349	4.9	64	1.9	0.2
26/03/18	2-MIB	S 1	146.5	9344	0.8349	4.9	70	0.8	0.1
26/03/18	2-MIB	R 2	378.8	10789	0.8349	4.9	72	1.8	0.2
26/03/18	2-MIB	S 2	177.1	13921	0.8349	4.9	72	0.7	0.1
26/03/18	2-MIB	R 1	54.7	1626.9	0.8329	4.9	66	1.6	0.2
27/03/18	2-MIB	S 1	30.9	1702.9	0.8329	4.9	68	0.9	0.1
27/03/18	2-MIB	RL 1	34.9	1790.5	0.8329	4.9	66	0.9	0.1
27/03/18	2-MIB	R 2	72.7	1891.8	0.8329	4.9	68	1.9	0.2
27/03/18	2-MIB	S 2	46	2378.8	0.8329	4.9	70	1	0.1
27/03/18	2-MIB	RL 2	47	2083	0.8329	4.9	70	1.1	0.1
27/03/18	2-MIB	R 1	48.3	1315.3	0.8329	4.9	66	1.7	0.2
28/03/18	2-MIB	S 1	30.4	1678.3	0.8329	4.9	68	0.9	0.1
28/03/18	2-MIB	RL 1	20.6	1768.1	0.8329	4.9	70	0.6	0.1
28/03/18	2-MIB	R 2	55.7	2174.8	0.8329	4.9	70	1.3	0.1
28/03/18	2-MIB	S 2	22.2	1965.4	0.8329	4.9	70	0.6	0.1
28/03/18	2-MIB	RL 2	45.4	2361.8	0.8329	4.9	68	0.9	0.1
27/02/18	GSM	R 1	1534	5893	0.8141	4.9	68	11.6	1.1
27/02/18	GSM	S 1	657.5	6813	0.8141	4.9	66	4.2	0.4
27/02/18	GSM	R 2	2075	8914	0.8141	4.9	68	10.4	1
27/02/18	GSM	S 2	901.3	8986	0.8141	4.9	68	4.5	0.4
28/02/18	GSM	R 1	1454	5749	0.803	4.9	66	11.1	1.1
28/02/18	GSM	S 1	527	6696	0.803	4.9	68	3.6	0.3
28/02/18	GSM	RL 1	455.1	7246	0.803	4.9	68	2.8	0.3
28/02/18	GSM	R 2	1680	9002	0.803	4.9	72	8.9	0.9
28/02/18	GSM	S 2	534	8860	0.803	4.9	62	2.5	0.2
28/02/18	GSM	RL 2	530.9	9263	0.803	4.9	66	2.5	0.2
1/03/18	GSM	R 1	2062	6342	0.8141	4.9	66	14.1	1.4
1/03/18	GSM	S 1	518.5	7235	0.8141	4.9	68	3.2	0.3
1/03/18	GSM	RL 1	498.8	7202	0.8141	4.9	70	3.2	0.3
1/03/18	GSM	R 2	2283	8490	0.8141	4.9	74	13.1	1.3

1/03/18	GSM	S 2	552.5	9531	0.8141	4.9	58	2.2	0.2
1/03/18	GSM	RL 2	460.2	5832	0.8141	4.9	70	3.6	0.3
2/03/18	GSM	R 1	2160	6252	0.7943	4.9	68	15.8	1.5
2/03/18	GSM	S 1	492.7	6984	0.7943	4.9	72	3.4	0.3
2/03/18	GSM	RL 1	426.4	7450	0.7943	4.9	72	2.8	0.3
2/03/18	GSM	R 2	3371	10136	0.7943	4.9	68	15.2	1.5
2/03/18	GSM	S 2	579.4	9275	0.7943	4.9	70	2.9	0.3
3/03/18	GSM	R 1	1921	6429	0.7943	4.9	68	13.7	1.3
3/03/18	GSM	S 1	559.8	6952	0.7943	4.9	68	3.7	0.4
3/03/18	GSM	RL 1	371.8	7647	0.7943	4.9	70	2.3	0.2
3/03/18	GSM	R 2	3442	9758	0.7943	4.9	68	16.1	1.5
3/03/18	GSM	S 2	629.7	9597	0.7943	4.9	62	2.7	0.3
3/03/18	GSM	RL 2	571.3	9922	0.7943	4.9	70	2.7	0.3
4/03/18	GSM	R 1	2150	7944	0.803	4.9	70	12.6	1.2
4/03/18	GSM	S 1	475.7	7538	0.803	4.9	72	3	0.3
4/03/18	GSM	RL 1	527.2	8055	0.803	4.9	70	3	0.3
4/03/18	GSM	R 2	2571	9001	0.803	4.9	70	13.3	1.3
4/03/18	GSM	S 2	444.9	9073	0.803	4.9	74	2.4	0.2
4/03/18	GSM	RL 2	418.4	7548	0.803	4.9	70	2.6	0.2
5/03/18	GSM	R 1	1033	3896	0.8092	4.9	72	12.6	1.2
5/03/18	GSM	S 1	441.2	5389	0.8092	4.9	74	4	0.4
5/03/18	GSM	RL 1	299.7	6361	0.8092	4.9	74	2.3	0.2
5/03/18	GSM	R 2	1702	8057	0.8092	4.9	64	8.9	0.9
5/03/18	GSM	S 2	661.1	9957	0.8092	4.9	74	3.2	0.3
5/03/18	GSM	RL 2	422.8	9146	0.8092	4.9	72	2.2	0.2
6/03/18	GSM	R 1	1684	7730	0.8092	4.9	70	10.1	1
6/03/18	GSM	S 1	385.9	8143	0.8092	4.9	70	2.2	0.2
6/03/18	GSM	RL 1	370.1	9130	0.8092	4.9	72	1.9	0.2
6/03/18	GSM	R 2	2818	13550	0.8092	4.9	68	9.3	0.9
6/03/18	GSM	S 2	572.8	12351	0.8092	4.9	72	2.2	0.2
6/03/18	GSM	RL 2	412.5	11674	0.8092	4.9	74	1.7	0.2
7/03/18	GSM	R 1	635.4	5290	0.8311	4.9	68	5.3	0.5
7/03/18	GSM	S 1	271.6	6733	0.8311	4.9	66	1.7	0.2
7/03/18	GSM	RL 1	271.6	6795	0.8311	4.9	72	1.9	0.2
7/03/18	GSM	R 2	668.7	7235	0.8311	4.9	72	4.3	0.4
7/03/18	GSM	S 2	619.8	7666	0.8311	4.9	72	3.7	0.4
7/03/18	GSM	RL 2	298.2	8514	0.8311	4.9	76	1.7	0.2
8/03/18	GSM	R 1	1074	4663	0.8311	4.9	70	10.4	1
8/03/18	GSM	S 1	343.3	6097	0.8311	4.9	72	2.6	0.3
8/03/18	GSM	RL 1	301.3	6623	0.8311	4.9	76	2.2	0.2
8/03/18	GSM	R 2	1496	6935	0.8311	4.9	72	10	1
8/03/18	GSM	S 2	370.8	8343	0.8311	4.9	74	2.1	0.2
8/03/18	GSM	RL 2	371.1	8162	0.8311	4.9	76	2.2	0.2
9/03/18	GSM	R 1	1555	6477	0.8035	4.9	70	11.2	1.1
9/03/18	GSM	S 1	464.3	7987	0.8035	4.9	72	2.8	0.3
9/03/18	GSM	RL 1	457.2	8720	0.8035	4.9	74	2.6	0.2
9/03/18	GSM	R 2	2071	9313	0.8035	4.9	74	10.9	1.1
9/03/18	GSM	S 2	491	9891	0.8035	4.9	72	2.4	0.2
9/03/18	GSM	RL 2	495.2	10033	0.8035	4.9	72	2.4	0.2
10/03/18	GSM	R 1	1554	5655	0.8311	4.9	68	12	1.2
10/03/18	GSM	S 1	353.2	6118	0.8311	4.9	70	2.6	0.2
10/03/18	GSM	R 2	2883	10365	0.8311	4.9	72	12.9	1.2
10/03/18	GSM	S 2	816.9	11378	0.8311	4.9	68	3.1	0.3
10/03/18	GSM	RL 2	528.8	11191	0.8311	4.9	74	2.2	0.2
11/03/18	GSM	R 1	2294	7117	0.8001	4.9	66	14.2	1.4
11/03/18	GSM	S 1	566.6	8835	0.8001	4.9	70	3	0.3
11/03/18	GSM	R 2	2526	11159	0.8001	4.9	72	10.9	1
11/03/18	GSM	S 2	677.3	9077	0.8001	4.9	70	3.5	0.3

12/03/18	GSM	R 1	2050	5052	0.8035	4.9	66	17.8	1.7
12/03/18	GSM	S 1	527.2	7572	0.8035	4.9	72	3.3	0.3
12/03/18	GSM	RL 1	435.7	8318	0.8035	4.9	66	2.3	0.2
12/03/18	GSM	R 2	2672	9264	0.8035	4.9	72	13.8	1.3
12/03/18	GSM	S 2	696.5	9154	0.8035	4.9	72	3.6	0.3
12/03/18	GSM	RL 2	656	9695	0.8035	4.9	70	3.2	0.3
13/03/18	GSM	R 1	1227	4008	0.8189	4.9	64	12.8	1.2
13/03/18	GSM	S 1	151	5378	0.8189	4.9	68	1.2	0.1
13/03/18	GSM	RL 1	386.7	6652	0.8189	4.9	72	2.7	0.3
13/03/18	GSM	R 2	2193	8903	0.8189	4.9	68	10.9	1
13/03/18	GSM	S 2	172.5	7706	0.8189	4.9	78	1.1	0.1
13/03/18	GSM	RL 2	439	7897	0.8189	4.9	60	2.2	0.2
14/03/18	GSM	R 1	1990	4843	0.8001	4.9	64	17.6	1.7
14/03/18	GSM	S 1	455.6	6033	0.8001	4.9	68	3.4	0.3
14/03/18	GSM	RL 1	431.9	5795	0.8001	4.9	68	3.4	0.3
14/03/18	GSM	R 2	2692	6672	0.8001	4.9	68	18.3	1.8
14/03/18	GSM	S 2	412.6	7704	0.8001	4.9	74	2.6	0.3
14/03/18	GSM	RL 2	457.2	8181	0.8001	4.9	68	2.5	0.2
15/03/18	GSM	R 1	1858	5561	0.8141	4.9	56	12.3	1.2
15/03/18	GSM	S 1	424.3	5804	0.8141	4.9	58	2.8	0.3
15/03/18	GSM	RL 1	379.8	6033	0.8141	4.9	62	2.6	0.2
15/03/18	GSM	R 2	2659	7836	0.8141	4.9	56	12.5	1.2
15/03/18	GSM	S 2	479.6	9114	0.8141	4.9	72	2.5	0.2
15/03/18	GSM	RL 2	493.4	8791	0.8141	4.9	62	2.3	0.2
16/03/18	GSM	R 1	1732	5432	0.8076	4.9	64	13.5	1.3
16/03/18	GSM	S 1	474.8	7252	0.8076	4.9	68	2.9	0.3
16/03/18	GSM	RL 1	414.6	7320	0.8076	4.9	68	2.5	0.2
16/03/18	GSM	R 2	2462	8241	0.8076	4.9	70	13.8	1.3
16/03/18	GSM	S 2	480.5	8492	0.8076	4.9	68	2.5	0.2
16/03/18	GSM	RL 2	478.3	8692	0.8076	4.9	70	2.5	0.2
17/03/18	GSM	R 1	2332	7160	0.8076	4.9	70	15.1	1.4
17/03/18	GSM	S 1	456.9	7325	0.8076	4.9	66	2.7	0.3
17/03/18	GSM	RL 1	543.4	8148	0.8076	4.9	70	3.1	0.3
17/03/18	GSM	R 2	2541	7474	0.8076	4.9	70	15.8	1.5
17/03/18	GSM	S 2	163.1	2118	0.8076	4.9	78	4	0.4
17/03/18	GSM	RL 2	462.2	9520	0.8076	4.9	74	2.4	0.2
18/03/18	GSM	R 1	306.1	1292.3	0.8449	4.9	64	9.6	0.9
18/03/18	GSM	S 1	31.5	1691.2	0.8449	4.9	68	0.8	0.1
18/03/18	GSM	RL 1	26.4	1705.9	0.8449	4.9	66	0.6	0.1
18/03/18	GSM	R 2	470	2122.1	0.8449	4.9	64	9	0.9
18/03/18	GSM	S 2	124.4	2317.3	0.8449	4.9	72	2.4	0.2
18/03/18	GSM	RL 2	47.3	739.5	0.8449	4.9	64	2.6	0.2
19/03/18	GSM	R 1	204	1292.3	0.6604	4.9	66	8.4	0.8
19/03/18	GSM	S 1	86.4	1533.6	0.6604	4.9	66	3	0.3
19/03/18	GSM	RL 1	95.3	1630.2	0.6604	4.9	66	3.1	0.3
19/03/18	GSM	R 2	261.3	1787.4	0.6604	4.9	66	7.8	0.7
19/03/18	GSM	S 2	64.5	1831.7	0.6604	4.9	70	2	0.2
19/03/18	GSM	RL 2	144.9	1844.9	0.6604	4.9	66	4.2	0.4
20/03/18	GSM	R 1	288.7	1215.3	0.6604	4.9	62	11.9	1.1
20/03/18	GSM	S 1	79.2	1582.1	0.6604	4.9	66	2.7	0.3
20/03/18	GSM	RL 1	48.3	1782.9	0.6604	4.9	70	1.5	0.1
20/03/18	GSM	R 2	408.1	1906.9	0.6604	4.9	60	10.4	1
20/03/18	GSM	S 2	98.2	1994.2	0.6604	4.9	68	2.7	0.3
20/03/18	GSM	RL 2	49.2	1767.7	0.6604	4.9	68	1.5	0.1
21/03/18	GSM	R 1	394.6	1528.6	0.8449	4.9	62	10.1	1
21/03/18	GSM	S 1	56.6	1654.4	0.8449	4.9	66	1.4	0.1
21/03/18	GSM	RL 1	57.3	1802.7	0.8449	4.9	66	1.3	0.1
21/03/18	GSM	R 2	451.7	2038	0.8449	4.9	68	9.5	0.9

21/03/18	GSM	S 2	75	2414.3	0.8449	4.9	66	1.3	0.1
21/03/18	GSM	RL 2	83	2019.4	0.8449	4.9	68	1.8	0.2
22/03/18	GSM	R 1	326.2	1556.9	0.8449	4.9	68	9	0.9
22/03/18	GSM	S 1	49.6	1850.7	0.8449	4.9	68	1.2	0.1
22/03/18	GSM	RL 1	43.1	1628.1	0.8449	4.9	68	1.1	0.1
22/03/18	GSM	R 2	347.5	1738.5	0.8449	4.9	68	8.6	0.8
22/03/18	GSM	S 2	110.7	1899.7	0.8449	4.9	70	2.6	0.2
22/03/18	GSM	RL 2	33.8	2153	0.8449	4.9	72	0.7	0.1
23/03/18	GSM	R 1	991.5	6728	0.8335	4.9	72	6.8	0.7
23/03/18	GSM	S 1	241.9	8598	0.8335	4.9	74	1.3	0.1
23/03/18	GSM	RL 1	459.3	9955	0.8335	4.9	76	2.2	0.2
23/03/18	GSM	R 2	1607	11106	0.8335	4.9	76	7.1	0.7
23/03/18	GSM	S 2	380.4	11780	0.8335	4.9	76	1.6	0.2
23/03/18	GSM	RL 2	541.7	10666	0.8335	4.9	68	2.2	0.2
23/03/18	GSM	R 1	2027	8149	0.7781	4.9	68	11.6	1.1
24/03/18	GSM	S 1	449.6	10135	0.7781	4.9	68	2.1	0.2
24/03/18	GSM	RL 1	371.5	10692	0.7781	4.9	72	1.7	0.2
24/03/18	GSM	R 2	2497	12269	0.7781	4.9	74	10.3	1
24/03/18	GSM	S 2	440.8	9351	0.7781	4.9	74	2.4	0.2
24/03/18	GSM	RL 2	340	8520	0.7781	4.9	70	1.9	0.2
24/03/18	GSM	R 1	536	1452.3	0.7948	4.9	64	15.9	1.5
25/03/18	GSM	S 1	74.8	1715.3	0.7948	4.9	62	1.8	0.2
25/03/18	GSM	RL 1	72.4	1871.3	0.7948	4.9	66	1.7	0.2
25/03/18	GSM	R 2	662.7	2201	0.7948	4.9	70	14.2	1.4
25/03/18	GSM	S 2	79	2051.6	0.7948	4.9	70	1.8	0.2
25/03/18	GSM	RL 2	62.1	2045.9	0.7948	4.9	66	1.3	0.1
25/03/18	GSM	R 1	1834	9138	0.7781	4.9	64	8.8	0.8
26/03/18	GSM	S 1	395.9	9344	0.7781	4.9	70	2	0.2
26/03/18	GSM	RL 1	261.8	8983	0.7781	4.9	70	1.4	0.1
26/03/18	GSM	R 2	1785	10789	0.7781	4.9	72	8.2	0.8
26/03/18	GSM	S 2	554.1	13921	0.7781	4.9	72	2	0.2
26/03/18	GSM	RL 2	420.1	13316	0.7781	4.9	72	1.6	0.1
26/03/18	GSM	R 1	217.1	1626.9	0.7945	4.9	66	5.9	0.6
27/03/18	GSM	S 1	90.4	1702.9	0.7945	4.9	68	2.4	0.2
27/03/18	GSM	RL 1	53.4	1790.5	0.7945	4.9	66	1.3	0.1
27/03/18	GSM	R 2	322.5	1891.8	0.7945	4.9	68	7.8	0.7
27/03/18	GSM	S 2	114	2378.8	0.7945	4.9	70	2.3	0.2
27/03/18	GSM	RL 2	70.5	2083	0.7945	4.9	70	1.6	0.2
27/03/18	GSM	R 1	345	1315.3	0.7945	4.9	66	11.6	1.1
28/03/18	GSM	S 1	57.6	1678.3	0.7945	4.9	68	1.6	0.2
28/03/18	GSM	RL 1	49.6	1768.1	0.7945	4.9	70	1.3	0.1
28/03/18	GSM	R 2	397.8	2174.8	0.7945	4.9	70	8.6	0.8
28/03/18	GSM	S 2	68.9	1965.4	0.7945	4.9	70	1.7	0.2
28/03/18	GSM	RL 2	69.8	2361.8	0.7945	4.9	68	1.4	0.1

2-MIB isotherm data:

PA_A	PA_{IS}	RF	C_{IS} ($\mu g\ L^{-1}$)	C_i ($ng\ cm^{-3}$)	V_{sup} (μL)	C_e ($ng\ cm^{-3}$)	+/- ($ng\ cm^{-3}$)	V_s (cm3)	V_c (cm3)	Q_e (ng/cm3)
367	1859	0.78	4.9	0.1	70	0.0106	0.0012	50	0.00035	12778
409	1906	0.78	4.9	0.1	70	0.0115	0.0013	50	0.00035	12646
1181	2245	0.78	4.9	0.25	74	0.0298	0.0035	50	0.00035	31463
1018	2111	0.78	4.9	0.25	72	0.0265	0.0031	50	0.00035	31924
2370	2365	0.78	4.9	0.5	70	0.0536	0.0062	50	0.00035	63766
2688	2090	0.78	4.9	0.5	68	0.0669	0.0078	50	0.00035	61874
4435	2417	0.78	4.9	1	78	0.1094	0.0127	50	0.00035	127227
5612	1954	0.78	4.9	1	76	0.1668	0.0194	50	0.00035	119022
20175	2391	0.78	4.9	2	72	0.4645	0.0539	50	0.00035	219355
12753	2227	0.78	4.9	2	68	0.2978	0.0345	50	0.00035	243173

GSM isotherm data:

PA_A	PA_{IS}	RF	C_{IS} ($\mu g\ L^{-1}$)	C_i ($ng\ cm^{-3}$)	V_{sup} (μL)	C_e ($ng\ cm^{-3}$)	+/- ($ng\ cm^{-3}$)	V_s (cm3)	V_c (cm3)	Q_e (ng/cm3)
34	1859	0.79	4.9	0.1	70	0.0009	0.0001	50	0.00035	14162
38	1906	0.79	4.9	0.1	70	0.0009	0.0001	50	0.00035	14151
174	2245	0.79	4.9	0.25	74	0.0039	0.0003	50	0.00035	35161
180	2111	0.79	4.9	0.25	72	0.0041	0.0004	50	0.00035	35122
375	2365	0.79	4.9	0.5	70	0.0075	0.0007	50	0.00035	70355
378	2090	0.79	4.9	0.5	68	0.0083	0.0007	50	0.00035	70239
523	2417	0.79	4.9	1	78	0.0114	0.0010	50	0.00035	141226
794	1954	0.79	4.9	1	76	0.0209	0.0018	50	0.00035	139873
3686	2391	0.79	4.9	2	72	0.0751	0.0065	50	0.00035	274983
2371	2227	0.79	4.9	2	68	0.0490	0.0043	50	0.00035	278716

Column dosing data:

t (min)	C_{in} ($ng\ L^{-1}$)	Analyte	Depth (cm)	PA_A	PA_{IS}	RF	C_{IS} ($\mu g\ L^{-1}$)	V_{sup} (μL)	C_f ($ng\ L^{-1}$)	+/- ($ng\ L^{-1}$)
0	50	2-MIB	0	2732.51	1913.01	0.8407	4.9	58	58.8	6.8
0	50	2-MIB	10	1787.62	1852.81	0.8407	4.9	68	46.5	5.4
0	50	2-MIB	20	1147.43	2072.65	0.8407	4.9	66	25.9	3.0
0	50	2-MIB	30	669.39	2213.01	0.8407	4.9	68	14.6	1.7
0	50	2-MIB	40	316.03	1641.24	0.8407	4.9	66	9.0	1.0
0	50	2-MIB	50	212.08	2083.37	0.8407	4.9	70	5.1	0.6
0	50	2-MIB	60	142.56	1996.41	0.8407	4.9	68	3.4	0.4
0	50	2-MIB	70	93.17	2260.44	0.8407	4.9	70	2.0	0.2
0	50	2-MIB	80	61.79	1942.57	0.8407	4.9	70	1.6	0.2
0	50	2-MIB	90	40.87	1836.06	0.8407	4.9	66	1.0	0.1
0	50	2-MIB	100	48.92	2653.48	0.8407	4.9	70	0.9	0.1
0	50	2-MIB	110	28.96	2510.54	0.8407	4.9	68	0.6	0.1
0	50	2-MIB	120	29.9	2251.18	0.8407	4.9	68	0.6	0.1
30	50	2-MIB	0	2854.53	1921.76	0.8407	4.9	66	69.5	8.1
30	50	2-MIB	10	2063.13	2033.65	0.8407	4.9	68	48.9	5.7
30	50	2-MIB	20	1137.12	2053.07	0.8407	4.9	66	25.9	3.0
30	50	2-MIB	30	598.28	1904.04	0.8407	4.9	70	15.6	1.8
30	50	2-MIB	40	332.45	1723.59	0.8407	4.9	68	9.3	1.1
30	50	2-MIB	50	178.28	2010.33	0.8407	4.9	70	4.4	0.5
30	50	2-MIB	60	147.07	1976.1	0.8407	4.9	70	3.7	0.4
30	50	2-MIB	70	114.57	2340.43	0.8407	4.9	66	2.3	0.3
30	50	2-MIB	80	59.38	2209.6	0.8407	4.9	70	1.3	0.2
30	50	2-MIB	90	54.06	1859.55	0.8407	4.9	68	1.4	0.2
30	50	2-MIB	100	48.43	2446.59	0.8407	4.9	68	1.0	0.1
30	50	2-MIB	110	34.59	2498.06	0.8407	4.9	70	0.7	0.1
30	50	2-MIB	120	33.79	2138.31	0.8407	4.9	70	0.8	0.1
0	50	GSM	0	2213.9	1913.01	0.8201	4.9	58	48.8	5.7
0	50	GSM	10	1196.58	1852.81	0.8201	4.9	68	31.9	3.7
0	50	GSM	20	620.82	2072.65	0.8201	4.9	66	14.4	1.7
0	50	GSM	30	329.01	2213.01	0.8201	4.9	68	7.4	0.9
0	50	GSM	40	93.65	1641.24	0.8201	4.9	66	2.7	0.3
0	50	GSM	50	61.47	2083.37	0.8201	4.9	70	1.5	0.2
0	50	GSM	60	41.29	1996.41	0.8201	4.9	68	1.0	0.1
30	50	GSM	0	2050.4	1921.76	0.8201	4.9	66	51.2	5.9
30	50	GSM	10	1282.34	2033.65	0.8201	4.9	68	31.2	3.6

30	50	GSM	20	634.69	2053.07	0.8201	4.9	66	14.8	1.7
30	50	GSM	30	293.35	1904.04	0.8201	4.9	70	7.8	0.9
30	50	GSM	40	99.77	1723.59	0.8201	4.9	68	2.9	0.3
30	50	GSM	50	52.14	2010.33	0.8201	4.9	70	1.3	0.2
30	50	GSM	60	44.72	1976.1	0.8201	4.9	70	1.2	0.1
0	150	2-MIB	0	5665.21	1929.76	0.8407	4.9	70	145.8	16.9
0	150	2-MIB	10	2837.27	2369.2	0.8407	4.9	72	61.2	7.1
0	150	2-MIB	20	1842.33	2335.55	0.8407	4.9	70	39.2	4.5
0	150	2-MIB	30	1054.93	1823.89	0.8407	4.9	74	30.4	3.5
0	150	2-MIB	40	704.45	2131.31	0.8407	4.9	72	16.9	2.0
0	150	2-MIB	50	440.96	1860.77	0.8407	4.9	70	11.8	1.4
0	150	2-MIB	60	344.86	1966.54	0.8407	4.9	68	8.5	1.0
0	150	2-MIB	70	145.78	1904.48	0.8407	4.9	72	3.9	0.5
0	150	2-MIB	80	165.1	2116.03	0.8407	4.9	72	4.0	0.5
0	150	2-MIB	90	132.92	2186.09	0.8407	4.9	72	3.1	0.4
0	150	2-MIB	100	107.76	2263.97	0.8407	4.9	70	2.4	0.3
0	150	2-MIB	110	56.03	2529.2	0.8407	4.9	72	1.1	0.1
0	150	2-MIB	120	50.53	2575.38	0.8407	4.9	70	1.0	0.1
0	150	2-MIB	130	37.7	2293.91	0.8407	4.9	74	0.9	0.1
0	150	2-MIB	140	29.45	2194.96	0.8407	4.9	72	0.7	0.1
0	150	2-MIB	150	25.34	2521.19	0.8407	4.9	72	0.5	0.1
30	150	2-MIB	0	5638.13	1883.33	0.8407	4.9	70	148.7	17.2
30	150	2-MIB	10	2807.53	2419.69	0.8407	4.9	70	57.6	6.7
30	150	2-MIB	20	1788.09	2148.57	0.8407	4.9	72	42.5	4.9
30	150	2-MIB	30	1188.16	2032.46	0.8407	4.9	70	29.0	3.4
30	150	2-MIB	40	713.52	2024.71	0.8407	4.9	72	18.0	2.1
30	150	2-MIB	50	454.05	1948.1	0.8407	4.9	72	11.9	1.4
30	150	2-MIB	60	357.86	2235.8	0.8407	4.9	72	8.2	0.9
30	150	2-MIB	70	169.59	2193.96	0.8407	4.9	72	3.9	0.5
30	150	2-MIB	80	164.45	2192.86	0.8407	4.9	70	3.7	0.4
30	150	2-MIB	90	127.12	2145.7	0.8407	4.9	72	3.0	0.4
30	150	2-MIB	100	92.79	2380.58	0.8407	4.9	70	1.9	0.2
30	150	2-MIB	110	68.3	2335.84	0.8407	4.9	74	1.5	0.2
30	150	2-MIB	120	52.22	2613.62	0.8407	4.9	70	1.0	0.1
30	150	2-MIB	130	36.19	2267.08	0.8407	4.9	72	0.8	0.1
30	150	2-MIB	140	26.94	2042.53	0.8407	4.9	70	0.7	0.1
30	150	2-MIB	150	27.03	2494.75	0.8407	4.9	72	0.6	0.1
0	150	GSM	0	5425.81	1929.76	0.8201	4.9	70	143.1	16.6
0	150	GSM	10	1968.99	2369.2	0.8201	4.9	72	43.5	5.0
0	150	GSM	20	1012.17	2335.55	0.8201	4.9	70	22.1	2.6
0	150	GSM	30	478.18	1823.89	0.8201	4.9	74	14.1	1.6
0	150	GSM	40	246.85	2131.31	0.8201	4.9	72	6.1	0.7
0	150	GSM	50	117.95	1860.77	0.8201	4.9	70	3.2	0.4
0	150	GSM	60	75.63	1966.54	0.8201	4.9	68	1.9	0.2
0	150	GSM	70	32.5	1904.48	0.8201	4.9	72	0.9	0.1
0	150	GSM	80	28.78	2116.03	0.8201	4.9	72	0.7	0.1
30	150	GSM	0	5526.53	1883.33	0.8201	4.9	70	149.4	17.3
30	150	GSM	10	2049.44	2419.69	0.8201	4.9	70	43.1	5.0
30	150	GSM	20	982.56	2148.57	0.8201	4.9	72	23.9	2.8
30	150	GSM	30	533.8	2032.46	0.8201	4.9	70	13.4	1.6
30	150	GSM	40	249.1	2024.71	0.8201	4.9	72	6.4	0.7
30	150	GSM	50	156.56	1948.1	0.8201	4.9	72	4.2	0.5
30	150	GSM	60	71.77	2235.8	0.8201	4.9	72	1.7	0.2
30	150	GSM	70	27.68	2193.96	0.8201	4.9	72	0.7	0.1
30	150	GSM	80	32.2	2192.86	0.8201	4.9	70	0.7	0.1

Example of an *R* script used for modelling 2-MIB and GSM:

This is an example of the code used to model GSM and 2-MIB removal within the pilot column. In this case, the Freundlich isotherm with second order kinetics is given as an example, using the adsorption parameters and data for 2-MIB.

```
##############################################################################
# Modeling of 2-MIB concentration through the depth of a GAC filter column #
##############################################################################

# Load the required libraries
library(tidyverse)
library(deSolve)
library(FME)

# Load the data to be used for fitting parameters. The file must be in the current working directory.
dataset <- read.csv("mib_h_mql.csv")

# Set constant parameters - change as required.
# These parameters are either known of measured experimentally.
# These must be changed depending on the analyte being modelled
Q <- 1000          # Flow rate (cm3/min)
A <- 88.36         # Cross sectional area of the filter media (cm2)
dx <- 0.12         # Change in depth through the column (cm) - This must be set based on
                   # the time step of deSolve solver
epsilon <- 0.65    # Void fraction of the filter media
K <- 4.36e5        # Adsorbate saturation concentration (from isotherm data)
n <- 0.6676        # Freundlich isotherm constant (from isotherm data)

# The system of differential equations to be solved - the appropriate kinetic model can be substituted
# into dy1 and dy2.
model <- function (time, y, parms, ...) {
  with(as.list(c(parms, y)), {

    if (time <= 0.01)
      lag1 = lagvalue(time,1)
    else
      lag1 <- lagvalue(time-0.01, 1)

   # Liquid phase concentration of the analyte = dC/dt
    dy1 <- (lag1 - y[1])*(Q/(A*dx*epsilon)) - (k*y[1]*((K*y[1]^n)-y[2]))*((1-epsilon)/((epsilon)))

    # Solid phase concentration of outer adsorption sites (dCs/dt)
    dy2 <- (k*y[1]*((K*y[1]^n)-y[2]))

    list(c(dy1,dy2))
  })}

# Write the parameters that are to be estimated to a list that is passed to the model function.
# These are the parameters that will also be estimated by the fitting routine.
parms <- c(k = 3e-5)

# Set the times that intergration will occur.
times <- seq(from = 0, to = 10, by = 0.01) #Times and change in time for each step (min)

# set the initial conditions - y1 is the influent liquid phase concentration (ng^cm-3).
y0 <- c(y1 = 0.1472, y2 = 0)

# Solve the model with deSolve using the delay differential equation solver
# using the initial conditions, times and parameters set previously.
out1 <- dede(y0, times, model, parms)

# Plot the data and the model with initial guesses listed in parms
plot(out1, obs = dataset)

# Model fitting
# A cost function that returns residuals and model cost (sum of squared residuals)
# between the model and data.
cost <- function(p) {
  out <- dede(y0, times, model, p)
  out[is.nan(out)] <- 0
  modCost(out, dataset, weight = "none")

# Fit the model to the data by minimising the output of the cost function by varying the parameters
# listed in parms.
# Gives an estimate of the best set of parameter values. Possible parameter values
# are constrained by "upper" and "lower" bounds.
fit <- modFit(f = cost, p = parms, lower = 0, upper = 1e-4, method = "bobyqa")

# Plot the data against the model with optimised parameters
par(mar=c(2, 2, 2, 2), xpd=FALSE)
out1 <- dede(y0, times, model, coef(fit))
plot(out1, obs=dataset, obspar=list(pch=16, col="red"))


# Summary of the output from the fitting routine
summary(fit)
```

Pilot column design:

Figure A2-1: Design of main column sections: Front† (top left), left side (top right), right side (bottom left) and cross section (bottom right). All units in cm.

† Note that all front sections indicate a hole (96.0 cm x 6.0 cm) where acrylic windows were fitted.

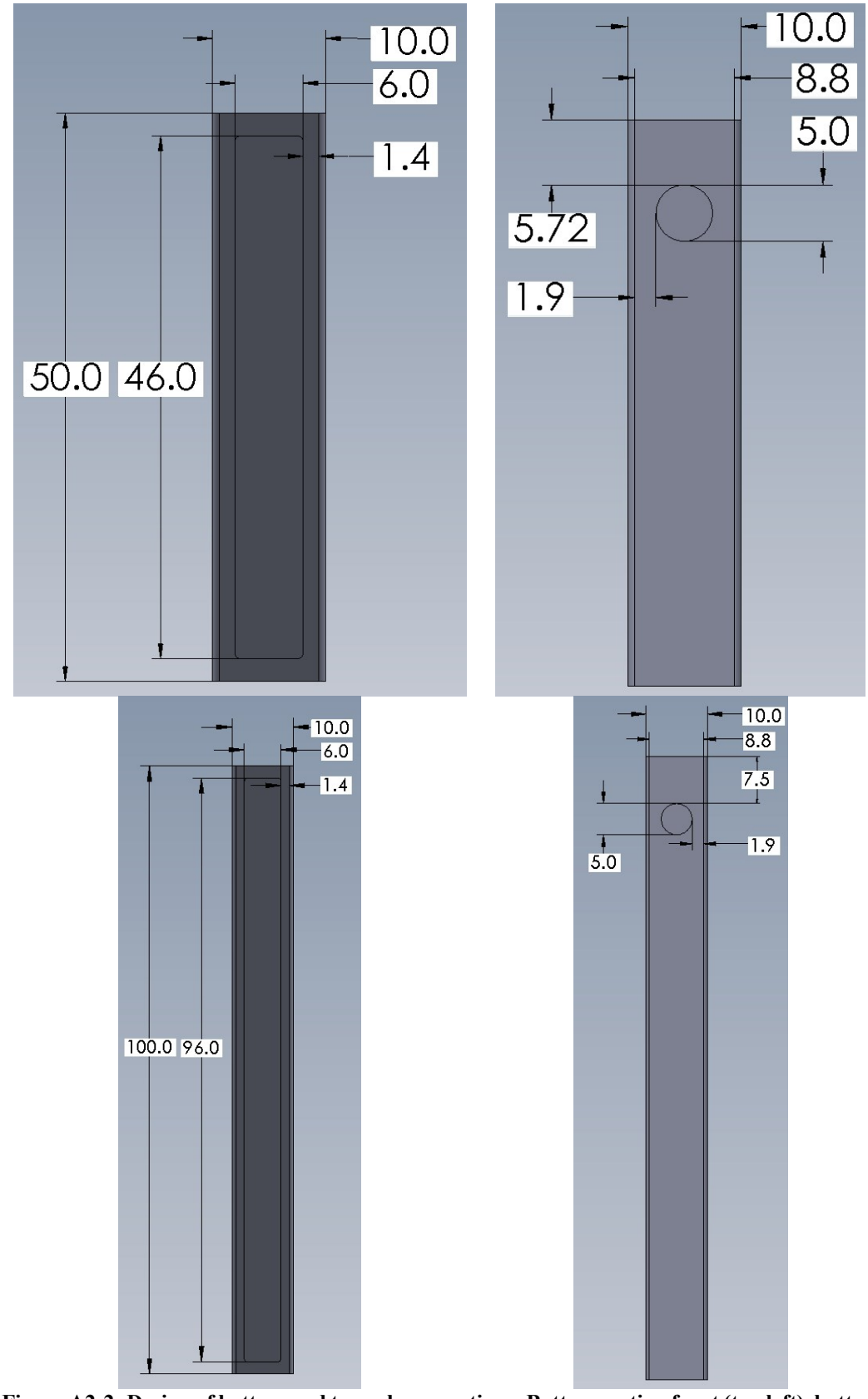

Figure A2-2: Design of bottom and top column sections: Bottom section front (top left), bottom section right side (top right), top section front (bottom left) and top section left side (bottom right). All units in cm.

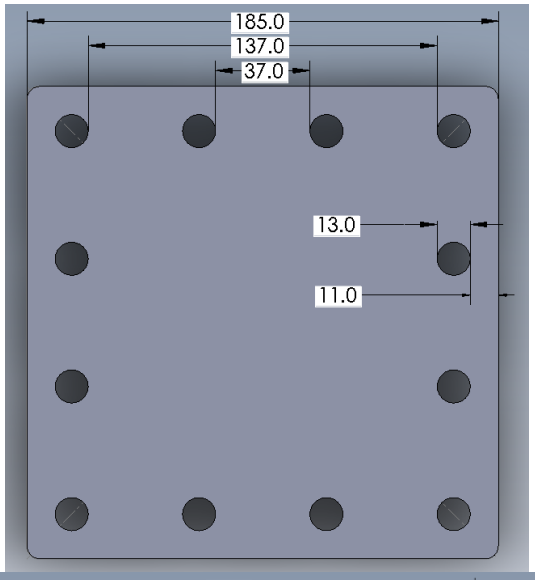

Figure A2-3: Design of bottom plate for bottom column section.

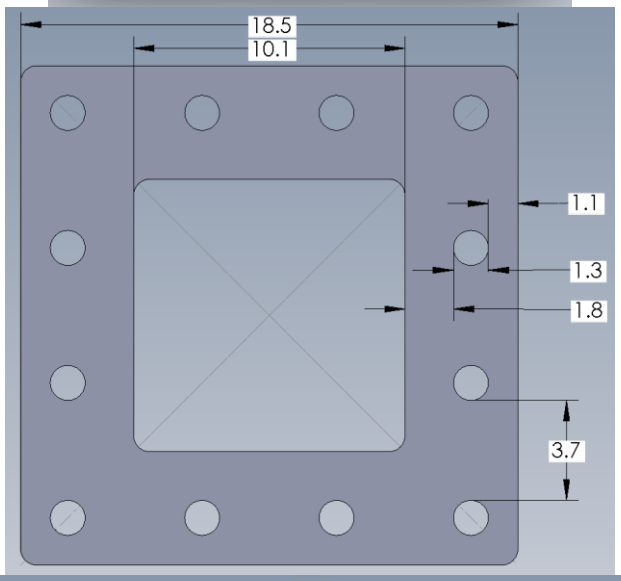

Figure A2-4: Design of flanges and gaskets for column sections

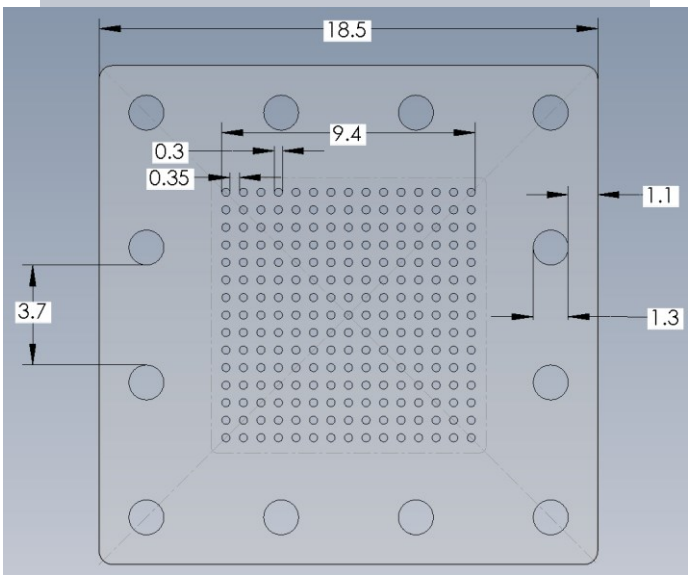

Figure A2-5: Design of grill to support the filter media.

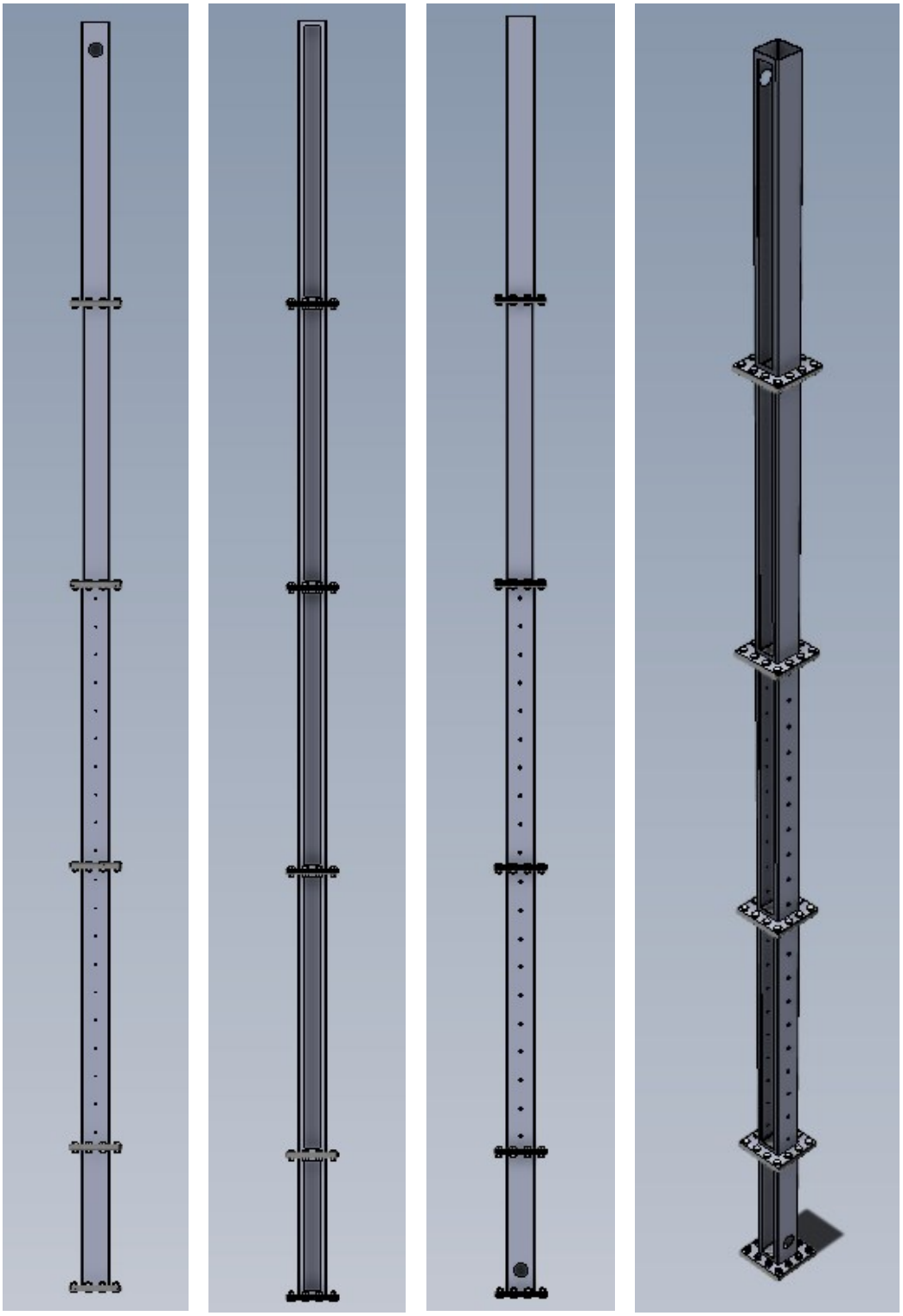

Fig A2-6: Left, front, right and isometric representations of the assembled column design.

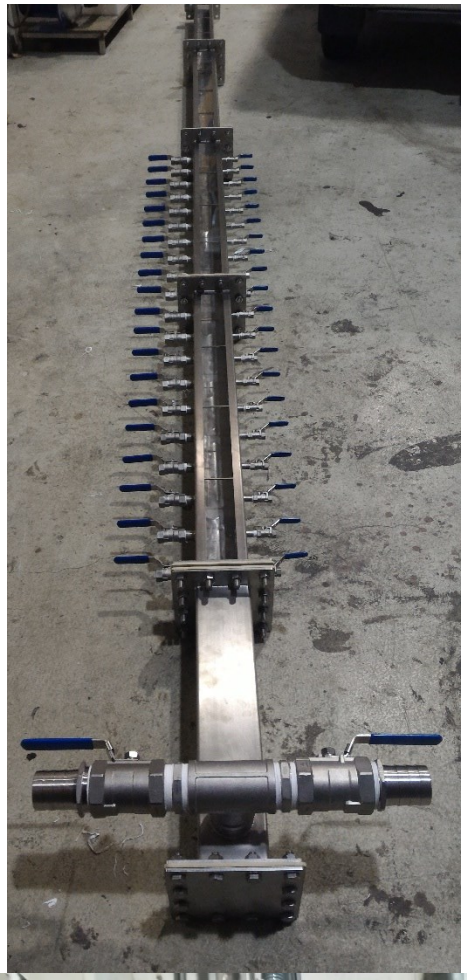

Fig A2-7: Some images of the completed and installed pilot column.

A-3 Chapter 5 Supplementary Information

TOC data:

Date	Location	TOC (mg L^{-1})	± (mg L^{-1})	Outlier
5/01/2018	R	1.35	0.03	No
5/01/2018	S	1.00	0.02	No
5/01/2018	RL	0.98	0.02	No
5/01/2018	G1	0.84	0.02	No
5/01/2018	G2	0.81	0.02	No
5/01/2018	G3	0.72	0.02	No
5/01/2018	G5	1.00	0.02	No
5/01/2018	G6	0.89	0.02	No
5/01/2018	PUV	1.06	0.02	No
5/01/2018	C	0.49	0.01	No
5/01/2018	F	1.87	0.04	Yes ($p < 2.2\ e^{-16}$)
31/01/2018	R	1.84	0.04	No
31/01/2018	S	0.95	0.02	No
31/01/2018	RL	0.56	0.01	No
31/01/2018	G1	0.80	0.02	No
31/01/2018	G2	0.84	0.02	No
31/01/2018	G3	1.19	0.03	No
31/01/2018	G5	1.27	0.03	No
31/01/2018	G6	1.08	0.02	No
31/01/2018	PUV	1.05	0.02	No
31/01/2018	C	0.85	0.02	No
31/01/2018	F	0.44	0.01	No
1/02/2018	R	1.45	0.03	No
1/02/2018	S	0.95	0.02	No
1/02/2018	RL	0.84	0.02	No
1/02/2018	G1	0.73	0.02	No
1/02/2018	G2	0.64	0.01	No
1/02/2018	G5	0.60	0.01	No
1/02/2018	G6	0.86	0.02	No
1/02/2018	PUV	0.76	0.02	No
1/02/2018	C	0.64	0.01	No
1/02/2018	F	0.50	0.01	No
2/02/2018	R	1.44	0.03	No
2/02/2018	S	0.86	0.02	No
2/02/2018	RL	0.91	0.02	No
2/02/2018	G1	0.84	0.02	No
2/02/2018	G2	0.69	0.02	No
2/02/2018	G3	0.60	0.01	No
2/02/2018	G5	0.86	0.02	No
2/02/2018	G6	0.78	0.02	No
2/02/2018	PUV	0.73	0.02	No
2/02/2018	C	0.49	0.01	No
2/02/2018	F	0.52	0.01	No
7/02/2018	R	1.32	0.03	No
7/02/2018	S	0.75	0.02	No
7/02/2018	RL	0.75	0.02	No
7/02/2018	G1	0.70	0.02	No
7/02/2018	G2	0.54	0.01	No
7/02/2018	G3	0.69	0.02	No
7/02/2018	G5	0.88	0.02	No
7/02/2018	G6	0.61	0.01	No
7/02/2018	PUV	0.61	0.01	No
7/02/2018	C	0.32	0.01	No
7/02/2018	F	0.47	0.01	No
9/02/2018	R	0.66	0.02	Yes ($p = 0.032$)
9/02/2018	S	0.51	0.01	No
9/02/2018	RL	0.57	0.01	No
9/02/2018	G1	0.42	0.01	No
9/02/2018	G3	0.30	0.01	No
9/02/2018	G5	0.63	0.01	No
9/02/2018	G6	0.37	0.01	No
9/02/2018	PUV	0.50	0.01	No
9/02/2018	C	0.22	0.01	No
9/02/2018	F	0.50	0.01	No
28/02/2018	R	1.49	0.03	No
28/02/2018	S	1.18	0.03	No
28/02/2018	RL	0.92	0.02	No

28/02/2018	G1	0.85	0.02	No
28/02/2018	G2	0.65	0.01	No
28/02/2018	G3	0.76	0.02	No
28/02/2018	G4	0.42	0.01	No
28/02/2018	G5	3.52	0.08	Yes ($p < 2.2\ e^{-16}$)
28/02/2018	G6	0.70	0.02	No
28/02/2018	PUV	0.76	0.02	No
2/03/2018	R	1.72	0.04	No
2/03/2018	S	1.08	0.02	No
2/03/2018	RL	1.26	0.03	No
2/03/2018	G1	0.88	0.02	No
2/03/2018	G2	0.85	0.02	No
2/03/2018	G3	0.97	0.02	No
2/03/2018	G4	0.63	0.01	No
2/03/2018	G5	1.21	0.03	No
2/03/2018	G6	1.00	0.02	No
2/03/2018	PUV	1.08	0.02	No
2/03/2018	C	0.71	0.02	No
3/03/2018	R	1.83	0.04	No
3/03/2018	S	1.25	0.03	No
3/03/2018	RL	1.04	0.02	No
3/03/2018	G1	0.86	0.02	No
3/03/2018	G2	0.50	0.01	No
3/03/2018	G3	0.84	0.02	No
3/03/2018	G4	1.01	0.02	No
3/03/2018	G5	1.22	0.03	No
3/03/2018	G6	0.90	0.02	No
3/03/2018	PUV	1.00	0.02	No
4/03/2018	R	1.47	0.03	No
4/03/2018	S	1.16	0.03	No
4/03/2018	RL	1.13	0.03	No
4/03/2018	G1	0.86	0.02	No
4/03/2018	G2	0.77	0.02	No
4/03/2018	G3	0.74	0.02	No
4/03/2018	G4	0.52	0.01	No
4/03/2018	G5	1.01	0.02	No
4/03/2018	G6	0.80	0.02	No
4/03/2018	PUV	0.86	0.02	No
5/03/2018	R	1.99	0.05	No
5/03/2018	S	1.28	0.03	No
5/03/2018	RL	1.20	0.03	No
5/03/2018	G1	0.83	0.02	No
5/03/2018	G2	0.82	0.02	No
5/03/2018	G3	0.80	0.02	No
5/03/2018	G4	0.35	0.01	No
5/03/2018	G6	0.87	0.02	No
5/03/2018	PUV	0.84	0.02	No
6/03/2018	R	1.45	0.03	No
6/03/2018	S	0.88	0.02	No
6/03/2018	RL	0.92	0.02	No
6/03/2018	G1	0.63	0.01	No
6/03/2018	G2	0.35	0.01	No
6/03/2018	G3	0.26	0.01	No
6/03/2018	G4	0.26	0.01	No
6/03/2018	G6	0.67	0.02	No
6/03/2018	PUV	0.64	0.01	No
15/03/2018	R	1.54	0.04	No
15/03/2018	S	0.69	0.02	No
15/03/2018	RL	0.47	0.01	No
15/03/2018	G1	0.47	0.01	No
15/03/2018	G2	0.40	0.01	No
15/03/2018	G3	0.25	0.01	No
15/03/2018	G4	-0.07	0.00	Instrument error
15/03/2018	G6	0.22	0.01	No
15/03/2018	PUV	0.35	0.01	No
16/03/2018	R	1.46	0.03	No
16/03/2018	S	1.25	0.03	No
16/03/2018	RL	0.72	0.02	No
16/03/2018	G1	0.93	0.02	No
16/03/2018	G2	0.47	0.01	No
16/03/2018	G3	0.34	0.01	No
16/03/2018	G4	0.22	0.01	No

16/03/2018	G6	0.50	0.01	No
16/03/2018	PUV	1.29	0.03	No
17/03/2018	R	1.60	0.04	No
17/03/2018	S	0.95	0.02	No
17/03/2018	RL	0.77	0.02	No
17/03/2018	G1	0.85	0.02	No
17/03/2018	G2	1.66	0.04	Yes (p = 0.0054)
17/03/2018	G3	0.46	0.01	No
17/03/2018	G4	0.58	0.01	No
17/03/2018	G6	0.86	0.02	No
17/03/2018	PUV	0.82	0.02	No

GAC TOC ANOVA results:

Anova: Single Factor

SUMMARY

Groups	*Count*	*Sum*	*Mean*	*Variance*
G1	15	11.52	0.77	0.023
G2	13	8.32	0.64	0.030
G3	14	8.91	0.64	0.081
G4	8	3.98	0.50	0.064
G5	9	8.69	0.97	0.060
G6	15	11.13	0.74	0.055
C	11	5.30	0.48	0.048

ANOVA

Source of Variation	*SS*	*df*	*MS*	*F*	*P-value*	*F crit*
Between Groups	1.65	6	0.28	5.50	8.66E-05	2.22
Within Groups	3.9	78	0.050			
Total	5.55	84				

GAC TOC Tukey HSD results:

Treatments pair	Tukey HSD Q statistic	Tukey HSD p-value	Tukey HSD inference
GAC1 vs GAC2	2.085	0.732	insignificant
GAC1 vs GAC3	2.188	0.691	insignificant
GAC1 vs GAC4	3.852	0.106	insignificant
GAC1 vs GAC5	2.970	0.364	insignificant
GAC1 vs GAC6	0.438	0.900	insignificant
GAC1 vs C	4.489	0.034	p<0.05
GAC2 vs GAC3	0.059	0.900	insignificant
GAC2 vs GAC4	1.994	0.769	insignificant
GAC2 vs GAC5	4.710	0.022	p<0.05
GAC2 vs GAC6	1.664	0.900	insignificant
GAC2 vs C	2.420	0.596	insignificant
GAC3 vs GAC4	1.970	0.779	insignificant
GAC3 vs GAC5	4.834	0.017	p<0.05
GAC3 vs GAC6	1.758	0.866	insignificant
GAC3 vs C	2.404	0.603	insignificant
GAC4 vs GAC5	6.048	0.001	p<0.01
GAC4 vs GAC6	3.487	0.186	insignificant
GAC4 vs C	0.205	0.900	insignificant
GAC5 vs GAC6	3.349	0.226	insignificant
GAC5 vs C	6.750	0.001	p<0.01
GAC6 vs C	4.086	0.071	insignificant

HWTS PARAFAC results:

Date	Sample	C1	C2	C3	B	T	A	M	C
5/01/2018	R	0.024	0.174	0.091	0.064	0.059	0.228	0.130	0.101
5/01/2018	S	0.023	0.160	0.098	0.089	0.068	0.199	0.123	0.093
5/01/2018	RL	0.051	0.112	0.049	0.077	0.032	0.170	0.080	0.067
5/01/2018	G2	0.026	0.089	0.047	0.048	0.026	0.151	0.060	0.046
5/01/2018	G3	0.045	0.240	0.078	0.096	0.047	0.253	0.176	0.114
5/01/2018	G5	0.046	0.119	0.045	0.061	0.018	0.152	0.088	0.068
5/01/2018	G6	0.008	0.051	0.040	0.011	0.019	0.111	0.044	0.032
5/01/2018	C	0.029	0.013	0.029	0.030	0.009	0.049	0.019	0.009
5/01/2018	F	0.408	0.038	0.023	0.105	0.029	0.112	0.035	0.020
13/01/2018	R	0.234	0.756	0.423	0.425	0.444	0.857	0.501	0.394
13/01/2018	S	0.161	0.206	0.153	0.190	0.122	0.264	0.160	0.106
13/01/2018	RL	0.154	0.369	0.329	0.219	0.293	0.462	0.297	0.202
13/01/2018	G2	0.212	0.161	0.131	0.220	0.113	0.225	0.117	0.084
13/01/2018	G3	0.167	0.155	0.168	0.239	0.165	0.230	0.111	0.081
13/01/2018	G5	0.218	0.526	0.240	0.276	0.220	0.553	0.361	0.246
1/02/2018	R	0.074	0.415	0.190	0.194	0.156	0.477	0.273	0.220
1/02/2018	S	0.040	0.120	0.066	0.064	0.035	0.162	0.091	0.067
1/02/2018	RL	0.038	0.213	0.088	0.115	0.051	0.250	0.157	0.116
1/02/2018	G2	0.050	0.083	0.056	0.104	0.043	0.133	0.060	0.049
1/02/2018	G3	0.086	0.073	0.038	0.088	0.045	0.127	0.051	0.041
1/02/2018	G5	0.070	0.298	0.097	0.076	0.063	0.311	0.183	0.134
1/02/2018	G6	0.062	0.131	0.065	0.098	0.068	0.181	0.098	0.068
1/02/2018	C	0.036	0.041	0.035	0.012	0.014	0.097	0.028	0.020
2/02/2018	R	0.469	0.252	0.208	0.305	0.232	0.287	0.167	0.141
2/02/2018	S	0.360	0.102	0.136	0.235	0.156	0.128	0.083	0.061
2/02/2018	RL	0.422	0.092	0.127	0.266	0.133	0.118	0.077	0.057
2/02/2018	G1	0.374	0.062	0.124	0.211	0.153	0.093	0.057	0.037
2/02/2018	G2	0.464	0.054	0.151	0.298	0.181	0.076	0.051	0.034
2/02/2018	G3	0.377	0.045	0.125	0.225	0.155	0.071	0.038	0.029
2/02/2018	G5	0.370	0.134	0.178	0.243	0.185	0.179	0.107	0.068
2/02/2018	G6	0.419	0.072	0.161	0.257	0.176	0.116	0.064	0.041
2/02/2018	PUV	0.412	0.022	0.113	0.252	0.138	0.071	0.028	0.017
2/02/2018	C	0.418	0.008	0.146	0.269	0.165	0.066	0.021	0.013
2/02/2018	F	0.345	0.015	0.081	0.204	0.116	0.078	0.023	0.012
8/02/2018	R	0.396	0.201	0.130	0.250	0.154	0.229	0.141	0.107
8/02/2018	S	0.408	0.140	0.199	0.270	0.199	0.160	0.113	0.084
8/02/2018	RL	0.375	0.118	0.152	0.248	0.163	0.141	0.099	0.070
8/02/2018	G1	0.350	0.055	0.102	0.211	0.132	0.086	0.047	0.034
8/02/2018	G2	0.377	0.044	0.104	0.221	0.139	0.085	0.038	0.025
8/02/2018	G3	0.376	0.042	0.106	0.229	0.148	0.079	0.037	0.023
8/02/2018	G5	0.351	0.170	0.143	0.232	0.161	0.188	0.110	0.081
8/02/2018	G6	0.380	0.067	0.121	0.238	0.164	0.100	0.058	0.041
8/02/2018	PUV	0.331	0.022	0.151	0.222	0.175	0.079	0.027	0.016
8/02/2018	C	0.379	0.005	0.146	0.220	0.148	0.077	0.024	0.012
8/02/2018	F	0.316	0.018	0.077	0.210	0.099	0.063	0.025	0.012
27/02/2018	R	0.319	0.269	0.168	0.226	0.186	0.293	0.182	0.147
27/02/2018	S	0.313	0.143	0.135	0.210	0.155	0.163	0.111	0.087
27/02/2018	G2	0.337	0.053	0.117	0.248	0.139	0.077	0.049	0.037
27/02/2018	G4	0.307	0.011	0.115	0.208	0.155	0.057	0.021	0.012
27/02/2018	G5	0.326	0.142	0.174	0.266	0.185	0.177	0.100	0.074
27/02/2018	G6	0.265	0.073	0.108	0.224	0.131	0.108	0.059	0.042
27/02/2018	PUV	0.370	0.070	0.133	0.266	0.160	0.106	0.057	0.044
28/02/2018	R	0.271	0.226	0.171	0.205	0.193	0.255	0.147	0.124
28/02/2018	S	0.236	0.135	0.127	0.155	0.136	0.169	0.104	0.086
28/02/2018	RL	0.243	0.105	0.091	0.161	0.113	0.144	0.080	0.064
28/02/2018	G1	0.248	0.072	0.117	0.154	0.125	0.103	0.054	0.041
28/02/2018	G2	0.216	0.065	0.096	0.140	0.111	0.097	0.048	0.037
28/02/2018	G3	0.268	0.059	0.082	0.163	0.106	0.088	0.044	0.032
28/02/2018	G4	0.243	0.009	0.088	0.152	0.111	0.040	0.016	0.010
28/02/2018	G5	0.300	0.177	0.146	0.202	0.164	0.204	0.118	0.083
28/02/2018	G6	0.216	0.059	0.088	0.148	0.106	0.096	0.046	0.033
28/02/2018	PUV	0.258	0.077	0.184	0.166	0.190	0.129	0.063	0.039
1/03/2018	R	0.445	0.257	0.199	0.315	0.243	0.292	0.171	0.142
1/03/2018	S	0.407	0.116	0.169	0.325	0.198	0.156	0.106	0.070
1/03/2018	RL	0.425	0.133	0.157	0.327	0.188	0.174	0.110	0.081
1/03/2018	G1	0.460	0.076	0.163	0.377	0.214	0.116	0.064	0.047
1/03/2018	G2	0.436	0.060	0.130	0.341	0.178	0.095	0.054	0.037
1/03/2018	G3	0.416	0.061	0.125	0.307	0.182	0.091	0.050	0.036
1/03/2018	G4	0.461	0.013	0.122	0.314	0.185	0.043	0.024	0.010

1/03/2018	G5	0.363	0.171	0.148	0.257	0.182	0.203	0.115	0.086
1/03/2018	G6	0.384	0.074	0.271	0.312	0.362	0.114	0.072	0.044
1/03/2018	PUV	0.341	0.073	0.159	0.228	0.213	0.124	0.062	0.041
1/03/2018	C	0.325	0.008	0.126	0.233	0.158	0.051	0.021	0.011
2/03/2018	R	0.407	0.288	0.186	0.270	0.231	0.329	0.195	0.158
2/03/2018	S	0.353	0.104	0.151	0.232	0.187	0.140	0.088	0.064
2/03/2018	RL	0.353	0.136	0.148	0.235	0.178	0.185	0.119	0.086
2/03/2018	G1	0.359	0.069	0.121	0.232	0.163	0.109	0.058	0.044
2/03/2018	G2	0.378	0.057	0.126	0.207	0.161	0.090	0.052	0.037
2/03/2018	G3	0.345	0.060	0.130	0.228	0.170	0.103	0.047	0.036
2/03/2018	G4	0.348	0.011	0.125	0.213	0.164	0.053	0.018	0.013
2/03/2018	G5	0.367	0.153	0.154	0.253	0.192	0.186	0.108	0.077
2/03/2018	G6	0.273	0.110	0.117	0.196	0.139	0.148	0.079	0.058
2/03/2018	PUV	0.406	0.079	0.120	0.244	0.148	0.124	0.068	0.045
2/03/2018	C	0.401	0.019	0.174	0.280	0.231	0.068	0.032	0.018
3/03/2018	R	0.298	0.278	0.213	0.250	0.237	0.300	0.185	0.150
3/03/2018	S	0.285	0.127	0.172	0.238	0.201	0.158	0.097	0.075
3/03/2018	RL	0.286	0.142	0.259	0.277	0.283	0.172	0.120	0.083
3/03/2018	G1	0.310	0.077	0.189	0.260	0.241	0.110	0.064	0.046
3/03/2018	G2	0.231	0.032	0.121	0.195	0.154	0.055	0.032	0.024
3/03/2018	G3	0.266	0.067	0.230	0.237	0.255	0.109	0.064	0.036
3/03/2018	G4	0.348	0.064	0.170	0.220	0.197	0.097	0.053	0.036
3/03/2018	G5	0.240	0.154	0.157	0.219	0.190	0.175	0.102	0.078
3/03/2018	G6	0.205	0.081	0.158	0.162	0.188	0.095	0.064	0.047
3/03/2018	PUV	0.225	0.084	0.096	0.179	0.115	0.109	0.064	0.047
4/03/2018	R	0.135	0.281	0.123	0.126	0.122	0.306	0.176	0.149
4/03/2018	S	0.176	0.120	0.100	0.129	0.102	0.153	0.094	0.071
4/03/2018	RL	0.367	0.136	0.121	0.247	0.145	0.156	0.110	0.079
4/03/2018	G1	0.317	0.074	0.093	0.220	0.123	0.101	0.059	0.040
4/03/2018	G2	0.369	0.061	0.116	0.237	0.156	0.100	0.055	0.038
4/03/2018	G3	0.284	0.061	0.109	0.197	0.135	0.102	0.057	0.037
4/03/2018	G4	0.343	0.014	0.089	0.218	0.143	0.051	0.025	0.016
4/03/2018	G5	0.342	0.175	0.116	0.230	0.150	0.193	0.119	0.087
4/03/2018	G6	0.405	0.085	0.113	0.260	0.157	0.111	0.069	0.046
4/03/2018	PUV	0.333	0.074	0.094	0.206	0.128	0.093	0.059	0.041
5/03/2018	R	0.282	0.250	0.188	0.251	0.203	0.272	0.168	0.130
5/03/2018	S	0.256	0.139	0.141	0.217	0.168	0.192	0.107	0.080
5/03/2018	RL	0.312	0.143	0.166	0.262	0.186	0.168	0.113	0.084
5/03/2018	G1	0.326	0.085	0.124	0.251	0.155	0.115	0.071	0.050
5/03/2018	G2	0.334	0.068	0.113	0.243	0.154	0.101	0.054	0.040
5/03/2018	G3	0.308	0.083	0.125	0.246	0.170	0.111	0.063	0.046
5/03/2018	G4	0.286	0.013	0.103	0.186	0.160	0.052	0.018	0.010
5/03/2018	G6	0.305	0.093	0.111	0.201	0.152	0.121	0.070	0.051
5/03/2018	PUV	0.237	0.060	0.101	0.187	0.129	0.087	0.043	0.038
5/03/2018	C	0.297	0.026	0.112	0.250	0.165	0.070	0.028	0.020
6/03/2018	R	0.395	0.292	0.153	0.282	0.194	0.322	0.194	0.155
6/03/2018	S	0.305	0.133	0.135	0.202	0.169	0.158	0.111	0.080
6/03/2018	RL	0.356	0.129	0.127	0.229	0.158	0.158	0.105	0.076
6/03/2018	G1	0.316	0.068	0.097	0.173	0.127	0.098	0.057	0.043
6/03/2018	G2	0.330	0.022	0.103	0.214	0.143	0.061	0.030	0.018
6/03/2018	G3	0.244	0.018	0.084	0.159	0.118	0.061	0.023	0.014
6/03/2018	G4	0.351	0.016	0.081	0.222	0.121	0.051	0.021	0.013
6/03/2018	G6	0.331	0.075	0.111	0.223	0.144	0.092	0.071	0.043
6/03/2018	PUV	0.322	0.054	0.121	0.205	0.169	0.089	0.047	0.033
6/03/2018	C	0.305	0.018	0.093	0.188	0.123	0.053	0.027	0.016
15/03/2018	R	0.302	0.216	0.172	0.271	0.204	0.247	0.144	0.115
15/03/2018	S	0.311	0.069	0.127	0.232	0.161	0.092	0.059	0.046
15/03/2018	RL	0.321	0.103	0.154	0.239	0.190	0.140	0.090	0.063
15/03/2018	G1	0.296	0.068	0.110	0.192	0.149	0.099	0.053	0.041
15/03/2018	G2	0.315	0.058	0.128	0.238	0.169	0.092	0.048	0.035
15/03/2018	G3	0.349	0.064	0.139	0.258	0.199	0.083	0.050	0.037
15/03/2018	G4	0.332	0.027	0.134	0.260	0.176	0.061	0.023	0.019
15/03/2018	G6	0.338	0.083	0.137	0.277	0.171	0.113	0.067	0.047
15/03/2018	PUV	0.376	0.059	0.123	0.271	0.177	0.085	0.051	0.037
15/03/2018	C	0.325	0.020	0.118	0.229	0.161	0.056	0.028	0.018
15/03/2018	F	0.224	0.028	0.084	0.167	0.101	0.078	0.028	0.020
16/03/2018	R	0.445	0.199	0.208	0.331	0.235	0.235	0.135	0.109
16/03/2018	S	0.244	0.082	0.179	0.218	0.176	0.125	0.068	0.050
16/03/2018	RL	0.319	0.103	0.168	0.222	0.208	0.136	0.082	0.063
16/03/2018	G1	0.352	0.073	0.161	0.240	0.192	0.124	0.062	0.043
16/03/2018	G2	0.350	0.060	0.179	0.273	0.223	0.093	0.054	0.039
16/03/2018	G3	0.319	0.061	0.188	0.290	0.226	0.105	0.048	0.036

16/03/2018	G4	0.383	0.031	0.140	0.257	0.198	0.079	0.036	0.022
16/03/2018	G6	0.349	0.067	0.182	0.257	0.230	0.100	0.053	0.039
16/03/2018	PUV	0.322	0.063	0.156	0.257	0.199	0.099	0.051	0.037
16/03/2018	C	0.326	0.018	0.152	0.215	0.179	0.069	0.023	0.018
16/03/2018	F	0.342	0.033	0.102	0.212	0.135	0.066	0.035	0.020
17/03/2018	R	0.399	0.208	0.187	0.333	0.233	0.245	0.144	0.112
17/03/2018	S	0.323	0.071	0.126	0.228	0.140	0.099	0.064	0.041
17/03/2018	RL	0.326	0.100	0.128	0.243	0.146	0.126	0.083	0.057
17/03/2018	G1	0.443	0.071	0.129	0.297	0.179	0.101	0.068	0.040
17/03/2018	G2	0.466	0.067	0.151	0.388	0.193	0.105	0.060	0.043
17/03/2018	G3	0.392	0.063	0.141	0.276	0.178	0.107	0.057	0.036
17/03/2018	G4	0.331	0.030	0.113	0.209	0.143	0.059	0.031	0.018
17/03/2018	G6	0.370	0.078	0.113	0.247	0.142	0.115	0.066	0.042
17/03/2018	PUV	0.321	0.056	0.133	0.218	0.166	0.075	0.051	0.033

HWTS PARAFAC components and TOC data:

Location	C1	C2	C3	TOC
R	0.024	0.174	0.091	1.35
S	0.023	0.160	0.098	1.00
RL	0.051	0.112	0.049	0.98
G2	0.026	0.089	0.047	0.81
G3	0.045	0.240	0.078	0.72
G5	0.046	0.119	0.045	1.00
G6	0.008	0.051	0.040	0.89
C	0.029	0.013	0.029	0.49
S	0.161	0.206	0.153	0.95
G2	0.212	0.161	0.131	0.84
G3	0.167	0.155	0.168	1.19
S	0.040	0.120	0.066	0.95
RL	0.038	0.213	0.088	0.84
G2	0.050	0.083	0.056	0.64
G6	0.062	0.131	0.065	0.86
C	0.036	0.041	0.035	0.64
R	0.469	0.252	0.208	1.44
S	0.360	0.102	0.136	0.86
RL	0.422	0.092	0.127	0.91
G1	0.374	0.062	0.124	0.84
G2	0.464	0.054	0.151	0.69
G3	0.377	0.045	0.125	0.60
G5	0.370	0.134	0.178	0.86
G6	0.419	0.072	0.161	0.78
PUV	0.412	0.022	0.113	0.73
C	0.418	0.008	0.146	0.49
F	0.345	0.015	0.081	0.52
R	0.271	0.226	0.171	1.49
S	0.236	0.135	0.127	1.18
RL	0.243	0.105	0.091	0.92
G1	0.248	0.072	0.117	0.85
G2	0.216	0.065	0.096	0.65
G3	0.268	0.059	0.082	0.76
G4	0.243	0.009	0.088	0.42
G6	0.216	0.059	0.088	0.70
PUV	0.258	0.077	0.184	0.76
R	0.407	0.288	0.186	1.72
S	0.353	0.104	0.151	1.08
RL	0.353	0.136	0.148	1.26
G1	0.359	0.069	0.121	0.88
G2	0.378	0.057	0.126	0.85
G3	0.345	0.060	0.130	0.97
G4	0.348	0.011	0.125	0.63
G5	0.367	0.153	0.154	1.21
G6	0.273	0.110	0.117	1.00
PUV	0.406	0.079	0.120	1.08
C	0.401	0.019	0.174	0.71
R	0.298	0.278	0.213	1.83
S	0.285	0.127	0.172	1.25
RL	0.286	0.142	0.259	1.04
G1	0.310	0.077	0.189	0.86
G2	0.231	0.032	0.121	0.50
G3	0.266	0.067	0.230	0.84

G4	0.348	0.064	0.170	1.01
G5	0.240	0.154	0.157	1.22
G6	0.205	0.081	0.158	0.90
PUV	0.225	0.084	0.096	1.00
R	0.135	0.281	0.123	1.47
S	0.176	0.120	0.100	1.16
RL	0.367	0.136	0.121	1.13
G1	0.317	0.074	0.093	0.86
G2	0.369	0.061	0.116	0.77
G3	0.284	0.061	0.109	0.74
G4	0.343	0.014	0.089	0.52
G5	0.342	0.175	0.116	1.01
G6	0.405	0.085	0.113	0.80
PUV	0.333	0.074	0.094	0.86
R	0.282	0.250	0.188	1.99
S	0.256	0.139	0.141	1.28
RL	0.312	0.143	0.166	1.20
G1	0.326	0.085	0.124	0.83
G2	0.334	0.068	0.113	0.82
G3	0.308	0.083	0.125	0.80
G4	0.286	0.013	0.103	0.35
G6	0.305	0.093	0.111	0.87
PUV	0.237	0.060	0.101	0.84
R	0.395	0.292	0.153	1.45
S	0.305	0.133	0.135	0.88
RL	0.356	0.129	0.127	0.92
G1	0.316	0.068	0.097	0.63
G2	0.330	0.022	0.103	0.35
G3	0.244	0.018	0.084	0.26
G4	0.351	0.016	0.081	0.26
G6	0.331	0.075	0.111	0.67
PUV	0.322	0.054	0.121	0.64
R	0.302	0.216	0.172	1.54
S	0.311	0.069	0.127	0.69
RL	0.321	0.103	0.154	0.47
G1	0.296	0.068	0.110	0.47
G2	0.315	0.058	0.128	0.40
G3	0.349	0.064	0.139	0.25
G6	0.338	0.083	0.137	0.22
PUV	0.376	0.059	0.123	0.35
R	0.445	0.199	0.208	1.46
S	0.244	0.082	0.179	1.25
RL	0.319	0.103	0.168	0.72
G1	0.352	0.073	0.161	0.93
G2	0.350	0.060	0.179	0.47
G3	0.319	0.061	0.188	0.34
G4	0.383	0.031	0.140	0.22
G6	0.349	0.067	0.182	0.50
PUV	0.322	0.063	0.156	1.29
R	0.399	0.208	0.187	1.60
S	0.323	0.071	0.126	0.95
RL	0.326	0.100	0.128	0.77
G1	0.443	0.071	0.129	0.85
G3	0.392	0.063	0.141	0.46
G4	0.331	0.030	0.113	0.58
G6	0.370	0.078	0.113	0.86
PUV	0.321	0.056	0.133	0.82

Pilot column PARAFAC results:

Date	Depth	C1	C2	C3	B	T	A	M	C
18/03/2019	0	0.0734	0.1397	0.0961	0.0785	0.0895	0.1340	0.0802	0.0569
18/03/2019	10	0.0608	0.0649	0.0703	0.0503	0.0652	0.0703	0.0404	0.0252
18/03/2019	20	0.2486	0.1371	0.1787	0.1935	0.1913	0.1248	0.0870	0.0534
18/03/2019	30	0.1427	0.1121	0.0882	0.1224	0.0926	0.1057	0.0653	0.0438
18/03/2019	40	0.0802	0.0901	0.0781	0.0694	0.0810	0.0879	0.0521	0.0350
18/03/2019	50	0.0663	0.0792	0.0727	0.0719	0.0737	0.0814	0.0439	0.0326
18/03/2019	60	0.0645	0.0732	0.0754	0.0709	0.0801	0.0746	0.0447	0.0297
18/03/2019	70	0.2302	0.0835	0.0976	0.1986	0.1220	0.0780	0.0559	0.0335
18/03/2019	80	0.0846	0.0737	0.0684	0.0735	0.0727	0.0753	0.0439	0.0310
18/03/2019	90	0.2430	0.0904	0.0868	0.1921	0.1205	0.0943	0.0575	0.0378
18/03/2019	100	0.0911	0.0682	0.0701	0.0650	0.0738	0.0788	0.0398	0.0278

18/03/2019	110	0.0667	0.0698	0.0721	0.0510	0.0676	0.0759	0.0407	0.0290
18/03/2019	120	0.0686	0.0573	0.0666	0.0611	0.0681	0.0655	0.0338	0.0249
18/03/2019	130	0.0556	0.0353	0.0552	0.0528	0.0594	0.0466	0.0231	0.0163
18/03/2019	140	0.0600	0.0479	0.0666	0.0661	0.0787	0.0547	0.0306	0.0200
18/03/2019	150	0.2201	0.0598	0.0706	0.1801	0.0961	0.0666	0.0413	0.0245
18/03/2019	160	0.0827	0.0595	0.0666	0.0619	0.0649	0.0679	0.0342	0.0252
18/03/2019	170	0.0644	0.0532	0.0581	0.0583	0.0610	0.0582	0.0312	0.0218
18/03/2019	180	0.0638	0.0587	0.0694	0.0599	0.0685	0.0681	0.0338	0.0237
23/04/2019	0	0.0607	0.0917	0.0686	0.0435	0.0719	0.0842	0.0559	0.0401
23/04/2019	10	0.0364	0.1036	0.0704	0.0279	0.0634	0.0979	0.0596	0.0426
23/04/2019	20	0.0366	0.0953	0.0663	0.0340	0.0635	0.0859	0.0576	0.0413
23/04/2019	30	0.0242	0.0783	0.0710	0.0197	0.0724	0.0741	0.0468	0.0339
23/04/2019	40	0.0331	0.0670	0.0510	0.0198	0.0540	0.0627	0.0429	0.0294
23/04/2019	50	0.1861	0.0484	0.0703	0.1398	0.0984	0.0509	0.0383	0.0239
23/04/2019	60	0.0575	0.0695	0.0630	0.0366	0.0630	0.0682	0.0445	0.0297
23/04/2019	70	0.0408	0.0631	0.0537	0.0275	0.0550	0.0609	0.0410	0.0264
23/04/2019	80	0.0355	0.0600	0.0519	0.0280	0.0614	0.0580	0.0404	0.0280
23/04/2019	90	0.0363	0.0662	0.0660	0.0252	0.0693	0.0652	0.0435	0.0269
23/04/2019	100	0.0318	0.0600	0.0518	0.0242	0.0529	0.0607	0.0386	0.0259
23/04/2019	110	0.0383	0.0568	0.0518	0.0327	0.0493	0.0562	0.0386	0.0249
23/04/2019	120	0.0323	0.0510	0.0504	0.0327	0.0492	0.0533	0.0319	0.0234
23/04/2019	130	0.0322	0.0302	0.0449	0.0293	0.0530	0.0380	0.0220	0.0162
23/04/2019	140	0.1673	0.0432	0.0801	0.1263	0.0994	0.0460	0.0348	0.0220
23/04/2019	150	0.0541	0.0498	0.0561	0.0364	0.0646	0.0547	0.0316	0.0219
23/04/2019	160	0.0471	0.0519	0.0549	0.0364	0.0548	0.0554	0.0320	0.0226
23/04/2019	170	0.0333	0.0453	0.0713	0.0327	0.0756	0.0466	0.0322	0.0192
23/04/2019	180	0.0372	0.0501	0.0541	0.0340	0.0545	0.0506	0.0308	0.0236
24/04/2019	0	0.0777	0.1482	0.0864	0.0637	0.0836	0.1366	0.0826	0.0606
24/04/2019	10	0.0572	0.1115	0.0784	0.0507	0.0880	0.1092	0.0616	0.0462
24/04/2019	20	0.0499	0.1016	0.0656	0.0466	0.0706	0.0945	0.0591	0.0425
24/04/2019	30	0.0470	0.0817	0.0620	0.0432	0.0682	0.0801	0.0470	0.0395
24/04/2019	40	0.0473	0.0851	0.0527	0.0448	0.0610	0.0843	0.0487	0.0351
24/04/2019	50	0.2033	0.0912	0.0666	0.1588	0.0922	0.0894	0.0583	0.0407
24/04/2019	60	0.0756	0.0823	0.0578	0.0518	0.0667	0.0805	0.0487	0.0341
24/04/2019	70	0.0565	0.0761	0.0559	0.0440	0.0609	0.0775	0.0425	0.0327
24/04/2019	80	0.0479	0.0691	0.0460	0.0384	0.0451	0.0702	0.0399	0.0311
24/04/2019	90	0.0465	0.0714	0.0540	0.0393	0.0532	0.0740	0.0387	0.0311
24/04/2019	100	0.0516	0.0677	0.0547	0.0377	0.0586	0.0679	0.0374	0.0298
24/04/2019	110	0.0502	0.0621	0.0430	0.0508	0.0524	0.0649	0.0347	0.0284
24/04/2019	120	0.2086	0.0712	0.0609	0.1512	0.0896	0.0707	0.0479	0.0321
24/04/2019	130	0.0772	0.0451	0.0537	0.0451	0.0645	0.0516	0.0288	0.0207
24/04/2019	140	0.0627	0.0443	0.0512	0.0497	0.0541	0.0480	0.0282	0.0216
24/04/2019	150	0.0552	0.0510	0.0424	0.0423	0.0553	0.0576	0.0296	0.0236
24/04/2019	160	0.0561	0.0558	0.0454	0.0442	0.0536	0.0615	0.0315	0.0266
24/04/2019	170	0.0496	0.0480	0.0417	0.0347	0.0482	0.0512	0.0270	0.0225
24/04/2019	180	0.0498	0.0534	0.0498	0.0400	0.0590	0.0547	0.0304	0.0242

Appendix B – Publications

THE UNIVERSITY OF WAIKATO
Te Whare Wānanga o Waikato

Co-Authorship Form

Postgraduate Studies Office
Student and Academic Services Division
Waharoa Ratonga Matauranga Akonga
The University of Waikato
Private Bag 3105
Hamilton 3240, New Zealand
Phone +64 7 838 4439
Website: http://www.waikato.ac.nz/sasd/postgraduate/

This form is to accompany the submission of any PhD that contains research reported in published or unpublished co-authored work. **Please include one copy of this form for each co-authored work.** Completed forms should be included in your appendices for all the copies of your thesis submitted for examination and library deposit (including digital deposit).

Please indicate the chapter/section/pages of this thesis that are extracted from a co-authored work and give the title and publication details or details of submission of the co-authored work.

Chapter 2 contains the original version of this review that resulted in the following conference paper:

Bernstein, Daniel; Glasgow, Graeme; Manley-Harris, Merilynn; Lay, Mark; Hu, Barry and Eriksen, Sven. Removal and monitoring of cyanobacterial metabolites in drinking water treatment - a review. In: Chemeca 2016: Chemical Engineering - Regeneration, Recovery and Reinvention. Melbourne, Vic.: Engineers Australia, 2016: 815-827

This is attached as appendix B-1 of the thesis.

Nature of contribution by PhD candidate	I reviewed the literature and wrote the manuscript.
Extent of contribution by PhD candidate (%)	70 %

CO-AUTHORS

Name	Nature of Contribution
Merylin Manley-Harris	Project discussion and paper revision
Graeme Glasgow	Project discussion and paper revision
Mark Lay	Project discussion and paper revision
Barry Hu	Project scoping and guidance on plant operation
Sven Eriksen	Project scoping and guidance on plant operation

Certification by Co-Authors

The undersigned hereby certify that:

- the above statement correctly reflects the nature and extent of the PhD candidate's contribution to this work, and the nature of the contribution of each of the co-authors; and

Name	Signature	Date
Merylin Manley-Harris	M. Manley-Harris	28/10/2020
Graeme Glasgow	G. Glasgow	27/10/20
Mark Lay		29/10/2020
Barry Hu	G Glasgow P.P. barry Hu	30/10/20
Sven Eriksen		6/10/2020

July 2015

THE UNIVERSITY OF WAIKATO
Te Whare Wānanga o Waikato

Co-Authorship Form

Postgraduate Studies Office
Student and Academic Services Division
Wahanga Ratonga Mataurange Akonga
The University of Waikato
Private Bag 3105
Hamilton 3240, New Zealand
Phone +64 7 838 4439
Website: http://www.waikato.ac.nz/sasd/postgraduate/

This form is to accompany the submission of any PhD that contains research reported in published or unpublished co-authored work. **Please include one copy of this form for each co-authored work.** Completed forms should be included in your appendices for all the copies of your thesis submitted for examination and library deposit (including digital deposit).

Please indicate the chapter/section/pages of this thesis that are extracted from a co-authored work and give the title and publication details or details of submission of the co-authored work.

Parts of this article were extracted from chapter 2, although the mejority of the content was not included in the final thesis. The article was published as the following review:

Bernstein, Daniel; Glasgow, Graeme; Manley-Harris, Merlyn; Lay, Mark; Biological activated carbon and advanced oxidation processes for the removal of cyanobacterial metabolites in drinking water treatment. Chemistry in New Zealand. 81(1), 13–18, 2017

This is attached as appendix B-2 of the thesis.

Nature of contribution by PhD candidate	I reviewed the literature and wrote the manuscript.
Extent of contribution by PhD candidate (%)	80 %

CO-AUTHORS

Name	Nature of Contribution
Merylin Manley-Harris	Reviewed and proofed manuscript
Graeme Glasgow	Reviewed/proofed manuscript, project ideation
Mark Lay	Reviewed and proofed manuscript

Certification by Co-Authors

The undersigned hereby certify that:

- the above statement correctly reflects the nature and extent of the PhD candidate's contribution to this work, and the nature of the contribution of each of the co-authors; and

Name	Signature	Date
Merylin Manley-Harris	M. Manley-Harris	28/10/2020
Graeme Glasgow	G. Glasgow	27/10/20
Mark Lay		29/10/2020

July 2015

B-1 Removal and monitoring of cyanobacterial metabolites in drinking water treatment – a review†

Paper no. 3405403

Chemeca 2016

25 – 28 September 2016, Adelaide, Australia

Removal and monitoring of cyanobacterial metabolites in drinking water treatment – a review

Daniel Bernstein[1*], Graeme Glasgow[2,3], Merilyn Manley-Harris[1,3], Mark Lay[2], Barry Hu[4], Sven Ericksen[4]

[1] School of Science, Faculty of Science and Engineering, University of Waikato, Private Bag 3105, Hamilton 3240, New Zealand
[2] School of Engineering, Faculty of Science and Engineering, University of Waikato, Private Bag 3105, Hamilton 3240, New Zealand.
[3] Environmental Research Institute, Faculty of Science and Engineering, University of Waikato, Private Bag 3105, Hamilton 3240, New Zealand
[4] Hamilton City Council, Private Bag 3010, Hamilton 3240, New Zealand

[*]Corresponding author: drbernstein1@gmail.com

Abstract: In 2006, activated carbon filters were commissioned in Hamilton, New Zealand as a means of controlling metabolites associated with cyanobacterial blooms. After this long service life, these filters are assumed to be operating as biological activated carbon (BAC) filters, and as such, the effectiveness and mechanism of action are likely to have changed. Current research into the removal of cyanobacterial metabolites using BAC while well developed in some areas, is lacking in others, and the performance of Hamilton's filters are at this point essentially unknown. As cyanobacterial blooms are seasonal events, the production of cyanobacterial metabolites during such events creates transient, high concentration conditions where the ability of BAC filters to respond dynamically is critical. Additionally, the transformation of cyanotoxins by bacteria is known to occur in natural waters and on biological sand filters, where less toxic analogues are metabolised into those which are more toxic. Prior to commencing research into the Hamilton City Water Treatment Plant, a review of the literature regarding the removal of taste and odour compounds, cyanotoxins and methods for monitoring these compounds was undertaken.

Keywords: drinking water treatment, BAC, AOPs, cyanobacterial metabolites, cyanotoxins, taste and odor, LC-MS, GC-MS.

1 Introduction

For the city of Hamilton, municipal drinking water supply is sourced from the Waikato River, which is New Zealand's longest river (442 km). The catchment for the Waikato River begins prior to Lake Taupo, on the eastern side of Mount Ruapehu as the Upper Waikato Stream, which joins with the Tongariro River before entering Lake Taupo. The Waikato River in its current course flows in a northerly direction from Lake Taupo and onward through the Waikato district before discharging into the Tasman Sea at Port Waikato (Figure 1) [1]. The total catchment area encompasses 11013 m^2 which drains from land used for various purposes. Based on 2008 data, land use is predominantly pastoral (44%), planted forest (41%) and indigenous forest (9%) with a small percentage (6%) which may include scrub, horticulture, inland water, willows and poplar [1]. However, there has recently been large scale conversion of planted forest to pasture, so these figures will have changed somewhat. Due to the varied land use, and in particular the intensive agriculture carried out along the course of the river, there are numerous point and non-point sources throughout the river system that contribute to the overall water quality by the time it reaches Hamilton for drinking water treatment.

Prior to distribution, municipal drinking water is treated at the Hamilton City Council (HCC) Drinking Water Treatment Plant (DWTP) (Figure 2). This plant was built in 1971 and was originally designed to produce 64 megalitres per day (ML D^{-1}). Over the years, the plant has been expanded to its current capacity, with a capability of producing 106 ML D^{-1} [2]. The plant consists of a series of individual

† This conference paper was originally published in Chemeca 2016: Chemical Engineering - Regeneration, Recovery and Reinvention. Melbourne, Vic.: Engineers Australia, **2016**: 815-827

processes designed to purify the source water and deliver it to the consumer (Figure 3) in a form that adheres to the Drinking Water Standards for New Zealand (DWSNZ,[3]).

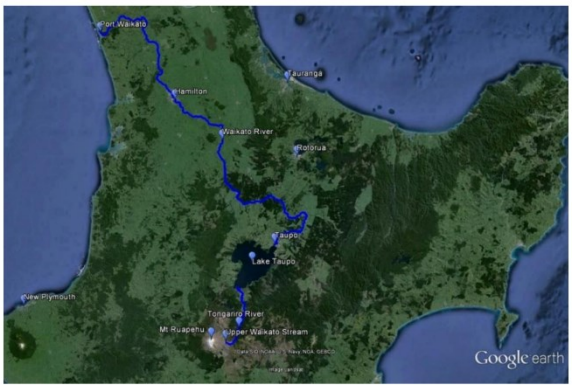

Figure 1: Map outlining the course of the Waikato River beginning from the Upper Waikato Stream (Source: 38o49'33.41" S 175o55'33.85" E. GOOGLE EARTH. October 4, 2013. December 14, 2015).

Figure 2: Aerial view of the Hamilton City Council Drinking Water Treatment Plant. Numbering reflects each process as numbered below (Source: 37°48'33.96" S 175°18'12.50" E. GOOGLE EARTH. January 5, 2013. October 23, 2015).

The main functions of each process are (Figures 2 and 3);

- Screening (1): Physical removal of large and small debris such as pieces of wood, leaves, aquatic weeds, etc.
- Flocculation and Sedimentation (2): Chemical precipitation of microorganisms, fluvic acids, humic acids, metals and other inorganic/organic compounds.
- Sand Filtration (3): Physical filtration of residual floc and any large residual material remaining after flocculation/sedimentation.
- Granular Activated Carbon (4): Removal of taste and odour compounds, residual microorganisms, cyanotoxins and other organic compounds via physicochemical adsorption.
- UV Disinfection (5): Kills residual protozoa.
- Chlorine Disinfection (6): Kills any remaining bacteria. The chlorinated water is allowed to dwell in a reservoir to allow for maximum chlorine contact and effectiveness. Water pumped to the city reservoirs contains residual chlorine as extra protection against bacterial growth
- Fluoride Dosing (7): Addition of Fluoride (as hexafluorosilicic acid) as per Council policy and Ministry of Health recommendations.

- pH Correction (8): Addition of lime to return pH to neutral as flocculation lowers pH.

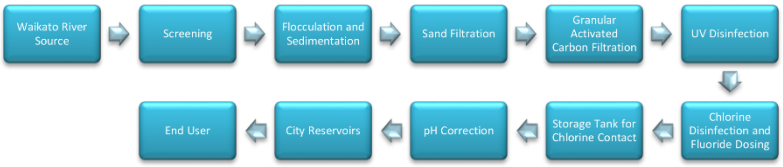

Figure 3: Basic process flow for the Hamilton City Council Drinking Water Treatment Plant (adapted from [2]).

Prior to 2006, the plant employed no Granular Activated Carbon (GAC) filtration. However, following a significant algal bloom of cyanotoxin-producing cyanobacteria in 2003, GAC filtration was implemented as part of a plant upgrade in 2006. This was aimed at removing cyanotoxins from drinking water during seasonal algal blooms while at the same time managing taste and odour problems typically associated with the presence of certain species of cyanobacteria [1,2,4,5]. Due to the prevalence of cyanobacterial blooms during low flow or drought conditions, the frequency and severity of such blooms is likely to increase in the future due to Climate Change/Global Warming and the prospect of longer, hotter summers in the region [5,6].

As the design of this particular GAC system makes replacement inherently difficult, and with GAC replacement being a rather expensive operation in general, the GAC present in the filters has not been replaced. Therefore, the absorption capacity of the GAC is likely to be almost entirely exhausted and the current system is likely to be operating more akin to a Biologically Activated Carbon (BAC) system with adsorption and transformation of chemical substrates present in the source water being carried out enzymatically by microorganisms attached to the GAC surface as a biofilm [7,8].

2 Biological Activated Carbon

Removal of organic compounds from source waters using GAC is achieved via physicochemical adsorption. Hence, once the adsorptive capacity of the GAC is exhausted, adsorption can no longer occur and breakthrough is observed [9]. To overcome this, the GAC must either be replaced or re-activated in order to restore its adsorption capacity. This is very labour intensive and costly, therefore in recent times, numerous investigations into the use of biological activated carbon (BAC or BGAC) have been carried out in various water treatment scenarios.

Biological activated carbon is activated carbon on which a biofilm has been allowed to accumulate with the aim of removing influent contaminants via biodegradation. Over the course of their life time, GAC filters are slowly converted to BAC as their adsorption capacity is depleted and a biofilm begins to accumulate. The term BAC (or BGAC) is also often used to refer to the combination of an advanced oxidation process (AOP) with a BAC reactor as a coupled process. Obviously, the effectiveness of a BAC reactor is dependent on the biodegradability of the target compound. In the case of poorly or non-biodegradable compounds, the implementation of an AOP prior to BAC aims to increase the biodegradability of the compounds by chemical oxidation.

In various parts of the world, some concerns have been raised by the public and regulatory bodies regarding the introduction of pathogens into the water supply via the sloughing of bacteria from biological filters. However, evidence suggests this concern is unwarranted [10]. Furthermore, in the case of Hamilton's DWTP, UV disinfection is carried out directly following the GAC/BAC filters as a direct measure to remove pathogens such as cryptosporidium.

Although the ideal scenario is the biodegradation of target compounds leading to complete mineralisation, partial degradation by a change in molecular functionality to give compounds that impart no or reduced deleterious aesthetic or toxicological qualities to a treated water is also acceptable [11]. However, the transformation of organic compounds, such as saxitoxins, into toxic or otherwise harmful products is a possibility that should not be overlooked [5].

2.1 Removal of taste and odour compounds using BAC

Many studies have been conducted in order to assess the effectiveness of BAC as a removal technology for taste and odour (T&O) compounds. These studies range from bench to full scale application and assess a wide range of operational conditions.

An early study by Yagi *et al.* [12] using bench scale GAC columns inoculated with Bacillus subtillus showed that biodegradation may indeed be a promising method for this purpose while at the same time extending the lifetime of GAC filters. This study investigated the biodegradation of geosmin and 2-methylisoborneol (2-MIB) as a primary substrate at relatively high concentrations (2 mg L^{-1}) compared to that typically found in natural waters encountered in drinking water treatment. The study showed that biodegradation of Geosmin and 2-MIB did indeed occur, indicating that the degradation of these compounds is possible when they are the sole carbon source.

A pilot scale investigation by Hrudey *et al.* [13] on raw waters containing geosmin at concentrations of 14 to 20 ng L^{-1} showed that BAC was effective at removing odour from the influent water when used in conjunction with pre-ozonation. However, bench scale studies carried out alongside the pilot study indicated that adsorption to the activated carbon may have been the primary mechanism for odour removal and it was concluded that biological removal of odours may not be a realistic approach. Despite this, more recent studies have indeed shown that the use of BAC is an effective treatment approach for T&O compounds.

An investigation by Nerenberg *et al.* [14] into the removal efficiency of a full scale plant employing conventional treatment with additional pre-ozonation and post-treatment BAC filtration showed that biological filtration was effective in the removal of 2-MIB. The study was prompted after a survey of the treatment plants in the area (Chicago, IL), showed that all except one plant was experiencing seasonal odour issues, based on both quantitative analysis and consumer complaints. Most plants in the area relied on powdered activated carbon (PAC) dosing to remedy seasonal odour events, which was deemed to be ineffective at affordable or practical doses. However, the one plant in the area that employed pre-ozonation and BAC filtration had no consumer complaints. Tracing the concentration of 2-MIB through the treatment process showed that the pre-ozonation removed 26% to 64% of the influent 2-MIB concentration, with the BAC removing a further 36% - 65% of the 2-MIB remaining after pre-ozonation and conventional treatment.

Elhadi *et al.* [15] carried out a study which investigated the transition from GAC to BAC using influent water containing spiked levels of 2-MIB (100 ng L^{-1}), geosmin (100 ng L^{-1}), and biodegradable organic matter (BOM; 1000 µg L^{-1}; formaldehyde, glyoxal, formate, and acetate). Fresh GAC filters were monitored for their removal efficiency for geosmin and 2-MIB, and as expected, the removal efficiency decreased over time as the adsorption capacity of the GAC became exhausted. The removal efficiency was then shown to increase as more time passed, indicating the establishment of a biofilm that was capable of biodegrading geosmin and 2-MIB. Using fresh GAC, complete removal of both compounds were observed for the first 7 days, dropping off over a two week period until it was clear that the adsorptive capacity had been compromised. After 42 days, the removal efficiencies of geosmin and 2-MIB were 76% and 47% respectively. The removal efficiency was then shown to increase, reaching removals of 87% for geosmin and 63% for 2-MIB by day 55 of the experiment. This suggested that biofilms are able establish themselves and acclimatise to the presence of these T&O compounds resulting in enhanced biological removal. Further experiments showed that acclimatised biofilms were able to maintain high removal efficiencies during transient T&O events. The filters were run with a hydraulic loading rate (HLR) of 7.5 m h^{-1}, corresponding to an empty bed contact time (EBCT) of 5.6 min. In a follow-up study [16], BAC was compared to biologically active anthracite in their ability to remove geosmin and 2-MIB in bench scale filter columns. The study also investigated the effect of temperature, geosmin/2-MIB concentration and BOM concentration on the effectiveness of the two media types. Overall, BAC was found to be more effective in the removal of these T&O compounds. Additionally, higher temperatures (20°C cf. 8°C), higher BOM concentration and higher T&O concentration resulted in a greater percentage removal for geosmin and 2-MIB, although at higher temperatures, BOM concentration became less important. At the lowest T&O concentration investigated (25 ng L^{-1}), the removal efficiency at 20°C was enough to produce an effluent water with concentrations of geosmin and 2-MIB that were within the odour concentration threshold for these compounds. At higher concentrations (100 ng L^{-1}), removals were found to be 60% for geosmin and 40% for 2-MIB.

Persson *et al.* [17,18] investigated the role of biodegradation on the removal of geosmin and 2-MIB by comparing BAC with biologically active expanded clay (EC). The removal efficiency of the BAC filter was found to be very high (≥ 97%) at low concentrations of influent geosmin and 2-MIB (20 ng L^{-1}) with an EBCT of 30 min and it was found to outperform the EC filter. In order to assess the extent of biodegradation, the filters were dosed with sodium azide (NaN_3) in order to suppress biological activity. Following this, the extent of removal in the EC filter was shown to diminish markedly, while the removal efficiency of the BAC remained largely unchanged (≥ 96%). This suggested that adsorption of T&O compounds to the GAC surface was still playing a major role even though the GAC medium had been in use for almost four years. As such, the results concerning the extent of biodegradation on the BAC filter in this study are complicated by the fact that significant adsorption was also occurring. It was

concluded that the use of BAC as a filtration medium was the more viable option based on the added robustness the GAC provided with the added removal mechanism of adsorption coupled with biodegradation.

Drikas *et al.* [19], during a study of the removal of geosmin and 2-MIB using GAC filters, noted that the removal efficiency of both T&O compounds increased over time, rather than the expected decrease due to the exhaustion of the GAC adsorption sites. This was attributed to the development of a biofilm over the course of the experiment, with the GAC media removing geosmin and 2-MIB via both adsorption and biodegradation. It was also shown that longer EBCT's were more effective, with an EBCT of 5 min resulting in breakthrough of geosmin and 2-MIB.

Ndiongue *et al.* [20] compared fresh GAC filters with GAC that had been in service for 3 years at various concentrations of geosmin and 2-MIB and also investigated the effect of the EBCT. Overall it was found that at higher influent concentrations, the percentage removal was higher. Additionally, longer EBCTs afforded greater removal efficiencies (EBCT = 2.8, 3.4, 5.0 or 7.5 min), provided that the removal efficiency at the shortest EBCT was good. If the performance of the filter at low EBCTs was poor (< 20%), increasing the EBCT had reduced or no effect. This may have been influenced by prior experiments preloading the GAC and reducing the adsorption capacity prior to the longer EBCT experiments. For the used GAC filter (BAC) removals of geosmin increased from 38% to 78% while 2-MIB removal increased from 14% to 43% as the EBCT was increased. The fresh GAC filters were shown to be more effective at removing both compounds although none of the filters in this study were able to provide effluent water containing the compounds at levels below their respective odour concentration thresholds.

In a pilot scale study, Yang *et al.* [21] compared GAC with an O_3/BAC process and their respective efficiencies in removing geosmin and 2-MIB. GAC alone was found to remove 83.1% and 92.0% of geosmin and 2-MIB respectively compared with 100% and 96.3% for the O_3/BAC process. In this study, O_3 was applied preceeding the BAC filter which was operated with an EBCT of 27.1 min. The raw water in this study also suffered from problems associated with trihalomethanes (THMs), haloacetic acids (HAAs) and salt water intrusion (increased bromides and increased brominated disinfection by products) for which nano and ultrafiltration membranes were investigated in addition to GAC and O_3/BAC.

Other studies that investigate the use of biological removal by biofilms attached to other media (sand, anthracite, expanded clay, tube systems etc.) have also been shown to be effective in the removal of T&O compounds [11,16-18,22-26].

2.2 Biodegradation of cyanotoxins

In freshwater environments, cyanotoxins are produced by cyanobacteria (sometimes called blue-green algae) [5]. The most common types of cyanotoxins include microcystins (MC), cylindrospermopsins (CYN), anatoxins (ATX), saxitoxins (STX) and nodularin (NOD), although NOD is generally found in brackish waters [5,27]. The occurrence of cyanobacterial blooms may be dominated by a single species or contain several species and in both cases a range of toxic metabolites will be produced. Favourable conditions that can lead to blooms include; stagnant or low flow water conditions, warm water (15 – 30 ^oC), neutral to alkaline pH (6 – 9), and high nutrient content (eutrophic) [28]. All cyanotoxins are known to be amenable to biodegradation in natural waters, although there are some complications that may limit the effectiveness of BAC in the removal of these compounds [5]. The DWSNZ state "Provisional Maximum Acceptable Values" (PMAVs) for cyanotoxins in treated water as listed in Table [3]. In drinking water treatment, certain processes may increase the concentration of dissolved cyanotoxins due to the lysing of cell membranes causing intracellular cyanotoxins to become part of the bulk liquid. As such, processes like pre-ozonation that promote the lysing of cells prior to removing intact cells from solution, for example by sedimentation or sand filtration, should be avoided during cyanobacterial blooms [29].

Table 1: PMAVs for cyanotoxins as stated in the DWSNZ [3].

Toxin	PMAV (µg L^{-1})
Anatoxin-a	6.00
Anatoxin-a(S)	1.00
Homoanatoxin-a	2.00
Cylindrospermopsin	1.00
Microcystins*	1.00
Saxitoxins**	3.00

* as MC-LR equivalent concentration (see section 3.2.1)
** as STX equivalent concentration (see section 3.2.2)

Microcystins have been shown to be biodegraded in natural water sources [30-36] and a number of individual species of bacteria capable of degrading MCs have been isolated [37-39]. The enzymatic pathway of biodegradation for MC-LR in *Sphingomonas spp.* was first put forward by Bourne *et al.* [39,40], showing the process involved at least three hydrolytic enzymes. The initial site of hydrolytic cleavage was shown to be at the ADDA-Arg peptide bond, resulting in ring opening and the loss of toxicity. The biodegradation products were found to be nontoxic in mouse bioassays. Other researchers [38] have since postulated that alternative metabolic pathways exist for other bacterial species.

While not as extensively studied as MCs, biodegradation of cylindrospermopsin has been shown to occur in natural waters and sludges [35,36,41,42]. To date, no degradation pathway has be proposed, although it has been shown to be biodegraded by MC degrading bacteria [42]. It has been shown that the toxicity of this compound requires the uracil moiety to remain intact and that oxidation processes can cause ring cleavage, resulting in non-toxic products [43]; the oxidants investigated in this study were chlorine, chlorine dioxide, and chloramine.

Although information regarding the biodegradation of anatoxins is sparse, although there is some evidence to suggest it does occur in natural waters and sludges [5]. Anatoxin-a and homoanatoxin-a are known to degrade in sunlight and at high pH to yield non-toxic dihydro and epoxy products [44,45].

At present, very little information on the biodegradation of saxitoxins in natural aquatic environments is available [46] with most investigations focussing on marine bacteria [47-50]. A common theme in the biodegradation of saxitoxins is the transformation of less toxic variants to more toxic ones. For example, Kotaki *et al.* [46] showed that marine and freshwater bacteria transformed GTX2 and GTX3 into STX. Similar phenomena have been documented in BAC and other biofilter filter studies involving saxitoxins. It is also known that C-toxins (C1, C2 etc. Figure 4) spontaneously degrade to GTXs, causing waters contaminated with C-toxins to become more toxic over time as the concentration of GTX, and possibly STX, variants increase. Conversely, a more recent study, Ho *et al.* [35] concluded that saxitoxins (C1, C2, GTX2, GTX3, STX) were non-biodegradable in an Australian source water (Myponga Resevoir, South Australia) at 14 ^{o}C and 24 ^{o}C from batch biodegradation experiments. This indicated that the degradation of saxitoxins is dependent on local conditions and perhaps the bacterial species present

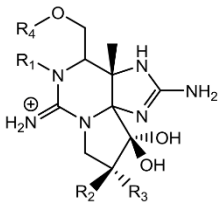

	Substituent Groups				
Toxin	R1	R2	R3	R4	TEF
STX	H	H	H	$CONH_2$	1.00
GTX2	H	H	OSO_3^-	$CONH_2$	0.40
GTX3	H	OSO_3^-	H	$CONH_2$	0.60
C1	H	H	OSO_3^-	$CONHSO_3^-$	0.01
C2	H	OSO_3^-	H	$CONHSO_3^-$	0.10
dcSTX	H	H	H	H	0.20
dcGTX2	H	H	OSO_3^-	H	0.40

Figure 4: General structure of saxitoxins, the substituents of some common analogues and their toxicity equivalency factors [5,51,52].

3 Quantitative analysis of cyanobacterial metabolites

In order to effectively monitor the presence of cyanobacterial metabolites in environmental samples and the performance of technologies designed for their removal from drinking water, there is a strong reliance on sensitive and robust quantitative analytical methods. Certain properties of these metabolites, such as their very low concentration, high solubility or high number of potential analogues, can pose significant challenges in developing suitable, yet practical methods.

3.1 Quantitative analysis of geosmin and 2-methylisoborneol

Quantitative analysis of geosmin and 2-MIB can be achieved with good accuracy and very low limits of detection (LOD) by employing the use of gas chromatography-mass spectrometry (GC-MS), which is the dominant chromatographic technique used in the quantitative analysis of these and other T&O compounds. Due to the very low odour concentration threshold (OCT) in humans for these types of chemicals (Table 2), the analytical method employed in the monitoring of processes designed to remove T&O compounds during drinking water treatment requires an LOD equal to, or preferably lower than, the OCT in order to ascertain as to whether the removal technology is performing acceptably. With GC-MS being by far the preferred instrumental technique, analytical methods in this area mainly differ in sample preparation and extraction methods.

Table 2: Odour concentration threshold values for geosmin and 2-MIB [53].

Compound	Odour concentration threshold (ng L^{-1})
Geosmin	6-10
2-MIB	2-20

Table 3: Chromatographic techniques, extraction methods and limits of detection for analytical methods employed in the monitoring of 2-MIB and geosmin.

Separation and Detection	Extraction Method*	Limit of Detection (ng L^{-1}) 2-MIB	Geosmin	Reference
GC-MS	CLS	0.80	0.80	*[54]*
GC-FID/ECD	CLS	-	-	*[55]*
GC-MS	LLE	20	20	*[56]*
GC-MS	CLS	-	-	*[57]*
GC-IT-MS	LLME	1.00	1.00	*[58]*
GC-CI/EI-IT-MS	SPME	1.00	1.00	*[59]*
GC-MS	SBSE	0.33	0.15	*[60]*
GC-MS	Ambersorb 572	1.00	1.00	*[61]*
GC-MS	SPE	0.10	0.10	*[62]*
GC-MS	LLME	0.10	0.10	*[63]*
GC-MS	SHS	0.36	0.14	*[64]*
GC-MS	SPME	0.59-0.66	0.44-0.49	*[65]*
GC-MS	SPME	0.15	0.16	*[66]*
GC-MS	PT	1.00	2.00	*[67]*
GC-MS	LVI-LLE	0.34	0.05	*[68]*
GC-MS	SPME	5.10	1.50	*[69]*
GC-MS	LLE	5.00	1.00	*[70]*
GC-MS	SPME	1.00	1.00	*[71]*
GC-MS	PT/SPE	0.87-1.00	0.50-0.62	*[72]*
GC-MS	USAD-LLME	9.00	5.00	*[73]*
GC-MS	PT	1.40	0.08	*[74]*
GC-MS	LLME	1.00	1.10	*[75]*
GC-MS/MS	SPME	8.00-20.00	0.10-2.00	*[76]*
GC-IT-MS/MS	SPME	1.40	0.40	*[77]*
GC-MS	SPME	0.25	0.58	*[78]*
GC-MS	SPE	0.50	0.50	*[79]*
GC-MS	SPME	0.60	0.40	*[80]*
GC-MS	SPME	0.13	0.04	*[81]*
GC-MS	SPME	4.12	3.60	*[82]*
GC-MS	SPME	0.50	0.20	*[83]*
GC-MS	SPME	0.50	0.20	*[84]*
GC-MS	NED	0.50	1.50	*[85]*
GC-MS/MS	SPE	5.50	0.90	*[86]*
GC-MS	HF-LPME	1.30	1.90	*[87]*

* CLS = Closed Loop Stripping; LLE = Liquid-Liquid Extraction; SPME = Solid Phase Micro-extraction; SBSE = Stir-Bar Sorptive Extraction; SPE = Solid Phase Extraction; LLME = Liquid-Liquid Micro-extraction; PT = Purge and Trap; LVI = Large Volume Injection Liquid Liquid Extraction; USAD = Ultrasound Assisted Dispersive; NED = Needle-Like Extraction Device; HF-LMPE = Hollow-Fiber Liquid-Phase Microextraction.

Due to the semi-volatile nature of both geosmin and MIB, headspace GC-MS analysis by solid phase micro-extraction (SPME) has been the method of choice for many researchers in this field of study *[59,65,69,71,76-83,88]*. However, the use of SPME requires the use of expensive extraction fibres, gives long sample turn-around times and requires manual injection of the sample into the GC if a specialised auto-sampler is not available. Other methods such as those that employ closed loop stripping as the extraction method suffer from similar drawbacks, with analysis being even more cumbersome and time consuming *[54,55,57]*. Similarly, purge and trap (PT) extractions requires specialized apparatus *[67,74]*.

Other extraction methods include stir-bar sorptive extraction (SBSE) *[60]*, static headspace (SHS) extraction *[64]* and needle-like extraction devices (NED) *[85]* which are based upon adsorption of the analyte to activated carbon packed needles. Again, these methods all require specialised equipment.

In efforts to reduce analysis times without resorting to expensive consumables and apparatus, a range of liquid-liquid micro-extraction (LLME) methods have been developed *[58,63,68,70,73,75,87]*. In

general, these methods involve the partitioning of the target analytes from a water sample into a small volume of organic extracting solvent (e.g. pentane or tetrachloroethylene) by salting out the aqueous phase with high concentrations of inorganic salts (e.g. NaCl and K_2HPO_4), mechanical agitation, dispersion using a co-solvent or some combination of these techniques. These methods have the advantage of not requiring special auto-samplers like SMPE, which makes the analysis of large numbers of samples more feasible with the use of a standard auto-sampler. The use of organic solvents may be regarded as a disadvantage, but the volumes used are typically very small (3-1000 µL). Similarly, methods that employ solid phase extraction (SPE) also do not require specialised auto-samplers, but require numerous consumable SPE cartridges and can require quite large amounts of solvent *[62,72,79,86]*.

Of the methods that have been developed to date, LODs are acceptable for most extraction procedures. Hence, the choice of method can be made based upon the available instrumentation or other restrictions regarding available apparatus or consumables. As many of these methods are also applicable to other T&O compounds the specific needs of the analysis (fitness of purpose) also need to be considered. A summary of analytical methods available in the literature is presented in Table 3.

3.2 Quantitative analysis of cyanotoxins

Quantitative analysis of cyanotoxins is usually achieved through the use of High Performance Liquid Chromatography (HPLC) with either MS (LC-MS) or Fluorescence detection (LC-FLD) depending on the class of the target cyanotoxin. These analytical techniques are known to provide good selectivity and low limits of detection. Other methods include mouse bioassays and various enzyme-linked immunosorbent assays (ELISA). However, while being simple to perform, these methods can suffer from numerous technical issues such as poor sensitivity, reproducibility, interferences, and false positive results *[52,89]*. A range of analytical methods are summarised in Table 4 *[52,90-104]*.

3.2.1 Microcystins, cylindrospermopsins and anatoxins

These cyanotoxins are usually quantified in aquatic environments using LC-MS or LC-MS/MS. In order to remove matrix effects and interferences, sample preparation usually involves some kind of SPE protocol. While early methods could only screen for single toxins or classes of toxin, recent developments allow for the analysis of multiple toxins simultaneously. However, due to the vast number of cyanotoxin analogues, particularly MCs, and the high cost of analytical standards, analysing each individual compound can either be an unfeasible or financially prohibitive task. In such cases, a small number of the most common analogues from a subgroup can be analysed and taken as an estimate of the total subgroup concentration. This is often the case with microcystins, for which the concentration is often reported as the MC-LR equivalent concentration. This is generally less problematic for ATXs and CYNs, as the number of known analogues is low and each can be quantified directly.

3.2.2 Saxitoxins

Saxitoxins require a separate quantitative chromatographic method from other cyanotoxins due to the unique challenges associated with this class of toxins. Due to their highly polarity (zwitterionic), the retention of these compounds on traditional reversed phase (usually octadecylsilane; C18) columns is very poor. In order to overcome this, chromatography is achieved using an ion-pairing reagent. The drawback of this is that it precludes the use of MS detection due to the severe signal suppression that occurs in the presence of ion-pairing reagents. As the detection of these compounds requires very low limits of detection, one way of overcoming this is to employ fluorescence detection. However, STXs do not possess functional groups that exhibit fluorescence. This requires either pre- or post-column oxidation (periodic acid, hydrogen peroxide or tert-butyl-peroxide) in order to yield reaction products that exhibit fluorescence. More recently, the use of hydrophilic interaction liquid chromatography (HILIC) has allowed for successful chromatography of STXs without the need for ion-pairing reagents which allows the use of sensitive MS detection. This removes the need for pre/post oxidation of STX's while still providing low limits of detection. As with MCs, a large number of STX analogues exist and analytical standards are expensive. Although methods exist to analyse many of these analogues, this is not always feasible or practical.

Table 4: Chromatographic techniques, extraction methods and limits of detection for analytical methods employed in the monitoring of cyanotoxins.

Separation	Detection	Toxins	LOD (ppb)	Extraction	Reference
RP PLRP-S Gradient*	ESI-MS	ATX, MCs	0.4 - 0.5	SPE	*[90]*
CEX+AEX Gradient*	FLD + ESI-MS	STXs	0.5 - 2	LSE + Filtration	*[91]*
RP C18 Gradient	Pre-oxidation FLD	STXs	20 - 100	SPE	*[92]*
RP C18 Gradient	Post-oxidation FLD	STXs	0.014 - 0.820	LSE + Filtration	*[93]*
HILIC Amide Gradient	ESI-MS/MS	STXs	0.1 - 101.2	HILIC SPE	*[94]*
RP C18 Gradient	ESI-MS/MS	MCs	0.01 - 0.03	SPE	*[95]*
RP C18 Gradient	ESI-MS/MS	MCs, ATX, CYN	0.17 - 0.21	Filtration	*[96]*
RP C18 Gradient	ESI-MS	MCs, ATX, CYN, NOD	0.002 - 0.1	SPE	*[97]*
HILIC Amide Gradient	ESI-MS/MS	STXs, ATX, CYN	0.002 - 0.527	LSE	*[98]*
RP C18 Gradient	ESI-MS/MS	MCs, NOD	0.002 - 0.527	LSE	*[98]*
RP C18 Gradient	Pre-oxidation FLD	STXs	0.5 - 13	LSE	*[99]*
RP C18 Gradient	ESI-MS/MS	MCs	0.0158 - 0.0317	SPE	*[100]*
RP C18 Gradient	UV-DAD	MC-LR	100	SPE	*[101]*
HILIC Amide Gradient	ESI-MS/MS	STXs	0.03 - 1.17	LSE + GC-SPE	[52]
RP C18 Gradient	ESI-MS/MS	MCs, ATX,CYN	0.01 - 0.02	SPE	*[102]*
RP C18 Gradient	ESI-MS/MS	MCs	0.01 - 0.012	ASE-SPE	*[103]*
RP C18 Gradient	ESI-MS/MS	MCs, ATX, CYN, NOD	0.1 - 0.5	Filtration + LVI	*[104]*

* PLRP-S = Polymeric Reversed Phase; CEX = Cation Exchange; AEX = Anion Exchange

4 Summary

As cyanobacterial metabolites are susceptible to biodegradation, it follows that their removal from drinking water using biological filtration such as BAC should be feasible, as evidenced by the extensive work in the area of taste and odour removal. However, the literature surrounding the removal of cyanotoxins is less well developed, and in some cases indicates that the use of biological filtration may prove detrimental. As Hamilton's BAC filters were implemented to address cyanobacterial metabolites specifically, a current assessment of the system is warranted. This research will aim to assess the current performance of Hamilton's full scale BAC filters alongside laboratory and pilot scale studies that will investigate biofilm kinetics, biofilm populations and characterisation, metabolic transformations of specific compounds and methods of improving the overall process including advanced oxidation processes (AOPs). It is hoped that this will provide added insight into the operation and performance of full scale BAC filters and expand on the current knowledge on the biodegradation of cyanobacterial metabolites at the molecular and biochemical level.

5 References

1. Collier, J. C.; Hamilton, D. P.; Vant, W. N.; Howard-Williams, C. Ed. *The Waters of the Waikato: Ecology of New Zealand's Longest River.* Environment Waikato and the Centre for Bioiversity and Ecology Research (The University of Waikato): Hamilton, New Zealand, 2010.
2. Hamilton City Council. River to the Tap: A guide to Hamilton's Water Supply. http://www.hamilton.govt.nz/our-services/water/water/Documents/RIVER%20TO%20TAP%20FOR%20WEB.pdf (accessed 23 October 2015)
3. Ministry of Health Drinking-Water Standards for New Zealand 2005 (Revised 2008). Government of New Zealand: Wellington (NZ), 2008.

4. Kouzminov, A.; Ruck, J.; Wood, S. A. New Zealand risk management approach for toxic cyanobacteria in drinking water. *Aust. N.Z. J. Public Health* **2007**, *31*, 275-281.
5. Ho, L.; Sawade, E.; Newcombe, G. Biological treatment options for cyanobacteria metabolite removal – A review. *Water Res.* **2012**, *46*, 1536-1548.
6. Clark, A.; Mullan, B.; Porteous, A. "Scenarios of Regional Drought under Climate Change," NIWA, 2011.
7. Cecen, F.; Aktas, O. *Activated Carbon for Water and Wastewater Treatment: Integration of Adsorption and Biological Treatment*; Wiley-VCH: Weinheim, Germany, 2012.
8. American Water Works Association *Water Quality and Treatment: A Handbook of Community Water Supplies. 5th Ed*; McGraw-Hill Publishing Co., 1999.
9. Digiano, F. A. Adsorption of Organic Substances in Drinking Water. In *Control of Organic Substances in Water and Wastewater*; B. B. Berger, Ed.; Noyes Data Corporation: NJ, USA, 1987.
10. Zhu, I. X.; Getting, T.; Bruce, D. Review of biologically active filters in drinking water applications. *J. - Am. Water Works Assoc.* **2010**, *102*, 67-77.
11. Rittmann, B. E., Gantzer, C.J., Montiel, A. Biological treatment to control taste-and-odor compounds in drinking water treatment. In *Advances in Taste-and-Odor Treatment and Control*; I. H. Suffet, Mallevialle, J., Kawczynski, E. , Ed.; American Water Works Association Research Foundation: Denver, USA, 1995; pp 290-246.
12. Yagi, M.; Nakashima, S.; Muramoto, S. Biological degradation of musty odor compounds, 2-methylisoborneol and geosmin, in a bio-activated carbon filter. *Water Sci. Technol.* **1988**, *20*, 255-260.
13. Hrudey, S. E.; Huck, P. M.; Mitton, M. J.; Kenefick, S. L. Evaluation of odor removal by pilot-scale biological treatment process trains during spring runoff in an ice-covered river. *Water Sci. Technol.* **1995**, *31*, 195-201.
14. Nerenberg, R.; Rittmann, B. E.; Soucie, W. J. Ozone/biofiltration for removing MIB and geosmin. *J. - Am. Water Works Assoc.* **2000**, *92*, 85-95.
15. Elhadi, S. L. N.; Huck, P. M.; Slawson, R. M. Removal of geosmin and 2-methylisoborneol by biological filtration. *Water Sci. Technol.* **2004**, *49*, 273-280.
16. Elhadi, S. L. N.; Huck, P. M.; Slawson, R. M. Factors affecting the removal of geosmin and MIB in drinking water biofilters. *J. - Am. Water Works Assoc.* **2006**, *98*, 108-119.
17. Uhl, W., Persson, F., Heinicke, G., Hermansson, M., and Hedberg, T. Removal of geosmin and MIB in biofilters-on the role of biodegradation and adsorption. In *Recent progress in slow sand and alternative biofiltration processes*; R. Gimbel; N. Graham and M. R. Collins, Eds.; IWA Publishing: London, UK, 2006.
18. Persson, F.; Heinicke, G.; Hedberg, T.; Hermansson, M.; Uhl, W. Removal of geosmin and MIB by biofiltration - an investigation discriminating between adsorption and biodegradation. *Environ. Technol.* **2007**, *28*, 95-104.
19. Drikas, M.; Dixon, M.; Morran, J. Removal of MIB and geosmin using granular activated carbon with and without MIEX pre-treatment. *Water Res.* **2009**, *43*, 5151-5159.
20. Ndiongue, S.; Anderson, W. B.; Tadwalkar, A.; Rudnickas, J.; Lin, M.; Huck, P. M. Using pilot-scale investigations to estimate the remaining geosmin and MIB removal capacity of full-scale GAC-capped drinking water filters. *Water Qual. Res. J. Can.* **2006**, *41*, 296-306.
21. Yang, J.-S.; Yuan, D.-X.; Weng, T.-P. Pilot study of drinking water treatment with GAC, O3/BAC and membrane processes in Kinmen Island, Taiwan. *Desalination* **2010**, *263*, 271-278.
22. Hattori, K. Water treatment systems and technology for the removal of odor compounds. *Water Sci. Technol.* **1988**, *20*, 237-244.
23. Lundgren, B. V.; Grimvall, A.; Saevenhed, R. Formation and removal of off-flavor compounds during ozonation and filtration through biologically active sand filters. *Water Sci. Technol.* **1988**, *20*, 245-253.
24. Urfer, D.; Huck, P. M.; Booth, S. D. J.; Coffey, B. M. Biological filtration for BOM and particle removal: a critical review. *J. - Am. Water Works Assoc.* **1997**, *89*, 83-98.
25. Ho, L.; Hoefel, D.; Bock, F.; Saint, C. P.; Newcombe, G. Biodegradation rates of 2-methylisoborneol (MIB) and geosmin through sand filters and in bioreactors. *Chemosphere* **2007**, *66*, 2210-2218.
26. McDowall, B.; Hoefel, D.; Newcombe, G.; Saint, C. P.; Ho, L. Enhancing the biofiltration of geosmin by seeding sand filter columns with a consortium of geosmin-degrading bacteria. *Water Res.* **2009**, *43*, 433-440.
27. World Health Organization *Toxic Cyanobacteria in Water: A Guide to their Public Health Consequences, Monitoring and Managment*, 1st ed.; E & FN Spon: London, 1999.
28. Clark, S.; Smith, D. W. Cyanobacteria toxins and the current state of knowledge on water treatment options: a review. *J. Environ. Eng. Sci.* **2004**, *3*, 155-185.
29. Merel, S.; Walker, D.; Chicana, R.; Snyder, S.; Baurès, E.; Thomas, O. State of knowledge and concerns on cyanobacterial blooms and cyanotoxins. *Environ. Int.* **2013**, *59*, 303-327.
30. Cousins, I. T.; Bealing, D. J.; James, H. A.; Sutton, A. Biodegradation of microcystin-LR by indigenous mixed bacterial populations. *Water Res.* **1996**, *30*, 481-485.
31. Jones, G. J.; Negri, A. P. Persistence and degradation of cyanobacterial paralytic shellfish poisons (PSPs) in freshwaters. *Water Res.* **1997**, *31*, 525-533.
32. Christoffersen, K.; Lyck, S.; Winding, A. Microbial activity and bacterial community structure during degradation of microcystins. *Aquat. Microb. Ecol.* **2002**, *27*, 125-136.
33. Holst, T.; Jorgensen, N. O. G.; Jorgensen, C.; Johansen, A. Degradation of microcystin in sediments at oxic and anoxic, denitrifying conditions. *Water Res.* **2003**, *37*, 4748-4760.
34. Bourne, D. G.; Blakeley, R. L.; Riddles, P.; Jones, G. J. Biodegradation of the cyanobacterial toxin microcystin LR in natural water and biologically active slow sand filters. *Water Res.* **2006**, *40*, 1294-1302.
35. Ho, L.; Tang, T.; Monis, P. T.; Hoefel, D. Biodegradation of multiple cyanobacterial metabolites in drinking water supplies. *Chemosphere* **2012**, *87*, 1149-1154.

36. Maghsoudi, E.; Fortin, N.; Greer, C.; Duy, S. V.; Fayad, P.; Sauvé, S.; Prévost, M.; Dorner, S. Biodegradation of multiple microcystins and cylindrospermopsin in clarifier sludge and a drinking water source: Effects of particulate attached bacteria and phycocyanin. *Ecotoxicol. Environ. Saf.* **2015**, *120*, 409-417.
37. Hu, L. B.; Yang, J. D.; Zhou, W.; Yin, Y. F.; Chen, J.; Shi, Z. Q. Isolation of a Methylobacillus sp that degrades microcystin toxins associated with cyanobacteria. *N. Biotechnol.* **2009**, *26*, 205-211.
38. Manage, P. M.; Edwards, C.; Singh, B. K.; Lawton, L. A. Isolation and identification of novel microcystin-degrading bacteria. *Appl. Eviron. Microbiol.* **2009**, *75*, 6924-6928.
39. Bourne, D. G.; Jones, G. J.; Blakeley, R. L.; Jones, A.; Negri, A. P.; Riddles, P. Enzymatic pathway for the bacterial degradation of the cyanobacterial cyclic peptide toxin microcystin LR. *Appl. Eviron. Microbiol.* **1996**, *62*, 4086-4094.
40. Bourne, D. G.; Riddles, P.; Jones, G. J.; Smith, W.; Blakeley, R. L. Characterisation of a gene cluster involved in bacterial degradation of the cyanobacterial toxin microcystin LR. *Environ. Tox.* **2001**, *16*, 523-534.
41. Smith, M. J.; Shaw, G. R.; Eaglesham, G. K.; Ho, L.; Brookes, J. D. Elucidating the factors influencing the biodegradation of cylindrospermopsin in drinking water sources. *Environ. Tox.* **2008**, *23*, 413-421.
42. Mohamed, Z. A.; Alamri, S. A. Biodegradation of cylindrospermopsin toxin by microcystin-degrading bacteria isolated from cyanobacterial blooms. *Toxicon* **2012**, *60*, 1390-1395.
43. Banker, R.; Carmeli, S.; Werman, M.; Teltsch, B.; Porat, R.; Sukenik, A. Uracil moiety is required for toxicity of the cyanobacterial hepatotoxin cylindrospermopsin. *J. Toxicol. Environ. Health A* **2001**, *62*, 281-288.
44. James, K. J.; Furey, A.; Sherlock, I. R.; Stack, M. A.; Twohig, M.; Caudwell, F. B.; Skulberg, O. M. Sensitive determination of anatoxin-a, homoanatoxin-a and their degradation products by liquid chromatography with fluorimetric detection. *J. Chromatogr. A* **1998**, *798*, 147-157.
45. James, K. J.; Crowley, J.; Hamilton, B.; Lehane, M.; Skulberg, O.; Furey, A. Anatoxins and degradation products, determined using hybrid quadrupole time-of-flight and quadrupole ion-trap mass spectrometry: Forensic investigations of cyanobacterial neurotoxin poisoning. *Rapid Commun. Mass Spectrom.* **2005**, *19*, 1167-1175.
46. Kotaki, Y. Screening of bacteria which convert gonyautoxin 2, 3 to saxitoxin. *Nippon Suisan Gakk.* **1989**, *55*, 1293-1293.
47. Smith, E. A.; Grant, F.; Ferguson, C. M. J.; Gallacher, S. Biotransformations of paralytic shellfish toxins by bacteria isolated from bivalve molluscs. *Appl. Environ. Microbiol.* **2001**, *67*, 2345-2353.
48. Vasama, M.; Kumar, H.; Salminen, S.; Haskard, C. A. Removal of paralytic shellfish toxins by probiotic lactic acid bacteria. *Toxins* **2014**, *6*, 2127-2136.
49. Donovan, C. J.; Ku, J. C.; Quilliam, M. A.; Gill, T. A. Bacterial degradation of paralytic shellfish toxins. *Toxicon* **2008**, *52*, 91-100.
50. Kotaki, Y.; Oshima, Y.; Yasumoto, T. Bacterial transformation of paralytic shellfish toxins in coral reef crabs and a marine snail. *Nippon Suisan Gakk.* **1985**, *51*, 1009-1013.
51. Quilliam, M. A.; Janecek, M.; Lawrence, J. F. Characterization of the oxidation products of paralytic shellfish poisoning toxins by liquid chromatography/mass spectrometry. *Rapid Commun. Mass Spectrom.* **1993**, *7*, 482-487.
52. Boundy, M. J.; Selwood, A. I.; Harwood, D. T.; McNabb, P. S.; Turner, A. D. Development of a sensitive and selective liquid chromatography–mass spectrometry method for high throughput analysis of paralytic shellfish toxins using graphitised carbon solid phase extraction. *J. Chromatogr. A* **2015**, *1387*, 1-12.
53. Omur-Ozbek, P.; Little, J. C.; Dietrich, A. M. Ability of humans to smell geosmin, 2-MIB and nonadienal in indoor air when using contaminated drinking water. *Water Sci. Technol.* **2007**, *55*, 249-256.
54. Hwang, C. J.; Krasner, S. W.; McGuire, M. J.; Moylan, M. S.; Dale, M. S. Determination of subnanogram-per-liter levels of earthy-musty odorants in water by the salted closed-loop stripping method. *Environ. Sci. Technol.* **1984**, *18*, 535-539.
55. Jüttner, F. Dynamics of the volatile organic substances associated with cyanobacteria and algae in a eutrophic shallow lake. *Appl. Eviron. Microbiol.* **1984**, *47*, 814-820.
56. Brownlee, B. G.; Gammie, L.; Gummer, W. D.; MacInnis, G. A. A simple extraction procedure for moderately volatile taste and odor compounds such as geosmin and 2-methylisoborneol - method and applications. *Water Sci. Technol.* **1988**, *20*, 91-97.
57. Hayes, K. P.; Burch, M. D. Odorous compounds associated with algal blooms in South Australian waters. *Water Res.* **1989**, *23*, 115-121.
58. Bao, M.-L.; Barbieri, K.; Burrini, D.; Griffini, O.; Pantani, F. Determination of trace levels of taste and odor compounds in water by microextraction and gas chromatography-ion-trap detection-mass spectrometry. *Water Res.* **1997**, *31*, 1719-1727.
59. McCallum, R.; Pendleton, P.; Schumann, R.; Trinh, M.-U. Determination of geosmin and 2-methylisoborneol in water using solid-phase microextraction and gas chromatography-chemical ionization/electron impact ionization-ion-trap mass spectrometry. *Analyst* **1998**, *123*, 2155-2160.
60. Nakamura, S.; Nakamura, N.; Ito, S. Determination of 2-methylisoborneol and geosmin in water by gas chromatography-mass spectrometry using stir bar sorptive extraction. *J. Sep. Sci.* **2001**, *24*, 674-677.
61. Palmentier, J. P. F. P.; Taguchi, V. Y. The determination of six taste and odour compounds in water using Ambersorb 572 and high resolution mass spectrometry. *Analyst* **2001**, *126*, 840-845.
62. Ikai, Y.; Honda, S.; Yamada, N.; Onuma, S.; Tomita, B.-i.; Kawamura, N.; Miyazaki, Y. Determination of geosmin and 2-methylisoborneol in water using solid phase extraction and headspace-GC/MS. *J. Mass. Spectrom. Soc. Jpn.* **2003**, *51*, 174-178.
63. Shin, H.-S.; Ahn, H.-S. Simple, rapid, and sensitive determination of odorous compounds in water by GC-MS. *Chromatographia* **2004**, *59*, 107-113.

64. Nakamura, S.; Sakui, N.; Tsuji, A.; Daishima, S. Determination of 2-methylisoborneol and geosmin in aqueous samples by static headspace-gas chromatography-mass spectrometry with ramped inlet pressure. *J. Sep. Sci.* **2005**, *28*, 2511-2516.
65. Sung, Y.-H.; Li, T.-Y.; Huang, S.-D. Analysis of earthy and musty odors in water samples by solid-phase microextraction coupled with gas chromatography/ion trap mass spectrometry. *Talanta* **2005**, *65*, 518-524.
66. Zhang, L.; Hu, R.; Yang, Z. Simultaneous picogram determination of "earthy-musty" odorous compounds in water using solid-phase microextraction and gas chromatography–mass spectrometry coupled with initial cool programmable temperature vaporizer inlet. *J. Chromatogr. A* **2005**, *1098*, 7-13.
67. Salemi, A.; Lacorte, S.; Bagheri, H.; Barceló, D. Automated trace determination of earthy-musty odorous compounds in water samples by on-line purge-and-trap–gas chromatography–mass spectrometry. *J. Chromatogr. A* **2006**, *1136*, 170-175.
68. Zhang, L.; Hu, R.; Yang, Z. Routine analysis of off-flavor compounds in water at sub-part-per-trillion level by large-volume injection GC/MS with programmable temperature vaporizing inlet. *Water Res.* **2006**, *40*, 699-709.
69. Boutou, S.; Chatonnet, P. Rapid headspace solid-phase microextraction/gas chromatographic/mass spectrometric assay for the quantitative determination of some of the main odorants causing off-flavours in wine. *J. Chromatogr. A* **2007**, *1141*, 1-9.
70. Ma, X.; Gao, N.; Chen, B.; Li, Q.; Zhang, Q.; Gu, G. Detection of geosmin and 2-methylisoborneol by liquid-liquid extraction-gas chromatograph mass spectrum (LLE-GCMS) and solid phase extraction-gas chromatograph mass spectrum (SPE-GCMS). *Front. Environ. Sci. Eng.* **2007**, *1*, 286-291.
71. Chang, J.; Biniakewitz, R.; Harkey, G. Determination of geosmin and 2-MIB in drinking water by SPME-PTV-GC-MS. *LC-GC Eur.* **2008**, 11-12.
72. Sibali, L. L.; Schoeman, C.; Morobi, J. S.; Molalatladi, B. S. Comparison of two selective methods for determination of geosmin (1,2,7,7-tetramethyl-2-norborneol) and 2-MIB (2-methylisoborneol) in drinking and raw water samples by capillary gas chromatography-mass spectrometry. *Water Qual. Res. J. Can.* **2010**, *45*, 491-497.
73. Cortada, C.; Vidal, L.; Canals, A. Determination of geosmin and 2-methylisoborneol in water and wine samples by ultrasound-assisted dispersive liquid-liquid microextraction coupled to gas chromatography-mass spectrometry. *J. Chromatogr. A* **2011**, *1218*, 17-22.
74. Deng, X.; Liang, G.; Chen, J.; Qi, M.; Xie, P. Simultaneous determination of eight common odors in natural water body using automatic purge and trap coupled to gas chromatography with mass spectrometry. *J. Chromatogr. A* **2011**, *1218*, 3791-3798.
75. Ma, J.; Lu, W.; Li, J.; Song, Z.; Liu, D.; Chen, L. Determination of geosmin and 2-methylisoborneol in water by headspace liquid-phase microextraction coupled with gas chromatography-mass spectrometry. *Anal. Lett.* **2011**, *44*, 1544-1557.
76. Machado, S.; Gonçalves, C.; Cunha, E.; Guimarães, A.; Alpendurada, M. F. New developments in the analysis of fragrances and earthy–musty compounds in water by solid-phase microextraction (metal alloy fibre) coupled with gas chromatography–(tandem) mass spectrometry. *Talanta* **2011**, *84*, 1133-1140.
77. Parinet, J.; Rodriguez, M. J.; Serodes, J.; Proulx, F. Automated analysis of geosmin, 2-methyl-isoborneol, 2-isopropyl-3-methoxypyrazine, 2-isobutyl-3-methoxypyrazine and 2,4,6-trichloroanisole in water by SPME-GC-ITDMS/MS. *Int. J. Environ. Anal. Chem.* **2011**, *91*, 505-515.
78. Ma, K.; Zhang, J. N.; Zhao, M.; He, Y. J. Accurate analysis of trace earthy-musty odorants in water by headspace solid phase microextraction gas chromatography-mass spectrometry. *J. Sep. Sci.* **2012**, *35*, 1494-1501.
79. Sun, W.; Jia, R.; Gao, B. Simultaneous analysis of five taste and odor compounds in surface water using solid-phase extraction and gas chromatography-mass spectrometry. *Front. Environ. Sci. Eng.* **2012**, *6*, 66-74.
80. Chen, X.; Luo, Q.; Yuan, S.; Wei, Z.; Song, H.; Wang, D.; Wang, Z. Simultaneous determination of ten taste and odor compounds in drinking water by solid-phase microextraction combined with gas chromatography-mass spectrometry. *J. Environ. Sci.* **2013**, *25*, 2313-2323.
81. Peng, S.; Ding, Z.; Xia, W.; Zheng, H.; Xia, Y.; Chen, X. Orthogonal design study on factors affecting the determination of common odors in water samples by headspace solid-phase microextraction coupled to GC/MS. *J. Anal. Methods Chem.* **2013**, 340658, 340610 pp.
82. Yuan, B.; Li, F.; Xu, D.; Fu, M.-L. Comparison of two methods for the determination of geosmin and 2-methylisoborneol in algae samples by stable isotope dilution assay through purge-and-trap or headspace solid-phase microextraction combined with GC/MS. *Anal. Methods* **2013**, *5*, 1739-1746.
83. Ding, Z.; Peng, S.; Xia, W.; Zheng, H.; Chen, X.; Yin, L. Analysis of five earthy-musty odorants in environmental water by HS-SPME/GC-MS. *Int. J. Anal. Chem.* **2014**, *2014*, 11.
84. Peng, S.; Ding, Z.; Zhao, L.; Fei, J.; Xuan, Z.; Huang, C.; Chen, X. Determination of seven odorants in purified water among worldwide brands by HS-SPME coupled to GC–MS. *Chromatographia* **2014**, *77*, 729-735.
85. Ueta, I.; Mitsumori, T.; Kawakubo, S.; Saito, Y. Determination of musty-odor compounds in water by gas chromatography-mass spectrometry with a needle-type sample-preparation device. *Anal. Sci.* **2014**, *30*, 979-983.
86. Wright, E.; Daurie, H.; Gagnon, G. A. Development and validation of an SPE-GC-MS/MS taste and odour method for analysis in surface water. *Int. J. Environ. Anal. Chem.* **2014**, *94*, 1302-1316.
87. Yu, S.; Xiao, Q.; Zhu, B.; Zhong, X.; Xu, Y.; Su, G.; Chen, M. Gas chromatography–mass spectrometry determination of earthy–musty odorous compounds in waters by two phase hollow-fiber liquid-phase microextraction using polyvinylidene fluoride fibers. *J. Chromatogr. A* **2014**, *1329*, 45-51.
88. Lin, T.-F.; Liu, C.-L.; Yang, F.-C.; Hung, H.-W. Effect of residual chlorine on the analysis of geosmin, 2-MIB and MTBE in drinking water using the SPME technique. *Water Res.* **2003**, *37*, 21-26.

89. Kaushik, R.; Balasubramanian, R. Methods and Approaches Used for Detection of Cyanotoxins in Environmental Samples: A Review. *Crit. Rev. Env. Sci. Technol.* **2013**, *43*, 1349-1383.
90. Hormazabal, V.; Ostensvik, O.; Underdal, B.; Skulberg, O. M. Simultaneous determination of the cyanotoxins anatoxin a, microcystin desmethyl-3, LR, RR, and YR in fish muscle using liquid chromatography-mass spectrometry. *J. Liq. Chromatogr. Relat. Technol.* **2000**, *23*, 185-196.
91. Jaime, E.; Hummert, C.; Hess, P.; Luckas, B. Determination of paralytic shellfish poisoning toxins by high-performance ion-exchange chromatography. *J. Chromatogr. A* **2001**, *929*, 43-49.
92. Lawrence, J. F.; Niedzwiadek, B. Quantitative determination of paralytic shellfish poisoning toxins in shellfish by using prechromatographic oxidation and liquid chromatography with fluorescence detection. *J. AOAC Int.* **2001**, *84*, 1099-1108.
93. Diener, M.; Erler, K.; Hiller, S.; Christian, B.; Luckas, B. Determination of paralytic shellfish poisoning (PSP) toxins in dietary supplements by application of a new HPLC/FD method. *Eur. Food. Res. Technol.* **2006**, *224*, 147-151.
94. Turrell, E.; Stobo, L.; Lacaze, J.-P. Optimization of hydrophilic interaction liquid chromatography/mass spectrometry and development of solid-phase extraction for the determination of paralytic shellfish poisoning toxins. *J. AOAC Int.* **2008**, *91*, 1372-1386.
95. Mekebri, A.; Blondina, G. J.; Crane, D. B. Method validation of microcystins in water and tissue by enhanced liquid chromatography tandem mass spectrometry. *J. Chromatogr. A* **2009**, *1216*, 3147-3155.
96. Oehrle, S. A.; Southwell, B.; Westrick, J. Detection of various freshwater cyanobacterial toxins using ultra-performance liquid chromatography tandem mass spectrometry. *Toxicon* **2010**, *55*, 965-972.
97. Yen, H.-K.; Lin, T.-F.; Liao, P.-C. Simultaneous detection of nine cyanotoxins in drinking water using dual solid-phase extraction and liquid chromatography-mass spectrometry. *Toxicon* **2011**, *58*, 209-218.
98. Lajeunesse, A.; Segura, P. A.; Gelinas, M.; Hudon, C.; Thomas, K.; Quilliam, M. A.; Gagnon, C. Detection and confirmation of saxitoxin analogues in freshwater benthic Lyngbya wollei algae collected in the St. Lawrence River (Canada) by liquid chromatography-tandem mass spectrometry. *J. Chromatogr. A* **2012**, *1219*, 93-103.
99. Harwood, D. T.; Boundy, M.; Selwood, A. I.; van Ginkel, R.; MacKenzie, L.; McNabb, P. S. Refinement and implementation of the Lawrence method (AOAC 2005.06) in a commercial laboratory: Assay performance during an Alexandrium catenella bloom event. *Harmful Algae* **2013**, *24*, 20-31.
100. Rodrigues, M. A.; Reis, M. P.; Mateus, M. C. Liquid chromatography/negative electrospray ionization ion trap MS2 mass spectrometry application for the determination of microcystins occurrence in Southern Portugal water reservoirs. *Toxicon* **2013**, *74*, 8-18.
101. de Andrade, F. M.; de Macedo, A. N.; Vieira, E. M. Determination of microcystin-LR in cyanobacterial blooms from the Mogi Guacu River (Brazil) by high-performance liquid chromatography. *J. Liq. Chromatogr. Relat. Technol.* **2014**, *37*, 1310-1319.
102. Fayad, P. B.; Roy-Lachapelle, A.; Duy, S. V.; Prevost, M.; Sauve, S. On-line solid-phase extraction coupled to liquid chromatography tandem mass spectrometry for the analysis of cyanotoxins in algal blooms. *Toxicon* **2015**, *108*, 167-175.
103. Zastepa, A.; Pick, F. R.; Blais, J. M.; Saleem, A. Analysis of intracellular and extracellular microcystin variants in sediments and pore waters by accelerated solvent extraction and high performance liquid chromatography-tandem mass spectrometry. *Anal. Chim. Acta* **2015**, *872*, 26-34.
104. Pekar, H.; Westerberg, E.; Bruno, O.; Lääne, A.; Persson, K. M.; Sundström, L. F.; Thim, A.-M. Fast, rugged and sensitive ultra high pressure liquid chromatography tandem mass spectrometry method for analysis of cyanotoxins in raw water and drinking water—First findings of anatoxins, cylindrospermopsins and microcystin variants in Swedish source waters and infiltration ponds. *J. Chromatogr. A* **2016**, *1429*, 265-276.

B-2 Biological activated carbon and advanced oxidation processes for the removal of cyanobacterial metabolites in drinking water treatment†

Chemistry in New Zealand *January 2017*

Article

Biological activated carbon and advanced oxidation processes for the removal of cyanobacterial metabolites in drinking water treatment

Daniel Bernstein,[1*] Graeme Glasgow,[2,3] Merilyn Manley-Harris,[1,3] Mark Lay[2]

[1] School of Science, Faculty of Science and Engineering, University of Waikato, Private Bag 3105, Hamilton 3240

[2] School of Engineering, Faculty of Science and Engineering, University of Waikato, Private Bag 3105, Hamilton 3240

[3] Environmental Research Institute, Faculty of Science and Engineering, University of Waikato, Private Bag 3105, Hamilton 3240 (email: *drbernstein1@gmail.com*)

Keywords: *water treatment, advanced oxidation, trace analysis, analytical chemistry*

Abstract

Biological activated carbon (BAC) and advanced oxidation processes (AOPs) are often used in conjunction during drinking water treatment for the removal of trace organic compounds that are not effectively removed during traditional treatment processes such as coagulation, flocculation and sand filtration. These trace organic compounds include toxic cyanobacterial metabolites such as saxitoxins and taste and odour (T&O) causing compounds like geosmin and 2-methylisoborneol (2-MIB) which are produced by a number of bacterial species including cyanobacteria. At present, the Hamilton Drinking Water Treatment Plant (HDWTP) employs the use of BAC as part of the final stage of drinking water treatment for its municipal water supply. This article provides a general overview of the chemical and physical processes involved and a review of the current state of AOP technology.

Introduction

The use of carbon as a means to purify water dates back to antiquity, with Hindu documents dating from around 450 BC making references to the use of charcoal filters for this purpose. The use of activated carbon for this purpose, however, is a more recent advance and it was first used as a means to dechlorinate chlorinated drinking water in 1910. Since then, it has been applied to a wide range of treatment problems including the removal of taste and odour – (T&O) causing compounds, synthetic organic contaminants (SOCs) and disinfection by-products (DBPs).[1]

Activated carbons (ACs) are porous carbonaceous materials capable of adsorbing a wide range of aqueous phase solutes. Because of their porosity and very high surface area (500-1500 m^2g^{-1}), they have the potential to adsorb very large amounts of material.[1,2]

The nature of the starting material, carbonisation conditions and activation process all contribute to the properties of the AC produced. Such properties include porosity, pore size, pore size distribution, surface functionality, and ash content.[1,2] The surface functionality of ACs plays an important role in the adsorption of organic solutes and is comprised mainly of oxygen based functional groups such as acidic groups including strong and weak carboxylic acids, phenols and carbonyls (α protons). Basic surface groups such as cyclic ethers are also generally present, with higher activation temperatures resulting in a more basic surface. Other components of ACs such as minerals, e.g. calcium, sulphate, and phosphate ions and ash (silica, alumina, iron oxides, and alkaline earth metals) also contribute to the surface activity.[1]

While activated carbon is very good at removing problematic compounds from drinking water sources, due to the physical nature of the process and the finite number of absorption sites, the surface of the AC becomes saturated over time. Once the surface of the AC is saturated, adsorption no longer occurs (or is substantially reduced) and breakthrough of previously adsorbed compounds is observed.[3] To remedy this situation, the AC must either be replaced or regenerated, both of which are costly processes.

A method to overcome this problem that has become increasingly exploited over the years, both in drinking and waste water treatment, is the use of biological activated carbon (BAC). In this mode of operation, microbial communities are allowed to colonise the AC media as the adsorption capacity becomes depleted. Once colonised, compounds that were previously removed by physical adsorption may now be metabolised enzymatically by the microorganisms that inhabit the AC surface.

Granular activated carbon in drinking water treatment

In drinking water treatment, the filter media in fixed bed carbon filters usually consists of granular activated carbon (GAC). Granular activated carbons generally have a particle size ranging from 0.2-5 mm and are designated by mesh sizes such as 8/20, 20/40, or 8/30 for such applications.[1,4]

The use of GAC in drinking water treatment is a very common practice and is implemented with the aim of removing unwanted contaminants from source water intended for use as drinking water that cannot be removed via primary treatment.[1,3,5] As such, the composition of the source water and the specific contaminants it may contain mean that GAC is employed for different reasons

† This article was originally published in Chemistry in New Zealand, 81(1), 13–18, **2017**

depending on location.[1,5] In Hamilton, GAC filtration was introduced as a precautionary measure for the removal of cyanobacterial metabolites, particularly cyanotoxins like microcystins (Fig. 1) and saxitoxins (Fig. 2), that may pose serious health risks during potential cyanobacterial blooms in the future.[6] Additionally, GAC is extremely effective in the removal of T&O causing compounds[1] such as geosmin and 2-methylisoborneol (GSM and 2-MIB; Fig. 3) which are known to be present in the Waikato River and were another reason for the initial implementation of GAC at the Hamilton plant.[7]

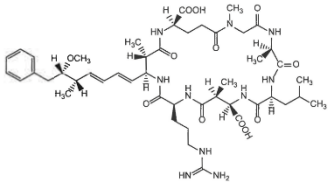

Fig. 1. Molecular structure of microcystin L-R

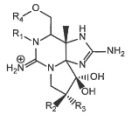

	Substituent Groups			
Toxin	**R1**	**R2**	**R3**	**R4**
STX	H	H	H	$CONH_2$
GTX2	H	H	OSO_3^-	$CONH_2$
GTX3	H	OSO_3^-	H	$CONH_2$
C1	H	H	OSO_3^-	$CONHSO_3^-$
C2	H	OSO_3^-	H	$CONHSO_3^-$
dcSTX	H	H	H	H
dcGTX2	H	H	OSO_3^-	H

Fig. 2. General structure of saxitoxins and the substituents of some common analogues[8-10]

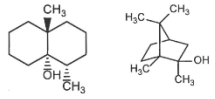

Fig. 3. Molecular structures of geosmin (left) and 2-methylisoborneol (right)

Biological activated carbon

The GAC filters currently in service at the HDWTP have been in use since 2007 following an extensive upgrade of the plant. Due to the length of time the filters have been operating, it is generally thought that adsorption processes have largely ceased and any removal of contaminants is a result of biological activity.[7] Indeed, the long term plan for the use of these filter was for them to operate as BAC filters once adsorption capacity was exhausted and a biofilm was gradually established.[11]

For successful operation of GAC filters operating in the BAC mode, certain operational criteria must be met in order to achieve sufficient removal of the target compounds. These criteria include ensuring the influent target compounds are in a form that is readily biodegradable (biodegradable organic matter; BOM) by the filter microorganisms and allowing sufficient contact time to permit diffusion of target compounds to the surface bound bacterial colony for metabolism to occur.

Usually, to increase the BOM fraction of influent dissolved organic matter (DOM), an advanced oxidation process (AOP) such as ozonation is implemented prior to the BAC filter, with the "BAC process" referring to the coupled mode of operation. While this was initially considered during the upgrade of the HDTWP, it was not implemented at the time. However, the design of the upgrade allowed contingency for the addition of such a process in the future if required.[11]

In order to provide sufficient time for the mass transport of these contaminants from the liquid phase into the bacterial cell for metabolism to occur, the contact time of water within the filter must be sufficiently long. In the operation of GAC and BAC filters, this is generally measured using the "effective empty bed contact time" (EBCT), which is a measure of the average time water would take to traverse the filter bed if the filter were empty. For BAC filters, an EBCT of greater than 7.5 minutes is generally thought to be sufficient if it is coupled to an AOP prior to the filter. Without the associated AOP, EBCTs of 10 minutes or more are considered more appropriate and this reflects the current operation of the filters at the HDWTP.

The general mechanism of removal of problematic compounds by bacteria occurs via secondary metabolic pathways acting upon the target compounds as secondary substrates due to their low concentration (ng L^{-1}), with the total organic carbon (TOC) which is present at much higher concentrations (mg L^{-1}) providing the primary substrate for primary metabolism. For example, GSM and 2-MIB are generally present in Hamilton source water at baseline levels of 5 to 50 ng L^{-1} which is noticeable to many people, imparting an earthy or musty character to the water (Table 1). Hence, the degree of removal needs to be very good and provide high percentages of removal even when the influent concentration is very low. The degree of removal is also very important for compounds like cyanotoxins which are covered under the Drinking Water Standards for New Zealand (DWSNZ) where, for example, the maximum acceptable value (MAV) for microcystins is set at 1 µg L^{-1}.[12]

Table 1. Odour concentration threshold values for geosmin and 2-MIB[13]

Compound	Odour concentration threshold (ng L^{-1})
Geosmin	6-10
2-MIB	2-20

While the desired outcome of metabolic transformation of target compounds is, at a minimum, the loss of chemical functionality that imparts undesired properties to finished drinking water (taste and odour, colour, toxicity, etc.), this may not always be the case. For example, there is some evidence to suggest that during the degradation

of saxitoxins in biological filters, those with lower relative toxicity like C1, C2, GTX2 and GTX3 (Fig. 2) are converted to the more toxic STX, potentially leading to an increase in toxicity following biological filtration and in other environmental contexts.[14-16] In situations where the influent water is known to contain high levels of saxitoxins, for example during a cyanobacterial bloom, it may be necessary to implement an AOP temporarily so as not to potentially exacerbate the problem.

Advanced oxidation processes

Advanced oxidation processes (AOPs) are often employed in drinking water treatment as a method of removing unwanted organic impurities and trace organic pollutants via chemical oxidation, with the ultimate aim of complete mineralization to C-O_2.[17] In particular, AOPs are a useful method for increasing the BOM fraction of the TOC prior to BAC or another type of bio-filtration system as a means of allowing compounds resistant to biodegradation to be metabolised more effectively by the biofilm. Of course, as a living biomass is involved, sufficient time must be allowed for the oxidant residual to decrease to a level that will not affect the health of the biological media following the AOP treatment.[18] Additionally, the AOP used must not contribute an increase in the trihalomethane (THM), haloacetic acid (HAA) or other disinfection by-product (DBP) formation potential, as these are tightly controlled under the DWSNZ.[12]

Although a range of AOPs are currently employed in various drinking and waste water treatment scenarios, almost all are based on the production of highly reactive radical intermediates, specifically the hydroxyl radical (•OH, Table 2).[19] Under most conditions, •OH will react via addition to unsaturated carbon-carbon bonds, aromatic substitution, hydrogen abstraction, or mono-electronic oxidation.[20]

Table 2. Standard half-cell potentials for some oxidants commonly used in water treatment[5,21,22]

Oxidant	Reduction half-reaction	E°_{red}(V)
Titanium dioxide "hole"*	$TiO_2 (h^+) + e^- \rightarrow TiO_2$	3.20
Hydroxyl radical	$^\bullet OH + H^+ + e^- \rightarrow H_2O$	2.85
Ozone	$^1/_3O_3 + H^+ + e^- \rightarrow {}^1/_2H_2 + {}^1/_2O_2$	2.08
Hydrogen peroxide	$^1/_2H_2O_2 + H^+ + e^- \rightarrow H_2O$	1.78

* h^+ = valence band hole produced by incident photons of sufficient energy

A range of AOPs are available and currently used in full-scale drinking water treatment plants worldwide. The use of AOPs as a mechanism for the removal of pollutants is applicable only in situations where the source water has a relatively low organic load (chemical oxygen demand; COD ≤ 5g L^{-1}). Hence, AOPs are ideally suited for the treatment of water intended for human consumption that has undergone primary treatment (coagulation, flocculation and filtration).[17] Current AOPs can be characterised as catalytic processes, ozone-based processes or UV-based processes.

Catalytic AOPs

Catalytic AOPs utilize H_2O_2, UV or a combination thereof in conjunction with a solid semi-conductor or transition metal catalyst to produce •OH. Catalytic AOPs such as the Fenton (Eq. 1) and Fenton-like processes (Eqs. 2-4) are often confined to waste water treatment, as the catalytic activity of Fe^{2+}/Fe^{3+} that is a feature of these processes requires strict pH control at fairly strong acidity (pH = 2.7-2.8) that is unlikely to be feasible for drinking water treatment applications.[17,22,23] The rate of degradation of organic pollutants by a Fenton-like mechanism can be increased by the use of UV light, giving the so-called photo-assisted Fenton processes. However, the pH requirements are the same as for more traditional Fenton-like processes.

$$Fe^{2+} + H_2O_2 \rightarrow Fe^{3+} + OH + {}^\bullet OH \quad \text{(Eq. 1)}$$

$$Fe^{3+} + H_2O_2 \leftrightarrows H^+ + [Fe - OOH]^{2+} \quad \text{(Eq. 2)}$$

$$[Fe - OOH]^{2+} \rightarrow HO_2^\bullet + Fe^{2+} \quad \text{(Eq. 3)}$$

$$Fe^{2+} + H_2O_2 \rightarrow Fe^{3+} + OH^- + {}^\bullet OH \quad \text{(Eq. 4)}$$

Photocatalysis: TiO_2/UV

More recently, photocatalytic AOPs based on TiO_2 (anatase) have been developed. The initial step in the TiO_2/UV type system involves the irradiation of TiO_2 followed by the formation of electron-hole pairs. This is achieved by employing incident photons of sufficient energy to produce conduction band electrons and valence band holes (Eq. 5).

$$TiO_2 + h\nu \rightarrow TiO_2^{h^+} + e^- \quad \text{(Eq. 5)}$$

The extremely high oxidation potential of holes (denoted h^+; Table 2) means that nearly all chemicals should be able to be oxidized, including the oxidation of adsorbed H_2O or OH^- to give •OH (Eqs. 6 & 7).

$$TiO_2^{h^+} + H_2O \rightarrow TiO_2 + {}^\bullet OH + H^+ \quad \text{(Eq. 6)}$$

$$TiO_2^{h^+} + OH^- \rightarrow TiO_2 + {}^\bullet OH \quad \text{(Eq. 7)}$$

Similarly, direct oxidation of pollutants may also occur, via adsorption and subsequent oxidation at the TiO_2 surface, although this process is thought to play a very minor role in the oxidation of organic components, with respect to •OH (Eq. 8).[22]

$$TiO_2^{h^+} + RX \rightarrow TiO_2 + RX^{+\bullet} \quad \text{(Eq. 8)}$$

Additionally, the electrons produced in the initial step are able to reduce some metals and dissolved O_2 to give the superoxide radical, $^\bullet O_2^-$.

This method has the advantage of potentially using solar radiation as a source of UV, thereby not requiring the implementation of UV lamps as part of the reactor. However, as this relies on consistently fine weather, this leads to inconsistent system performance. Additionally, standard TiO_2 only absorbs a narrow bandwidth of the total solar spectrum, meaning the overall quantum yield is low. To overcome this, the development of doped TiO_2 that is able to more effectively utilise wavelengths of the

solar spectrum available at ground level have been investigated as a means of reducing the need for specialised UV reactors.[17,24] TiO_2-based AOPs have been investigated by a number of researchers as a means to remove cyanotoxins from drinking water including microcystins (Fig. 1), cylindrospermopsins and nodularins (Fig. 4) with good results.[25-28]

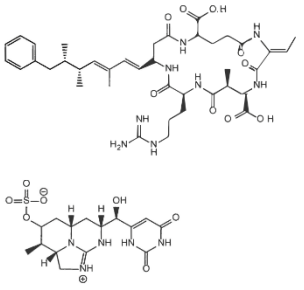

Fig. 4. Molecular structures of nodularin-R (top) and cylindrospermopsin (bottom)

Ozone- and UV-based AOPs

Ozone-based processes rely on the decomposition of ozone (O_3) to produce •OH. The yield of •OH can be increased by the use of H_2O_2 or UV in the system. The production of •OH in aqueous systems can also be achieved without the use of O_3 as is the case with UV-based processes like H_2O_2/UV and Cl_2/UV-based AOPs.

Ozone-based processes

The use of O_3 as an oxidant requires the implementation of an on-site O_3 generator. Ozone is usually generated by an electrical discharge (8-20 kV) applied to molecular oxygen, air or oxygen enriched air as per Eqs. 9 & 10.[5]

$$O_2 + \text{energy} \rightarrow O + O \qquad \text{(Eq.9)}$$

$$O + O_2 \rightarrow O_3 \qquad \text{(Eq.10)}$$

The O_3 that is generated can then be introduced into solution via a suitable gas transfer device such an in-line gas injection system or a multistage bubble contactor.[5]

O_3 is highly reactive towards many compounds found in drinking water that contain specific functional groups including alkenes, activated aromatics, amines, sulfides and other organic compounds containing electron rich moieties.[29,30] While this means direct use of ozone is likely to be minimally effective for the removal of many T&O causing compounds (Fig. 3), cyanotoxins are likely to be effectively oxidised due to their wide range of susceptible functionalities (Figs. 1,2,5).

Under the right conditions, O_3 will also spontaneously decompose via a chain reaction mechanism, which includes the production of •OH and •OOH (hydroperoxyl) radicals that are much less selective oxidants according to Eqs. 11-17.

$$HO^- + O_3 \rightarrow O_2 + HO_2^- \qquad \text{(Eq.11)}$$

$$HO_2^- + O_3 \rightarrow HO_2^\bullet + O_3^{\bullet -} \qquad \text{(Eq.12)}$$

$$HO_2^\bullet \rightarrow H^+ + O_2^{\bullet -} \qquad \text{(Eq.13)}$$

$$O_2^{\bullet -} + O_3 \rightarrow O_2 + O_3^{\bullet -} \qquad \text{(Eq.14)}$$

$$O_3^{\bullet -} + H^+ \rightarrow HO_3^\bullet \qquad \text{(Eq.15)}$$

$$HO_3^\bullet \rightarrow HO^\bullet + O_2 \qquad \text{(Eq.16)}$$

$$HO^\bullet + O_3 \rightarrow HO_2^\bullet + O_2 \qquad \text{(Eq.17)}$$

The chain reaction can be initiated in various ways including the presence of natural organic matter (NOM), Fe^{2+}, H_2O_2, UV radiation and OH^- (Eq. 11; pH ≥ 8.5).[5,17,23,30]

For example, the production of HO_2^- from H_2O_2 in aqueous solution (Eq. 18) illustrates how the initiation of the chain decomposition to produce •OH may be enhanced, by increasing the quantity of HO_2^- available to react with O_3 (Eq. 12).[17,22,30]

$$H_2O_2 \leftrightarrows HO_2^- + H^+ \qquad \text{(Eq.18)}$$

Hence, oxidation by O_3 can be enhanced by the addition of H_2O_2 into the system. This can be achieved by directly introducing H_2O_2 into the system (O_3/H_2O_2), or by producing H_2O_2 *in situ* from O_3 using UV radiation (O_3/UV system).[22,30] This is achieved via the UV irradiation of ozone, which produces molecular oxygen and excited singlet state oxygen ($O(^1D)$). The singlet oxygen rapidly combines with water to produce hydrogen peroxide (Eq. 19).

$$O_3 \xrightarrow{UV} O_2 + O(^1D) \xrightarrow{H_2O} H_2O_2 \qquad \text{(Eq.19)}$$

The H_2O_2 that is produced can then dissociate (Eq. 18) and initiate the chain reaction decomposition of O_3 (Eqs. 12-17).

The use of additives such as H_2O_2 or UV overcomes the need to maintain the O_3 system at low pH while still producing an adequate concentration of •OH to effect a reasonable rate of oxidation for a wide range of target contaminants. Reaction rates of oxidation by •OH of some T&O causing compounds are generally much higher than O_3 (Table 3), with the faster reaction rates of oxidation with O_3 limited to alkenes and activated aromatic compounds.[29]

UV-based processes

UV-based processes forego the use of ozone as an oxidant and instead aim to form •OH or other radical species from other oxidising agents or from water directly. These include UV/H_2O_2, UV/Cl_2 and vacuum UV (VUV).

UV/H_2O_2

This process aims to produce •OH from H_2O_2 by exploiting the absorption of UVC radiation by H_2O_2 between 100 and 280 nm.[20] As Hg lamps produce an emission line at 253.6 nm, these are most commonly used for this purpose.[20,22] Initiation of the chain propagation reaction begins with homolytic photolysis of H_2O_2, yielding two •OH (Eq. 20), which then undergo a radical chain reaction via the Haber-Weiss mechanism (Eqs. 21 & 22).[22,31]

Table 3. Reaction rate constants of taste and odour compounds via oxidation with O_3 or $^{\bullet}OH$[29]

Compound	Reaction rate constant (k) O_3	$^{\bullet}OH$
β-cyclocitral	3890 $M^{-1} s^{-1}$	7.42 x 10^9 $M^{-1} s^{-1}$
geosmin	0.10 $M^{-1} s^{-1}$	7.80 x 10^9 $M^{-1} s^{-1}$
3-hexen-1-ol	5.4 x 10^5 $M^{-1} s^{-1}$	7.45 x 10^9 $M^{-1} s^{-1}$
β-ionone	1.6 x 10^5 $M^{-1} s^{-1}$	7.79 x 10^9 $M^{-1} s^{-1}$
2-isopropyl-3-methoxypyrazine	50.2 $M^{-1} s^{-1}$	4.91 x 10^9 $M^{-1} s^{-1}$
2-methylisoborneol	0.35 $M^{-1} s^{-1}$	5.09 x 10^9 $M^{-1} s^{-1}$
2,6-nonadienal	8.7 x 10^5 $M^{-1} s^{-1}$	10.49 x 10^9 $M^{-1} s^{-1}$
1-penten-3-one	5.9 x 10^4 $M^{-1} s^{-1}$	4.71 x 10^9 $M^{-1} s^{-1}$
2,6-di-*tert*-butyl-4-methylphenol	7.4 x 10^4 $M^{-1} s^{-1}$	3.20 x 10^9 $M^{-1} s^{-1}$
2,4,6-tribromoanisole	0.020 $M^{-1} s^{-1}$	3.74 x 10^9 $M^{-1} s^{-1}$
2,4,6-trichloroanisole	0.057 $M^{-1} s^{-1}$	5.10 x 10^9 $M^{-1} s^{-1}$

$$H_2O_2 + h\nu \rightarrow 2HO^{\bullet} \quad \text{(Eq.20)}$$

$$H_2O_2 + HO^{\bullet} \rightarrow HO_2^{\bullet} + H_2O \quad \text{(Eq.21)}$$

$$HO_2^{\bullet} + H_2O_2 \rightarrow H_2O + O_2 + HO^{\bullet} \quad \text{(Eq.22)}$$

Stoichiometrically, it would seem that the photolysis of 1 mol of H_2O_2 would yield 2 mol of $^{\bullet}OH$, and experiments in the gas phase do agree with this where the quantum yield of $^{\bullet}OH$ ($\Phi^{\bullet}_{OH}$) has been shown to be 2.09 ± 0.36. However, in the liquid phase this is not true, where $\Phi^{\bullet}_{OH} \approx 1$ and this indicates that only approximately 50% of H_2O_2 is converted to free $^{\bullet}OH$. This is often explained by the solvent "cage" effect, whereby newly created radicals in the liquid phase are surrounded by a solvent cage which promotes recombination of the radical species (Eq. 23).[20,22,31]

$$H_2O_2 + h\nu \leftrightarrows (HO^{\bullet} + HO^{\bullet})_{aq} \rightarrow HO^{\bullet} \quad \text{(Eq.23)}$$

The UV/H_2O_2 system is quite commonly used, and has the advantage of requiring fewer oxidants and dosage systems compared with O_3/H_2O_2 systems, while still providing high enough concentrations of $^{\bullet}OH$ to achieve reasonable degrees of removal of pollutants at the commonly used dosages in water treatment of 2 – 10 mg L^{-1}.[22]

UV/Cl_2

The UV/Cl_2 process is based on UV-induced photo-dissociation of species present in aqueous solutions of chlorine which is produced by introducing chlorine gas to water (Eqs. 24 – 28).[32,33]

$$Cl_2 + H_2O \rightarrow HOCl + HCl \quad \text{(Eq.24)}$$

$$HOCl \xrightarrow{UV} HO^{\bullet} + Cl^{\bullet} \quad \text{(Eq.25)}$$

$$HOCl \leftrightarrows H^+ + OCl^- \quad \text{(Eq.26)}$$

$$OCl^- \xrightarrow{UV} O^{\bullet} + Cl^{\bullet} \quad \text{(Eq.27)}$$

$$O^{\bullet} + H_2O \rightarrow HO^{\bullet} + HO^- \quad \text{(Eq.28)}$$

While the yield of $^{\bullet}OH$ is theoretically higher than the UV/H_2O_2 process, the UV/Cl_2 process is pH dependent, with optimum yield being realised at pH < 6.[32] As the pH of the influent water used at the HDWTP is approximately 7,[34] pH adjustment would be required to achieve optimum $^{\bullet}OH$ yield. However, at neutral pH, the process is kinetically comparable to the UV/H_2O_2 in the oxidation of trace organic contaminants.[32] Additionally, as many water treatment plants, including Hamilton, already employ Cl_2 as a disinfectant, this method may provide a cost effective alternative AOP to O_3 and H_2O_2 based processes which require the installation of new infrastructure. Although this may be a good option in some cases, and has been shown to degrade GSM and 2-MIB quite effectively,[32] it may be more prone to radical scavengers and quenching than the UV/H_2O_2 process, depending on the composition of the influent water.[35]

Vacuum UV

Vacuum UV (VUV) is an "oxidant free" AOP that degrades organic pollutants by the formation of reactive species like $^{\bullet}OH$, $^{\bullet}H$, $e^-_{(aq)}$, $^{\bullet}HO_2$ and $^{\bullet}O_2$ via the direct photolysis of water by irradiation with short wavelength (< 200 nm) UV radiation.[22]

Two main reactions initiate a series of chain reactions (Eqs. 29 & 30).

$$H_2O + h\nu_{<200nm} \rightarrow HO^{\bullet} + H^{\bullet} \quad \text{(Eq.29)}$$

$$H_2O + h\nu_{<200nm} \rightarrow HO^{\bullet} + H^+ + e^-_{aq} \quad \text{(Eq.30)}$$

Photons with wavelengths in the VUV region can be produced in a number of ways, most commonly via the use of excimer (excited dimer) lamps and low-pressure Hg lamps (VUV-Hg). Excimer lamps, which contain inert gases like xenon, argon and krypton, emit VUV radiation at various wavelengths, depending on the gas used. For example, Xe_2-excimer lamps emit at 172 nm with around 5 to 40% efficiency. One problem with the use of these lamps is the fact that water has a very high absorptivity (550 cm^{-1}) at this wavelength. While VUV-Hg lamps provide radiation at 185 nm where the absorptivity of water is lower (1.80 cm^{-1}), this still means that most of the emitted photons are absorbed within 0.3 cm of the water surface. Possible ways to circumvent this problem may be to increase the level of turbulence in the VUV reactor or bubbling oxygen or air through the system via some form of diffuser or aerator.[22,36,37]

More than 30 reactions are known to occur during VUV photolysis of water, and while the direct photolysis of dissolved organic compounds is possible, it is unlikely to be significant compared to the oxidation of these compounds by the radicals produced from water during the VUV process, which is present at a concentrations many orders of magnitude higher.[22]

At present, VUV technology is still at the laboratory stage and in pilot plant development for application to large scale water treatment, although it looks to be a promising technology for future applications in this area.

Summary

AOPs provide a means of mineralising problematic organic contaminants commonly associated with cyanobacteria. When complete mineralisation is not achieved, AOPs may also pre-treat influent water for a downstream bio-filtration system such as BAC by oxidising these problematic compounds and presenting them in a more biodegradable form. While some of these AOPs are well established and used routinely in full scale treatment facilities, some promising new technologies are emerging that minimise the use of chemical oxidants or employ photocatalytic reagents providing greener, more sustainable options.

References

1. Cecen, F.; Aktas, O. *Activated carbon for water and wastewater treatment: Integration of adsorption and biological treatment*, Wiley-VCH: Weinheim, Germany, 2012.
2. Marsh, H.; Rodriguez-Reinoso, F. *Activated carbon*, Elsevier: Amsterdam; London, 2006.
3. Digiano, F. A. Adsorption of organic substances in drinking water. In *Control of organic substances in water and wastewater*; B. B. Berger, Ed.; Noyes Data Corporation: NJ, USA, 1987.
4. Davis, M. L. *Water and wastewater engineering*, McGraw-Hill: New York, 2010.
5. American Water Works Association *Water quality and treatment: A handbook of community water supplies. 5th ed*, McGraw-Hill Publishing Co., 1999.
6. Kouzminov, A.; Ruck, J.; Wood, S. A., *Aust. N.Z. J. Public Health*, **2007**, *31*, 275-281.
7. Porter, M.; Rose, R., *Hamilton's water treatment plant - a review of recent performance*, Rotorua, New Zealand, 2011.
8. Ho, L.; Sawade, E.; Newcombe, G., *Water Res.*, **2012**, *46*, 1536-1548.
9. Quilliam, M. A.; Janecek, M.; Lawrence, J. F., *Rapid Commun. Mass Spectrom.*, **1993**, *7*, 482-487.
10. Boundy, M. J.; Selwood, A. I.; Harwood, D. T.; McNabb, P. S.; Turner, A. D., *J. Chromatogr. A*, **2015**, 1387, 1-12.
11. Porter, M.; Carne, S.; Muntisov, M.; Shaw, M.; Harty, T.; Mould, M., *Hamilton WTS upgrade – the future for water treatment in NZ?*, Bendigo Exhibition Centre, VIC, Australia, 2007.
12. Ministry of Health, *Drinking-water standards for New Zealand 2005 (revised 2008)*, Government of New Zealand, Wellington (NZ), 2008.
13. Omur-Ozbek, P.; Little, J. C.; Dietrich, A. M., *Water Sci. Technol.*, **2007**, *55*, 249-256.
14. Kayal, N.; Newcombe, G.; Ho, L., *Environ. Tox.*, **2008**, *23*, 751-755.
15. Kotaki, Y.; Oshima, Y.; Yasumoto, T., *Nippon Suisan Gakk.*, **1985**, *51*, 1009-1013.
16. Kotaki, Y., *Nippon Suisan Gakk.*, **1989**, *55*, 1293-1293.
17. Andreozzi, R.; Caprio, V.; Insola, A.; Marotta, R., *Catal. Today*, **1999**, *53*, 51-59.
18. Urfer, D.; Huck, P. M.; Booth, S. D. J.; Coffey, B. M., *J. Am. Water Works Assoc.*, **1997**, *89*, 83-98.
19. Black & Veatech Corporation *White's handbook of chlorination and alternative disinfectants (5th edition)*, John Wiley & Sons, Inc., 2010.
20. Gligorovski, S.; Strekowski, R.; Barbati, S.; Vione, D., *Chem. Rev.*, **2015**, *115*, 13051-13092.
21. Nakata, K.; Fujishima, A., *J. Photochem. Photobiol. C*, **2012**, *13*, 169-189.
22. Linden, K. G.; Mohseni, M. Advanced oxidation processes: Applications in drinking water treatment. In *Comprehensive water quality and purification*; S. Ahuja, Ed.; Elsevier: Waltham, 2014; pp 148-172.
23. Munter, R., *Proc. Est. Acad. Sci. Chem.*, **2001**, *50*, 59-80.
24. Henderson, M. A., *Surf. Sci. Rep.*, **2011**, *66*, 185-297.
25. Feitz, A. J.; Waite, T. D.; Jones, G. J.; Boyden, B. H.; Orr, P. T., *Environ. Sci. Technol.*, **1999**, *33*, 243-249.
26. Liu, I.; Lawton, L. A.; Bahnemann, D. W.; Robertson, P. K. J., *Appl. Catal., B*, **2005**, *60*, 245-252.
27. Pestana, C. J.; Edwards, C.; Prabhu, R.; Robertson, P. K. J.; Lawton, L. A., *J. Hazard. Mater.*, **2015**, 300, 347-353.
28. Wu, C.-C.; Huang, W.-J.; Ji, B.-H., *J. Environ. Sci. Health, Part A: Toxic/Hazard. Subst. Environ. Eng.*, **2015**, *50*, 1116-1126.
29. Peter, A.; Von Gunten, U., *Environ. Sci. Technol.*, **2007**, *41*, 626-631.
30. Hoigne, J. Chemistry of aqueous ozone and transformation of pollutants by ozonation and advanced oxidation processes. In *Quality and treatment of drinking water II*; D. J. Hrubec, Ed.; Springer, 1998; pp 83-141.
31. Lunak, S.; Sedlak, P., *J. Photochem. Photobiol., A*, **1992**, *68*, 1-33.
32. Watts, M. J.; Hofmann, R.; Rosenfeldt, E. J., *J. Am. Water Works Assoc.*, **2012**, *104*, 47-48.
33. Jin, J.; El-Din, M. G.; Bolton, J. R., *Water Res.*, **2011**, *45*, 1890-1896.
34. Hamilton City Council "Waikato river and treated drinking water comprehensive analysis report 2013/14," 2014.
35. Jin, J.; El-Din, M. G.; Bolton, J. R., *Water Res.*, **2011**, *45*, 1890-1896.
36. Oppenländer, T.; Walddörfer, C.; Burgbacher, J.; Kiermeier, M.; Lachner, K.; Weinschrott, H., *Chemosphere*, **2005**, *60*, 302-309.
37. Oppenländer, T. *Photochemical purification of water and air - advanced oxidation processes (AOPs): Priciples, reaction mechanisms, reactor concepts*, Wiley-VCH: Darmstadt, Germany, 2003.